FACULTY OF SCIENCES

SCK•CEN ACADEMY FOR NUCLEAR SCIENCE AND TECHNOLOGY

DEPARTMENT OF ANALYTICAL CHEMISTRY

EXPERIMENTAL DETERMINATION AND RE-EVALUATION OF NUCLEAR DATA FOR THE PARAMETRIC AND k_0-STANDARDIZATION OF NEUTRON ACTIVATION ANALYSIS

Word count: 109708

Fulvio Farina Arboccò
Student number: 00814488

Supervisor(s): Prof. Dr. Karel Strijckmans, Ir. Peter Vermaercke

A dissertation submitted to Ghent University in partial fulfilment of the requirements for the degree of Doctor of Sciences: Chemistry

Academic year: 2016 – 2017

GHENT UNIVERSITY

SCK•CEN
STUDIECENTRUM VOOR KERNENERGIE
CENTRE D'ETUDE DE L'ENERGIE NUCLEAIRE

Acknowledgements

This work is the result of the successful collaboration between several people. Each one deserves an explicit mention and my deepest gratitude.

The most crucial person for the realization of this work is Peter Vermaercke, my co-promoter. He opened me the door of opportunity some time ago, so I could work on my first thesis. He also found me a job on the highly interesting and challenging topic of uranium fission. Later, he prepared 2 Doctoral research projects, so even if the first proposal failed to be approved (as it happened) I could still have a unique second chance to be recipient of a full-time scholarship. That was only the beginning in a series of generosities and favours during all these years to help me become a better scientist.

I am indebted to the three angular stones of this work: Mrs. Katrien Smits, Ing. Liesel Sneyers and Ing. Leen Verheyen, for all their tremendous effort and hard work. Coordination and preparation of all these samples, rabbits and their unconditional assistance at every step of the PhD stage was just a part of all the valuable things you did for me. I thank Mr. Eddy Daniels for being part of that wonderful group.

It is due to Prof. Karel Strijckmans that I had the pleasure and opportunity to be part of this Alma Mater. Thanks to his continuous advices, support and help, half of what seemed impossible became possible and half of what could have gone wrong did not.

This work would have not been possible without the help and financial funding from the SCK•CEN Direction, the SCK•CEN Scientific Committee, and the SCK•CEN Academy. I will be forever indebted with this institute workforce.

Needless to say that I am in deep gratitude with Dr. M. Bruggemann for his advices, scientific and technical wisdom handsomely irradiated to me; to Mrs. G. Sibbens, Mr. A. Moens and Dr. J. Wagemans for providing me with the greatest quality and most suited materials we could get for this work. I would like to thank the technical staff: Mr. I. Verwimp, Mr. B. Van Houdt, Mr. P. Vandycke, Mr. S. Van Bijlen and Mr. J. Leeuws for making the irradiations possible and for their skilful help during these exercises. Special gratitude goes out to Dr. G. Vittiglio for his help and provided reactor time. I would like to thank Dr. F. De Corte, Dr. G. Kennedy, Dra. C. Chilian, Mr. W. De Boek, Mr. R. Van Sluijs, Dr. D. Bossus, Dr. A. Chatt and Dr. A. Trkov for their valuable insight and important key remarks during these years.

Thanks to the final and important remarks from Dr. A. Simonits, Dr. N. Otsuka, Dr. S. Pommé, Dr. P. Bode, Prof. Dr. H. Thierens, Prof. Dr. W. Maenhaut and Prof. Dr. L. Vincze I could improve the content of this book.

A mi madre Liliana, mis hermanos Oriana y Gianluca, mis amigos F. Mata, A. Bencid, Dr. A. Peralta, Dr. H. Barros, Dr. G. Husband, L. Bonet, A. Mora, A. Godoy, J. A. Mesa, S. González, G. Macsotay, A. Ostapovich y K. Contreras, porque fueron, son y seguirán siendo mis constantes. De las constantes nucleares se puede dudar, pero de la constancia de vuestro amor nunca.

Thank you for making this work possible,

Fulvio Romano Farina Arboccò

Caracas, Venezuela

To my mother, sister and brother,

the true constants of my life

“Per aspera ad astra”

List of Abbreviations

A = Atlas of Neutron Resonances [1, 2]

A = saturated γ (or X) ray induced activity; $A = I_\gamma A_{Sat}$; section 2.1

a = (induced) activity concentration $A/\hat{w}$; see eq. (2.61); section 2.9.2

AA = Alfa Aesar (UK); Thermo Fisher scientific brand

ADC = Analog-to-Digital Converter; section 3.2

ADS = Activation-Decay Scheme; section 2.14

A_{Sat} = saturated induced activity; section 2.1

AVG = arithmetic mean

AW = standard atomic weight of the element; dimensionless

α = irradiation channel and position specific parameter to account for $1/E^{(1+\alpha)}$ deviations of the epithermal neutron fluence rate; dimensionless; see eq. (2.17); section 2.4

B = uranium results reported by Blaauw et al. in reference [3]

β_α = the inverse of the modified spectral index (r_α); defined in eq. (2.68); section 2.10

C = Calculated value derived with the aid of the absolute nuclear constants compiled in Table 10.21 (when Lit values were not found). Nuclear data obtained from [1, 2, 4–10]

Cavity = highly-thermalized irradiation channel with characteristics given in Table 6.6. and Figure 6.7

CENDL = Chinese Evaluated Nuclear Data Library as compiled in reference [2]

Ch = the number of channels from the multi-channel data analyser employed in the spectrum acquisition

CFY = cumulative fission yield factors adopted from references [11, 12]

COI = γ-ray coincidence correction factor; see eq. (3.20)

CRP = Coordinated Research Project from the IAEA

C_t = counting factor; see eq. (2.7)

C_α = corrected C_0 parameter for a specific channel and irradiation position; defined in eq. (2.42); section 2.8

C_0 = a correction factor for I_0 related to the ratio between 2 convened reference neutron energies E_0 and E_{Cd}; defined in eq. (2.43); section 2.8

DC = values reported by F. De Corte in his Habilitation thesis [13]

DDEP = Decay Data Evaluation Project [8]

D_t = decay factor; defined in eq. (2.7)

Δ = usually the relative difference between the results of this work and other authors; can have other meanings (per section)

Δa = Cd-subtracted activity concentration; see eq. (2.63); section 2.9.2

EAF =The European Activation File [14]

E_{Cd} = Cadmium cut-off energy for Cd-covers of 1 mm thickness; 0.55 eV by convention

EENL = evaluated or experimental nuclear data libraries: ENDF, JEFF, ROSF, CENDL, EAF, JENDL databases in references [2, 4, 6–8, 15]

ENDF = Evaluated Nuclear Data File

$E_{r,j}$ = resonance energy of a given target isotope for a radiative neutron capture at neutron energy j

$\bar{E}_r$ = effective resonance energy; weighted average from all $E_{r,j}$; see eq. (2.48); section 2.8

$\bar{E}_{r,\alpha}$ = correction to the effective resonance energy when $\alpha \neq 0$; see eqs. (2.45) and (2.46); section 2.8

ε_γ = efficiency for the detection of a γ or X-ray of a given energy E_γ at a specific sample-detector configuration and distance

$\varepsilon_{\gamma,\mathrm{ref}} = \varepsilon_\gamma$ at reference position, i.e. detector calibration configuration

F = a metal (pure or alloy) foil

f = thermal-to-epithermal conventional fluence rate ratio; dimensionless; see eq. (2.26); section 2.4

F_i = decay branching factor (or I.T. coefficient) from a given nucleus state to another one.

F_{Cd} = Cadmium transmission factor for cadmium covers 1 mm thick and 2:1 cylindrical size; see eq. (2.50)

FN = formed nuclide

FWHM = full width at half maximum

G_e = epithermal neutron self-shielding correction factor; sections 2.5 and 4.2

GF = GoodFellow (USA); standards and materials provider

G_{mod} = neutron moderation correction factor; sections 2.5, 4.3 and 4.5

g_T = Westcott factor; correction factor for non-1/v nuclides; see eq. (2.67); section 2.10

G_{th} = thermal neutron self-shielding correction factor; sections 2.5 and 4.1

H = Holden N. E. [16]

HDPE = high-density PE

HP = high-purity; hyper-pure

IAEA = International Atomic Energy Agency (Austria)

IRMM = Institute for Reference Materials and Measurements (Belgium)

IUPAC = International Union of Pure and Applied Chemistry (Switzerland)

IUPAC1 = IUPAC Technical Report from Wieser et al. [17]

IUPAC2 = IUPAC Technical Report from Berglund et al. [10]

JEFF = Joint Evaluated Fission and Fusion Nuclear Data Library as compiled in reference [2]

JENDL = Japanese Evaluated Nuclear Data Library [7]

k = Coverage factor for a 95% confidence level

k = The Boltzman constant; $k = 8.6173324(78) \times 10^{-5}$ eV.K^{-1}

KFKI = Központi Fizakai Kutató Intézet; Atomic Research Institute (Hungary; now AEKI)

k_0 = (experimentally found) composite nuclear data ratio from standard and single-comparator radiative (γ or X-ray) thermal neutron capture effective yields; see eq. (2.38); section 2.7; dimensionless; generally tabulated for natural (terrestrial) isotopic abundances for production of a ground, metastable or an effective radionuclide state; ADS-dependent

k_0-ISC = The International k_0 Scientific Committee

k_0-UNAA = k_0-NAA for the analysis of multielemental samples containing U; see Chapter 5

K1 = Kennedy et al. in reference [18]

K2 = Kennedy et al. in reference [19] by means of Cd-ratios

K3 = Kennedy et al. in reference [19] by means of the two-channel method

L = the thermal-to-fast conventional neutron fluence rate ratio; see eq. (2.104); section 2.13

LFC = Loss Free Counting; correction method for (pulse) count losses; section 3.9

Lit = the k_0-ISC recommended k_0 literature or k_0-libraries (2003-2012) in references [20–24]

LP = Liquid pipetted on a cylindrical paper filter; as described in Figure 6.5; section 6.8

λ = decay constant of a given radionuclide (in s^{-1}); other generalizations see eqs. (2.121); section 2.15

M = the molar mass of the element (in g.mol^{-1})

m = the different number of standards or materials employed

MCA = Multi-Channel Analyzer; section 3.2

ND = Nudat 2.6 database [6]

NIST = National Institute of Standards and Technology (USA)

N_{Ch} = the number of channels

N_m = the number of bare or Cd-covered samples irradiated per channel

N_p = number of detected X or γ-ray radioisotope emissions of a given energy, i.e. the area of a (deconvoluted) photopeak. Must be corrected for pulse pile-up, dead-time, burn-up, γ-ray coincidence; see Chapter 3.

PE = polyethylene; $(C_2H_4)_n$; 0.88–0.96 g/cm^3; CAS number 9002-88-4

Q_0 = (experimentally found) ratio between the evaluated resonance integral I_0 per an idealized $1/E$ epithermal neutron distribution and the thermal neutron cross-section σ_0; dimensionless; see eq. (2.44); section 2.8; for production of a ground, metastable or an effective radionuclide state; ADS-dependent

$Q_{\alpha\,=}$ corrected Q_0 the irradiation channel and position employed; see eq. (2.41); section 2.8

R_{Cd} = Cd-ratio; ratio between the activities of a bare and a Cd-covered replicate sample; see eq. (2.49); section 2.8

r_{Cd} = normalized Cd-Ratio; this work definition; given in eqs. (2.51) to (2.53); section 2.9.1

R_H = normalized (n,γ) reaction rate per nuclide according to the modified Høgdahl convention; see eq. (2.31); section 2.4

Risø = Danmarks Tekniske Universitet (DTU) National Laboratory for Sustainable Energy (Denmark; dissolved in 2012)

ROSF = Russian Evaluated Data Libraries as compiled in reference [2]

RV = Revised Values / Recommended Data in reference [8]

R_W = normalized (n,γ) reaction rate per nuclide according to the modified Westcott formalism; see eq. (2.65); section 2.10

SA = Sigma-Aldrich Corporation (USA); standards and materials provider

S_t = saturation factor; defined in eq. (2.5); dimensionless

SPEB = square PE bag of 0.1 mm thickness; see Figure 6.6, section 6.8

SWX = Shieldwerx (USA); materials provider

S84 = irradiation channel with characteristics given in Table 6.6. and Figure 6.7; section 6.9

s_0 = equivalent to the Q_0 factor for use under the modified Westcott formalism; see eq. (2.70) of section 2.10

$s_{\alpha\,=}$ corrected s_0 the irradiation channel and position employed; see eq. (2.69); section 2.10

σ_0 = radiative neutron capture cross-section for neutrons in thermal equilibrium with the moderator (T_0 = 293.6 K) at an energy of $E_0 = kT_0$ = 25.3 meV, (velocity v_0 = 2200 m.s^{-1}); see eq. (2.18); section 2.4.

θ = isotopic abundance (fraction); dimensionless

TI = target isotope

Tkv = values calculated by Trkov et al. with the aid of the ENDF/B-VII.1b4 in the report "Supplementary Data for Neutron Activation Analysis" [25], submitted to the CRP of the IAEA

Trkov = values reported by A. Trkov in a personal communication to the k_0-ISC (2011)

TW = this work; this book results

$T_{1/2}$ = half-life of a given radionuclide (in s); related to λ by means of eq. (2.4); section 2.1

T_j = Temporal factor $T = S_{ti}D_{td}C_{tc}$ for the radionuclide j; see eq. (2.122); section 2.15

T_{yz} = Temporal factor according to the ADS decay type y and scenario z; see Table 10.3

Others = Values calculated by A. Trkov with data from the ENDF library [4] or compiled from other sources by him in [25]

ω_{Cd} = ratio of r_{Cd} values for the analyte and the comparator; given in eq. (2.57). It is the proportionality constant between Q_α factors (for the analyte and comparator)

W = a metal (pure or alloy) wire

w = mass of the element of interest (in g)

$\hat{w}$ = sample mass (in g)

W' = small correction factor for a non-1/v behaviour when $\alpha = 0$; see eq. (2.79); section 2.10.2

W'_α = correction to the W' parameter when $\alpha \neq 0$; see eq. (2.78); section 2.10.2

ρ = can be: 1) fraction of the element in the sample (in $\mu g.g^{-1}$); 2) the density of the sample/material

X26 = irradiation channel with characteristics given in Table 6.6. and Figure 6.7; section 6.9

Y4 = irradiation channel with characteristics given in Table 6.6. and Figure 6.7; section 6.9

ZDT = Zero Dead-Time; section 3.9

Contents

1. Introduction

Some ancient people attributed to deities or to the “quintessence” the power of transforming objects that seemed unable to be changed by any circumstance (immutable) and the power to impart incorruptibility, to keep them from rotting [26]. Several of our ancestors believed in the existence of a “lapis philosophorum”, a legendary chemical substance said to be capable of turning metals such as lead or mercury into gold or silver (transmutation) [27]. For centuries, this achievement would be the most important goal in “Alchemy”, a metaphysical precursor of modern chemistry. In 1886 the prolific chemist Hermann Kopp said about the centuries long failed attempts to transmute elements that “the history of Alchemy is the history of an error” [28].

Less than a century ago (1932) Sir James Chadwick discovered the “neutron”, a nuclear particle with no charge and a building block of the atomic nucleus [29]. Two years later Enrico Fermi [30] and Amaldi et. al [31] showed that bombardment of rare earth elements such as lanthanum, gadolinium and europium with free neutrons induced the transmutation of a nuclide into another. Thus, the possibility of nuclidic transmutation was demonstrated and it was clearly within the technological reach. The elusive and for centuries sought qualities of the “philosopher’s stone” were apparently found in the form of neutrons. The bombardment of elements with high-energy charged particles and light demonstrated these capabilities as well, but the great majority of the newly discovered transmutations could be easily induced with neutrons.

During each transmutation process, high energy radiation was produced (i.e. energetic light or fast particles were emitted) and due to the quantum (discrete) nature of the phenomena, the radiation emitted by a given "radioactive element", radioisotope or radionuclide, had always the same energy.

By 1936 Hevesy and Levi found that the number of radionuclides induced decreased with time, with a specific half-time for each given radionuclide. These observations allowed them to propose "the analysis by radioactivation" for the identification and quantification of trace elements in materials along with the employment of radionuclides as tracers [32]. Thus, the foundations for a new analytical technique were laid: Neutron Activation Analysis (NAA; see Figure 1.1). Yet, radiochemical separation of the formed species was tedious and inefficient. Stronger neutron sources were needed for the technique to gain sensitivity. By the year 1952 the Oak Ridge National Laboratory made available an "activation analysis service" for the public and from that moment the technique gained widespread interest [33]. In NAA the primary reaction of interest is therefore the "radiative neutron-capture": the capture of a neutron by a nucleus and the monitoring of the released electromagnetic radiation by (radioactive) de-excitation of the radionuclide formed.

Unfortunately for NAA, not all the elements can be transmuted when exposed to a neutron fluence rate. When a neutron collides with a nucleus, it can only be scattered or end up being absorbed. It is important then to assign a probability to each outcome and for each bombarded nucleus of analytical interest. Formally known as "neutron cross-sections", these capture probabilities also depend (among other things) on the energy of the incident neutron, neutron-nucleus spins and atomic bound state [34]. For instance, slow or low-energy neutrons will spend more time near a given nucleus, therefore increasing their chances of being absorbed.

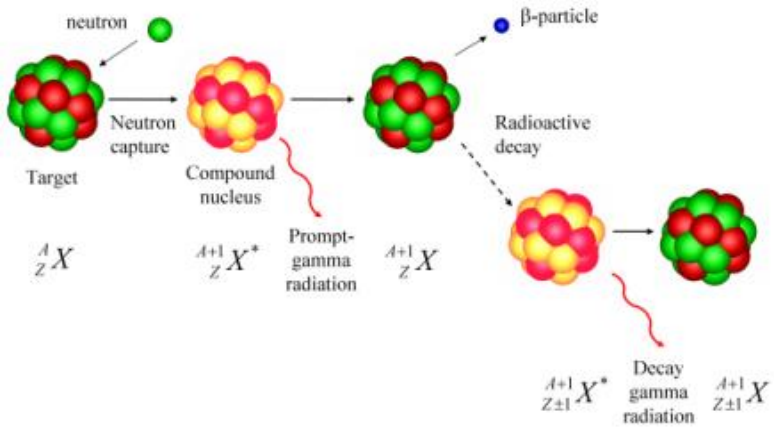

Figure 1.1: The neutron capture by the target nuclide $^{A}X_{Z}$ with atomic number Z and isotopic number A leading to the compound nucleus $^{A+1}X_{Z}$ which is unstable. A primary release of energy (de-excitation) in the form of γ rays occurs (Prompt-γ radiation), followed by a delayed de-excitation and transmutation of the compound nucleus into $^{A+1}X_{Z\pm1}$ by emission of a $\beta^{\pm}$ particle and more X or γ-rays (Delayed-γ). The NAA analytical nuclear technique consist in the identification and quantification of $^{A}X_{Z}$ in a sample by detection of either emitted radiation, yet the experimental procedure, instruments required and energy range of interest varies significantly between the Prompt-γ and Delayed-γ methods, which are considered 2 separate (but complementary) techniques. This work deals with Delayed-γ NAA only. Figure extracted from reference [35]**.**

Although these neutron cross-sections are modelled (i.e. idealized) functions of many parameters, the scientific community provides several specific definitions and evaluations of its functional form for each isotope, reaction channel and neutron energy of interest. The practical approach is to tabulate in the literature these energy and reaction-specific cross-sections as

"absolute nuclear constants" and to determine them experimentally at various independent facilities from time to time. Thus, although these parameters are usually referred as "constants", the literature values might differ between authors per the different neutron energy regions of interest investigated and the mathematical framework introduced for the determinations.

The accurate knowledge of these cross-sections is the key ingredient for the success of NAA as a nuclear analytical technique since it has some main advantages over other analytical methods are [34, 36]:

- It is non-destructive. Although radioactivity in samples is induced, it is usually minimal and it usually decreases considerably with time, allowing for examination of e.g. forensic evidence, archeological samples, historic artifacts, jewelry, paintings, etc.
- Since the neutrons interact only with the atomic nucleus, these wave-particles can penetrate most sample matrices with relative ease, and therefore, most samples do not require chemical separation of the analyte. When no chemical digestion, leaching, etc. is required, the chances of mass losses during the sample preparation and the workload is minimized.
- It is multi-elemental (panoramic) and very sensitive. NAA allows for the characterization of more than 70 elements, from which a high percentage could be determined with one neutron-bombardment experiment. The detection limits can be e.g. 1 to 10^7 picograms under a 10^{13} $cm^{-2}.s^{-1}$ fluence rate.

The NAA analyst would usually adopt these cross-sections and several other nuclear constants from the latest literature, but sometimes their metrological traceability and/or measurement accuracy are dubious as other correlated and/or adopted reference values may differ greatly between authors. Some reported values are imprecise or the spread of the results between authors is higher than desired. Sometimes no uncertainty is provided or the results

come from the average of just a few determinations, triggering the need for further investigation.

The work by De Corte et al. [37, 38], Simonits et al.[39] and Moens et al. [40] showed that these cross-sections and several other nuclear constants employed by the technique could be grouped together into composite factors or "k_0 factors" for each reaction of interest and emitted radiation.

The k_0-factors solved the inconveniences of laboratory-specific constants like the "*k* factors" previously introduced by Girardi et al. [41], by being normalized against the conditions of their determination [13]. Hence, these k_0 factors could be experimentally determined first by specialized laboratories, with overall uncertainties of ≤5% (at 95% confidence level) and could be later used by other NAA laboratories abroad, by adopting the k_0-standardization framework which aimed to be simple and versatile at the same time [13].

The k_0-standardization was also a simple alternative to the rigid methodology employed in the relative standardization: which avoids the use of cross-sections and other parameters by co-irradiating standards that would replicate all the important characteristics of the sample in question. Additionally, accurate experimental k_0 factors could serve as a reference for other nuclear techniques that employed neutron cross-sections [42].

The first k_0 factors were determined during 1980-90 mainly by 2 institutes: the Instituut Nucleaire Wetenschappen (INW) at the UGent Universiteit Gent (Belgium) and the Központi Fizakai Kutató Intézet (KFKI) Atomic Research Institute (Hungary; now AEKI), with the occasional collaboration of Risø at the Danmarks Tekniske Universitet (DTU) National Laboratory for Sustainable Energy (Denmark; dissolved in 2012) [36, 40, 43, 44]. During the '90s the worldwide reception and application of the k_0-standardization method cemented its transcendence into the neutron activation community [45, 46].

Each decade there were revisions, redeterminations of its core values by the same authors or independent ones (≤ 2014) [3, 18–20, 23, 24, 47–63] however it can be seen from the latest recommended compilation in 2014 [23] that some of these k_0 factors have been determined only once ~35 years ago and have not been experimentally redetermined even if these factors has been quoted as candidates for a redetermination since 1987. Some k_0 values are correlated to other parameters that were adopted from imprecise literature available before 1990. The traceability of some factors could be compromised since in the latest two compilations [20, 23] the are no fundamental and correlated F_{Cd} factors provided.

Some of the independent results ≤ 2014 already available [18, 19, 58–60, 64–66] have not been weighted yet into the latest recommended library since another reason manifesting the need for a broad re-determination of the k_0 factors is that after more than 30 years since the method was introduced there is a noticeable lack of a robust statistical pool of experimental (and independent) k_0-data from which the k_0-community can draw conclusions about the accuracy of the current database.

Finally, the technological advances in gamma spectrometry hardware (resolution) [67–69], computing power and software [70–72], the reviews and proposal of updated NAA-conventions [48, 73, 74], new methods for calculation of neutron self-shielding effects [75–79] as well as today's usually more detailed, precise standards certificates (up to trace content) are to be considered as a motivating advantage over experimentally determined data from decades ago.

The Studiecentrum voor Kernenergie or Centre d'Étude de l'énergie Nucléaire (SCK•CEN) institute and the UGent Universiteit Gent (both in Belgium) have joined forces for launching a broad experimental redetermination and compilation of k_0 nuclear data through this work. Among the k_0-determination methods, the Cd-subtraction technique was chosen in virtue of its better precision and because it avoids the employment

of calibrated/modelled parameters in the computations. This technique was applied to 92% of all studied target isotopes [62, 80, 81].

The fundamentals of NAA, the parametric method, the relative and the k_0-standardization of NAA under the Høgdahl convention, the modified Westcott formalism and a hybrid approach are given in Chapter 2. Inspection of the different Activation-Decay schemes and primary interferences of interest are discussed in the last part. The Chapter 3 on the other hand gives the fundamentals of γ-spectrometry and the results from the calibration and fine-tuning of all the HPGe γ-ray detectors and measurement setups employed.

The undesired phenomena of neutron moderation and neutron self-shielding was kept minimal by employing mostly Al-alloys of minor quantities of the analyte (typically 0.1 to 5%) and by avoiding thick sample containers. However, the corrections were duly accounted for on all materials (e.g. pure metals, compounds) employed in this work by means of more recent semi-empirical calculation methods described in Chapter 4 [82–84]. As a comparison, during the launch of the k_0-method most samples were prepared by diluting pure compounds until these effects were considered negligible under some criteria. This was justified in the view that earlier calculation models were known to be inaccurate and/or that the nuclear data for a proper calculation was missing. As the work involved in the dilution of a pure compound might lead to mass losses (e.g. inefficient or partial dilution, pipetting, evaporation, transfer between containers, etc.), these days one might favour the employment of purer materials when the self-shielding effects can be estimated or are found to be negligible. In this work, we also pipetted and dried some diluted solutions of 0.1 to 1% analyte content but these liquids were certified reference materials, therefore the number of intermediary steps for sample preparation is kept low. The Chapter 4 also describes the calibration of the neutron irradiation channels.

The use of k_0-NAA for the determination of the $n(^{235}U)/n(^{238}U)$ isotopic ratio in multi-elemental samples containing uranium is explored in Chapter 5 [85]. The k_0-UNAA proposed method can be successfully applied in homeland security, nuclear forensics, environmental monitoring for safeguards or biomonitoring in order to determine the U content and ^{235}U enrichment level at the ppm to ppb level [86, 87].

A multi-channel approach proposed first in 1984 by Simonits et al. [88] is redefined in Chapter 6 and extended for the case of an α-dependent behaviour of the effective resonance energy [89]. This method was also applied for 70% of the studied cases for the re-determination of effective resonance energies and Q_0 factors, which are a fundamental part of the k_0-standardization [62, 89]. We also aimed at taking advantage of all current technological advances from software development in state-of-the-art programing languages for our determinations (e.g. Visual C# and its native connectivity to SQL) [90].

The nuclides of interest were investigated in typically up to three irradiation channels by means of highly-diluted and high-quality certified standards, while a fourth irradiation channel with a highly thermalized neutron fluence rate was employed in some cases in which undesired resonance phenomena had to be avoided. The choice of formalism and a discussion about their equivalence, the materials and methods are discussed also in Chapter 6 while the calculation of the uncertainties is given in a separate chapter (Chapter 7).

The experimental k_0 nuclear data resulting from the investigation of 78 target isotopes, the monitoring of 97 (n,γ) formed states and 20 ^{235}U fission products is discussed in Chapter 8, along with the results and recommended average values from other authors, but the compendium with the results and the derived nuclear data is given in Chapter 10, which also contains a summary of Chapter 8. To enhance the overall k_0-standardization (through k_0-UNAA) the Chapter 10 also provides recommended k_0 and k_0-fission factors for ^{235}U and ^{238}U characterization and correction for ^{235}U fission

interferences in complex multi-elemental samples containing uranium from the average of the results for up to 3 authors [91].

A final summary of this work is provided in Chapter 9 and a dutch version in Chapter 11.

2. Neutron Activation Analysis

2.1 The induced activity

Not all particles in nature are stable, some, for example de W and Z bosons have a transient existence [34]. The "mean life" is the time τ that a particle exists in isolation, before it undergoes radioactive decay into i.e. other component particles. If we define P_t as the probability that a particle exists for a time interval t and we assume that the particle has a constant probability $\lambda = (1/\tau)$ per unit time of decaying, then the probability of the particle surviving (or existing) for an additional interval of time dt is:

$$P_{t+dt} = P_t - P_t(\lambda dt) \tag{2.1}$$

Rearranging eq. (2.1) in terms of λ:

$$\frac{1}{P_t}\frac{(P_{t+dt} - P_t)}{dt} = \frac{1}{P_t}\frac{dP_t}{dt} = -\lambda \tag{2.2}$$

Integration of differential eq. (2.2) gives:

$$P_t = P_0 e^{-\lambda t} \tag{2.3}$$

where $P_0 = 1$ since at time $t = 0$ the particle exists in totality. If one in interested in finding at what time $T_{1/2}$ the particle has a 50% probability of existence $P_{T1/2} = 0.5$, substitution of these values into eq. (2.3) introduces the relationship:

$$\lambda = \frac{\ln(2)}{T_{1/2}} \tag{2.4}$$

The $T_{1/2}$ is then inversely proportional to λ and is defined as the "half-life" of an unstable particle.

The eq. (2.3) is the familiar "exponential-decay law" for an unstable particle, although related forms of this function are commonly seen in the treatment of statistical quantities such as the decay of a mass of radioactive nuclei [34], determination of the time of death in forensics [92] and the growth/decay of populations of viruses and bacteria [93]. In our topic of interest, the number N of nuclei of the same kind existing (or surviving) at time t is found from (N_0P_t) with N_0 the number of radionuclei at the initial time $t = 0$.

The "activity" (from radioactivity) is defined as the number of disintegrations per unit time (in s^{-1} or Bq = Becquerel) and is equal to the product (λN). The activity defined in this way depends on the number of radioactive nuclei present at a given instant of time. The law of radioactive decay on the other hand states that the activity after an interval t of time is (λN_0P_t), where λN_0 is the activity at the initial time $t = 0$.

When irradiating a sample with neutrons (see Figure 1.1), a portion of the radioactive nuclei that are being created are also decaying. In this work we define the saturation factor S as the probability of finding one (induced) radionuclide after an irradiation time t_i [34]:

$$S_{t_i} \equiv 1 - P_{t_i} \tag{2.5}$$

Suppose that we irradiate a sample for a sufficiently long time as to obtain the maximum attainable induced activity for that neutron source, irradiation position, radioisotope and sample characteristics, which we will denominate the "saturation" activity A_{sat}. According to eq. (2.5) if the irradiation is stopped at time t_i the induced activity is at that moment $A_{sat}S_{ti}$ but after the sample has "cooled" (decayed) during an interval t_d while it was transported

to the measurement system the remaining activity will be $(A_{sat}S_{ti})P_{td}$. Finally, after measuring the sample with a detection system for an interval t_c of time, the remaining activity would be $[(A_{sat}S_{ti})P_{td}]P_{tc}$. The difference between the last 2 activities is the activity variation during the measurement process ΔA:

$$\begin{aligned}\Delta A = \lambda \Delta N &= \left(A_{sat} S_{t_i} P_{t_d}\right) - \left(A_{sat} S_{t_i} P_{t_d} P_{t_c}\right) \\ &= A_{sat} S_{t_i} \left(P_{t_d}\right)\left(1 - P_{t_c}\right)\end{aligned} \tag{2.6}$$

with ΔN the number of nuclei that decayed during the measurement.

If we define the decay and counting factors D and C (probabilities) as:

$$\begin{aligned} D &\equiv P_{t_d} \\ C &\equiv \left(1 - P_{t_c}\right)\left(1/\lambda t_c\right)\end{aligned} \tag{**2.7**}$$

then eq. (2.6) can be written as:

$$\Delta N = A_{sat}\left(S_{t_i} D_{t_d} C_{t_c}\right) t_c \tag{2.8}$$

If our detector has an efficiency ε for detecting these nuclides, the number of detected decays should be $(\Delta N\varepsilon)$ under ideal conditions, that is, if there no loss on detected decays due to other unaccounted factors. In NAA one can use one or several detectors of different kinds for measuring the radiation emitted by the radioactive sample (i.e. beta, alpha, gamma radiation detectors). In the k_0-standardization and in INAA in general, one is interested in the emitted γ-ray from the sample and the employed detectors have a specific detection efficiency ε_γ for each γ-ray of a given energy, which is strongly correlated to the crystal properties and attached circuitry (current, temperature, voltage specifications, etc.). The detection efficiency topic will be dealt in more detail in Chapter 3.

When considering ε_γ and the probability of emission of a γ-ray I_γ one has from eq. (2.6):

$$N_p \equiv \Delta N \varepsilon_\gamma I_\gamma \equiv \left(A_{sat} I_\gamma\right)\left(S_{t_i} D_{t_d} C_{t_c}\right)\left(\varepsilon_\gamma t_c\right) \tag{2.9}$$

with N_p equal to the number detected γ-rays (or counts) of a given energy during the measurement time interval t_c. In terms of the saturation γ-ray activity $A = I_\gamma A_{sat}$ [34] one has from eq. (2.9):

$$\frac{N_p}{t_c \varepsilon_\gamma} = A\left(S_{t_i} D_{t_d} C_{t_c}\right) \tag{2.10}$$

Finally, one obtains from the previous equation the following general relationship between the saturated γ-ray activity and the measured count-rate (N_p/t_c) for a given radioisotope X [13, 36, 38, 44, 45]:

$$A_X = \frac{1}{f\left(S,D,C\right)_X}\left(\frac{N_p}{\varepsilon_\gamma t_c}\right)_X \tag{2.11}$$

The saturation S, decay D and counting C correction factors in the denominator of eq. (2.10) were combined in a unique function *f(S,D,C)* that is different for each activation-decay scheme (ADS) involved in the production and measurement of a radionuclide [36]. The description of the activation-decay pathways for the $x \rightarrow X$ process and associated *f(S,D,C)* formulae for several reactions are compiled for instance in reference [20] but these will be discussed in the section 2.14.

It must be remarked that N_p (or A) must have been corrected for γ-ray coincidence summing effects or pulse losses, burn-up of investigated or intermediary nuclide and detector dead-time, in order for eq. (2.11) to be a valid equality. These corrections are discussed in reference [13] but will be dealt in the next chapters. Note that eq. (2.11) implies that A is a partly-modelled and a partly-measured parameter.

2.2 The Activation Equation

The saturation activity A_{sat} of radioisotope X obtained from the irradiation of n atoms of isotope x with neutrons can be modelled according to [34]:

$$A_{sat,X} = n_x R'_{x,X} \tag{2.12}$$

The R' function is defined as the neutron-capture reaction rate per nuclide x for the particular neutron-source (in Bq), leading directly or indirectly to the formation of X, i.e. $x(n,\gamma)X$ or $x(n,\gamma)X' \rightarrow X$. The eq. (2.12) is commonly known as the general form of the "Activation Equation".

The number of atoms is defined in terms of the mass w (in g) and the molar mass M (in g.mol^{-1}) of the element associated to the isotope x having isotopic abundance θ [34]:

$$n_x = w \frac{N_A}{M} \theta_x \tag{2.13}$$

with N_A the Avogadro constant. Combining the previous equations and in terms of the saturation γ-ray activity A one arrives at:

$$w = \left(\frac{A_X}{R'_{x,X}} \right) \frac{M}{N_A \theta_x I_{\gamma,X}} \tag{2.14}$$

The main goal of the Neutron Activation Analysis technique (NAA) is to find the mass of an element (or the amount of an isotope) on an unknown sample, employing its measured neutron-induced activity, a mathematical or empirical model of the reaction rate and, e.g. the substitution for the I_γ constants and mean θ, M values from ranges typically found in nature, which are tabulated elsewhere in the literature.

2.3 About the notation

In this work the indexes *x* and *X* are used to emphasize that the physical quantity in question is related to the target *x* and/or to the formed radionuclide *X* involved in the $x \rightarrow X$ process. The index *x* might also be used for an element-specific physical quantity from which *x* is the isotope of interest.

The *x,X* indexes will be employed at first introduction of a physical quantity or when considered necessary but in general the index *x* alone can replace the use of these double indexes or be neglected when tacit for the sake of clarity.

2.4 The modified Høgdahl convention

The radiative neutron-capture or (n,γ) reaction rate per nuclide is expressed in its general form as [13, 34]:

$$R'_x = \int_0^\infty \phi'_E \sigma_{E,x} dE \tag{2.15}$$

with σ_E defined as the neutron cross-section for a $x(n,\gamma)X$ reaction for neutrons incoming at energy *E* (in eV). The σ_E function is a "probability" having area units, i.e. an "effective" area (in barn or b; $1b = 10^{-24}\ cm^2$) that is different for each neutron energy. The ϕ'_E function is the neutron fluence rate per unit energy interval (given in $cm^{-2}.s^{-1}eV^{-1}$). Figure 2.1 shows a schematic representation of the typical shape of the ϕ'_E function for a reactor irradiation channel.

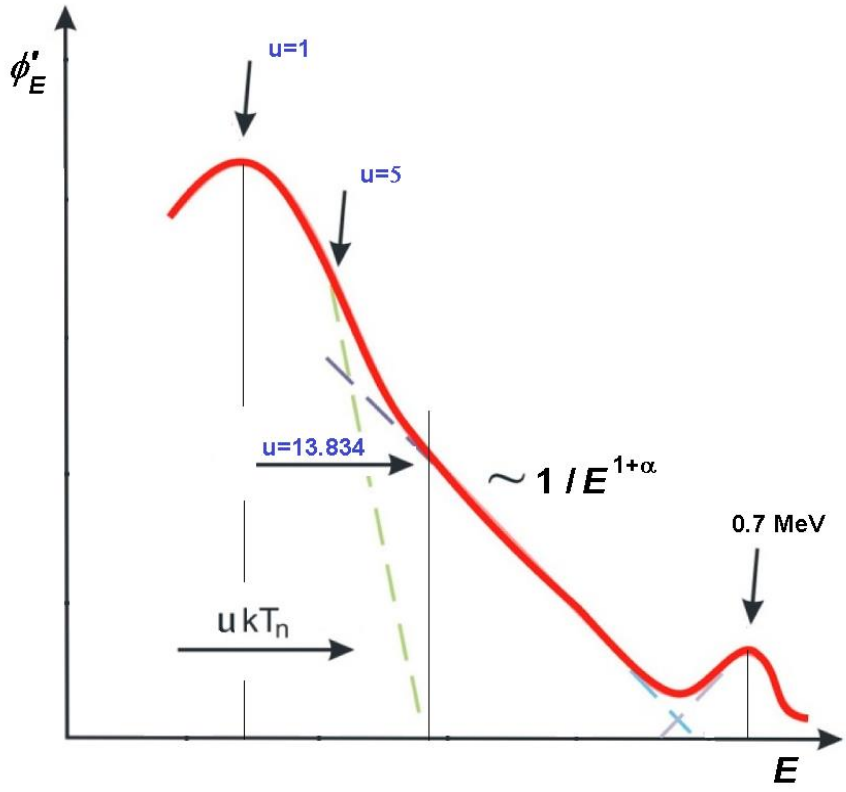

Figure 2.1: Typical representation of the neutron fluence rate per unit energy interval (ϕ'_E) as a function of the neutron energy (E) for a reactor irradiation channel. The axis units are arbitrary (not scaled) but delimiters are given in the text. See also the text for a description of the symbols.

In Figure 2.1 the ϕ'_E function is subdivided into three sections, given by the neutron energy (E) range.

First, one can observe a spectrum of low-energetic neutrons that after colliding repeatedly with the channel surroundings (moderator) are in thermal equilibrium with it. The neutron fluence rate distribution in this

energy range is usually described by a Maxwell-Boltzmann distribution (left part) [34]. The Maxwell-Boltzmann distribution has a maximum for neutrons with average neutron energy $E_n = ukT_n$, where k is the Boltzmann constant $k = 8.6173324(78) \times 10^{-5}$ eV.K^{-1}, T_n is the average neutron or moderator temperature (in K) and u = 1 is a dimensionless auxiliary parameter employed in Figure 2.1 to map other neutron energies in terms of this maximum. If the reactor moderator is at 293.6 K (or $T_0 = 20.4$ °C), the average energy of the neutrons in equilibrium with the moderator is 25.3 meV.

Secondly, one observes a spectrum of medium energetic neutrons that are being slowed down by the moderator. This spectrum is usually described by a $\sim E^{-(1+\alpha)}$ distribution with α being a channel-specific parameter that also depends on the irradiation position inside the channel (or its centre part) [13]. This distribution starting point can be approximated at neutron energies 5 times greater than the previous distribution maximum ($u \geq 5$; junction point), although as we shall see later, a higher starting point is adopted by convention.

Finally, one observes a third and last spectrum of fast neutrons from ^{235}U fission showing a maximum at 0.7 MeV and usually described by a Watt-representation (right part) [94].

A 1 mm thick, high-purity Cd-foil (index *Cd*) can absorb all the neutrons with energy $E < 0.2$ eV from a mono-energetic beam that collides in a direction normal to its surface, mainly due to the very high σ_E value for ^{113}Cd at $E = 0.178$ eV (or u = 7.04) [13, 34] (see Figure 2.2).

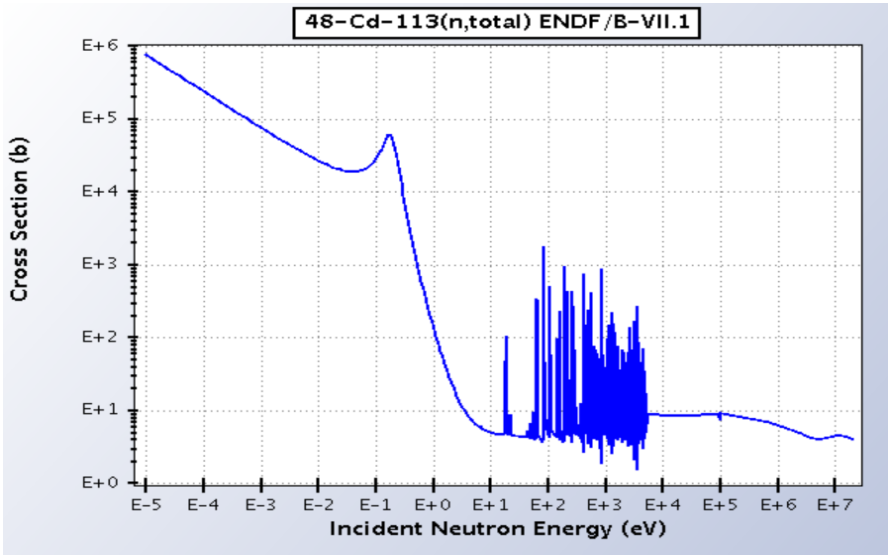

Figure 2.2: Total cross-section function for ^{113}Cd as a function of neutron energy E [15]. The highest resonance occurs at E = 0.178 eV.

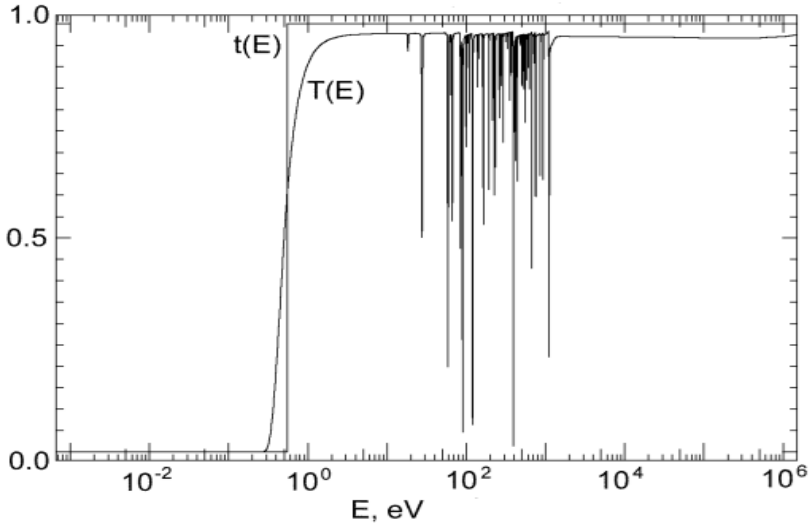

Figure 2.3: Actual (T_E) and idealized (t_E) transmission function for Cd-covers of 1 mm thickness as a function of the neutron energy (E), as reported in [95]**.**

A transmission function T_E for neutrons (as a function of their energy) through a Cd-cover of thickness d (in cm) can be approximated to:

$$T_E = \exp\left(-dn_{Cd}\sum_i \theta_i \sigma_{tot,E,i}\right) \tag{2.16}$$

where $\sigma_{tot,E,i}$ is the total cross-section function for the i isotope of Cd (in b) and n_{Cd} is the number density of Cd atoms (4.63 x10^{22} atoms.cm^{-3}).

The actual T_E approximates to unity for $E > 1.5$ eV and $l = 1$ mm as shown by the Figure 2.3, but it is possible to idealize the actual transmission function into a step-function t_E. The step-function has the value $t_E = 0$ at $E < E_{Cd}$ and $t_E = 1$ at $E > E_{Cd}$, with $E_{Cd} = 0.55$ eV accepted internationally as the Cd cut-off energy (u = 21.7) [13]. But this is only possible as long as the following conditions for a reactor irradiation channel neutron spectrum are satisfied [13, 36, 96]:

$$\phi'_E \rightarrow \begin{cases} \phi'_v \propto n_v v & \text{if } E \le E_{Cd} \\ \phi'_E \propto \dfrac{1\text{eV}^{\alpha}}{E^{1+\alpha}} & \text{if } E > E_{Cd} \end{cases} \tag{2.17}$$

$$\sigma_{v,x} \propto \frac{v_0}{v}\sigma_{0,x} \quad \text{if } v \equiv \sqrt{\frac{2E}{m_n}} \le v_{Cd} \tag{2.18}$$

where v is the neutron velocity (in cm.s^{-1}), m_n its rest mass (in amu), n_v is the neutron density per unit of velocity interval (in cm^{-4}.s) at neutron velocity v (in cm.s^{-1}). The σ_0 parameter is the neutron capture cross-section (in b) for neutrons at an average energy of $E_0 = 25.3$ meV ($T_0 = 293.6$ K), that is, neutrons with velocity $v_0 = 2200$ m/s. These reactor channel neutrons are commonly called “thermal” neutrons ($E \le E_{Cd}$).

The eq. (2.18) shows that the σ_v function must follow a $1/v$ dependence (or law) for $v \le v_{Cd}$ (the velocity of neutrons with energy E_{Cd}), but in practice this requirement should be satisfied for up to 1.5 eV (u > 50), where the true T_E function approaches unity. Also, the neutron fluence rate ϕ'_E should be

homogeneous and isotropic, and the condition imposed in eq. (2.17) must be actually satisfied for E down to 0.35 eV (u = 13.834), where T_E approaches zero [13]. In eq. (2.17) α is a channel-specific parameter (dimensionless) that depends on the irradiation position as well.

With the employment of the idealized t_E function it is possible to separate the integral in eq. (2.15) near $E = E_{Cd}$:

$$R'_x = \int_0^{v_{Cd}} \phi'_v \sigma_{v,x} dv + \int_{E_{Cd}}^{\infty} \phi'_E \sigma_{E,x} dE \tag{2.19}$$

and with the aid of the approximations in eqs. (2.17) and (2.18), one obtains [13]:

$$R'_x = \sigma_{0,x} \left\{ v_0 \int_0^{v_{Cd}} n_v dv \right\} + \varphi_e \left\{ (1\text{eV})^{\alpha} \int_{E_{Cd}}^{\infty} \frac{\sigma_{E,x}}{E^{1+\alpha}} dE \right\} \tag{2.20}$$

The bracket at the left of eq. (2.20) is defined as the conventional thermal fluence rate (index *th*; in $cm^{-2}.s^{-1}$):

$$\varphi_{th} \equiv v_0 \int_0^{v_{Cd}} n_v dv \tag{2.21}$$

while the right-side bracket is instead condensed into a single parameter:

$$I_{\alpha,x} \equiv (1\text{eV})^{\alpha} \int_{E_{Cd}}^{\infty} \frac{\sigma_{E,x}}{E^{1+\alpha}} dE \tag{2.22}$$

The I_α parameter is the evaluated resonance integral (in b) for neutrons with energies $E > E_{Cd}$ following an approximate $\sim 1/E^{1+\alpha}$ group distribution, for a reactor channel with specific α-parameter. The α parameter is not constant but a function of spatial gradients within the channel and hence, of the target position. Modelling the spatial dependence of the α parameter for a given channel might be difficult, for which standardized irradiation positions are usually employed in practice.

The $E > E_{Cd}$ energy region corresponds to the "epicadmium" or "epithermal" neutron spectrum of the channel. Mathematically, the conventional epithermal fluence rate (index *e*; in $cm^{-2}.s^{-1}$) is defined as:

$$\varphi_e \equiv \frac{\alpha}{(1\text{eV})^{\alpha}} \left(\frac{\int_{E_1}^{E_2} \phi'_E dE}{(-E)^{-\alpha}\Big|_{E_1}^{E_2}} \right) \tag{2.23}$$

with E_2 and E_1 as the upper and lower energy limits of the epithermal spectrum.

In its compact form, eq. (2.20) is written as:

$$\begin{aligned} R'_x &= \{\sigma_{0,x}\varphi_{th}\} + \{\varphi_e I_{\alpha,x}\} \\ &\equiv R'_{th,x} + R'_{e,x} \end{aligned} \tag{2.24}$$

The thermal and the epithermal conventional neutron fluence rates can be determined experimentally by irradiating a given isotope with known σ_0 and I_α values, i.e. cross-section standards such as ^{197}Au, ^{232}Th, etc.

Equivalently to eq. (2.24), *R'* can be re-arranged as:

$$R'_x = \sigma_{0,x}\varphi_{th}\left(1 + \frac{Q_{\alpha,x}}{f}\right) \tag{2.25}$$

Where, according to references [13, 36], *f* is defined as the ratio between the thermal (*th*) and the epithermal (*e*) conventional neutron fluence rates (φ) as given in eqs. (2.21) and (2.23):

$$f \equiv \frac{\varphi_{th}}{\varphi_e} \tag{2.26}$$

while the Q_α factor has been defined as the effective resonance integral (I_α) to thermal neutron cross-section (σ_0) ratio:

$$Q_{\alpha,x} \equiv \frac{I_{\alpha,x}}{\sigma_{0,x}} \tag{2.27}$$

The Q_0 determination methods are discussed in sections 2.9.1 and 6.3. The f and α determination methods are described at the end of this chapter.

2.5 Neutron self-shielding

In this work, we refer to thermal neutron self-shielding as the loss of thermal neutron fluence rate due to the sample nuclear density, target thickness and the macroscopic thermal cross-section that results after considering all the absorbers of thermal neutrons within the sample. On the other hand, neutron moderation is considered as the reduction of the speed of fast neutrons, thereby turning them into thermal neutrons [97–101]. The "effective" thermal shielding correction factor ($G_{th,\text{eff}}$) accounts for shielding and/or moderation of thermal neutrons, because the conventional thermal fluence rate detected by the monitor ($\varphi_{th,\text{eff}}$) is related to the "true" conventional thermal fluence rate of the irradiation channel by:

$$\begin{aligned} \varphi_{th,\text{eff}} &= G_{th,\text{eff}}\varphi_{th} \\ &= \left(G_{th}G_{\text{mod}}\right)\varphi_{th} \end{aligned} \tag{2.28}$$

The correction factor G_{th} is considered ≤ 1 and > 0 while the neutron moderation correction factor G_{mod} (as defined in this work) can be higher than unity if the net effect was an increase in φ_{th} [102, 103].

Epithermal neutron self-shielding is more complicated and depends on the nuclear density and on epithermal resonance parameters [55, 101, 104]. The correction factor $G_e \leq 1$ is introduced to account for an effective Q_α factor:

$$Q_{\alpha,\text{eff}} = G_e Q_\alpha \tag{2.29}$$

After considering both neutron self-shielding effects, an "effective" form of eq. (2.25) is typically used instead:

$$R' \rightarrow R'_{\text{eff}} = \sigma_0 \varphi_{th} R_H \tag{2.30}$$

where the auxiliary parameter R_H is defined as a dimensionless equivalent to the (n,γ) reaction rate of a given nuclide in an irradiation channel:

$$R_{H,x} \equiv G_{th,\text{eff}} + \left(\frac{Q_{\alpha,x}}{f} \right) G_{e,x} \tag{2.31}$$

The G_i correction factors are calculated from different empirical or analytical models [13, 78, 101], which are described thoroughly in 4. The index "eff" will be dropped from the following equations as it is understood that one should employ the "effective" correction factor from the combination of all undesired thermal neutron losses in the reaction rate.

2.6 Two methods for solving the Activation Equation

As mentioned before, the main goal of NAA is to find the mass of an element (or isotope) on an unknown sample. Different methods are summarized in the literature for this task [13, 34].

2.6.1 The Parametric method

After substituting for the modelled reaction rate per nuclide *R'* of eq. (2.30) into eq. (2.14), the "Parametric (or Absolute) method" consist in calculating *w* from:

$$w = \left(\frac{A_X}{\kappa_{x,X}} \right) \left(\frac{1}{N_A \varphi_{th} R_{H,x}} \right) \tag{2.32}$$

with κ defined as a composite nuclear constant that is calculated from absolute nuclear data from the literature:

$$\kappa_{x,X} \equiv I_{\gamma_X} \left(\theta \sigma_0 \right)_x \frac{1}{M} \tag{2.33}$$

and R_H is given by eq. (2.31).

2.6.2 The Comparator and/or Relative methods

If we co-irradiate the unknown sample with a "comparator", that is, a standard of well-known nuclear data and mass *w'* of the element associated with an isotope *c* (from which radioisotope *C* is induced; $c \rightarrow C$), then, by writing eq. (2.32) for both samples and dividing one against the other, the technique known as the "Comparator method" gives [13, 40]:

$$w_x = w_c \left(\frac{A_X}{A_C} \right) \frac{\left(\kappa \, \varphi_{th} R_H \right)_c}{\left(\kappa \, \varphi_{th} R_H \right)_x} \tag{2.34}$$

If we chose a comparator such that $x = c$ and $X = C$, we obtain:

$$w_x = w_c \left(\frac{A_X}{A_C} \right) \frac{\left(\varphi_{th} R_H \right)_c}{\left(\varphi_{th} R_H \right)_x} \tag{2.35}$$

Furthermore, if:

- the samples are prepared in such a manner that $G_{i,x} = G_{i,c}$, i.e. same matrix composition, packing or if both samples are sufficiently diluted $G_i = 1$ and,

- both samples are irradiated at the same position, where gradients in *f* and α in their vicinity are negligible ($f_x = f_c$ and $\alpha_x = \alpha_c$), then eq. (2.34) simplifies to:

$$w_x \cong w_c \left(\frac{A_X}{A_C} \right) \tag{2.36}$$

The previous expression can be reduced further if both samples are irradiated, cooled (let decay) and measured during the same amount of time and under the same practical geometrical conditions, i.e. same detector and sample-detector separation. Note that we have assumed that there was no variability in the κ constants between the sample and the standard employed, which might not hold true in the analysis of non-local objects (i.e. meteorites, space dust, etc.) i.e. when there is a huge spread in the natural isotopic abundance range for the given isotope [13, 40].

In practice, it is rather expensive and difficult to opt for such high metrological work and to prepare mono and/or multi-standards matching most of the stringent conditions of this "Relative method". Furthermore, if the sample contains an element for which there was no equivalent standard co-irradiated, it would not be possible to quantify it. Thus, usually either eq. (2.32) can be employed with the use of absolute nuclear data or the full form of eq. (2.34) is taken instead, with κ_c/κ_x ratios substituted by experimental equivalents that were accurately determined, under the highest metrological level attainable at a given NAA-laboratory. The latter process is known as "the k_0-standardization of the comparator method" [13, 36, 38, 40, 44, 45].

2.7 The k_0-standardization method

The k_0-standardization method (or k_0-method) consist in co-irradiating a standard (index *s*) and a comparator (index *c*) in order to determine from each saturation γ-ray activity ratio, the respective ratio between kappa-values defined in eq. (2.33). This is performed through eq. (2.34) written for the standard and the comparator:

$$k_{0,s,S,c,C} \equiv \frac{\kappa_{s,S}}{\kappa_{c,C}} = \frac{w_c}{w_s}\frac{A_S}{A_C}\frac{R_{H,c,C}}{R_{H,s,S}} \qquad \textbf{(2.37)}$$

Thus, a k_0 factor is a composite nuclear constant by definition:

$$k_{0,s,S,c,C} \equiv \frac{I_{\gamma,S}\left(\theta\sigma_0/M\right)_s}{I_{\gamma,C}\left(\theta\sigma_0/M\right)_c} \qquad \textbf{(2.38)}$$

These experimental values can be tabulated for each $s \rightarrow S$ reaction and for each γ-ray of S of analytical interest [13, 20, 36, 38, 40, 44, 45]. The k_0 factors are experimentally found composite nuclear constants that have been normalized against any contribution from the laboratory conditions of their determination.

The amount of an element of interest in a sample (analyte; $b \rightarrow B$) that has tabulated k_0 factors in the literature (index $s_1 = b$) can be calculated by employing a co-irradiated monitor ($m \rightarrow M$) with known k_0 factors as well (index $s_2 = m$):

$$w_b = w_m \frac{A_B}{A_M}\frac{R_{H,m}}{R_{H,b}}\frac{k_{0,s_2,c}}{k_{0,s_1,c}} \qquad (2.39)$$

This is possible by taking advantage of the equality:

$$\frac{1}{k_{0,b,m}} = \frac{k_{0,s_2,c}}{k_{0,s_1,c}} \qquad (2.40)$$

and the assumption that there was no isotopic variability between the standards employed for the standardization and the samples under current investigation (i.e. $\theta_b = \theta_{s1}$ and $\theta_m = \theta_{s2}$).

The k_0 factors are tabulated in the literature for θ and M associated to natural isotopic abundances [20]. Usually the same comparator reaction that was employed for a standardization (e.g. ^{197}Au(n,γ)^{198}Au at 411.8 keV γ-ray) can be employed as the routine monitor, therefore $m = s_2 = c$ and the numerator on the right-hand of eq. (2.40) reduces to unity.

The shape of eq. (2.31) shows that R_H is correlated to f and Q_α and thus, an accurate k_0 determination will also depend on the accurate knowledge (or modelling) of these parameters. Because the development of the k_0-method was focused in providing a simple framework for the widespread-adoption of INAA [13], a standardized Q_α computation method was adopted from Ryves [105] that has been exploited by other authors [106, 107].

2.8 The Q_0 factor and the effective resonance energy

The work of Ryves introduced the idea of an "effective" resonance energy $\bar{E}_r$ (in eV), which corresponds to a hypothetical resonance that gives the same contribution to the epithermal reaction rate as all the true resonances [105–107]:

$$Q_\alpha \equiv \left\{ \left(Q_0 - C_0\right)\left(\bar{E}_r\right)^{-\alpha} \left(1\text{eV}\right)^{\alpha} \right\} + C_\alpha \qquad \textbf{(2.41)}$$

where C_α is a channel and irradiation position-specific quantity (dimensionless):

$$C_\alpha \equiv \frac{C_0}{\left(2\alpha+1\right) {E_{Cd}}^{\alpha}} \left(1\text{eV}\right)^{\alpha} \qquad \textbf{(2.42)}$$

that fine-tunes the idealized correction factor:

$$C_0 \equiv 2\sqrt{\frac{E_0}{E_{Cd}}} = 2\sqrt{\frac{25.3}{550}} = 2\sqrt{0.046} \cong 0.42895 \qquad \textbf{(2.43)}$$

That is, according to eq. (2.41) a fixed ($\sigma_0 C_0$) band where the Maxwellian tail and the start of the convened epithermal region join is first subtracted from the idealized evaluated resonance integral. The resulting value is

evaluated by means of the effective resonance energy to obtain an effective but reduced resonance integral for that channel and irradiation position. The band is fine-tuned ($\sigma_0 C_\alpha$) and added back to the result to obtain an accurate I_α value. The term $(1\text{eV})^\alpha$ in eq. (2.42) can be dropped as long as the $\bar{E}_r$ is always inputted in eV.

The Q_0 factor is an α-independent composite nuclear constant, defined as [13]:

$$Q_0 \equiv \frac{I_0}{\sigma_0} \tag{2.44}$$

where I_0 (in barn) is the evaluated resonance integral per an idealized ~1/E distribution of neutrons in a reactor channel with energy $E > E_{Cd}$ = 0.55 eV (epithermal neutrons). The resonance integral I_0 (or equivalently, Q_0) can be found experimentally by means of the cadmium-ratio.

By definition the $\bar{E}_r$ is given by [107]:

$$\left(\bar{E}_{r,\alpha}\right)^{-\alpha} \equiv \frac{I'_\alpha}{I'_0} \tag{2.45}$$

with $\bar{E}_{r,\alpha}$ a function of the parameter α and I_0' the reduced resonance integral (see further in the text). In terms of the Breit-Wigner expression quoted in reference [107] as:

$$\left(\bar{E}_{r,\alpha}\right)^{-\alpha} \equiv \frac{1}{\sum_i w_i}\left\{\sum_i w_i \left(\bar{E}_{r,\alpha,i}\right)^{-\alpha}\right\} \tag{2.46}$$

with w_i a weight factor for each i-resonance, given by:

$$w_i = \left\{\frac{(2J+1)}{(2I+1)}\left(\frac{1}{\bar{E}_r^{\,2}}\right)\left(\frac{\Gamma_n \Gamma_\gamma}{\Gamma}\right)\right\}_i \tag{2.47}$$

where the Γ_n is the neutron resonance, Γ_γ the radiative and Γ the total resonance widths, while $\bar{E}_{r,i}$ is the energy at the peak (centroid) of the i

resonance. with J and I the spins of the resonance state and target nucleus. It was shown by Moens et al. [108] that $\bar{E}_{r,\alpha}$ can be approximated by an α-independent expression:

$$\ln\left(\bar{E}_r\right) \cong \left(\frac{1}{\sum_i w_i}\right) \sum_i w_i \ln\left(\bar{E}_{r,i}\right) \qquad \textbf{(2.48)}$$

By means of eq. (2.48) it was estimated that $\bar{E}_{r,\alpha}$ and $\bar{E}_r$ values might differ by up to 20% for $\alpha = 0.1$.

2.9 Cd-covered irradiations

2.9.1 The Cd-Ratio for Q_0 determination

The Cd-ratio R_{Cd} is the ratio between the saturated γ-ray activity A of a radioisotope in a sample and, the corresponding value of a replicate sample irradiated at the same irradiation position but inside a cylindrical (and hermetic) 1 mm thick Cd-cover. This Cd-cover served as a filter for all the thermal neutrons ($\varphi_{th} = 0$) [13, 34]:

$$R_{Cd} \equiv \frac{\left(\rho\hat{w}\right)_{Cd}}{\rho\hat{w}} \left(\frac{A}{A_{Cd,\text{obs}}}\right) \qquad \textbf{(2.49)}$$

with $\hat{w}$ the sample mass (in g) and ρ the mass fraction of the analyte in the sample (in µg/g), that is $w = \rho\hat{w}$. Since the samples are replicates then $\rho = \rho_{Cd}$ but the sample mass should be kept in the equation because of possible differences that can be expected during the samples preparation. If the samples were not prepared from the same standard, the eq. (2.49) must employ ρ for each sample. The index "obs" is introduced to account for the

fact that in some cases the observed A_{Cd} is lower than expected. This occurs when the neutron resonances of the target isotope are overlapped by the resonances from the Cd-isotopes, withdrawing those neutrons from the epithermal fluence rate:

$$A_{Cd} F_{Cd} = A_{Cd,\mathrm{obs}} \tag{2.50}$$

The cadmium transmission factor (dimensionless) F_{Cd} is a correction factor that is usually equal to unity for Cd-covers of 1 mm thickness for the majority of the isotopes of analytical interest, except for a few cases quoted for instance in [21, 38, 40, 44, 45], that are unfortunately not listed anymore in the 2003 and 2012 k_0-compilations in [20] or [22]. The F_{Cd} factor can also be higher than unity if e.g. neutrons of 234 eV are scattered by the Cd resonance at 233.4 eV and end up being absorbed by the ^{65}Cu resonance at 230 eV [13].

By employing the following definition of a normalized R_{Cd}:

$$r_{Cd} \equiv \left(R_{Cd} F_{Cd} \right) - 1 \tag{2.51}$$

we have that per eqs. (2.30) and (2.32) applied to both samples and knowing that $\varphi_{th} = 0$ for the Cd-covered irradiation, the r_{Cd} factor is also equivalent to the following expression:

$$r_{Cd} \equiv \frac{G_{th}}{G_e} \left(\frac{\varphi_{th}}{\varphi_e} \frac{\sigma_0}{I_\alpha} \right) \equiv \frac{G_{th}}{G_e} \frac{f}{Q_\alpha} \tag{2.52}$$

on condition that the epithermal self-shielding and neutron fluence rate for the Cd-covered sample did not differ significantly from the epithermal self-shielding and neutron fluence rate for the bare sample. If this is not the case and $G_{e,Cd} \neq G_e$, then one must calculate r_{Cd} as:

$$r_{Cd,corrected} \equiv \left(R_{Cd} F_{Cd} \frac{G_{e,Cd}}{G_e} \right) - 1 \tag{2.53}$$

If $\alpha = 0$, the r_{Cd} factor is inversely proportional to the Q_0 factor, as substitution of eq. (2.41) into eq. (2.52) gives an expression for Q_0 or q_0 determination:

$$\begin{aligned} q_0 &\equiv \left(Q_0 - C_0\right) \equiv \left(Q_\alpha - C_\alpha\right)\left(\bar{E}_{r,\alpha}\right)^{\alpha}\left(1\text{eV}\right)^{-\alpha} \\ &\equiv q_\alpha \left(\bar{E}_{r,\alpha}\right)^{\alpha}\left(1\text{eV}\right)^{-\alpha} \end{aligned} \tag{2.54}$$

which is found experimentally through the q_α factor:

$$q_\alpha = \left\{\frac{G_{th}}{G_e}\frac{f}{r_{Cd}}\right\} - C_\alpha \tag{2.55}$$

On the other hand, one could also co-irradiate each sample with a comparator and substitute f by means of the same eq. (2.52) written for the comparator:

$$f = \left(\frac{G_e}{G_{th}}\right)_c r_{Cd,c} Q_{\alpha,c} \tag{2.56}$$

Then one can calculate a value ω_{Cd} which is a found experimentally from a ratio of Cd-Ratios:

$$\omega_{Cd,x,c} \equiv \left(\frac{G_{th,x}}{G_{e,x}}\frac{f}{Q_{\alpha,c}}\right)\left(\frac{1}{r_{Cd,x}}\right) \equiv \left(\frac{G_{e,c}}{G_{e,x}}\frac{G_{th,x}}{G_{th,c}}\right)\left(\frac{r_{Cd,c}}{r_{Cd,x}}\right) \tag{2.57}$$

This value is the proportionality constant between the analyte and the comparator Q_α factors:

$$Q_\alpha = \omega_{Cd,c} Q_{\alpha,c} \tag{2.58}$$

From the definitions in eq. (2.54) and (2.58) one arrives at the experimental (classical) equation for Q_0 determination:

$$Q_0 = \left(\omega_{Cd,c} Q_{\alpha,c} - C_\alpha\right)\left(\bar{E}_{r,\alpha}\right)^{\alpha}\left(1\text{eV}\right)^{-\alpha} + C_0 \tag{2.59}$$

2.9.2 The Cd-subtraction technique: k_0 determination

The Cd-covered irradiations are not only useful for Q_0 determination as a function of the f, α and $\bar{E}_r$ parameters, they also provide the researcher with a method for k_0 determination without the need for Q_0, f, α and $\bar{E}_r$ parameters. The eq. (2.52) substituted into eq. (2.37) gives:

$$k_{0,s,S,c,C} = \left(\frac{\rho_c}{\rho_s}\right)\left(\frac{a_{s,S}}{a_{c,C}}\right)\left(\frac{G_{th,c}}{G_{th,s}}\right)\left(\frac{1+\left(1/r_{Cd}\right)_{c,C}}{1+\left(1/r_{Cd}\right)_{s,S}}\right) \qquad \textbf{(2.60)}$$

where we have introduced for simplicity the following auxiliary parameter:

$$a_{x,X} \equiv \left(\frac{A}{\hat{w}}\right)_{x,X} \qquad (2.61)$$

Physically, the parameter a is to be understood as the activity concentration (of the analyte) in the sample.

As long as the bare and Cd-covered samples are made from the same standard (i.e. the samples share the same ρ) the eq. (2.60) can be written in condensed form as:

$$k_{0,s,S,c,C} = \left(\frac{\rho_c}{\rho_s}\right)\left(\frac{\Delta a_{s,S}}{\Delta a_{c,C}}\right)\left(\frac{G_{th,c}}{G_{th,s}}\right) \qquad \textbf{(2.62)}$$

with the introduction of the auxiliary parameters:

$$\begin{aligned} f_{Cd,x} &\equiv \left(F_{Cd}\,\frac{G_{e,Cd}}{G_e}\right)_x \\ \Delta a_{x,X} &\equiv \left(a - \frac{a_{Cd}}{f_{Cd}}\right)_{x,X} \end{aligned} \qquad (2.63)$$

The Δa is the Cd-subtraction of the activities concentrations for the bare and Cd-covered standard (or comparator) and f_{Cd} as an "effective" Cd-

transmission factor in the case that the bare and Cd-covered samples are not replicates, i.e. when $G_{e,Cd} \neq G_e$.

The eq. (2.60) (or eq. (2.62)) is known as the Cd-subtraction technique [109] and it minimizes the introduction of uncertainties into the k_0 factor from most of the modelled parameters employed in the calculation of the (n,γ) reaction rate, which are typically of greater magnitude than the uncertainties on the r_{Cd}, A and A_{Cd} values.

The Cd-subtraction technique also turns the correlation in terms of the ultimate comparator experimental data (on which the method is based) and since the comparator was co-irradiated next to the sample, it would be a better indicator of the neutron fluence rates at that time and position than a f factor obtained by a calibration curve, which is instead correlated to the nuclear data and mean result from other isotopes.

If f has (unknowingly) changed during calibration and k_0 determination, the employment of this modelled parameter would introduce a bias. But on the other hand, if any meaningful fluence rate variation has occurred during the irradiation of bare and Cd-covered samples, the Cd-subtraction technique would also bias the analytical result. Hence, it is recommended to perform the bare irradiations and to follow them immediately or within days of separation by the Cd-covered ones. The k_0 method requires the use of channels with negligible fluence rate variations or, that these effects are corrected for in the employment of eq. (2.37) or in the alternate eq. (2.60).

2.9.3 The use of highly-thermalized channels

For highly-thermalized irradiation channels, i.e. $\varphi_{th} >> \varphi_e$, eq. (2.60) can be employed assuming $A_{Cd} = 0$, leading to:

$$k_{0,s,S,c,C} = \left(\frac{\rho_c}{\rho_s}\right)\left(\frac{a_{s,S}}{a_{c,C}}\right)\left(\frac{G_{th,c}}{G_{th,s}}\right) \tag{2.64}$$

The previous equation shows that the uncertainty on the k_0 determination improves considerably with these type of channels as it manly depends on the ratios between the specific activities, but the information about the resonance phenomena is completely sacrificed.

Unfortunately, not all the k_0-NAA specialized laboratories in the world have highly-thermalized irradiation channels at disposition, nor are all of them suited for Cd-covered irradiations, as too high conventional fluence rates might lead to the dangerous radiation exposure of the analyst and reactor staff to the Cd-radionuclides formed in these (bulky) Cd-covers. Therefore, the f, α parameters and the $\bar{E}_r$ factors are inherently necessary for a wide-spread adoption of the k_0-standardization at the international level: for its versatility as an analytical technique or as a reactor irradiation channel calibration method; for its consistency and metrological traceability in the determination of k_0 and Q_0 factors that can be employed in other related nuclear disciplines.

2.10 The modified Westcott formalism

2.10.1 Changes to the (n,γ) dimensionless reaction rate

The majority of the previous equations were written after assuming that the neutron cross-section of a given isotope in the thermal region is inversely proportional to the neutron velocity (1/v-law) for up to 1.5 eV neutron energy (the modified Høgdahl convention [96]). To account for deviations from this norm, the modified Westcott formalism was necessarily introduced into the k_0-standardization in references [45, 48], almost 20 years after the

introduction of the k_0-method. Under this convention, R_H in eq. (2.31) should be replaced by R_W:

$$R_{H,x} \rightarrow R_{W,x} \equiv \left(G_{th} g_{T,x} + G_{r,x} \frac{s_{\alpha,x}}{\beta_\alpha} \right) \qquad \textbf{(2.65)}$$

where:

- G_r is the resonance self-shielding correction factor. It is related to the epithermal self-shielding correction factor G_e by means of [48]:

$$G_{r,x} = G_{e,x} - \varepsilon\left(1 - G_{e,x}\right) \qquad (2.66)$$

under the assumption that only resonances outside of the 1/v-tail (see Figure 2.1) are taking part in the self-shielding phenomena. The ε parameter is the fraction of the 1/v contribution to the epithermal activation [48]. To a good approximation one can assume $G_e >> \varepsilon(1- G_e)$ and thus, $G_r \approx G_e$ for practical purposes.

- g_T (the Westcott factor) is a function of the neutron temperature T_n and corrects the deviation of the thermal neutron cross-section from the 1/v law. It can evaluate as $g_T > 1$ or $g_T < 1$ depending on the isotope, while it is considered equal to 1 when no deviation is expected. It is defined in the following way [48]:

$$g_{T,x} \equiv \frac{1}{\sigma_{0,x} v_0} \int_0^\infty \left[2z - \left(\frac{v^2}{v_T^3} \right) \exp\left\{ -\left(\frac{v}{v_T} \right)^2 \right\} \right] \sigma_{v,x} v dv \qquad (2.67)$$

where $z = (2/\sqrt{\pi}) \approx 1.1284$

- β_α is a channel-specific parameter, dependent on α, defined here as the inverse of the more commonly known "modified spectral index" (r_α) given in references [45, 48]:

$$\beta_\alpha \equiv \frac{1}{r_\alpha}\sqrt{\frac{T_0}{T_n}} \equiv \left\{\frac{1}{r}\frac{C_\alpha}{C_0}\left(\frac{E_{Cd}}{\mu k T_n}\right)^\alpha\right\}\sqrt{\frac{T_0}{T_n}} \qquad \textbf{(2.68)}$$

with μ the coefficient of the cut-off value kT_n giving the joining point between the neutron energy regions, i.e. between the thermal and the low-energy end of the epithermal spectrum. The μ and r values are both channel-specific constants, with Westcott proposing μ = 3.7 for a graphite or heavy-water moderator and μ = 2.1 for a water moderator [48, 110]. This parameter is not required for the computation of β_α since the latter is usually found experimentally by means of a comparator as in eq. (2.151).

- s_α factors in lieu of Q_α factors, which are calculated from [45, 48]:

$$s_{\alpha,x} \equiv s_{0,x}\left(\bar{E}_{r,\alpha}\right)_x^{-\alpha}\left(1\text{eV}\right)^\alpha \qquad \textbf{(2.69)}$$

with the s_0 factor defined as:

$$s_{0,x} \equiv \left(\frac{2}{\sqrt{\pi}}\right)\frac{I'_{0,x}}{\sigma_{0,x}} = z\frac{I'_{0,x}}{\sigma_{0,x}} \qquad \textbf{(2.70)}$$

where $I_0{}'$ is the "reduced" resonance integral, defined as:

$$I'_{0,x} \equiv \int_0^\infty \left[\sigma_{E,x} - g_{T,x}\left(\frac{\sigma_{0,x}v_0}{v}\right)\right]\rho_E dE \qquad (2.71)$$

and where ρ_E is the "joining" function (of E) of the reactor spectrum, i.e. the shape of the low-energy end of the reactor epithermal neutron spectrum. It has been shown by De Corte et al. in [48] from the Westcott formulae in [110], that the previous integral can be rewritten as:

$$I'_0 \equiv \int_{E=\mu k T_n}^\infty \left[\sigma_{E,x} - g_{T,x}\left(\frac{\sigma_{0,x}v_0}{v}\right)\right]\frac{dE}{E} \qquad (2.72)$$

Thus, the I'_0 factor can be understood as a 1/v-tail subtracted I_0 factor.

By means of the Cd-ratios (or r_{Cd} values), the s_0 factors can be experimentally determined from the following relationship derived in this work from references [45, 48]:

$$s_{\alpha,x} \equiv \frac{g_{T,x}}{r_{Cd,x} G_{r,x}} \left[G_{th} \beta_\alpha + z_{Cd,x} \left(W'_{\alpha,x} - C'_\alpha \right) \right] \qquad \textbf{(2.73)}$$

where we have introduced the auxiliary parameters:

$$z_{Cd,x} \equiv \left(r_{Cd,x} + 1 \right) z \qquad \textbf{(2.74)}$$

The equivalence between C'_α and C_α:

$$C'_\alpha \equiv \frac{C_\alpha}{z \mathrm{K} C_0} \equiv C_\alpha \qquad \textbf{(2.75)}$$

was derived in this work from the definition of K given in reference [48]:

$$\mathrm{K} \equiv \frac{1}{2z} \sqrt{\frac{E_{Cd}}{E_0}} \equiv \frac{1}{z C_0} = \frac{\sqrt{\pi}}{2} \frac{1}{C_0} \qquad (2.76)$$

A quick computation of eq. (2.76) shows that K ≈ 2.07, although it is mentioned in reference [48] that Westcott et al. proposed the value K = 2.29 for Cd-covers of 1 mm thickness, which would mean that $C'_\alpha \neq C_\alpha$:.

From eq. (2.73), the β_α parameter can be found from the Cd-ratios of isotopes with known s_α values (similarly to f and eq. (2.52)):

$$\frac{1}{\beta_\alpha} \equiv r_\alpha = \frac{G_{th}}{\left\{ G_r \, r_{Cd} s_\alpha / g_T \right\}_x - z_{Cd,x} \left\{ W'_{\alpha,x} + C_\alpha \right\}} \qquad \textbf{(2.77)}$$

It must be noted that the eq. (2.69) derived in this work is significantly different than the one proposed in reference [20], which was compiled by the same author of the reference [48]. We believe that the equations in reference [48] are correct and that there were some typographic errors when transcribed later into reference [20].

In eq. (2.69) another parameter is defined in this work slightly different than in reference [48]:

$$W'_{\alpha,x} \equiv \frac{G_{W,x}}{g_{T,x}} W'_x \left(\bar{E}_{r,\alpha}\right)_x^{-\alpha} \left(1\text{eV}\right)^{\alpha} \qquad \textbf{(2.78)}$$

where W' is a small correction factor for a non-1/v cross-section behaviour in the [μkT_n, E_{Cd}] energy region and G_W is a correction factor for self-shielding effects in that energy region (G_W = 1 for sufficiently diluted samples) [48]. The W' is defined as:

$$W'_x \equiv \frac{1}{\sigma_{0,x}} \int_{\mu kT_n}^{E_{Cd}} \left[\sigma_{E,x} - g_{T,x}\left(\frac{\sigma_{0,x} v_0}{v}\right)\right] \frac{dE}{E} \qquad (2.79)$$

2.10.2 Non-1/v isotopes as channel temperature monitors

The eq. (2.71) shows that while g_T increases (diverges from unity), the s_α by means of eq. (2.70) decreases. However, the eq. (2.71) also shows that I'_0 is still a function of the neutron temperature T_n and, to a lesser extent, of the chosen μ parameter (of the reactor moderator), therefore the s_0 factor cannot be considered a "true" nuclear constant, unless $g_T \approx 1$ but that would mean that the adoption of such formalism was not necessary [48].

Because of the temperature dependence, the modified Westcott formalism was not meant for s_0 determination. Furthermore, the determination of s_0 factors by means of eq. (2.73) requires Cd-covered irradiations and the accepted Cd cut-off energy E_{Cd} = 0.55 eV is bound to the condition that the neutron cross-section of the isotope must follow the 1/v-law up to ~1.5 eV [48]. For strong non-1/v absorbers this is clearly not the case, invalidating the expected accuracy of eq. (2.73).

The idea of the Westcott formalism was to co-irradiate a reference isotope showing a strong g_T variation with temperature such as ^{176}Lu and/or ^{151}Eu (index *x*), along with a typical 1/*v*-isotope and, to calculate the channel temperature T by means of [48]:

$$g_{T,x} = \left(\frac{A}{w}\right)_x \left(\frac{w}{A}\right)_{1/v} \left(\frac{k_{0,1/v}}{k_{0.x}}\right)\left(\frac{1}{G_{th}}\right)_x R_{W,1/v} - \left(\frac{G_r}{G_{th}}\frac{s_\alpha}{\beta_\alpha}\right)_x \qquad (2.80)$$

The channel temperature is found by interpolation of the resulting $g_{T,x}$ value with reported $g_{T,x}$ tables as a function of T_n, which are for instance published in references [2, 13, 16, 48, 111]. Clearly, the $s_{0,x}$, $k_{0,x}$ and $k_{0,1/v}$ factors in eq. (2.80) would need to be adopted or calculated from the literature, while the $s_{0,1/v}$ factor could be calculated from its known Q_0 factor (since $g_{T,1/v} = 1$) [48]:

$$s_{0,1/v} = z\left(Q_{0,1/v} - C_0\right) \qquad \textbf{(2.81)}$$

Once the average irradiation channel T_n is known, the $g_{T,y}$ values for another non-1/*v* nuclide *y* can be adopted (from the literature), for the experimental determination of its $k_{0,y}$ factors (or vice versa).

The Table 2.1 compiles the Westcott g_T factors at T = 20 ºC for isotopes of analytical interest in NAA from references [2, 13, 16, 48, 111], having the highest deviations from unity ($g_T \neq 1$) and the highest g_T variation over the 20-100 ºC neutron temperature range ($g_{\Delta T}$):

$$g_{\Delta T} = \left(g_{100} - g_{20}\right)/g_{20} \qquad (2.82)$$

The most significant cases are the target isotopes: ^{176}Lu, ^{204}Hg, ^{151}Eu, ^{168}Yb and ^{36}S (in that order), but not only because of the magnitude of their g_T deviation from unity at 20 ºC (see Table 2.1 for values). Their high g_T variation of 3 to 32% between the temperature range of 20-100 ºC (usually found in practice) is also of great concern, as neglecting this variation in routine analysis or k_0 calculations would lead to values that differ

significantly between irradiation channels at different average neutron temperatures. The use of the modified Westcott formalism as given in this section or in reference [48] or the use of a "simplified Westcott method" as proposed in reference [74] is therefore strictly necessary when dealing with these cases.

The relative difference on a k_0 determination that makes use of the modified Westcott formalism (or R_W) as compared to the modified Høgdahl convention (or R_H) is obtained from eq. (2.37) in its general form:

$$\frac{k_{0,s,c,W}}{k_{0,s,c,H}} = \left(\frac{R_W}{R_H}\right)_c \left(\frac{R_H}{R_W}\right)_s = \frac{R_{H,s}}{R_{H,c}} \frac{R_{W,c}}{R_{W,s}} \tag{2.83}$$

The Table 2.2 shows the percent relative differences that are expected in the experimental k_0 factors for some non-1/v nuclides of Table 2.1, when adopting the modified Westcott formalism ($k_{0,W}$) vs. the modified Høgdahl convention ($k_{0,H}$), for irradiations over 3 different irradiations channels with extreme f and α parameters but equal average neutron temperature (20 ºC).

For the strong non-1/v nuclides ^{176}Lu, ^{151}Eu, ^{153}Eu and ^{168}Yb, the differences of -42%, 12%, 3% and -5% (respectively) are too high to be acceptable, even for T = 20 ºC channels. The Westcott formalism must be adopted for these cases, as mentioned in the previous section.

Table 2.1: Reported Westcott g_T-factors at T = 20 ºC for target isotopes of analytical interest in NAA with the highest g_T deviations from unity and, the highest $g_{\Delta T}$ variation over the 20 - 100 ºC range ($g_{\Delta T}$).

		Target Isotope			
Reference	**Year**	**Lu-176**	**Eu-151**	**Yb-168**	**Eu-153**
De Corte [13]	1987	1.691	0.902	1.050	1.029
De Corte et al. [48]	1994	1.746	0.901	1.050	
Holden [16, 112]	1999	1.746	0.901		0.974
IAEA [111]	2007	1.752	0.900	1.057	0.966
Pritychenko et al. [2]	2012	1.758	0.894		0.986
Van Sluijs et al. [113]	2015	1.708	0.946	1.057	0.986
$g_{\Delta T}$ (%)		32.3	-6.9	4.7	-1.2
		Target Isotope			
Reference	**Year**	**Hg-204**	**S-36**	**Rh-103**	**Ir-193**
De Corte [13]	1987			1.023	1.022
De Corte et al. [48]	1994			1.025	1.022
Holden [16, 112]	1999			1.025	
IAEA [111]	2007		1.014	1.023	1.017
Pritychenko et al. [2]	2012			1.024	1.018
Van Sluijs et al. [113]	2015	1.114	1.014	1.022	1.018
$g_{\Delta T}$ (%)		10.9	2.6	1.8	1.4

Calculated g_T variation according to eq. (2.82) and values from references [16, 111].

Table 2.2: Expected % relative differences in experimental k_0 factors for some non-1/v nuclides of Table 2.1 when adopting the modified Westcott formalism ($k_{0,W}$) as compared to the modified Høgdahl convention ($k_{0,H}$), for irradiations on 3 irradiation channels with extreme f and α parameters but equal average neutron temperature (of 20 ºC).

							f = 16.4; α = -0.0034 β_α = 19			f = 38.2; α = 0.066 β_α = 43.6			f = 95; α = 0.11 β_α = 114		
TI	**FN**	$\bar{E}_r$ **(eV)**		s_0		g_{20}	R_H	R_W	$k_{0,W}$ / $k_{0,H}$	R_H	R_W	$k_{0,W}$ / $k_{0,H}$	R_H	R_W	$k_{0,W}$ / $k_{0,H}$
^{176}Lu	^{177}Lu	0.158	(-)	1.67	(10)	1.746	1.12	1.84	-40%	1.05	1.79	-41%	1.02	1.77	-42%
^{168}Yb	^{169}Yb	0.61	(-)	4.97	(-)	1.057	1.29	1.33	-3%	1.13	1.18	-4%	1.05	1.11	-5%
^{153}Eu	^{154}Eu	5.8	(4)	5.90	(10)	0.974	1.35	1.29	3%	1.13	1.10	3%	1.05	1.02	3%
^{151}Eu	^{152}Eu	0.448	(-)	1.25	(-)	0.901	1.09	0.97	12%	1.04	0.93	11%	1.02	0.91	12%
^{197}Au	^{198}Au	5.650	(7)	17.2	(2)	1.007	1.96	1.94	0%	1.37	1.36	0%	1.14	1.14	0%

Nuclear data adopted from the recommended literature [23], uncertainties in % at the 1*s* confidence level.

R_H calculated according to eq. (2.31); R_W calculated according to eq. (2.65).

TI = Target Isotope; FN = Formed Nuclide.

The g_{20} factor is the Westcott g_T factor at T = 20 ºC, taken from references [2, 16, 111, 112] (see Table 2.1).

2.11 About the equivalence between formalisms: the hybrid approach

There is no exact equivalence between the modified Westcott and Høgdahl conventions, as the latter approach to the problem neglects the effect of the irradiation channel (neutron) temperature on the (n,γ) reaction rate.

It is natural to question the need of 2 different formalisms if, in principle, the modified Westcott formalism could be used for the 1/v cases ($g_T = 1$) as well by performing the corresponding conversion of Q_α (or q_α) to s_α factors by means of the eqs. (2.81), (2.69) and (2.41):

$$\begin{aligned} s_{\alpha,1/v} &= s_{0,1/v}\left(\bar{E}_{r,\alpha}\right)^{-\alpha}\left(1\text{eV}\right)^{\alpha} = zq_\alpha \\ &= zq_0\left(\bar{E}_{r,\alpha}\right)^{-\alpha}\left(1\text{eV}\right)^{\alpha} \\ &= z\left(Q_\alpha - C_\alpha\right) \end{aligned} \tag{2.84}$$

From eqs. (2.65) and (2.84), the R_W dimensionless reaction rate for a 1/v isotope is expressed as:

$$R_{W,1/v} = g_{T,1/v}G_{th} + G_{r,1/v}\frac{q_{\alpha,1/v}}{\beta_\alpha}z \tag{2.85}$$

where we have kept the g_T factor in the formula as it can be later set to unity.

If the g_T factor of a given isotope remains relatively constant or "flat" over the typical temperature range, i.e. with just ±1% relative fluctuation between 20-100 ºC, then these isotopes having "flat g_T factors" can be idealized as 1/v-isotopes as well. The 1/v index can be dropped and the previous relation can be written in the same notation as in the modified Høgdahl convention:

$$R_W \cong R_{W\to H} \equiv g_T G_{th} + G_e\frac{q_\alpha}{f^*} \tag{2.86}$$

where it was assumed that $G_r \approx G_e$ and the auxiliary parameter f^* was defined as:

$$f^* \equiv \frac{\beta_\alpha}{z} = \frac{\sqrt{\pi}}{2}\beta_\alpha \qquad \textbf{(2.87)}$$

The eq. (2.86) should not be employed for strong non-1/v absorbers. It should be understood as a "hybrid" equation for isotopes following the 1/v-law with (at worst) ±2% variation over the 20-100 ºC temperature range (i.e. $g_T \neq 1$ but relatively constant). The "approximately equal" symbol is introduced to differentiate this R_W from its strict definition provided in eq. (2.65).

The g_T factor in eq. (2.86) can be factorized and assimilated temporarily into the q_α factor. That is, a change of variable $Q_0^* = (Q_0/g_T)$ can be performed in:

$$\begin{aligned} \frac{q_\alpha}{g_T} &\cong \left(Q_0^* - C_0\right)\left(\bar{E}_r\right)^{-\alpha}\left(1\text{eV}\right)^\alpha \\ &\cong q_\alpha^* \end{aligned} \qquad (2.88)$$

by considering that the error introduced from performing a $C_0^* = (C_0/g_T) \approx C_0$ approximation will be poorly propagated to q_α unless the $Q_0 \leq C_0$ (as with ^{174}Yb, ^{45}Sc and ^{164}Dy) [23].

Thus, from eq. (2.86) one has:

$$\begin{aligned} R_W &\cong g_T\left(G_{th} + G_e\frac{q_\alpha^*}{f^*} + G_e\left\{\frac{C_\alpha}{f^*}\right\} - G_e\left\{\frac{C_\alpha}{f^*}\right\}\right) \\ &\cong g_T\left(\left\{G_{th} + G_e\left(\frac{Q_\alpha^*}{f^*}\right)\right\} - G_e\left\{\frac{C_\alpha}{f^*}\right\}\right) \end{aligned} \qquad (2.89)$$

A linear relation between the modified Westcott (R_W) formalism and the ("effective") Høgdahl (R_H^*) convention (n,γ) reaction rate is found for

isotopes following the 1/v-law and, for those non-1/v nuclides having "flat" g_T factors within the temperature range of interest:

$$R_W \cong R_{W\to H} \equiv g_T \left({R_H}^* - G_e \left\{ \frac{C_\alpha}{f^*} \right\} \right) \qquad \textbf{(2.90)}$$

The asterisk superscript (*) is kept to emphasize the potential difference between f^* and f, as well as between the ${Q_\alpha}^*$ and Q_α factors.

For an epithermal channel with f = 15, $\alpha \approx 0$, with $Q_0 \approx f$ and a g_T factor ±2% different than unity, the (R_W/R_H) ratio varies between 0.975 and 0.995 (0.5-2.5% relative change). On the contrary, for highly thermalized irradiation channels the term (C_α/f^*) vanishes and for a sufficiently low Q_0 factor:

$$R_W \approx g_T {R_H}^* \approx g_T R_H \qquad \textbf{(2.91)}$$

implying that the difference between R_W and R_H would be approximately of the order of the g_T factor deviation from unity.

The recent work from van Sluijs et al. (2014; index *vS*) [74] presents a similar approach to the problem of the equivalence between the formalisms, although they recommend the use of:

$$R_{W,vS} \cong g_T G_{th} + G_e \frac{Q_\alpha}{f^*} \qquad (2.92)$$

The main difference with the $R_{W\to H}$ parameter from eq. (2.86) or eq. (2.90) is that the correction term (C_α/f^*) is absent in their relation, since they proposed the employment of Q_α instead of q_α. Additionally, van Sluijs et al. [74] proposed $f^* \approx f$ for practical reasons, since they found that the (f^*/f) ratios from 5 reactor irradiation channels employed in reference [45] were within an average 2.6% deviation from unity (0 - 5% range). They showed that the expected error in the analytical result when employing their formulae was generally within 1% and rarely within 2%, validating its accuracy.

The relative difference on a k_0 determination that makes use of the modified Westcott formalism (or R_W) vs. the modified Høgdahl convention (or R_H) is obtained for these cases from eqs. (2.83) and (2.90):

$$\left(\frac{k_{0,s,c,W}}{k_{0,s,c,H}}\right)=\frac{g_{T,c}}{g_{T,s}}\frac{R_{H,s}}{R_{H,c}}\frac{\left\{R_{H,c}{}^{*}-\left(C_\alpha / f^{*}\right)\right\}}{\left\{R_{H,s}{}^{*}-\left(C_\alpha / f^{*}\right)\right\}} \tag{2.93}$$

For highly thermalized channels and/or sufficiently low Q_0 factors ($R_H \approx R_H{}^{*}$) the previous equation is reduced to:

$$k_{0,s,c,H} \approx \frac{g_{T,s}}{g_{T,c}} k_{0,s,c,W} \tag{2.94}$$

The g_T factors from the previous equation can be absorbed temporarily into the k_0 definition of eq. (2.38), that is, $(g_T.k_0) \rightarrow k_0{}^{*}$, meaning that the strict application of the Høgdahl convention for the determination of k_0 nuclear data for non-1/v isotopes would result (approximately) into "effective" $k_0{}^{*}$ and $Q_0{}^{*}$ values (i.e. *T*-dependent). These values need to be normalized by the respective g_T factor to tabulate the g_T-independent definitions.

The Table 2.3 quotes target isotopes with Westcott g_T factors at T = 20 ºC showing a 1-2% deviation from unity and ±1.6% g_T variation over the 20-100 ºC range. For this group of "flat g_T factor" isotopes: ^{113}In, ^{187}Re, ^{232}Th, ^{175}Lu and ^{191}Ir, the g_T factors are barely <0.6% different than unity, therefore the final impact on the accuracy of the k_0 factors determined by adopting the formal Høgdahl convention is expected to be small in sufficiently thermalized irradiation channels. In fact, the modified Høgdahl convention seemed justified at the time of the first k_0 determinations [36, 38, 40].

The Table 2.4 shows the percent relative differences in k_0 factors for some of the nuclides of the Table 2.3, when adopting the formal modified Westcott ($k_{0,W}$) formalism vs. the formal modified Høgdahl convention ($k_{0,H}$). These differences were estimated for determinations in 3 irradiation channels with extreme *f* and α parameters but equal average neutron temperature (20 ºC).

For production of ^{114m}In, ^{186}Re there would be no difference in k_0 factors at this temperature (<0.5%). For production of ^{188m}Re/^{188}Re and ^{16m}In the difference would be ±1%, meaning that the use of the formal modified Høgdahl convention is acceptable but the approximation of eq. (2.90) is preferable. A 2% impact on the k_0 factors is estimated for production of ^{165m}Dy/^{165}Dy and ^{175}Hf, therefore the adoption of the Westcott formalism is preferable over the Høgdahl convention.

Assuming that $f^* \approx f$ is valid within the uncertainty range, then eq. (2.90) would imply that even for 1/v isotopes the R_W parameter would be lower in magnitude than R_H by a channel (and irradiation position) specific small quantity (C_α/f), which is maximum for poorly thermalized channels and minimum for highly thermalized ones. This becomes clear from:

$$R_W - R_H \cong \left\{ g_T {R_H}^* - R_H \right\} - \left\{ g_T G_e \frac{C_\alpha}{f^*} \right\} \tag{2.95}$$

and in the case that $g_T = 1$, $f^* \approx f \rightarrow {R_H}^* = R_H$ and $G_e = 1$ one obtains:

$$R_W - R_H \approx -\left(\frac{C_\alpha}{f} \right) \tag{2.96}$$

The C_α term is lower than $C_0 = 0.429$ for $\alpha > 0$ and higher than this value for $\alpha < 0$. An α value in the [-0.1;0.1] range would imply a C_α value in the [0.50;0.38] range. If for instance $f = 15$ and $C_\alpha = 0.45$ then one obtains (C_α/f) = 0.03. This means that for $Q_0 \approx C_0$, one would obtain $Q_\alpha \approx C_\alpha$ and the difference in magnitude between R_W and R_H would be at a maximum (in this case ~3%). This is the case for 1/v isotopes like ^{174}Yb, ^{45}Sc and a "flat" g_T factor isotope as ^{164}Dy.

From eq. (2.93) and assuming $f^* \approx f$, the ratio between the k_0 factors computed through both formalisms would yield for 1/v isotopes ($g_T = 1$):

$$\left(\frac{k_{0,s,c,W}}{k_{0,s,c,H}}\right)_{1/v} \approx \left\{1-\frac{C_\alpha}{R_{H,c}\,f}\right\} \Big/ \left\{1-\frac{C_\alpha}{R_{H,s}\,f}\right\} \qquad (2.97)$$

thus, the difference would be at a maximum for poorly thermalized channels and at a minimum for highly thermalized ones (see Figure 2.4). The eq. (2.97) would also correspond to the ratio in the computed elemental content of the analyte, as obtained by both conventions (w_W/w_H).

The correction term (C_α/f^*) can lead to ~3% differences between R_W and R_H in an epithermal channel as in our previous example, but the impact in the analytical result such as the elemental content or a k_0 factor is expected to be lower given the shape of eq. (2.97). When adopting the recommended nuclear data from the literature [23] and assuming that $f^* \approx f$, the Figure 2.4 illustrates that for a poorly thermalized channel with $f = 16.4$ and $\alpha = -0.0034$, the expected percent relative differences between k_0 factors (calculated through both conventions) can be as high as 1.6% for low Q_0 factors ($Q_0 < 2$). The relative difference decreases with increasing Q_0 factor and can change sign, with -0.5% for $Q_0 = 60$.

For a sufficiently thermalized channel with $f = 38.3$ and $\alpha = 0.066$, the difference decreases linearly from 0.8% for $Q_0 < 2$, to 0.3% for $40 < Q_0 < 60$. For a highly thermalized channel ($f = 95$; $\alpha = 0.011$) the difference remains constant at ~0.6% at the same Q_0 range. Only 2 isotopes in the k_0-NAA literature have a $Q_0 > 60$ (^{96}Zr and ^{238}U), therefore the Q_0 axis in Figure 2.4 covers the usual range of analytical interest.

It is therefore noted from Figure 2.4 that:

- if the k_0 and Q_0 factors for 1/v nuclides were experimentally determined through one given convention, then one should later employ the same convention (for which these factors are correlated) in the analytical determinations. This is recommended at least for poorly thermalized channels and low Q_0 factors;

- since the eq. (2.92) proposed by van Sluijs et al. [74] reduces to R_H for $g_T = 1$ (for $f^* = f$ as suggested), the differences shown by the figure would also correspond to differences between our "hybrid" $R_{W\rightarrow H}$ parameter of eq. (2.86) and their parameter $R_{W,vS}$ of eq. (2.92).

Whether eq. (2.97) is valid and whether the $f^* \approx f$ approximation holds for our irradiation channels as well will be discussed later in this work. In the case that $f^* > f$ then the differences in Figure 2.4 should be lower unless the Q_0 (or s_0) factor is high.

Table 2.3: Reported Westcott g_T-factors at T = 20 ºC for target isotopes of analytical interest in NAA with 1-2% deviation from unity and less than ±1.6% g_T variation within the 20-100 ºC temperature range ($g_{\Delta T}$).

Reference	Year	Target Isotope					
		Dy-164	**In-113**	**Re-187**	**Th-232**	**In-115**	**Au-197**
De Corte [13]	1987	0.988		0.982		1.018	1.004
De Corte et al. [48]	1994	0.988			1.000	1.020	1.007
Holden [16, 112]	1999	0.988		0.996		1.021	1.007
IAEA [111]	2007	0.988	1.012	0.982	0.995	1.019	1.005
Pritychenko et al. [2]	2012	0.987	1.006	0.994	0.998	1.020	1.005
Van Sluijs et al. [113]	2015	0.988	1.013	0.995	0.995	1.020	1.006
$g_{\Delta T}$ (%)		-1.0	1.0	-0.4	-0.5	1.6	0.4

Reference	Year	Target Isotope				
		Hf-174	**Os-190**	**Hg-196**	**Lu-175**	**Ir-191**
De Corte [13]	1987				0.977	1.033
De Corte et al. [48]	1994				0.977	1.033
Holden [16, 112]	1999				0.977	
IAEA [111]	2007	0.986		0.988	0.976	0.996
Pritychenko et al. [2]	2012	0.977				0.996
Van Sluijs et al. [113]	2015	0.987	0.988	0.988	1.003	0.996
Δg (%)		-1.1	-1.0	-1.0	0.2	-0.3

Calculated g_T variation according to eq. (2.82) and values from references [16, 111].

Table 2.4: Expected % relative differences in experimental k_0 factors for some "flat g_T factor" nuclides of Table 2.3, when adopting the modified Westcott formalism (R_W) as compared to the modified Høgdahl convention (R_H), for irradiations on 3 irradiation channels with extreme f and α parameters but equal average neutron temperature (20 ºC). Values calculated assuming that $f^* \approx f \rightarrow \beta_\alpha \approx zf$.

							f = 16.4; α = -0.0034			f = 38.2; α = 0.066			f = 95; α = 0.11		
TI	**FN**	$\bar{E}_r$ **(eV)**		Q_0		g_{20}	R_H	R_W	$k_{0,W}$ / $k_{0,H}$	R_H	R_W	$k_{0,W}$ / $k_{0,H}$	R_H	R_W	$k_{0,W}$ / $k_{0,H}$
^{115}In	^{116m}In	1.56	(7)	16.8	(2)	1.021	2.03	2.02	-1%	1.43	1.44	-1%	1.17	1.19	-1%
^{113}In	^{114m}In	6.41	(15)	24.2	(2)	1.006	2.48	2.46	0%	1.56	1.56	0%	1.21	1.21	0%
^{185}Re	^{186}Re	3.40	(4.1)	15.4	(3)	1.007	1.94	1.92	0%	1.37	1.37	0%	1.14	1.14	0%
^{187}Re	^{188m}Re	41.1	(3.9)	4.57	(3)	0.996	1.28	1.25	1%	1.09	1.08	1%	1.03	1.03	1%
	^{188}Re			4.35	(10)		1.27	1.24	1%	1.09	1.08	1%	1.03	1.02	1%
^{164}Dy	^{165}Dy	224	(5)	0.19	(10)	0.988	1.01	0.97	3%	1.01	0.98	2%	1.00	0.99	2%
^{174}Hf	^{175}Hf	29.6	(7)	0.78	(10)	0.986	1.05	1.01	3%	1.02	0.99	2%	1.01	0.99	2%
^{197}Au	^{198}Au	5.650	(7)	15.70	(2)	1.007	1.96	1.94	0%	1.37	1.36	0%	1.14	1.14	(-)

Nuclear data adopted from the recommended literature [23]. Uncertainties given at the 1s confidence level.

The s_0 factors were calculated from eq. (2.81), i.e. assuming a "flat g_T factor" approximation (see text).

The g_{20} factor is the Westcott g_T factor at T = 20 ºC, taken from references [2, 16, 111, 112] (see Table 2.3).

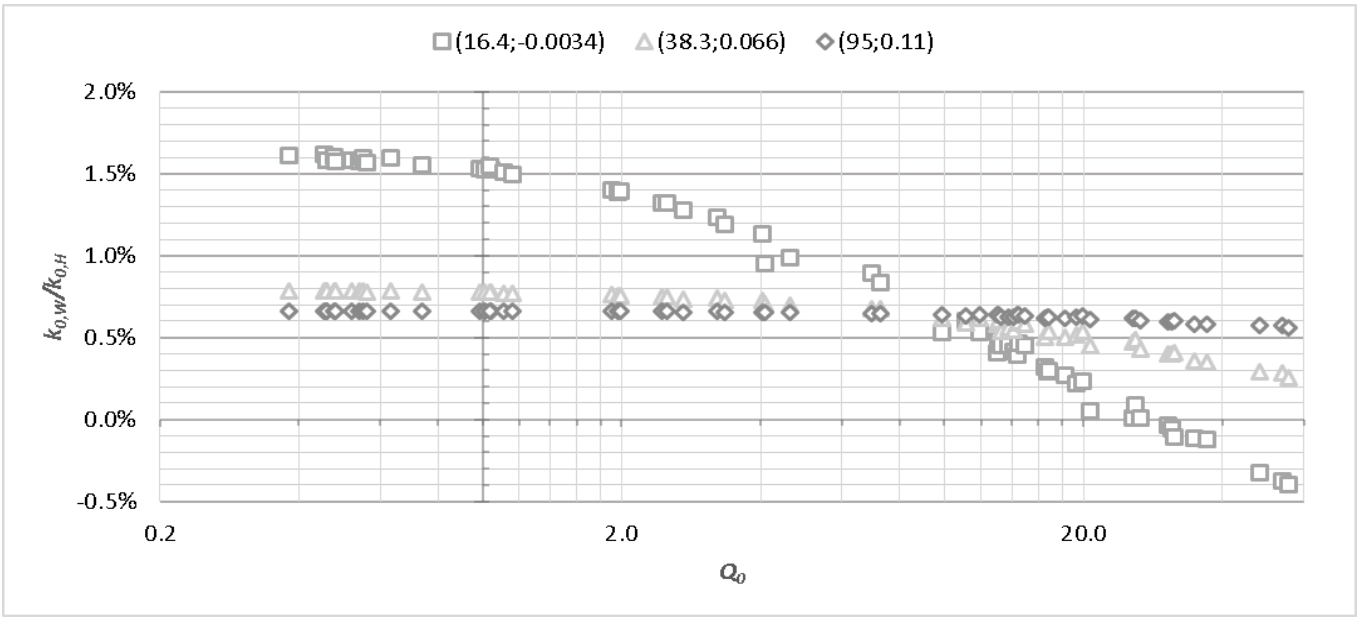

Figure 2.4: Expected % relative differences in experimental k_0 factors for several 1/v-nuclides (g_T = 1), when adopting the modified Westcott formalism ($k_{0,W}$) as compared to the modified Høgdahl convention ($k_{0,H}$), as a function of the Q_0 factor, for irradiations on 3 irradiation channels with extreme f and α parameters. Values calculated assuming that $f^* \approx f \rightarrow \beta_\alpha \approx zf$.

2.12 The two-channel method

In the section 2.9 it was shown that Cd-covered irradiations play a fundamental role in Q_0 and k_0 determination, by filtering the thermal contribution to the total reaction rate. The eqs. (2.55) and (2.59) allow for the computation of the Q_0 factor either by employment of the modelled/calibrated f parameter and/or the equivalent f as seen by the comparator during the bare a Cd-covered irradiations. In the modified Westcott formalism, one could determine instead s_0 factors from eq. (2.69), although as previously mentioned, the s_0 factors are by definition a function of the channel temperature.

Another possibility for Q_0 (or s_0) determination is known as the "two channel method" [114], that employs eq. (2.37) written for replicate samples irradiated in two different irradiation channels, from which a relationship in terms of f_1, f_2 (or $\beta_{\alpha 1}$, $\beta_{\alpha 2}$) and α_1, α_2 is obtained:

$$\frac{R_{H,s,2}}{R_{H,s,1}} = \left[\frac{w_c}{w_s}\frac{A_S}{A_C}\right]_2 \left[\frac{w_s}{w_c}\frac{A_C}{A_S}\right]_1 \frac{R_{H,c,2}}{R_{H,c,1}} \tag{2.98}$$

with the due substitution of the R_H parameter (or R_W) by eq. (2.31) (or eq. (2.65)) for each case. With this method the Q_0 for the standard (index s) is found in terms of the comparator (index c) nuclear and experimental data from the two channels. In any of these methods however, the knowledge of the effective resonance energy $\bar{E}_r$ of the target isotope of analytical interest is required.

2.13 Interferences

The monitoring of a radionuclide X produced by a (n,γ) reaction on the target isotope x can be "spectrally interfered" when some (or all) of the

characteristic radiation from the decay of *X* is also emitted by other radionuclides present in the sample. If the analyst has other means to quantify the interfering radioisotope (e.g. with other interference-free radiation, an elemental content certificate for the interfering species, etc.), then the problem is reduced to the application of a few simple correction algorithms, given for instance in reference [115]. If the monitored and interfering radionuclide differ significantly in terms of half-lives, then cooling and re-measurement of the sample until either nuclide has completely decayed is the standard practice. Finally, if the spectral interferences cannot be avoided and/or corrected, the analyst could also perform a radioanalytical separation of the species of interest.

On the other hand, if the monitored radionuclide *X* is also produced by a neutron induced reaction different than the radiative neutron capture process of analytical interest, that is, by a (n,n'), (n,2n), (n,f), (n,p) or (n,α) reaction on an isotope *y* that is present in the sample, then one is posed with the problem of a "reaction interference".

The (n,p) and (n,α) reaction interferences are known as "threshold reactions" because of the minimum incident neutron energy that is required for the reaction to occur. The threshold energies are characteristic of the target isotope and reaction mechanism, spanning a 0.1 - 20 MeV neutron energy range. In a U-fuelled nuclear reactor, the 0.1 - 10 MeV "fast" component of the neutron fluence rate is commonly known as the ^{235}U fission neutron spectrum, and has been typically described by a Watt distribution centred at 0.7 MeV [94] (see Figure 2.1 and Figure 2.5). Similarly, a Maxwellian distribution centred at 1.2 MeV has also been applied to model the ^{235}U fission spectrum in the 0.28 to 1.8 MeV region [116].

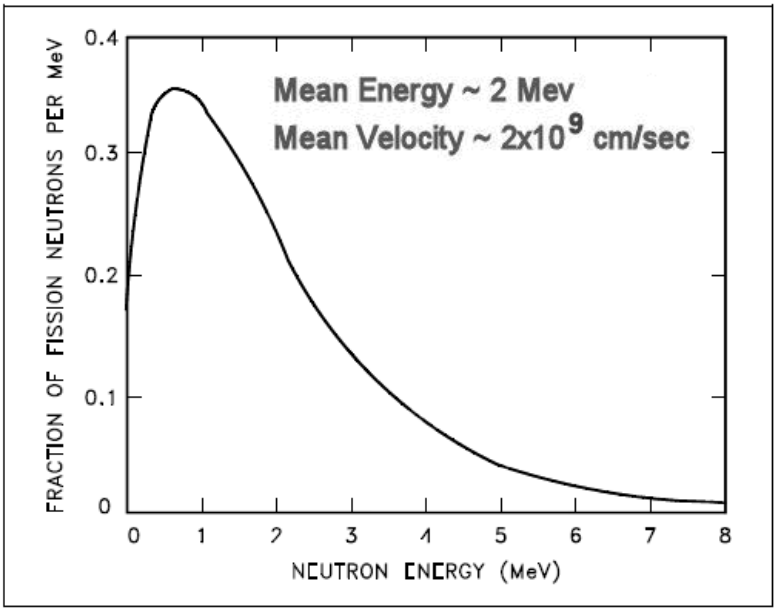

Figure 2.5: Typical ^{235}U fission (fast) neutron spectrum of an irradiation channel of a U-fueled reactor. The center of the Watt distribution is observed at 0.7 MeV, while the mean neutron energy is at 2 MeV [117]**.**

The (n,n') and (n,2n) reactions are threshold reactions as well, but these are instead grouped as "primary interferences" because the target *y* nuclide in either case is an isotope of the element of analytical interest.

To account for a threshold or primary reaction on a target isotope *y* that interferes in the characterization of a radioisotope *X*, the Activation Equation in eq. (2.12) needs to be corrected:

$$\begin{aligned} A_{sat,X} &= n_x R'_{x,X} + n_y R'_{y,X} \\ &= n_x \left[R'_{x,X} + \left(\frac{n_y}{n_x} \right) R'_{y,X} \right] = n_x R'_{eff,x} \end{aligned} \tag{2.99}$$

where the effective reaction rate R'_{eff} is defined as the quantity between brackets.

To determine R'_{eff} we borrowed the idea exposed for instance in reference [95], i.e. that the neutron fluence rate per unit energy interval in eq. (2.15) (ϕ'_E; in $cm^{-2}.s^{-1}eV^{-1}$) at energies $E>E_{Cd}$ can be replaced by:

$$\phi'_E \rightarrow \phi'_{r,E} + h\phi'_{f,E} \tag{2.100}$$

with h a scaling factor ("ad hoc" constant) between the epithermal or "resonance" ($\phi'_{r,E}$; index r) and fast ($\phi'_{f,E}$; index f) neutron fluence rates per unit energy interval (in $cm^{-2}.s^{-1}eV^{-1}$) [95].

The R'_{eff} can be expressed as having a thermal, epithermal and fast component:

$$\begin{aligned} R'_{eff,x} &= R'_{th,x} + R'_{e,x} + \left(\frac{n_y}{n_x} \right) R'_{f,y} \\ &= \left(\int_0^{v_{Cd}} \phi'_v \sigma_{v,x} dv \right) + \left(\int_{E_{Cd}}^{\infty} \phi'_{r,E} \sigma_{E,x} dE \right) \\ &\quad + \left(\frac{n_y}{n_x} \right) \left(h \int_{E_{Cd}}^{\infty} \phi'_{f,E} \sigma_{E,y} dE \right) \end{aligned} \tag{2.101}$$

The general "effective fission spectrum integral" or "fast spectrum averaged cross-section" $\sigma_{y,(n,z)}$ for an isotope y undergoing a (n,z) reaction (in b) can be defined similarly to the evaluated resonance integral I_α as shown in [95]. In this work, we follow the approach that the last integral at the right-hand side can be expressed as the product:

$$\varphi_f \sigma_{y,(n,z)} \equiv h \int_{E_{Cd}}^{\infty} \phi'_{f,E} \sigma_{E,y} dE \tag{2.102}$$

with the introduction of φ_f the conventional fast neutron fluence (in $cm^{-2}.s^{-1}$). In this way, the corrected reaction rate R'_{eff} in eq. (2.101) can be expressed as:

$$R'_{eff,x} = \left\{\varphi_{th}\sigma_{0,x}\right\} + \left\{\varphi_e I_{\alpha,x}\right\} + \left(\frac{n_y}{n_x}\right)\left\{\varphi_f \sigma_{y,(n,z)}\right\} \tag{2.103}$$

Similarly, to the *f* parameter, a dimensionless parameter *L* can be defined as the thermal-to-fast conventional neutron fluence rate ratio:

$$L \equiv \frac{\varphi_{th}}{\varphi_f} \tag{2.104}$$

and the dimensionless quantity $\delta_{x,y,z}$ as the ratio:

$$\delta_{x,y,z} \equiv \frac{\theta_y}{\theta_x}\frac{\sigma_{y,(n,z)}}{\sigma_{0,x}}\frac{M_x}{M_y} \tag{2.105}$$

Hence, from eq. (2.103) and when considering corrections for neutron self-shielding one obtains:

$$R'_{eff,x} = \sigma_{0,x}\varphi_{th}\left(G_{th} + G_{e,x}\left\{\frac{Q_{\alpha,x}}{f}\right\} + G_{f,y}\left\{\frac{w_y}{w_x}\frac{\delta_{x,y,z}}{L}\right\}\right) \tag{2.106}$$

with the introduction of the fast (G_f) neutron self-shielding correction factor. In this way, the problem is shifted to the experimental determination of *L* and not to the determination of φ_f or the scaling factor *h*.

The Figure 2.6 shows an example of the neutron cross-section function dependence on the incident neutron energy for (n,*z*) inelastic reactions on ^{77}Se (*z* = n', 2n, p, etc.) obtained from the Japanese Evaluated Nuclear Data Library (JENDL-4.0) [45].

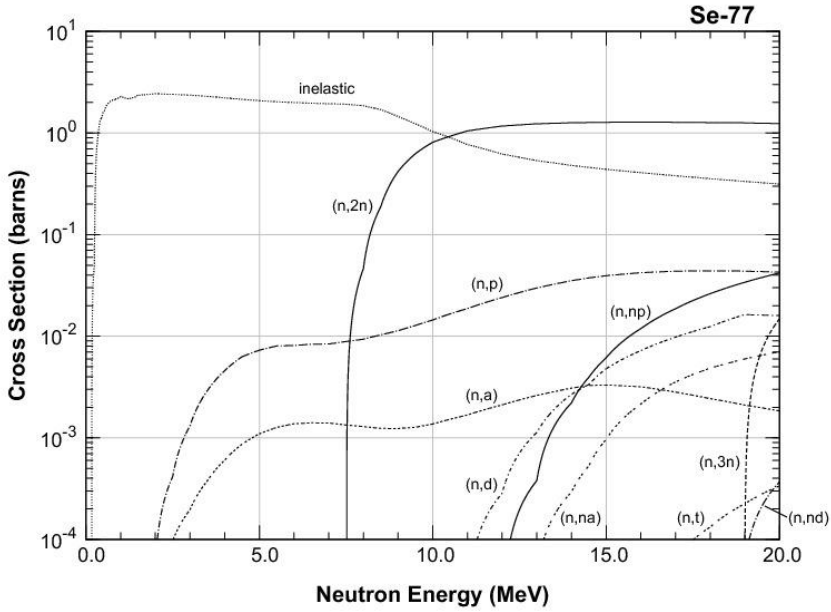

Figure 2.6: Example graph of the neutron cross-section function dependence on incident neutron energy for (n,*z*) inelastic reactions on ^{77}Se (*z* = n', 2n, p, etc.) [7].

2.13.1 Single interference

From the previous equation, the "corrected" (*) dimensionless reaction rate (in a reactor) for a given x(n,γ)X reaction that is single-interfered by a y(n,z)X reaction can be expressed according to the modified Høgdahl convention (R_H^*) as:

$$R_{H,x}^{*} \equiv G_{th} + G_{e,x}\left\{\frac{Q_{\alpha,x}}{f}\right\} + G_{f,y}\left\{\frac{w_y}{w_x}\frac{\delta_{x,y,z}}{L}\right\} \qquad \textbf{(2.107)}$$

and per the modified Westcott formalism (R_W^*) as:

$$R_{W,x}^{\ *} \equiv G_{th}\left\{g_{T,x}\right\} + G_{r,x}\left\{\frac{s_{\alpha,x}}{\beta_\alpha}\right\} + G_{f,y}\left\{\frac{w_y}{w_x}\frac{\delta_{x,y,z}}{L}\right\} \qquad \textbf{(2.108)}$$

2.13.2 Multiple interferences

When there are several simultaneous threshold and/or primary reactions of different kind because of the presence of several interfering target isotopes y_1, y_2, …, y_n, then the last term at the right-hand side of eqs. (2.106) and (2.107) should be replaced by an "effective" $\Delta_{w,x}$ parameter:

$$G_{f,y}\frac{w_y}{w_x}\delta_{x,y,z} \rightarrow \Delta_{w,x} \qquad (2.109)$$

with:

$$\Delta_{w,x} \equiv \sum_{y}^{n}\Delta_{w,x,y} \equiv \sum_{y=1}^{n}\sum_{z} G_{f,y,z}\frac{w_y}{w_x}\delta_{x,y,z} \qquad (2.110)$$

Once more, if one includes $y_0=x$ into the set, the sum will also contain the fast to thermal cross-section ratio term. Therefore, from eqs. (2.107) or (2.108) with the substitution suggested in eq. (2.109) with obtain a general expression for the calculation of the corrected reaction rate when dealing with multiple interferences (y_1, y_2, …, y_n) and a significant fast neutron spectrum contribution ($y_0=x$). That is, in the Høgdahl convention:

$$R_{H,x}^{\ *} \equiv R_{H,x} + \left\{\frac{1}{L}\sum_{y=0}^{n}\Delta_{w,x,y}\right\} \qquad \textbf{(2.111)}$$

or with the substitution $H \rightarrow W$ if the Westcott formalism is preferred. The R_H or R_W is calculated as before, according to eq. (2.31) or eq. (2.65).

2.13.3 Threshold interferences for fast fluence rate monitoring

From the ratio between activities of a "pure fast fluence rate monitor" such as: ^{58}Ni(n,p)^{58}Co or ^{90}Zr(n,2n)^{89}Zr and a "pure thermal/epithermal fluence rate monitor" such as the ultimate comparator (index *c*), the thermal-to-fast conventional neutron fluence rate ratio defined by eq. (2.104) is found experimentally from:

$$L = \frac{w_y}{w_c}\frac{A_c}{A_y}\frac{G_{f,y}}{R_{H,c}}k_{0,y(n,z),c} \qquad \textbf{(2.112)}$$

where we introduced a k_0 factor for the "fast" y(n,z) reaction of interest (z = p, α but also n', 2n) as:

$$k_{0,y(n,z),c} \equiv \frac{I_{\gamma,y}}{I_{\gamma,c}}\delta_{c,y,z} \qquad \textbf{(2.113)}$$

It seems that as of 2014, there is no peer-reviewed published literature providing a recommended set of experimental "fast k_0 factors". In principle these values can be calculated from experimental or evaluated fast neutron integrals reported for instance in references [13, 118, 119].

In the case of routine k_0-NAA, by substituting the R'_{eff} parameter from eq. (2.106) into the eq. (2.99), Lin et al. proposed a way for the analyst to determine the (erroneous) excess mass content of the element of the isotope *x* of interest that would be observed for each mass unit of the element of the interfering isotope *y* [118]:

$$\frac{\varepsilon_{w_x}}{w_y} = \frac{w_{x,int} - w_{x,true}}{w_y} = \frac{\delta_{x,y,z}}{L}\frac{G_{f,y}}{R_{H,x}} \qquad (2.114)$$

The eq. (2.114) is useful for instance in the analysis of ^{54}Mn and/or ^{51}Cr in samples with a high iron content, due to the expected ^{54}Fe(n,p)^{54}Mn and/or ^{54}Fe(n,α)^{51}Cr interferences for samples irradiated under poorly thermalized channels. Alternatively, the eq. (2.114) shows that if $w_{x,true}$ = 0 as when

irradiating a high-purity standard of the element of the isotope *y* (e.g. a high-purity Fe wire) for which the $x(n,\gamma)X$ is not expected (e.g. null Cr content), then *L* can also be computed from the same equation by inputting the observed "apparent" (index *apa*) mass content that would have been obtained from (erroneously) computing it as a (n,γ) reaction. That is, *L* is computed for instance from the "apparent" Cr mass content per Fe mass unit:

$$L = \left(\frac{w_y}{w_{x,apa}} \right) \delta_{x,y,z} \frac{G_{f,y}}{R_{H,x}} \tag{2.115}$$

with $x = {}^{50}Cr$, $y = {}^{54}Fe$ and $z = \alpha$.

The Table 2.5 shows some threshold reactions that are usually considered "interfering reactions" but that can be employed instead in the irradiation of high-purity materials (of the interfering isotope) for the determination of the *L* parameter of an irradiation channel by eq. (2.115), when inputting the observed "apparent" mass contents. The isotopic abundances (θ) for the target isotopes (TI) and atomic weights (*AW*) for the elements were adopted from the IUPAC references [49], [50], while the neutron cross-sections for the (n,γ) and (n,z) reactions leading to the formed nuclide (FN) were taken from the Atlas of resonances [42] (A) and the JENDL database [46]. The $\delta_{x,y,z}$ values were calculated according to eq. (2.105). The relative uncertainties in the $\delta_{x,y,z}$ values are estimated at 6% (at 1*s*).

For the "pure" fast fluence rate monitors ${}^{58}Ni(n,p){}^{58}Co$ and ${}^{90}Zr(n,2n){}^{89}Zr$ the $\delta_{x,y,z}$ values of Table 2.5 were tabulated against the comparator nuclear data ${}^{197}Au(n,\gamma){}^{198}Au$, for which "fast" k_0 factors can be obtained with the aid of the I_γ values from e.g. references [6, 8].

The uncertainties on the θ and *M* "natural" (or terrestrial) values are insignificant, thus, the precision in the $\delta_{x,y,z}$ values will depend mainly on the adopted σ constants for the (n,*z*) reactions, as Table 2.5 shows that for (n,γ) reactions the σ uncertainties are usually ≤ 2% (relative) at the 1*s* confidence level. The JENDL database [46] does not provide the uncertainty on the

$\sigma_{y,(n,z)}$ values. Assuming that the relative uncertainty in R_H (or R_W) is ~6% and the computed $\delta_{x,y,z}$ values from Table 2.5 is 5-10% uncertainty at 1*s* confidence level, then one would expect an 8-12% uncertainty on the *L* parameter.

In this work, we aimed at the metrological determination of nuclear constants by irradiation of high-quality mono-standards with very low quantities of trace elements or quantities below detectable limits, avoiding the need for corrections from spectral and threshold interferences. Unfortunately, the phenomena of primary reactions such as (n,n') and (n,2n) reactions cannot be avoided in routine analysis because the analyst usually deals with samples having elements with natural (or terrestrial) isotopic abundances. In the metrological determination of k_0 nuclear data, one could employ certified isotopic standards depleted in the interfering isotope, to avoid or minimize the interferences, but that kind of standards are generally very expensive and sometimes not fully suited for the intended purpose. The corrections to experimentally determined k_0 and Q_0 factors affected by primary interferences are proposed in the next section.

Table 2.5: Threshold and (n,γ) reactions that can be employed in high-purity materials for the determination of the *L* parameter of an irradiation channel according to eq. (2.115) and nuclear data from references [1, 2, 7, 10, 17, 120]**. See text for symbols and references.**

TI	Reaction	FN	θ (%)		σ (mb) A / JENDL	AW^*	$\delta_{x,y,z}$
^{19}F	**(n,γ)**	**^{20}F**	100		9.51 (9)	18.998	**5.85E-02**
^{23}Na	**(n,α)**		100		0.673	22.989	
^{23}Na	**(n,γ)**	**^{24}Na**	100		517 (4)	22.989	**1.13E-03**
^{27}Al	**(n,α)**		100		0.6877	26.982	
^{27}Al	**(n,γ)**	**^{28}Al**	100		231 (3)	26.982	**2.27E-02**
^{28}Si	**(n,p)**		92.223	(19)	5.919	28.085	
^{26}Mg	**(n,γ)**	**^{27}Mg**	11.01	(3)	38.4 (6)	24.306	**9.13E-01**
^{27}Al	**(n,p)**		100		4.284	26.982	
^{45}Sc	**(n,γ)**	**^{46}Sc**	100		27200 (200)	44.956	**3.75E-05**
^{46}Ti	**(n,p)**		8.25	(3)	13.1	47.867	
^{55}Mn	**(n,γ)**	**^{56}Mn**	100		13360 (50)	54.938	**7.14E-05**
^{56}Fe	**(n,p)**		91.754	(36)	1.057	55.845	
^{58}Ni	**(n,p)**	**^{58}Co**	68.077	(19)	107.2	58.693	**2.48E-03**
^{90}Zr	**(n,2n)**	**^{89}Zr**	51.45	(40)	0.083	91.224	**9.35E-07**
^{197}Au	**(n,γ)**	**^{198}Au**	100		98659 (138)	196.967	

* Negligible uncertainty (last significant digit).

The relative uncertainties in the $\delta_{x,y,z}$ values are estimated at 6% (at 1*s*).

2.13.4 Primary interferences

The Evaluated Nuclear Data Libraries (ENDL) [15], the Japanese Experimental Nuclear Data Library (JENDL) [7] and the Experimental Nuclear Reaction Data (EXFOR) [121] databases provide a great deal of information concerning (n,n') and (n,2n) reactions, but nowadays the data is still incomplete, i.e. the $\sigma_{f,E}$ function has not been fully mapped for all the interesting cases and neutron energies of interest. For instance, for several isotopes the evaluated and/or experimental data-points were obtained from incident neutron energies above 4 MeV, while other cases were investigated at 14 MeV and 20 MeV only. Finally, one must note that some reported

values have no uncertainties or are imprecise, sometimes greatly scattered between authors, as seen when exploring the nuclear databases [7, 15, 121].

When considering the recommended k_0 literature as of 2012 [23], a close examination of the ENDL [15], JENDL [7] or EXFOR [121] databases shows that for the application of the k_0-method, the most significant primary interferences on irradiations in poorly thermalized channels are expected for: ^{77m}Se, ^{87m}Sr, ^{135m}Ba and ^{117m}Sn, because of the ^{77}Se(n,n')^{77m}Se, ^{87}Sr(n,n')^{87m}Sr, ^{135}Ba(n,n')^{135m}Ba and ^{117}Sn(n,n')^{117m}Sn reactions (see Figure 2.7 to Figure 2.9). Interferences such as ^{111}Cd(n,n')^{111m}Cd or ^{137}Ba(n,n')^{137m}Ba, are of no analytical interest (yet) in k_0-NAA, as there is no k_0 nuclear data published for the ^{110}Cd(n,γ)^{111m}Cd and ^{137}Ba(n,γ)^{137m}Ba reactions and because other radioisotopes are tipically monitored which are free from these problematic interferences: ^{115}Cd/^{115m}In, ^{117m,g}Cd/^{117m,g}In, ^{131}Ba, ^{133m}Ba and ^{139}Ba.

The Cd-subtraction technique provides a means for determining k_0 factors that are automatically corrected from these threshold interferences, since they are equally present under bare and/or Cd-covered irradiation conditions. In this respect, a k_0 factor determined according to eq. (2.60) can be denoted as $k_{0,true}$, while employment of eq. (2.37) (with R_H or R_W) would result in a biased k_0 factor (uncorrected; $k_{0,int}$), because it would not take into account the fast contribution to the reaction rate.

The ratio between the uncorrected and corrected k_0 values is related to the thermal-to-fast conventional neutron fluence rate ratio in the following way [13]:

$$\frac{k_{0,int}}{k_{0,true}} - 1 = \frac{\delta_{x,y,z}}{L} \frac{G_{f,y}}{R_{H,x}} \qquad \textbf{(2.116)}$$

where for instance, y = ^{117}Sn (or ^{135}Ba) and x = ^{116}Sn (or ^{134}Ba). Clearly, R_H can be substituted by R_W under the modified Westcott formalism.

It must be noted that $\delta_{x,y,z}$ is considerably simplified in the case of primary interferences (z = n',2n):

$$\delta_{x,y,z}\Big|_{z=n',2n} \equiv \frac{\theta_y}{\theta_x}\frac{\sigma_{y,(n,z)}}{\sigma_{0,x}}\Bigg|_{z=n',2n} \qquad \textbf{(2.117)}$$

The δ values can be calculated from nuclear data reported for instance in reference [13]. The adoption of the Q_0 factor from the literature [20] would be necessary in order to estimate the channel L parameter by means of eq. (2.116), as the Q_0 factor determined with the Cd-ratio (r_{Cd}) definition given in eq. (2.52) is still interfered ($Q_{0,int}$). This is because an accurate Q_0 calculation ($Q_{0,true}$) is actually given by:

$$Q_{\alpha,x,true} = \frac{f}{G_{e,x}}\left(G_{t,x}\left\{\frac{1}{r_{Cd,x}}\right\} - G_{f,y}\left\{\frac{\delta_{x,y,z}}{L}\right\}\right) \qquad \textbf{(2.118)}$$

which itself depends on the knowledge of L. An alternative would be to employ highly thermalized channels ($L>>\delta$) for Q_0 determination [13].

The Table 2.6 compiles k_0 nuclear data for the most important primary interferences to expect during the standardization of the related (n,γ) reaction according to the k_0 method. The isotopic abundances (θ) for the target isotopes (TI) were adopted from the IUPAC reference [17].The neutron cross-sections for the (n,γ) and (n,z) reactions were taken from reference [13]. The Q_0 and $\bar{E}_r$ values were taken from references [20, 23], except for the ^{134}Ba and ^{110}Cd isotopes, which were adopted from reference [13]. The $\delta_{x,y,z}$ values were calculated per eq. (2.117). The relative uncertainties in the $\delta_{x,y,z}$ values are estimated at 6% (at 1s).

To illustrate the impact of these interferences in typical irradiation setups, the Figure 2.11 to Figure 2.10 show the magnitude of the correction (in %) expected from eq. (2.116), that should be applied to a k_0 factor computed

without the fast neutron component, as in eq. (2.37) (interfered; $k_{0,int}$), in order to obtain its true value ($k_{0,true}$).

As observed in Figure 2.11 to Figure 2.10, the primary reactions ^{137}Ba(n,n')^{137m}Ba and ^{117}Sn(n,n')^{117m}Sn are by far the most significant ones and that the magnitude of the correction increases with decreasing thermal-to-fast conventional fluence rate ratios. These significant reactions (>5% correction) are followed by the ^{111}Cd(n,n')^{111m}Cd reaction (<5%), which is not tabulated in the recommended k_0 literature, and by the ^{77}Se(n,n')^{77m}Se and ^{87}Sr(n,n')^{87m}Sr reactions with less than 1% correction each. It must be noted that L = 20 and/or L = 50 for an irradiation channel with f = 100 are not realistic examples, but are kept to illustrate some extremes.

For all the (n,2n) interfering reactions of Table 2.6, the previous figures have shown that even if L = 20 the corrections would be lower than 1% for any of our hypothetical irradiation channels.

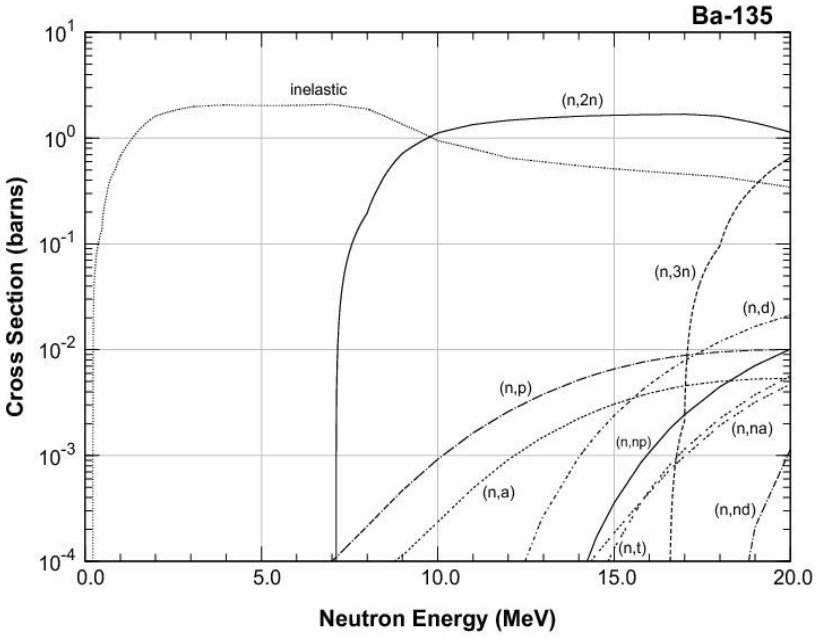

Figure 2.7: Graph of the neutron cross-section for (n,*z*) inelastic reactions on ^{135}Ba (*z* = n', 2n, p, etc.) as a function of neutron energy, from the JENDL-4.0 database [7].

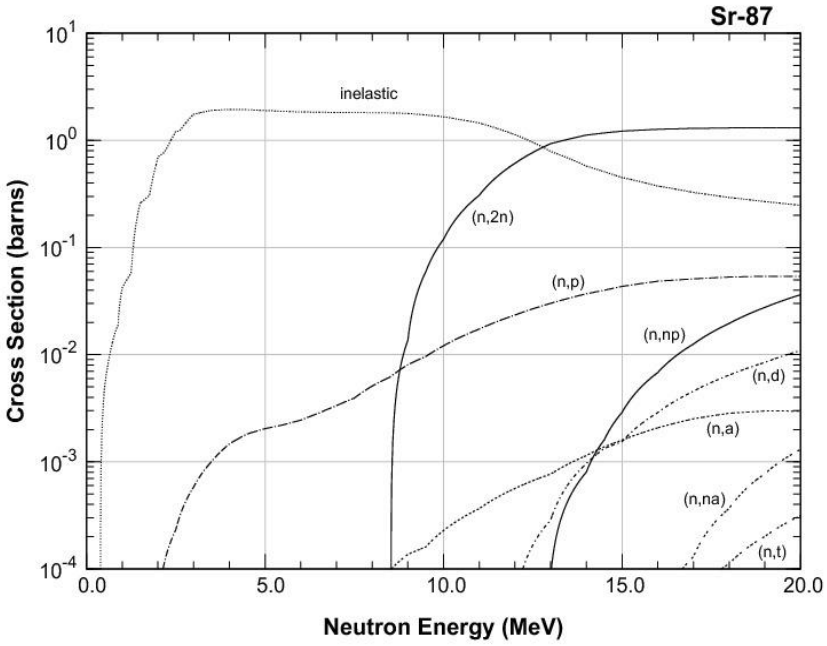

Figure 2.8: Graph of the neutron cross-section for (n,*z*) inelastic reactions on ^{87}Sr (*z* = n', 2n, p, etc.) as a function of neutron energy, from the JENDL-4.0 database [7].

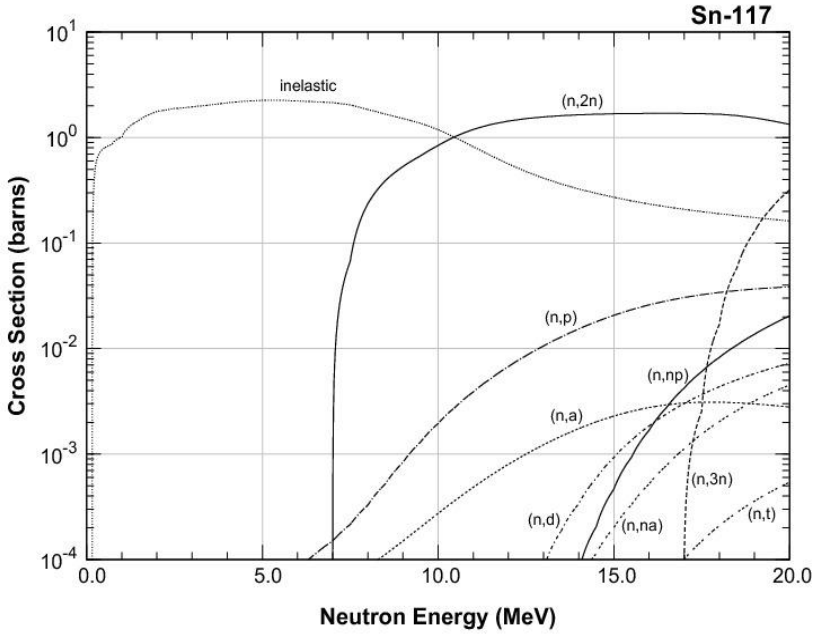

Figure 2.9: Graph of the neutron cross-section for (n,*z*) inelastic reactions on ^{117}Sn (*z* = n', 2n, p, etc.) as a function of neutron energy, from the JENDL-4.0 database [7].

Table 2.6: Examples of primary (n,n') and (n,2n) reaction interferences of interest in the determination of k_0 nuclear data. For the study of ^{235}U one is interested in the contribution to the fission products from ^{238}U fission with fast neutrons (n,f). See text for symbols and references.

TI	θ (%)		Reaction	FN	σ (mb)		Q_0 (%; 1s)		$\bar{E}_r$ (eV)	$\delta_{x,y,z}$
^{76}Se	9.37	(29)	(n,γ)	^{77m}Se	22000	(-)	0.77	10	577	
^{77}Se	7.63	(16)	(n,n')		733	(-)				2.71E-02
^{78}Se	23.77	(28)	(n,2n)		0.275	(-)				3.00E-05
^{86}Sr	9.86	(1)	(n,γ)	^{87m}Sr	770	7	4.11	2	795	
^{87}Sr	7.00	(1)	(n,n')		112	(-)				1.03E-01
^{88}Sr	82.58	(1)	(n,2n)		0.197	(-)				2.14E-03
^{110}Cd	12.49	(18)	(n,γ)	^{111m}Cd	140	(-)	21.4	(-)	125	
^{111}Cd	12.8	(12)	(n,n')		228	(-)				1.67
^{112}Cd	24.13	(21)	(n,2n)		0.977	(-)				1.35E-02
^{116}Sn	14.54	(9)	(n,γ)	^{117m}Sn	5.96	12	56.3	2	128	
^{117}Sn	7.68	(7)	(n,n')		95	(-)				8.42
^{118}Sn	24.22	(9)	(n,2n)		0.962	(-)				2.69E-01
^{134}Ba	2.417	(18)	(n,γ)	^{135m}Ba	53	(-)	55.8	(-)	115	
^{135}Ba	6.592	(12)	(n,n')		300	(-)				15.44
^{136}Ba	7.854	(24)	(n,2n)		1.12	(-)				6.87E-02
^{235}U	0.7204	(6)	Thermal fission	Fission	585100	(-)	0.47	(-)	59	
^{235}U	0.7204	(6)	Fast fission	Fission	1201	(-)				2.05E-03
^{238}U	99.274	(1)	Fast fission	Fission	294.5	(-)				6.94E-02

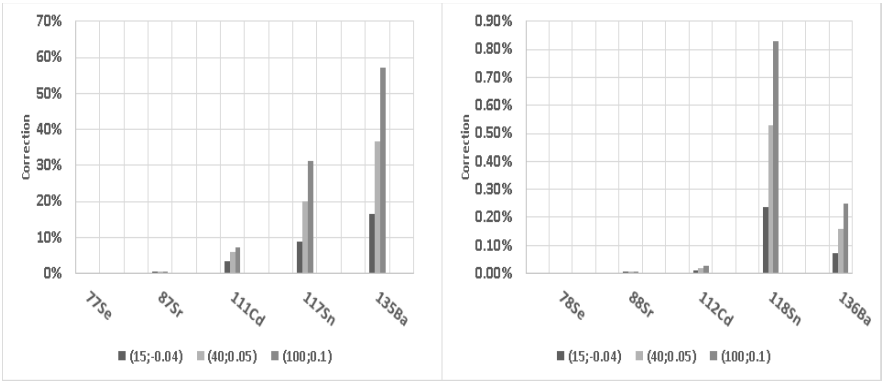

Figure 2.10: Bias (%) in a k_0 factor from its true value when neglecting the (n, n') and the (n, 2n) reaction interferences of Table 2.6 (left and right), for 3 typical irradiation channel parameters (f;α) and L = 20.

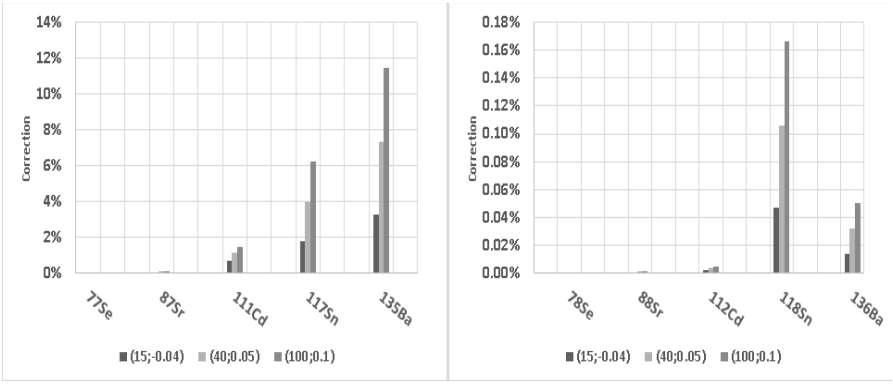

Figure 2.11: Bias (%) in a k_0 factor from its true value when neglecting the (n, n') and the (n, 2n) reaction interferences of Table 2.6 (left and right), for 3 typical irradiation channel parameters (f;α) and L = 100.

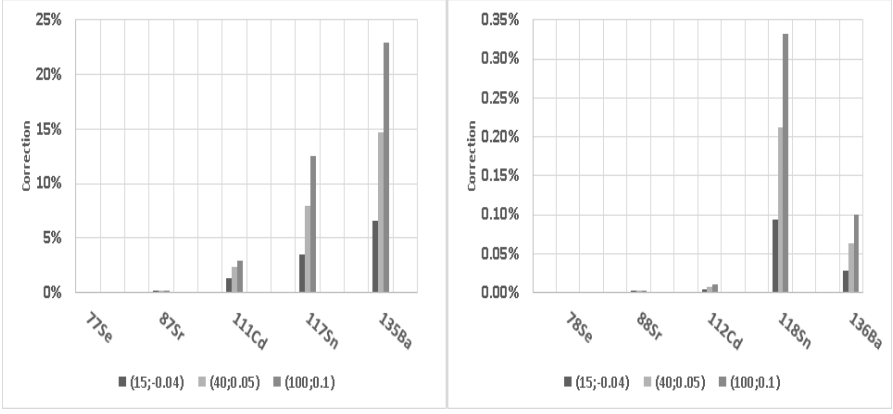

Figure 2.12: Bias (%) in a k_0 factor from its true value when neglecting the (n, n') and the (n, 2n) reaction interferences of Table 2.6 (left and right), for 3 typical irradiation channel parameters (f;α) and L = 50.

2.14 Fast contribution to the radiative neutron capture

Discarding any primary or threshold single-interference, if the averaged fast neutron (n,γ) cross-section $\sigma_{x,(n,\gamma),fast}$ for the target isotope of interest x is also known and is not negligible, setting $x=y$ in the eqs. (2.107) or (2.108) gives the full reaction rate value for the whole reactor channel neutron spectrum. For instance, in the Høgdahl convention:

$$R_{H,x} = G_{th} + G_{e,x}\left\{\frac{Q_{\alpha,x}}{f}\right\} + G_{f,x}\left\{\frac{\sigma_{x,(n,\gamma),fast}}{\sigma_{0,x}}\frac{1}{L}\right\} \qquad (2.119)$$

and in the modified Westcott formalism:

$$R_{W,x} \equiv G_{th}\left\{g_{T,x}\right\} + G_{r,x}\left\{\frac{s_{\alpha,x}}{\beta_{\alpha}}\right\} + G_{f,y}\left\{\frac{\sigma_{x,(n,\gamma),fast}}{\sigma_{0,x}}\frac{1}{L}\right\} \qquad (2.120)$$

2.15 The Activation-Decay Schemes in k_0-NAA

A large compendium of NAA formulae per activation-decay scheme is given by Pommé et al. in [122].

Each ADS compiled in the recommended k_0-literature [20, 21] was reviewed in this work in order to discard typographic errors, inconsistencies, etc. that could be present in the relevant formulae that could have been introduced during transcriptions through the years. Since there is no dedicated open source software available for computing these *f(S,D,C)* functions it was felt necessary to introduce our own series of algorithms that were to be equivalent to the existing equations, but in a notation that could result easier to code in a software from our perspective. It was felt that the amount of equations and their shape as proposed in the latest recommended references

[20, 24] could be reduced and simplified as similar functions and terms are repeated several times. The first step would consist in defining the following sets of scalars and functions:

Lamda factors

$$\begin{aligned} \lambda_i &\equiv \ln(2)/T_{1/2,i} \\ \lambda_{ij} &\equiv \lambda_i - \lambda_j \\ \lambda_{ijk} &\equiv \frac{\lambda_j \lambda_k}{\lambda_{ij} \lambda_{ik}} \end{aligned} \tag{2.121}$$

Temporal factors

$$\begin{aligned} T_i &\equiv S_i D_i C_i \\ T_{ij} &\equiv \frac{\lambda_i T_j - \lambda_j T_i}{\lambda_{ij}} \\ T_{ijk} &\equiv T_i \lambda_{ijk} \end{aligned} \tag{2.122}$$

where *S*, *D*, *C* are given in eqs. (2.5) and (2.7).

Each *i*, *j* and *k* index represents a radionuclide involved in a decay chain (e.g. if mother = *i* and daughter = *j*; $i \rightarrow j$). By employing positive integer values, we can constrain the calculation of all Lamda or Temporal factors to the condition $i = 1 < j = 2 < k = 3$. It is also possible to define Lamda or Temporal factors with more indexes but we shall see that for our library purposes it is sufficient with these three. Note that any λ or T factor with at least 2 indexes is a combination of λ_i or T_i factors and that ultimately all these factors are functions of the half-life $T_{1/2}$ of the radionuclides involved. Some

relationships when permuting indexes are observed in the previous equations:

$$\begin{aligned} \lambda_{ij} &\equiv -\lambda_{ji} \\ \lambda_{ijk} &\equiv \lambda_{ikj} \\ T_{ij} &\equiv T_{ji} \\ T_{ijk} &\equiv T_{ikj} \end{aligned} \tag{2.123}$$

and one can also note that for instance if $\lambda_i >> \lambda_j$ and $T_i = 0$ one obtains $T_{ij} = T_j$.

About the notation

We can rewrite each of the time-related ADS equations *f*(*S*,*D*,*C*) from the recommended library in [20, 21] as linear combinations of the Temporal factors of eq. (2.122). There are 7 types of ADS in the library traditionally labelled with roman numerals. Each ADS type can have a maximum of 4 possible scenarios labelled *a*, *b*, *c*, *d*. For consistency with the recommended library we will keep the letter *T* with indexes *y* = *I*, *II*, ... , *VII* and *z* = *a*, *b*, *c*, *d* for labelling each $f_{yz}(S,D,C) = T_{yz}$ function from the library and at the same time we will employ *T* with positive integers *i*, *j* and *k* as indexes for the equivalent combination of Lambda and Temporal factors defined in this work.

Additionally, the following auxiliary constants are employed:

$$\iota_{ij} \equiv \frac{I_{\gamma,i}}{I_{\gamma,j}}; \quad \eta_{ij} \equiv \frac{\sigma_{0,i}}{\sigma_{0,j}}; \quad \mathrm{O}_{ij} \equiv \eta_{ij} \frac{R_{H,i}}{R_{H,j}} \tag{2.124}$$

Note that in the modified Westcott formalism, R_H must be substituted by R_W as in eq. (2.65). The different types of ADS in reference [20] are described next.

ADS Type I

The simplest of all the ADS consists in the production of radionuclide (2) from the activation of target nuclide (1), which has a neutron-capture probability of $\sigma_{0,1}$ for thermal and of $I_{0,1}$ for epithermal neutrons.

$$1 \xrightarrow[\sigma_{0,1}, I_{0,1}]{} [2]_{\gamma_2, \lambda_2}$$

Figure 2.13: Diagram of the ADS type I

The measurement of nuclide (2) through its emitted γ_2-ray (decay constant λ_2), requires the substitution of the $T_I = f(S,D,C)_I$ parameter from the recommended library by the Temporal factor T_2:

$$T_I = T_2 = S_2 D_2 C_2 \tag{2.125}$$

ADS Type II

The ADS type II corresponds to the activation of nuclide (1) and the direct production of a mother radionuclide (2). The mother nuclide decays with decay constant λ_2 and fraction F_2 into the daughter radionuclide (3). The radionuclide (3) is then monitored through the γ_3-ray emitted during its decay (decay constant λ_3).

$$1 \xrightarrow[\sigma_{0,1}, I_{0,1}]{} 2 \xrightarrow{F_2, \lambda_2} [3]_{\gamma_3, \lambda_3}$$

Figure 2.14: Diagram of the ADS type II

The measurement of (3) can be done according to these scenarios:

a) while the mother nuclide (2) is present. In this case the change of notation implies:

$$T_{IIa} = T_{23} = \frac{\lambda_2 T_3 - \lambda_3 T_2}{\lambda_{23}} = \frac{\lambda_2 T_3 - \lambda_3 T_2}{\lambda_2 - \lambda_3} \tag{2.126}$$

b) when $\lambda_2 >> \lambda_3$ and the mother nuclide has decayed ($T_2 = 0$):

$$T_{IIb} = T_3 \tag{2.127}$$

c) when it is in transient equilibrium with the mother nuclide ($\lambda_2 < \lambda_3$; $T_3 = 0$):

$$T_{IIc} = \left(\lambda_3 / \lambda_{32}\right) T_2 \tag{2.128}$$

d) similar to a) but the mother nuclide also emits a γ_2-ray that interferes with the γ_3-ray:

$$T_{IId} = T_{23} + \left(\frac{\iota_{23}}{F_2}\right) T_2 \tag{2.129}$$

It was observed that none of the radionuclides tabulated in the recommended library [20, 21, 23] requires the ADS type II/c.

ADS Type III

The ADS type III corresponds to the activation of (1) and the direct production of the radionuclide (2). The radionuclide (2) has a probability F_{24} of decaying into the measured radionuclide (4) as well as a F_2 probability of decaying into (a proxy) radionuclide (3). The decay of (3) contributes with branching factor F_3 and decay constant λ_3 to the formation of the measured radionuclide (4).

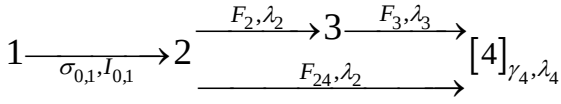

Figure 2.15: Diagram of the ADS type III

The measurement of a γ_4-ray emitted by (4) (decay constant λ_4) is performed under the following scenarios:

a) while radionuclides (2) and (3) are present. In this case:

$$T_{IIIa} = \left(\frac{F_{24}}{F_2 F_3}\right) T_{24} + \{T_{234} + T_{324} + T_{423}\} \tag{2.130}$$

b) a special case of scenario a) with $F_{24} = 0$:

$$T_{IIIb} = T_{234} + T_{324} + T_{423} \tag{2.131}$$

c) while nuclide (2) is present but nuclide (3) has decayed ($T_3 = 0$), $\lambda_3 >> \lambda_2$ and λ_4. With $F_3 = 1$ and $F_2 + F_{24} = 1$, one has:

$$T_{IIIc} = T_{24} \tag{2.132}$$

ADS Type IV

This ADS corresponds to the activation of target nuclide (1) and the direct production of a radionuclide in two possible energy states: metastable (m or 2) and ground (g or 3), with probabilities $\sigma_{0,2}$ and $\sigma_{0,3}$ for thermal and $I_{0,2}$ and $I_{0,3}$ for epithermal neutrons (respectively). The metastable state (2) decays with probability F_2 and decay constant λ_2) into the ground state (3) which is monitored through its emitted γ_3-ray.

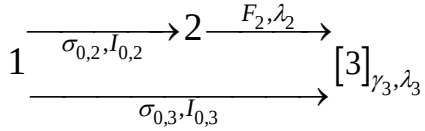

Figure 2.16: Diagram of the ADS type IV

The measurement of radionuclide (3) (decay constant λ_3) is performed under the following scenarios:

a) while the isomer is present, in which case T is replaced by:

$$T_{IVa} = F_2 T_{23} O_{23} + T_3 \tag{2.133}$$

b) after the isomer has decayed ($T_2 = 0$) and $\lambda_2 >> \lambda_3$, leading to:

$$T_{IVb} = T_3 \tag{2.134}$$

c) when it is in transient equilibrium with the isomer ($\lambda_2 < \lambda_3$; $T_3 = 0$):

$$T_{IVc} = \left(\lambda_3 / \lambda_{32}\right) T_2 \tag{2.135}$$

d) in the case the isomer emits a γ_2-ray of roughly the same energy as the γ_3-ray emitted by the ground state:

$$T_{IVd} = \{\iota_{23} T_2 + F_2 T_{23}\} O_{23} + T_3 \tag{2.136}$$

According to the official literature [20, 21], none of the tabulated radionuclides are quoted under the ADS type IV/c.

ADS Type V

This ADS corresponds to the activation of target nuclide (1) and the direct production of a radionuclide in two (energy) states: metastable (m or 2) and ground (g or 3) with radiative capture probabilities $\sigma_{0,2}$ and $\sigma_{0,3}$ for thermal neutrons and $I_{0,2}$ and $I_{0,3}$ for epithermal neutrons. The isomer (2) decays with probability F_2 into the ground state (3), which in turn decays with probability F_3 to a measured radionuclide (4) that emits a γ_4-ray.

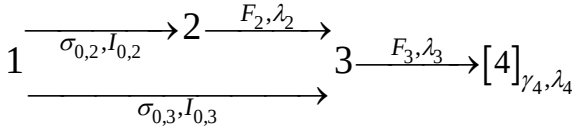

Figure 2.17: Diagram of the ADS type V

The measurement of the radionuclide (4) is performed under the following scenarios:

a) while the isomer (2) and the ground state (3) are populated:

$$T_{Va} = F_2 \{T_{234} + T_{324} + T_{423}\} O_{23} + T_{34} \tag{2.137}$$

b) after the isomer and ground states have decayed ($T_2 = T_3 = 0$), with $\lambda_4 << \lambda_2$ and λ_3, leading to:

$$T_{Vb} = T_4 \tag{2.138}$$

c) in the case the isomer has decayed ($T_2 = 0$) and $\lambda_3 << \lambda_2$ and $\lambda_3 << \lambda_4$ in which case one needs to employ:

$$T_{Vc} = T_3 \tag{2.139}$$

d) after the isomer has decayed ($T_2 = 0$) and $\lambda_3 < \lambda_2$, leading to:

$$T_{Vd} = T_{34} \tag{2.140}$$

ADS Type VI

Under this ADS the production of a measured radionuclide (4) is achieved by a three-fold activation of the target nuclide (1) leading to:

- the mother radionuclides (2) (or isomer m2) and (3) (or isomer m1) that can decay with branching probabilities F_{24} and F_3 (respectively) directly into the radionuclide (4). A fraction F_2F_3 of radionuclide (2) also contributes to the formation of radionuclide (4) via the proxy radionuclide (3);

- the direct formation of nuclide (4) (or ground state).

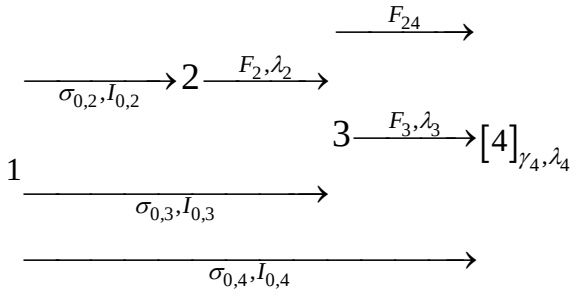

Figure 2.18: Diagram of the ADS type VI

With the ADS type VI defined in this way we have the following scenarios for measurement of radionuclide (4):

a) while nuclides (2) and (3) are present, in which case one needs to employ:

$$T_{VIa} = \left\{F_{24}T_{24} + F_2F_3\left\{T_{234} + T_{324} + T_{423}\right\}\right\}O_{24} + F_3T_{34}O_{34} + T_4 \quad (2.141)$$

b) after nuclides (2) and (3) have completely decayed ($T_2 = T_3 = 0$) and $\lambda_4 < \lambda_2$ and λ_3. In this case one can employ:

$$T_{VIb} = T_4 \quad (2.142)$$

c) a special case of the *b*-scenario with $F_{24} = 0$, for which we would obtain:

$$T_{VIc} = T_4 \quad (2.143)$$

This third scenario, described in this work as VI/c is the only one proposed in the current k_0-literature under the label "ADS type VI" [20, 21].

The production of ^{131}I from the fission of ^{235}U and from the decay of its mother nuclide ^{131}Te (or its isomer ^{131m}Te; both also fission products) has not been dealt properly in the k_0 recommended literature according to the ADS type VI definition provided in references [20, 21, 54]. The scenario VI proposed in these references (equivalent to VI/c here) is valid for instance in the analysis of the (n,γ) reaction on the target ^{123}Sb and the measurement of ^{124}Sb, but it is not valid for the monitoring of ^{131}I since it is known that for this radionuclide $F_{24} \neq 0$ from the (n,γ) production data compiled in the same references and/or from an independent reference such as [6].

It must be also noted that the k_0 and Q_0 definitions for this ADS reported in the references [20, 21] have a typographic error: F_2 is missing in the k_0 definition and appears to be multiplying the "m1" (3) physical quantities in both the k_0 and Q_0 definitions, instead of multiplying the "m2" (2) quantities as expected. This does not mean that the experimental k_0-fission factors for ^{131}I in the recommended literature are necessarily biased, it is the relationship with the absolute nuclear constants provided in these references which is not correct.

ADS Type VII

It corresponds to the activation of a target nuclide (1) and the formation of both the metastable (2) and ground (3) states of the corresponding radioisotope. Both states will further decay with branching factors F_{24} and F_3 (respectively) into the same daughter nuclide (4), which is then measured. The probability F_2 corresponds to that of an Internal Transformation (I.T.) from the metastable to the ground state.

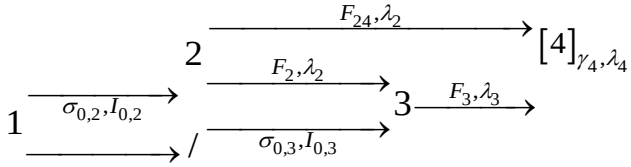

Figure 2.19: Diagram of the ADS type VII

The measurement of nuclide (4) can be performed under the following scenarios:

a) while nuclides (2) and (3) are present, for which it would be necessary to replace T by:

$$T_{VIIa} = \left[\left\{F_{24}/F_3\right\}T_{24} + F_2\left\{T_{234} + T_{324} + T_{423}\right\}\right]\mathrm{O}_{23} + T_{34} \quad (2.144)$$

b) while nuclides (2) and (3) are present but there is no I.T. from the metastable to the ground state ($F_2 = 0$). In which case eq. (2.144) is simplified into:

$$T_{VIIb} = \left\{F_{24}/F_3\right\}T_{24}\mathrm{O}_{23} + T_{34} \quad (2.145)$$

c) when $\lambda_4 << \lambda_2, \lambda_3$ and nuclides (2) and (3) have completely decayed ($T_2 = T_3 = 0$):

$$T_{VIIc} = T_4 \tag{2.146}$$

The only studied case satisfying scenario "c" corresponds to the monitoring of ^{111}Ag from the decay of its parent nuclides: ^{111m}Pd and ^{111}Pd, which are produced by neutron bombardment on ^{110}Pd. The conditions for the scenario VII/c are satisfied just after ≥ 0.6 times the ^{111}Ag half-life (see nuclear data compilations for half-lives). For this particular case we have F_{24} = 0.27, F_2 = 0.73 and F_3 = 1 [6] while the η_{ij} value, as defined in eq. (2.124), can be calculated from cross-section data in [1, 2, 6]or, after the k_0 and Q_0 factors for ^{111m}Pd and ^{111}Ag are experimentally found, as in this work.

2.16 Reactor channel calibration

In NAA with nuclear reactors the characterization of the neutron spectrum of a given channel is usually performed by the co-irradiation of "flux monitors" (standards), with well-known nuclear data and a given set of nuclear properties that comprises the neutron energy-range of analytical interest [108, 123, 124].

It was shown by De Corte et al. [123] that knowledge of the conventional thermal and epithermal neutron fluence rates can be obtained with good precision and accuracy by replacing most of the absolute nuclear data by experimentally-determined k_0 and Q_0 factors with ≤ 2% and ≤ 10% relative uncertainty (respectively) [20].

Making use of three multi-isotopic methods involving bare and cadmium (Cd) covered irradiations, the k_0-standardization of NAA provides a way to characterize the neutron spectrum (thermal and epithermal parts) through the f and α parameters. Basically, these three methods consist in plotting an expression of the form [13, 123]:

$$\ln\left[B_j \left(\bar{E}_r\right)^{-\alpha} \left(1\text{eV}\right)^{\alpha} \right] \text{ vs. } \ln\left[\bar{E}_r\right] \tag{2.147}$$

where the B_j term is itself a function of α, the saturated γ-ray activity A_j, the corresponding $k_{0,j}$ and $Q_{0,j}$ composite nuclear constants and the effective resonance energy $\bar{E}_{r,j}$ (in eV) of the radioisotope j in the set of N calibration isotopes. The slope of the resulting linear fit (equal to $-\alpha$) is used in an iterative process until no more significant variation is observed.

2.16.1 The Cd-covered method

The activation of flux monitors inside a 1 mm thick Cd-cover will be only due to epithermal capture of neutrons. If all the monitors have a $1/v$ dependence of the thermal cross-section for up to 1.5 eV neutron energy, the shape of B_j is given by:

$$B_j \equiv \left(\frac{A_{Cd,\text{obs}}}{k_{0,c} F_{Cd} G_e Q_\alpha} \right)_j \tag{2.148}$$

when setting $\varphi_{th} = 0$ in eq. (2.49).

Similarly, in the modified Westcott formalism [48]:

$$B_{W,j} \equiv \left(\frac{A_{Cd,\text{obs}}}{k_{0,c} F_{Cd} \left\{ G_r s_\alpha - g_T \left(W'_\alpha + C_\alpha \right) \right\}} \right)_j \tag{2.149}$$

with s_α defined as in eq. (2.69).

2.16.2 The Cd-Ratio method

This method is intended when the reactor neutron fluence rate characteristics are known to be sufficiently stable as a function of time. In this case B_j is

just inversely proportional to the thermal-to-epithermal conventional fluence rate ratio f as seen by the j-monitor:

$$B_j \equiv \left(\frac{G_{th}}{G_e} \frac{1}{\{Q_\alpha r_{Cd}\}} \right)_j \equiv \frac{1}{f_j} \tag{2.150}$$

Similarly, one can write in the modified Westcott formalism for a given channel [48]:

$$B_{W,j} \equiv \left(\frac{G_{th}}{G_r \{r_{Cd} s_\alpha / g_T\} - z_{Cd} \{W'_\alpha + C_\alpha\}} \right)_j \equiv \frac{1}{\beta_{\alpha,j}} \tag{2.151}$$

with β_α defined as in eq. (2.68). Both channel-specific constants can be determined experimentally from eqs. (2.150) and (2.151) written for e.g. the comparator.

2.16.3 The Bare method

By combining ratios from a subset of epithermal fluence rate monitors (monitors activated mostly by epithermal neutrons; high Q_0 factor) versus a "reference" thermal fluence rate monitor (low Q_0 factor), f and α can be obtained without the need of a Cd-covered irradiation. In the Bare method, the B_j term is a function of the chosen "reference" monitor as well:

$$B_j \equiv \frac{\left(\frac{A}{k_{0,c}} \right)_j - \left(\frac{A}{k_{0,c}} \right)_{\text{ref}}}{\left(\frac{G_e}{G_{th}} Q_\alpha \right)_j - \left(\frac{G_e}{G_{th}} Q_\alpha \right)_{\text{ref}}} \tag{2.152}$$

Similarly, in the modified Westcott formalism [48]:

$$B_{W,j} = \frac{\left(\frac{k_{0,c,\mathrm{ref}}}{k_{0,c,j}}\right)\left(G_{th}g_T\right)_{\mathrm{ref}} - \left(\frac{A_{\mathrm{ref}}}{A_j}\right)\left(G_{th}g_T\right)_j}{\left(\frac{A_{\mathrm{ref}}}{A_j}\right)\left(G_r s_\alpha\right)_j - \left(\frac{k_{0,c,\mathrm{ref}}}{k_{0,c,j}}\right)\left(G_r s_\alpha\right)_{\mathrm{ref}}} \tag{2.153}$$

2.16.4 About the choice of (*f*, *α*)-determination method

The choice of a given *(f, α)*-determination method and the number of monitors to irradiate depends on the channel characteristics, aimed accuracy and precision. If *f* and *α* are stable in time, then the Cd-Ratio method is recommended since it is expected to give lower uncertainties than the Bare method [123]. In fact, uncertainty propagation of the relevant formulae reveals that the overall uncertainty for a given method and channel is dependent on sensitivity coefficients (see Chapter 7) as e.g. $c_\alpha(A_j)$, that accounts for the uncertainty contribution of the saturated γ-ray activity into the *α* uncertainty [13, 123]:

$$c_\alpha\left(A_j\right)_{\text{Cd-Covered}} \propto \frac{1}{|\alpha|} \tag{2.154}$$

$$c_\alpha\left(A_j\right)_{\text{Cd-Ratio}} \propto c_\alpha\left(A_j\right)_{\text{Cd-Covered}} R_{H,j} \tag{2.155}$$

$$c_\alpha\left(A_j\right)_{\text{Bare}} \propto c_\alpha\left(A_j\right)_{\text{Cd-Ratio}} f \tag{2.156}$$

Indistinctly from the chosen method, a channel with $\alpha \approx 0$ bears an intolerable uncertainty in this value, for all of them assume $\alpha \neq 0$.

Although in the Cd-Ratio method most of the uncertainty contributions in the saturated γ-ray activities cancel by taking ratios, relation (2.155) shows that a high uncertainty on *α* is to be expected for low *f* and high Q_α factors [123]. However, this method is superior in precision to the Bare method as

shown by eq. (2.156), but suffers more from fluctuations in the reactor neutron spectrum.

In the Bare method, the uncertainty propagation factors for the "reference" isotope must be included as well, aggravating the overall uncertainty. An optimization of the Bare method can be achieved by irradiating a large set monitors with low, middle and high Q_0 factors, alternating the reference isotope in each (f, α)-determination. Due to a singularity in the B_j term for $Q_{\alpha,j} \approx Q_{\alpha,ref}$ the number of possible combinations for a given set is inherently reduced, for the chosen "reference" monitor must be so that no other isotope from the set has a comparable Q_0 factor. This method is more suited for "reference" monitors having a low Q_0 factor (thermal monitors) with all other monitors having much higher ones (epithermal monitors), since this combination differentiates better the thermal and epithermal contributions to the total reaction rate [123].

For these methods to be accurate, f and α should remain constant during irradiation and the samples must be irradiated in the same irradiation positions [13, 123]. In fact, if no computational or experimental method is applied to account for the impact of the irradiation containers and for the shape and chemical composition of the monitors, the resulting f and α will remain linked to the monitor's conditions of their determination. This illustrates the importance of avoiding excessively massive vials/containers or spacers to position the monitors inside the channel and of using sufficiently diluted monitors to prevent thermal and epithermal neutron self-shielding [13, 123].

3. Detection of γ and X-rays

The γ-rays are electromagnetic waves, i.e. discrete wave-packets or "photons" of energy $E_\gamma = h\upsilon$ (with h the Planck's constant; in $m^2 \cdot kg.s^{-1}$) [125–127], each one having a wave-frequency υ (in s^{-1} or Hz) that is typically higher than 10^{19} Hz [128] although in this work we dealt with photons with energies ≥ 58 keV. By means of the relation $v = \upsilon\lambda$ where v is the velocity of the wave (the light speed in air) this corresponds to wave-lengths λ (in m) of less than 10 pm, which are smaller than the diameter of an atom. Some radionuclides of interest in NAA also emit X-rays, which have a wavelength in the range of 0.01 to 10 nm [128], corresponding to frequencies in the range of 3×10^{16} to 3×10^{19} Hz or, energies in the range of 100 eV to 100 keV. Thus, the X-rays are usually less energetic than γ-rays although their distinction is not based on their energy but mainly because X-rays are caused by electron energy transfer, while γ-rays are caused by the atomic nucleus energy transfer [129].

3.1 Interaction of the X and γ-rays with matter

There are three main interaction mechanisms between radiation and matter:

3.1.1 The photoelectric effect

The photoelectric effect (see Figure 3.1) allows for the full absorption of the incoming photon by a bound (atom) electron inside the detector crystal, resulting in the electron being ejected from the material at a kinetic energy $T = E_\gamma - W$ where W is the minimum energy necessary to remove the electron from the crystal (binding energy of the electron; material dependent) [127]. Full absorption is also possible when a series of these interaction mechanisms take place within the detector volume. On the other hand, when a γ-ray undergoes a Compton interaction [130, 131] or an electron-positron pair-production [132], a portion of the energy of the photon escapes from the detector active volume without being absorbed, while only the residual energy from these interactions is inevitably processed (Background or noise signal).

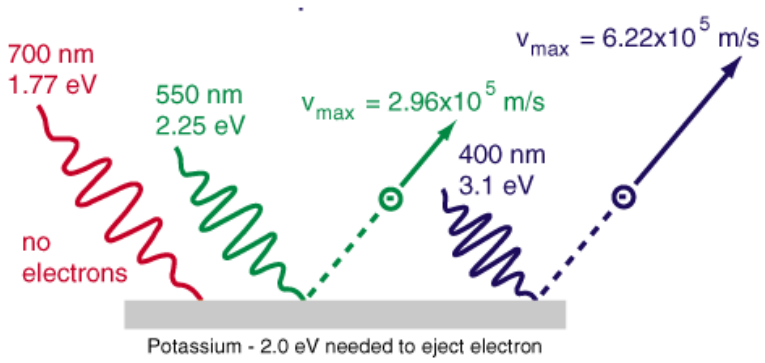

Figure 3.1: Diagram of the photoelectric effect on a pure K sheet of material [133]**.**

3.1.2 Compton scattering

In a Compton scattering process (see Figure 3.2), the photon collides with a bound (atom) electron and the amount of energy exchanged varies with angle of deflection θ. The final photon energy (E'_γ) is:

$$E'_\gamma = \frac{E_\gamma}{1+\frac{(1-\cos\theta)E_\gamma}{m_e c^2}} \tag{3.1}$$

where m_e is the mass of the electron and c is the speed of light [130].

For cos(θ = 180) the maximum amount of energy is transferred into the material:

$$\left(E_\gamma - E'\right)_\gamma\Big|_{\max} = \frac{2E_\gamma^2}{2E_\gamma + m_e c^2} \tag{3.2}$$

hence a sharp cut-off at this energy is statistically observed when measuring e.g. a high-yield mono-energetic photon for enough time.

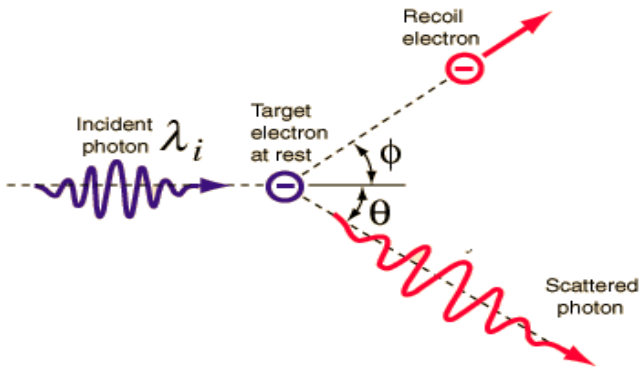

Figure 3.2: Diagram of the Compton scattering interaction [134].

3.1.3 Pair production and annihilation

A γ-ray pair-production is a photon-nucleus interaction that can only occur if the photon has an energy exceeding twice the rest energy of an electron ($m_e c^2$ = 0.511 MeV; E_γ = 1.022 MeV), since an electron and a positron (the electron's antiparticle) are simultaneously created out of the photon's energy. By momentum conservation the particles would have opposite traveling directions and one particle might escape the active volume without detection. The positron soon encounters matter around it and it is eventually stopped by an electron in an annihilation process that results in the production of two photons of 0.511 MeV each (see Figure 3.3). Therefore, one always observes an energy distribution around 511 keV, 1022 keV and, at single and double escape peaks when measuring a sample, either because of a sample high-energy γ-rays or because of background radiation.

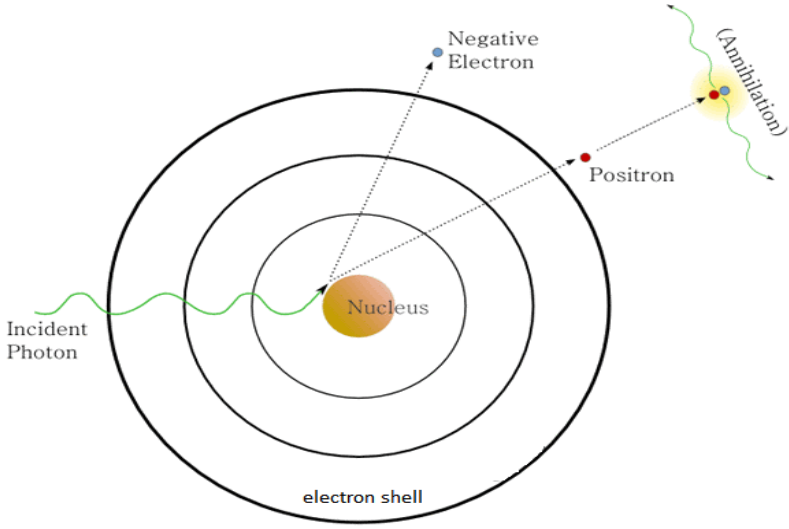

Figure 3.3: Diagram of the pair-production and annihilation process [135].

3.2 Spectrometry

In eq. (2.11) the detection efficiency for a γ-ray of a given energy (ε_γ) was introduced to account for the fact that in practice not all γ-rays emitted by the sample during the measurement process would be fully detected and/or processed by the measurement system. If 100 γ-rays are emitted by the sample and only one is detected, one would say that the "relative" detection efficiency for that γ-ray is 1%.

While a sample is viewed as an isotropic γ-rays source, a detector typically employed in NAA is basically a cylindrical crystal (a γ-ray absorber) separated at a given distance from the source, therefore only the γ-rays that are emitted within an "effective" solid angle between the sample and the detector surface will interact with it (see Figure 3.4). Even if a perfectly spherical detector surrounds the source, the detection efficiency is still inherently correlated to the crystal material properties and quality of the detector assembly, as well as to the readiness and accuracy of the attached electronics, which are responsible of the overall signal processing. Additionally, from these 3 radiation-matter interaction mechanisms in nature, two are inevitably responsible for losses of detectable γ-rays.

In the case of semi-conductor detectors, as with the High Purity Germanium HPGe employed in this work, the initial chain of photoelectric and Compton scattered electrons are rapidly captured by a higher voltage difference applied through electrodes that are attached to the crystal itself. Since these electrodes will also capture thermionic electrons [136], cryogenic refrigeration of the semi-conductor crystal is required, while in the case of scintillator detectors this is not necessary.

The signal pulse produced by the detector (or by the photomultiplier in a scintillation detector) is shaped by the pre-amplifier before it enters a multichannel analyser (MCA). The MCA takes the small signal produced by

the detector and reshapes it into a Gaussian or trapezoidal shape (a pulse), to convert the signal into a digital one by means of an Analog-to-Digital Converter (ADC). In some systems, the ADC conversion is performed before the signal is reshaped. The MCA also sorts the pulses by their height, having specific numbers of "bins" into which the pulses can be sorted; these bins represent the channels in the spectrum. The choice of number of channels depends on the resolution of the system and the energy range being studied. The MCA output is sent to a computer, which stores and displays the data. Thus, the screen display of the number of counts vs. channel number is a histogram of the number of counts versus the pulse height, i.e. a pulse-height spectrum. The range of pulse heights to be analysed can be set via upper and lower level discriminators at the input. A variety of software packages are available from each detector manufacturer. These typically include γ-ray spectrometry analysis tools such as energy and efficiency calibration, peak area calculation and resolution analysis.

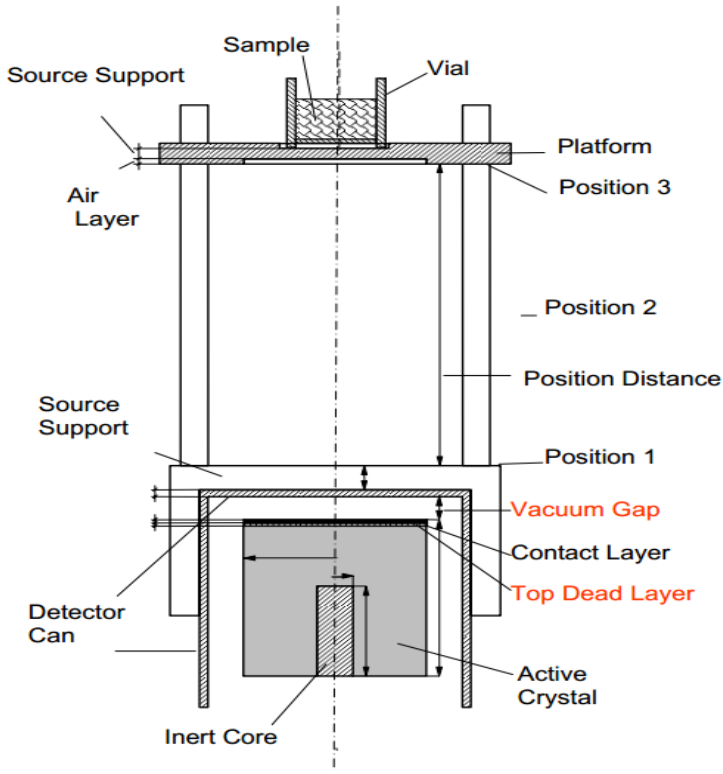

Figure 3.4: Diagram of some constituent parts of the measurement setup: detector active crystal, cavity core, top dead and contact layers, sample, sample platform and holder.

The energy calibration is performed by mapping the MCA channels (*Ch*) corresponding to the centroids of the observed histogram peaks arising from the measurement of known multi-γ sources (see Figure 3.5). A quadratic polynomial or a linear function is then adjusted on the resulting E_γ vs. Ch plot:

$$E_\gamma = b_0 (Ch)^2 + b_1 (Ch) + b_2 \tag{3.3}$$

with b_0, b_1 and b_2 (in keV) as the parameters of the fit.

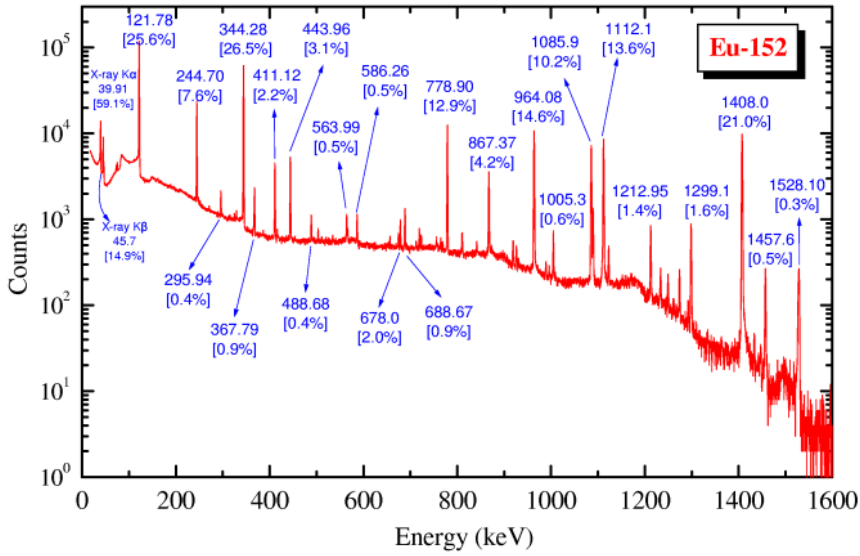

Figure 3.5: A γ-ray spectrum of ^{152}Eu [137]**. The pulses generated from the detection of γ-rays are distributed in channels (bins) per the pulse-height (voltage), i.e. a pulse-height spectrum. A conversion from channels to γ-ray energy is performed by mapping the channels in the centroids of the histogram peaks to the known energies of a measured multi-γ source (as ^{152}Eu).**

The eq. (3.3) is not just detector-specific, it also depends on the source-detector separation, since at closer geometries some undesired effects such as X and γ-ray cascade coincidence, pile-up of detected pulses and detector dead-time can alter fundamentally the shape (i.e. the width) of the expected histogram peaks. An accurate determination of the centroid of the histogram peak (its expected value) and its uncertainty requires finding the full width at half-maximum amplitude (FWHM) of the adjusted density function of the peak (e.g. a Gaussian; see Figure 3.6). This task is nowadays performed by spectrometry software that employs iterative procedures for achieving the histogram peak deconvolution, but the success of the algorithms relies on the

accurate determination of the peaks tails, skewness and kurtosis, which is not always guaranteed at close-in geometries.

Once a polynomial fit on a FWHM vs. *Ch* plot is obtained, by e.g. measuring the FWHM values of the adjusted Gaussians on a known multi-γ source spectrum, then one can proceed with the energy calibration proposed in eq. (3.3). The FWHM calibration curve is usually expressed as a function of E_γ:

$$FWHM = a_1 \cdot E_\gamma^{1/2} + a_2 \tag{3.4}$$

with a_1 and a_2 the parameters of the fit.

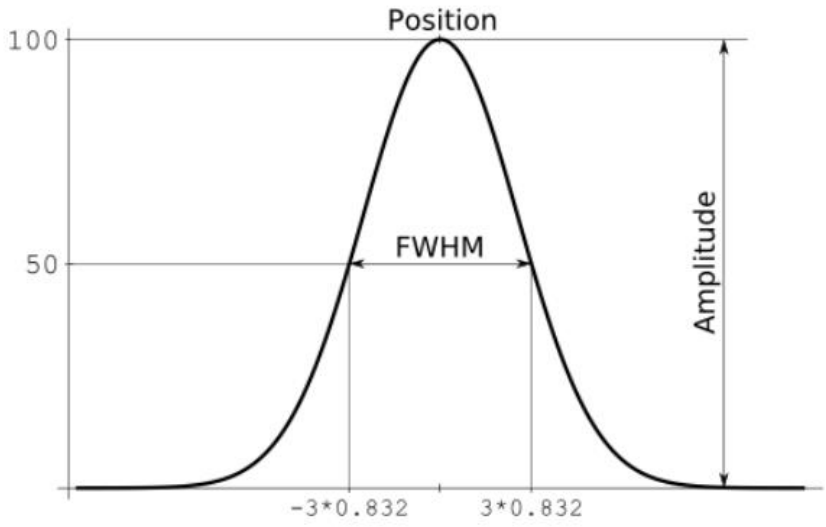

Figure 3.6: Diagram of the FWHM: the full width of a Gaussian curve at half its maximum amplitude at the curve centroid.

3.3 Histogram peak deconvolution

For the deconvolutions of the histogram peaks one can make use of open-source or commercial software packages. In this work we employed the state-of-the-art commercial software package HyperLab version 2009 from HyperLabs Software (Hungary) [138]. The Figure 3.7 shows the main window of this software spectrum peak evaluator (1). The residuals window (2) displays the difference between the experimental values and the fitted peak curves.

The red triangles mark the positions of the suspected photo-peaks (their centroids) based on the intensity-background ratios, the Energy calibration and FWHM calibration. The deconvolution employs the FWHM calibration to find an initial estimate of the photopeak width, with a default tolerance of ± 30%.

The actual deconvolution process can be initiated by drawing a horizontal line from left to right over the suspected peak regions (see Figure 3.8), having care in specifying a sufficiently wide background margin that must be peak-free for the different peak-fitting algorithms to work properly. The functions are described in the next sections.

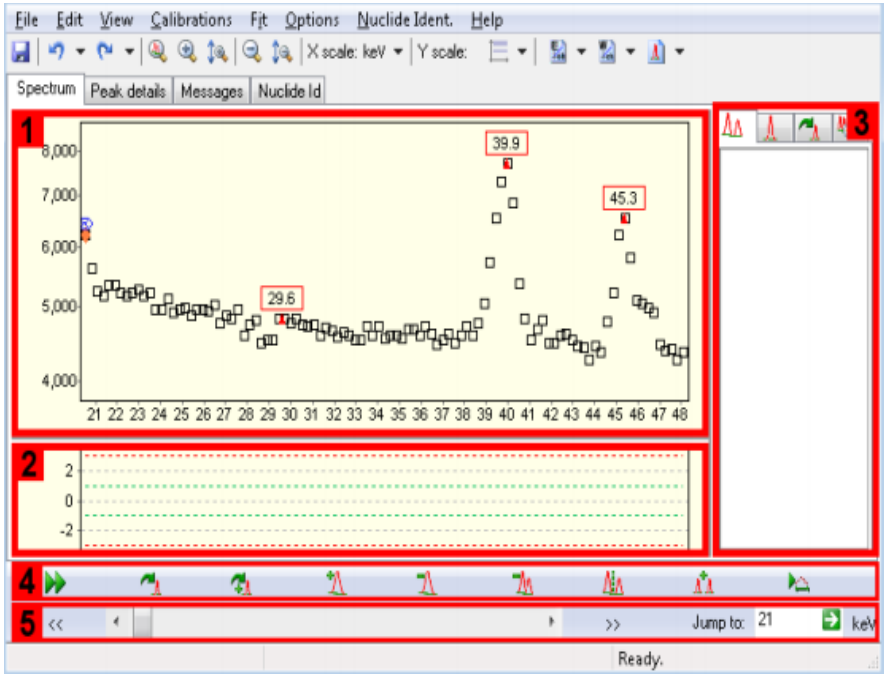

Figure 3.7 The HyperLab (version 2009) spectrometry software main window for histogram peak deconvolutions [138]**. Spectrum (1) and the residuals window (2); Spectrum regions list (3); Peak-evaluator fine tuning toolbar (4); Spectrum navigation toolbar (5).**

3.3.1 Gaussian peak fit functions

The following function describes a Gaussian function of arbitrary real constants a, x_c and Δ employed by HyperLab [139]:

$$F(x) = ae^{-\frac{(x-x_c)}{\Delta}} \tag{3.5}$$

where x corresponds to the channel, x_c the peak centroid, a the Gaussian amplitude and Δ is the peak-width parameter such that FWHM = $2\Delta(\text{Log}(2))^{½}$. See for instance the Figure 3.6.

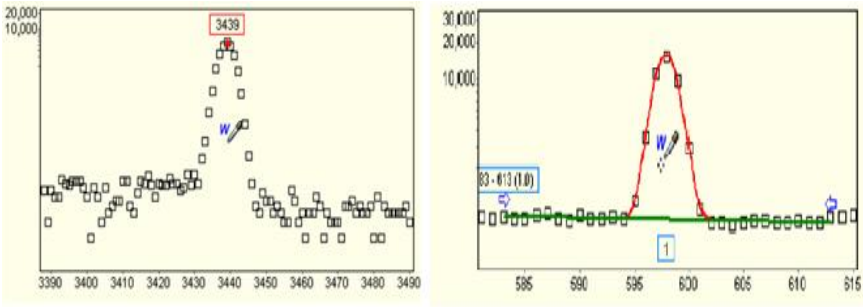

Figure 3.8 The histogram peak deconvolution process in HyperLab is performed by drawing a horizontal line from left to right over the suspected peak region, specifying a sufficiently wide background margin that is peak-free. The Gaussian peak-fitting equations applied by this software are given by eqs. (3.5) to (3.10).

Since in practice incomplete charge collection in the detector crystal and pile-up effects alter the shape at the left and right of the Gaussian function (see Figure 3.9) the HyperLab software applies 2 additional functions to perform a more realistic deconvolution. For the Left skew (S_L) Gaussian function of Figure 3.9 [139], one has:

$$S_{L,x} = a\frac{\sqrt{\pi}}{2}S_{LA}\left[e^{\left(\frac{\Delta}{2S_{LS}}\right)^2+\frac{(x-x_c)}{S_{LS}}}\right]ercf\left(\frac{\Delta}{2S_{LS}}+\frac{(x-x_c)}{\Delta}\right)\Delta \quad (3.6)$$

and for the Right skew Gaussian function, the number of counts at channel x (S_R) is:

$$S_{R,x} = a\frac{\sqrt{\pi}}{2}S_{RA}\left[e^{\left(\frac{\Delta}{2S_{RS}}\right)^2-\frac{(x-x_c)}{S_{RS}}}\right]ercf\left(\frac{\Delta}{2S_{RS}}-\frac{(x-x_c)}{\Delta}\right)\Delta \quad (3.7)$$

where S_{LA} and S_{RA} correspond to the Left and Right skew amplitudes (from 0 to 0.75), S_{LS} and S_{RS} are the Left and Right skew slopes (from 0.3 to 2) and *ercf* is the standard complimentary error function.

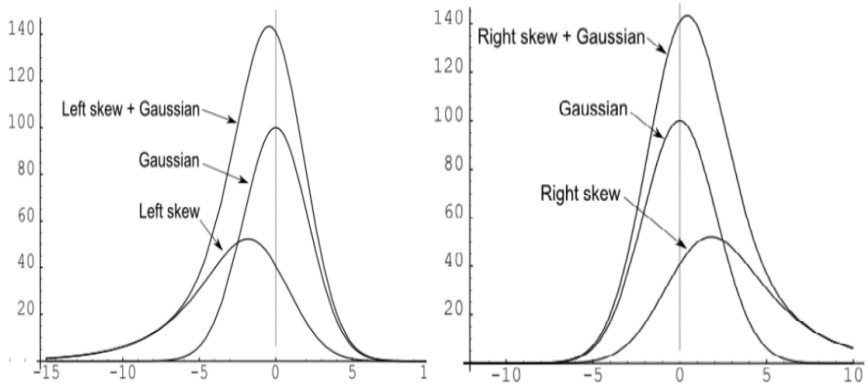

Figure 3.9 Left and Right skew functions employed by HyperLab for a realistic histogram peak deconvolution due to an incomplete charge (or collection in the detector crystal (left) and pile-up effects (right) [139]**.**

3.3.2 Background fit functions

In order to characterize a continuous and slowly changing curved (or parabolic) background under the peaks, HyperLab implements a 2nd order polynomial to determine the number of background counts (B_p) at the channel position x_p within the fitted region [139]:

$$B_p = l + sx_p + cx_p^2 \tag{3.8}$$

where l is the constant background level (positive only), s is the background slope and c is the background curvature (see Figure 3.10). The 1st channel of the region is x_1=0.

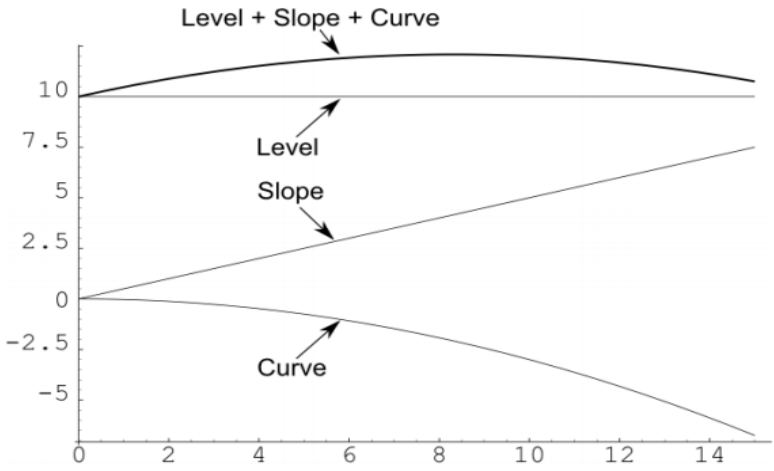

Figure 3.10 Modelling of a continuous and slowly changing background by HyperLab as a function of 3 terms: a level (*l*=10), a slope (*s*=0.5) and a curve (*c*=-0.03) as in eq. (3.8) [139]**.**

In the case that a sharp background step is observed under a peak (e.g. a Compton edge; see Figure 3.11) the program offers the following function to calculate the step counts (B_S) at channel x in terms of the background step amplitude relative to that of the Gaussian (B_{SA}) [139]:

$$B_{S,x} = a\frac{\sqrt{\pi}}{2} B_{SA} ercf\left(\frac{x}{\Delta}\right)\Delta \tag{3.9}$$

On the other hand, a slowly decreasing exponential background (or tail component) can be assumed under the low energy side of the peak, as in eq. (3.6), to compensate for some detector surface effects [139]. The number of tail component counts (B_T) at channel x is found from:

$$B_{T,x} = a\frac{\sqrt{\pi}}{2} B_{TA}\left[e^{b^2+\frac{(x-x_c)}{B_{TS}}}\right] ercf\left(b+\frac{(x-x_c)}{\Delta}\right)\Delta \tag{3.10}$$

where B_{TA} is the background tail amplitude relative to that of the Gaussian (from 0 to 0.01) and:

$$b \equiv \frac{\Delta}{2B_{TS}} \tag{3.11}$$

with B_{TS} is the background tail slope (see Figure 3.11).

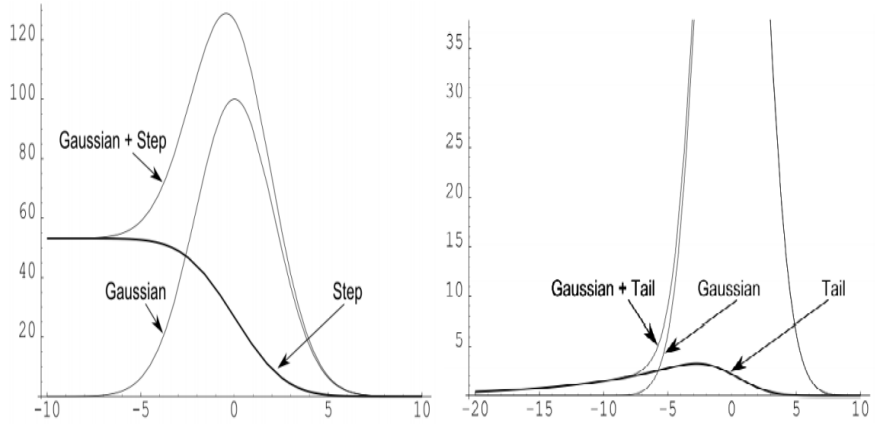

Figure 3.11 Step (left) and tail (right) background functions of channel position modelled by the HyperLab peak evaluator by means of eqs. (3.9) and (3.10) [139]**.**

Because of to the statistical nature of the measurement process the standard Chi-squared value (χ^2) is employed to show the significance of the difference between the experimental and fitted counts. The χ^2 considers the statistical variance of each measured count value instead of the absolute value alone:

$$\chi^2 = \sum_{x=1}^{n} \frac{\left(N_x - Y_x\right)^2}{\sigma_x^{\,2}} \tag{3.12}$$

where N is the number of counts, Y the sum of peak and background functions and σ^2 is the variance in N at the (region) channel x. The integer n is the number of channels in the region.

The Figure 3.12 and Figure 3.13 shows that $\chi^2 = 1$ limit is designated by a green dashed line, while a red dashed line shows the $\chi^2 = 3$ limit. As a rule of thumb, if the absolute value of the difference is greater than 3, closer inspection is needed near that channel. A normalized χ^2 value is also computed for a whole region from the sum of all the χ^2 values (*RXSQ*; see Figure 3.16).

The Figure 3.12 to Figure 3.15 show 4 cases where a region deconvolution results in χ^2 values outside of the expected range, indicating (respectively) the need for: 1) a region split; 2) a multiplet introduction instead of a singlet; 3) a resizing of the background margins and 4) variable width Gaussian fits.

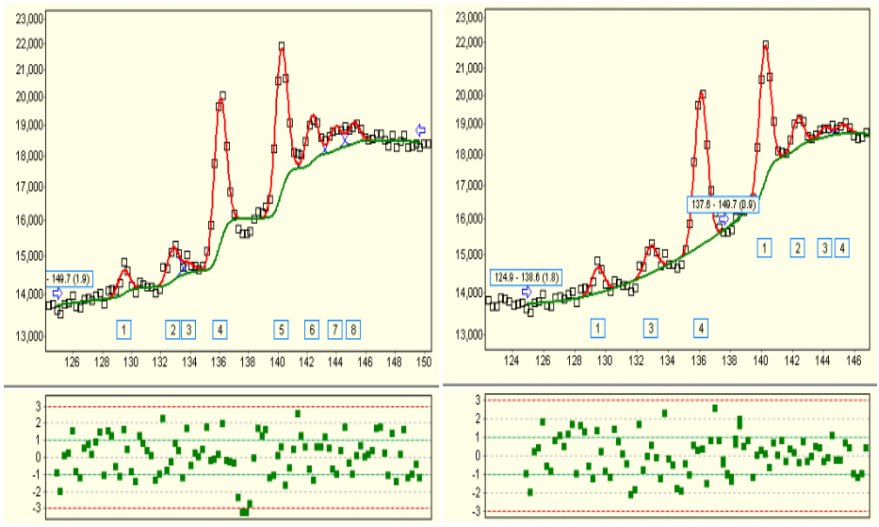

Figure 3.12 Deconvolution of a large region (channels 124 to 150) with residuals outside of the expected range in the middle of the region (channels 136 to 140; $\chi^2 > |\pm 3|$; left) and the corresponding residuals inside the expected range when splitting this region into 2 smaller ones.

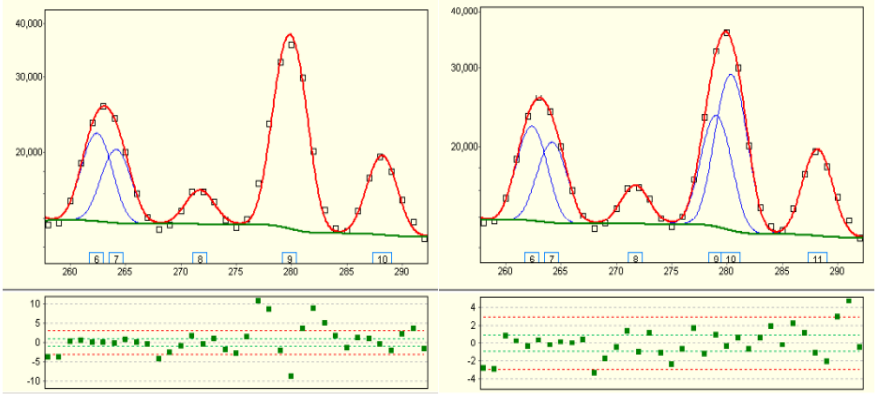

Figure 3.13 Deconvolution of a region with residuals outside of the expected range (χ^2>>|±3|) for an assumed single peak with centroid at channel 280 (left; singlet) and the corresponding residuals within the expected range (χ<|±2|) when considering a multiplet instead (right).

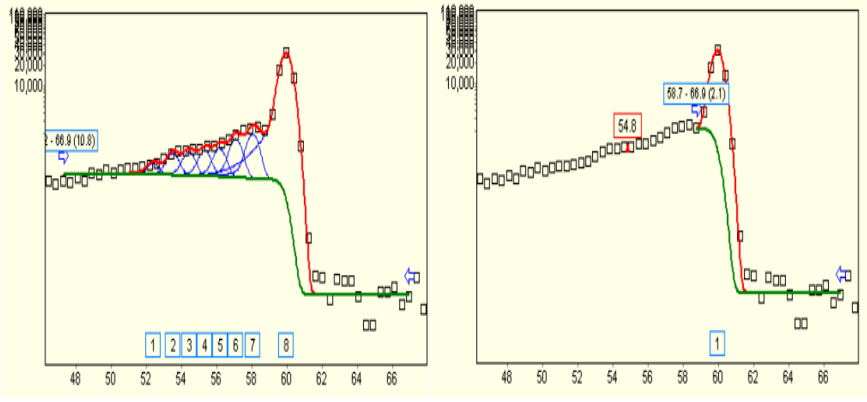

Figure 3.14 Spectrum of ^{241}Am with 59 keV peak distortion due to a high-count rate at a close detector-sample distance. Artificial peaks introduced by the HyperLab automatic evaluation algorithm (left). A more realistic deconvolution can be obtained manually by reducing the background region when moving the blue arrow from the left to the right, at the expenses of a small increase in the uncertainty in the photopeak area.

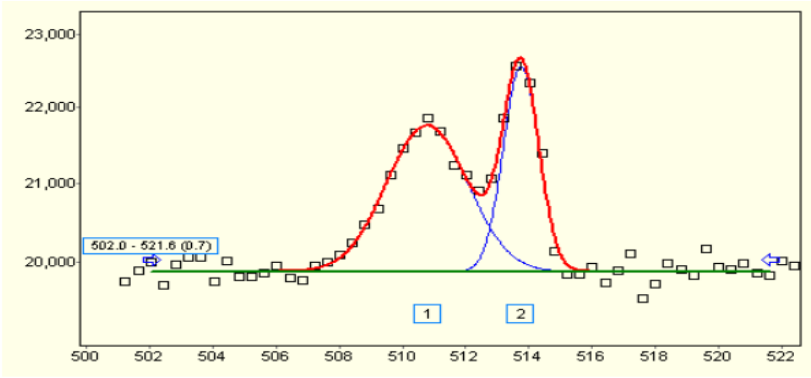

Figure 3.15 Example of variable width Gaussian fits for the 511 keV annihilation peak and a considerably narrower 514 keV peak next to it. This is achieved by increasing the default FWHM tolerance from ± 30% to ± 400% [139]**.**

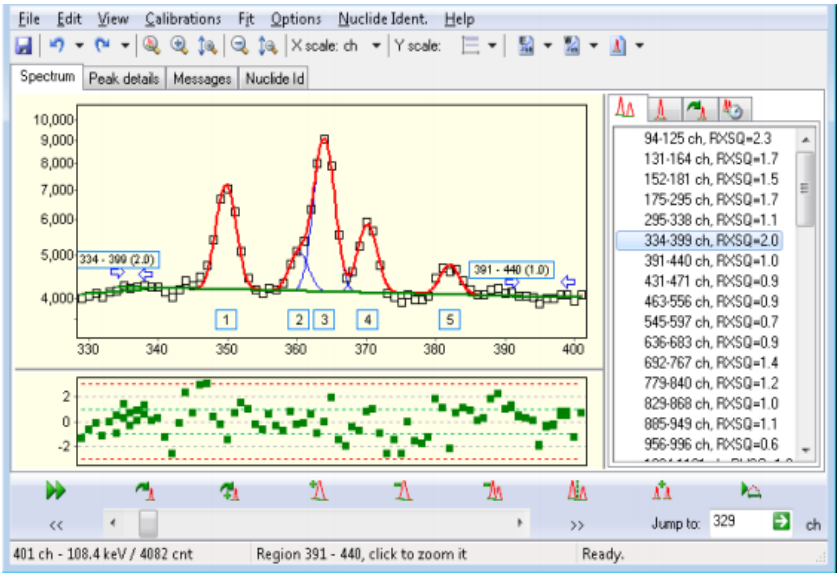

Figure 3.16 HyperLab version 2009 main window showing the resulting normalized χ^2 value (RXSQ = 2) for the deconvoluted region between channels 334 and 399.

3.3.3 Peak area and uncertainty

When the iterative fit reaches a minimum χ^2, the peak area is calculated from:

$$N_p = a\Delta\sqrt{\pi}\left(1 + S_{LA}S_{LS}\Delta + S_{RA}S_{RS}\Delta\right) \tag{3.13}$$

Also, HyperLab calculates the inverse of the covariance matrix M for all fitted parameters p_k ($k = 1, \ldots, m$) through:

$$M_{kr} = \sum_{x=1}^{n}\left(\frac{1}{\sigma_x{}^2}\frac{\partial\chi^2}{\partial p_k}\frac{\partial\chi^2}{\partial p_r}\right) \tag{3.14}$$

The inverse of M contains the covariances (and variances; $k = r$) for the p_k parameters. The uncertainty in the histogram peak area is calculated by means of:

$$\sigma_{N_p} = \sqrt{\sum_{k,r}^{n}\left(\frac{\partial N_p}{\partial p_k}\left(M^{-1}{}_{kr}\right)\frac{\partial N_p}{\partial p_r}\right)} \tag{3.15}$$

According to the HyperLab creators, in terms of their Monte Carlo simulation results the eq. (3.15) is a good representation of the real peak area uncertainty and considerably more accurate than other spectrometry programs [139].

3.4 Efficiency calibration

The γ-ray detection efficiency determination is performed by measuring certified single and multi-γ point-sources at sufficiently far (or "reference") source-detector distances where complex γ-attenuation, cascading coincidence γ-summing and losses effects are negligible [13]. The functional relationship is usually established as a n-degree polynomial fit $y(x)$ on a Log(ε_γ) vs. Log(E_γ) plot:

$$y = \sum_{i=0}^{n} a_i x^i \tag{3.16}$$

with $y = \mathrm{Log}(\varepsilon_\gamma)$ and $x = \mathrm{Log}(E_\gamma)$.

The Table 3.2 summarizes the point-sources employed in this work for the energy, FWHM and efficiency calibration of 6 HPGe semi-conductor detectors at the SCK•CEN. The Table 3.1 summarizes the typical FWHM values (in keV) and relative efficiencies (in %) at 2 reference γ-ray energies. The Figure 3.17 shows a diagram of the typical measurement setup used at this institution. A sample holder as depicted in Figure 3.4 was also employed on each detector, having 5 different sample-platform distances to the detector top-can, which are summarized in Table 3.3).

Table 3.1: FWHM values and relative efficiencies for all employed detectors in this work (detectors A, P, C, O, H, E) as specified by the vendor's datasheet.

Detector, FWHM (keV) and relative efficiencies[*]

Detector	FWHM at 122keV (Co-57)	FWHM at 1332keV (Co-60)	Absolute efficiency at 1332keV (%)
P	0.83	1.83	40.6
C	0.83	1.80	40.0
H	0.88	1.80	40.0
A	0.84	1.77	38.2
E	1.00	1.90	60.0
O	1.10	2.10	80.0

[*] Efficiencies relative to a similar size NaI(Tl) detector at 25 cm detector-source separation.

The certified sources of Table 3.2 consisted in a drop of 22 to 28 mg.cm^{-2} radioactive solution spiked inside 2 circular Mylar® Biaxially-oriented

polyethylene terephthalate (BoPET) layers of 0.1 mm thickness and 25 mm diameter (mass density ρ = 1.39 g/cm^3 at 20°C). The spiked drop had a maximum 2 mm diameter and was situated at a 1.85 mm height from the sample platform.

Figure 3.18 to Figure 3.22 show the reference efficiency curves for the 6 HPGe detectors employed at the SCK•CEN, obtained from the measurement of the point-sources quoted in Table 3.2 at the "reference" position 5, that is, 230 to 276.8 mm of platform-to-detector top can separations (see Table 3.3 for positions). The energy range covers the 50 keV to 3 MeV spectra. The figures also show the relative differences between the experimental and the fitted points: (exp/fit)-1 (in %) as indicators on the accuracy of the fit. A ≤1.5% relative difference is observed on average for most points on every curve and even lower for high-yield γ-rays, while a >2% uncertainty is observed for some secondary γ-rays. It must be remarked that in k_0 determination one is interested in the uncertainty contribution from the ratios of efficiency values (for the standard and the comparator γ-rays) and, with the measurement of high-yield γ-rays mainly (for sensitivity purposes) thus for these cases the accuracy can be estimated to be 1% under proper conditions, but that also depends on the difference in γ-energies and sample geometry, as well as the detector distances at which these samples were measured.

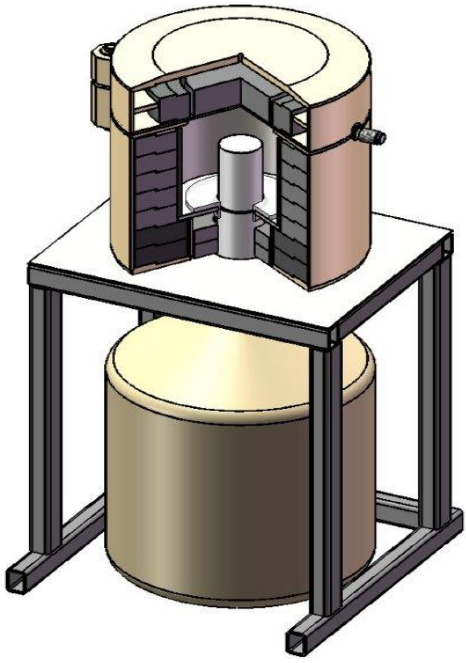

Figure 3.17: Diagram of a semi-conductor detector enclosed inside a hollow lead cylinder (shielding) and its cryostat (Dewar container; down) [140]**. Measurement setup typically employed at the SCK•CEN.**

Table 3.2: Certified γ sources (in radioisotope activity; *A*) employed in this work for the calibration of 6 HPGe semi-conductor detectors at the SCK•CEN.

Provider	Source		Half-life		Ref.	*A*	Unc.	Certified on
PTB	ML	^{133}Ba	10.52	y	217-90	141.8	1.5	07/09/94
					2003-1009	4.91	1.02	01/01/03
					527-83	49.9	1.5	29/03/88
		^{152}Eu	13.53	y	429-83	342	2.0	01/01/84
					229-94	47.6	2.0	01/01/95
					103-89	306	2.0	01/05/94
					231-86	32	2.0	29/03/88
		^{88}Y	106.6	d	2008-1166	18.05	1	01/03/08
		^{60}Co	5.271	y	270-93	5.83	0.69	01/01/00
		^{134}Cs	2.062	y	159-93	10.75	1.02	01/12/01
		^{226}Ra	1601	y	412-84	148.2	2	01/01/90
	SL	^{241}Am	432.6	y	252-90	194.4	1.5	01/05/94
					147-86	87.6	1.5	01/01/90
		^{109}Cd	1.267	y	2005-1113	0.848	1.77	01/09/06
		^{137}Cs	30.15	y	315-99	6.46	1.08	01/01/00
					193-90	155.4	1.50	01/07/94
		^{22}Na	2.602	y	317-97	4.74	0.84	01/12/01
AREVA	ML	^{88}Y	106.6	d	50101	48.1	2.3	11/09/09
		^{60}Co	5.271	y	50223	38.68	1.5	11/09/09
	SL	^{65}Zn	244.1	d	2004-1019	18.83	1.43	08/12/04
		^{85}Sr	64.85	d	40262	49.8	1.5	11/09/09
		^{113}Sn	115.09	d	50005	35.4*	1.5	15/05/09
		^{22}Na	2.603	y	50067	42	2	11/09/09
		^{54}Mn	312.13	d	50073	31.96	1.5	11/09/09
		^{137}Cs	30.05	y	50480	39.1	2	11/09/09
		^{51}Cr	27.703	d	50063	51.6	2	11/09/09
		^{139}Ce	137.64	d	50008	31.3*	1.5	15/05/09
		^{57}Co	271.8	d	50203	45.3	1.7	11/09/09
		^{241}Am	432.6	y	50125	41	3.5	11/09/09

ML = Multiple-line; SL = Single-line emitters

* Value corresponds to gamma-ray activity ($4\pi.s^{-1}$).

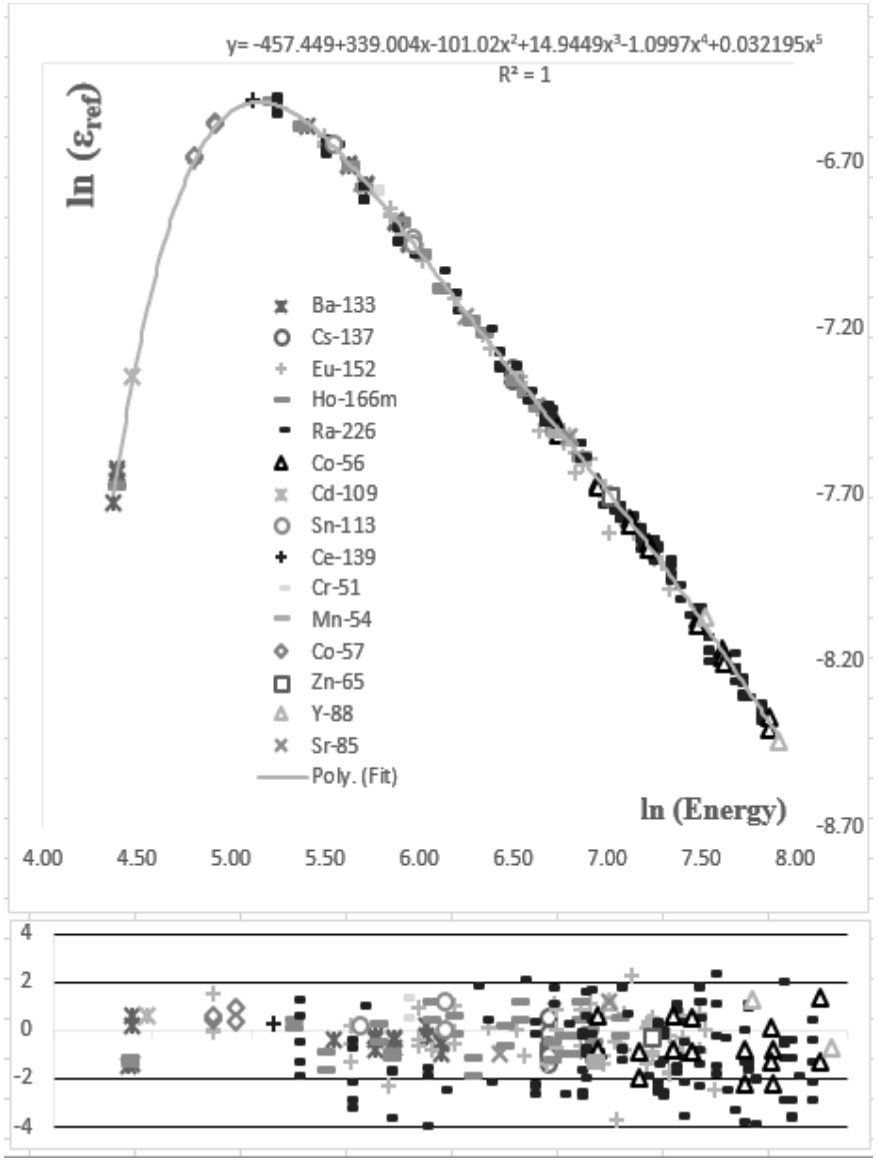

Figure 3.18: Reference efficiency curve for detector P as a function of the γ-ray energy (50 to 2734 keV). Residuals between the experimental points and the polynomial fit.

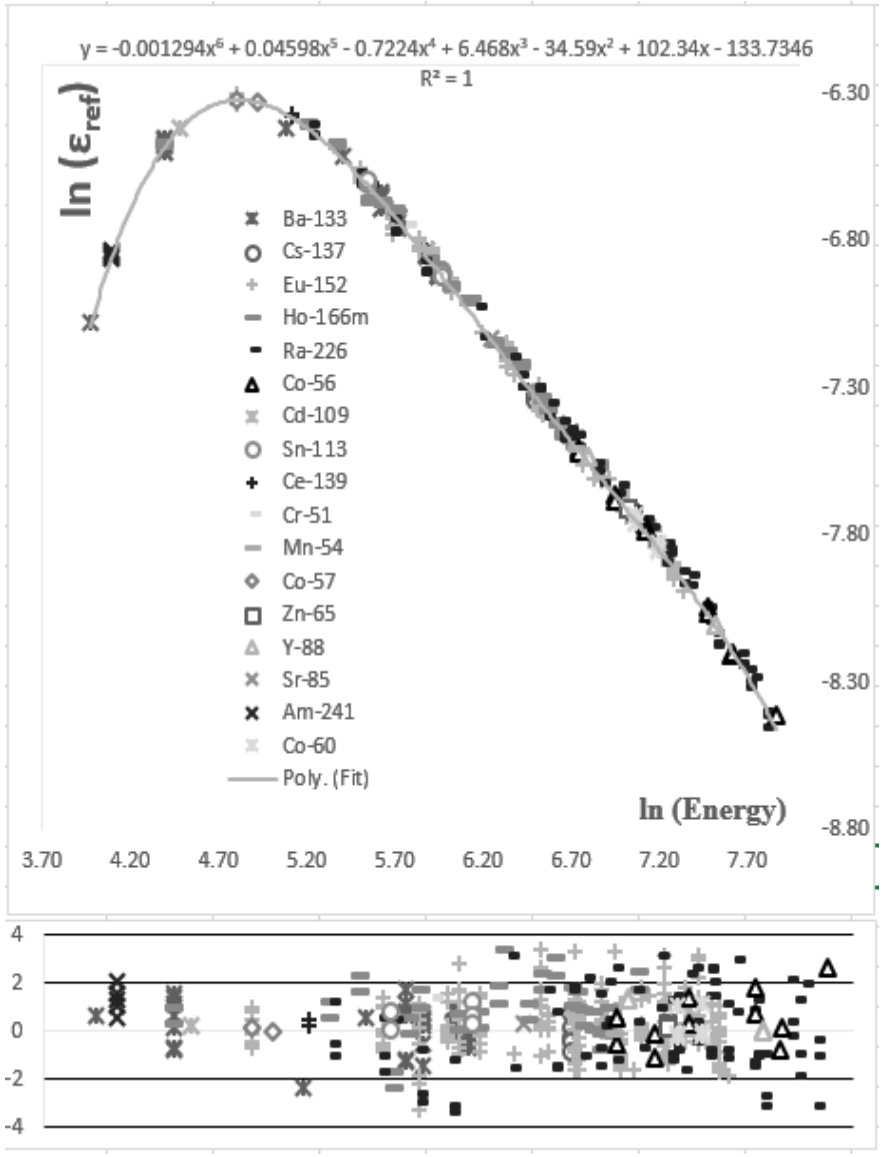

Figure 3.19: Reference efficiency curve for detector C as a function of the γ-ray energy (50 to 2734 keV). Residuals between the experimental points and the polynomial fit.

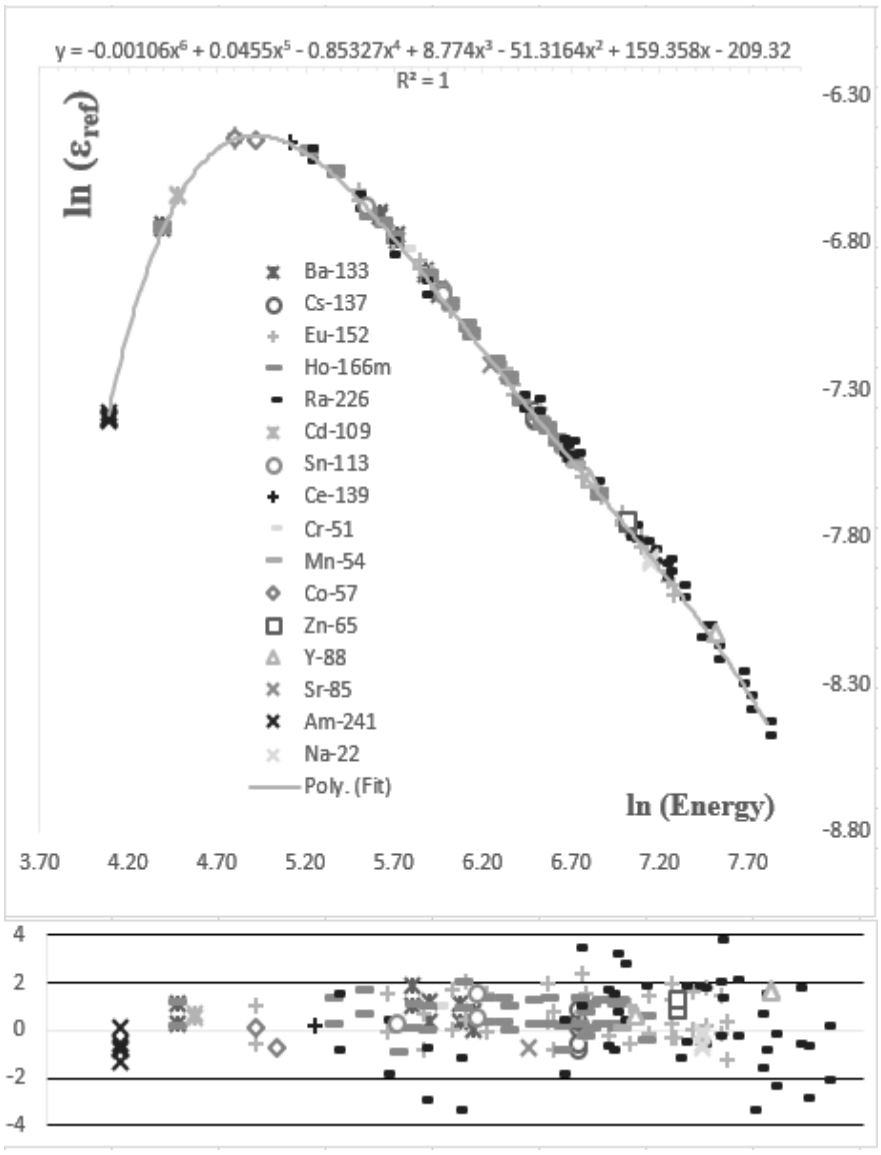

Figure 3.20: Reference efficiency curve for detector H as a function of the γ-ray energy (50 to 2734 keV). Residuals between the experimental points and the polynomial fit.

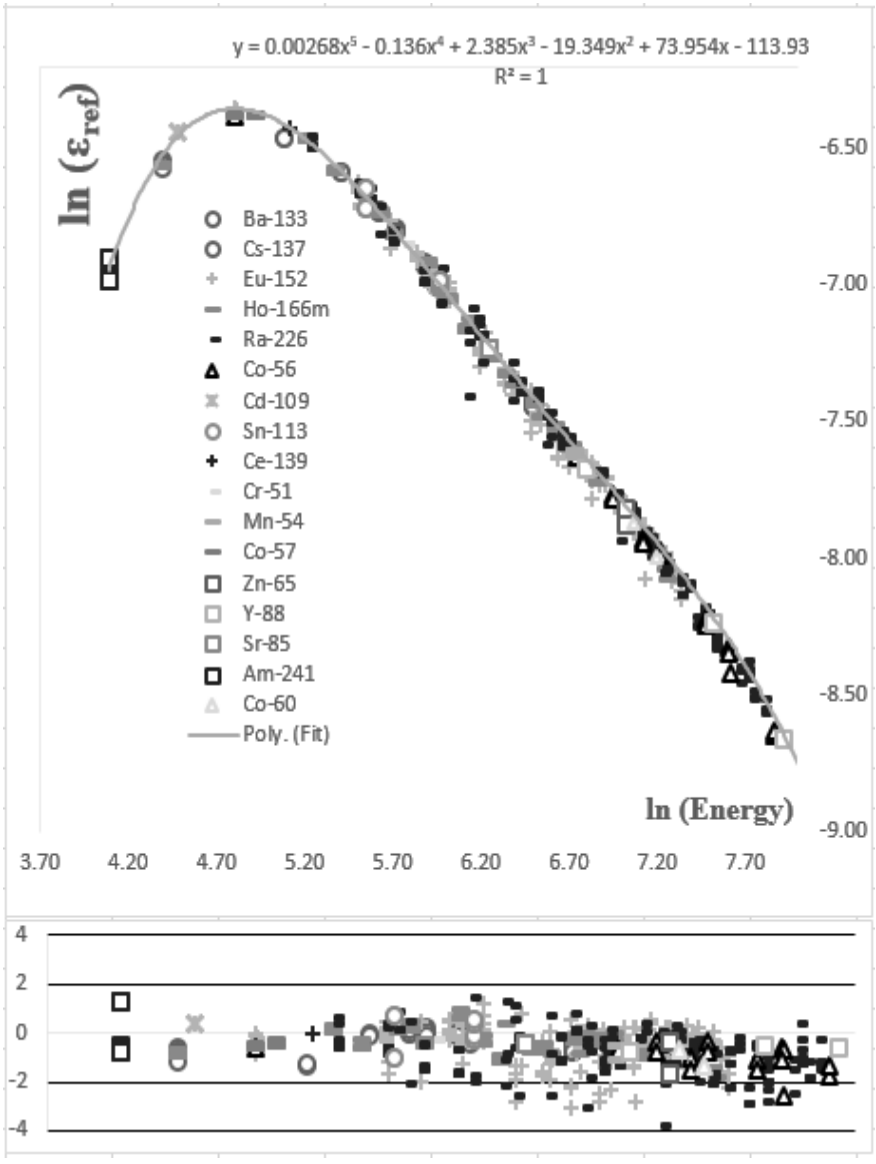

Figure 3.21: Reference efficiency curve for detector A as a function of the γ-ray energy (50 to 2734 keV). Residuals between the experimental points and the polynomial fit.

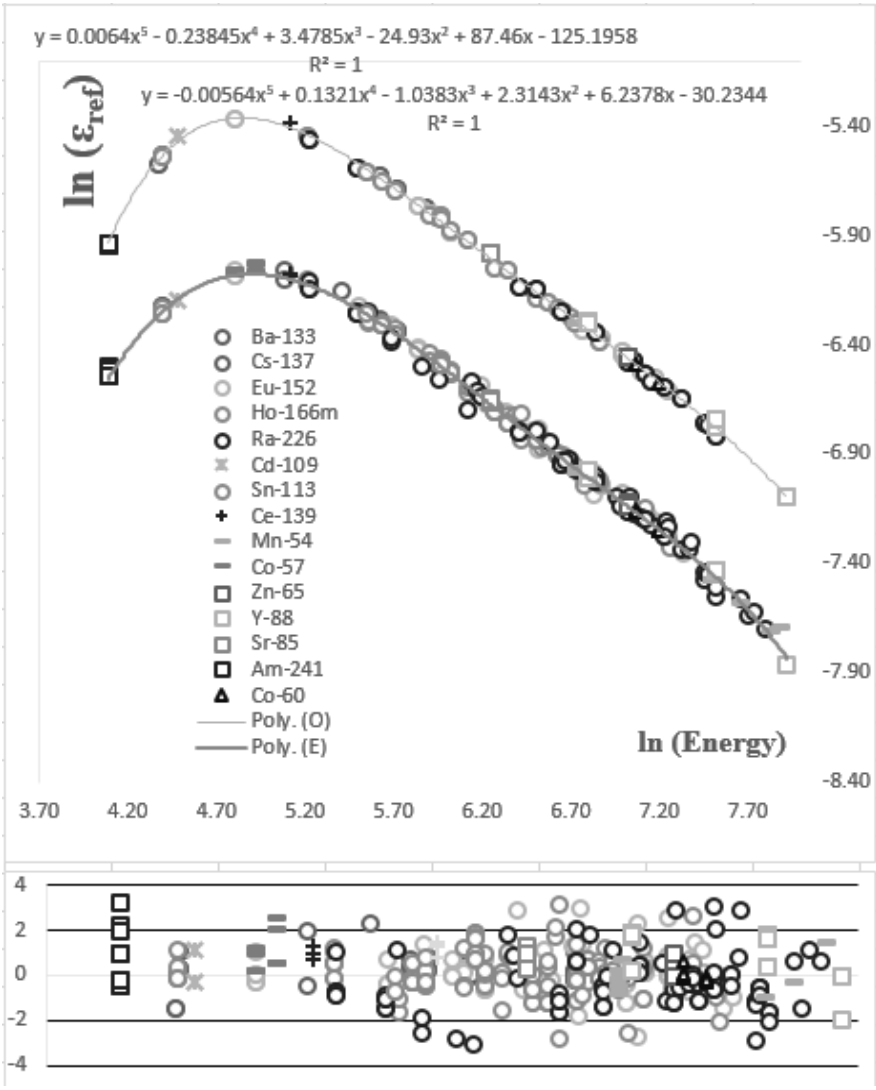

Figure 3.22: Reference efficiency curves for detectors O (up) and E (down) as a function of the γ-ray energy (50 to 2734 keV). Residuals between the experimental points and the polynomial fit, with black circles for detector O and light grey circles for detector E. Superposition of circles are given in dark-gray.

Table 3.3: Sample support (holder platform) distances to the detector top can (in mm).

	Detector					
Position	**P**	**C**	**H**	**A**	**E**	**O**
1	0	0	0	0	0	0
2	25	25.5	25	26.7	25	25
3	65	65.5	65	56.7	65	65
4	125	125.5	125	117.0	125	125
5	275	275.5	275	276.8	275	205

3.5 Efficiency transfer

Since the preparation and measurement of a single-γ certified source designed to replicate each sample of analytical interest is not feasible, a procedure for efficiency transformation from a "reference" efficiency point $\varepsilon_{\gamma,\text{ref}}$ (or curve; as with Figure 3.18) to a γ-ray efficiency point for the sample geometry of interest $\varepsilon_{\gamma,\text{geo}}$ was proposed by Moens et al. [141, 142] that has been tested extensively in the literature and applied in the determination of the first generation of k_0 factors [13, 36, 38, 40, 44]. The relationship proposed was [141, 142]:

$$\varepsilon_{\gamma,\text{geo}} = \varepsilon_{\gamma,\text{ref}} \frac{\Omega'_{\text{geo}}}{\Omega'_{\text{ref}}} \tag{3.17}$$

Where Ω*'* is the "effective" solid angle subtended at the source by the detector [13, 141, 142]. The Ω*'* values for the reference source and sample geometry setup can be calculated for each γ-ray energy of analytical interest by means of:

$$\Omega' = \int F_e F_a d\Omega \tag{3.18}$$

where F_e is the probability for a photon of energy $E_{\gamma,}$ emitted within an infinitesimal solid angle and that impinges on the detector, to interact incoherently (e.g. by means of Compton scattering) with the detector crystal. The F_a is the probability of attenuation of the γ-ray caused by incoherent interactions in the absorbing materials interposed between the radiation source and the detector (source matrix, container, platform support, holder support, detector can, etc.). Integration of eq. (3.18) is done by means of the Gauss-Legendre quadrature for sources and detectors having axial symmetries (e.g. cylinders) [141, 142]. The F_i values of eq. (3.18) are determined by means of the X-ray and γ-ray mass-attenuation coefficients (in $cm^2.g^{-1}$) as a function of the photon energy, which are available for instance in the NIST XCOM Internet database [143].

Dedicated commercial software such as Kayzero/SOLCOI© uses the provided detector specifications, the source and sample dimensions, the source-detector separations and the reference efficiency curves to solve eq. (3.17) [71, 144]. Other commercial codes are available elsewhere but these have not been validated for as many years as the Kayzero/SOLCOI© package since its introduction in the ‘90s [70, 71]. Table 3.4 summarizes the dimensions and technical specifications for the 7 HPGe detectors employed in this work.

Table 3.4: Specifications for the constituent parts of the measurement setup per detector. All values are in mm, except for PS which is given in µs.

D	CR	CH	Cav R	Cav H	TDL	HS	OA	PS	VG	CT
P	34.0	51.0	4.5	24.0	0.502	3	1	6	8.120	1.0
C	30.5	60.0	4.5	46.0	0.521	3	0	4	8.378	1.0
H	30.5	61.0	4.5	47.0	0.509	3	0	6	8.251	1.0
A	29.0	59.0	4.5	39.0	0.467	3	0	4	7.070	1.5
E	37.5	75.5	11.5	35.0	0.872	3	0	4	12.954	1.5
O	37.0	83.5	5.0	70.5	0.509	3	0	4	6.947	1.5

OA = other absorber thickness; PS = pulse shaping.

All other abbreviations in the table are defined in the diagram of Figure 3.4.

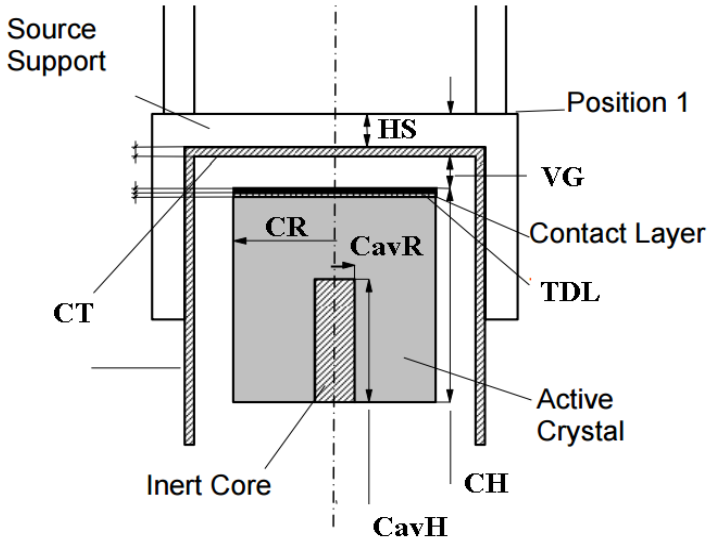

Figure 3.23: Diagram of some constituent parts of the measurement setup whose dimensions are reported in Table 3.4. These are defined as: D = detector; CR = crystal radius; CH = crystal height; CavR = core cavity radius; CavH = core cavity height; TDL = top dead-layer thickness; HS = holder support thickness; VG = vacuum gap; CT = can top thickness.

The crystal matrix of every detector consisted in hyper-pure (HP) Germanium, with a mass density ρ = 5.35 g/cm^3. The can top was made of high-purity Al (ρ = 2.7 g/cm^3), except for the detector P, which has a can top of high-purity Cu (ρ = 8.94 g/cm^3) and an additional internal layer of Teflon (24% C, 76% F; ρ = 2.2 g/cm^3). The holder matrix consisted of PMMA (Polymethyl methacrylate, also known as acrylic or acrylic glass, as well as the trade names Plexiglass, Acrylite, Lucite and Perspex ($C_5H_8O_2$; ρ = 1.19 g/cm^3).

The calculation of eq. (3.18) (for a given geometry) by the Kayzero/SOLCOI© software is performed for only 17 data-points by default, distributed with usually ≥ 100 keV intervals for covering the whole energy spectrum of interest (50 to 3000 keV). On request, the value for a specific energy of interest can be calculated as well ("Direct Solcoi" option), but only during k_0-NAA related elemental content calculations. However, since it is a commercial software, the exact algorithms used in the computations are obfuscated, as one would expect. The source code and exact data for their mass attenuation coefficients is unknown. Yet, it is known that the software uses some sort of local file library of photon linear attenuation coefficients from NIST XCOM, that might not be as updated as the NIST XCOM Internet database [143]. This is especially true when considering that the attenuation coefficients are discontinuous at absorption edges at low energies and more than 17 pre-defined energies are necessary for accurately mapping the energy regions of interest. The development of a new software for the efficiency calculations was not feasible during the given time-span for attaining the main objectives of this work.

Fortunately, the Kayzero/SOLCOI© software User's guide gives a detailed description on how some key input and output files are constructed [144]. Since it performs these computations in separate steps, providing intermediate output files in the process, it was possible for us to develop a home-made software that recreates structural copies of these input and

output files, but containing instead updated mass-attenuation coefficients that were obtained on run-time per each γ or X-ray of interest from the NIST XCOM Internet database. This was achieved by means of iterative HTTP "Post" requests.

The batch application of computational algorithms designed for the execution, data reading and SQL-database storing of the Kayzero/SOLCOI© results allowed us to obtain more precise and smooth Ω' vs. E_γ curves than previously allowed by this software package. These were obtained from calculated data-points in increments of 0.1 keV (30000 total data-points), for all geometries and γ-ray energies dealt in this work during our k_0 and Q_0 determinations.

For comparison, we calculated the solid angles for the 366.3 keV line of ^{65}Ni with both codes for a pure metal 0.1 mm thin sample inside a HDPE vial (dimensions given in section 6.8.3) at our farthest sample-detector distance (position 5). With our tweaked version of SOLCOI we found that it was 0.6500, while the original SOLCOI code gives 0.6566 for the same exact input data. The difference corresponds to 1%. For a high-energy line, such as the 1481.8 keV the difference was just 0.2% (0.5672 vs. 0.5687).

3.6 Correction for X and γ-ray coincidence effects

The X and γ-ray coincidence effects occur when two or more cascading radiations from a given sample, emitted within a negligible time delay, give raise to a total or partial energy deposition in the detector crystal [13]. Therefore, the coincidence effects are responsible for the loss and increase of the number of detected counts of a given photo-peak in the spectrum.

Coincidence effects with the energetic electrons from the radioactive decay (β particles) or with bremsstrahlung are usually considered negligible [13].

The treatment and extensive formulae for the correction of coincidence effects has been dealt in detail elsewhere in the literature [141, 145, 146]. A calculated correction factor *COI* is applied to the number of detected γ-ray of a given energy N_p' in order to obtain the correct number of γ-rays that should have been detected [13]:

$$N_p = \frac{N_p'}{COI} \tag{3.19}$$

The *COI* correction factor is computed from:

$$COI = \left(1 - L_\gamma\right)\left(1 + S_\gamma\right) \tag{3.20}$$

Where L_γ and S_γ are the total probabilities for coincidence loss and summing (respectively), which can be computed with the aid of computational software that employs the relations exposed in e.g. reference [13].

These L_γ and S_γ probabilities are functions of absolute nuclear constants (e.g. I_γ values, internal conversion coefficients) and the detector efficiency. For coincidence summing the ε_γ value for the actual geometry in question must be supplied. In the case of coincidence loss effects the calculation of the *COI* correction factor requires the total detector efficiency ε_t instead, which can be calculated from the ε_γ by means of:

$$\varepsilon_t = \frac{\varepsilon_\gamma}{\left(P/T\right)} \tag{3.21}$$

where the (*P/T*) factor is the peak-to-total ratio, a measurable quantity which is, for a given detector, dependent on the following parameters: the photon energy, the distance between the source and the detector, the source geometry and composition, as well as any absorbing or scattering materials interposed between the source and the detector [13].

A *P/T* curve as a function of the energy is obtained by measuring single-γ sources covering the energy region of interest. These sources are required because these are free from coincidence γ or X-rays effects. A polynomial fit $y(x)$ as in eq. (3.16) is obtained from a Log(*P/T*) vs. Log(E_γ) plot, where each y = Log(*P/T*) value was found after a subtraction of all background radiation contributions in the spectra and, after taking into account an estimated contribution for the low-energy photons that were filtered by the pulse-discriminator, by means of a linear extrapolation to zero energy. In the case of sources giving rise to an histogram photo-peak at an energy other than the one of interest, e.g. the 511 keV annihilation photons from an antimatter emitter such as ^{65}Zn or ^{22}Na, one must subtract this contribution as well [13]. The a_i coefficients for the n-degree polynomials of the 6 detectors employed in this work at the SCK•CEN are summarized in Table 3.5. The accuracy of these curves was found to be within 2% for positions 4 and 5, 3% for position 3 and up to 5% for positions 1 and 2.

Table 3.5: The a_i coefficients (i = 0, … , n) for the y = log(*P/T*) vs. x = log E_γ fitted polynomial of eq. (3.16) for each detector and for each standardized source-detector position employed at the SCK•CEN, obtained from the measurement of the single-γ sources of Table 3.2.

Detector	E_γ range		a_0	a_1	a_2	a_3	Position
H	55.0	486.5	-14.008	17.0322	-6.812	0.87147	5
	486.5	3500	1.03725	-0.5779			
	55.0	486.5	-15.304	19.248	-7.984	1.0678	4
	486.5	3500	1.11995	-0.6095			
	55.0	502.3	-12.12	15.0948	-6.210	0.81757	3
	502.3	3500	0.96665	-0.559			
	55.0	505.6	-8.8329	10.7494	-4.333	0.54992	2
	505.6	3500	0.90909	-0.5477			
	55.0	507.5	-13.684	17.282	-7.222	0.9673	1
	507.5	3500	0.77161	-0.5193			

Detector	E_γ range		a_0	a_1	a_2	a_3	Position
C	55.0	491.7	-20.535	25.0458	-10.12	1.33028	5
	491.7	3500	0.96279	-0.5577			
	55.0	473.1	-19.13	23.806	-9.79	1.30505	4
	473.1	3500	0.96664	-0.5571			
	55.0	466.6	-18.227	22.859	-9.507	1.28334	3
	466.6	3500	0.957	-0.5622			
	55.0	620.2	-9.8706	12	-4.83	0.62	2
	620.2	3500	1.085	-0.606			
	55.0	576.0	-17.996	22.5359	-9.366	1.26077	1
	576.0	3500	1.02136	-0.5979			
A	55.0	563.2	-11.292	13.406	-5.231	0.64579	5
	563.2	3500	1.14925	-0.6203			
	55.0	673.4	-10.865	13.2025	-5.282	0.67041	4
	673.4	3500	1.16048	-0.6242			
	55.0	673.4	-9.8706	12.0457	-4.854	0.61921	3
	673.4	3500	1.09205	-0.6057			
	55.0	676.7	-9.8706	12	-4.83	0.62	2
	676.7	3500	1.085	-0.606			
	55.0	579.0	-9.5464	11.9929	-5.042	0.67396	1
	579.0	3500	1.04768	-0.6259			
P	60.0	497.6	-4.6671	5.86355	-2.410	0.29656	5
	497.6	3500	1.07382	-0.6079			
	60.0	526.1	-3.5661	4.50851	-1.852	0.21948	4
	526.1	3500	0.97556	-0.5752			
	60.0	673.4	-7.2896	9.52361	-4.068	0.5401	3
	673.4	3500	1.03601	-0.6027			
	60.0	673.3	-5.506	7.32382	-3.183	0.4219	2
	673.3	3500	1.00024	-0.6044			
	60.0	644.8	-10.14	13.2549	-5.717	0.77759	1
	644.8	3500	1.05242	-0.6535			

Detector	E_γ range		a_0	a_1	a_2	a_3	Position
O	50.0	437.0	0.42813	-1.2035	0.714	-0.14602	5
	437.0	3500	0.99203	-0.5495			
	50.0	460.3	-9.7968	12.4807	-5.307	0.72541	4
	460.3	3500	0.87035	-0.5144			
	50.0	456.6	-2.4191	2.56353	-0.957	0.09818	3
	456.6	3500	0.87621	-0.5263			
	50.0	394.0	-3.0261	3.38402	-1.334	0.15316	2
	394.0	3500	0.59939	-0.4421			
	50.0	483.0	-4.8642	6.05426	-2.58	0.34041	1
	483.0	3500	1.06246	-0.6264			
E	50.0	476.3	-14.179	17.5292	-7.216	0.96622	5
	476.3	3500	0.84556	-0.476			
	50.0	463.9	-10.899	13.3685	-5.439	0.7112	4
	463.9	3500	0.89533	-0.4999			
	50.0	480.1	-5.9502	6.99345	-2.776	0.34699	3
	480.1	3500	0.86474	-0.4974			
	50.0	492.9	-3.2823	3.40044	-1.166	0.10532	2
	492.9	3500	0.98409	-0.5586			
	50.0	573.2	-9.9757	12.3281	-5.067	0.65978	1
	573.2	3500	1.23619	-0.6922			

The accuracy of these curves was found to be within 2% for positions 4 and 5, 3% for position 3 and up to 5% for positions 1 and 2.

3.7 Detector Fine-tuning

The accuracy of the efficiency transfer calculations can be improved by fine-tuning the detector top dead-layer thickness and the vacuum gap separations between the crystal and the top can. To empirically find the adequate

dimensions, the measurement of single-γ sources is performed at every source platform standardized position (see Table 3.3). The ratio between the efficiency experimental data-points from two different positions must be equal to the corresponding ratio between calculated efficiency data-points. By changing these layers' dimensions within an estimated range in an iterative process, the optimal values are obtained when the differences between experimental and calculated efficiency data-points is minimized. These dimensions are provided in Table 3.4. The Table 3.6 lists the radioactive single-γ sources employed for the fine-tuning of the detectors top dead-layer and vacuum gap.

Figure 3.24 shows the percent deviations between the calculated and the experimental efficiency ratios during the fine-tuning of detectors P, H, C and A. Given the top dead-layers and vacuum gaps proposed in Table 3.4, the maximum observed deviation was ± 1%.

Table 3.6: Certified single-γ sources (in γ-ray activity; A_γ) from AREVA employed in this work for the fine-tuning of the top dead-layer and vacuum gap dimensions of 6 HPGe detectors. These sources are different than in Table 3.2.

Source	Half-life		A_γ ($4\pi.s^{-1}$)		Unc. (%; 3*s*)	Certified on
^{65}Zn	244.01	d	22634	3.34E+04	1.5	15/05/09
^{85}Sr	64.85	d	40202	3.29E+04	2.3	16/05/09
^{113}Sn [a]	115.09	d	50005	3.54E+04	2	17/05/09
^{54}Mn	312.13	d	50009	4.22E+04	1.5	18/05/09
^{137}Cs	30.05	y	50463	3.56E+04	1.5	19/05/09
^{51}Cr	27.703	d	50111	2.43E+04	1.5	20/05/09
^{57}Co [b]	271.8	d	50075	3.62E+04	2	22/05/09
^{57}Co [c]			50075	4.53E+03	2	23/05/09
^{139}Ce	137.641	d	50008	3.13E+04	1.5	24/05/09
^{109}Cd	461.4	d	21851	3.49E+04	2	25/05/09
^{241}Am	432.6	y	50123	2.96E+04	3.5	26/05/09

[a] For the 392 keV line.

[b] For the 122 keV line.

[c] For the 136 keV line.

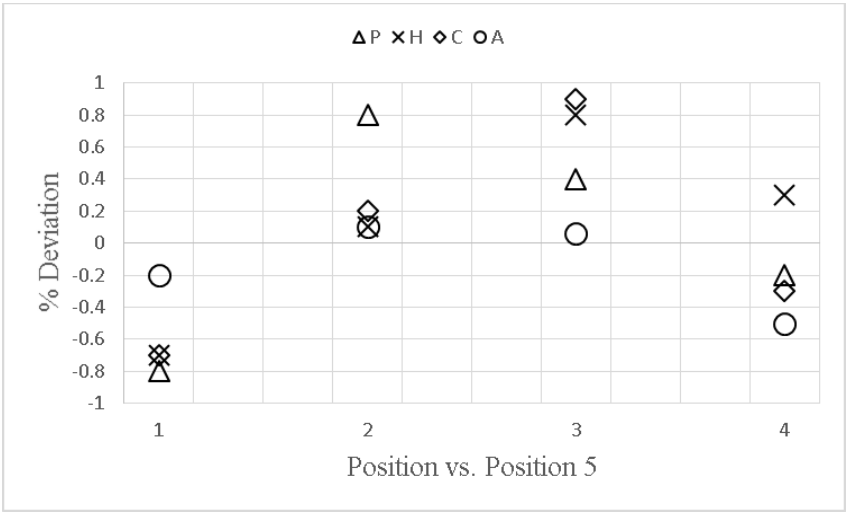

Figure 3.24: Percent deviation between the experimental and the calculated efficiency ratios for a given position against the reference position 5, when inputting the top dead-layer, vacuum gaps, crystal parameters and source platform to detector separations summarized in Table 3.3 and Table 3.4.

3.8 Validation of the efficiency transfer

For the validation of our efficiency transfer and *COI* computations for other source-detector separations (or positions) and geometries of interest, we proceeded by measuring the induced γ-ray activity on typical samples employed in routine analysis, which consisted in 100 μL aliquots of ICP standards (with 0.1% elemental content), spiked on cylindrical paper filters of 1.25 mm thickness and 7.5 mm diameter. These paper filters (cellulose; 100% $C_6H_{10}O_5$) were packed and inside small high-density polyethylene (HDPE) vials of 0.65 mm side thickness, 0.45 mm bottom thickness and 8.1 mm diameter for their irradiation of 7 hours inside the irradiation channel Y4 of the BR1 reactor at the SCK•CEN. These samples were later measured on 3 different detectors at the standardized position 4 inside these HDPE vials. Channel Y4 has a thermal conventional fluence rate of ~$1x10^{11}$ $n.cm^2.s^{-1}$ and an epithermal conventional fluence rate which is (approximately) 40 times lower.

From eq. (2.11) it is possible to estimate the γ-ray detection efficiency for the geometry in question if the γ-ray activity is well-known. However, if the source of radiation is a multi-γ source, when writing eqs. (2.11) and (3.19) for two different γ-rays "1" and "2" of the same nuclide and sample, one obtains:

$$\frac{A_2}{A_1} = \frac{(SDC)_1}{(SDC)_2}\left(\frac{N'_p}{COI\,\varepsilon_\gamma t_c}\right)_2\left(\frac{COI\,\varepsilon_\gamma t_c}{N'_p}\right)_1 \tag{3.22}$$

When considering the previous ratio for the same spectrum, the expression is simplified:

$$\frac{I_{\gamma,2}}{I_{\gamma,1}} = \left(\frac{N'_{p,2}}{N'_{p,1}}\right)\left(\frac{COI_1\varepsilon_{\gamma,1}}{COI_2\varepsilon_{\gamma,2}}\right) \tag{3.23}$$

Hence, the exact weight elemental content and other parameters are not required to determine $\varepsilon_{\gamma,1}$ (or $\varepsilon_{\gamma,2}$) as a function of $\varepsilon_{\gamma,2}$ (or $\varepsilon_{\gamma,1}$). By inserting a calculated ε_γ x *COI* value for a given γ-ray, one can find the experimental ε_γ x *COI* value for a secondary γ-ray and, compare it with its corresponding calculated ε_γ x *COI* value. In this way it was possible to estimate the accuracy of our efficiency transfer and *COI* calculations for HDPE-covered cylindrical samples used in routine analysis at the SCK•CEN. Figure 3.25 to Figure 3.27 show these results for detectors P, C and H at positions 4, 3 and 3, respectively. The accuracy of our efficiency transfer plus COI calculations is estimated to be 1.5% for positions 3, 4 and typically 0.5 to 1.5% for position 5. Therefore, for these positions one can later adopt a half-width uncertainty of 1% for efficiency transfer and 0.5% for COI correction (see section 7.2.1).

Our results for the lower positions 1 and 2 are estimated to be accurate within 5% on average and 10% at worst, therefore in this work only measurements at positions 4 and 5 will be employed for k_0 determination. All positions can be employed for Q_0 determination, although pulse pile-up and dead-time will be different for bare and Cd-covered irradiated samples and position 3 is preferable when possible.

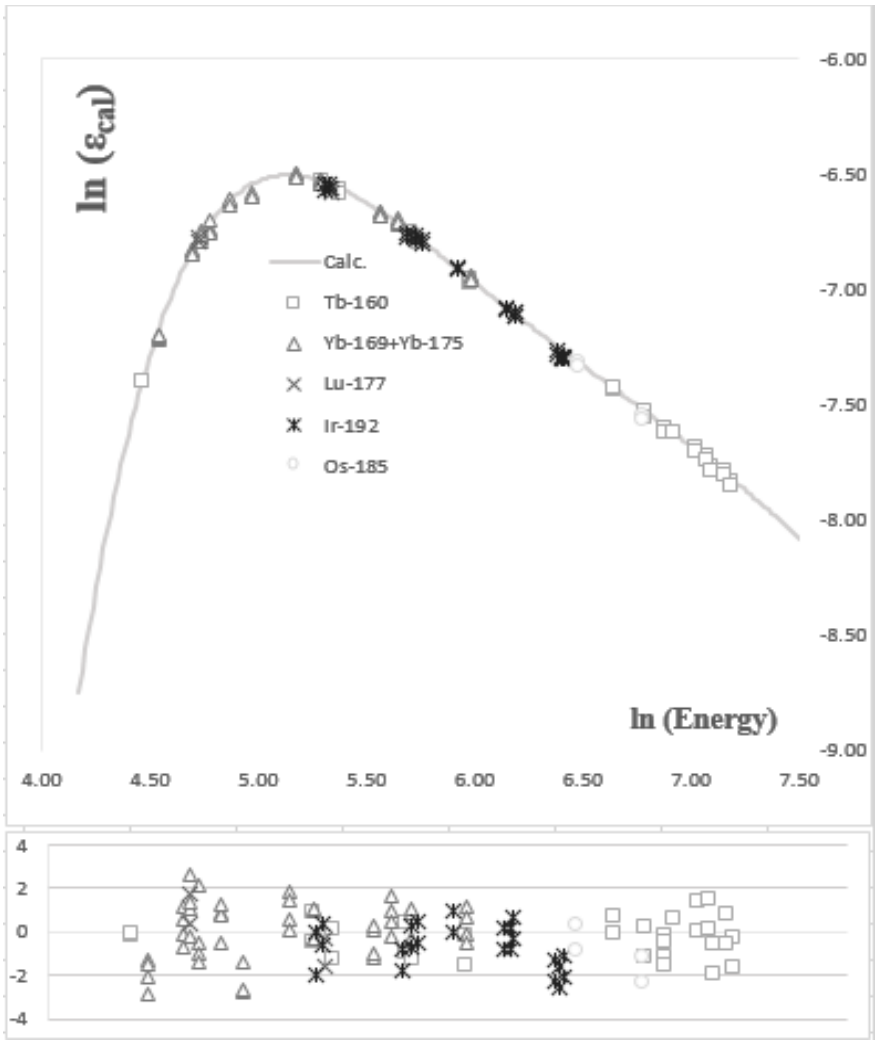

Figure 3.25: Calculated ε_γ curve for paper filters packed inside HDPE vials at the measurement position 4 of detector P (see text). Expected ε_γ x *COI* data-points are found in a relative way, by employment of eq. (3.23) and the calculated ε_γ x *COI* values for a reference γ-ray of the same radionuclide. Residuals between the expected points and the calculated ones. Here 2σ corresponds to 1.5%.

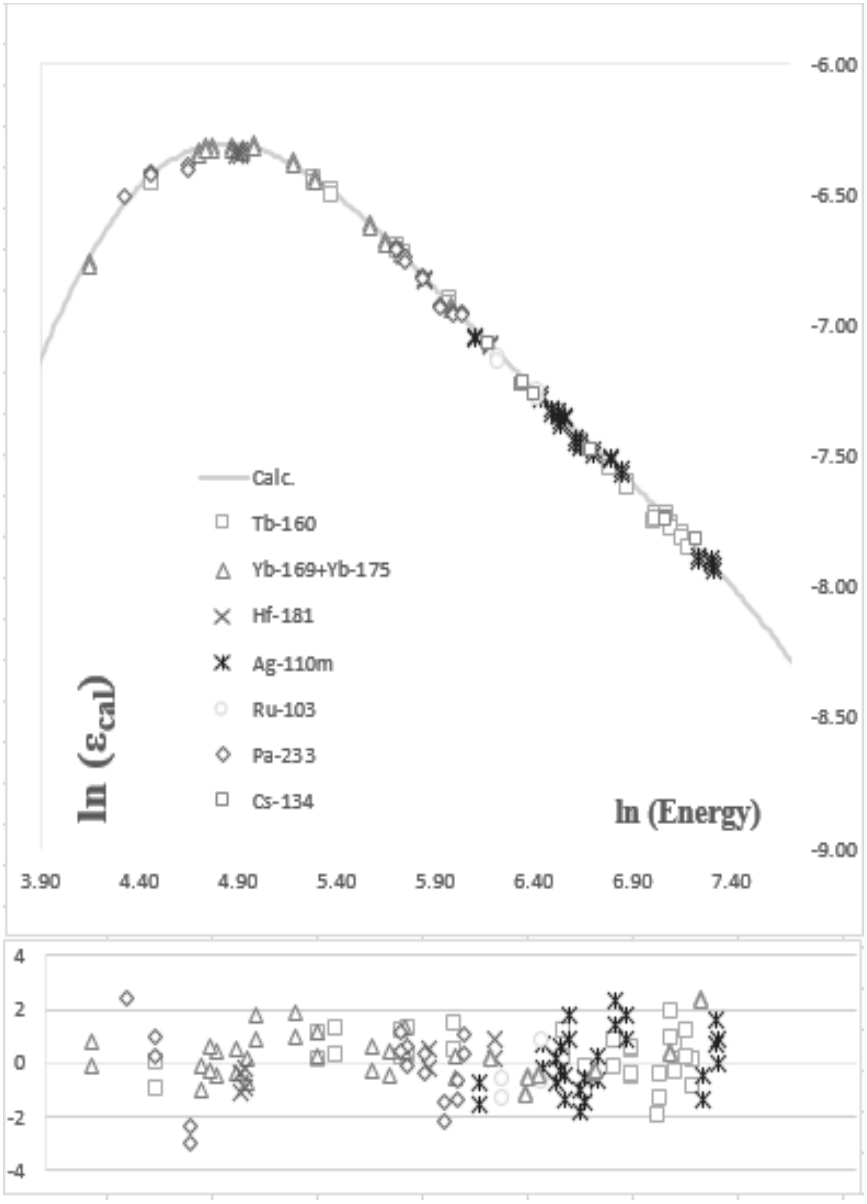

Figure 3.26: Calculated ε_γ curve for paper filters packed inside HDPE vials at the measurement position 3 of detector C. See text and Figure 3.25.

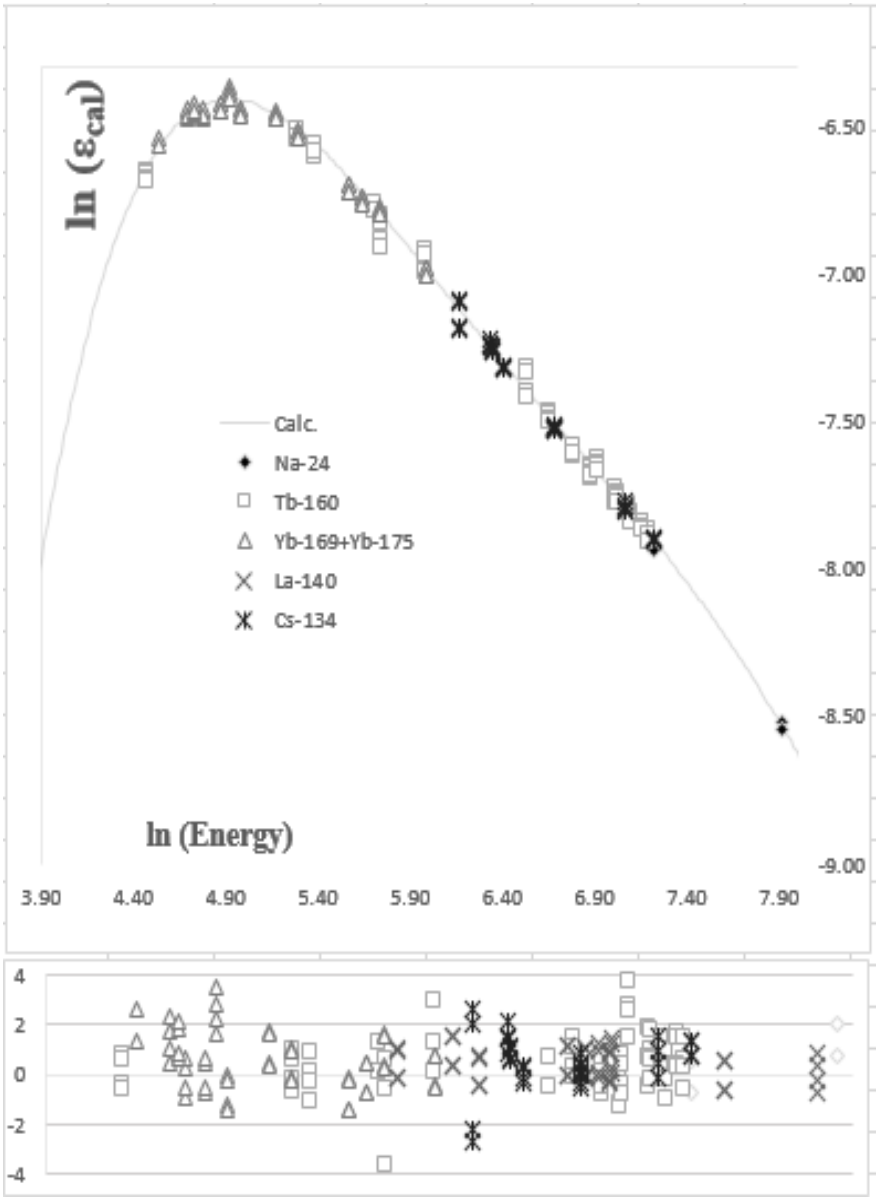

Figure 3.27: Calculated ε_γ curve for paper filters packed inside HDPE vials at the measurement position 3 of detector H. See text and Figure 3.25.

3.9 Dead-time and pulse pile-up corrections

For detection systems that record discrete events, the dead-time is the period of time after each event during which the (detection) system is busy and is not able to record another event [147]. When the dead-time is not prolonged by the arrival of a new pulse it is called “non-extending”. In a system with “extending” dead-time, each (incoming) event prolongs the dead-time by a given amount of time [148].

The total dead-time of a detector is mainly due to:

- Intrinsic dead-time (due to the detector physical characteristics);

- the conversion time of the ADC and the readout and storage times.

Another count loss mechanism, pulse pile-up, occurs when a new event (pulse) can pass through the amplifier when the ADC is still processing a first one. The combination of pulses leads to the count being assigned to another (higher-energy) channel. A hardware setup between these chain elements is usually employed for pile-up rejection [149] but as mentioned by Pommé et al. in [148] it must be distinguished from extending dead-time because during rejection both pulses are being discarded. Several correction methods for both count loss mechanism are compiled and discussed in [148, 150].

A Loss-Free counting module (LFC) is an electronic apparatus designed to insure that at the end of any data acquisition interval, the electronics have accumulated all of the events that occurred regardless of any dead-time that may have been present [68, 151].

The LFC is based on the concept that by adding "n" counts per event to an MCA register, rather than digitizing and storing a single count at a time, a "zero dead time" (ZDT) energy spectrum can be accumulated that assures all counts are included in the spectrum. If "n" is correctly derived, that is n = 1

plus a "weighting parameter" representing the number of events that were lost since the last event was stored, and if the data is truly random in nature, the concept is statistically valid [152].

The factor "n" is derived on a continuous basis by examining the state of the detector amplifier and ADC every 200 ns [68]. The elapsed time during which the amplifier and ADC are processing a pulse provides a measure for the magnitude of the weighting factor, which is updated every 20 ms on average [68].

The scattering of the n factor has been found to be $\approx (n\text{-}1)^{1/2}$ by Pommé et al. in reference [151].

The usual assumption used by all peak fitting algorithms is that of Poisson statistics [153], i.e. the uncertainty of the peak area is proportional to the square root of this area. Unfortunately, the counting statistics of a measurement performed in a LFC detection system cannot be obtained from the corrected spectrum as it has been artificially manipulated. To properly quantify the uncertainty of a histogram-peak (photo-peak), the peak fitting program must have access to both the corrected and the uncorrected spectrum and to take the counting statistics from the latter. Therefore one usually speaks of a "Dual-LFC" spectrum, containing the corrected and uncorrected spectrum parts [68]. The *A*, *C*, *P* and *D* detectors employed in this work employed separate LFC modules model 556A from Canberra (Australia) [67], while the detectors *O* and *E* employed the Lynx Digital Signal Analyzer latest MCA with integrated LFC module from Canberra [69].

For the validation of the dead-time corrections performed by the LFC module of a detector we proceeded with the measurement of the sole photo-peak of a certified ^{137}Cs radioactive source in the presence of low to very high detection dead-times. This is possible by measuring first the ^{137}Cs source alone on a given standardized position and by measuring the same

source but with the incremental addition of other radioactive sources (^{133}Ba and ^{152}Eu) to the setup. For our detector O, the Figure 3.28 shows the observed percent deviation between the expected and actual peak-areas as a function of the detector dead-time. For dead-times between 60 to 80%, the observed deviation was 1 - 1.5% meaning that even under these extreme measuring conditions the accuracy of the determination is not being sacrificed.

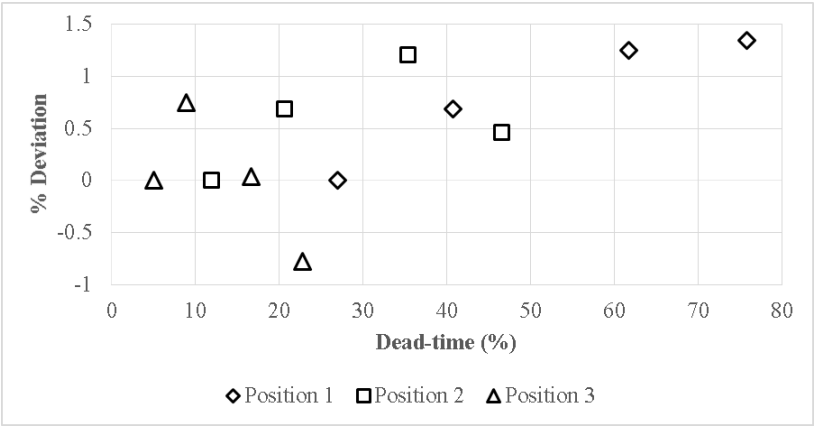

Figure 3.28: Percent deviation in the expected measured activity as a function of the dead-time of the detector O (up to 0.7%, 1.2% and 1.4% for positions 3, 2 and 1; respectively).

4. Other factors affecting the (n,γ) reaction rate

Although the neutron absorption process is the key process in INAA, it is to be expected that sometimes an excess of it can be a serious disadvantage. When irradiating a sample with neutrons, the presence of the nuclei themselves perturbs the neutron fluence rate, and if the sample is not sufficiently small, diluted and homogenous, the inner layers will perceive a lower neutron fluence rate than the outer ones. This effect of fluence rate depression is historically known as "neutron self-shielding" and has been studied widely during the last fifty years.

To avoid this undesired effect, it would be ideal that the sample is made sufficiently diluted and homogenous, guaranteeing that the presence of strong neutron absorbers within the matrix will not alter (shield) the fluence rate significantly. In practice this is not always possible and one must account for this undesired fluence rate depression.

This chapter reviews some methods currently available in the literature for thermal and epithermal self-shielding calculation, focusing on their origins, corrections and/or improvements over time. An experimental validation of these methods by irradiation of different strong thermal and epithermal absorbers with different scattering to absorption cross-section ratios and resonances is performed through the comparison of the calculated results to

experimentally determined ones, aiming at estimating the importance of the phenomena and overall accuracy of each calculation method.

4.1 Thermal neutron self-shielding

4.1.1 Analytical expressions

The first algorithms for modelling this phenomenon were proposed for instance, by Case et al. [154], Dwork [155], Nisle [97], Baumann [99] and were mainly focusing on thermal neutrons. However, scattering effects were neglected in these models.

The research from Stewart and Zweifel [156, 157] is constantly referenced in the literature because they derived "exact" expressions to calculate the perturbed-to-unperturbed thermal reaction rate ratio (or "thermal self-shielding factor"; $G_{th} \leq 1$) for various sample geometries.

The formula derived by Stewart and Zweifel was founded on the assumption that the neutron fluence rate is isotropic and scattering within a body does not change the neutron energy. They also integrated the effects of Doppler broadening and offered a correction for the calculated self-shielding factor when scattering effects are not negligible, based upon Wachspress [158]. The general function proposed in references [156–160] is:

$$G_{th} = \frac{G_0}{1 - \frac{\sum_s}{\sum_t}(1 - G_0)} \tag{4.1}$$

where Σ_s and Σ_t are the scattering and total macroscopic cross-sections (respectively) and G_0 is an initial parameter, a partial self-shielding factor that is calculated without considering scattering in the sample, for the

specific geometry of interest. The geometry-specific G_0 functions were briefly compiled by Gilat et al. [159, 160], Flemming [98] and later integrated by De Corte in reference [13]. For instance, for the following three geometries [98]:

Slab of thickness *d*:

$$G_0 = \frac{1}{x}\left(\frac{1}{2} - E_{3,x}\right)\Bigg|_{x=d\Sigma_a} \tag{4.2}$$

Sphere of radius *R:*

$$G_0 = \frac{3}{x^3}\left(\frac{x^2}{2} - 1 + \left(1+x\right)e^{-x}\right)\Bigg|_{x=2R\Sigma_a} \tag{4.3}$$

Infinite cylinder of radius *R*:

$$G_0 = \frac{2x}{3}\left(y_x - K_{0,x}I_{1,x} + K_{1,x}I_{0,x}\right)\Big|_{x=R\Sigma_a} \tag{4.4}$$

with the auxiliary parameter:

$$y_x = 2\left(xK_{1,x}I_{1,x} + K_{0,x}I_{0,x} - 1\right) + \frac{1}{x}K_{1,x}I_{1,x} \tag{4.5}$$

and the introduction of the Modified Bessel functions of the First and Second kind ($I_{n,x}$ and $K_{n,x}$) and the exponential integral ($E_{n,x}$) which are available in the literature [161–163]. A dimensionless parameter is introduced to replace the independent variable *x* in all relevant formulae:

$$\xi = \frac{2V}{S}\Sigma_a = \frac{2V}{S}\left(\sum_i^n N_A \frac{m_i}{V}\frac{\sigma_{a,i}}{M_i}\right) = \frac{2N_A}{S}\left(\sum_i^n m_i \frac{\sigma_{a,i}}{M_i}\right) \tag{4.6}$$

V and *S* are the volume and surface of the sample and Σ_a is the macroscopic absorption cross-section from *n* contributing absorbers in the sample. The latter value depends on the Avogadro's constant N_A, the microscopic

absorption cross-section σ_a for neutrons at 2200 m/s, molar mass M and elemental mass m of each absorber.

It is straightforward to show that, for eqs. (4.2) to (4.4):

$$\begin{aligned} x_{slab} &= \xi/2 \\ x_{sphere} &= 3\xi \\ x_{cyl,\infty} &= \xi \end{aligned} \tag{4.7}$$

4.1.2 Improvements to the Stewart-Zweifel model

Gilat et al. concluded in references [159, 160] that the scattering correction seldom exceeds 10% and it is important only for highly scattering samples. De Corte et al. agreed with this conclusion during the launch of the k_0-standardization [13]. Scattering effects could be important because the neutrons will lose energy on each collision until they eventually escape the sample region or, reach the specific energy range where their probability of being absorbed is high.

According to eq. (4.1), Stewart and Zweifel assumed that the scattering of neutrons should diminish the thermal self-shielding effect (G_{th}), based on the logical reasoning that a perfect scatterer in an isotropic neutron field has no absorption and thus, no self-shielding, therefore a body that absorbs and scatters neutrons should have intermediate effects. In the case of spherical samples under an impinging neutron beam, Fleming proposed that the total cross-section (absorption plus scattering) should be used instead of the absorption cross-section, although he could not demonstrate this empirical correction. He assumed that the self-shielding would be the same under a neutron beam or an isotropic neutron field because of symmetry considerations [98].

In 1995, Blaauw [164] found that some corrections were needed to eq. (4.6) because experimentally, the scattering in spheres amplified the self-shielding instead of diminishing it. He derived again the relationship provided by Stewart and Zweifel, arriving at the demonstration that the total cross-section rather than only the absorption should be inputted in eq. (4.6), that is, that G_0 needs to be calculated with scattering in mind, giving insight to the discrepancy observed by Fleming. Later on, Blaauw clarifies some concepts about what cross-sections values should be used in these computations [165].

Based on theoretical derivations, experimental results and Monte Carlo data, Blaauw concluded that eq. (4.6) should be replaced by a temperature-dependent expression [165], re-adapted in this work as:

$$\xi_{B,T,s} = b^s \sqrt{\frac{T_0}{T}} \frac{2V}{S} \Sigma_t \tag{4.8}$$

Where $b = 2/\sqrt{\pi}$, $s = 1$ for thin (or small) samples and $s = -1$ for thick (or larger) ones. As before, the resulting partial self-shielding factor G_0 must be later inserted in eq. (4.1) to obtain the final thermal self-shielding correction factor G_{th}.

Recently Trkov et al. [101] compiled the Stewart and Zweifel algorithms (including the correction suggested by Blaauw) into an open-source FORTRAN code. Furthermore, Trkov et al. proposed a fine-tuning for eq. (4.1):

$$G_{th} = \frac{G_0}{1 - W \frac{\Sigma_s}{\Sigma_t}(1 - G_0)} \tag{4.9}$$

which merely consisted in replacing (Σ_s/Σ_t) by $W(\Sigma_s/\Sigma_t)$, where the factor W is an adjustable constant that depends on the irradiation channel configuration. Trkov et al. explained that $W = 1$ matches the original expression and corresponds to an irradiation channel with an isotropic neutron current. For a cylindrical neutron current, the empirical values $W =$

0.93 or W = 0.67 should be used (respectively) for parallel (co-axial) or perpendicularly placed cylindrical samples [101].

4.1.3 A universal curve: The Sigmoid method

The Monte Carlo N-Particle (MCNP) transport code can probably perform the most sophisticated and rigorous computations related to neutron transport, if a detailed and accurate model for the neutron source and sample configuration is inputted. If the desired accuracy is high and computation time is not a problem one should opt for it, but in routine INAA the number of samples to deal with can render it impractical.

In an effort to provide an "universal" curve for self-shielding calculations, Salgado et al. [76, 166] combined eq. (4.1) and Blaauw results for spheres [164], noticing that a sigmoid (or logistic) function with a few empirical parameters can also yield the same results. Per them, G_{th} can be calculated for a variety of samples from:

$$G_{th,S} = \frac{1}{1+\left(\frac{\xi_S}{x_0}\right)^p} \tag{4.10}$$

where the experimentally determined parameters p = 1.061 (or p = 1.009) and x_0 = 0.635 (or x_0 = 0.643) were proposed for cylindrical samples on two different publications [76, 166]. These parameters were obtained after inputting in eq. (4.8):

$$\xi_{S,cyl} = \frac{1}{b}\xi_{B,T_0,s=1}\left(\frac{\Sigma_a}{\Sigma_t}\right)^c = \frac{2V_{cyl}}{S_{cyl}}\Sigma_t\left(\frac{\Sigma_a}{\Sigma_t}\right)^c \tag{4.11}$$

with c = 0.85 ± 0.05. In their work they concluded that the b term is not necessary and can be dropped [76, 166]. However, it must be remarked that their c factor was empirically determined from their fits to the results of

Blaauw [76, 166], who clearly focused on the use of b [164] and that these values are correlated. This also means that eq. (4.10) is related to the algorithm for spheres as proposed by Stewart and Zweifel in references [156, 157].

4.1.4 The Chilian method

Chilian et al. extended the research on the sigmoid function and its applications on the resonance self-shielding phenomena, proposing that one might want to keep x_0 not so universal [77, 78, 104, 167]. They concluded that x_0 could be channel-specific but once determined for a given irradiation channel, the Sigmoid method can be applied to other elements. Additionally, Chilian et al. introduced a similar form of eq. (4.10) for resonance self-shielding calculations and their idea of a channel-specific parameter proved very useful in the experimental determination of "effective" resonance cross-sections [77, 78, 104].

The form of eq. (4.10) proposed by Chilian et al. for thermal self-shielding calculation was not derived in references [77, 78, 104], but one can demonstrate that from eqs. (4.6) and (4.11):

$$\begin{aligned}\xi_{S,cyl} &= \frac{2V_{cyl}}{S_{cyl}}\Sigma_t\left(\frac{\Sigma_a}{\Sigma_t}\right)\left(\frac{\Sigma_a}{\Sigma_t}\right)^{c-1} \\ &= \frac{1}{\pi}\frac{N_A}{r(r+h)}\sum_i^n\frac{m_i\sigma_{a,i}}{M_i}\left(\frac{\Sigma_t}{\Sigma_a}\right)^{1-c}\end{aligned} \tag{4.12}$$

with r the radius and h the height of the cylinder. Chilian et al. first proposed the independent variable:

$$\xi_{Ch} = \frac{N_A}{r(r+h)}\sum_i^n\frac{m_i\sigma_{a,i}}{M_i}\left(\frac{\Sigma_t}{\Sigma_a}\right)^{1-c} \tag{4.13}$$

and assumed that since the scattering is usually negligible, the term between parentheses at the right-hand side of eq. (4.13) could be dropped [104]. By setting c = 1 we obtain:

$$\frac{1}{x_{0,cyl}}\xi_{S,cyl}\Big|_{c=1} = \left(\frac{1}{\pi x_{0,cyl}}\right)\xi_{Ch}\Big|_{c=1} \tag{4.14}$$

Finally, the form of eq. (4.10) proposed by Chilian et al. was:

$$G_{th,Ch} = \frac{1}{1+\left(k_{th}\xi_{Ch}\right)^{p'}} \tag{4.15}$$

where the term defined as k_{th} is the channel-specific constant proposed by Chilian et al. that must be determined [104] with the aid of known neutron absorbers.

In terms of equivalence with the eq. (4.10) from Salgado et al. in [76, 166], although Chilian et al. rather used p' = 0.964 in their research [104], we propose the initial value:

$$k_{th,0} = \left(\pi x_{0,cyl}\right)^{-1} = \left(0.643\pi\right)^{-1} = 0.5 \tag{4.16}$$

in the calculations, per their Sigmoid method. This will allow after few iterations, to determine the "true" or final adjusted k_{th} value for the irradiation channel of interest.

4.2 Epithermal neutron self-shielding

When the fluence rate depression is due to the presence of strong resonance absorbers, that is, an isotope-specific phenomenon, it is known as "epithermal" (or resonance) self-shielding. Resonance neutron capture is a rather complex process. To accurately calculate the self-shielding effects, it is necessary to compute the sample geometry, composition and to model the

neutron transport from the neutron source through the sample with the help of powerful statistical techniques such as Monte Carlo, but this requires a great amount of computing time. Recently, two calculation methods of far more simplicity have been proposed for calculating the shielding effects to expect when irradiating samples of cylindrical shape, which is the sample geometry of practical choice in Neutron Activation Analysis [76–78, 101, 104, 166].

4.2.1 The MatSSF method

The method proposed by Trkov et al. makes use of analytical expressions to determine the ratio of the perturbed-to-unperturbed neutron reaction rates due to resonance capture ($G_e \leq 1$; epithermal self-shielding correction factor) by means of a FORTRAN code [79, 101]. This code employs a library of pre-calculated G_e factors that were tabulated against the microscopic dilution cross-section for the single-resonance absorber $\sigma_0 = \Sigma_0/n$, where n is the number density of the absorber nuclei (absorber per unit volume) and Σ_0 is the macroscopic dilution cross-section for the absorber.

When the sample dimensions and composition are given, a "generalized" mean chord length l is computed and added to the moderator macroscopic cross-section $\sum_m$ in order to obtain the microscopic dilution cross-section σ of the sample [79, 101]:

$$\sigma = n^{-1}\left(\Sigma_m + a^*/l\right) \tag{4.17}$$

In eq. (4.17) a^* is the Bell factor. The G_e factors for the single-resonance absorber are finally obtained by interpolation with the values in the MatSSF library. If necessary, the software employs a Multi-group approximation when other resonance absorbers admixed in the sample can cause interferences, but the Trkov et al. derivations will not be dealt in this work.

The generalized mean chord length l is calculated in MatSSF for three different neutron source-sample configurations (see Figure 4.1):

a) when the source is isotropic (*M0*);

b) when the source is of cylindrical shape and the (cylindrical) sample is oriented perpendicularly (*M1*) or;

c) it is oriented parallel to the source axis (co-axial; *M2*).

For an isotropic neutron fluence rate (*M0*), the generalized mean chord length of a sample of volume V and surface S is calculated as:

$$l_{M_0} = \frac{4V}{S} = \frac{2rh}{r+h} \tag{4.18}$$

with r and h the radius and height of the cylinder.

For the other configurations (*M1* and *M2*) the channel dimensions must be supplied and the shape of l is more complex. For the perpendicular case (*M1*):

$$l_{M_1} = \frac{h(\pi r)^2 y}{2\left((2rh)g_y + \pi r^2\left(\frac{s}{\sqrt{1+s^2}}\right)\right)} \tag{4.19}$$

and for the co-axial case (*M2*):

$$l_{M_2} = \frac{(\pi rh)y\sqrt{1+s^2}}{2hs + \pi r\left(\sqrt{1+s^2}-1\right)} \tag{4.20}$$

With the s, y and g_y auxiliary parameters given by:

$$y = \arctan(s)$$
$$s = \left(\frac{H}{2R}\right) \tag{4.21}$$
$$g_y = \int_0^{\pi/2} d\varphi \int_0^{y} \sqrt{\cos^2\theta\cos^2\varphi + \sin^2\theta}\, d\theta$$

where R and H the radius and height of the cylindrical neutron source.

The adopted Bell factor is identical for the isotropic and co-axial configurations ($a^* = 1.16$) but different for the perpendicular case (see Table 4.1) [79, 101].

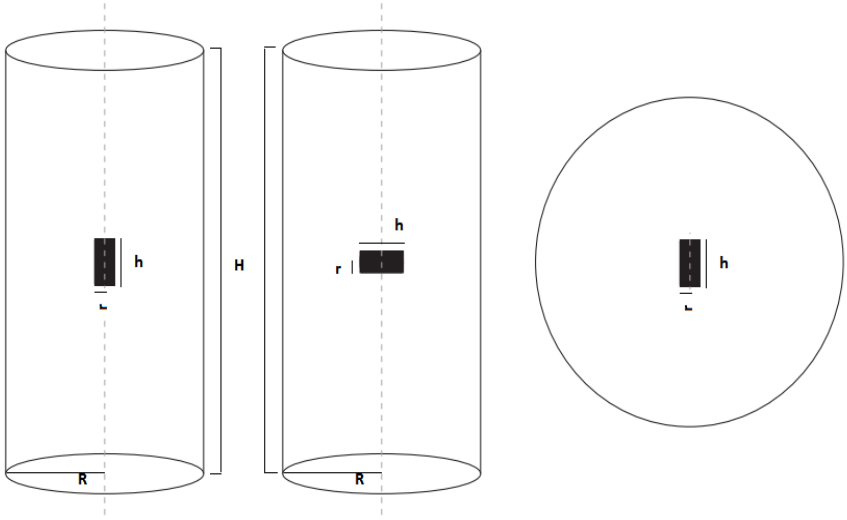

Figure 4.1: The three neutron source-sample configuration in MatSSF [79, 101]**: cylindrical source with sample lying co-axial to the channel axis (left; *M2*), cylindrical source with sample axis perpendicular to the channel axis (middle; *M1*) and, spherical isotropic source (right; *M0*).**

Table 4.1: Bell factor for each neutron source-sample configuration in MatSSF [79, 101].

source-sample configuration	a*
M0 (isotropic)	1.16
M1 (perpendicular)	$1.30 + 0.5\Sigma_s/\Sigma_t$
M2 (co-axial)	1.16

4.2.2 The Sigmoid method for single-resonances

The second method is semi-empirical, introduced and studied by Salgado, Martinho and Gonçalves for different sample geometries and single-resonances [75, 76, 166, 168–171]. It was born from the repeated observations that a Sigmoid (or logistic) function can accurately describe the self-shielding effects for several absorbers with the aid of a few experimentally determined parameters. In terms of a generalized sigmoid function, G_e can be calculated from:

$$G_e = \frac{A_1 - A_2}{1 + \left(\xi_{S,e}\right)^p} + A_2 \tag{4.22}$$

For cylinders, it has been suggested the use of the experimentally determined parameters $A_1 = 1$, $A_2 = 0.06$ and $p = 0.82$. In the case of a single-resonance under an isotropic neutron fluence rate, Salgado, Martinho and Gonçalves introduced the following variable [75, 76, 166, 168–171]:

$$\xi_{S,e} = \frac{1}{z_0} n \frac{2V_{cyl}}{S_{cyl}} \left(\frac{\Gamma_\gamma}{\Gamma}\right)^{1/2} \sigma_{t,res} \tag{4.23}$$

with $\sigma_{t,res}$ being the microscopic total cross-section at the resonance peak, Γ_γ the radiative and Γ the total resonance widths. The value z_0 is found empirically and is in principle different for each sample geometry (spheres, foils, wires, cylinders).

For a cylinder of radius r and height h, it is possible to write eq. (4.23) as a function of the mass of the element m and the isotopic abundance θ with the aid of the molar mass M and Avogadro's number N_A:

$$\xi_{S,e} = \left(\frac{N_A}{M}\frac{m}{r(r+h)}\right)\left(\frac{\theta}{\pi z_0}\right)\sigma_{t,res}\left(\frac{\Gamma_\gamma}{\Gamma}\right)^{1/2} \tag{4.24}$$

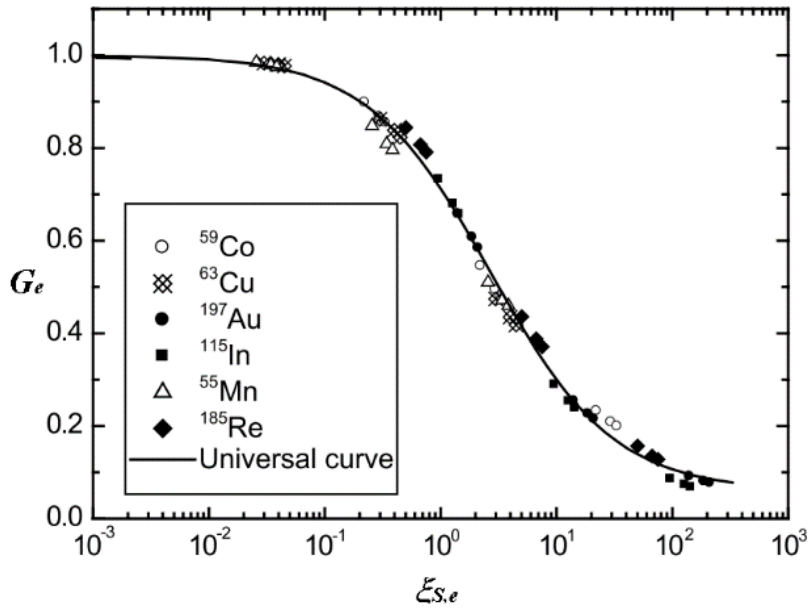

Figure 4.2: The universal or Sigmoid curve for single resonances found by Gonçalves et al. [168].

4.2.3 The Chilian method for multiple resonances

The Sigmoid method for single-resonances was later redefined and further improved by Chilian et al. [78, 104] for samples of cylindrical shape. Chilian et al. proposed to condense the isotope-specific data (right bracket) into a

single composite nuclear constant, an "effective" resonance absorption cross-section $\sigma_{e,abs}$ that accounts for *n*-resonances [104]:

$$\sigma_{e,abs} = \left(\frac{1}{\pi z_0}\right)\theta \frac{\sum_i^n w_i \left(\sigma_{t,res,i}\left(\frac{\Gamma_\gamma}{\Gamma}\right)^{1/2}\right)}{\sum_i^n w_i} \tag{4.25}$$

This parameter could be calculated using the weight factors w_i given in reference [78] exactly as:

$$w_i = \left(\frac{(2J+1)}{(2I+1)}\frac{\Gamma_n}{E_{res}^2}\frac{\Gamma_\gamma}{\Gamma}\right)_i \tag{4.26}$$

with *J* and *I* the spins of the resonance state and target nucleus. The Γ_n is the neutron resonance width and E_{res} is the energy at the peak (centroid) of the resonance.

Experimentally, these $\sigma_{e,abs}$ values can be found by solving eq. (4.24) for cylinders of a pure element having different mean chord lengths. The value z_0 = (2.7/1.65) = 1.636 for cylindrical samples was found by Salgado, Martinho and Gonçalves et al. [75, 76, 166, 168–171] and has been adopted by Chilian et al. on their first generation of calculated and/or experimentally determined $\sigma_{e,abs}$ values [77, 78, 104]. In brief, the latest idea consists in employing these values to obtain the epithermal self-shielding factors from eq. (4.22) after inputting:

$$\begin{aligned}\xi_{Ch,e} &= \left(\frac{N_A}{M}\frac{m}{r(r+h)}\right)k_e\sigma_{e,abs} \\ &= Zk_e\sigma_{e,abs}\end{aligned} \tag{4.27}$$

for the geometry of interest. The left bracket of eq. (4.27) has been associated here as the *Z* variable, an auxiliary parameter that contains information about the sample geometry (i.e. radius, height and mass). The correction factor k_e

was introduced by Chilian et al. to account for possible channel-specific deviations of epithermal neutron spectrum nature that might influence the accuracy of the calculations due to of the adopted effective resonance absorption cross-section. This value might be in principle equal to unity and is believed to be independent of the nature of the moderator/reflector at the irradiation site [78, 104].

4.3 Neutron moderation

Neutron moderation is considered as the reduction of the speed of fast neutrons, thereby turning them into thermal neutrons [102, 103]. Practical conditions of analysis involve irradiation of samples packed into polyethylene (PE) or aluminium containers which might alter the irradiation conditions as compared to the ones at the time of the reactor channel calibration. As such, a systematic error might be introduced in the analytical result if the impact of these containers is not considered.

Figure 4.3 shows the Monte Carlo simulation of paths taken by neutrons of 1 MeV kinetic energy after being scattered and absorbed when entering parallel to the axis of cylinders of different materials [102].

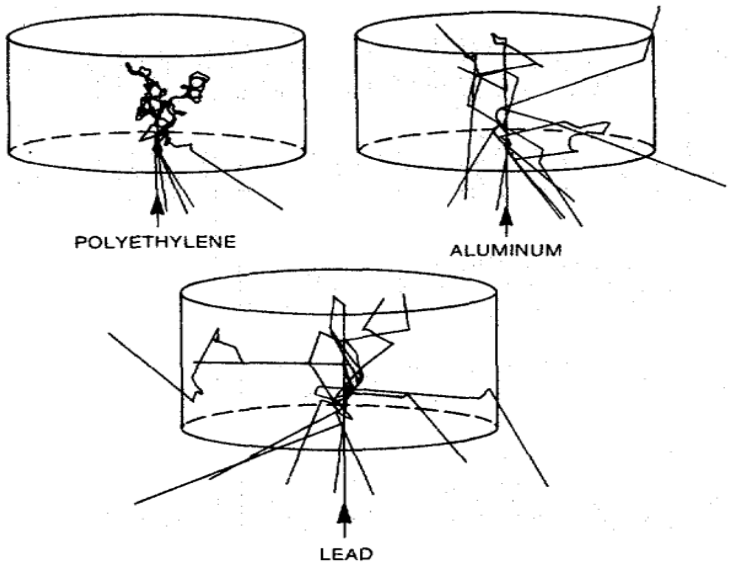

Figure 4.3: Neutrons with 1 MeV kinetic energy are shown entering cylinders of different materials from the bottom (parallel to the cylinder axis) and then being scattered and absorbed. The paths were calculated with the Monte Carlo technique [102]**.**

Under equal conditions of irradiation and measurement, differences in (f, α)-determination between identical sets of bare and PE-covered monitors can only be attributed to neutron moderation and/or shielding effects due to the PE hydrogen-rich content. If the PE is very pure (trace elements are negligible) this should remain the only variable affecting f and α.

4.4 Burn-up effects

Burn-up is defined as the significant disappearance of a target isotope or a directly formed nuclide by further (n,γ) reactions on these nuclides. It is a phenomenon that is limited to a few cases, e.g. the loss of the formed nuclide

^{165}Dy from activation of ^{164}Dy, due to the high σ_0 value for ^{165}Dy, which is of the same order of magnitude as the effective σ_0 (metastable plus ground state) value for ^{164}Dy. Thus, the burn-up effect is mainly sensed for nuclides with high neutron cross-section values or of comparable magnitude to the nuclides involved in the activation-decay chain [13].

The burn-up correction factor F_b is usually introduced into the observed (saturation) γ-ray activity to obtain the "true" A value [13]:

$$A = \frac{A_{obs}}{F_b} \tag{4.28}$$

By assigning "1" to the target isotope and "2" to the formed nuclide, we have, for the case of burn-up of target and/or directly formed nuclide:

$$F_b = \frac{\lambda_2 \exp\left(-R_1' t_i\right)\left[1-\exp\left(\left\{R_1' - R_2' - \lambda_2\right\} t_i\right)\right]}{\left\{R_2' - R_1' + \lambda_2\right\}\left[1-\exp\left(-\lambda_2 t_i\right)\right]} \tag{4.29}$$

For other cases, such as the burn-up of a daughter nuclide, the shape of F_b is more complicated as it is a function of the activation-decay scheme of the nuclides involved. The functions for several cases are compiled for instance by De Corte in reference [13] or in a larger compendium of NAA formulae by Pommé et al in [122]. The impact of burn-up in the ultimate comparator, i.e. ^{197}Au(n,γ)^{198}Au(n,γ) ^{199}Au, for several simulated neutron fluence intensities is given by Pommé et al. in [172] that were later validated by experiments. The burn-up topic will not be dealt with in this work, as it is clear from the same references that the F_b factor would only diverge from unity for neutron fluence rates $\geq 10^{13}$ cm^{-2}.s^{-1}. For instance F_b = 0.976 for a 2.2 x 10^{13} cm^{-2}.s^{-1} fluence rate and ~24 hour irradiation [172].

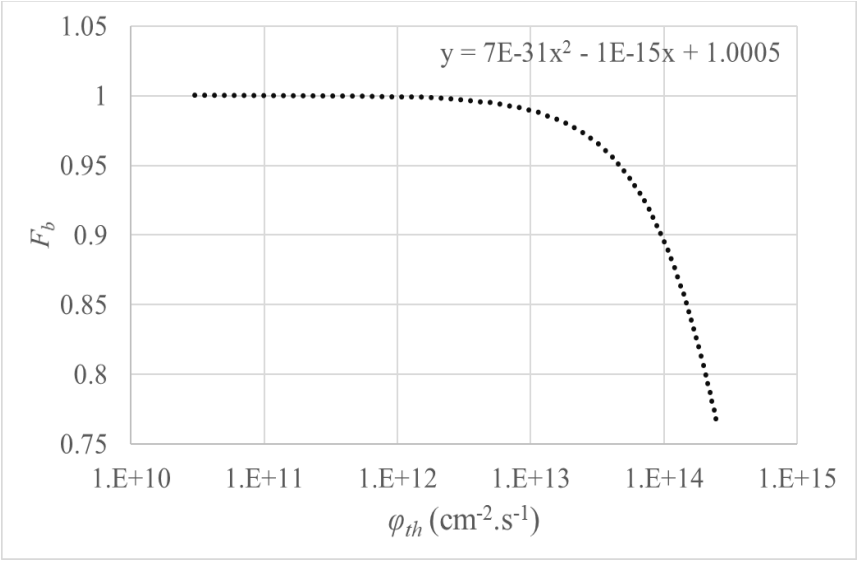

Figure 4.4: Calculated burn-up correction factor for the ^{197}Au(n,γ)^{198}Au(n,γ)^{199}Au as a function of the φ_{th} with the eqs. given by Pommé et al. in [172]**.**

The Figure 4.4 provides a quick formula for computation of the burn-up correction factor for the ultimate comparator reaction as a function of the (conventional) thermal neutron fluence rate. At the institute where our k_0 determination took place the highest employed neutron fluence rate was 2 orders of magnitude lower, i.e. 10^{11} cm^{-2}.s^{-1} and the maximum irradiation time was ~7h. Therefore the value F_b = 1.000 was obtained as expected for ^{198}Au(n,γ) burn-up ($A = A_{obs}$).

4.5 Impact of typical PE-vials in the channel calibration

4.5.1 Experimental

The experiments aimed at studying the impact of typical NAA PE-vials (1 mm wall thickness) in reactor channel characterization (calibration) by applying the (f, α)-determination methods to three different irradiation channels of the BR1 reactor at the SCK•CEN. A given set of fluence rate monitors ranging from low to high Q_0 factors was irradiated: bare, inside PE-vial, bare inside Cd-cover and inside PE-vial placed inside Cd-cover.

The set of monitors (standards) employed for these exercises were Mn, Co, Zn, Zr, Mo, La, Lu and Th. More information about the standards catalog numbers, typical sample masses and sizes and reactions employed in this work can be found later in the text in Table 6.3. Foils of Al-1% Lu were added for reactor-channel temperature monitoring purposes by employing the Westcott factors for ^{176}Lu reported by Holden [16].

The calculation of thermal and epithermal self-shielding correction factors for these monitors was performed using the Chilian method and the MatSSF code developed by Trkov et al. [78, 79, 101]. The G_{th} was found to be ≈ 1 for all materials and with both methods. The G_e factors were quite similar with both methods and lower than 3% for ^{98}Mo although we adopted the MatSSF results as the final ones (see values in Table 6.3). Epithermal self-shielding effects due to the polyethylene components are insignificant (the impurities in the PE are given later in Table 6.2).

We employed the irradiation channels S84, Y4 and X26 for these experiments which are discussed in sections 6.9 and 6.12.

For all irradiation channels an identical set of monitors were irradiated:

1) bare (without covers);

2) inside high-density PE cylindrical vials (~1 mm wall thickness, 950 kg/m^3 density);

3) bare but inside the Cd-cover (1 mm Cd thickness, 20 mm diameter, 40 mm height);

4) inside high-density PE cylindrical vials placed inside the Cd-cover.

These sets were placed inside larger PE irradiation containers. The effects of these larger containers can be incorporated into the channel parameters or vice versa. Since they were present in every single irradiation they will not account for observed differences between bare and PE-covered monitors.

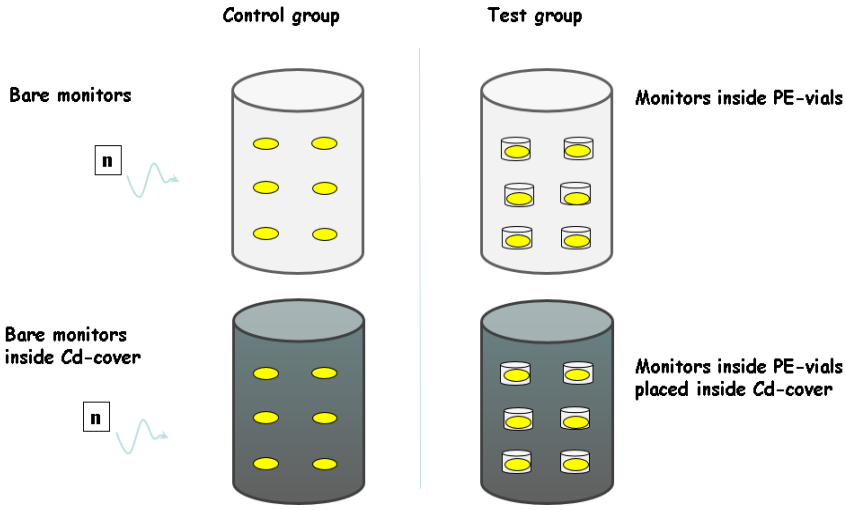

Figure 4.5: Scheme of the irradiation containers and samples packing employed for the investigation of the impact of 1 mm thick vials polyethylene vials. See text for more information.

In channel Y4 the monitors were irradiated for 7 hours which is the maximum irradiation time routinely employed in this channel and because the monitors studied produce medium to long-lived radioisotopes. Although channel S84 is usually employed for the study of short-lived radioisotopes, the irradiations were performed in that channel for 5.5 hours and in channel X26 for 6 hours during the same day to keep uniform the effect of the fluence variability dependence (on the irradiation time) between the different irradiation channels. That is, all replicate sets of monitors should have observed simultaneously the same proportion of fluctuations in the reactor power (neutron fluence rate) at their respective irradiation positions for similar amounts of time.

To reduce the overall uncertainty in the measurement system in terms of detector efficiency, pulse losses, etc., the monitors' γ-ray spectra were taken at 5 HPGe detectors recently re-calibrated (40 to 80% absolute efficiency), equipped with Dual- LFC modules and Lynx® Digital Signal Analysers. The detectors were weekly verified with QA calibrated sources.

About 3-10 measurements per monitor were made at the detector reference position, where gamma-ray cascade coincidence effects are negligible (~27 cm monitor-detector distance), obtaining ≤ 0.3% uncertainty in counting statistics, except for the Cd-covered monitors irradiated in X26, for which we obtained ≤ 1% uncertainty. For the Cd-Ratio method, the measurements were made at the same detector and positions, minimizing the efficiency transfer uncertainty contribution and allowing for measurements at closer monitor-detector distances (better counting statistics). Efficiencies and coincidence factors for the geometries in question were calculated with the KAYZERO/SOLCOI® software [70, 71, 144]. All the required k_0 nuclear data employed in the calculations was adopted from the 2003 recommended k_0-literature [20, 21].

4.5.2 Results

The approach used in this work was to neglect the neutron moderation effects due to the PE-vials in all the calculations. It was expected that the (f, α) calculated values from the PE-irradiations (with or without Cd-covers) would have been noticeably different from the ones calculated from the bare-irradiations (with or without Cd-covers) considered as the "Control group". Specifically, the neutron moderation correction factor G_{mod} can be estimated from:

$$f_{PE} = G_{\text{mod}} f_C \tag{4.30}$$

where the C index corresponds to the Control group.

The Table 4.3, Table 4.5 and Table 4.7 summarize the results of applying the *(f,α)*-determination methods to channels Y4, S84 and X26 (respectively), either by employing the Control group or, by employing only PE-covered samples. The results were obtained with the aid of a home-made software that allowed for large data treatment, specifically developed for the application of the 3 *(f,α)*-determination methods and for the calculation of the associated uncertainties by the error propagation formulae exposed by e.g. De Corte et al. in reference [123]. However the reported uncertainties in f, α for each calibration method were not obtained from standard uncertainties as guided by the reference [109], but were calculated from "estimate uncertainties" (e.g. a half-width or a SD) without the due type-A or type-B evaluation. On the other hand, the "Total" results report the percent SD from averaging the results of the 3 calibration methods and is taken as our best estimate of the uncertainty in these parameters from the irradiation exercises.

The Table 4.4, Table 4.6 and Table 4.8 summarize the relative differences in f and α between the PE-covered monitors and the Control group per each calibration method. The Table 4.2 provides a summary of the relative

differences, reported SD from the calibration methods and test for significance within a 95% confidence level.

In the Cd-Ratio method the PE-covered monitors were compared against their respective PE+Cd-covered monitors as to demonstrate more the impact of the vials in a method that assumes $f = 0$, i.e. the thermal conventional fluence rate is null due to the strong absorption of neutrons from Cd-covers. This latter assumption might not hold because of the thermalization effect on the epithermal and fast neutron fluence rates due to the PE.

Underestimation of α was observed in all the employed methods and in every channel when compared to their respective Control group. This underestimation varied between irradiation channels and chosen method.

Table 4.2: Relative difference Δ between the PE-covered monitors and the Control group, SD from the average of all calibration methods employed and expanded uncertainty *U* from the historic records of independent calibrations performed at the BR1. Significance of the observed relative difference (Δ) and coverage factor k at the 95% confidence level.

Channel		*f*	*FC*	*α*	*Source*
Y4	Δ	7	-6	-28	Table 4.4
	SD	6	2	7	Table 4.3
	U	5.3	5.0 *	5.3	Table 6.4
	k	2.306	4.303	2.306	
	t-statistic	3.05	-5.20	-12.18	
	significant?	Yes	Yes	Yes	
S84	Δ	-4	4	-35	Table 4.6
	SD	3	2	35	Table 4.5
	U	3.6	5.0 *	50	Table 6.4
	k	2.517	4.303	2.517	
	t-statistic	-2.80	3.46	-1.76	
	significant?	Yes	No	No	
X26	Δ	6	-6	-11	Table 4.8
	SD	7	2	14	Table 4.7
	U	61.4 *	5.0 *	34.8 *	Table 4.7
	k	12.41	4.303	4.303	
	t-statistic	10.64	-5.20	-1.36	
	significant?	No	Yes	No	

* From N = 3 and N = 2 independent calibrations.

The "t-statistic" refers to the two-tailed t-test.

Channel Y4

Per Table 4.4 and the Bare method, the relative 8% difference in α is statistically significant when considering U = 5.6% (k=2.306) from Table 6.4 (historic records). Per the Cd-Ratio and Cd-covered methods the impact of the PE was very significant, with a 40% decrease in α when considering isotopes belonging to either the low or high Q_0 factor categories. When averaging over all methods employed in Y4, the total underestimation on α of about 30% is statistically significant either by considering the uncertainties in Table 6.4 or Table 4.3.

A relative difference of ~7% was observed for the f parameter (i.e. G_{mod} = 1.07). This difference is statistically significant at the 95% confidence level if one adopts U = 5.6% (k = 2.306) from Table 6.4 as the best estimate uncertainty for this parameter.

A positive bias in f and a negative one in α was also observed for Y4 as reported by Vermaercke et al. [173, 174] when synthetic multi-element standards irradiated under PE-vials were compared to results from bare-irradiated Au - Zr foils, although to a higher degree (43%) than in the present work (30%). In their study, a 3% impact on isotopes with either low or high Q_0 was expected in calculated elemental concentrations for a 15% overestimation on f. The reason for their higher discrepancies in α can be due to the use of bigger samples for reactor characterization: 10 mm length for SMELS compared to 0.1 mm for foils. This assumption is based on the logic that the larger the sample, the higher the PE amount directly influencing the neutron fluence in the sample matrix.

The temperature for this channel was found to be 27 ± 2°C therefore no impact due to the ^{197}Au deviation from the ~1/v law was expected in our results (Westcott factor ~1) [13, 16, 48]. Furthermore, any non-1/v deviation should have the same effect for PE-covered monitors and the Control group.

Channel S84

For a more "epithermal" channel like S84 (see Table 4.6) the Bare method based on low-to-mid Q_0 factors (up to ^{198}Au; Bare A) reported a 50% underestimation on α when employing PE-covered monitors. The Cd-methods for channel S84 showed differences in α of 15 to 35%. These results are not statistically significant at the 95% confidence level if one considers U = 50.1% (k=2.571) from the historic records of Table 6.4 or the 35% SD reported in Table 4.5. The low f and α observed in this channel bears an inherently high uncertainty as shown from eqs. (2.154) to (2.156).

On the contrary, the 4% discrepancy in f for PE-covered monitors is statistically significant at the 95% confidence level (G_{mod} = 0.96) if one considers a U = 3.6% (k=2.571) from Table 6.4. When ^{56}Mn is used as the "reference" isotope we observed a relative difference of 8% in this parameter, probably due to its low Q_0 factor and therefore its greater sensitivity to the PE impact inside the Cd-cover (if $f \neq 0$). Hence, for ^{56}Mn as reference monitor the discrepancy in f is also statistically significant.

The temperature for this channel was found to be 50 ± 4 °C, which is consistent with the fact that this channel is very close to the reactor core. A 1% 1/v-law deviation for ^{197}Au was taken into account in the calculations [16, 48].

Channel X26

The Table 4.8 illustrates that for channel X26 the relative differences on f and α of 6% and 11% (respectively) between the Control group and PE-covered monitors were not statistically significant per any calibration method given the respective 7% and 14% SD reported in Table 4.7. Since there is historic record for this channel, no comparison can be made with a better estimate of the uncertainty for these parameters.

For the Bare A method, the underestimation in α was 15% and the overestimation in f was 14% (G_{mod} 1.14), while for the Bare B method the differences were lower but both differences are not statistically significant as previously mentioned. It was observed that the f-determination per the Bare method formulae is strongly α-sensitive for such channel: a 40% lower input α-value used for the iteration translates into a 30% higher f, and that the Cd-based methods gave lower relative differences, considering that there is no special reason for which an analyst would pick a specific Bare A or Bare B monitor set combination. This confirms the conclusions by Dung and Sasajima [175] that the Cd-based methods are better suited for characterizing channels with $f \geq 70$ and $\alpha \geq 0.10$. The Cd-subtraction technique is also better suited for k_0 determination on these channels since it makes no use of f and α in the calculations and is not sensitive to the correlation between these parameters. The neutron temperature was 25 ± 2 °C, therefore there was no expected impact on ^{198}Au production from its Westcott factor [16, 48].

From Table 4.2 and the significances observed for channels Y4 and S84 is possible to assume that the presence of PE-spacers inside Cd-covers does thermalize further the epithermal and fast fluence rates before they arrive at the sample. It seems a better option to avoid the use PE-vials inside Cd-covers.

The impact of the PE vial on normal irradiations, i.e. typical irradiations without Cd-covers, can be estimated when comparing the f and α value

obtained from the Cd-ratio of the Control group against the one resulting from the Cd-ratio of the PE-covered monitors vs. the Cd-covered bare monitors of the Control group.

When comparing the PE results from Figure 4.6 to the ones obtained from the Control group (see Figure 4.7), it can be seen that for channels S84, Y4 and X26, the net impact of the PE-vials on the α values resulted in net differences of 0.5%, 1% and -1.6% respectively, meaning that the PE-vials did not affect α significantly under normal irradiation conditions (bare irradiations). The f parameter for each case can be extracted from the "intercepts" in Figure 4.6 and Figure 4.7.

Using eq. (4.30) we obtained from the PE vials against the bare monitors G_{mod} = 0.995 for S84 and G_{mod} = 0.990 for Y4 and G_{mod} = 1.009 for X26. Thus, the net impact of these PE vials seems negligible in normal irradiations and is observable (although not significant) when PE-vials are employed inside Cd-covers in ENAA. However, the uncertainty on the determined G_{mod} values (~7%; 2s) is much higher than the observed ≤1% net moderation and the result is not conclusive. A net decrease in f would physically mean that there was more net gain on epithermal neutrons due to fast neutrons moderation than gain on thermal neutron fluence rate. The epithermal neutron fluence rate was: ϕ_e ~1x10^{10} cm^{-2}.s^{-1} for channel Y4, ϕ_e ~1x10^{10} cm^{-2}.s^{-1} for channel S84 and ϕ_e ~7.5x10^{8} cm^{-2}.s^{-1} for channel X26.

Op De Beeck [176] observed that the "average" α-value derived from a log-log plot like equation (2.147) is not a good approximation of the actual α-value because the increase on α with neutron energies is not negligible for large positive α-values. In our experiments, with $\alpha \approx 0.12$ and up to neutron energies of 6260 eV, this effect was not confirmed.

Finally, the observed f and α values for channels Y4 and S84 were in good agreement with previously reported values listed in Table 6.4 from other authors. This is especially true with the latest 2006 values were the latest

recommended k_0-nuclear data was employed at the time. This is logical since the BR1 has not changed its configuration significantly in the last decades.

Table 4.3: Results from (*f*, *α*)-determinations performed on channel Y4 by employing the Control group and the PE-covered monitors (with or without Cd-covers).

			Control group (%; 1*s*)				PE-covered (%; 1*s*)			
	Set	vs. Ref.	*α*	*f*	*FC* [a]		*α*	*f*	*FC* [a]	
Bare	^{233}Pa	^{95}Zr	0.063 (9)	38.9 (8)	2890		0.062 (9)	40.5 (8)	2800	
	^{198}Au	^{56}Mn	0.061 (9)	39.6 (8)	2850		0.054 (9)	43.1 (9)	2656	
	^{99}Mo	^{60}Co	0.060 (9)	39.8 (8)	2832		0.056 (10)	42.4 (9)	2695	
	^{97m}Nb	^{140}La	0.063 (9)	39.0 (8)	2884		0.057 (9)	42.0 (9)	2710	
		^{65}Zn	0.063 (7)	39.0 (8)	2880		0.055 (7)	41.0 (7)	2750	
		^{69m}Zn	0.063 (9)	39.1 (8)	2884		0.060 (9)	40.8 (8)	2770	
		Total	0.062 (9)	39.2 (8)	2870		0.057 (10)	41.6 (8)	2730	
Cd-Ratio		Low Q_0 [b]	0.073 (7)	36.5 (5)	3074		0.044 (7)	38.8 (5)	2877	
		High Q_0 [b]	0.052 (9)	39.2 (5)	2815		0.032 (17)	40.5 (5)	2670	
		All except ^{97m}Nb	0.069 (5)	37.0 (2)	3023		0.040 (6)	39.7 (3)	2800	
Cd-Covered		All except ^{97m}Nb	0.065 (5)		2922		0.044 (5)		2800	
		^{198}Au, ^{233}Pa, ^{99}Mo	0.067 (7)		3053		0.040 (6)		2791	
	Total		**0.065 (7)**	**38.1 (6)**	**2938**		**0.047 (7)**	**40.7 (6)**	**2777**	

[a] *FC* or "comparator" factor, directly proportional to the conventional epithermal fluence rate [12]. The typical standard uncertainty is $u(F_C) \approx 2\%$.

[b] Isotopes with low Q_0 factors are less sensitive to epithermal neutrons. High Q_0 means more epithermal (and overall) sensitivity [3,6].

Table 4.4: Percent relative differences (Δ) in *f*, *α* and *FC* values obtained from the PE-covered monitors as compared to the Control group, for the same irradiation position of channel Y4 (see Table 4.3).

			Δ (%)		
	Set	**vs. Ref.**	Δ_f	Δ_{FC}	Δ_α
Bare	^{233}Pa	^{95}Zr	4	-3	-2
	^{198}Au	^{56}Mn	9	-7	-11
		^{60}Co	6	-5	-7
	^{99}Mo	^{140}La	8	-6	-10
		^{65}Zn	5	-5	-13
	^{97m}Nb	^{69m}Zn	4	-4	-5
	Total		6	-5	-8
Cd-Ratio	Low Q_0		6	-6	-40
	High Q_0		3	-5	-38
	All except ^{97m}Nb		7	-7	-42
Cd-Cov.	All except ^{97m}Nb			-4	-32
	^{198}Au, ^{233}Pa, ^{99}Mo			-9	-40
	Total		**7**	**-6**	**-28**

Table 4.5: Results from (*f*, *α*)-determinations performed on channel S84 by employing the Control group and the PE-covered monitors (with or without Cd-covers). Symbols explained in Table 4.3.

			Control group (%; 1*s*)			PE-covered (%; 1*s*)		
	Set	**vs. Ref.**	***α***	***f***	***FC***	***α***	***f***	***FC***
Bare A	^{233}Pa, ^{198}Au	^{56}Mn	-0.040 (11)	17.3 (2)	2880	-0.021 (11)	16.0 (2)	3100
		^{60}Co	-0.042 (11)	17.0 (4)	2900	-0.019 (10)	16.2 (2)	3052
		^{140}La	-0.040 (11)	17.5 (2)	2865	-0.018 (12)	16.4 (3)	3028
		^{69m}Zn	-0.041 (12)	17.5 (3)	2894	-0.016 (14)	17.0 (3)	2981
		^{95}Zr	-0.041 (12)	17.3 (2)	2890	-0.018 (12)	16.6 (2)	3019
	Total		-0.041 (11)	17.3 (3)	2886	-0.018 (12)	16.4 (2)	3036
Bare B	^{99}Mo, ^{97m}Nb	^{56}Mn	-0.003 (75)	16.2 (2)	3100	0.005 (44)	15.0 (2)	3300
		^{60}Co	-0.003 (75)	16.2 (2)	3102	0.002 (66)	15.5 (3)	3200
		^{140}La	-0.003 (80)	16.2 (2)	3108	0.002 (66)	15.6 (3)	3200
		^{69m}Zn	-0.007 (30)	17.0 (2)	3006	-0.003 (66)	16.6 (2)	3080
		^{95}Zr	-0.012 (17)	17.8 (3)	2928	-0.007 (34)	17.0 (3)	3027
	Total		-0.006 (60)	16.7 (2)	3049	0.000 (56)	15.9 (3)	3161
Cd-Ratio	^{60}Co,^{65}Zn,^{69m}Zn ^{198}Au,^{233}Pa		-0.023 (7)	18.5 (2)	2802	-0.022 (10)	17.9 (3)	2910
	Previous + ^{95}Zr		-0.010 (11)	17.7 (3)	2900	-0.008 (16)	16.9 (3)	3026
Cd-Cov.	^{60}Co,^{65}Zn,^{69m}Zn ^{198}Au,^{233}Pa		-0.022 (11)		2820	-0.019 (10)		2930
	Previous + ^{95}Zr^{P}		-0.012 (15)		2900	-0.008 (16)		3026
	Total		**-0.019 (17)**	**17.6 (3)**	**2893**	**-0.013 (35)**	**16.8 (3)**	**3015**

Table 4.6: Percent relative differences (Δ) in *f*, *α* and *FC* values obtained from the PE-covered monitors as compared to the Control group, for the same irradiation position of channel S84 (see Table 4.5).

			Δ (%)		
	Set	**vs. Ref.**	Δ_f	Δ_{FC}	Δ_α
Bare A	^{233}Pa, ^{198}Au	^{56}Mn	-8	8	-48
		^{60}Co	-5	5	-55
		^{140}La	-6	6	-55
		^{69m}Zn	-3	3	-61
		^{95}Zr	-4	4	-56
		Total	-5	5	-55
Bare B	^{99}Mo, ^{97m}Nb	^{56}Mn	-7	6	-267
		^{60}Co	-4	3	-167
		^{140}La	-4	3	-23
		^{69m}Zn	-2	2	-53
		^{95}Zr	-4	3	-41
		Total	-4	4	-110
Cd-Ratio	^{60}Co,^{65}Zn,^{69m}Zn ^{198}Au,^{233}Pa		-4	4	-4
	Previous + ^{95}Zr^{Sa95}Zr		-5	4	-20
Cd-Covered	^{60}Co,^{65}Zn,^{69m}Zn ^{198}Au,^{233}Pa			4	-14
	Previous + ^{95}Zr			4	-33
Total			**-4**	**4**	**-35**

Table 4.7 Results from (*f*, *α*)-determinations performed on channel X26 by employing the Control group and PE-covered monitors (with or without Cd-covers). Symbols explained in Table 4.3

			Control group (%; 1*s*)			PE-covered (%; 1*s*)		
	Set	**vs. Ref.**	***α***	***f***	***FC***	***α***	***f***	***FC***
Bare A	^{99m}Tc	^{95}Zr	0.116 (9)	98 (8)	177	0.101 (7)	110 (6)	163
		^{95}Nb	0.118 (9)	96 (8)	185	0.097 (7)	112 (8)	160
	^{99}Mo	^{60}Co	0.138 (12)	83 (7)	207	0.102 (13)	108 (6)	164
	^{97m}Nb	^{140}La	0.130 (14)	90 (7)	192	0.108 (16)	103 (9)	171
		^{65}Zn	0.120 (10)	96 (7)	182	0.117 (13)	99 (10)	180
	^{97}Nb	^{69m}Zn	0.125 (10)	93 (7)	188	0.112 (15)	100 (8)	176
	^{198}Au							
	Total		0.125 (11)	93 (7)	189	0.106 (12)	105 (7)	169
Bare B	Low Q_0	^{198}Au	0.115 (15)	97 (9)	182	0.110 (33)	99 (9)	180
		^{97m}Nb	0.132 (8)	93 (8)	190	0.141 (7)	90 (8)	196
		^{99m}Tc	0.116 (15)	97 (9)	180	0.101 (17)	101 (9)	176
	Total		0.121 (13)	95 (7)	184	0.117 (22)	97 (8)	184
Cd-Ratio	All		0.125 (7)	83 (5)	217	0.112 (6)	86 (6)	205
Cd-Covered	All		0.129 (6)		218	0.107 (6)		200
Total			**0.125 (10)**	**90 (7)**	**202**	**0.111 (14)**	**96 (7)**	**190**

Table 4.8: Percent relative differences (Δ) in *f*, *α* and *FC* values obtained from the PE-covered monitors as compared to the Control group, for the same irradiation position of channel X26 (see Table 4.7).

			Δ (%)		
	Set	**vs. Ref.**	Δ_f	Δ_{FC}	Δ_α
Bare A	^{99m}Tc	^{95}Zr	12	-8	-13
	^{99}Mo	^{95}Nb	17	-14	-18
		^{60}Co	30	-21	-26
	^{97m}Nb	^{140}La	14	-11	-17
		^{65}Zn	3	-1	-2
	^{97}Nb	^{69m}Zn	8	-6	-10
	^{198}Au				
		Total	14	-10	-15
Bare B	Low Q_0	^{198}Au	2	-1	-4
		^{97m}Nb	-3	3	7
		^{99m}Tc	4	-2	-13
		Total	1	0	-3
Cd-Ratio		All	4	-6	-10
Cd-Covered		All		-8	-17
	Total		**6**	**-6**	**-11**

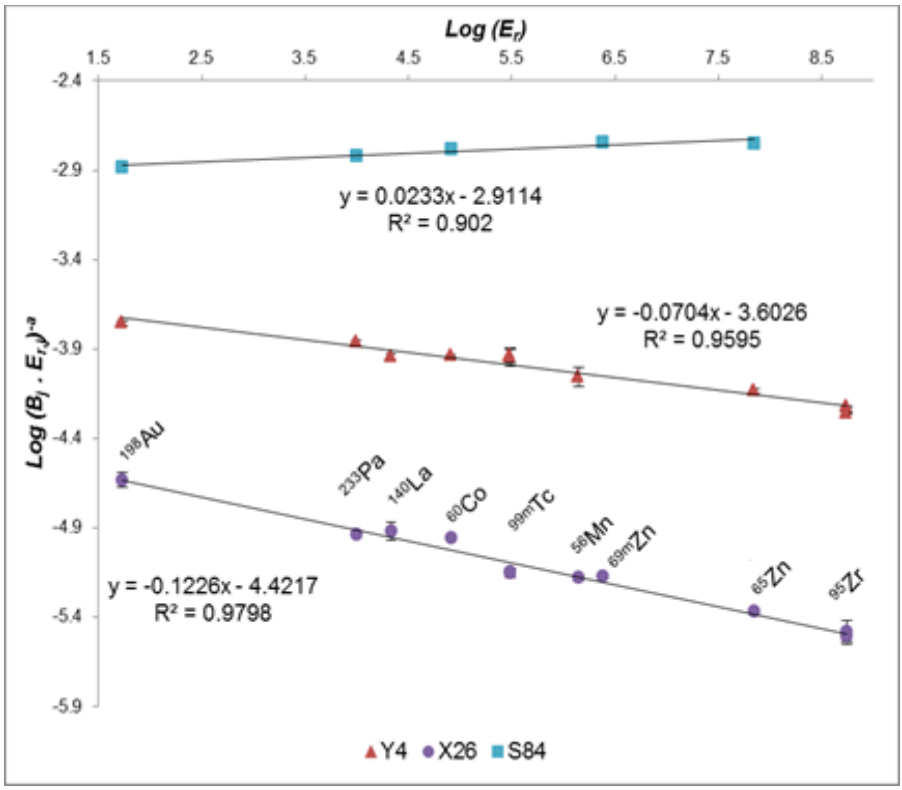

Figure 4.6: Results from the Cd-Ratio method applied to the Y4, X26 and S84 irradiation channels from the PE-covered monitors against (bare) monitors inside a Cd-cover.

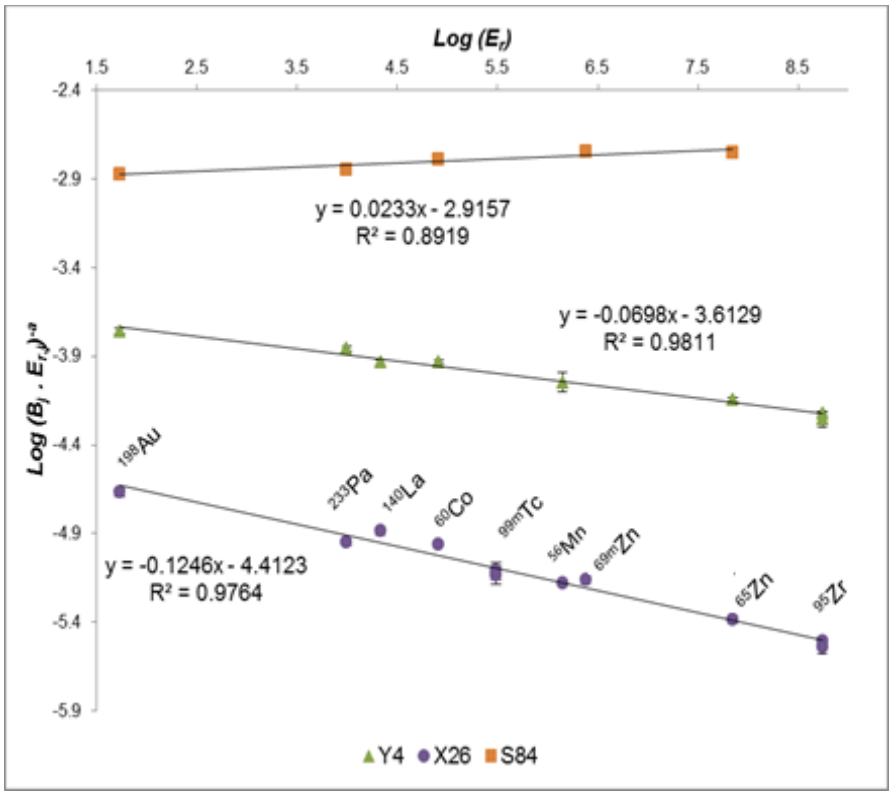

Figure 4.7: Results from the Cd-Ratio method applied to the Y4, X26 and S84 irradiation channels from the Control group (bare samples only).

4.5.3 Conclusions

The overall impact of neglecting the moderation effects due to the employment of PE vials (~1 mm thick) showed an obvious inconsistency in the results between the Bare and Cd-based methods for any given channel. These inconsistencies were statistically significant for channels Y4 and S84 when one considers the expanded standard uncertainty *U* obtained from different calibrations performed by different authors from 1992 until the realization of this work (2012). However, the discrepancies were not statistically significant for *f* when considering the high observed SD between the calibration methods in this exercise. The PE impact was particularly observable from the SD of Cd-covered samples packed inside PE-vials, i.e. PE-covered ENAA probably due to the thermalization of the epithermal and fast fluence rates, resulting in a $f \neq 0$ contrary to the ideal situation. It is recommendable that all (f, α)-determination must be pooled and thin monitors should be employed for channel characterization if the use of PE-vials is unavoidable and cannot be accounted for, to obtain a better estimate of the true f and α channel-specific parameters. An estimated 1% of effective thermal moderation effect was observed by use of this kind of PE vials under normal NAA (not involving Cd irradiations), i.e. these PE vials will not affect the analytical results in normal NAA.

The use of PE-vials could pose a threat to the accuracy of the analytical results, for instance when only one (f, α)-determination method is applied for channel characterization with bare monitors and later, the analyst employs these PE-containers for the irradiation of unknown samples. It follows that the analyst should employ the PE-covered monitors for reactor calibration if he/she intends to use these PE-covers for routine analysis.

Irrespective of the chosen method and its accuracy and considering that the set of monitors fully covered the thermal and epithermal neutron spectrum, the following behaviour was observed:

First, in channels with low or high *f* and α-values (S84 or X26; our extreme channels), the Cd-based methods were less sensitive to the PE-vial impact, giving a lower relative difference to the "true" α value (from our Control group) than the Bare method. In the case of high *f* this confirms the observations reported by Dung and Sasajima [175]. In contrast, for a channel with average *f* and α-values (Y4), the Bare method gave lower relative differences to the Control group values than the Cd-based methods. The same effect was observed in a previous work by Vermaercke et al. [173, 174] when using more bulky synthetic multi-elemental standards inside PE-vials for channel calibration, although their observed variation in the *f* and α values was higher, probably due to their use of bigger samples and thus bigger PE-containers.

Secondly, the *f* and α values obtained for three different channels confirmed once more the consensus: higher neutron thermalization (high *f*) yields a higher α-value (viewed as a softening of the epithermal spectrum) while more "epithermal" channels can even have negative α-values (viewed as a hardening of the epithermal spectrum).

4.6 Variability of the neutron fluence

The Table 4.9 shows the observed variation in the epithermal fluence rate of channel Y4 during a 9-month period between September 2011 and June 2012 (3 seasons; A, B and C). The results were obtained from the monitoring of bare and Cd-covered ultimate comparators (IRMM-530R; Table 6.3) at 3 different positions within a rabbit (Top, Middle and Bottom). A description of the rabbits is given in 6.10. The variation is reported as the SD in the φ_e results between 2 monitors that were irradiated separately but in the same position within a rabbit for 2 randomly-picked dates of each season. The results are given for the 4 rabbit irradiation positions in the metal ship shown

in Figure 4.8. Similarly, the Table 4.10 reports the SD in the φ_e results between 12 randomly-picked monitors during the full 9-month period for each monitor position inside the rabbit.

4.6.1 Spatial variability in the neutron fluence

The Table 4.9 also provides the combined spatial φ_e variability observed at the irradiation geometry in terms of the observed SD along the axis of each rabbit and radially between all 4 rabbit irradiation positions. These values are tabulated as Axial and Radial SD (respectively). Therefore, channel Y4 fluence stability is demonstrated close to the core and middle of the BR1 reactor. It is sufficient to extend the validity of these results to the other channels as well. Axially and radially, a maximum 0.5% SD was observed for the 4 rabbit irradiation positions.

4.6.2 Temporal variability in the neutron fluence

Since in Table 4.10 the comparison of φ_e values was made between monitors at the same position within a rabbit, the $\leq$ 0.5% SD gives an indication of the temporal variability in the neutron fluence, but one has to consider that this SD also contains other significant sources of variability such as counting geometry (different detectors), moderator temperature and counting statistics that should be subtracted [177]. The SD was also $\leq$0.5% for Cd-covered irradiations.

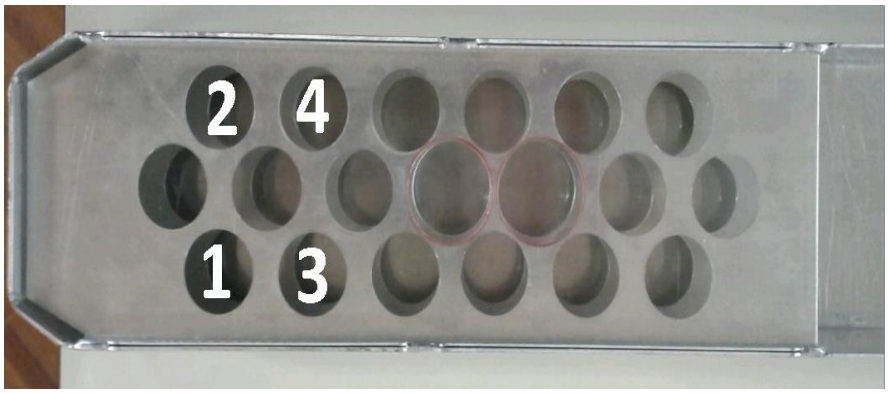

Figure 4.8: Metal ship (irradiation main container) on which the rabbits containing the samples were always placed (holes 1, 2, 3 and 4) for irradiations on channel Y4. The use of these four positions simultaneously was avoided, to minimize the impact on the neutron fluence rate due to the presence of a contiguous rabbit. Therefore, either positions 1 and 4 were employed simultaneously or positions 2 and 3 were used instead (two-rabbit irradiations). The α value for channel Y4 corresponds to the average result from these four positions, by monitors irradiated under the same pattern. Inclusion of rabbits/samples from routine analysis experiments by third parties was also avoided and, when not possible, the holes at the far right were used for these experiments.

Table 4.9: SD (in %) in the conventional epithermal fluence rate (φ_e) of channel Y4 as determined by 2 monitors irradiated separately in time but at the same position, for each of the 3 different positions employed within a rabbit (Top, Middle and Bottom) and for the 4 rabbit irradiation positions depicted in Figure 4.8. Values reported for bare (N) and Cd-covered (E) irradiations on 3 different periods/seasons (A, B, C) with the ultimate comparator as the fluence monitor (IRMM-530R; Table 6.3).

	Position 1		**Position 2**		**Position 3**		**Position 4**		***Radial SD %***	
Period – Rabbit Position	***N***	***E***	***N***	***E***	***N***	***E***	***N***	***E***	***N***	***E***
A - Top	0.4	0.3	0.5	0.4	0.4	0.3	0.5	0.3	***0.4***	***0.4***
B - Top	0.4	0.5	0.2	0.2	0.4	0.5	0.2	0.4	***0.4***	***0.5***
C - Top	0.5	0.5	0.4	0.5	0.2	0.3	0.1	0.5	***0.4***	***0.4***
A - Middle	0.4	0.5	0.3	0.3	0.4	0.5	0.5	0.3	***0.5***	***0.4***
B - Middle	0.4	0.3	0.4	0.3	0.5	0.3	0.3	0.1	***0.5***	***0.2***
C - Middle	0.2	0.5	0.4	0.4	0.4	0.5	0.2	0.3	***0.5***	***0.3***
A - Bottom	0.4	0.5	0.3	0.4	0.2	0.3	0.2	0.3	***0.4***	***0.3***
B - Bottom	0.5	0.4	0.2	0.3	0.4	0.4	0.1	0.5	***0.4***	***0.4***
C - Bottom	0.3	0.3	0.4	0.3	0.4	0.5	0.3	0.4	***0.5***	***0.3***
Axial SD %	***0.5***	***0.4***	***0.4***	***0.3***	***0.4***	***0.5***	***0.3***	***0.4***		

A = September-December 2011 (Fall); B = January-March 2012 (Winter); C = April–June 2012 (Spring).

N = bare irradiation; E = Cd-covered irradiation

Radial SD = SD between the results of all 4 rabbits at a given period for monitors at the same location within a rabbit.

Axial SD = SD between the results for the different periods (A, B and C) for all the monitors inside a given rabbit.

Table 4.10: SD (in %) in the conventional epithermal fluence rate (φ_e) of channel Y4 as determined by 12 monitors irradiated separately in time but at the same position for each of the 3 different positions within a rabbit (Top, Middle and Bottom) and for the 4 rabbit irradiation positions depicted in Figure 4.8. Values reported for bare (NAA) and Cd-covered (ENAA) irradiations performed during 9 months with the ultimate comparator as monitor (IRMM-530R; Table 6.3).

	Position 1		**Position 2**		**Position 3**		**Position 4**	
Rabbit Position	***NAA***	***ENAA***	***NAA***	***ENAA***	***NAA***	***ENAA***	***NAA***	***ENAA***
Top	0.4	0.5	0.5	0.5	0.4	0.5	0.4	0.3
Middle	0.4	0.5	0.5	0.5	0.5	0.5	0.4	0.2
Bottom	0.5	0.4	0.4	0.5	0.4	0.3	0.4	0.3

4.7 Threshold interferences

The Table 4.11 compiles the threshold and primary reactions employed in this work for the determination of the thermal-to-fast conventional neutron fluence rate ratio *L* for channels S84, Y4 and X26 during the years 2006 and 2011. These *L* parameters were calculated by means of eqs. (2.112) and (2.115) when inputting the quoted $\delta_{x,y,z}$ values of Table 2.5 and Table 2.6, with the aid of I_γ and $T_{1/2}$ values from references [6, 8, 20]. The relative uncertainty in *L* factors is estimated at 10% at the 1*s* confidence level, based on a 6% relative uncertainty in R_H, a 7% uncertainty in $\delta_{x,y,z}$ and a 4% uncertainty contribution from other terms, such as e.g. the fast neutron self-shielding correction factor and activities ratios.

When comparing the 2006 average and SD value of L = 18.3(17) with the 2011 value of L = 24.3(26) for channel S84 (at the 1*s*), the 30% relative increment in the magnitude of *L* from 5 years ago suggests that there has been a decrease in the fast fluence rate since then because the thermal-to-

epithermal conventional fluence rate ratio has fluctuated just 5% as shown in Table 6.4 and as discussed in that section. However, the difference in L results is statistically not significant at the 95% confidence level considering that we only have 2 records. Between 2006 and 20011, the channel Y4 shows a relative increment of 15% in the magnitude of the L parameter, clearly not significant at 95% confidence level as well because of the previous reason. There is no L history for channel X26 before 2011.

In this work we employed the Cd-subtraction technique or eq. (2.60) to determine the $k_{0,true}$ value for the $^{116}Sn(n,\gamma)^{117m}Sn$ reaction, that is, without contributions from the interfering $^{117}Sn(n,n')^{117m}Sn$ reaction, since the fast component of the induced activity is subtracted along its epithermal part. Next, by adopting its Q_0 factor from the recommended literature [20, 23] (or $Q_{0,true}$), the $k_{0,int}$ value was calculated according to eq. (2.37). From the ratio between corrected and uncorrected k_0 factors and the $\delta_{x,y,z}$ values from Table 2.6, it was possible to find the L parameter for channels Y4 and X26 (see Table 4.11), and to estimate later a correction for our Q_0 results from the Cd-ratio and eq. (2.118).

The L parameter from channel Y4 was also found by means of the threshold reactions $^{27}Al(n,\alpha)^{24}Na$ and $^{58}Ni(n,p)^{58}Co$. The $^{27}Al(n,\alpha)^{24}Na$ reaction might have been interfered by activation of trace Na content in the sample, which could explain its higher result (10%) as compared to the ^{58}Co and ^{117m}Sn ones. For this reason, the L value from the $^{27}Al(n,\alpha)^{24}Na$ threshold reaction was not employed in our calculations, but just as a validation of the magnitude of our employed ^{58}Co and ^{117m}Sn average and SD of $L = 100 \pm 3$.

With the aid of these L parameters, the $Q_{0,true}$ factors for the $^{134}Ba(n,\gamma)^{135m}Ba$ and the $^{86}Sr(n,\gamma)^{87m}Sr$ interfered reactions we found after by performing the correction described in eq. (2.118). The $k_{0,true}$ factors were found by the Cd-subtraction technique. On the other hand, from the ^{135m}Ba corrected results it was possible to calculate the L value for the irradiation channel S84, as shown in Table 4.11.

The Table 4.12 shows the neutron cross-sections for the (n,γ) reactions of interest as obtained in this work (TW) and, as reported by other authors [1, 2, 13]. Our results are systematically 2-3% higher than in these references. The corrected (or "true") k_0 and Q_0 factors are given further in the text in Table 10.15.

Table 4.11: The thermal-to-fast conventional neutron fluence rate ratio (*L*) values obtained for the irradiation channels Y4, S84 and X26 of the BR1 reactor, from the employment of the high-purity materials of Table 6.3 and the nuclear data of Table 2.5.

Reaction			Y4	S84	X26	Year
^{23}Na	(n,α)	^{20}F		+		2011
^{27}Al	(n,α)	^{24}Na	**89**	**20**		2006
^{27}Al	(n,p)	^{27}Mg		**17**		2006
^{27}Al	(n,α)	^{24}Na	**110**	**28**		2011
^{27}Al	(n,p)	^{27}Mg		**22**		2011
^{28}Si	(n,p)	^{28}Al		**18** #		2006
^{46}Ti	(n,p)	^{46}Sc	*			2011
^{56}Fe	(n,p)	^{56}Mn	*		*	2011
^{58}Ni	(n,p)	^{58}Co	**97**	**23**		2011
^{90}Zr	(n,2n)	^{89}Zr	*	*	*	2011
^{117}Sn	(n,n')	^{117m}Sn	**103**		**126**	2011
^{135}Ba	(n,n')	^{135m}Ba		**24**		2011

* Not observed or below detection limits.

+ Failure to obtain good counting statistics due to the short ^{20}F half-life of $T_{1/2}$ = 11.16 s. [20].

Determined by Peter Vermaercke with a high-purity Silicon block prior to this work.

The standard uncertainty in *L* factors is estimated at 10% at the 1*s* confidence level

Table 4.12: Thermal neutron cross-sections for the (n,γ) reactions from De Corte [13] (DC), the Atlas of resonances [1] (A), and as obtained in this work (TW), after the proper corrections were estimated from eq. (2.116) with the k_0 factors provided in Table 10.15.

		Neutron cross-section (in mb; 1*s*)			
FN	**TI**	**Reaction**	**DC**	**A**	**TW**
^{87m}Sr	**^{86}Sr**	**(n,γ)**	770(7)	770(60)	**791(9)**
^{117m}Sn	**^{116}Sn**	**(n,γ)**	5.96(12)	6.0(20)	**6.16(2)**
^{135m}Ba	**^{134}Ba**	**(n,γ)**	53	134(24)	**54(1)**

4.8 Fast-fission contributions in the analysis of uranium

In the analysis of uranium samples one must consider the contribution to fission products not only from thermal fission of ^{235}U, but also for fast neutron fission of ^{238}U and ^{235}U as well. To illustrate this, according to the correction term introduced in eq. (2.110) for multiple interferences, for the fast fission contribution from ^{235}U and ^{238}U one has:

$$\begin{aligned}\Delta_{w,5} &\equiv \sum_{y}^{n} \Delta_{w,5,y} \equiv \Delta_{w,5,5} + \Delta_{w,5,8} \\ &= G_{f,5}\delta_{5,5,f} + G_{f,8}\delta_{5,8,f} \\ &= G_{f,5}\left(\frac{\sigma_{5,(\mathrm{n,f}),\,fast}}{\sigma_{0,5}}\right) + G_{f,8}\left(\frac{\theta_8}{\theta_5}\frac{\sigma_{8,(\mathrm{n,f}),\,fast}}{\sigma_{0,5}}\right)\end{aligned} \tag{4.31}$$

For a natural ^{235}U sample the calculated $\delta_{x,y,z}$ values are given in Table 2.6. The impact of the correction will depend on the L factor of the irradiation channel as i.e. determined in the previous section.

In our case, the fast fluence rate in channel Y4 can account to maximum 1% of the thermal fluence rate (e.g. see L values in Table 4.11), but given the

lower ^{235}U neutron cross-section for fast neutrons and the lower fission yields as compared to the respective values for thermal fission [1, 2], the overall contribution from fast fission is negligible. Assuming no fast-neutron self-shielding ($G_{f,5}$= $G_{f,8}$=1) and adopting L=100 for channel Y4 (see Table 4.11):

$$\frac{\Delta_{w,5}}{L} = \left(\frac{2.05 * 10^{-3}}{100} \right) + \left(\frac{6.94 * 10^{-2}}{100} \right) = 7.15 * 10^{-4} \qquad (4.32)$$

which translates into a 0.07% (or < 0.1%) contribution to the (uncorrected) reaction rate, due mostly to ^{238}U. Clearly, the correction term will be lower for a sample enriched in ^{235}U. Channel S84 the correction would be ~4 times higher ($L \approx 25$).

4.9 Validation of the thermal self-shielding calculation methods

4.9.1 Experimental

For the experimental validation of some thermal self-shielding calculation methods for cylindrical samples we selected the materials listed in Table 4.13. The respective nuclear data was taken from [178] except for hydrogen, where we referred to [15] due to discrepancies found in the primary source. The different heights were obtained after compactly stacking several Dy-Al foils (or NaCl disks) inside polyethylene vials, or in the case of the PVC powder samples, by filling polyethylene vials of different heights.

Figure 4.9 shows a diagram of PE-vials being filled by stacked foils. The NaCl and PVC materials were especially selected due to their high scattering-to-absorption cross-section ratios.

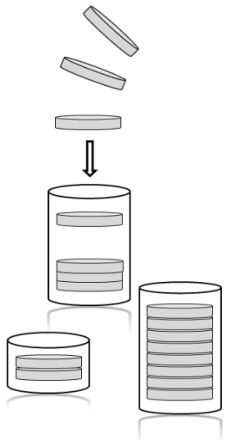

Figure 4.9: A diagram of our cylindrical samples. High purity single-element circular foils (or disks) were compactly stacked together inside cylindrical polyethylene vials of different heights.

The Dy - Al alloy samples were irradiated by duplicates in channels X26, Y4 and S84 of the BR1. The NaCl samples were irradiated by duplicates in channels Y4 and S84 while the PVC samples were only irradiated in channel S84. Each sample was co-irradiated with one Al - 0.1% Au (or one Al - 1% Mn) monitor to verify the magnitude of the neutron fluence rate at which the samples were exposed. These monitors were positioned at least 5 cm away from the sample.

The rabbits containing the samples and monitors were irradiated separately when possible and otherwise with at least 10 cm of separation to avoid mutual self-shielding effects. The fluence rate variations within these irradiation positions were found to be negligible. The samples were later counted on 6 HPGe detectors equipped with LFC modules at 27 cm sample-detector distance (to minimize the uncertainty contribution due to gamma

coincidence effects) and until less than 0.4% statistical uncertainty was reached at the photo-peaks areas of interest.

In the calculations according to Trkov et al. [101] for an impinging cylindrical neutron flux, approximate knowledge of the channel dimensions is required [79, 100]. Channels X26 and S84 have cylindrical shapes with Ø = 80 mm and 300 mm of length while channel Y4 has square dimensions but can be approximated to a cylinder of Ø = 100 mm and 500 mm of length. Channels X26 and Y4 are horizontal but perpendicular to each other. Channel S84 is vertical and perpendicular to both channels X26 and Y4.

Finally, since all the irradiated samples and monitors are standards, experimentally determined self-shielding factors were obtained when comparing the induced specific activity of a given sample to that of its co-irradiated monitor.

Table 4.13: Selected materials for the thermal self-shielding experiments. Respective absorption (*a*), scattering (*s*) and total (*t*) thermal neutron cross-sections for the elements and their atomic weights (AW), adopted from references [15, 17, 178]**. The radius (r) and height (h) of the samples.**

Material	Provider	Element	σ_a (b)	σ_s (b)	σ_t (b)	AW (g/mol)	r (mm)	h (mm)
5.00 to 29.20% Dy-Al	IRMM	Al	0.23	1.50	1.73	26.98	4	0.1 to 0.8
		Dy	994	90.3	1084.3	162.50		
NaCl HP disks	Shield-werx	Na	0.53	3.28	3.81	22.99	6.35	1.91 to 7.62
		Cl	33.5	16.8	50.3	35.45		
PVC in powder	DSM	H	0.33	30.28	30.61	1.01	4.1 to 4.6	3.5 to 20
		C	0.0	5.55	5.55	12.01		

4.9.2 Results and discussion

For the thermal self-shielding calculations according to the Sigmoid method [76–78, 104, 166], the use of relation (4.12) with three different values of the c parameter allowed us to obtain independent variables ξ_S that were directly proportional to: the total (c = 0; Figure 4.10); the effective (c = 0.85; Figure 4.1) and; the absorption (c = 1; Figure 4.12) macroscopic cross-section. Table 4.14 summarizes the results of plotting our experimentally determined G_{th} factors versus these independent variables for the three irradiation channels employed (S84, Y4 and X26). Table 4.14 also contains the results from fitting the sigmoid function in eq. (4.10) with p = 0.964 to the experimental data: the adjusted channel-specific x_0 values with their standard errors (SE) and the mean x_0 value (AVG) and SD from all materials tested.

Figure 4.10 shows that when use is made of an independent variable ξ_S which is only proportional to the total macroscopic cross-section (c = 0), there is no coherence between the obtained channel-specific x_0 values for the different samples and irradiation channels employed. This means that is not possible to establish one "universal" curve or relationship based only on the total cross-section. Instead, when the independent variable is proportional to the absorption (c = 1) or the effective macroscopic cross-section (c = 0.85), universality is reached. Table 4.14 shows that the scenario with c = 1 (Figure 4.12) gives a slightly lower SD between x_0 values of different materials than the scenario with c = 0.85 (Figure 4.11), however, the latter figure shows that as the independent variable increases, the scenario with c = 0.85 or "b", as proposed by Salgado et al. in [76, 166], gives G_{th} factors in better agreement with the experiments. Therefore, we would adopt c = 0.85 and x_0 = 0.55 ± 0.04 in our calculations related to the Sigmoid method. It seems that x_0 should be kept channel-specific as it was proposed by Chilian et al. [104] since there is no exact value of x_0 that could be employed for all possible irradiation channels in the world. In this work, we tested 3 channels that are

related in terms of the moderator material, observing up to 7% SD on x_0 from the mean between channels, which is acceptable due to its small propagation into the G_{th} factor. Also, it must be remarked that their proposed value of p = 0.964 gave a better fit to the experimental data than $p \geq 1$.

The k_{th} values can be obtained from the x_0 values with the aid of eq. (4.16). Chilian et al. informed us in a personal communication in 2011 that the k_{th} channel-specific parameter seems to vary from 0.46 to 1.1 (or even more), depending on sample size and on the neutron reflecting materials (rabbits, vials) surrounding the sample. They think that k_{th} can be modelled as a sum of factors, each one accounting for these reflections. This confirms the observation that the x_0 (or k_{th}) values obtained for our three irradiation channels are similar between each other: graphite is the common neutron reflector in these channels and their dimensions are quite similar as well. On the other hand, channel X26 uses a PE rabbit that is 3 times thicker than the ones employed on Y4 and S84. From the results of the Dy-Al samples studied at channel X26 a higher x_0 value is observed.

For the thermal self-shielding calculations according to the Stewart and Zweifel method without corrections due to scattering effects we used the KAYZERO/SOLCOI® software [71, 144]. For the calculations that take into account these scattering events we employed the program MATSSF [79] developed by Trkov et al. [101]. These results, expressed as percent differences relative to our experimentally determined G_{th} factors, are listed in Table 4.16 for different values of the independent variable ξ_S (with c = 0.85). The results obtained from the MATSSF program corresponds to three different neutron source-sample arrangements: an isotropic neutron source and a cylindrical neutron current impinging on: parallel (or co-axial; ‖) and perpendicularly-axial samples (⊢). The percent relative differences against the Sigmoid method (with c = 0.85 and p = 0.964) are also listed in Table 4.16**.**

Table 4.16 shows that the Stewart and Zweifel method gives good results if the samples are kept small and/or the scattering contribution is negligible (Dy - Al foils; with $\xi_S < 0.07$). However, when scattering starts playing an important role (NaCl disks) but is not considered in the computations, these percent relative differences can go as high as 24% (for $\xi_S \geq 0.07$).

On the other hand, when scattering is included in the computations the percent relative differences listed in Table 4.16 are minimized but can still go as high as 13% for an isotropic neutron source arrangement, which is the expected source orientation in a nuclear reactor. The tweak to eq. (4.1) proposed by Trkov et al. offered an improvement in the accuracy of the Dy - Al calculated self-shielding factors, as a perpendicular-axial source-sample model for channels Y4 and S84 lowered these relative differences. On the other hand, the co-axial source-sample model worked better for the NaCl disks, meaning that the *W* parameter introduced by Trkov et al. might not be a constant.

Finally, the percent relative differences between the experimental G_{th} factors and those obtained from the Sigmoid method (eqs. (4.10) and (4.11) with $c = 0.85$ and $p = 0.964$) were just as high as 2% for any kind of samples, demonstrating its great accuracy and versatility in thermal self-shielding calculations.

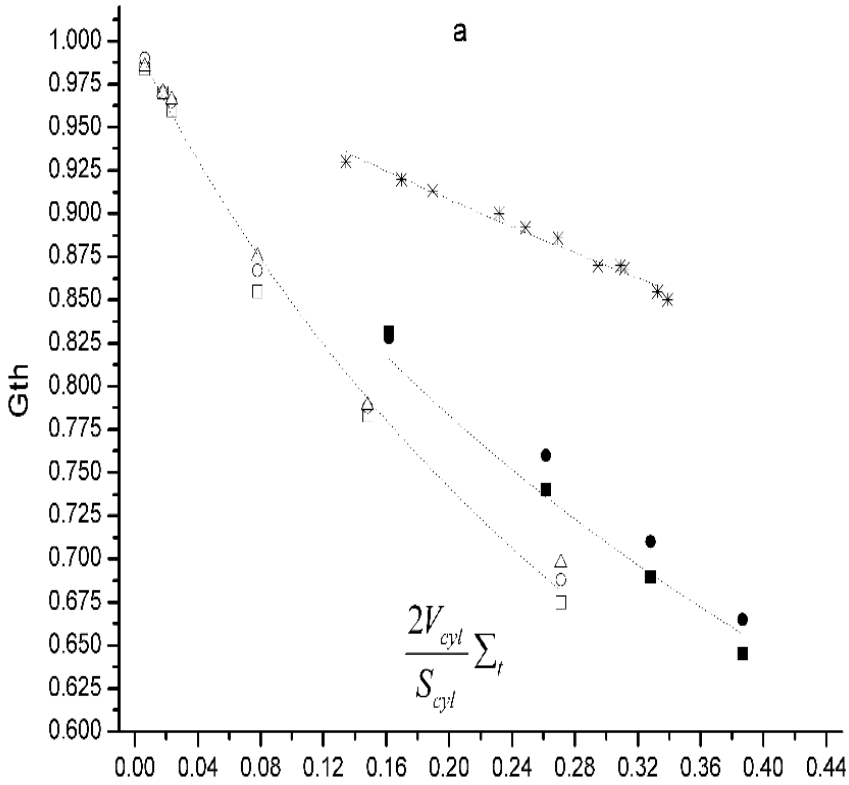

Figure 4.10: Experimentally determined G_{th} factors versus ξ_S with c = 0 for the different materials tested in the irradiation channels Y4 (square), S84 (circle) and X26 (triangle). Empty data-points correspond to the Dy - Al alloy foils, filled (black) ones correspond to the NaCl disks. The asterisk data-points correspond to PVC samples irradiated in channel S84.

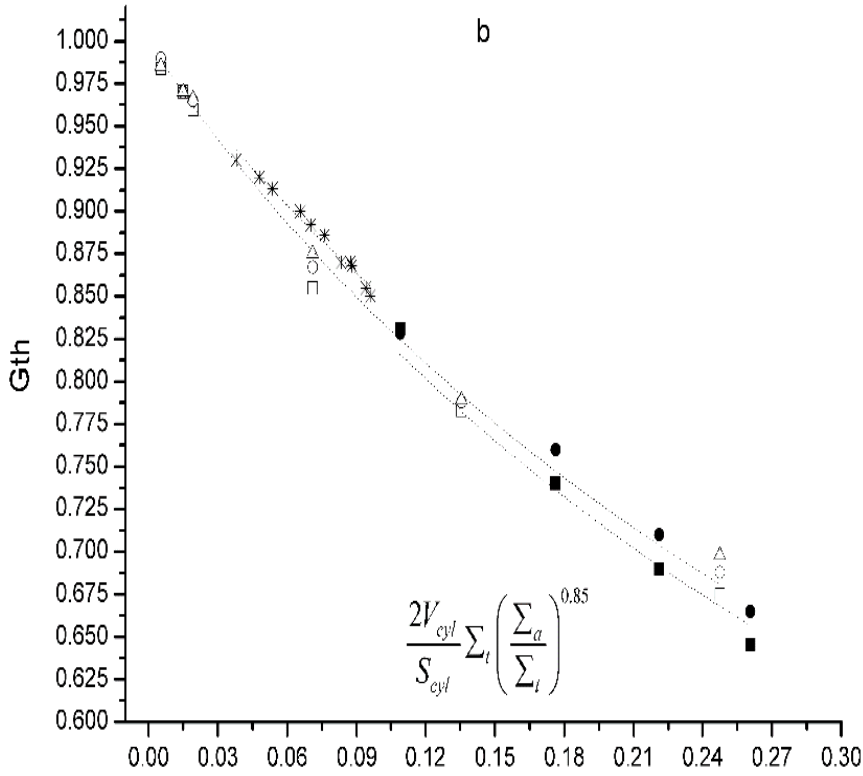

Figure 4.11: Experimentally determined G_{th} factors versus ξ_S with c = 0.85 for the different materials tested in the irradiation channels Y4 (square), S84 (circle) and X26 (triangle). Symbols explained in the Figure 4.10 caption.

Table 4.14: Channel-specific x_0 values and standard errors when adjusting the data to the sigmoid function from eq. (4.10) with p = 0.964. Data for 3 irradiation channels and materials employed.

		$x_0 \pm \Delta x_0$					
	Channel	**with c = 0**		**with c = 0.85**		**with c = 1**	
Al - Dy foils	Y4	0.56	0.02	0.51	0.01	0.50	0.01
	S84	0.60	0.01	0.54	0.01	0.53	0.01
	X26	0.62	0.02	0.56	0.01	0.56	0.01
NaCl disks	Y4	0.76	0.02	0.51	0.02	0.48	0.01
	S84	0.82	0.02	0.56	0.01	0.52	0.01
PVC	S84	2.16	0.03	0.61	0.01	0.49	0.01

Table 4.15: Mean channel-specific x_0 values for each irradiation channel employed when averaging the results from Table 4.14.

	$x_0 \pm \Delta x_0$					
Channel	**with c = 0**		**with c = 0.85**		**with c = 1**	
Y4	0.66	0.14	0.51	0.01	0.49	0.02
S84	1.19	0.84	0.57	0.04	0.51	0.02
X26	0.62	0.02	0.56	0.01	0.56	0.01
Mean	0.82(32)		0.55(3)		0.52(3)	

The uncertainties in the mean values are SDs quoted for the last significant digit.

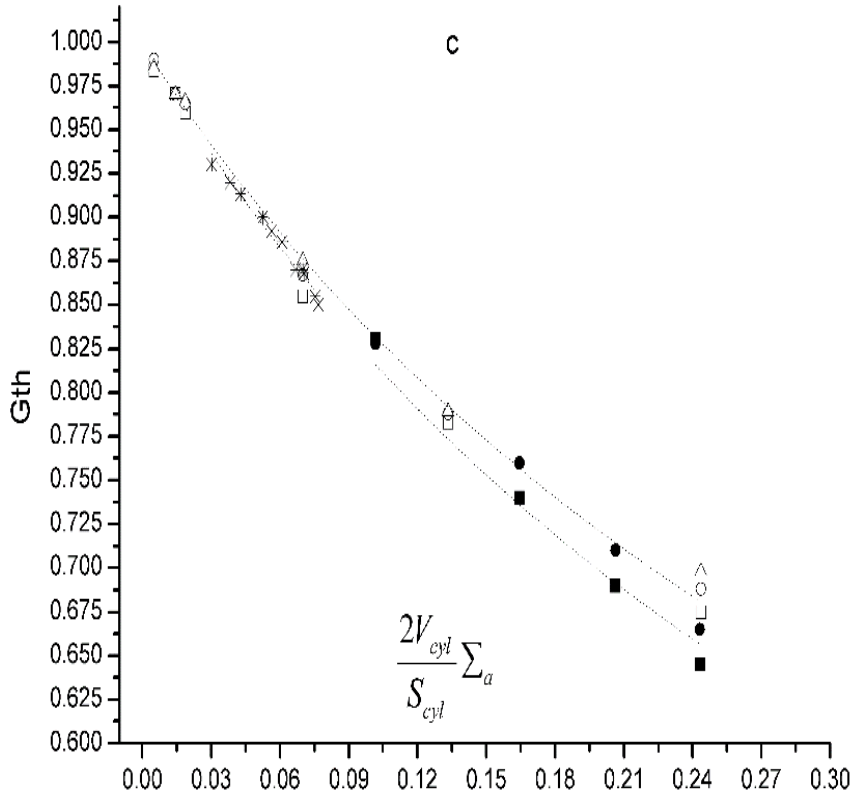

Figure 4.12: Experimentally determined G_{th} factors versus ξ_S with c = 1 for the different materials tested in the irradiation channels Y4 (square), S84 (circle) and X26 (triangle). See Figure 4.10 caption.

Table 4.16: Percent differences relative to our experimental G_{th} factors when applying the Sigmoid method and the Stewart & Zweifel method (with or without scattering considerations) for different source-sample arrangements.

		Stewart and Zweifel method								**Sigmoid method**	
		with scattering						**without scattering**		**p = 0.964**	
		Isotropic		**⊢ axes**		**‖ axes**				**c = 0.85**	
	ξ_S	Y4	S84	Y4	S84	Y4	S84	Y4	S84	Y4	S84
	c = 0.85										
A	0.005	0.1	-0.5	0.0	-0.6	0.2	-0.4	0.7	0.1	0.4	-0.1
	0.015	-0.6	-0.6	-0.9	-0.8	-0.5	-0.5	0.7	1.1	-0.2	0.0
	0.019	-0.4	-0.9	-0.8	-1.2	-0.3	-0.9	1.3	0.8	-0.1	-0.4
	0.071	2.5	1.1	1.4	0.3	3.5	1.8	8.7	7.5	1.8	1.1
	0.135	2.9	2.2	1.3	1.1	4.5	3.4	13.8	14.1	-0.1	0.5
	0.248	5.7	3.7	3.5	2.2	7.8	5.2	20.6	20.1	-1.0	-1.1
B	0.109	1.1	1.5	-0.3	0.3	0.0	0.0	9.1	9.9	-1.8	0.0
	0.176	5.6	2.9	3.9	1.5	3.4	0.4	15.5	13.8	-0.5	-1.2
	0.221	8.8	5.7	7.1	4.3	5.6	2.4	19.3	17.5	0.2	-0.3
	0.258	12.7	9.3	11.1	7.9	8.6	5.2	23.6	22.0	2.1	1.7

A = Dy - Al alloy foils; B = NaCl disks

4.9.3 Conclusions

It has been fifty years since the Stewart and Zweifel algorithms were introduced for thermal self-shielding calculations for a variety of samples. It is clear from the work of Blaauw and our experimental observations that scattering plays an important role and should not be neglected in the computations, in the case of samples with high scattering-to-absorption cross-section ratios. Otherwise, the accuracy of the resulting G_{th} factor will be affected.

The Sigmoid method is a semi-empirical form of the Stewart and Zweifel algorithm for spheres that has been adapted to cylindrical samples by Salgado et al. and later refined and extended by Chilian et al. It might not be an "exact" analytical expression but its great simplicity and versatility in thermal self-shielding calculations for cylindrical samples and up to 40% thermal self-shielding is clear: different materials with different scattering-to-absorption cross-section ratios agreed on the value of the x_0 (or k_{th}) channel-specific parameter for 2 irradiation channels.

If one is seeking an alternative and quicker method than the MCNP code for thermal self-shielding calculations, we propose the use of the Sigmoid function (or universal curve) through eqs. (4.10) and (4.11) with $c = 0.85$ as suggested by Salgado et al. However, one should use $p = 0.964$ and treat x_0 (or k_{th}) as a channel-specific parameter as it was addressed by Chilian et al. The procedure would be: to determine the x_0 value for the channel of interest and later introduce this parameter for calculations related to any other set of cylindrical samples. The nature of x_0 (or k_{th}) is being investigated by Chilian et al. as a function of the moderator and channel-specific parameters, meaning that this method for thermal self-shielding calculation will be further improved.

4.10 Validation of the epithermal self-shielding calculation methods

4.10.1 Experimental

Up to 20 high-purity Zr foils (Goodfellow) of Ø = 8 mm and 0.127 mm thickness were compactly stacked together for attaining different mean chord lengths. The same procedure was repeated with the same amount of high-purity Mo foils (Goodfellow) of the same diameter but of 0.025 mm thickness. These small cylinders (or thick foils) were packed inside 0.7 mm thickness high-density PE vials keeping the foils compactly stacked (see Figure 4.9). The materials were selected due to the accurate knowledge of the strong resonance cross-sections for ^{96}Zr and ^{98}Mo and the lack of thermal self-shielding effects contributing to the loss of the total reaction rate. An approximated 20% epithermal self-shielding impact was expected for each isotope.

The samples were irradiated by duplicates in channels Y4 and S84 of the BR1 reactor. Each sample was co-irradiated with one Al - 0.1% Au (or one Al - 1% Mn) monitor to check the magnitude of the neutron fluence rate at which the samples were exposed. These monitors are known to be exempt from self-shielding effects. The rabbits containing the samples were separated by 10 cm and the monitors were positioned at least 5 cm away from each sample. The fluence rate variations within these irradiation positions are known to be negligible.

The samples were later counted on several HPGe detectors equipped with the LFC modules at 27 cm sample-detector distance (to minimize the uncertainty contribution from gamma coincidence effects) until less than 0.4% statistical uncertainty was reached at the photo-peak areas of interest.

Finally, since all the irradiated samples and monitors are standards, experimental self-shielding factors G_e were obtained when comparing the induced specific activity of a given sample to that of its co-irradiated monitor. These values were compared to the MatSSF calculated G_e factors for an isotropic (*M0*) and an impinging cylindrical neutron current that is perpendicular (*M1*) or co-axial (*M2*) to the sample cylinder axis. For these arrangements, the channel dimensions were supplied for channels S84 (Ø = 8, 30 cm of length) and Y4 (Ø = 10, 50 cm of length).

Use was made of eq. (4.27) and the $\sigma_{e,abs}$ values provided by Chilian et al. [78, 104], to calculate the G_e factors according to the Sigmoid (or Chilian) method and compare them to our experimental values. Retrospectively, a logistic or sigmoid fit as in eq. (4.22) on the observed G_e factors vs. the Z variable allowed us to determine $k_e\sigma_{e,abs}$ values instead, and check whether the condition $k_e \approx 1$ is satisfied by comparison with available $\sigma_{e,abs}$ values.

4.10.2 Results and discussion

Figure 4.13 and Figure 4.14 show our experimentally observed G_e factors for ^{98}Mo and ^{96}Zr isotopes as compared to the calculated ones obtained from the MatSSF and Sigmoid methods (with $k_e = 1$), as a function of the sample-related Z variable. The calculated values per the Sigmoid method [3,6] are in good agreement with the experimental data for both irradiation channels (S84 and Y4). The relative differences amount to just 2% in the case of ^{98}Mo and up to 6% for ^{96}Zr.

The calculated value $\sigma_{e,abs}$ = 21(2) b for ^{98}Mo (by applying eq. (4.25)) gives sufficiently accurate self-shielding factors when $k_e = 1$ is assumed on both channels. This is not the case for ^{96}Zr, since the experimental value $\sigma_{e,abs}$ = 10.3(8) b proposed in [78, 104] overestimates the calculated G_e factor. The $\sigma_{e,abs}$ value proposed by Chilian et al. differs from the calculated one ($\sigma_{e,abs}$ = 8 b) in 28%. When the calculated value is employed, the relative difference

is reduced to just 2%. This somehow motivates the question of what k_e value should be applied for our channels. If a $k_e \neq 1$ is assumed in favour of the reported $\sigma_{e,abs}$ value for ^{96}Zr by Chilian et al., then a bias would be introduced later on our ^{98}Mo results. From a logistic sigmoid fit of G_e vs. Z it was possible to extrapolate $k_e\sigma_{e,abs}$ factors and to tabulate them (see further).

Assuming a k_e = 1 for our irradiation channels (within a 10% uncertainty), our experimental $\sigma_{e,abs}$ values for ^{98}Mo and ^{96}Zr are compiled in Table 4.17 along previous values from references [168, 169]. For the Beryllium site (k_e = 1) and for the Water irradiation sites 6 and 8 (k_e = 0.93 both) studied by Chilian et al. [104], their reported $\sigma_{e,abs}$ values were normalized to k_e = 1 and are tabulated as such. New proposed values are given per the average of all values reported.

The proposed value of $\sigma_{e,abs}$ = 8.8(4) b at the 1*s* confidence level for ^{96}Zr is 9% lower than the one reported by Chilian et al. after the due k_e re-normalization. By comparison, the proposed $\sigma_{e,abs}$ value is 10% higher than the calculated one. With this new value ~2.3% relative difference is observed between the calculated and our experimental G_e factors per the Chilian sigmoid method. The differences between Chilian et al. results and ours are not statistically significant at the 95% confidence level. The 16% discrepancy with our $\sigma_{e,abs}$ results for ^{96}Zr could be due to the fact that this isotope is very sensitive to deviations from the ideal 1/E epithermal fluence rate distribution of each channel, i.e. high Q_0 factor > f for any irradiation channel employed. In this work we dealt with 2 target isotopes and very small samples as compared to the ones employed by Chilian et al. in [104]. Therefore, further work is required to study the behaviour of the k_e parameter imposed by the model.

For ^{98}Mo the proposed value $\sigma_{e,abs}$ = 22.3(7) is only 6% different than the calculated one and it is not significant at the 95% confidence level. This translates into an accuracy of 1.5% on the calculated self-shielding factors

for ^{98}Mo. No experimental $\sigma_{e,abs}$ values for this isotope have been published so far for use in the Sigmoid method.

When analysing the results from the MatSSF method (Figure 4.13 and Figure 4.14), a ~2% relative difference is also obtained between the calculated and experimental values when applying the perpendicular source-sample axial configuration *(M1)*. This holds for the 2 irradiation channels and the 2 isotopes tested. On the other hand, the isotropic *(M0)* and co-axial *(M2)* configurations overestimated the self-shielding effects in both channels, up to 5% for ^{98}Mo and 10% for ^{96}Zr.

The neutron fluence rate or the neutron self-shielding effect in a nuclear reactor has been found to be isotropic [77, 83, 100] so one would expect that the *M0* configuration would give the most accurate results among the others. The overestimation observed by applying the *M0* and *M2* configurations is of the same magnitude, hence the deviations due to their different "generalized" mean chord length definitions cannot account for their overall bias. The reason of this discrepancy could be related to the Bell factors adopted for those configurations, since the factors for the *M0* and *M2* setups are identical but significantly different than the one adopted in the *M1* configuration.

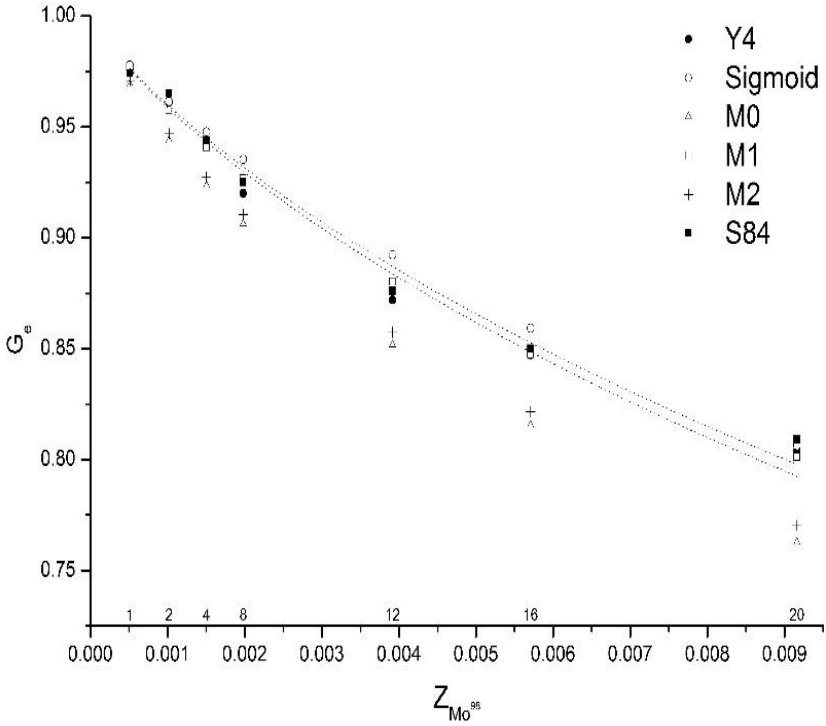

Figure 4.13: Experimental and calculated G_e factors for ^{98}Mo when plotted against the Z independent variable in eq. (4.27) from 1 up to 20 compactly stacked high-purity Mo foils (Ø = 8 mm, 0.025 mm thick) and by adopting the experimental $\sigma_{e,abs}$ values from Chilian et al. of Table 4.17. The dotted lines represent sigmoid fits on the results from channels Y4 (upper) and S84 (lower) from which $k_e\sigma_{e,abs}$ values are obtained per eqs. (4.22) and (4.27).

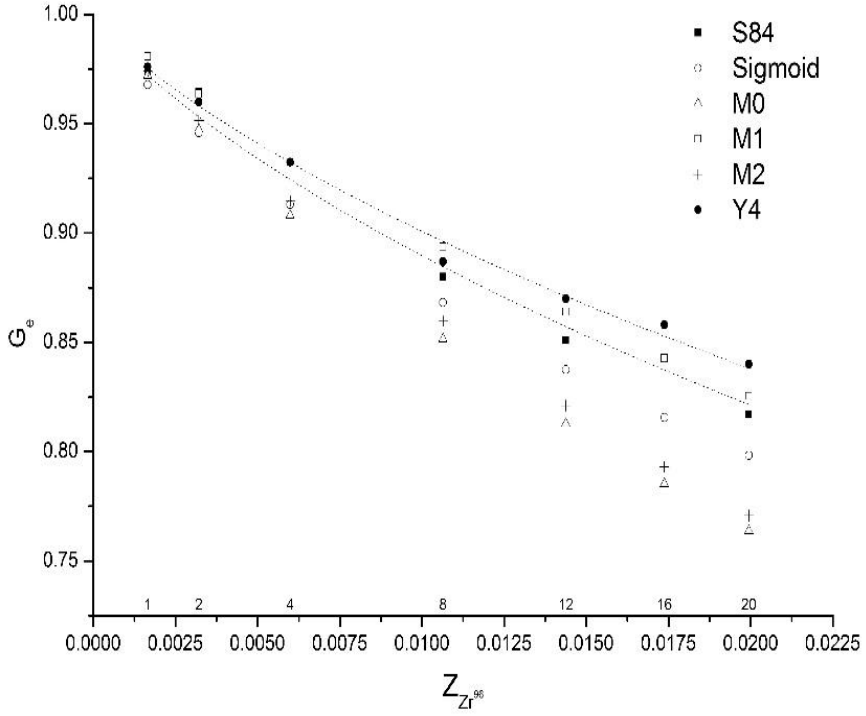

Figure 4.14: Experimental and calculated G_e factors for ^{96}Zr when plotted against the Z independent variable in eq. (4.27) for 1 up to 20 compactly stacked pure Zr foils (Ø = 8 mm, 0.127 mm thick) and by adopting the experimental $\sigma_{e,abs}$ values from Chilian et al. of Table 4.17. The dotted lines represent sigmoid fits on the results from channels Y4 (upper) and S84 (lower) from which $k_e\sigma_{e,abs}$ values are obtained per eqs. (4.22) and (4.27).

Table 4.17: Calculated and experimental $\sigma_{e,abs}$ values (in barn; 1 b = 10^{-28} m^2) from the literature and from this work.

	Chilian et al. [104]			**This work**			
	Be site 1	**Water site 6**	**Water site 8**	**Calc.**	**S84**	**Y4**	**Proposed**
^{98}Mo	-	-	-	21.0(10)	22.7(11)	23.3(11)	22.3(7)*
^{96}Zr	10.3(8)	9.6(8)	9.6(8)	8.0(8)	8.6(7)	7.4(8)	8.8(4)**

All quantities are expressed in barns along their uncertainty in absolute value for the last significant digit at the 1*s* confidence level.

* SD of the mean (N = 3). Use k = 4.303 for a 95% confidence level.

** SD of the mean (N = 6). Use k = 2.571 for a 95% confidence level.

4.10.3 Conclusions

The Chilian (or Sigmoid) and the MatSSF methods were of great simplicity and versatility for epithermal self-shielding modelling of cylindrical samples. The Chilian method provided us with epithermal self-shielding corrections factors in good agreement with the experimental ones for ^{98}Mo and ^{96}Zr when adopting their $\sigma_{e,abs}$ values (2.2 and 6% relative difference; respectively). The small difference with the experimental results for both isotopes on 2 irradiation channels favours the idea that although k_e might be channel-specific, it can be equaled to unity within a 10% uncertainty ($0.9 \leq k_e \leq 1.1$). This seems to hold as a valid argument for water, beryllium and graphite moderators/reflectors. By fixing $k_e = 1$, its estimated 10% variation is moved toward our experimental $\sigma_{e,abs}$ values instead. A 20% overall uncertainty on the $\sigma_{e,abs}$ value would propagate to the self-shielding factors into a 6% bias, which is accurate enough for routine analysis. One must consider that the uncertainty introduced by the self-shielding factor is further reduced toward the analytical result.

It is possible to achieve 2% relative difference for ^{98}Mo and ^{96}Zr with the Sigmoid method by employing our proposed $\sigma_{e,abs}$ values. These were averaged over other independent experimental results and agree with the calculated or theoretical ones.

The MatSSF method gave a 2% relative difference between calculated and experimental values for both irradiation channels Y4 and S84 and for both isotopes, but only for the perpendicular source-sample axial configuration. However, the relative differences were as high as 10% for both isotropic and co-axial sample-source configurations and for both isotopes.

Since the neutron fluence rate of several reactors has been shown to be isotropic, a Bell factor $a^* \approx 1.3$ would tune the MatSSF results for the isotropic and co-axial cases in favour of a better agreement with our experiments.

For small single-element samples and up to 20% self-shielding effect, both methods are accurate and precise within a 6% uncertainty. This can also be improved further by tuning the empirical parameters these methods employ. Their versatility and short computing time might be excellent substitutes for a MCNP model in routine analysis.

5. The k_0-NAA of multi-elemental samples containing uranium (k_0-UNAA)

Characterization of rare earth elements in samples containing uranium by Neutron Activation Analysis (NAA) is known to be severely interfered by neutron-induced fission of ^{235}U, for this phenomenon produces the same radioisotopes that are usually monitored for their quantification [54, 179, 180]. After an initial overview of the relevant nuclear data to account for these ^{235}U interferences [180, 181] and the introduction of the k_0-standardization of NAA in 1975 [39], efforts have been made to provide the NAA community with more accurate (experimentally determined) nuclear data for these cases [54, 115].

Current uranium data presented in the k_0-literature is related to ^{235}U-fission interfered radioisotopes of analytical interest (e.g. for the analysis of soils, rocks) and are correlated to ^{235}U and ^{238}U natural abundances [20, 54]. In this chapter, however, we aim at using this data for determining the $n(^{235}U)/n(^{238}U)$ ratio of the sample by means of a simple algorithm. For this we need to assume that at least one of the monitored radioisotopes comes exclusively from the ^{235}U fission. This means that the observed ^{235}U fission and ^{238}U activation are now our subject of analytical interest and the activation of rare earth elements is considered as the interfering problem.

5.1 Principles of k_0-UNAA

In NAA of samples containing uranium (UNAA), the U content (m_U; in mg) is usually determined by monitoring the decay γ-rays from ^{239}U and/or ^{239}Np (index 9) produced from the activation of ^{238}U (index 8). In the modified Høgdahl convention use is made of the following relation (see section 2.4):

$$m_U = A_9 \left(\frac{M_U}{I_{\gamma,9}\theta_8 N_A} \right) \left(\frac{1}{G_{th}\varphi_{th}\sigma_{0,8} + G_{e,8}\varphi_e I_{\alpha,8}} \right) \tag{5.1}$$

Additionally, by monitoring the γ-rays from the decay of the radioisotopes produced by fission of ^{235}U (index 5), a similar alternative method for the determination of the U content is possible (in the same convention):

$$m_U = A_F \left(\frac{M_U}{I_{\gamma,F}\theta_5 N_A Y_F} \right) \left(\frac{1}{G_{th}\varphi_{th}\sigma_{0,5} + G_{e,5}\varphi_e I_{\alpha,5}} \right) \tag{5.2}$$

where the index F = ^{95}Zr, ^{99m}Tc, ^{103}Ru, …, ^{141}Ce and Y_F is their respective cumulative fission yield.

Combining eq. (5.1) with eq. (5.2) and, considering that the observed U content should be the same regardless of the monitored radioisotope, the $n(^{235}\mathrm{U})/n(^{238}\mathrm{U})$ isotopic ratio in the sample can be determined from:

$$\frac{n\left(^{235}\mathrm{U}\right)}{n\left(^{238}\mathrm{U}\right)} = \frac{\theta_5}{\theta_8} = \frac{A_F}{A_9}\frac{I_{\gamma,9}}{I_{\gamma,F}}\frac{1}{Y_F}\left(\frac{G_{th}\varphi_{th}\sigma_{0,8} + G_{e,8}\varphi_e I_{\alpha,8}}{G_{th}\varphi_{th}\sigma_{0,5} + G_{e,5}\varphi_e I_{\alpha,5}} \right) \tag{5.3}$$

By introducing the k_0 and k_0-fission factors definitions [54]:

$$\begin{aligned} k_{0,8,9,c} &\equiv \left(I_{\gamma,9}\theta_{8,n}\sigma_{0,8}M_{c,n} \big/ \gamma_c \theta_{c,n}\, \sigma_{0,c}M_{U,n} \right) \\ k_{0,5,F,c} &\equiv \left(I_{\gamma,F}\theta_{5,n}\sigma_{0,5}Y_F M_{c,n} \big/ \gamma_c \theta_{c,n}\, \sigma_{0,c}M_{U,n} \right) \end{aligned} \tag{5.4}$$

And with the index *n* introduced to emphasize the correspondence to natural isotopic abundances, then eqs. (5.1), (5.2) and (5.3)can be rewritten in the k_0-formalism as:

$$m_{\mathrm{U}} = \frac{A_9}{A_c}\frac{1}{k_{0,8,9,c}}\frac{R_{H,c}}{R_{H,8}}\left(\frac{\theta_{8,n}}{\theta_8}\frac{M_{\mathrm{U}}}{M_{\mathrm{U},n}}\right), \tag{5.5}$$

$$m_{\mathrm{U}} = \frac{A_F}{A_c}\frac{1}{k_{0,5,F,c}}\frac{R_{H,c}}{R_{H,5}}\left(\frac{\theta_{5,n}}{\theta_5}\frac{M_{\mathrm{U}}}{M_{\mathrm{U},n}}\right) \tag{5.6}$$

and,

$$\frac{n\left(^{235}\mathrm{U}\right)}{n\left(^{238}\mathrm{U}\right)} = \frac{\theta_5}{\theta_8} = \left[\frac{A_F}{A_9}\frac{k_{0,8,9,c}}{k_{0,5,F,c}}\frac{R_{H,8}}{R_{H,5}}\right]\left(\frac{\theta_{5,n}}{\theta_{8,n}}\right) \tag{5.7}$$

The index *c* refers to the co-irradiated monitor (comparator) for which the k_0 and k_0-fission factors were tabulated. Notice that if the expression between brackets in eq. (5.7) is less than unity the sample is depleted in ^{235}U, while if greater than unity the sample is enriched in ^{235}U. In case it equals unity the isotopic ratio corresponds to the natural one: 0.00725262 (negligible uncertainty) [10].

Chronologically, equations (5.5) and (5.6) shall be solved after (5.7) is known. If the amounts of other U isotopes in the sample are not known, use can be made of the following approximation:

$$\begin{aligned}&\theta_8 + \theta_5 + \ldots + \theta_4 \cong \theta_5 + \theta_8 \cong 1\\ &\theta_8 M_8 + \theta_5 M_5 + \ldots + \theta_4 M_4 \cong \theta_8 M_8 + \theta_5 M_5 \cong M_{\mathrm{U}}\end{aligned} \tag{5.8}$$

knowing that ^{234}U is the third most abundant one (0.0054%; natural abundance) [10] but that its presence is usually negligible in comparison to the ^{235}U and ^{238}U.

It must be remarked that the ^{235}U-fission shows a slight deviation from the ~1/v ideal cross-section behaviour in the thermal neutron energy region and

the use of the modified Westcott formalism should be adopted instead (see $R_H \rightarrow R_W$ substitution in eq. (2.65)). Considering that the ^{235}U Westcott g_T factor is ~2% different from unity for neutron temperatures between 20 to 40 °C [16] and, that the k_0-fission factors were experimentally determined through the modified Høgdahl formalism [54], the use of the latter convention is justified for not too extreme channel temperatures. An additional undesired phenomenon would be epithermal neutron self-shielding due to a strong ^{238}U resonance at 6.7 eV [182], which can be avoided by sufficient sample dilution.

5.2 An algorithm for complex interferences

The determination of the $n(^{235}U)/n(^{238}U)$ isotopic ratio in multi-elemental samples containing uranium would be interfered if the fission products were additionally produced by (n,γ) reactions on other isotopes occurring in the sample (e.g. ^{141}Ce produced by (n,γ) reactions on ^{140}Ce). This is because the current k_0-fission literature was intended for interference corrections and not for ^{235}U determination. There is no k_0-fission data currently available for radionuclides produced only by fission of ^{235}U.

The k_0-literature contains 9 k_0 factors for ^{238}U determination and 36 k_0-fission factors [20, 23] and since this accounts for up to 324 experimentally determinable isotopic ratios, selection of reliable data through a computer code is required. Rejection of interfered values can be achieved by means of a filtering algorithm, based on the idea that the calculated U content from a fission product by eq. (5.6) should be the same no matter which radioisotope was monitored. For each fission product, a weighted average of the U content can be calculated from all measured γ-rays (weighed per e.g. the counting statistics). A set of elemental U values from the monitoring of fission products ($F = a, b, \ldots, n$) can be constructed:

$$\bar{m}_{U,5} = \left\{ \bar{m}_{U,5,a}, \bar{m}_{U,5,b}, ..., \bar{m}_{U,5,n} \right\} \tag{5.9}$$

Clearly, the minimum of this set would correspond to the less biased (or interfered) monitored fission product, if the accuracy of the data is not suspected. For a given set, the following filtering algorithm can be employed to test the accuracy of each result *F* in the set:

$$\frac{\bar{m}_{U,5,F} \pm \Delta_{\bar{m}_{U,5,F}}}{\min\left\{\bar{m}_{U,5}\right\} \pm \Delta_{\min\{\bar{m}_{U,5}\}}} \leq 1 + \delta \tag{5.10}$$

Where Δ is the weighted SD of the corresponding weighted average and δ is an analyst-defined test gap (e.g. δ = 0.1 equals a 10% max. expected bias). A frequency (or ranking) factor is assigned to every fission product that satisfies eq. (5.10) each time δ is slowly decreased in an iterative process, until the set of outliers and a set of reliable values is finally constructed. Once a first averaged $n(^{235}U)/n(^{238}U)$ value is calculated it can be used for determining the amount of the interfering isotopes naturally occurring in the sample, allowing for the set of reliable data to be expanded further, until no variation of the isotopic ratio is observed within its overall uncertainty region.

This filtering process can be improved if one takes into account that ^{131}I, a fission product and daughter of ^{131}Te (and its isomer), is usually not interfered from (n,γ) reactions on ^{130}Te, since tellurium is apart from the precious metals, the rarest stable solid element in the earth's crust [183]. Its abundance by mass is less than 1 ng/g. By comparison, even the rarest of the lanthanides have crustal abundances of 0.5 mg/kg [184]. One can logically expect that the observed ^{131}I was produced exclusively from the ^{235}U fission, making it our first unbiased estimator of choice.

Another useful radioisotope would be ^{140}La ($T_{1/2}$ = 1.678 days), produced by ^{235}U(n,f)^{140}Ba ($T_{1/2}$ = 12.75 days) → ^{140}La and/or by ^{139}La(n,γ)^{140}La [20]. Its activity increments in time when produced through the decay of the fission

product ^{140}Ba, instead of decreasing as in the case of (n,γ) reactions on ^{139}La. After a cooling period of ≈10 half-lives of ^{140}La (≈17 days), the observed activity is practically unbiased from (n,γ) contributions, while >50% of the produced ^{140}Ba has decayed into ^{140}La.

5.3 Validation of k_0-UNAA

For testing the applicability and reproducibility of the adopted analytical method and the proposed data filtering algorithm, the certified uranium isotopic standards of Table 5.1 were selected, ranging from 0.5 to 10% ^{235}U enrichment. The five NBS standards were diluted in nitric acid matrix as to obtain three solutions of different elemental U content for each standard. The solutions were spiked on paper filters, dried at room temperature over two days and later packed into cylindrical polyethylene vials. To summarize, three samples for each standard were prepared with around 200 µg, 2 µg and 0.2 µg of elemental uranium content (respectively), giving a total of 15 NBS samples.

Table 5.1: Uranium materials selected for testing the k_0-UNAA approach.

Material	Nominal $n(^{235}U)/n(^{238}U)$	Description
NIST-005	0.004919	
NIST-010	0.010140	
NIST-020	0.02081	highly purified U_3O_8; powder
NIST-050	0.05278	
NIST-100	0.11360	

All values have a 0.1% uncertainty (at the 1*s* confidence level)

The samples were co-irradiated in the year 2009 with several fluence rate monitors (Al - 0.1% Au foils; IRMM 530) for 7 hours inside channel Y4 of the BR1 reactor (SCK•CEN, Belgium) with parameters f = 37.5 and α =

0.062 (2009; see Table 6.4), in three separate irradiations. After a minimum cooling period of 24 hours the samples were measured every three days (with a total of 6 measurements per sample) and long enough as to achieve less than 1% uncertainty in the photo-peak areas of analytical interest. Three HPGe detectors and different sample-detector distances (up to 27.5 cm) where employed. At the farthest distances the detection efficiency is accurately known and true-coincidence effects are negligible, but at lower distances the true-coincidence effects were accounted with the aid of KayWin/SOLCOI® software package [52, 71]. For spectrum analysis, the program HyperLab 2005® was used [185] while for calculation of the $n(^{235}U)/n(^{238}U)$ ratios and selection of reliable data, a home-made software in C++ was developed, based on the k_0-library and activation-decay schemes available in the recommended literature [20]. Neutron self-shielding effects in the samples were believed to be negligible at these low U concentrations and therefore were not considered. These experiments were performed in the year 2009, before the complete recalibration of the SCK•CEN laboratory detectors and irradiation channel positions (described in sections 3.4, 2.16 and 4.5) was performed.

Every experimentally (index *e*) determined isotopic ratio was normalized against its nominal (certified; index *s*) value per:

$$R_{e,s} = \left(\frac{\theta_5}{\theta_8}\right)_e \left(\frac{\theta_8}{\theta_5}\right)_s \tag{5.11}$$

The Table 5.2 shows that with current k_0 nuclear data [20] an overestimation of the isotopic ratio by 3% is systematically observed for several isotopes but not for all monitored lines. The choice of the 277.6 keV line as "reference" was based on several aspects: it is interference-free, has a high γ-ray abundance and it has a recommended k_0-factor (with the lowest uncertainty from the ^{239}Np set). For ^{147}Nd we observe and underestimation of 3% instead. The observed discrepancies between fission products cannot

be attributed merely to neutron self-shielding or burn-up effects since these were observed systematically at different ^{235}U enrichments levels for a given nuclide.

Table 5.3 shows that the observed $n(^{235}U)/n(^{238}U)$ isotopic ratios are also overestimated for other ^{239}Np gamma-rays in the same proportion as for the 277.6 keV line, although with a lower overestimation: for the 209.8 keV line it is just ~1% and for the 315.9 and 334.2 keV it is ~2%, while for the 106.1 keV the overestimation is higher: ~4%. None of these results are statistically significant at the 95% confidence level.

From the study on the applicability and reproducibility of the k_0-UNAA method at our institute, a total overestimation of isotopic ratio was found at 2.3% when considering all ^{239}Np gamma-rays and the current k_0-literature [20]. This discrepancy is within our k_0-UNAA uncertainty budget of 2-3% at the 1*s* confidence interval. However, if we consider the results from the fission products separately, the observed discrepancies suggest that a re-determination of the k_0-fission factors is necessary as to increase the accuracy and reliability of the filtering algorithm. This conclusion is based on the following aspects:

- all the ^{235}U-fission products share the same Q_0 factor, differing fundamentally in their k_0-fission factor definition;

- the different ^{239}Np gamma-rays reported correlated results, meaning that any systematic bias in the ^{238}U analysis is propagated equally to all ratios from the different fission products.

The observed differences between the different ^{239}Np gamma-rays also suggest that a re-determination of their k_0 factors is desirable.

The ^{131}I was demonstrated as a reliable (unbiased) ^{235}U-fission monitoring radioisotope in all samples. The k_0-fission factors for nuclides that are only produced by ^{235}U fission (i.e. ^{140}Ba, ^{135}I, etc.) should be determined to increase the statistical pool of unbiased estimators.

Table 5.2: $R_{e,s}$ values obtained from the monitored ^{235}U-fission products (FP) versus the ^{239}Np at 277.6 keV line for each investigated NIST standard

		$R_{e,s}$ (% SD)					
FP	**γ (keV)**	**NSB-005**	**NBS-010**	**NBS-020**	**NBS-050**	**NBS-100**	**TOTAL**
^{143}Ce	293.3	1.038 (0.4)	1.035 (0.3)	1.038 (0.2)	1.040 (0.6)	1.038 (0.2)	1.038 (0.1)
	350.6	1.036 (0.6)	1.055 (0.5)	1.052 (0.7)	1.047 (0.8)	1.052 (0.7)	1.049 (0.8)
	664.6	1.039 (0.5)	1.076 (1.5)	1.061 (1.5)	1.072 (1.6)	1.061 (1.5)	1.047 (1.9)
^{131}I	364.5	0.990 (1.0)	1.010 (1.0)	1.000 (1.0)	0.990 (1.0)	1.010 (1.0)	1.000 (1.0)
^{140}La	487.0	1.046 (1.4)	1.041 (1.4)	1.048 (0.6)	1.046 (0.4)	1.048 (0.6)	1.046 (0.2)
	815.8	1.036 (0.7)	1.035 (1.0)	1.033 (1.0)	1.038 (0.8)	1.033 (1.0)	1.035 (0.2)
^{97m}Nb	743.4	1.011 (1.5)	1.022 (0.2)	1.017 (0.8)	1.024 (0.5)	1.017 (0.8)	1.021 (0.3)
^{147}Nd	91.1	0.961 (0.8)	0.954 (1.5)	0.980 (1.0)	0.979 (1.0)	0.980 (1.0)	0.971 (1.2)
	531.0	0.973 (1.4)	0.971 (1.4)	0.987 (1.0)	0.977 (1.1)	0.987 (1.0)	0.981 (0.8)
^{103}Ru	497.1	1.019 (0.9)	1.027 (1.4)	1.036 (1.0)	1.027 (0.5)	1.036 (1.0)	1.028 (0.7)
^{95}Zr	724.2	1.042 (0.4)	1.049 (0.3)	1.038 (0.5)	1.038 (0.1)	1.038 (0.5)	1.040 (0.5)
	756.7	1.003 (0.6)	1.017 (1.0)	1.015 (0.5)	1.018 (0.8)	1.015 (0.5)	1.013 (0.6)

Table 5.3: $R_{e,s}$ values obtained from the monitored ^{235}U-fission products (FP) versus the remaining ^{239}Np lines.

		$R_{e,s}$ (% SD)							
TI	**γ (keV)**	**106.1 keV**		**209.8 keV**		**315.9 keV**		**334.2 keV**	
^{143}Ce	293.3	1.04	(0.5)	1.01	(0.3)	1.02	(0.6)	1.04	(3.9)
	350.6	1.06	(0.4)	1.03	(1.7)	1.04	(1.1)	1.05	(1.2)
	664.6	1.07	(1.2)	1.04	(1.4)	1.05	(0.8)	1.05	(1.5)
^{131}I	364.5	0.99	(1.5)	0.95	(1.1)	0.97	(0.9)	0.96	(1.6)
^{140}La	487.0	1.06	(0.7)	1.02	(0.6)	1.03	(0.5)	1.03	(2.8)
	815.8	1.05	(0.8)	1.01	(0.9)	1.02	(1.2)	1.02	(3.8)
^{97m}Nb	743.4	1.03	(1.0)	1.00	(0.7)	1.01	(0.4)	1.00	(1.9)
^{147}Nd	91.1	0.99	(1.6)	0.94	(1.9)	0.96	(0.3)	0.97	(1.0)
	531.0	1.00	(0.5)	0.95	(1.3)	0.97	(0.1)	0.98	(0.7)
^{103}Ru	497.1	1.04	(0.3)	1.01	(1.1)	1.01	(0.5)	1.02	(1.5)
^{95}Zr	724.2	1.05	(0.1)	1.02	(1.0)	1.03	(1.2)	1.03	(1.5)
	756.7	1.02	(0.8)	1.00	(0.5)	1.01	(0.6)	1.01	(0.1)

6. Materials and Methods

The recommended k_0 nuclear data from 2003 [20] has been re-investigated by some authors during the last decades [3, 18, 19, 58–61, 63–65, 85, 186], motivated by some discrepancies that were systematically observed during their analysis. Their significant findings have not been included (yet) in a newer compilation (2012) [23], as it is difficult to draw conclusions on the accuracy of k_0 and Q_0 factors when the statistical population of independent experimental values is quite scarce.

In some cases, it is considerably difficult to compare the different results observed by independent laboratories, since a strong correlation to the adopted Q_0 factor means that a direct comparison between the results of different authors is not exact if the data required for a proper renormalization was not provided.

At the SCK•CEN and UGent we would like to supply the k_0-community with the nuclear data of 76 (n,γ) target isotopes, for a total of 95 radionuclides and 364 k_0 factors. The isotopes were investigated in up to 4 channels of the BR1 reactor at the SCK•CEN, obtaining k_0 values with < 2% uncertainty. A multi-channel approach is proposed (the α-vector), which allowed us to determine the Q_0 factors and effective resonance energies for 55 (n,γ) reactions.

In order to improve the reliability of the k_0-UNAA method exposed in Chapter 5, the k_0 and k_0-fission factors for the characterization of ^{235}U and ^{238}U were also re-determined for the majority of the γ-lines of interest, while new k_0 fission factors are proposed that are only linked to the fission of ^{235}U

that could serve as unbiased estimators in the determination of the $n(^{235}U)/n(^{238}U)$ isotopic ration during the analysis of multi-elemental samples containing uranium.

The materials, irradiation channels, models and methods employed are discussed in this chapter. The next chapter provides the uncertainty calculations while our results are discussed and compared to the literature elsewhere in Chapter 8.

6.1 A general need for the redeterminations

The accuracy of the k_0-standardization of Neutron Activation Analysis (k_0-NAA) relies on periodic revisions, re-evaluations and/or redeterminations of its experimental core-values. Since the introduction of the first generation of k_0 nuclear data in [13, 36, 38, 40, 43, 44], updated versions of the library have been published each decade [3, 20–23, 45]. Yet it is clear from examining the latest validated compilations (digital) in [20, 22, 23], that some values were experimentally determined only once, at the UGent and the KFKI approximately 30 years ago and have not been re-determined or updated since then. For instance, the library Q_0 factors for ^{50}Cr, ^{102}Ru, ^{152}Gd, ^{164}Dy,^{174}Hf, ^{181}Ta and ^{84}Sr were "adopted", obtained by averaging the literature data available at that time (<1980) and were therefore reported with a high relative uncertainty (10%). Some of their k_0 factors were quoted as "not recommended" and as candidates for a re-determination [13, 36, 38, 40, 43, 44]. After three decades the metrological traceability of this nuclear data can get affected as well, since the values F_{Cd} factors for all nuclides are reported in the first libraries [13, 38, 44, 45] but not anymore in the latest ones [20, 22, 23].

Some laboratories have re-investigated the k_0 nuclear data for the aforementioned isotopes during the last decade [18, 19, 59, 60, 64]. Their

findings have not been included yet in the latest library, probably because of the small pool of experimental (and independent) data that is available for comparison. Averaging results is not straightforward when the data are scattered and/or are strongly correlated to other values that were not equally adopted between authors.

The quantification of caesium is performed by inducing neutron capture on ^{133}Cs, followed by γ-spectrometry on the formed ^{134}Cs and/or its nuclear isomer ^{134m}Cs. The monitoring of the metastable nuclide is more promising because its half-life of $T_{1/2}$ = 2.903 hours [20] makes it considerable short-lived as compared to its ground state half-life of $T_{1/2}$ = 2.065 years [20]. This allows for a faster analysis by means of short neutron irradiations. Additionally, its recommended k_0 nuclear data has been experimentally determined with a relative standard deviation <2% [13, 20]. On the other hand, the monitoring of ^{134}Cs relies on imprecise nuclear data as shown by references [13, 20, 23], namely:

- adopted Q_0 factors from older literature (10% uncertainty) for both activation-decay schemes (*ADS*) type *IV/a* and *IV/b*, corresponding to the monitoring of the ground state during and/or after the excited level has completely decayed (after ~20 half-lives of ^{134m}Cs);

- experimentally determined k_0 factors for the *IV/a* and *IV/b* cases that are inherently correlated to other adopted (imprecise) factors, such as the Q_0 factors and the metastable-to-ground thermal neutron cross section ratio (η).

Nonetheless, the accurate knowledge of k_0 nuclear data for ^{134}Cs is of great interest since its theoretical sensitivity is 10 times greater than for ^{134m}Cs. Furthermore, this sensitivity remains constant over long cooling times.

Another radionuclide for which it would be possible to have both *ADS* type *IV/a* and *IV/b* data and, for which there is currently imprecise data in the literature [20, 23] for the scenario “a” and, no data at all for the scenario “b”

is: ^{188}Re. Its isomer has a half-life of 18.59 m, significantly shorter than the 17.01 h of the ground state.

For production of ^{134m}Cs and ^{188m}Re one is interested in determining:

$$Q_{0,m} = \frac{I_{0,m}}{\sigma_{0,m}} \tag{6.1}$$

while for production of ^{134}Cs and ^{188}Re according to the activation-decay scheme *IV/b* (see Section 2.14) one seeks to determine:

$$Q_{0,m+g} = \frac{I_{0,m}F_2 + I_{0,g}}{\sigma_{0,m}F_2 + \sigma_{0,g}} = \frac{F_2\eta_{mg}Q_{0,m} + Q_{0,g}}{F_2\eta_{mg} + 1} \tag{6.2}$$

with $F_2 = 1$ being the probability for the metastable (m) to ground (g) internal transition (I.T.) in those cases. With the following definition:

$$\eta_{mg} \equiv \left(\sigma_0^m / \sigma_0^g\right) \tag{6.3}$$

the Q_0 factor for the ground state (*IV/a*) can be extrapolated from the previous equations if η is known. The recommended literature proposes the adopted value of $\eta = 0.087$ for the computations related to decay scheme *IV/a* [2]. Similarly, in terms of k_0 factors, for ^{134m}Cs and ^{188m}Re one seeks to determine (with *c* as the comparator index):

$$k_{0,m,s,c} = \left(\frac{\sigma_{0,m}\theta I_\gamma}{M}\right)_s \left(\frac{M}{\sigma_{0,g}\theta I_\gamma}\right)_c \tag{6.4}$$

with θ being the isotopic abundance of ^{133}Cs, I_γ the emission probability for the respective γ transition and M the molar mass of the element. For ^{134}Cs on the other hand, one needs to determine a pair of k_0 factors for each γ line. For the activation-decay scheme *IV/a* one has:

$$k_{0,g,s,c} = \left(\frac{\sigma_{0,g}\theta I_{\gamma'}}{M}\right)_s \left(\frac{M}{\sigma_{0,g}\theta I_\gamma}\right)_c \tag{6.5}$$

and for the activation-decay scheme *IV/b:*

$$k_{0,m+g,s,c} = \left(\frac{\left(\sigma_{0,m} F_2 + \sigma_{0,g}\right)\theta I_{\gamma'}}{M} \right)_s \left(\frac{M}{\sigma_{0,g}\theta I_{\gamma}} \right)_c \tag{6.6}$$

This means that by performing the ratio between eqs. (6.5) and (6.6) one obtains, after considering the definition of η_{mg} given in eq. (6.3):

$$\frac{k_{0,m+g,s,c}}{k_{0,g,s,c}} = \eta_{mg} + 1 \tag{6.7}$$

For ^{134}Cs or ^{188}Re under the activation-decay scheme *IV/a*, the computation of a k_0 factor is not straightforward. For this case *A* is itself a function of the adopted η, f, α and both Q_0 factors for the metastable and ground states as shown in the Section 2.14. This problem must be solved iteratively. For a given η, the Q_0 for the ground state is calculated with the aid of its definition and the experimental Q_0 results from the metastable (*I*) and the *IV/b* cases (metastable and ground). These Q_0 factors along f, α and η are then employed for the determination of the k_0 factors for the *IV/a* case. Combining these experimental results (*IV/a*) with the ones from the *IV/b* case allows for the determination of an intermediate η' value (iteration result) by the experimental definition given in the eq. (6.7). The η' is substituted as η in the previous calculations for the recalculation of the Q_0's and k_0's. A new iteration process is therefore initiated, stopping when no further variance is observed between the last two iterations.

In the case of the Ba radionuclides, their Q_0 factors are adopted as thus imprecise while their k_0 factors have been experimentally determined only once. For ^{130}Ba, the reported Q_0 value in the recommended literature is incorrect [20, 23]. An error was identified as early as 1994 by Smodis et al. and its Q_0 factor was redetermined [49]. Unfortunately, the Q_0 factor was not updated in the 2003 k_0-library [20].

Apart from Kennedy et al. [19] (2006) the accuracy of the ^{130}Ba(n,γ)^{131}Ba data was also suspected by Lin et al. [64] (2007). Although its nuclear data has been reviewed by De Corte in reference [187] (2010), as of today the

values remain unchanged in the 2012 k_0-library [23]. In this work, we aim at validating their proposed values by means of its Q_0 and k_0 redetermination.

The nuclear data for ^{135m}Ba is listed for instance in reference [13] but is not listed anymore in the latest recommended libraries. Since it is strongly (n,n') interfered, it can be used for fast fluence rate monitoring.

In the case of ^{109m}Ag, a discrepancy between the k_0 factors for two different activation-decay schemes has been identified by Blaauw et al. and the need for a redetermination was evidenced [3]. The k_0 data for ^{111}Ag (daughter of ^{111}Pd) could offer another mechanism for Pd characterization. The ^{125}Sb radionuclide can be investigated as an alternative for Sn determination. It is also noticeable that the k_0 nuclear data for ^{196}Pt (n,γ)^{197}Pt (and/or its isomer) is absent from the literature, which could be determined with the aid of the ^{198}Pt (n,γ)^{199}Pt→^{199}Au reaction as internal comparator (recommended data).

6.2 Correlation to the ultimate comparator

If the Q_0 or k_0 factor is computed with the aid of f estimated from a calibration curve, the result will be correlated to the average neutron fluence rate perceived by the calibration isotopes and, to their nuclear data. By withdrawing the ultimate comparator from this set, it is possible to compute a Q_0 factor with no correlation to the ultimate comparator (see eq. (2.54)).

While the use of several calibration isotopes can provide a robust f average parameter, it is only relative to the ultimate comparator (i.e. to a single comparator) to which the k_0 factors are defined and experimentally determined. Since the successful application of the k_0-method in typical reactor irradiation channels that are found in practice relies not just on accurate k_0 factors but also on Q_0 and $\bar{E}_r$ factors, the correlation between all these experimental constants should be kept in favour of the ultimate comparator nuclear data as much as possible, as it is the standard that should

be in principle later adopted by other laboratories in routine analysis. The use of an *f* value obtained from the average Cd-ratio of the co-irradiated comparators that were "sandwiching" the sample seems to be the best alternative for Q_0 determination.

On the other hand, the introduction of the *f* parameter for Q_0 (and k_0) determination is inevitable when Cd-covered irradiations were not performed.

6.3 The α-vector method for Q_0, s_0 and $\bar{E}_r$ determination

Most of the Q_0 factors in the recommended literature [20, 23] are correlated to $\bar{E}_r$ values that were first calculated in references [106, 107] (during 1979-87) with the aid of known resonance data at that time and, by employing eq. (2.48) as an analytical expression that was derived after assuming that a Breit-Wigner distribution describes any resonance accurately. In 1984, a method for the simultaneous experimental determination of Q_0 and $\bar{E}_r$ factors as a linear functional relationship to the α values from multi-channel results was introduced by Simonits et al. in [88], but it seems it has not been exploited in the literature since that publication, on which 11 (n,γ) reactions were investigated.

In this work we have derived and extended this method for the case of a non-linear α-relationship of the $\bar{E}_r$ parameter as a function of an isotope-specific *p* value, a parameter that was first proposed in reference [107] (1987). In that reference the following α-dependence was introduced to determine the actual $\bar{E}_r$ value to employ later in the calculations:

$$\bar{E}_{r,p,\alpha} = \bar{E}_r \exp\left(-\alpha\, p\right) \tag{6.8}$$

In this work, "the α-vector method" consists in calculating an experimental parameter Y_α, derived from eq. (2.41), defined for a given isotope and irradiation channel as a function of the comparator data and the normalized Cd-ratios (r_{Cd} or ω_{Cd} values; see eqs. (2.53) or (2.57)):

$$\begin{aligned} Y_\alpha &\equiv \ln\left\{\left(\omega_{Cd,c}Q_{\alpha,c}\right)-C_\alpha\right\} \\ &= \ln\left\{\omega_{Cd,c}\left(Q_0-C_0\right)_c\,\bar{E}_{r,p,\alpha,c}{}^{-\alpha}+\left(\omega_{Cd,c}-1\right)C_\alpha\right\} \\ &\equiv \ln\left\{Q_\alpha-C_\alpha\right\} \end{aligned} \tag{6.9}$$

According to eq. (2.41) and the substitution of the $\bar{E}_r$ function given in eq. (6.8), Y_α is also equivalent to a second order polynomial of α:

$$\begin{aligned} Y_\alpha &= p\alpha^2-\alpha\ln\left\{\bar{E}_r\right\}+\ln\left\{Q_0-C_0\right\} \\ &= p_3\alpha^2+p_2\alpha+p_1 \end{aligned} \tag{6.10}$$

where we made the change of variables:

$$\begin{aligned} Q_0 &\equiv \exp(p_1)+C_0 \\ \bar{E}_r &\equiv \exp(-p_2) \\ p &\equiv p_3 \end{aligned} \tag{6.11}$$

For $N\geq 2$ irradiation channels we would obtain the following transcendental system of equations:

$$\begin{pmatrix} Y_{\alpha_1} \\ \vdots \\ Y_{\alpha_N} \end{pmatrix} = \begin{pmatrix} p_3\alpha_1+p_2 & \cdots & 0 \\ \vdots & \ddots & \vdots \\ 0 & \cdots & p_3\alpha_N+p_2 \end{pmatrix}\begin{pmatrix} \alpha_1 \\ \vdots \\ \alpha_N \end{pmatrix}+\begin{pmatrix} p_1 \\ \vdots \\ p_1 \end{pmatrix} \tag{6.12}$$

It is clear that in order for eq. (6.12) to be solved, at least 2 irradiation channels are needed if we assume that $p_3\approx 0$ (negligible) or substitute it by its known numerical value. If the p_3 value is unknown and is not negligible,

then at least 3 irradiation channels are necessary for a simultaneous p_1, p_2 and p_3 determination.

The expansion of Y_α in power series of α (centred at α = 0) for a given channel, satisfies:

$$\begin{aligned}\exp\{Y_\alpha\} &= \exp\left\{\sum_{n=1}^{N} p_n \alpha^{n-1}\right\} \\ &= \prod_{n=1}^{N} \exp\left(p_n \alpha^{n-1}\right) \\ &= Q_\alpha - C_\alpha\end{aligned} \tag{6.13}$$

where the last equality is found if we assume that p_i = 0 (or negligible) for $i \geq 4$.

However, with the employment of N irradiation channels it is mathematically possible to find all the p_i coefficients up to p_N, being these factors negligible or not, after calculating the inverse of the non-singular A_M matrix in the following system:

$$\begin{aligned}\vec{Y}_\alpha &= \begin{pmatrix} Y_{\alpha_1} \\ \vdots \\ Y_{\alpha_N} \end{pmatrix} \\ &= \begin{pmatrix} {\alpha_1}^0 & \cdots & {\alpha_1}^{N-1} \\ \vdots & \vdots & \vdots \\ {\alpha_N}^0 & \cdots & {\alpha_N}^{N-1} \end{pmatrix} \begin{pmatrix} p_1 \\ \vdots \\ p_N \end{pmatrix} = \mathrm{A}_M \vec{p}\end{aligned} \tag{6.14}$$

and its corresponding multiplication with the Y_α-vector. The inverse of A_M needs to be calculated only once. It is also possible to obtain the p_i coefficients from a (N-1) degree polynomial regression on a Y_α versus α plot.

It is usually assumed that the p_3 values are zero for most the isotopes. This was the rule of thumb applied during the first compilations [36, 38, 40, 44,

45] as there was no reason to doubt the α-independence of the effective resonance energy. By forcing $p_3 = 0$, the Q_0 and $\bar{E}_r$ values can be calculated, for instance, from the least-squares linear fit method [188]:

$$\begin{aligned} p_2 &= \frac{S_{\alpha,Y_\alpha}}{S_\alpha} \\ p_1 &= \bar{Y}_\alpha - p_2\bar{\alpha} \end{aligned} \tag{6.15}$$

with the substitution of the mean values for Y_α and α (dashed), and the factors:

$$\begin{aligned} S_\alpha &= \langle \vec{\alpha} | \vec{\alpha} \rangle - N\bar{\alpha}^2 \\ S_{\alpha,Y_\alpha} &= \langle \vec{\alpha} | \vec{Y}_\alpha \rangle - N\bar{\alpha}\bar{Y}_\alpha \\ S_{Y_\alpha} &= \langle \vec{Y}_\alpha | \vec{Y}_\alpha \rangle - N\bar{Y}_\alpha{}^2 \end{aligned} \tag{6.16}$$

where the bracket notation means the inner product of the two vectors. The standard errors (SE) on the parameters p_1 and p_2 can be calculated from:

$$\begin{aligned} \mathrm{SE}_{p_1} &= s'\sqrt{(1/N) + \left(\bar{\alpha}^2/S_\alpha\right)} \\ \mathrm{SE}_{p_2} &= s'\left(1/\sqrt{S_\alpha}\right) \end{aligned} \tag{6.17}$$

With s' an estimator for the variance in the error between the actual Y_α point and its fitted value:

$$s' = \sqrt{\left(S_{Y_\alpha} - p_2 S_{\alpha,Y_\alpha}\right)/\left(N-2\right)} \tag{6.18}$$

The quality of the fit is measured by the correlation coefficient r^2:

$$r^2 = \frac{S_{\alpha,Y_\alpha}{}^2}{S_\alpha S_{Y_\alpha}} \tag{6.19}$$

If $W' = 0$, then eq. (6.9) can be written under the modified Westcott formalism (index W) as:

$$\begin{aligned} Y_{W\alpha} &\equiv \ln\left\{ s_0 \bar{E}_{r,p',\alpha}{}^{-\alpha} \right\} \\ &= \ln\left\{ g_T \right\} + \ln\left\{ G_t \beta_\alpha - z_{Cd} C_\alpha \right\} - \ln\left\{ G_r r_{Cd} \right\} \end{aligned} \tag{6.20}$$

which can be generalized to N channels as in eq. (6.14) but with $s_0 = \exp(p_1)$ instead.

6.3.1 Using the α-vector method for channel calibration

Clearly, if the Q_0 and $\bar{E}_r$ (or p_1 and p_2) values are well-known, the α-vector method can be reverse-engineered for α-calibration. If we assign the index i = 1,2 for two calibration isotopes (e.g. ^{94}Zr and ^{96}Zr), from eq. (6.10) we obtain the following expression when neglecting all p_3 values:

$$\begin{aligned} Y_{\alpha,i} &= \left(\alpha p_2 + p_1 \right)_i \\ &= \ln\left\{ 1 + \Omega_{Cd,i,c} D_{\alpha,c} \right\} + \ln\left\{ \omega_{Cd,i,c} \right\} + \left(p_1 + \alpha p_2 \right)_c \end{aligned} \tag{6.21}$$

where we have defined the auxiliary parameters:

$$\begin{aligned} D_{\alpha,c} &\equiv \exp\left(-Y_{\alpha,c} \right) = \frac{1}{\left(\dfrac{Q_{\alpha,c}}{C_\alpha} \right) - 1} \\ \Omega_{Cd,i,c} &\equiv 1 - \left\{ 1 / \omega_{Cd,i,c} \right\} \end{aligned} \tag{6.22}$$

If we subtract the eq. (6.21) for isotope "a" from the eq. (6.21) of isotope "b", we can obtain α numerically, from the following transcendental relation:

$$\alpha\left(\Delta p_2 \right) + \Delta p_1 = \ln\left\{ \left(\frac{1 + \Omega_{Cd,\mathrm{b}} D_\alpha}{1 + \Omega_{Cd,\mathrm{a}} D_\alpha} \right) \left(\frac{1 - \Omega_{Cd,\mathrm{a}}}{1 - \Omega_{Cd,\mathrm{b}}} \right) \right\}_c \tag{6.23}$$

that makes use of the following auxiliary definition:

$$\Delta p_j \equiv p_{j,\mathrm{b}} - p_{j,\mathrm{a}} \tag{6.24}$$

From the $\ln(1 + x^b) \leq bx$ identity for any $x \geq 0$ and $b \geq 1$, we obtain:

$$\alpha \leq \frac{1}{\Delta p_2}\left[\left(\Omega_{Cd,\mathrm{b}} - \Omega_{Cd,\mathrm{a}}\right)_c D_\alpha + \ln\left\{\frac{1-\Omega_{Cd,\mathrm{a}}}{1-\Omega_{Cd,\mathrm{b}}}\right\}_c\right] - \Delta p_1 \tag{6.25}$$

as a delimiter. Note that in eqs. (6.23) or (6.25), only the D_α and C_α parameters change on each iteration, while the ω_{Cd} values defined in eq. (2.57) are the only experimental (but fixed) parameters.

6.4 Experimental k_0 determination

By employing the Cd-subtraction technique [13] in up to 3 irradiation channels of the BR1 reactor, it was possible to determine the k_0 nuclear data for the characterization of up to 76 target isotopes of analytical interest (excluding uranium; see section 6.7). This method avoids the introduction of the modelled parameters *f, α, Q_o* and $\bar{E}_r$ and their uncertainties into the analytical result, which are of greater magnitude than the typical uncertainties of the other terms (see Chapter 7).

Since the application of k_0-NAA relies on the specific activities from a comparator that was co-irradiated next to the sample, it follows that its Cd-ratio would be a better indicator of the neutron fluence rate in that specific region. This alternative bears the lowest uncertainty and maintains the correlation in favour of the comparator results and its nuclear data. In this work, almost all our reported k_0 values were determined with the Cd-subtraction technique (see eq. (2.60)). These k_0 factors are therefore independent from the chosen *f, α,* Q_0 and $\bar{E}_r$ values. The few exceptions that required Q_0 or s_0 adoption for k_0 determination, as in eq. (2.37) with R_H or R_W as given in eqs. (2.31) or (2.65), will be quoted later in the text.

Still, although most of the Q_0 and $\bar{E}_r$ factors were not required for a k_0 determination, the k_0 factors from this work were tabulated along these quantities to have a complete self-consistent library of data. A verification of our results with the usual f (or β_α) and α-dependent relations of eqs. (2.31) or (2.65) was performed.

A fourth channel having a "pure" thermal neutron spectrum (the Cavity) was employed when feasible, which was especially suited for k_0 determination due to the absence of resonance contributions to the activation rate.

6.5 On the hybrid approach

In the section 2.11 we introduced some formulae to establish an equivalence between the modified Westcott and Høgdahl formalisms for 1/v isotopes and, for non-1/v isotopes having "flat" g_T factors, i.e. having a small g_T variation in the 20-100 ºC neutron (or channel) temperature region of interest.

One of the questions that remained was the validity of the $f^* \approx f$ approximation in eq. (2.97). The Figure 6.1 shows a graph of ln (f_α) or ln (β_α) versus the α parameter for the irradiation channels S84, Y4 and X26 and irradiation positions employed.

A polynomial fit of second order to the experimental points of the Figure 6.1 allowed us to obtain an empirical equation describing f_α (or β_α) as a function of α for the employed channels and irradiation positions at the institute.

Knowing that for a given function Y_x:

$$Y_x = \mathrm{e}^{Ax^2+Bx+C} = \mathrm{e}^{C}\,\mathrm{e}^{Ax\left(x+\frac{B}{A}\right)} \tag{6.26}$$

then we can write:

$$f_\alpha = f_0 \exp\left[\alpha\left(\alpha + zd_f\right)x_f\right] \tag{6.27}$$

with f_0 = 16.8, x_f = 74.8 and d_f = 0.0894. Similarly:

$$\beta_\alpha = z\beta_0 \exp\left[\alpha\left(z\alpha + d_\beta\right)x_\beta\right] \tag{6.28}$$

with β_0 = 17.2, x_β = 76.9 and d_β = 0.0854.

In the previous equations we introduced the constant $z = (2/\sqrt{\pi})$ ad hoc, which in eq. (6.27) is multiplying d_f while in eq. (6.28) is multiplying α. This was done to obtain similar (x, d) parameters on both fits (see Figure 6.1). In this way one can approximate $x_f \approx x_\beta$ and $d_f \approx d_\beta$, reducing therefore the number of parameters to just two, the average values x = 75.85 and d = 0.0874. The uncertainties for these parameters is not provided as one can take the uncertainty in f_α or $ß_\alpha$ from the classical (f ,α) calibration results instead, as given for instance in Table 6.6.

This set of (x, d) numbers characterizes the full (f, α) and/or ($ß$, α) range of the 3 irradiation channels at the BR1 reactor, under both adopted formalisms described in this work. Yet, the previous empirical "BR1 equations" were not derived to be used for k_0 and Q_0 calculations, but just to describe in a holistic approach the behaviour of f_α (or β_α) in our graphite-moderated research reactor and covered α range. Clearly, the validity of the previous empirical equations remains to be tested on other irradiation channels (and positions) of the same BR1 reactor, as well as in other NAA-capable nuclear reactors, to study other possible moderator/reflector dependences.

When computing the ratio between eqs. (6.27) and (6.28) one has:

$$\frac{\beta_\alpha}{f_\alpha} = z\left(\frac{\beta_0}{f_0}\right)\left(\frac{e^{z\alpha+d}}{e^{\alpha+zd}}\right)^{\alpha x} \tag{6.29}$$

and per the definition of f^* given in eq. (2.87), the previous equation can be written as:

$$\frac{f_\alpha^{\,*}}{f_\alpha} = \left(\frac{\beta_\alpha}{z}\right)\left(\frac{1}{f_\alpha}\right) = \left(\frac{\beta_0}{f_0}\right) e^{(z-1)(\alpha-d)(\alpha x)} \tag{6.30}$$

The Table 6.1 shows the numerical values for the terms in eq. (6.30). It can be seen that the condition $f^* \approx f$ is valid for our 3 irradiation channels, within an average 2.8% deviation from unity (0-5% full range), confirming what was observed by van Sluijs et al. in reference [45] for 5 irradiation channels: an average 2.6% deviation from unity in a full 0-5% range.

Table 6.1: Numerical values for the terms of eq. (6.30).

	S84	**Y4**	**X26**
$e^{(\alpha-d)(z-1)(\alpha x)}$	**1.003**	**0.986**	**1.025**
f_α^* / f_α	**1.027**	**1.008**	**1.049**

The term β_0/f_0 is constant and equal to 1.024

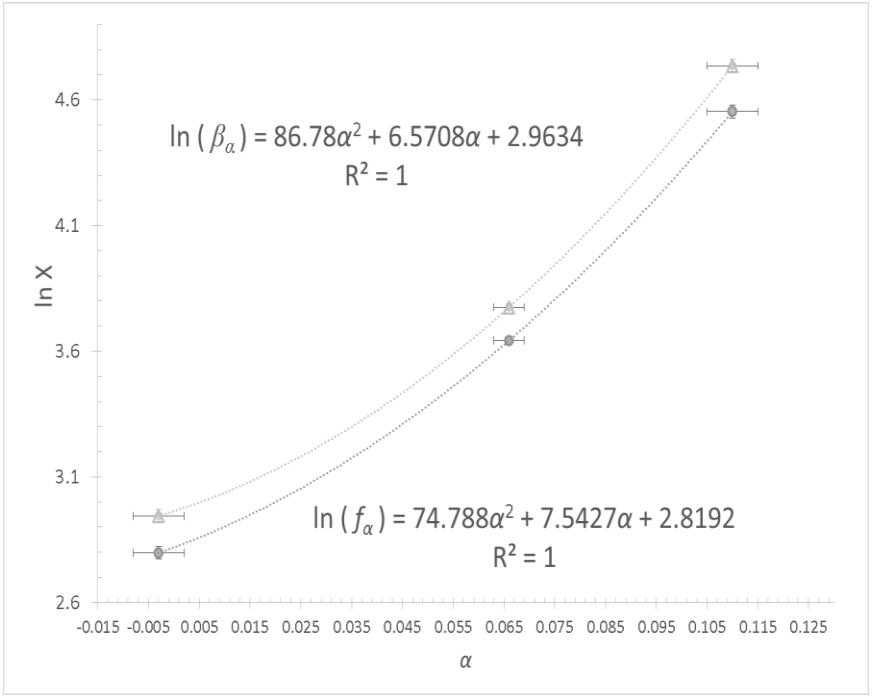

Figure 6.1: Graph of ln (f_α) and ln (β_α) vs. the α parameter for the BR1 reactor irradiation channels: S84, Y4 and X26 at the irradiation positions employed (see Table 6.6). A polynomial fit of 2nd order shows an empirical equation describing f_α (or β_α) as a function of α.

6.5.1 For 1/v nuclides

Since the Table 6.1 shows that $f^* > f$ for our irradiation channels of interest, then the approximation given in eq. (2.97) and the resulting Figure 2.4 are not quite accurate in providing the relative differences to expect for k_0 determination according to both formalisms (due to $R_H^* \neq R_H$). A better approximation is obtained for 1/v isotopes from eq. (2.93) by setting $g_T = 1$:

$$\left(\frac{k_{0,s,c,W}}{k_{0,s,c,H}}\right)_{1/v} \approx \frac{R_{H,s}}{R_{H,c}} \frac{\left\{R_{H,c}^{\ *} - \left(C_\alpha / f^*\right)\right\}}{\left\{R_{H,s}^{\ *} - \left(C_\alpha / f^*\right)\right\}} \tag{6.31}$$

where it is now clear that $(R_H^*/R_H) < 1$ for all isotopes (comparator and standard).

The Figure 6.2 shows that by adopting the modified Westcott convention for k_0 determination of typical 1/v cases, one is expected to observe differences of up to 0.4% for channel S84 and 0.6% for channel Y4, irrespectively of the Q_0 (or s_0) factor. For channel X26 on the other hand, the differences are expected to be up to 0.6% for isotopes with $Q_0 \leq 20$. For this channel, it can be as high as 1.4% for $Q_0 > 20$ and $Q_0 < 60$. The higher impact for high Q_0 factors on a thermalized channel as X26 when compared to a less thermalized channel as Y4, seems counter-intuitive, but a closer look indicates that this is because the (Q_α/f) term in R_H is higher than the (s_α/β_α) term in R_W by ~5% for X26, due to the $(f^*/f) = 1.05$. On the other hand, for Y4 the difference is just ~1% due to $(f^*/f) = 1.01$ (see Table 6.1).

The Figure 6.2 indicates that although up to 1.4% difference is expected, the adoption of the modified Westcott formalism for 1/v isotopes instead of the modified Høgdahl convention will not be statistically significant for k_0 (or elemental content) determinations at the 2s confidence level.

Employing 1 formalism only for all non-1/v and 1/v cases seems the next logical step, but given the fact that the much simpler Høgdahl convention

was already employed during the first k_0 determinations, we opted to keep (and recommend the use of) this convention for all 1/v cases and to report Q_0 factors as well.

6.5.2 For non-1/v cases

For the strong non-1/v isotopes of Table 2.1 the modified Westcott convention will be the only option for s_0 and k_0 determination, due to the significant differences to expect that were quoted in Table 2.2.

For the isotopes having "flat" g_T factors of Table 2.3 we shall apply both conventions aiming at reporting s_0 and Q_0 factors. However it was clear from the discussion in section 2.11 and the results in Table 2.4, that the g_T-independent R_H parameter from eq. (2.31) is not sufficiently accurate and should be substituted by the $R_{W\to H}$ parameter of eq. (2.86) in all related calculations:

$$R_{W\to H} = g_T G_{th} + G_e \frac{q_\alpha}{f^*} \tag{6.32}$$

with the employment of the actual f^* values quoted in Table 6.1. That is, the following change must be made for Q_0 determination from bare and Cd-covered irradiations:

$$q_0 = Q_0 - C_0 = g_T \left(\frac{G_{th}}{G_e} \frac{f^*}{r_{Cd}} \right) \left(\bar{E}_r \right)^\alpha \left(1\text{eV} \right)^{-\alpha} \tag{6.33}$$

while for proper k_0 determination per the Cd-subtraction technique or eq. (2.60) it is not difficult to show from eqs. (6.32) and (2.91) that one must use:

$$k_{0,s,c} = \frac{g_{T,c}}{g_{T,s}} k_{0,s,c,H} \tag{6.34}$$

with $k_{0,H}$ calculated according to the Høgdahl convention as in eq. (2.60).

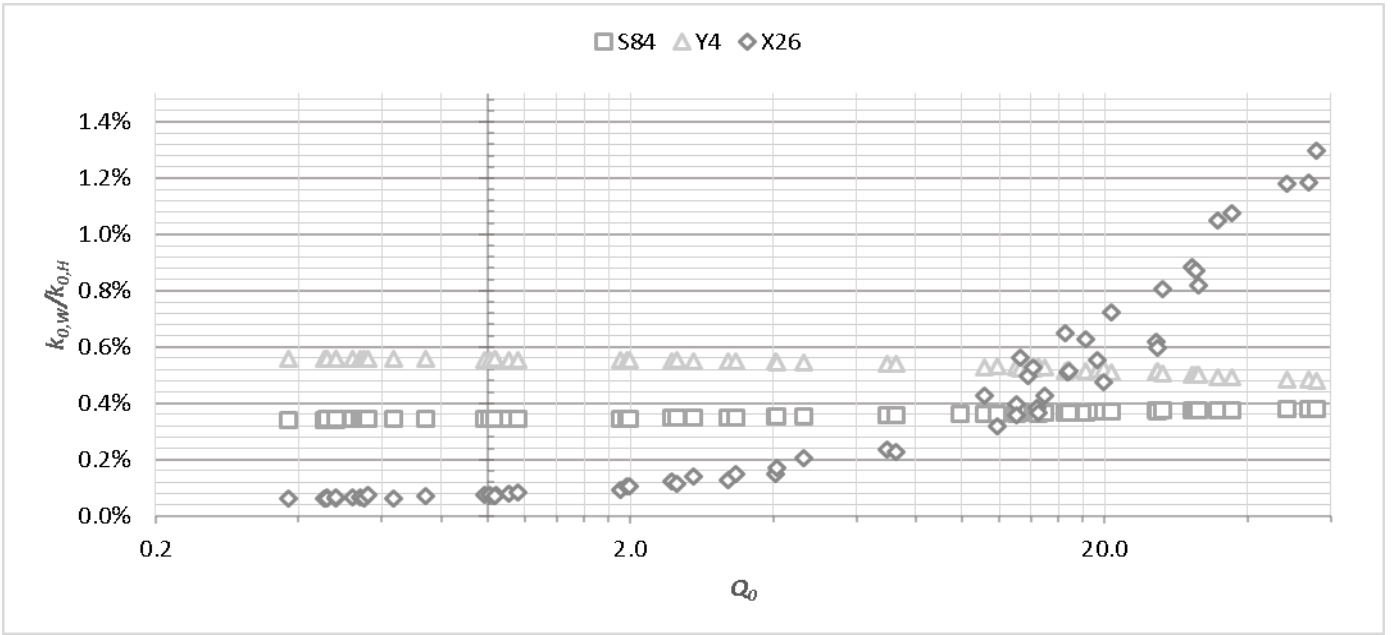

Figure 6.2: Expected % relative differences in experimental k_0 factors for several 1/v-nuclides (g_T = 1), when adopting the modified Westcott formalism ($k_{0,W}$) as compared to the modified Høgdahl convention ($k_{0,H}$), as a function of the Q_0 factor and for irradiations on 3 channels of the BR1 reactor covering the f, β_α and α ranges of interest.

6.6 Estimation of Cd-ratios

For Cd-covered irradiations the BR1 equations can provide a means to trace our R_{Cd} results. From eq. (2.52) we know that the Cd-ratio for any given radioisotope varies between irradiation channels and positions, i.e. it depends on α:

$$r_{Cd,\alpha} \equiv \frac{f_\alpha}{Q_\alpha}\left(\frac{G_t}{G_e}\right) \tag{6.35}$$

We can define for $\alpha = 0$:

$$r_{Cd,0} \equiv \frac{f_0}{Q_0}\left(\frac{G_t}{G_e}\right) \tag{6.36}$$

When combining the previous equation to our empirical relation in eq. (6.27) we obtain:

$$f_\alpha = \left(\frac{G_e}{G_t}\right) Q_0 r_{Cd,0}\left[\mathrm{e}^{\alpha\left(\alpha+zd_f\right)x_f}\right] \tag{6.37}$$

implying that:

$$\frac{r_{Cd,\alpha}}{r_{Cd,0}} = \frac{Q_0}{Q_\alpha}\left[\mathrm{e}^{\alpha\left(\alpha+zd_f\right)x_f}\right] \tag{6.38}$$

In this way one can estimate the r_{Cd} value to expect for a given radioisotope in any channel and position for which the multi-channel f_α function of eq. (6.27) has been determined, provided that the Q_0 and $\bar{E}_r$ factors are known. Thus, the k_0 community should be able to quickly estimate the r_{Cd} factors observed in this work, by inputting our experimentally determined Q_0 and $\bar{E}_r$ factors along the empirical curves for f (or β_α) described in eqs. (6.27) and (6.28).

6.7 Determination of k_0 and k_0-fission factors for k_0-UNAA

In 2010 some inconsistencies in the 2003 k_0-library were identified and studied by Blaauw et al. in [3] and a redetermination of the k_0-fission factors was also performed. They concluded that their results were consistent with literature factors except for the 610.3 keV line of ^{103}Ru, although several of their k_0 results were within a 3-4% relative difference with the k_0-literature (in a few cases even higher) and hence, in line with our observed overestimation in the previous section [85]. After performing a recalibration of our laboratory detectors (section 3.4), irradiation channel positions (sections 2.16 and 4.5) and, the gain in experience in the determination of k_0 nuclear data, we proceeded to perform the redetermination of the k_0 factors for the characterization of ^{238}U and ^{235}U. The goal was to introduce new k_0-fission factors for some radioisotopes that are only produced by fission of ^{235}U, mainly those for which our instruments were sensitive enough under the stringent irradiation and measurement conditions that are usually required for this kind of metrological work and for those γ-lines that are believed to be free from spectral interferences (or that could be corrected).

The ADS type VI currently exposed in the k_0-literature in [20, 21] was reviewed in section 2.12, due to inconsistencies found in its application to the ^{131}I case. The correct ADS type for the measurement of ^{131}I is denoted in this work as “VI/b”.

6.8 Standards and sample preparation

6.8.1 For the study of (n,γ) reactions

For the determinations of (n,γ) reactions we employed the standards listed in the Table 6.3. The standards matrices consisted in pure compounds, pure and metal alloys in thin sheets, plates and wires; water solutions at 5 to 10% acid content from different well-known providers. These standards are Certified Reference Materials (CRMs), i.e. these materials were fabricated for checking the quality and metrological traceability of products, validation of analytical techniques, measurement methods, calibration of instruments, etc.

Some standards from the Institute of Reference Materials and Measurements (IRMM) in the Table 6.3 are labelled NOC for "Not on Catalog". These materials were fabricated between 1966-1976 when the institute was known as the Central Bureau for Nuclear Measurements (CBNM) and currently there is no catalog number or official certificate available other than a digital catalog file from mail correspondences with Goedele Sibbens (same institute provider) and Joseph Oeyens (SCK•CEN provider). Although an official certificate is required by the CRM definition given in International Organization for Standardization (ISO) guide ISO30:2015 [189] these materials are especially suited for absolute nuclear data measurements as explained by Lamberti et al. in "Reference materials: from CBNM to IRMM" because at that time great metrological focus and new techniques were developed in order to provide the nuclear community with the reference materials needed for the determination of nuclear data [190]. The main advantage of employing them for this work is that most of them consisted in metal Al alloys with sufficiently diluted quantities of the analyte as to avoid any significant neutron self-shielding but at the same time be detectable with good statistics at far sample-detector distances.

The Table 6.3 also details the kind of sample, typical mass and shape obtained from the respective standard. A discussion about weighing, moisture, drying and packaging is given in the next sections. There were 3 groups of samples prepared from all the standards classified per their matrix type, namely:

a) Pure or metal alloys that were shaped as thin foils (F), wires (W), thin disks and "dots". The foils and disks were of varying thickness, typically ≤ 0.1 mm and Ø = [7;9] mm with some having Ø = [4;14] mm. The wires were of varying length, typically ≤ 2 cm and Ø = [0.5;1] mm and were rolled up in spiral (RUIS) when necessary or when large enough to be bendable mainly because the SOLCOI code is meant for calculations on cylindrical samples with their axis parallel to the detector crystal axis and not for wires lying flat along that axis (perpendicular cylinders). The few samples regarded as "dots" were ≤ 2 mm in length and diameter but were modelled as cylinders as any other sample.

b) Liquids on paper disks (LP): Aliquots of typically 100 µL of water with 5 to 10% acid solution (i.e. 90-110 mg) having ≤ 1% analyte content (i.e. ≤ 1.1 mg) were deposited from a polyethylene pipette onto ~1.25 mm thick cylindrical cellulose filters of Ø = 7 mm, ~32 mg and $\rho \approx 0.67$ g.cm^{-3}. The samples were dried at room temperature (see further).

c) High-purity (HP) powder compounds with no sample preparation other than moisture analysis (%L), weighing and packaging into typically ≤ 1 x 1 cm^2 square polyethylene bags of 0.1 mm thickness (SPEB).

The comparator consisted mainly in 0.1% Au Al-alloy foils of 0.1 mm thickness and 8 mm diameter (IRMM 530R) with occasional use of 1% Au Al-alloy foils (IRMM TP 695 and TP 1511) with the same dimensions. For irradiations in the thermal Cavity, the comparator consisted in a high-purity Au wire (Goodfellow AU0005150).

6.8.2 For ^{235}U fission and ^{238}U activation

For the determination of the ^{235}U k_0-fission factors and the k_0-factors for the radiative neutron capture of ^{238}U we employed 3 different uranium standards:

- the 1 mm diameter Al-alloy wire with 0.1% U content (IRMM SP 89010; 0.6% uncertainty at 1*s*) used in the first k_0-fission factors determination in [54] (later compiled in references [20, 21, 23]). This standard has a U isotopic composition of 5.834% ^{238}U, 0.227% ^{236}U, 93.155% ^{235}U, 0.781% ^{234}U, less than 0.0001% for both ^{232}U and ^{233}U, and a U molar mass of 235.211;

- the liquid standard with 9.993 ± 0.017 mg/g of U content (assumed natural; NIST SRM 3164) used in the 2010 k_0-fission factors redetermination performed by Blaauw et al. [3];

- the 0.1 mm thick Al-alloy foil with 0.2% U content (IRMM NS 20017) used in the first (and until now only) determination of k_0 factors for the (n,γ) capture of ^{238}U [13]. This material has a U isotopic composition of 99.9520% ^{238}U, 0.0375% ^{235}U, less than 0.0005% both ^{236}U and ^{234}U, and a U molar mass of 237.973.

6.8.3 Weighing, moisture analysis and drying

The balance employed in this work (see Figure 6.4) was from manufacturer Mettler-Toledo (Switzerland) model XP Ultra-microbalance, which offers a 0.1 μg readability and 0.25 μg repeatability [191]. The liquids on papers, compounds and respective containers were weighed 3 times during packaging. Foils and wires were weighed 2 times when cut prior packaging and 2 times during packaging. The moisture percent (%L) in each powder compound (see the Table 6.3) was found with the aid of an infrared moisture analyser model MA100H from manufacturer Sartorius (Germany) [192],

operating in constant heating mode over 2.6 minutes at a temperature of 180 ºC and 1-2 g samples.

The preparation of the liquids on paper disks is depicted in the Figure 6.5. The papers disks (A) were placed inside 2.5 mm height and Ø = 8.1 mm cylindrical HDPE vials (B; ~168 mg; $\rho \approx 0.95$ g.cm^{-3}) before being pipetted with the 100 µL aliquots (C) and were later dried at room temperature (20 ºC) for 24-36 h under the controlled environment (D) provided by a partially recirculating downflow cabinet from LAF Technologies (Australia) model "AURA Mini" (see Figure 6.3). This workstation employs a High-efficiency Particulate Air H14 filter with 99.995% overall collection efficiency on 0.1-0.2 µm particles at 0.45 m/sec [193].

Figure 6.3 The partially recirculating downflow cabinet from LAF Technologies (Australia) model AURA Mini employed in this work for sample drying at room temperature (20 ºC) for 24-36 hours. The cabinet complies with a Class 100 (FED STD 209E) - ISO 5 (ISO 14644-1 Standard) environment throughout the work area [193]**.**

Figure 6.4 The Sartorius Infrared Moisture Analyzer MA100H (left) and the Mettler Toledo XP Ultra-microbalance (right) employed in this work for moisture and sample mass determinations [191, 192]**.**

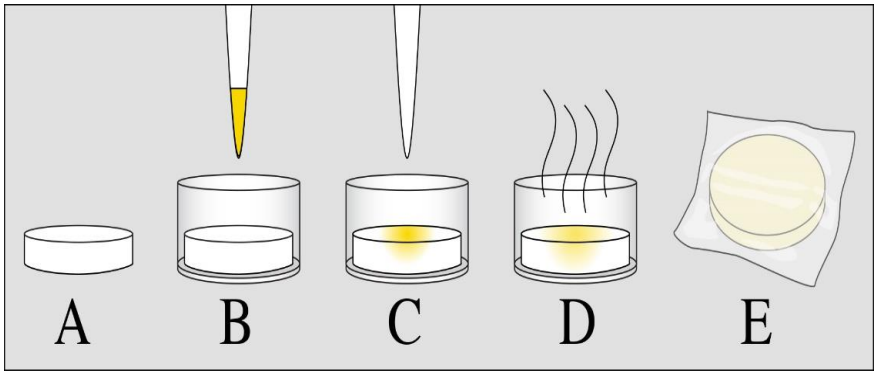

Figure 6.5: The preparation and packaging of the liquids on paper disks samples. Explanation of the A, B, C, D, E figures is given in the text.

6.8.4 Packaging and blanks

For irradiation of the bare and Cd-covered samples, the paper disks, compounds, foils, disks and wires were packed twice directly into (0.7 x 0.7) up to (2 x 2) cm^2 square polyethylene plastic bags (SPEB; see Figure 6.6) of 0.1 mm thickness instead of employing the typical HDPE vials:

- to avoid further thermalization of the neutron flux or (f, α) variations as in the case of samples placed inside Cd-covers ($f = 0$) and for low-Q_0 isotopes ($f \approx Q_\alpha$) where the reaction ratio is susceptible to a small $f \neq 0$;

- to avoid additional scattering of neutrons by the container walls, which cannot be modelled by the neutron self-shielding calculation methods adopted in this work;

- to keep the sample geometry simple to model, i.e. small, thin and as similar as the comparator geometry as possible (i.e. a 0.1 mm foil), to minimize errors due to the efficiency transfer calculations and the effect of neutron flux gradients.

In the case of the paper disks one must consider that it is possible that the solution content was not fully (and uniformly) absorbed by the matrix (see Figure 6.5; E). Therefore, the respective HDPE vials employed at the time of pipetting (see Figure 6.5; B or C) were packed separately along blank paper disks for irradiation and counting. This procedure allowed us to later determine and subtract the induced activity of any residual amount of analyte left over in the respective HDPE vial and any trace amount already present in the blank paper disks. The Table 6.2 shows the average elemental content found in these blanks.

Table 6.2. Average elemental content found in the blanks which consisted on paper disks and the HDPE containers employed when pipetting the liquids on the paper disks (see Figure 6.5; D). Uncertainties are half-widths estimated from the range of observed values.

	Content in µg/g	
Element	**Paper disk (~32 mg)**	**HDPE vial (~168 mg)**
Na	< 6	
Al	0.155(2)	0.065(8)
Cl	< 5	0.7(2)
K		n.d.
Cr		0.35(4)
Mn	0.0060(6)	
Co	0.0050(5)	
As		< 1
Br	0.010(1)	< 0.1
Rb		n.d.
Ru		n.d.
Cd		n.d.
Cs		< 1
Pt		n.d.
Eu		< 3
Yb		< 2

The worst blank subtraction was ≤ 0.05% for some Eu samples based on ~1 mg calculated deposited analyte in the paper disk. Some elements were not detected (n.d.), i.e. were below our detection limits.

Figure 6.6. A sample of high-purity BaO powder packed into a 2 x 2 cm^2 square PE bag of 0.1 mm thickness. This picture corresponds to the biggest sample size obtained at 660 mg with h = 0.4 + 2(0.1) mm = 0.6 mm total thickness for irradiations under the channel Cavity. Most samples were ≤ 1 x 1 cm^2 and 0.15 to 0.3 mm thick.

6.8.5 Self-shielding correction factors

The thermal and epithermal neutron self-shielding correction factors G_{th} and G_e reported in the Table 6.3 were obtained through the Chilian et al. [77, 78, 104] and the MatSSF [79, 101] methods described in the sections 4.1.4 and 4.2.1. These approaches were adapted for our specific experimental conditions for G_{th} and G_e computations [83, 84] (see sections 4.9 and 4.10).

We gave more weight to the Chilian et al. method for the G_{th} results since we determined experimental x_{th} factors for channels S84, Y4 and X26 in section 4.9 and demonstrated that it is more accurate than the MatSSF code for these specific calculations.

On the other hand, we gave more weight to the G_e correction factors from MatSSF because the code showed to be more accurate than the Chilian et al. method (see section 4.10).

The correction factors were negligible for most of the samples with ≤ 5% thermal self-shielding expected on the samples employed for Sr, Pd, Cd, In, Sn, Ga, Ta, Pt investigation. The epithermal self-shielding effects were neutralized for Sr, Pd, Dy and Ta by irradiating the samples in a "pure" thermal channel (the Cavity) and/or by irradiating sufficiently diluted standards when possible.

For the comparator employed in the channel Cavity (GF AU0005150) the thermal self-shielding was estimated experimentally at G_{th} = 0.87(7) with the aid of a 5% Au Al-alloy material (IRMM TP1002) that was "free" of thermal self-shielding effects. For the uranium materials both correction factors were negligible for the depleted and enriched Al-alloys. For the for the NIST liquid solution one can estimate G_e = 0.97 for ^{238}U.

The work from Trkov et al. showed that the MatSSF and Chilian et al. methods are < 0.8% different than the results from a Monte Carlo transport code for metal alloys with 5% neutron self-shielding (as in this work) [101].

Table 6.3: Materials employed in this work for the study of 52 elements: provider and catalog number, typical amount of standard applied (mg), sample geometry, sample matrix and the standard elemental content (% weight). The parameter *h* is either the diameter (for wires) or the sample thickness (for all other geometries) and is tabulated next to the calculated G_{th} and G_e values for each material, target isotope and formed nuclide.

Provider / Sample	Matrix	Element	%	h (mm)	G_{th}	G_e	TI	FN
HF 31434 * 10 to 24 mg (0.1 to 0.23 mm) in (0.7 x 0.7) cm^2 SPEB ρ = 2.16 $g.cm^{-3}$ (NaCl) 1.9% %L	HP NaCl 99.5%	Na	39.14	0.15	0.97	0.99	^{23}Na	^{24}Na
SWX 543b * 521 mg (Ø=12.7 mm) ρ = 2.16 $g.cm^{-3}$ (NaCl) 0.08% %L	Disk, NaCl 99.95+%		39.32	1.905	0.81	0.92		
AA 013832 * 100 mg (Ø=7 mm) Na_2CO_3 in H_2O 5% HNO_3	LP		0.1	1.25	1.00	1.00		

Provider / Sample	**Matrix**	**Element %**		**h (mm)**	G_{th}	G_e	**TI**	**FN**
GF MG000320 * 44 mg (Ø=8 mm) ρ = 1.738 g.cm^{-3}	Disk, HP Mg	Mg	99.99+	0.5	1.00	1.00	^{26}Mg	^{27}Mg
GF AL000391 * 2.1 mg (Ø=8 mm) ρ = 2.7 g.cm^{-3}	F, Al metal	Al	99.99+	0.015	1.00	1.00	^{27}Al	^{28}Al
IRMM NOC * 3.4 mg (Ø=4 mm) ρ = 2.7 g.cm^{-3}	F, Al metal		99.99+	0.1	1.00	1.00		
HF 31434 * 9 to 25 mg (0.1 to 0.23 mm) in (0.7 x 0.7) cm^2 SPEB ρ = 2.16 g.cm^{-3} (NaCl) 1.9% %L	HP NaCl 99.5%	Cl	60.36	0.15	0.97	1.00	^{37}Cl	^{38}Cl
AA 13866 * 100 mg (Ø=7 mm) KNO_3 in H_2O 5% HNO_3	LP	K	0.1	1.25	1.00	1.00	^{41}K	^{42}K

Provider / Sample	Matrix	Element	%	h (mm)	G_{th}	G_e	TI	FN
IRMM NOC * 17 mg (Ø=9 mm) ρ = 2.985 g.cm^{-3} (Sc) ρ = 2.7 g.cm^{-3} (Al/Sc)	F, Al/Sc alloy	Sc	1	0.1	1.00	1.00	^{45}Sc	^{46}Sc
IRMM NOC * 62 mg (Ø=14 mm) ρ = 4.506 g.cm^{-3}	F, Ti metal	Ti	99.99	0.1	0.99	1.00	^{50}Ti	^{51}Ti
GF V000310 * 4.25 mg (Ø=3 mm) ρ = 6.0 g.cm^{-3}	F, V metal	V	99.8	0.125	0.99	1.00	^{51}V	^{52}V
IRMM SP2440 * 12 mg (Ø=5 mm) ρ = 6.02 g.cm^{-3} (V/Co)	F, V/Co alloy	V Co	99 1	0.1	0.99	1.00 0.99	^{51}V ^{59}Co	^{52}V ^{60}Co

Provider / Sample	Matrix	Element %		h (mm)	G_{th}	G_e	TI	FN
GF CR000190 * 22 mg (Ø=9 mm) ρ = 7.1 g.cm^{-3}	F, Cr metal	Cr	99.99	0.05	1.00	1.00	^{50}Cr	^{51}Cr
IRMM NOC * 29 mg (Ø=4 mm) * 45 mg (Ø=5 mm) ρ = 2.88 g.cm^{-3} (Al/Cr)	Slab, Al/Cr alloy		10	0.8	1.00 0.99	1.00 1.00		
IRMM SP 89069 * 3.4 mg (Ø=4 mm) * 13 mg (Ø=8 mm) ρ = 7.43 g.cm^{-3} (Mn) ρ = 2.705 g.cm^{-3} (Al/Mn)	F, Al/Mn alloy	Mn	1	0.1	1.00	1.00	^{55}Mn	^{56}Mn

Provider / Sample	Matrix	Element	%	h (mm)	G_{th}	G_e	TI	FN
IRMM NOC * 54 mg (25 mm) RUIS ρ = 7.87 g.cm^{-3} (Fe) ρ = 2.752 g.cm^{-3} (Al/Fe)	W, Al/Fe alloy	Fe	1	1	1.00	1.00	^{58}Fe	^{59}Fe
GF FE000406 * 198 mg (Ø=8 mm) ρ = 7.87 g.cm^{-3}	F, Fe metal		99.99+	0.5	0.97	1.00		
GF FE000401 * 99 mg (Ø=8 mm) ρ = 7.87 g.cm^{-3}	F, Fe metal		99.99+	0.25	0.98	1.00		
IRMM 528R * 10.5 mg (Ø=7 mm) * 13.5 mg (Ø=8 mm) ρ = 8.9 g.cm^{-3} (Co) ρ = 2.762 g.cm^{-3} (Al/Co)	F, Al/Co alloy	Co	1	0.1	1.00	0.99	^{59}Co	^{60}Co
GF CO005110 * 3.5 mg (2 mm) dots ρ = 8.9 g.cm^{-3}	W, Co metal		99.99+	0.5	0.90	0.54		

Provider / Sample	Matrix	Element %		h (mm)	G_{th}	G_e	TI	FN
IRMM NOC * 45 mg (Ø=8 mm) ρ = 8.908 g.cm^{-3}	F, Ni metal	Ni	99.99+	0.1	0.99	1.00	^{64}Ni	^{65}Ni
IRMM NOC * 22 mg (Ø=10 mm) ρ = 8.96 g.cm^{-3} (Cu) ρ = 3.33 g.cm^{-3} (Al/Cu)	F, Al/Cu alloy	Cu	10	0.1	1.00	1.00 1.00	^{63}Cu ^{65}Cu	^{64}Cu ^{66}Cu
GF CU005295 * 7 mg (1 mm) dots ρ = 8.96 g.cm^{-3}	W, Cu metal		99.99+	1	0.98	0.78 0.95	^{63}Cu ^{65}Cu	^{64}Cu ^{66}Cu
IRMM 522A * 11 mg (Ø=4 mm) * 45 to 57 mg (Ø=8 to 9 mm) ρ = 8.96 g.cm^{-3}	F, Cu metal		99.99+	0.1	0.99	0.88 0.98	^{63}Cu ^{65}Cu	^{64}Cu ^{66}Cu
GF ZN000220 * 9 mg (Ø=8 mm) ρ = 7.14 g.cm^{-3}	F, Zn metal	Zn	99.95+	0.025	1.00	1.00 1.00	^{64}Zn ^{68}Zn	^{65}Zn ^{9m}Zn

Provider / Sample	Matrix	Element	%	h (mm)	G_{th}	G_e	TI	FN
IRMM NOC * 36.5 mg (17 mm) * 53.6 mg (25 mm) RUIS ρ = 5.907 g.cm^{-3} (Ga) ρ = 2.732 g.cm^{-3} (Al/Ga)	W, Al/Ga alloy	Ga	1	1	1.00	0.99	^{71}Ga	^{72}Ga
SCP CLAS2-2Y * 50 - 100 mg (Ø=7 mm) As metal in H_2O 2% HNO_3	LP	As	0.1	1.25	1.00	1.00	^{75}As	^{76}As
NIST SRM 3103a * 100 mg (Ø=7 mm) As metal in H_2O 10% HNO_3	LP		1	1.25	1.00	0.98		

Provider / Sample	Matrix	Element	%	h (mm)	G_{th}	G_e	TI	FN
SCP ASBR9-2Y * 100 mg (Ø=7 mm) NaBr in H_2O	LP	Br	0.1	1.25	1.00	0.99	^{81}Br	^{82}Br
AA 40013 * 19 to 26 mg (0.15 mm) in (0.7 x 0.7) cm^2 SPEB * 76 to 99 mg (0.3 mm) in (1 x 1) cm^2 SPEB * 163 to 229 mg (0.5 to 0.7 mm) in (1 x 1) cm^2 SPEB ρ = 3.27 $g.cm^{-3}$ 0.06% %L	HP $KBrO_3$ 99.8%		47.75	0.15 0.3 0.7	1.00 0.99 0.98	0.86 0.77 0.65		
NIST SRM 3145a * 100 mg (Ø=7 mm) Rb metal in H_2O 1% HNO_3	LP	Rb	1	1.25	1.00	1.00 1.00	^{85}Rb ^{87}Rb	^{86}Rb ^{88}Rb

Provider / Sample	**Matrix**	**Element %**		**h (mm)**	G_{th}	G_e	**TI**	**FN**
SA 204455	HP $SrCO_3$	Sr	59.35	0.15	1.00	1.00	^{84}Sr	^{85}Sr
* 41 to 88 mg	99.995%			0.25	1.00	1.00		
(0.15 to 0.25 mm)				0.6	0.99	0.99		
in (1 x 1) cm^2 SPEB				1.2	0.99	0.99		
* 165 mg (0.5 mm)								
in (1 x 1) cm^2 SPEB								
ρ = 3.5 $g.cm^{-3}$				0.15		0.98	^{86}Sr	^{87}Sr
0.13% %L				0.25		0.96		
				0.6		0.92		
* 250 to 600 mg				1.2		0.87		
(0.5 to 1 mm)								
in (1.3 x 1.3) cm^2 SPEB								

Provider / Sample	Matrix	Element	%	h (mm)	G_{th}	G_e	TI	FN
IRMM NOC * 23 mg (Ø=8 mm) * 29 mg (Ø=9 mm) ρ = 4.47 g.cm^{-3} (Y) ρ = 4.49 g.cm^{-3} (Y/Ta)	F, Y/Ta alloy	Y	99.3	0.1	1.00	0.98	^{89}Y	^{90m}Y
SA 205168 * 60 to 75 mg (0.15 mm) in (1 x 1) cm^2 SPEB * 120 to 150 mg (0.25 to 0.3 mm) in (1 x 1) cm^2 SPEB * 170 to 340 mg (0.15 to 0.3 mm) in (1.5 x 1.5) cm^2 SPEB ρ = 5.01 g.cm^{-3} 0.03% %L	HP Y_2O_3 99.99%		78.74	0.15 0.3 0.6	1.00 1.00 0.99	0.98 0.96 0.93		
AA 10594 * 41 mg (Ø=8 mm) * 53 mg (Ø=9 mm) ρ = 6.52 g.cm^{-3}	F, Zr metal	Zr	99.5	0.127	1.00	0.98 0.97	^{94}Zr ^{96}Zr	^{95}Zr ^{97}Zr

Provider / Sample	Matrix	Element	%	h (mm)	G_{th}	G_e	TI	FN
IRMM NOC * 22 mg (Ø=10 mm) ρ = 2.7 g.cm^{-3}	F, Al/Nb alloy	Nb	10	0.1	1.00	1.00	^{93}Nb	^{94m}Nb
IRMM 525A * 12 mg (Ø=9 mm) ρ = 8.57 g.cm^{-3}	F, Nb metal		99.99+	0.022	1.00	0.98		
K 366/013/74/G * 33 mg (Ø=8 mm)	F, Nb metal		99.99+	0.076	1.00	0.95		
GF MO000220 * 7.5 mg (Ø=6 mm) * 13 mg (Ø=8 mm) ρ = 10.28 g.cm^{-3}	F, Mo metal	Mo	99.9	0.025	1.00	0.97 0.98	^{98}Mo ^{100}Mo	^{99}Mo ^{101}Mo
AA 42686 * 99 mg (Ø=11 mm) ρ = 12.45 g.cm^{-3} (Ru) ρ = 20.75 g.cm^{-3} (Pt/Ru)	F, Pt/Ru alloy	Ru	4.6	0.05	1.00	1.00 1.00 1.00	^{96}Ru ^{102}Ru ^{104}Ru	^{97}Ru ^{103}Ru ^{105}Ru
AA 035767 * 100 mg (Ø=7 mm) $RuCl_3$ in H_2O 20% HNO_3	LP		0.1	1.25	1.00	1.00 1.00 1.00	^{96}Ru ^{102}Ru ^{104}Ru	^{97}Ru ^{103}Ru ^{105}Ru

Provider / Sample	Matrix	Element	%	h (mm)	G_{th}	G_e	TI	FN
GF PD0005145 * 5 mg (2 mm) “dots” * 55 mg (23 mm) RUIS ρ = 12.023 g.cm^{-3}	W, Pd metal	Pd	99.99+	0.5	0.98	0.31 0.97	^{108}Pd ^{110}Pd	^{109}Pd ^{111m}Pd
GF AG007100 * 16.7 mg tube crunched into 0.46 mm (thick) x 2 mm “dots” ρ = 10.49 g.cm^{-3}	Tube, Ag metal	Ag	99.95+	0.46	0.81	0.58 0.20	^{107}Ag ^{109}Ag	^{108}Ag ^{110m}Ag
IRMM TP1248 *13 mg (Ø=8 mm) ρ = 2.78 g.cm^{-3} (Al/Ag)	F, Al/Ag alloy		1	0.1	1.00	1.00 0.99	^{107}Ag ^{109}Ag	^{108}Ag ^{110m}Ag
IRMM TP1187 * 21 mg (Ø=10 mm) ρ = 2.71 g.cm^{-3} (Al/Ag)	F, Al/Ag alloy		0.1	0.1	1.00	1.00 1.00	^{107}Ag ^{109}Ag	^{108}Ag ^{110m}Ag
IRMM TP514 * 16 mg (30 mm) RUIS ρ = 2.78 g.cm^{-3} (Al/Ag)	W, Al/Ag alloy		1	0.5	1.00	1.00 0.98	^{107}Ag ^{109}Ag	^{108}Ag ^{110m}Ag
IRMM SP1819 * 16 mg (30 mm) RUIS	W, Al/Ag alloy		1	0.5	1.00	1.00 0.98	^{107}Ag ^{109}Ag	^{108}Ag ^{110m}Ag

Provider / Sample	Matrix	Element	%	h (mm)	G_{th}	G_e	TI	FN
NIST SRM 3108 * 100 mg (Ø=7 mm) Cd metal in H_2O 10% HNO_3	LP	Cd	1	1.25	0.96	1.00	^{114}Cd	^{114}Cd
IRMM TP705 * 37 mg (Ø=8 mm) ρ = 7.31 g.cm^{-3} (Sn/In)	F, Sn/In alloy	In	15.4	0.1	0.97	1.00 0.50	^{113}In ^{115}In	^{114m}In ^{116m}In
IRMM TP704 * 37 mg (Ø=8 mm) ρ = 7.31 g.cm^{-3} (Sn/In)	F, Sn/In alloy		5.15	0.1	0.99	1.00 0.71	^{113}In ^{115}In	^{114m}In ^{116m}In
IRMM TP702 * 13.6 mg (Ø=8 mm) * 3.4 mg (Ø=4 mm) ρ = 2.75 g.cm^{-3} (Al/In)	F, Al/In alloy		1	0.1	1.00	1.00 0.97	^{113}In ^{115}In	^{114m}In ^{116m}In
IRMM NOC * 13 mg (Ø=8 mm) * 30 mg (Ø=12 mm) ρ = 2.701 g.cm^{-3} (Al/In)	F, Al/In alloy		0.017	0.1	1.00	1.00 1.00	^{113}In ^{115}In	^{114m}In ^{116m}In

Provider / Sample	**Matrix**	**Element %**		**h (mm)**	G_{th}	G_e	**TI**	**FN**
IRMM TP705	F, Sn/In alloy	Sn	84.6	0.1	0.97	0.99	^{112}Sn	^{113}Sn
* 37 mg (Ø=8 mm)						0.89	^{116}Sn	^{117m}Sn
ρ = 7.31 g.cm^{-3} (Sn/In)						1.00	^{124}Sn	^{125}Sn
IRMM TP704	F, Sn/In alloy		94.85	0.1	0.99	0.99	^{112}Sn	^{113}Sn
* 37 mg (Ø=8 mm)						0.88	^{116}Sn	^{117m}Sn
ρ = 7.31 g.cm^{-3} (Sn/In)						0.99	^{124}Sn	^{125}Sn
IRMM NS99025	F, Al/Sb alloy	Sb	1	0.1	1.00	1.00	^{121}Sb	^{122}Sb
* 13.6 mg (Ø=8 mm)						1.00	^{123}Sb	^{124}Sb
* 31 mg (Ø=12 mm)								
ρ = 6.684 g.cm^{-3} (Sb)								
ρ = 2.74 g.cm^{-3} (Al/Sb)								
NIST SRM 3111a	LP	Cs	1	1.25	1.00	0.98	^{133}Cs	^{134}Cs
* 100 mg (Ø=7 mm)								
Cs salt in H_2O								
1% HNO_3								

Provider / Sample	Matrix	Element	%	h (mm)	G_{th}	G_e	TI	FN
SA 554847 * 67 to 172 mg (0.15 to 0.3 mm) in (1 x 1) cm^2 SPEB * 250 to 300 mg (0.2 mm) in (1.5 x 1.5) cm^2 SPEB * 660 mg (0.4 mm) in (2 x 2) cm^2 SPEB ρ = 5.72 $g.cm^{-3}$ 0.15% %L * 540 mg (1.2 mm) inside PE vial (Ø=8 mm) for channel Cavity	HP BaO 99.99%	Ba	89.57	<0.6 1.2	1.00 0.99	1.00 0.99 0.99 1.00 0.97	All ^{130}Ba ^{132}Ba ^{134}Ba ^{138}Ba	 ^{131}Ba ^{133m}Ba ^{135m}Ba ^{139}Ba
IRMM TP781 * 13.6 mg (Ø=8 mm) ρ = 6.15 $g.cm^{-3}$ (La) ρ = 2.74 $g.cm^{-3}$ (Al/La)	F, Al/La alloy	La	1	0.1	1.00	1.00	^{139}La	^{140}La

Provider / Sample	Matrix	Element	%	h (mm)	G_{th}	G_e	TI	FN
IRMM NOC * 13 mg (6 mm) * 26 mg (12 mm) * 52 mg (24 mm) RUIS ρ = 6.77 g.cm^{-3} (Pr) ρ = 2.751 g.cm^{-3} (Al/Pr)	W, Al/Pr alloy	Pr	1.25	1	1.00	0.99	^{141}Pr	^{142}Pr
IRMM NOC * 23 mg (20 mm) * 46 mg (40 mm) RUIS ρ = 7.52 g.cm^{-3} (Sm) ρ = 2.7 g.cm^{-3} (Al/Sm)	W, Al/Sm	Sm	0.008	0.74	1.00	1.00	^{152}Sm	^{153}Sm
AA 035753 * 100 mg (Ø=7 mm) Eu_2O_3 in H_2O 5% HNO_3	LP	Eu	0.1	1.25	0.98	1.00	^{151}Eu ^{153}Eu	^{152}Eu ^{154}Eu
IRMM NOC * 285 mg (Ø=9 mm) ρ = 7.895 g.cm^{-3} (Gd) ρ = 2.702 g.cm^{-3} (Al/Gd)	Disk, Al/Gd alloy	Gd	0.03	1.6	0.95	1.00 1.00	^{152}Gd ^{158}Gd	^{153}Gd ^{159}Gd

Provider / Sample	Matrix	Element	%	h (mm)	G_{th}	G_e	TI	FN
IRMM NOC * 27 mg (2 x 2 mm) dots * 60 mg (3 x 3 mm) dots ρ = 8.23 g.cm^{-3} (Tb) ρ = 2.76 g.cm^{-3} (Al/Tb)	Slabs, Al/Tb alloy	Tb	1	3	0.99	1.00	^{159}Tb	^{160}Tb
IRMM TP780 * 17 mg (Ø=8 mm) * 32 mg (Ø=11 mm) ρ = 8.54 g.cm^{-3} (Dy) ρ = 3.31 g.cm^{-3} (Dy/Al)	F, Al/Dy alloy	Dy	27	0.1	0.93	0.99	^{164}Dy	^{165}Dy
IRMM TP1611 * 20 mg (Ø=9.5 mm) ρ = 2.80 g.cm^{-3} (Dy/Al)	F, Al/Dy alloy		5	0.1	0.98	1.00		
IRMM SP237 * 20 mg (Ø=9.5 mm) ρ = 2.71 g.cm^{-3} (Dy/Al)	F, Al/Dy alloy		0.127	0.1	1.00	1.00		
IRMM TP1838 * 40 mg (Ø=13.5 mm) ρ = 8.79 g.cm^{-3} (Ho) ρ = 2.8 g.cm^{-3} (Ho/Al)	F, Al/Ho alloy	Ho	5	0.1	1.00	0.98	^{165}Ho	^{166}Ho

Provider / Sample	Matrix	Element	%	h (mm)	G_{th}	G_e	TI	FN
AA 13824 * 100 mg (Ø=7 mm) Tm_2O_3 in H_2O 5% HNO_3	LP	Tm	0.1	1.25	1.00	1.00	^{169}Tm	^{170}Tm
AA 13819 * 100 mg (Ø=7 mm) Yb_2O_3 in H_2O 5% HNO_3	LP	Yb	0.1	1.25	0.99	1.00 1.00 1.00	^{168}Yb ^{174}Yb ^{176}Yb	^{169}Yb ^{175}Yb ^{177}Yb
IRMM NS20018 * 21 mg (Ø=10 mm) * 31 mg (Ø=12 mm) ρ = 9.84 g.cm^{-3} (Lu) ρ = 2.71 g.cm^{-3} (Lu/Al)	F, Al/Lu alloy	Lu	0.1	0.1	1.00	1.00	^{176}Lu	^{177}Lu

Provider / Sample	Matrix	Element	%	h (mm)	G_{th}	G_e	TI	FN
IRMM SP1823	W, Al/Hf alloy	Hf	5	1	0.99	1.00	^{174}Hf	^{175}Hf
* 10 mg (4.5 mm)						0.98	^{179}Hf	^{180m}Hf
* 31 mg (14 mm)						0.97	^{180}Hf	^{181}Hf
RUIS								
ρ = 13.31 g.cm^{-3} (Hf)								
ρ = 2.81 g.cm^{-3} (Hf/Al)								
IRMM NOC	W, Al/Hf alloy		0.1	1	1.00	1.00	^{174}Hf	^{175}Hf
* 64 mg (30 mm) RUIS						1.00	^{179}Hf	^{180m}Hf
ρ = 2.711 g.cm^{-3} (Hf/Al)						1.00	^{180}Hf	^{181}Hf

Provider / Sample	Matrix	Element %		h (mm)	G_{th}	G_e	TI	FN
GF TA000490 * 84 mg (Ø=8 mm) for channel Cavity ρ = 16.69 g.cm^{-3} (Ta)	F, Ta metal	Ta	99.9	1	0.97	0.36	^{181}Ta	^{182}Ta
IRMM NOC * 23 mg (Ø=8 mm) * 29 mg (Ø=9 mm) ρ = 4.49 g.cm^{-3} (Y/Ta)	F, Ta/Y alloy		0.7	0.1	1.00	0.99		
NIST SRM 3155 * 100 mg (Ø=7 mm) Ta metal in H_2O; 10% HNO_3 + 1% HF	LP		1	1.25	1.00	0.96		

Provider / Sample	Matrix	Element	%	h (mm)	G_{th}	G_e	TI	FN
IRMM NS 00043 * 6 mg (20 mm) RUIS ρ = 2.702 g.cm^{-3} (Al/W)	W, Al/W alloy	W	0.01	0.37	1.00	1.00	^{186}W	^{187}W
IRMM NOC * 31 mg (Ø=12 mm) ρ = 2.733 g.cm^{-3} (Al/W)	F, Al/W alloy		0.2	0.5	1.00	1.00		
IRMM TP932 * 31 mg (Ø=12 mm) ρ = 2.87 g.cm^{-3} (Al/W)	F, Al/W alloy		1	0.1	1.00	1.00		
IRMM TP1448 * 32 mg (Ø=12 mm) ρ = 19.25 g.cm^{-3} (W) ρ = 3.53 g.cm^{-3} (Al/W)	F, Al/W alloy		5	0.1	1.00	0.97		
IRMM NOC * 43 mg (20 mm) * 64 mg (30 mm) * 86 mg (40 mm) RUIS ρ = 21.04 g.cm^{-3} (Re) ρ = 2.722 g.cm^{-3} (Al/Re)	W, Al/Re alloy	Re	0.118	1	1.00	1.00 1.00	^{185}Re ^{187}Re	^{186}Re ^{188}Re

Provider / Sample	Matrix	Element %		h (mm)	G_{th}	G_e	TI	FN
GF PT0005145 * 4-9 mg (1-2 mm) dots ρ = 21.45 g.cm^{-3}	W, Pt metal	Pt	99.99+	0.5	0.97	0.83 0.63	^{196}Pt ^{198}Pt	^{197m}Pt ^{199}Pt
AA 42686 * 99 mg (Ø=11 mm) ρ = 20.75 g.cm^{-3} (Pt/Ru)	F, Pt/Ru alloy		95.35	0.05	0.99	0.88 0.88	^{196}Pt ^{198}Pt	^{197m}Pt ^{199}Pt
AA 13827 * 100 mg (Ø=7 mm) Pt metal in H_2O 20% HCl	LP		0.1	1.25	1.00	1.00 1.00	^{196}Pt ^{198}Pt	^{197m}Pt ^{199}Pt
IRMM SP 91091 * 23 mg (10 mm) * 30 mg (13 mm) RUIS ρ = 11.724 g.cm^{-3} (Th) ρ = 2.774 g.cm^{-3} (Al/Th)	W, Al/Th alloy	Th	0.819	1	1.00	1.00	^{231}Th	^{233}Pa

Provider / Sample	Matrix	Element %		h (mm)	G_{th}	G_e	TI	FN
IRMM SP 89010 * 20 mg (10 mm) RUIS ρ = 2.716 g.cm^{-3} (Al/U)	W, Al/U alloy; enriched ^{235}U	U	0.1	1	1.00	1.00 1.00	^{238}U ^{235}U	^{239}U FP
NIST SRM 3164 * 100 mg (Ø=7 mm) U in H_2O 10% HNO_3	LP; natural		1	1.25	1.00	0.97 1.00	^{238}U ^{235}U	^{239}U FP
IRMM NS 20017 * 32 mg (Ø=12 mm) ρ = 2.733 g.cm^{-3} (Al/U)	F, Al/U Alloy; depleted ^{235}U		0.2	0.1	1.00	1.00 1.00	^{238}U ^{235}U	^{239}U FP
See text for more U material info								

Provider / Sample	Matrix	Element %		h (mm)	G_{th}	G_e	TI	FN
GF AU0005150 * 4-8 mg (1-2 mm) dots ρ = 19.3 g.cm^{-3}	W, Au metal	Au	99.99+	0.5	0.83	0.15	^{197}Au	^{198}Au
IRMM TP1002 * 32 mg (Ø=12 mm) * 14 mg (Ø=8 mm) ρ = 3.53 g.cm^{-3} (Al/Au)	F, Al/Au alloy		5	0.1	1.00	0.93		
IRMM TP1511 * 14 mg (Ø=8 mm) ρ = 2.866 g.cm^{-3} (Al/Au)	F, Al/Au alloy		1	0.1	1.00	0.99		
IRMM TP 695 * 14 mg (Ø=8 mm) ρ = 2.866 g.cm^{-3} (Al/Au)	F, Al/Au alloy		1	0.1	1.00	0.99		
IRMM 530R * 14 mg (Ø=8 mm) ρ = 2.717 g.cm^{-3} (Al/Au)	F, Al/Au alloy		0.1	0.1	1.00	1.00		

Providers: GF = Goodfellow; AA = Alfa Aesar; IRMM = Institute for Reference Materials and Measurements; NIST = National Institute of Standards and Technology; SA = Sigma-Aldrich; K = Kawecki; SWX = Shieldwerx; SCP = SpexCertiPrep.
NOC = Not on catalogue (see text for more information).
W = Wire; F = Foil; LP = Liquid pipetted on a cylindrical paper filter; HP = High-purity; SPEB = Square polyethylene bag of 0.1 mm thickness; RUIS = Rolled-up in spiral; FP = fission product.
%L = moisture content in the compound (in %).
The provided sample mass, wire lengths and neutron self-shielding correction factors are typical values (i.e. averaged and/or rounded; informative). The exact applied figures for each sample were inputted in the database and/or calculated on run-time based on the accurate knowledge of the matrix, geometry, compound purity and (adopted) standard elemental content.

6.9 The irradiation channels

The BR1 is a graphite moderated and air-cooled research reactor working with natural uranium at 4 MW. The channels X26 and S84 are pneumatically-driven, while channel Y4 is not (see Figure 6.7). For the irradiations in channel Y4 the samples are loaded before the reactor start. After 420 minutes, the reactor is shut down and the samples are dismantled the next morning (> 16 h decay). Considering the ramping up and down of the neutron fluence rate, the irradiations on this channel are usually fixed at 429(5) minutes each.

Both channels X26 and S84 use a pneumatic system that allows one rabbit per irradiation, thus only one irradiation position is employed for these channels. Channel Y4 on the other hand makes use of a metal ship as depicted in Figure 4.8.

The Table 6.4 shows previously reported f and α values for channels Y4 and S84 over the years and in this work [172, 193, 194].

If the expanded standard uncertainty in the determination of f for channel Y4 is assumed at U = 5.3% at the 95% confidence level (k = 2.306; N = 9) based on the historic records in Table 6.4, then the 11% relative difference between the 1996 [194] and 2006 [195] mean values is statistically significant at this confidence level when performing a two-tailed t-test (t = 4.78). The difference could be due to changes in the nuclear data, instruments or reactor changes over these 10 years [173, 194, 195]. Yet, when comparing our results with the latest independent calibrations of 2006 and 2008, the relative differences of 0.5% and 2% for channel Y4 are not statistically significant (t = 0.22 and t = 0.87; respectively). The expanded standard uncertainty for the parameter α of channel Y4 is coincidentally equal to that of f (with same coverage factor).

For channel S84, if we assign an expanded uncertainty U = 3.6% in the determination of the f parameter at the 95% confidence level (k=2.517; N = 6), then the 5% difference between the 1996 and 2006 results is statistically significant at this confidence level (t = 3.57). The 6% difference between our result and the 2008 independent calibration is also statistically significant (t = 4.28), but it is not when compared to the 2006 result instead (1.5% difference; t = 1.07). Curiously between 1993 and 1996 one also observes a significant 4% variation, thus the records might suggest an average 5% flip-flop in the magnitude of f at intervals of 2-3 years for this channel. The expanded standard uncertainty for the parameter α of channel S84 is on the other hand U = 19.5% (k = 2.517).

In general, our latest (2011) results for channel Y4 and S84 are not statistically significant when compared to results from the last 5 years. There was no published data available for channel X26 prior to this work.

Table 6.4: Previously determined f and α values for channels Y4 and S84 of reactor BR1 over the past years and in this work [173, 194, 195]**.**

Y4		**S84**		
f	***α***	***f***	***α***	**Year**
32.8	0.060			1992
32.7	0.072	16.8	-0.01	1993
35.4	0.063	17.5	-0.006	1996 [194]
35.8	0.061			1996 [194]
33.4	0.069			1996 [194]
37.5	0.062	16.1	-0.009	2006 [195]
39.4	0.059	17.2	-0.016	2006 [195]
37.5	0.062	17.4	-0.013	2008
38.2	*0.066*	*16.4*	*-0.0034*	*2011 (TW)*
35.9	**0.064**	**16.9**	**-0.010**	Mean
6.9%	6.8%	3.3%	47.8%	% SD
2.3%	**2.3%**	**1.4%**	**19.5%**	u = % SD/$\sqrt{N}$; Gaussian
2.306	*2.306*	*2.571*	*2.571*	k for 95% confidence
9		**6**		***N***

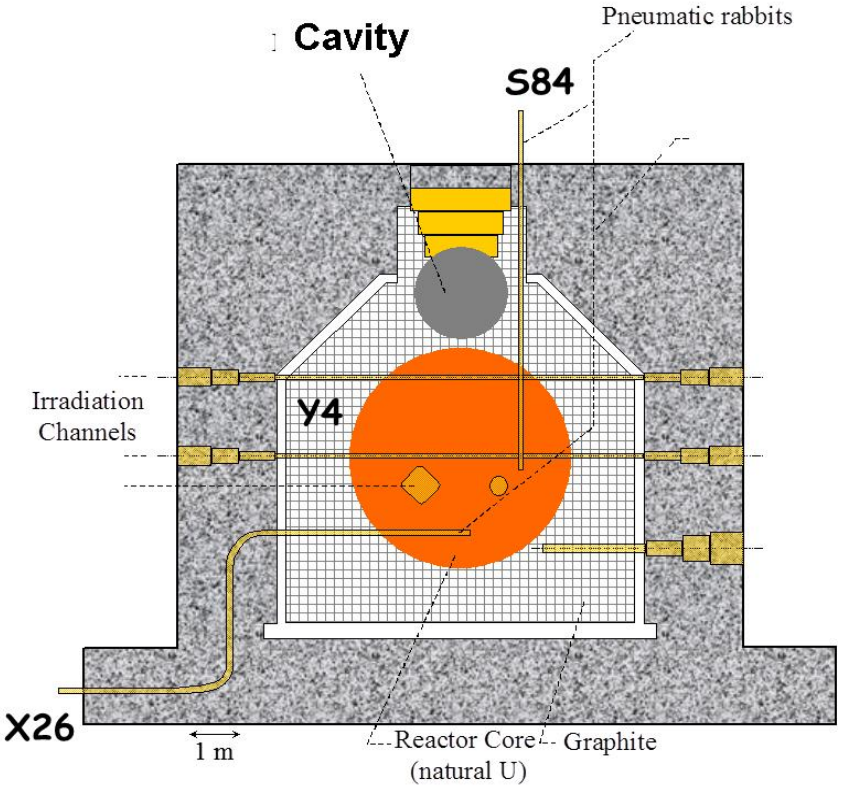

Figure 6.7: Representation of the reactor BR1 at the SCK•CEN and the 4 irradiation channels employed in this work. Channel Y4 is horizontal (yellow; middle of the picture) and perpendicular to both channels S84 (vertical) and X26 (horizontal and curved). The Cavity channel is, as its name suggest, a hollow sphere in the thermal column of the reactor. Channel dimensions given in Table 6.6)

6.10 Rabbits

On average 8 samples were prepared per irradiation channel per investigated element. Half of these samples were placed along the axis of a cylindrical polyethylene irradiation container or "rabbit", while the other samples were covered in hollow Cd-cylinders of 1 mm wall thickness. Inside the rabbit, each sample was sandwiched between 2 comparators within 2 cm separation to each one. See Figure 6.8 and Figure 6.9 for a graphic description.

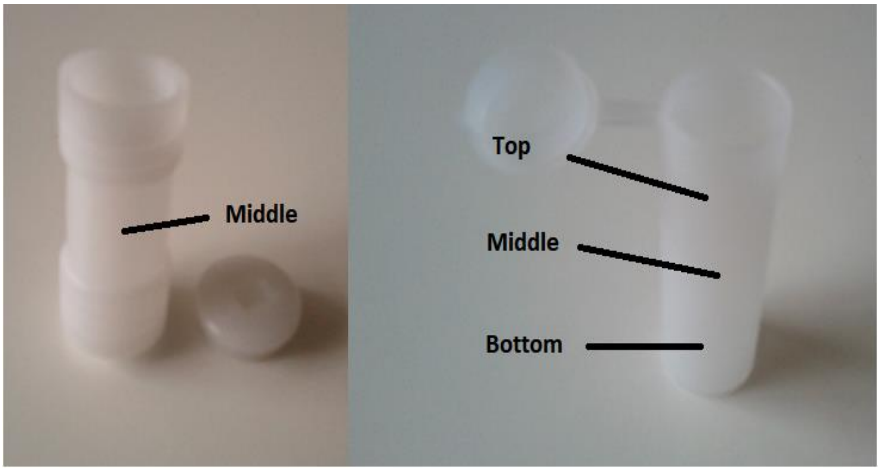

Figure 6.8: Rabbits employed for the irradiation of samples in the pneumatic channel S84 (left; Ø=2 cm and 5.3 cm length) and for the manually loaded metal ship of channel Y4 (right; Ø=2.2 cm and 7.1 cm length; see Figure 4.8). Top, middle and bottom positions are equidistant within 2 cm.

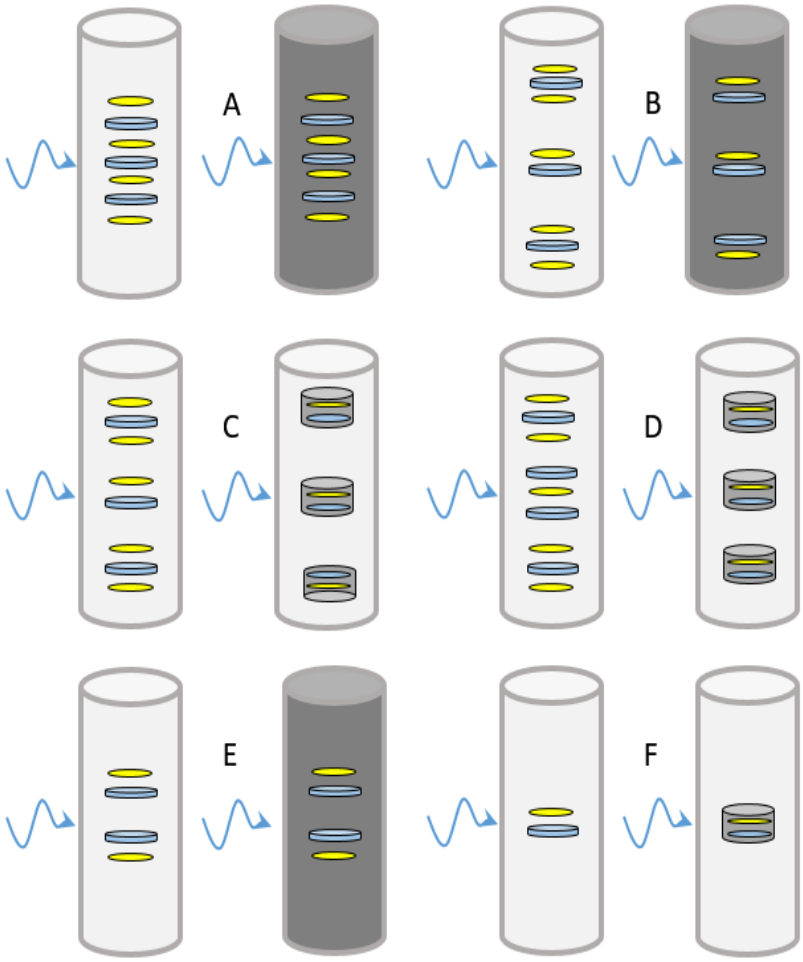

Figure 6.9: Sample packaging inside the HDPE rabbit for the different configurations employed for the irradiations in channels X26 (A and B), Y4 (C and D) and S84 (E and F). Sample positioning within the rabbit was achieved with the aid of small quantities of tissue paper. Yellow and Blue samples are the comparator and the analyte sample (respectively).

6.11 Irradiations and total samples

The rabbits were irradiated under the full extent of the neutron fluence rate of channels S84, Y4, X26 and the thermal Cavity at the BR1. The Cd-covered rabbits were irradiated within 30 min, 1 hour and 1 day separation to the normal rabbits for channels S84, X26 and Y4 (respectively).

Each experiment was fully repeated on each irradiation channel 2-3 times at different epochs, meaning that up to 8 samples per irradiation channel were tested. This translates in up to 24 samples (excluding the comparators) irradiated over 3 irradiation channels at the BR1 during these three years of experiments. Some targets were investigated in a fourth channel (the Cavity).

It is important to note that each standard is usually a mono-element or isotopic standard and that it will be useful in the study of 1, 2 and rarely 3 radioisotopes of interest. For the study of the 52 elements, the sample preparation of 412 to 1248 samples and twice the number of comparators would be required (average 2490). The actual number of samples irradiated in this work was 1923 since one must consider that not all elements were tested in all the channels and that the pure and metal alloy samples such as the comparator and others with short to medium lived radioisotopes can be reused after 20 half-lives. Realistically, this kind of research keeps the detectors busy for long periods since although comparators can be measured rather quickly some samples required 1 and up to 4 week long measurements and not all radioisotopes can be measured at the desired times. Although we aimed at the most metrological care, mistakes can happen when dealing with the preparation, irradiation, measurement and calculation of an average ~12.3 samples per (full) week on a 3-year frame. This justified the strong need for the development of a software with algorithms that kept track of scheduled measurements, database changes and probable inputted typos.

For the experiments related to ^{235}U and ^{238}U k_0-nuclear data determination 4 samples of each material were prepared, with masses of 20 to 32 mg for the Al-alloy materials (12 mm diameter foils; 1 cm long wires) and typically 100 µL for the liquid standard spiked on cylindrical paper disks as with the other samples (1.25 mm thickness and 7 mm diameter).

Since we employed 3 materials for U, half of the samples (6) were placed along the axis of a cylindrical polyethylene irradiation container or "rabbit", sandwiched between at least two comparators with a 2 cm separation to each one, while the other half were packed similarly in another rabbit for a replicate neutron irradiation 2 weeks later. These two irradiations were carried under the full extent of the neutron fluence rate of channel Y4 at the SCK•CEN BR1 reactor in the year 2012.

6.12 Channel parameters

The Table 6.6 summarizes the BR1 reactor irradiation channels characteristics, the typical irradiation times and rabbit sizes employed.

From the bare irradiations of the Al-Lu material and eq. (2.80) it was possible to estimate the g_T Westcott factors for the four irradiation channels (Y4, S84, X26 and the thermal Cavity) employed in this work. After comparing these values to the values reported by Holden for $^{176}Lu(n,\gamma)^{177}Lu$ as a function of the average neutron temperature [16], we extrapolated the channel temperatures quoted in Table 6.5.

The channels f, β_α and α characteristics reported in Table 6.6 might be slightly different than the exact values reported during our calibration experiments in the tables of section 4.5. This is because the former calibration experiments were performed between 2009 and 2010, and by the time of our Q_0 (or s_0) redetermination experiments (2011-2012) a re-monitoring of the fluence rate parameters for these channels was clearly

necessary to obtain the most representative channel parameters at the irradiations positions employed and, to discard significant gradients in the channel parameters during these irradiations. For Q_0 determination we opted to employ the Cd-ratios from the ^{197}Au results as the substitute for the f (or β_a) parameter in the calculations, to keep the correlation to the comparator nuclear data. This is performed by means of eqs. (2.56) and (6.9). For k_0 determination per the Cd-subtraction technique, the knowledge on the f (or β_a) parameter is not required.

Table 6.5: Experimental g_T Westcott factors obtained in this work for the four irradiation channels employed (Cavity, Y4, S84 and X26), from the analysis of the ^{176}Lu(n,γ)^{177}Lu non-1/*v* reaction and the quoted γ-rays.

	g_T (% SD; 1*s*)							
γ (keV)	**Cavity**		**Y4**		**S84**		**X26**	
112.9	1.78	(1.0)	1.82	(0.5)	1.99	(0.8)	1.79	(0.9)
208.4	1.75	(1.0)	1.79	(0.6)	1.95	(0.8)	1.76	(0.8)
AVG	1.77	(1.2)	1.80	(1.4)	1.97	(1.4)	1.78	(1.2)
Temperature (°C)	**23**	**± 2**	**27**	**± 2**	**50**	**± 4**	**25**	**± 2**

Temperatures were obtained by comparison with the g_T factors from Holden [16] and the uncertainties are expanded uncertainties at the 95% confidence level (k = 3.182).

Values between parentheses are relative SD (in %) from different determinations.

Table 6.6: Neutron parameters (f, α, βα, Cα) for the BR1 irradiation channels employed in this work (Y4, S84, X26 and the Cavity). Radius r and length l of these channels (first line) and rabbits (second line) in mm, with the typical irradiation time t_{irr} applied to each rabbit. Uncertainties at the 1*s* confidence level.

Y4		**S84**		**X26**		**Cavity**	
f	*α*	*f*	*α*	*f*	*α*	*f*	*α*
38.2(9)	0.066(3)	16.4(4)	-0.003(5)	95.0(23)	0.110(5)	70000	-
β_α	C_α	β_α	C_α	β_α	C_α	β_α	C_α
43.6(6)	0.40	19.0(5)	0.43	114(3)	0.38	-	-
r	*l*	*r*	*l*	*r*	*l*	*r*	*l*
50	500	40	300	40	300	40	300
11.1	71	10	53	20	80	15	60
t_{irr} = *429(5) m*		t_{irr} = *3600(2) s*		t_{irr} = *180(1) m*		t_{irr} = *240(1) m*	

The recalibration of our channels was performed by employing the set of monitors: ^{55}Mn, ^{59}Co, ^{64}Zn, ^{98}Mo and ^{232}Th (along the comparator ^{197}Au) as basis. The target isotope ^{176}Lu was employed as temperature monitor (see eq. (2.80)). This set of monitors is slightly different than the one employed in section 4.5. The target isotope ^{96}Zr was not included in our new set of calibration monitors because for all our employed channels the $Q_\alpha >> f$ and our results would be subject of too much uncertainty. The target isotope ^{94}Zr was not included in our calibration set because we found more recent measurements of its decay branching factors (F_i) in reference [8] that we could employ for its Q_0 and k_0 redetermination instead. After observing that our Q_0 results for ^{58}Fe, ^{81}Br and other recommended target isotopes such as ^{93}Nb and ^{159}Tb confirmed the recommended literature with sufficient accuracy (as shown by our results in section 10.6), these target isotopes were therefore added to our calibration set for increasing the robustness of our fits and to verify if the withdrawal of ^{94}Zr and ^{96}Zr from the calibration set could influence drastically our results. Thus, Table 6.6 contains our most

representative α values at the time of k_0 and Q_0 determination. The f (or β_α) values reported in there are representative of the neutron fluence rates as observed by the ultimate comparator.

For channel X26 we observed a variation of 10% in α between our results in Table 10.3 and our more recent results, but it did not seem to be related to either ^{94}Zr and/or ^{96}Zr inclusion in the set. For channel S84 the α parameter is close to 0, thus its inherent uncertainty is too high as to conclude if these two monitors had an impact on it.

Burn-up effects are negligible under a thermal fluence rate of the order of ~1x10^{11} cm^{-2}.s^{-1} for a 7h irradiation time as shown in section 4.4. That is, for all channels employed in this work we did not expect any loss of analyte due to this undesired effect.

6.13 Measurements

Between 12-18 measurements per sample were taken, distributed through 3-6 different HPGe detectors attached to Dual LFC modules for dead-time correction. For Q_0 determination the samples were measured at 1, 15, 20 and 27 cm sample-detector separations, while for k_0 determination only the measurements at the farthest distances were considered (15 to 27 cm), corresponding to multisource-calibrated (or reference) positions where the coincidence gamma effects are negligible (or easy to model) and efficiency calculations are more accurate (see section 3.4 to 3.9). The linear mass-attenuation coefficients were taken from the online NIST XCOM database [143] and the solid angles were taken for the specific energy of interest by a software adaptation of SOLCOI [71]. This software uses the method described in [13, 141, 142] for efficiency transfer. The deconvolutions were performed with the HyperLab 2009 spectrometry software [138] (see section 3.3).

For the experiments related to uranium, a total of 15 measurements per sample were taken during the span of 3 months, distributed through 3 different detectors. The measurements were done at 27 cm sample-detector separation as before. Unfortunately, at this distance from the detector crystal and after at least 16 h decay, our sensitivity was greatly reduced for fission products with < 4 h half-life, which were not dealt with in this work.

6.14 Data-handling

For all the computations, a home-made software in C# 4.0 programming language [90] was developed. It was focused around the concept of using SQL databases [196] (e.g. nuclear and laboratory libraries) for the fast storing and querying of great amounts of data points.

Secondly, the software was focused in the implementation of several constraints (algorithms) for reducing the chances of systematic errors in the data input (e.g. data-redundancy). Thirdly, it was focused in the automation and coupling of the detection system (e.g. measurement labelling, logging, scheduling) and lastly, in the use of intensive NAA calculation (and/or verification) routines, which were to be triggered as soon as any correlated parameter has been updated in any given database. Such state-of-the-art programming environments were chosen in view of their data crunching advantages and multi-interfacing capabilities [90, 196, 197].

Figure 6.10 to Figure 6.13 show the screenshots (pictures) of some modules of the developed software that were designed for data-input and/or computations. Unfortunately, due to time and budget constrains the software did not reach the required maturity /stability for public release (no detailed user-guide, major and minor user-interface modifications remaining etc.), although all core algorithms were fully developed and tested for all related

computations in this work. The description of these software modules is given in the figures.

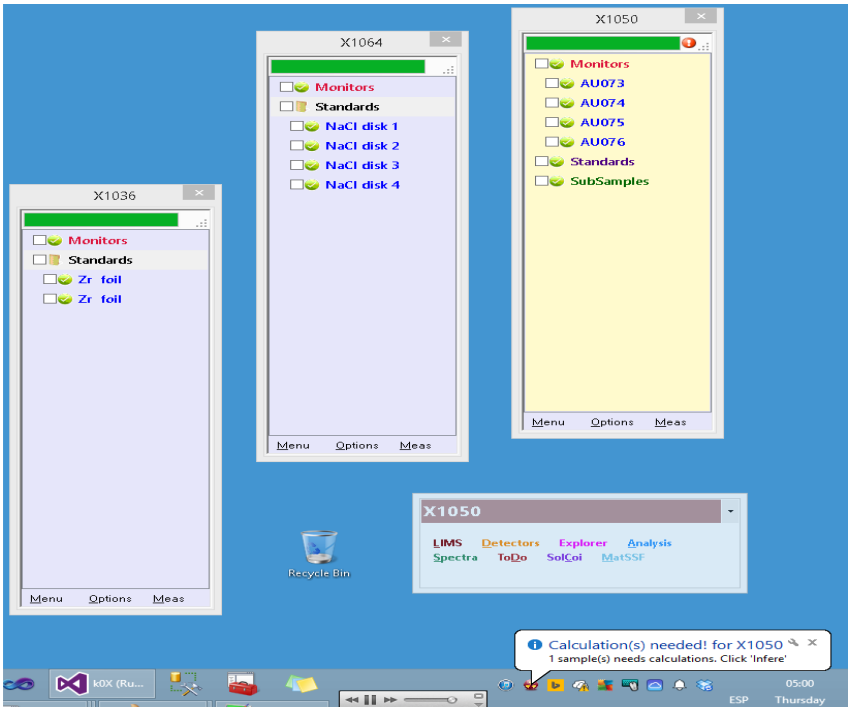

Figure 6.10: Screenshot of the software for k_0 nuclear data determination developed in this work. A rectangular menu provides a link to several user-friendly sub-modules (LIMS, Detectors, Explorer, etc.) where the databases can be filled, linked and manipulated (see Figure 6.11). Three "virtual rabbits" are shown, corresponding to three separated irradiation exercises (X1036, 64 and 50) which are being processed at the same time (multi-tasking). Colors where employed for special identification purposes, e.g. the gray background indicates that the rabbit was Cd-covered. A pop-up notification from "the assistant" (a context programmable shell; red ball lower icon), indicates that project X1050 has still one sample with pending calculations. This notification is raised when the program cannot "deduce" (by algorithms) all the information required to perform the required calculations, and that it needs further attention from the analyst (i.e. red warning icon at the X1050 right top).

Figure 6.11: Menu interface for the Laboratory Information Management System (LIMS). Each icon links to other user interfaces where the respective sub-databases are filled in with content. Some data could be automatically filled in (and verified) by a series of algorithms designed to exploit e.g. the sample, measurements and irradiations labelling systems employed at the SCK•CEN for data-inference (measurement positions, detectors employed, parent irradiation, Cd-covered or bare condition, etc.).

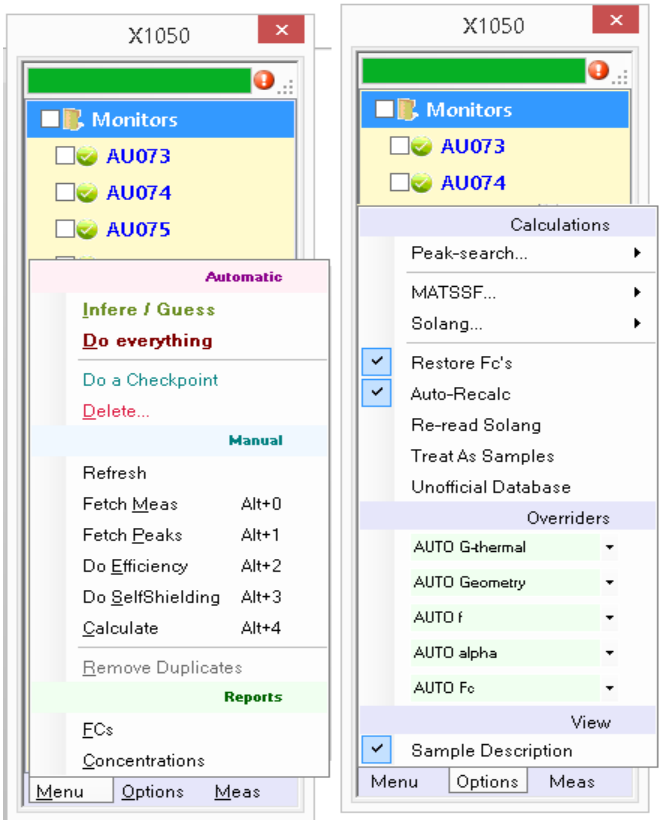

Figure 6.12: Screenshot of a "virtual rabbit" and its sub-menus for related NAA calculations: measurement and photo-peak search (data collection) from the HyperLab 2009 [138] **database, Solid angles (Solang), γ-ray coincidence correction, efficiency transfer and neutron self-shielding calculations (e.g. MATSSF). Several sub-menus contained tunable options (e.g. peak search window, miscellaneous MatSSF and Solang configurations, etc.). Other options pertained the overriding of automatically adopted values for versatility (e.g. actual *f* and *α* values, actual sample geometry and/or neutron self-shielding correction factors). Each sample can be analyzed separately with the select/reject module (see Figure 6.13).**

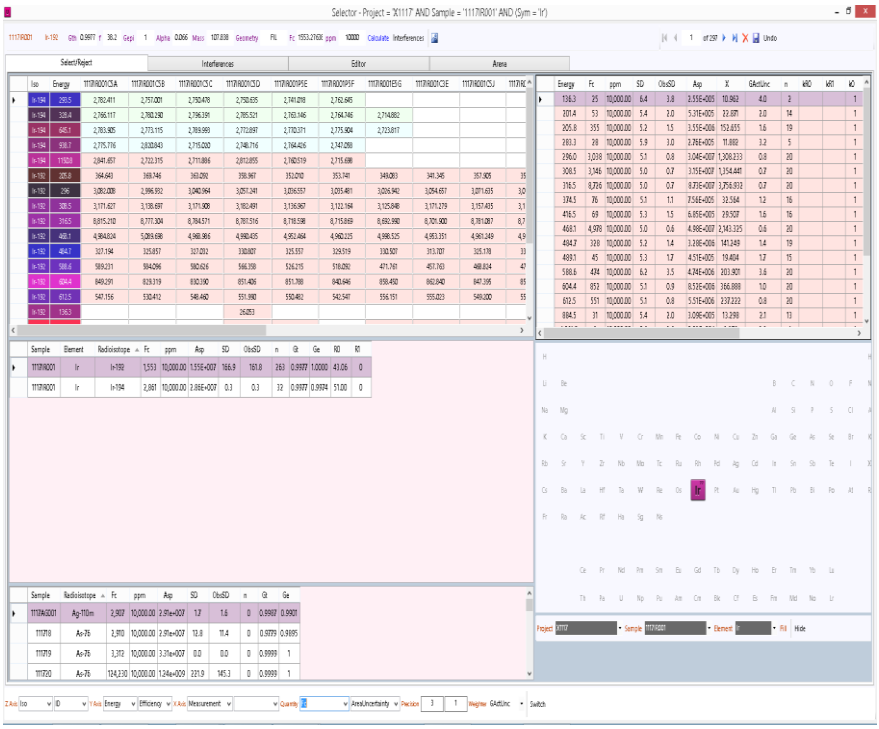

Figure 6.13: Screenshot of the software module developed for the rejection/inclusion of analytical results of interest into further calculations. The red cell background indicates that the current k_0-literature factor is not recommended. Each cell with value can be manually (de)activated and hence, withdrawn from the overall calculation. The results (e.g. peak area, Fc, k_0, geometry efficiency) are distributed into a cross-table Y vs. X, from which the Y or X quantities of choice can be selected in the bottom menu bar. This allowed for real-time custom cross-table arrangements: e.g. the k_0 or activity values per γ-line vs. each measurement. The advantages of this module over commercial software such as KayZero or spreadsheets are numerous: unlimited data-points (e.g. measurements), customizable Y vs. X representations for easier analysis, real-time modification/recollection of any input parameter of interest.

7. Calculation of uncertainties

This chapter seeks to provide:

1) A short summary of the main relations employed for the determination of the combined (standard) uncertainty in a given physical quantity from the different influence quantities by following the recommendations given in the "Guide to the expression of the uncertainty in measurement" [109].

2) A decomposition of the different uncertainty components contributing to the uncertainty in a k_0, Q_0 factor or neutron cross-section by following the recommendations given in "Neutron activation analysis: A primary method of measurement" [177]. That is, an uncertainty budget is provided for influence quantities grouped per its nature: spectrometry, neutronics, calibrations and certificates as well as for the main physical quantities of interest.

The (arithmetic) mean from N observations x_i ($i = 1, \ldots, N$) of a quantity x is given by:

$$\overline{x} = \frac{1}{N}\sum_{i=1}^{n} x_i \tag{7.1}$$

and it is considered an estimate of the expectation μ_x of x. The (experimental) standard deviation (SD) of N observations of a quantity x is calculated in this work (with the Bessel correction) as:

$$SD_x = +\sqrt{\frac{1}{N-1}\sum_{i=1}^{n}\left(x_i - \bar{x}\right)^2} \tag{7.2}$$

The SD characterizes the dispersion of the x_i values about their mean, while for a Gaussian or normal distribution the (experimental) SD of the mean:

$$s_x = \frac{SD_x}{\sqrt{N}} \tag{7.3}$$

characterizes how well the mean value estimates the expectation μ_x of x. Either SD, from eq. (7.2) or eq. (7.3) can be employed as a measure of the uncertainty in x [109]. The quantity s_x does not necessarily need to be a SD or an approximation to the (estimate of the) SD and it is generally regarded (e.g. as in this work) as an estimate of the uncertainty in the parameter x (see further).

According to reference [109] the estimate of the variance of an output quantity F that depends on z input parameters with estimates a_i (i.e. mean values) is calculated as:

$$s_F^2 = \sum_{i=1}^{z}\left(\frac{\delta F}{\delta a_i}\right)^2 s_{a_i}^2 + 2\sum_{i=1}^{z-1}\sum_{j=i+1}^{z}\left(\frac{\delta F}{\delta a_i}\frac{\delta F}{\delta a_j}\right)s_{a_i}s_{a_j}p_{ij} \tag{7.4}$$

where p_{ij} is the correlation coefficient of a_i and a_j and s_{ai} is the positive square-root of the estimate variances of a_i.

Neglecting any correlation between the estimates a_i (i.e. $p_{ij} = 0$ for every i and j), then eq. (7.4) reduces to:

$$s_F^2 \cong \sum_{i=1}^{z}\left(\frac{\delta F}{\delta a_i}\right)^2 s_{a_i}^2 \tag{7.5}$$

The term $(\delta F/\delta a_i)$ is known as the sensitivity coefficient for the parameter a_i. In terms of relative uncertainties (index r; relative to the mean value), the previous expression can be written as:

$$s_{r,F}{}^2 \equiv \left(\frac{s_F}{F}\right)^2 \cong \sum_{i=1}^{z}\left(\frac{a_i}{F}\frac{\delta F}{\delta a_i}\right)^2\left(\frac{s_{a_i}}{a_i}\right)^2 \tag{7.6}$$

We define the relative sensitivity coefficient $c_{F,ai}$ as:

$$c_{F,a_i} \equiv \left|\frac{a_i}{F}\frac{\delta F}{\delta a_i}\right| \tag{7.7}$$

Therefore eq. (7.6) can be expressed in a condensed form:

$$s_{r,F}^2 \cong \sum_{i=1}^{z}\left(c_{F,a_i}s_{r,a_i}\right)^2 = \sum_{i=1}^{z} s_{r,a_i,F}^2 \tag{7.8}$$

The definition:

$$s_{r,a_i,F} \equiv c_{F,a_i}s_{r,a_i} \tag{7.9}$$

is to be understood as the relative uncertainty associated with the output estimate F due to the relative uncertainty associated with the input estimate a_i.

According to reference [109] one must replace the (relative) uncertainty $s_{r,ai}$ by the (relative) "standard uncertainty" $u(a_i)$ obtained from performing a type-A or type-B uncertainty evaluation of it. That is, the $s_{r,ai}$ value must be either:

- a SD obtained from N repeated measurements (type-A evaluation; e.g. normal, Poisson) or;

- converted into a SD per the (assumed) distribution of the random variable a_i (type-B evaluation). In this case $s_{r,ai}$ should represent the half-width of a known uncertainty interval. Two typical assumed distributions are the rectangular (or uniform) when only the minimum and maximum values are known (conservative approach) and the triangular, when also a mean or mode is known (less conservative).

First one defines $u(a_i,F)$ as the relative standard uncertainty associated with the output estimate F due to the relative standard uncertainty associated with the input estimate a_i [109]:

$$u(a_i, F) \equiv c_{F,a_i} u(a_i) \tag{7.10}$$

When performing the conversion $s_{r,ai,F} \rightarrow u(a_i,F)$ and keeping in mind no correlations between the a_i input quantities, the eq. (7.8) becomes:

$$u^2(F) \cong \sum_{i=1}^{z} u^2(a_i, F) \tag{7.11}$$

The quantity $u(F)$ is known as the "combined standard uncertainty" in F due to all a_i uncertainty contributions.

It is important to remark that since in this work we split the uncertainty analysis in F components which are discussed in different sections by means of several tables, we will ambiguously employ the letter u to refer to the standard uncertainty of 1 given influence quantity $u(a_i,F)$ as given in eq. (7.10) or to the combined uncertainty $u(F)$ as given in eq. (7.11) from all the uncertainty components detailed in its specific section. The distinction is given through the text or table.

Similarly, the letter s is ambiguously employed for expressing an uncertainty that has not been converted to its standard form, i.e. a half-width or an approximate SD. As a distinction, if s is a raw input uncertainty then the assumed distribution is specified and the value has not been weighted per the sensitivity coefficient (i.e. $s = s_{r,ai}$). On the other hand, if s is calculated by means of error propagation, then $s = s_{r,ai,F}$ as given in eq. (7.9), i.e. it has been weighted according to its (specified) sensitivity coefficient.

7.1 In the sample mass

The main contributors to the $u(\hat{w})$ are the uncertainties from mass losses during drying (for liquids pipetted on paper filters), packaging, transport to (and from) the irradiation facility and volatilization during irradiation. The Table 7.1 summarizes the relative half-widths or uncertainty contributions estimated in this work and the corresponding $u(\hat{w})$ for the mass content determination in 1 sample.

The moisture corrections were ≤ 0.15% for all compounds except for the Honeywell Fluka NaCl standard with a correction of 1.9%. We assumed a half-width of 0.15% for our budget and a triangular distribution leading to u = 0.06% from moisture correction.

For pure metals and alloys, it is reasonable to assume that the mass loss during any of the previously mentioned stages is null. Weighing of a randomly picked metal sample before and after irradiation gave a SD of the same magnitude as our uncertainty from weighing alone. For paper disks and compounds inside plastic bags, the mass loss is unknown and we assign a 0.15% relative half-width uncertainty due to all mass losses mechanisms combined (a value adopted from our moisture correction uncertainty). This translates per the uniform distribution into a u = 0.04% for each of the 4 mass loss mechanisms mentioned in Table 7.1. A neglected contributor to the uncertainty is the mass loss due to Hot-atom transfer, i.e. the recoil during decay that forces some atoms in the vicinity to fall outside of the container.

A relative difference was calculated from weighing twice a given Al-alloy foil. The probability histogram for this variable from 128 results is shown in the Figure 7.1. Assuming a normal distribution, a u= 0.008% is assigned from weighing.

From Table 7.1 the combined standard uncertainty for estimating the mass of the sample is $u(\hat{w}) = 0.11\%$ for liquids and compounds and $u(\hat{w}) = 0.01\%$ for metal samples such as foils and wires.

Table 7.1: Relative *s* and *u* in the terms contributing to the combined uncertainty in the sample weight $u(\hat{w})$. All the sensitivity coefficients $c = 1$.

Contribution from:	*s (%)*	Distribution	*u (%)*	Type / Comment
Preparation				
Sample weighing	0.008	normal	0.008	A; *N*=128; k=1.984
Mass loss: packaging (PF & C)	0.075	uniform	0.04	B
Mass loss: transport (PF & C)	0.075	uniform	0.04	B
Blank subtraction (PF)	0.05	uniform	0.03	B
Others				
Mass loss: irradiation (PF & C)	0.075	uniform	0.04	B
Mass loss Hot-atom transfer	0	uniform	0	B
Mass loss: Drying (PF)	0.075	uniform	0.04	B
Moisture content (C)	0.15	triangular	0.06	B
Total				
PD & C	*0.22*		***0.11***	*1 sample*
FW	*0.01*		***0.01***	

PD = Paper disk; C = Compound; FW = metal samples such as foils and wires (Pure / Alloy).

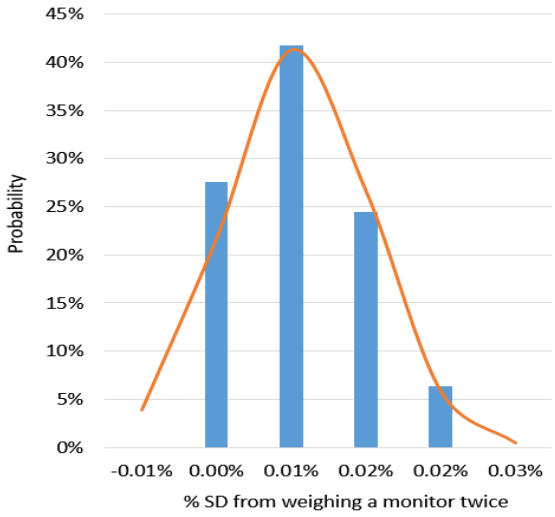

Figure 7.1: The probability histogram for the observed difference between 2 weights of a given Al-alloy foil for a sample size N = 128. Assuming a normal distribution, a u = 0.008% is adopted from weighing.

7.2 In the induced activity

7.2.1 Uncertainty in the activity from spectrometry

The Table 7.2 summarizes the uncertainty contributions in the calculation of $u(A)$ due to the different γ-spectrometry components:

a) There are contributions from calibration components: the efficiency and PTT calibrations at the reference positions, fine-tuning of the dead-layer and vacuum gap of the detector (see values in Chapter 3).

Some minor contributions from background subtraction, γ and X-ray self-absorption in the material and sample positioning were calculated or adopted. The combined standard uncertainty from calibration components is estimated at $u = 0.62\%$.

b) There are uncertainty contributions from hardware and software components in the detection system. Hardware-related uncertainty components are dead-time, LFC corrections and pulse pile-up (see section 3.9). From Figure 3.28 the correction from dead-time and pulse pile-up combined was estimated at 0.7% at position 3 (6.5 cm separation from the detector crystal) from 60% dead-time experiment. This leads to $s = 0.5\%$ assigned to each count loss mechanism. Thus, $u = 0.2\%$ from dead-time per a triangular distribution and $u = 0.3\%$ from pulse pile-up per a (conservative) uniform distribution.

Uncertainty contributions due to software (modelling) are: Efficiency transfer calculations, γ-coincidence corrections and photo-peak deconvolutions. These values are based on results discussed in sections 3.5 to 3.8. The efficiency transfer uncertainty was estimated from relative differences in Figure 3.25 to Figure 3.27. For paper disks and thick disks, the combined standard uncertainty is $u = 0.58\%$ while for foils, wires,

compounds and other small samples we estimate a combined standard uncertainty of u = 0.46% from hardware and software.

c) There are uncertainty contributions from sample decay (or cooling) and measurement. That is, from $u(D)$ and $u(C)$ due to timing and $u(\lambda)$, as well as the uncertainty from the counting statistics of the photopeak $u(N_p)$.

Following the definitions given in eq. (2.7), one has:

$$\begin{aligned} c_{S,t_i} &\equiv \left|\frac{t_i}{S}\frac{\delta S}{\delta t_i}\right| = \left|\left(\frac{1}{S}-1\right)\lambda t_i\right| \\ c_{D,t_d} &\equiv \left|\frac{t_d}{D}\frac{\delta D}{\delta t_d}\right| = \left|\lambda t_d\right| \\ c_{C,t_c} &\equiv \left|\frac{t_c}{C}\frac{\delta C}{\delta t_c}\right| = \left|\left(\frac{1}{C}-\lambda t_c\right)\left(1-\frac{1}{\lambda t_c}\right)\right| \end{aligned} \tag{7.12}$$

In terms of a fraction n of the half-life, i.e. $t = nT_{1/2}$, one has from de definition of λ in eq. (2.121) that $\lambda t = \ln(2^n)$, then the sensitivity coefficients can be expressed as:

$$\begin{aligned} c_{S,t_i} &= \left|\left(\frac{2^n}{2^n-1}-1\right)\ln\left(2^n\right)\right|_{n=n_i} \\ c_{D,t_d} &= \left|\ln\left(2^n\right)\right|_{n=n_d} \\ c_{C,t_c} &= \left|\left(\frac{2^n}{2^n-1}-1\right)\left(\ln\left(2^n\right)-1\right)\right|_{n=n_c} \end{aligned} \tag{7.13}$$

The reader can verify that for propagation of $u(\lambda)$ one arrives at the same expressions with the substitution $\lambda \rightarrow t$ for calculation of c_λ (for each *S, D or C* parameter). Suppose that $n_i = n_d = n_c = 0.5$, i.e. the sample was irradiated, cooled and counted for equal amounts of time that corresponded to 50% of the $T_{1/2}$ of the radioisotope of interest, then c_{ti} = 0.84, c_{td} = 0.35 and c_{tc} = 1.58.

Consider for instance the analysis of ^{28}Al with $T_{1/2}$ = 2.241 m and a cooling period of ~45 seconds (33%; c_{td} = 0.23) then a $s(t_d)$ of 1 second on cooling (2.2%) propagates as $u(D)$ = 0.21% as shown in Table 7.2. If the sample is counted for 2 half-lives of ^{28}Al then a $s(t_c)$ of 1 second in the counting time (0.37%) propagates as $u(C)$ = 0.02% (c_{tc} = 0.13). For ^{28}Al determination the uncertainty contribution to the induced activity from *D*, *C* and the counting statistics amounts to a u = 0.37%. The analysis of the uncertainty contribution from *S* is given in the next section.

The combined contribution to $u(A)$ due to spectrometry components is 0.9%.

Table 7.2: Relative *s* and *u* in the terms contributing to *u*(*A*) due to spectrometry components.

Contribution from:	*s (%)*	Distribution	*u (%)*	Type / Comment
Detectors				
Reference efficiency	0.50	triangular	0.20	B
Certified activity	0.50	normal	0.50	B
Peak-to-total calibration	0.50	triangular	0.20	B
Fine-tuning	0.50	triangular	0.20	B
γ and X-ray self-absorption	0.05	uniform	0.03	B
γ and X-ray angular correlation	0	uniform	0	B
Background subtraction	0.05	triangular	0.02	B
Sample positioning	0.10	uniform	0.06	B
Sub-total	*1.0*		***0.6***	*1 detector*
Hardware & Software				
Dead-time / LF Counting	0.50	triangular	0.20	B
Photo-peak deconvolution	0.20	triangular	0.08	B
Pulse pile-up	0.50	uniform	0.29	B
COI corrections	0.50	triangular	0.20	B
Sub-total	*0.9*		*0.4*	
Efficiency transfer (PD)	1.00	triangular	0.41	B
Efficiency transfer (FW)	0.50	triangular	0.20	B
Efficiency transfer (C)	0.50	triangular	0.20	B
Sub-total	-			
PD	*1.3*		***0.6***	*1 detector (middle position)*
FW	*1.0*		***0.5***	
C	*1.0*		***0.5***	
Counting				
Timing decay	2.22	triangular	0.21	B; c = 0.23; t = 33% of $T_{1/2}$ *i.e. Al-28*
Half-life impact on *D*	0.10	triangular	0.01	
Timing counting	0.34	triangular	0.02	B; c = 0.13; t = 200% of $T_{1/2}$ *i.e. Al-28*
Half-life impact on *C*	0.10	triangular	0.01	
Counting statistics	0.30	Poisson	0.30	A
Sub-total	*0.6*		***0.4***	*1 measurement*
Total				
PD	*1.8*		***0.9***	*1 measurement in 1 detector (middle position)*
FW & C	*1.6*		***0.9***	

PD = Paper disk; C = Compound; FW = metal samples such as foils and wires (Pure / Alloy)

7.2.2 Uncertainty in the activity from neutronics

The Table 7.3 shows some of the uncertainty components from neutronics contributing to $u(A)$.

Following the case for ^{28}Al determination in the previous section, consider for instance an irradiation period of 2 half-lives ($c_{ti} = 0.46$). A $s(t_i) = 1$ second uncertainty on the irradiation (0.34%) propagates as $u(S) = 0.06\%$ as shown in Table 7.3. We estimated a $u = 0.11\%$ total contribution from the half-life, irradiation timing and ramping up/down of the neutron fluence during the start and end of the irradiations.

Another $u = 0.11\%$ contribution was also found (as shown in Table 7.3) from all sources of interferences discussed in the section 2.13 and later on sections 4.7 and 4.8. The combined contribution to $u(A)$ from all the neutronics components in the Table 7.3 amounts to 0.15%.

Table 7.3: Relative *s* and *u* in the terms contributing to *u*(A) due to neutronics.

Contribution from:	*s* (%)	Distribution	*u* (%)	Type / Comment
Neutronics: Timing				
Half-life impact on *S*	0.10	triangular	0.02	B; c = 0.46; t = 200% of $T_{1/2}$ *i.e. Al-28*
Timing irradiation	0.34	triangular	0.06	
Ramping up/down fluence start-end	0.20	triangular	0.08	B
Sub-total	*0.26*		***0.11***	*1 irradiation*
Neutronics: Interferences				
Primary	0.20	triangular	0.08	B
Threshold	0.05	triangular	0.02	B
Double neutron capture [a]	0.05	triangular	0.02	B
Vicinity of other samples	0.10	uniform	0.06	B
Burn-up	0.05	triangular	0.02	B
Sub-total	*0.24*		***0.11***	*any channel*
Total	*0.35*		***0.15***	

[a] The only interesting case is for ^{199}Au monitoring (i.e. Pt analysis) and the interference from trace contents of ^{197}Au(n,γ)^{198}Au → ^{198}Au(n,γ)^{199}Au in the material.

7.3 In the activity concentration

From the results in Table 7.2 and Table 7.3 one can calculate the combined contribution from spectrometry and neutronics to $u(A)$ and along with Table 7.1 the combined standard uncertainty in the γ activity concentration $u(a) = u(A/\hat{w})$. This is shown in Table 7.4 for paper disks (PF), metal samples such as foils and wires (FW) and compounds (C).

Table 7.4: Relative *s* and *u* in the terms contributing to the combined standard uncertainty in the induced γ activity concentration $u(a) = u(A/\hat{w})$.

Contribution from:	*s (%)*	*u (%)*	Type / Comment
Sample mass (ŵ)			
PD & C	0.22	**0.11**	1 sample
FW	0.01	**0.01**	
γ activity A (spectrometry)			
PD	1.78	**0.92**	1 measurement in 1 detector (middle position)
FW & C	1.55	**0.85**	
γ activity A (neutronics)	0.35	**0.15**	1 channel exercise
γ activity concentration (a=A/ŵ)			
PD	*1.8*	***0.9***	
FW	*1.6*	***0.9***	
C	*1.6*	***0.9***	

PF = Paper disk; C = Compound; FW = metal samples such as foils and wires (Pure / Alloy).

All the sensitivity coefficients $c = 1$. Uncertainty components from Table 7.1 to Table 7.3.

7.4 From ratios between influence quantities

The k_0-NAA method is a single-comparator method, therefore it is fundamentally based on the experimental determination of ratios between different quantities.

Some influence quantities are only evident when considering the ratios between parameters. For instance, it is in theory assumed that a standard irradiated bare and its replicate irradiated under a Cd-cover are indistinguishable and that certain ratios such as the $G_{e,Cd}/G_e$ correction that appears in the eq. for k_0-determination by means of Cd-subtraction is equal to 1. This was the rule of thumb applied during the first k_0-determinations. In practice, when performing ENAA on low-Q_0 isotopes it is usually necessary to increase the mass and therefore size of the "replicate" sample by a considerable factor. This means that $G_{e,Cd}/G_e \neq 1$ and that other aspects such as sample geometry and neutron fluence differences within the matrix of the sample or between irradiation positions (spatial) are also relevant when taking ratios between induced activities. Additionally, since bare and Cd-covered irradiations as well as repeats are performed separately in time, it is necessary to consider the uncertainty from the temporal neutron fluence variability between these irradiations.

7.4.1 Westcott g_T and neutron self-shielding correction factors

According to the reference [13] the uncertainty in the thermal and epithermal self-shielding corrections factors can be estimated as a 10% of the correction term. We can estimate then a $s(G_{th})$ = 0.3% for some Na, Cl, Fe, Cd, In, Sn, Ta and Pt materials. It would be $s(G_{th})$ = 0.5% for Gd, 0.7% for Dy, 1% for Co and 2% for the pure Ag and Au materials, based on the results shown in the Table 6.3. Since we also irradiated other (diluted) materials with no G_{th} corrections needed for these elements except for Gd, we adopt a $s(G_{th})$= 0.5% in our budget leading to $u(G_{th})$ = 0.2% per a triangular distribution.

For scattering and neutron moderation we can adopt a $s(G_{mod})$ = 0.1% from the 10% of a 1% correction obtained from the observed differences between bare and PE-covered vials 1 mm thick (see section 4.5). As mentioned before, our samples were not irradiated inside these PE vials but inside 0.1

mm thin PE bags to avoid introducing scattering and undesired moderation effects. Nonetheless, we would like to introduce a $s(G_{mod})$ =0.05% leading to $u(G_{mod})$ = 0.02% in our budget.

The Table 7.5 summarizes the uncertainty contributions from the ratios between epithermal and "effective" thermal self-shielding correction factors. The later includes the contributions from neutron scattering/moderation and Westcott g_T factors. We assumed that the g_T factor for a non-1/v absorber has a half-width uncertainty equivalent to 20% of the correction term (g_T = 1), that is s = 0.2% leading to u = 0.12% when assuming the uniform distribution.

Table 7.5: Relative *s* and *u* in the values and ratios between the neutron self-shielding and Westcott g_T correction factors.

Contribution from:	*s* (%)	Distribution	*u* (%)	Type / Comment
Neutron self-shielding				
Epithermal self-shielding (G_e)	0.30	triangular	**0.12**	B
Scattering/moderation (G_{mod})	0.05	triangular	0.02	B
Thermal self-shielding (G_{th})	0.50	triangular	0.20	B
Westcott g_T factor (non-1/v isotopes)	0.20	uniform	0.12	B
G_{th} effective = G_{th} * g_T * G_{mod}	*0.54*		***0.24***	*B*
Total (from Ratios)				
(G_{th}) / (G_e) (effective)	*0.62*		***0.27***	*1 material*
($G_{e,Cd}$) / (G_e)	*0.42*		***0.17***	*different samples*
($G_{th,s}$) / ($G_{th,c}$) (effective)	*0.76*		***0.33***	

7.4.2 Temporal variability in the neutron fluence

Table 4.9 and Table 4.10 showed the observed variation in the epithermal fluence rate of channel Y4 during a 9-month period between September 2011 and June 2012. Since the comparisons were made between monitors at the same position within a rabbit, if we consider the max 0.5% SD reported in

Table 4.10 and subtract (quadratically) the typical 0.3% uncertainty due to counting statistics then with a sample size N = 12 the standard uncertainty due to temporal fluence variability is calculated at u = 0.12% (k = 2.201 for a 95% confidence level).

7.4.3 Spatial variability in the neutron fluence

From Table 4.9 results, the axial fluence variability of ≤ 0.5% SD translates after subtraction of counting statistics into a $u \approx 0.09\%$. This uncertainty was obtained from 18 determinations (k = 2.11 for a 95% confidence level). From the same table, the radial fluence variability of ≤ 0.5% SD translates (after the due correction) into $u \approx 0.14\%$. This uncertainty on the other hand was found from 8 determinations (k = 2.365 for a 95% confidence level).

7.4.4 Cd-covers, sample-rabbit configuration and volume differences between replicates

The uncertainty from geometry (or volume) differences between replicates can be estimated from the weights of a batch of 11 replicate monitors that were cut together into 7 mm diameter foils during the same day. A u = 0.18% is assigned from volume differences between replicates, obtained from the SD of the mean (0.6%/√11). The coverage factor is k = 2.23 for a 95% confidence level.

The uncertainty from the impact of the Cd-cover and the choice of sample-rabbit configuration can be estimated from comparison of Cd-ratios between different Cd-covers employed (for e.g. the comparator). We estimate a 0.45% half-width uncertainty leading to u = 0.18% per a triangular distribution.

The combined standard uncertainty from the contributions listed in Table 7.6 is estimated at $u = 0.33\%$ and a coverage factor of k = 2 for a 95% confidence level is given from the effective degrees of freedom obtained ($v_{eff} = 53$). This value is to be added quadratically to the uncertainty from ratios between activities, to the r_{Cd} and/or to ω_{Cd} when calculating the uncertainty in a k_0 or Q_0 determination. This will be shown in the corresponding sections.

Table 7.6: Relative *s* and *u* from geometry differences between standards, from the neutron (spatial & temporal) fluence variability between standards and for Cd-covered irradiations.

Contribution from:	*s* (%)	Distribution	*u* (%)	Type / Comment
Fluence variability: spatial				
between standards (spatial axial)	0.09	normal	0.09	A; N=18; k=2.11
between standards (spatial radial)	0.14	normal	0.14	A; N=8; k=2.365
Volume differences for replicates	0.18	normal	0.18	A; N=11; k=2.23
Sub-total	*0.25*		***0.25***	v_{eff} =25; k=2.06
Fluence variability: temporal				
between 2 irradiations	0.12	normal	0.12	A; N=12; k=2.201
Impact of the Cd-cover and rabbit configuration	0.45	triangular	0.18	B
Sub-total	*0.47*		***0.22***	v_{eff} =52; k=2
Total	*0.58*		***0.33***	v_{eff} =53; k=2

The coverage k factor is provided to obtain a U = k*u* at the 95% confidence level.
v_{eff} = effective degrees of freedom.

7.5 From the certified elemental content

The lowest uncertainty from all the standards employed correspond to the NIST SRM liquids with relative $u(\rho)$ = 0.15 to 0.30%. For most pure

compounds and pure metals with no specific certificate other than an assay of its high-purity we assumed a uniform distribution with half-width uncertainty of 0.75% leading to $u(\rho)$ = 0.43% in the adopted elemental content. This is shown in Table 7.7.

The highest uncertainty corresponds to some Alfa Aesar Specpure liquids with $u(\rho)$ = 1% and the IRMM NOC materials with $u(\rho)$ = 1.15%. The uncertainty in the IRMM NOC standards was estimated from the worst reported uncertainty of 2.3% at 95% confidence level (k=2) for other known aluminum alloy certified materials fabricated contemporarily during 1966-1976 by levitation melting in argon as performed by the authors of reference [198]. For the Alfa Aesar liquids (AA) where the certified elemental content is given in (µg/ml) instead of (µg/g) we adopted an additional u = 0.56% from unit conversion, which was estimated from a 1% half-width uncertainty and a rectangular distribution. This leads to a combined $u(\rho)$ = 1.15% as with the IRMM NOC materials.

The $u(\rho)$ is assumed negligible when performing the Cd-ratio since the material is assumed homogeneous and the fraction of the element cancels from the R_{Cd} factor computation. This is not the case for mass losses which might be clearly different between samples (for any given material) or when computing a R_{Cd} factor between different materials which is not advised unless the added uncertainty is not a concern.

7.5.1 Uncertainty due to isotopic variability

Greenberg et al. provides in reference [177] a compilation of relative standard uncertainties for ratios between isotopic abundances for unknown samples and standards typically studied by NAA. Most of the standard uncertainties for these ratios are well below u = 0.33% and only 11 cases (from the ones investigated in this work) display higher values:

- ^{168}Yb (11%), ^{152}Gd (7%), ^{114}Cd (2%), ^{84}Sr and ^{98}Mo (1.5%);

- ^{176}Lu, ^{110}Pd, ^{94}Zr, ^{116}Sn and ^{152}Sm (≤1%);

- ^{102}Ru (0.6%).

Our standards are certified in elemental and not in isotopic content. We assume that the isotopic abundance of the studied target isotopes in every sample corresponds to that of its (natural) terrestrial abundance as given in i.e. reference [10]. For a k_0 determination we will adopt the previous limit value u = 0.33% due to isotopic variability between different standards of the same analyte (see Table 7.7). Since the ratio between the isotopic abundances of standard and comparator is contained within the k_0 definition, the isotopic variability might be the main cause of possible discrepancies with other authors for the 11 target isotopes previously mentioned, as it is a common uncertainty when working with samples not certified in isotopic content. For a Q_0 determination, which involves replicate samples of the same standard (irradiated bare and Cd-covered) the uncertainty contribution due to isotopic variability can be neglected.

Table 7.7: Relative *s* and *u* from the isotopic variability and the certified elemental content.

Contribution from:	*s (%)*	Distribution	*u (%)*	Type / Comment
Material				
Isotopic variability	0.57	uniform	**0.33**	B
Certified content (PD, FW & C)	0.75	uniform	**0.43**	B
Certified content (IRMM NOC & AA)	1.15	normal	**1.15**	B; k=2

PD = Paper disk; C = Compound; FW = metal samples such as foils and wires (Pure / Alloy).

IRMM NOC = IRMM materials from 1966-1976 with no official catalog number or certificate other than a catalog file from mail correspondence with Goedele Sibbens (same institute provider) or with Joseph Oeyens (SCK•CEN provider).

AA = Alfa Aesar (Specpure) plasma standard solutions (liquids on paper filter). Includes uncertainty from ml → g (unit) conversion.

7.6 In a k_0 determination with the Cd-subtraction technique

From eq. (2.62) and the eq. (7.11) the sensitivity coefficients for the calculation of $u(\Delta a)$ due to the uncertainty in the activity concentrations a, a_{Cd} and the effective f_{Cd} factor are:

$$
\begin{aligned}
c_{\Delta a,a} &\equiv \left| \frac{a}{\Delta a} \frac{\delta \Delta a}{\delta a} \right| = \left| \frac{a}{\Delta a} \right| \\
c_{\Delta a,a_{Cd}} &\equiv \left| \frac{a_{Cd}}{\Delta a} \frac{\delta \Delta a}{\delta a_{Cd}} \right| = \left| \frac{a_{Cd}}{f_{Cd}} \frac{1}{\Delta a} \right| \\
c_{\Delta a,f_{Cd}} &\equiv \left| \frac{f_{Cd}}{\Delta a} \frac{\delta \Delta a}{\delta f_{Cd}} \right| = c_{\Delta a,a_{Cd}}
\end{aligned}
\qquad (7.14)
$$

If one assumes that the bare activity concentration is n times the Cd-covered activity concentration, i.e. that $a = n\,(a_{Cd}/f_{Cd})$, then the sensitivity coefficients are:

$$c_{\Delta a,a} = \left|\frac{n}{n-1}\right| = |n|\,c_{\Delta a,a_{Cd}}$$
$$c_{\Delta a,a_{Cd}} = c_{\Delta a,f_{Cd}} = \left|\frac{1}{n-1}\right| \tag{7.15}$$

It is possible to estimate the previous sensitivity coefficients from the ratio f/Q_α since in virtue of eqs. (2.51) and (2.52) when neglecting the self-shielding correction factors:

$$n-1 \cong \left(R_{Cd}F_{Cd}-1\right) \cong \frac{f}{Q_\alpha} \tag{7.16}$$

For channels S84, Y4 and X26 one obtains for the ultimate comparator $n \approx 2.14$, $n \approx 3.3$ and $n \approx 5.6$ (respectively). The Table 7.8 provides the combined standard uncertainty in a "single determination" of a k_0 factor according to the Cd-subtraction method of eq. (2.62). A single determination corresponds to the computation of a k_0 factor from the results of 1 material (analyte and comparator; 1 sample) co-irradiated once bare and once Cd-covered in 1 channel and as measured by 1 detector at the reference position. We can estimate when assuming no correlation between the variables [109] that our expected precision for a single determination is $u(k_0) \approx 2.4\%$. We believe this uncertainty budget is suited for most of the studied cases, but is clearly bound to some assumptions, such as:

- The standard and comparator materials were estimated as having uncertainties of 0.5% and 0.3% from thermal ($G_t = 0.95$) and epithermal self-shielding ($G_e = 0.97$) corrections (respectively), but these corrections were negligible for most materials;

- A small estimate uncertainty due to neutron interferences, burn up and F_{Cd} factor is given. However, most the investigated nuclides satisfy $F_{Cd} = 1$ and $g_T = 1$, did not suffer from burn-up due to the magnitude of our neutron fluences ($\leq 10^{11}$ $s^{-1}.cm^{-2}$) or from interferences since the Cd-subtraction avoids them. The adopted $s(F_{Cd}) = 0.3\%$ is taken from the 10% of the correction term for i.e. ^{181}Ta ($F_{Cd} = 0.972$), ^{187}Re ($F_{Cd} = 0.98$) and ^{65}Cu ($F_{Cd} = 1.034$) and clearly also covers cases such as ^{121}Sb ($F_{Cd} = 0.99$), ^{165}Ho ($F_{Cd} = 0.99$) and the ultimate comparator ($F_{Cd} = 0.991$). This uncertainty adoption is recommended by De Corte in [13]. The $u(k_0)$ remains almost unchanged at 2.5% for cases such as ^{186}W ($F_{Cd} = 0.908$) and ^{115}In ($F_{Cd} = 0.927$) which have $s(F_{Cd}) \leq 1\%$. Only ^{114}Cd has an imprecise F_{Cd} factor, with $F_{Cd} = 0.45$ quoted in [13]. The value $F_{Cd} = 0.40$ was found in this work (12.5% relative difference) and is statistically significant assuming $s(F_{Cd})= 6\%$. For a determination of ^{114}Cd then one obtains $u(k_0) = 5.7\%$ for irradiations on channel S84, $u(k_0) = 3.4\%$ for Y4 and $u(k_0) = 2.4\%$ for X26.

- A small estimate $s(g_T) = 0.2\%$ was adopted for a non-1/v absorber. If we consider instead $s(g_T) = 2\%$ for a strong non-1/v absorber, then one obtains $u(k_0) \approx 2.9\%$. This budget would be suited for strong non-1/v isotopes such as ^{151}Eu and ^{168}Yb although Cd-subtraction is not recommended for these targets and the calculation of a k_0 factor by means of adoption of a s_0 factor is preferred.

- The sensitivity coefficients for Δa are estimated for a determination in our most epithermal channel (S84) and for an analyte with $Q_0 \approx 5$ such as ^{95}Zr, ^{153}Eu or ^{187}Re (see Table 7.9 for other cases);

- ^{28}Al is employed to obtain the worst estimate uncertainty on the decay parameter D for irradiations in S84. Determination of ^{42}K could be an example of a worst estimate of uncertainty on the parameters S and C for irradiations in Y4. From our calculations for t_i =7h, t_d = 16h and t_c = 1h, the estimate for a k_0 determination of ^{42}K in channel Y4 increases to $u(k_0) \approx$ 2.7%.

- The full $u(N_p)$ = 0.3% from the counting statistics of 1 measurement is considered and not the reduced uncertainty obtained from 8 to 12 measurements.

- The uncertainty contribution from COI corrections, pulse pile-up and dead-time was estimated at position 3, i.e. just 6.5 cm sample-detector separation and 60% dead-time. Most k_0 measurements were done at position 5 instead (27.5 cm separation) and we aimed at a maximum 15% dead-time, although occasionally some low activity measurements had to be carried out at position 3.

The Table 7.9 shows that for channels Y4 and up to $Q_0 \approx 30$ and for channel X16 and up to $Q_0 \approx 80$ our precision in a single k_0 determination remains $\leq$ 2.5% at the 1*s* confidence level. That is, this reported precision is suited for all studied cases (except i.e. ^{96}Zr and ^{238}U).

Table 7.8: Relative *s* and *u* contributions to $u(\Delta a)$ and $u(k_0)$ for a single determination on our most epithermal channel (S84) per the Cd-subtraction technique. Estimate for a target isotope with $Q_0 \approx 5$ such as ^{95}Zr, ^{153}Eu or ^{187}Re.

Contribution from:	***s (%)***	**Distribution**	***u (%)***	**Type / Comment**
($G_{e,Cd}$ / G_e)	0.42		**0.17**	not exact replicates
F_{Cd} factor	0.30	triangular	**0.12**	B
f_{Cd} factor	0.52		**0.21**	from previous 2 terms
a_{Cd}/f_{Cd} factor				see Table 7.4.
PD	1.90		**0.97**	
FW & C	1.69		**0.90**	
$\Delta a = a - (a_{Cd}/f_{Cd})$ factor analyte				*n*=4.33; *c*=1.3 (bare)
PD	2.44		**1.26**	$Q_0 \approx 5$
FW & C	2.15		**1.17**	e.g. Eu-153, Re-187
$\Delta a = a - (a_{Cd}/f_{Cd})$ factor comparator				*n*=2.14; *c*=1.88 (bare)
PD	0.73		**1.96**	$Q_0 \approx 15.7$
FW & C	0.85		**1.82**	i.e. Au-197

Contribution from:	***s (%)***	**Distribution**	***u (%)***	**Type / Comment**
($G_{th,s}$ / $G_{th,c}$) (effective)	0.76		**0.33**	includes unc. in g_T
FV: spatial	0.25		**0.25**	see Table 7.6
FV: temporal & others	0.47		**0.22**	
Material			→	see Table 7.7
k_0 factor				***Single determination***
PD	*3.72*		***2.4***	*1 channel exercise;*
FW & C	*3.34*		***2.3***	*1 detector;*
IRMM NOC & AA	*3.56*		***2.6***	*(1 sample)*

See the uncertainty contributions reported in Table 7.1 to Table 7.7 for more information on components, symbols and abbreviations.

FV = neutron fluence variability.

No correlation was considered between the variables.

See text for more information on the sensitivity coefficients and the overall uncertainty budget.

Table 7.9: Combined standard uncertainty (in %) for a single determination of a k_0 factor per the Cd-subtraction technique. Values for 3 irradiation channels, i.e. for different values of n (or sensitivity coefficients) for the analyte.

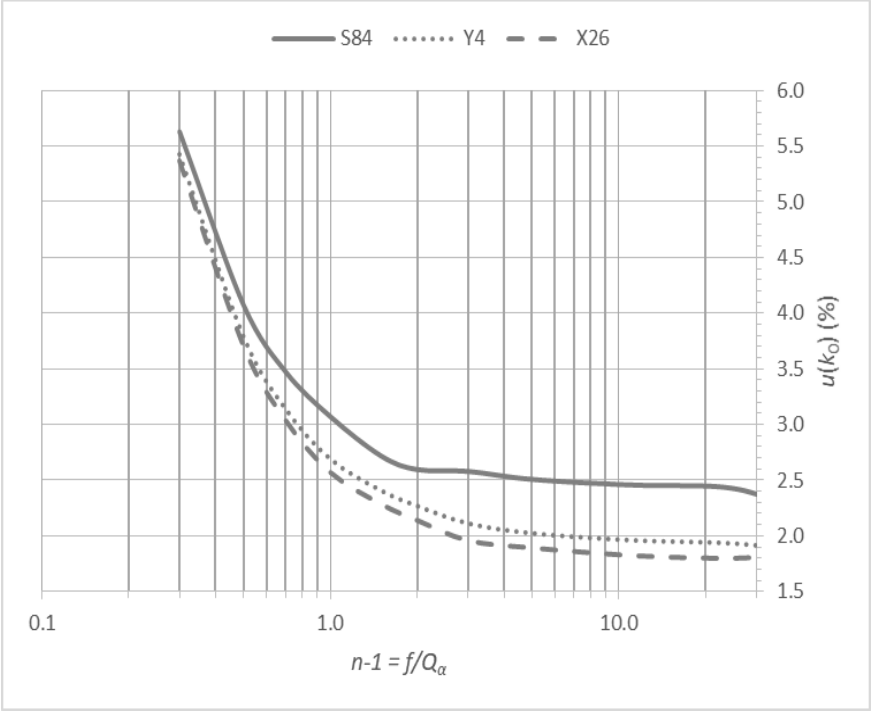

$n = (f/Q_\alpha) + 1 =$		1.3	1.5	1.7	2	2.5	3	4	6	12	24	35
combined *u*	*S84*	**5.6**	**4.1**	**3.5**	**3.1**	**2.7**	**2.6**	**2.6**	**2.5**	**2.5**	**2.4**	**2.3**
in a single	*Y4*	**5.4**	**3.8**	**3.1**	**2.7**	**2.4**	**2.3**	**2.1**	**2.0**	**2.0**	**1.9**	**1.9**
k_0 determination	*X26*	**5.4**	**3.7**	**3.0**	**2.6**	**2.3**	**2.1**	**2.0**	**1.9**	**1.8**	**1.8**	**1.8**

The uncertainty contribution from the comparator was calculated with $n \approx 2.14$, $n \approx 3.3$ and $n \approx 5.6$ for channels S84, Y4 and X26 (respectively).

See this section text for more information.

7.7 In a Q_0 determination

For the calculations concerning the $^{197}Au(n,\gamma)^{198}Au$ comparator reaction we employed $Q_0 = 15.7 \pm 0.3$ and $\bar{E}_r = 5.65 \pm 0.4$ eV from the recommended literature [3, 20, 54, 85], with the quoted uncertainties corresponding to half-widths.

7.7.1 Uncertainty in the q_α factor for the analyte

For the calculation of $u(q_\alpha)$ for the analyte according to eq. (2.59), one needs to consider the uncertainty in the experimental ω_{Cd} factor, $u(Q_\alpha)$ for the comparator and $u(C_\alpha)$. The sensitivity coefficients are:

$$
\begin{aligned}
c_{q_\alpha,\omega_{Cd}} &\equiv \left|\frac{\omega_{Cd}}{q_\alpha}\frac{\delta q_\alpha}{\delta \omega_{Cd}}\right| = \left|\frac{Q_{\alpha,c}}{q_\alpha}\omega_{Cd}\right| = |n|\, c_{q_\alpha,C_\alpha} \\
c_{q_\alpha,Q_{\alpha,c}} &\equiv \left|\frac{Q_{\alpha,c}}{q_\alpha}\frac{\delta q_\alpha}{\delta Q_{\alpha,c}}\right| = c_{q_\alpha,\omega_{Cd}} \\
c_{q_\alpha,C_\alpha} &\equiv \left|\frac{C_\alpha}{q_\alpha}\frac{\delta q_\alpha}{\delta C_\alpha}\right| = \left|\frac{C_\alpha}{q_\alpha}\right| = \left|\frac{1}{n-1}\right|
\end{aligned}
\tag{7.17}
$$

where we have set $\omega_{Cd} = n(C_\alpha/Q_{\alpha,c})$ for simplicity. Since the ratio $(C_\alpha/Q_{\alpha,c})$ is always small independently of α, for instance $(C_\alpha/Q_{\alpha,c}) = 36.6$ for $\alpha = 0$, the major contributors to the Q_0 factor uncertainty are the ω_{Cd} and $Q_{\alpha,c}$ factors, which are discussed next.

7.7.2 Uncertainty in the ω_{Cd} factor

According to eq. (2.57) the $u(\omega_{Cd})$ is obtained from the uncertainty in the ratios between neutron self-shielding correction factors and the $u(r_{Cd})$ values for standard and comparator (with sensitivity coefficients equal to 1).

The uncertainty in the r_{Cd} factor is on the other hand obtained from $u(R_{Cd})$ and $u(F_{Cd})$. The sensitivity coefficients for the calculation of the uncertainty in the r_{Cd} factor are:

$$c_{r_{Cd},R_{Cd}} \equiv \left|\frac{R_{Cd}}{r_{Cd}}\frac{\delta r_{Cd}}{\delta R_{Cd}}\right| = \left|\frac{R_{Cd}F_{Cd}}{r_{Cd}}\right| = \left|1+\frac{1}{r_{Cd}}\right|$$
$$c_{r_{Cd},F_{Cd}} \equiv \left|\frac{F_{Cd}}{r_{Cd}}\frac{\delta r_{Cd}}{\delta F_{Cd}}\right| = c_{r_{Cd},R_{Cd}} \quad (7.18)$$

Table 7.10: Combined standard uncertainty $u(\omega_{Cd})$ from the uncertainty contributions due to the ratio between r_{Cd} factors and other components discussed in section 7.4.

Contribution from:	*s (%)*	*u (%)*	Type / Comment
Fluence variability: spatial	0.25	**0.25**	*into the ω_{Cd}*
Fluence variability: temporal & others	0.47	**0.22**	*into the r_{Cd}*
r_{Cd} comparator	2.37	**1.27**	FW; IRMM-530R
r_{Cd} analyte	2.67	**1.37**	PD
	2.38	**1.27**	FW & C
$(G_{th,s})$ / $(G_{th,c})$ (effective)	0.76	**0.33**	includes unc. in g_T
$(G_{e,s})$ / $(G_{e,c})$	0.42	**0.17**	
ω_{Cd} factor	*3.7*	***1.9***	*PD*
	3.5	***1.9***	*FW & C*

PD = Paper disk; C = Compound; FW = metal samples such as foils and wires (Pure / Alloy)

The $u(R_{Cd})$ is obtained from the uncertainty on the γ activity concentrations for the bare and Cd-covered samples (sensitivity coefficients = 1). The uncertainty contribution due to temporal neutron fluence variability, the impact of the Cd-cover, the sample-rabbit configuration and the volume differences between replicates discussed in section 7.4 can be added (quadratically) to $u(r_{Cd})$. Later, the uncertainty due to spatial neutron fluence variability between standard and comparator is incorporated into the $u(\omega_{Cd})$.

The Table 7.10 reports a combined standard uncertainty of $u(\omega_{Cd}) \approx 1.9\%$ independently of the chosen material. It must be noted that this uncertainty contains contributions from the ratios between the effective $G_{th,\mathrm{eff}} = g_T * G_{th} * G_{mod}$ and G_e correction factors reported in Table 7.5 and $u(\hat{w})$.

7.7.3 Uncertainty in the Q_α factor

For the comparator

For the calculation of the $u(Q_\alpha)$ for the comparator it is necessary to know the uncertainty in $q_{\alpha,c}$ and C_α. The sensitivity coefficients are:

$$\begin{aligned} c_{Q_{\alpha,c},q_{\alpha,c}} &\equiv \left| \frac{q_{\alpha,c}}{Q_{\alpha,c}} \frac{\delta Q_{\alpha,c}}{\delta q_{\alpha,c}} \right| = \left| \frac{q_{\alpha,c}}{Q_{\alpha,c}} \right| = |n| \, c_{Q_{\alpha,c},C_\alpha} \\ c_{Q_{\alpha,c},C_\alpha} &\equiv \left| \frac{C_\alpha}{Q_{\alpha,c}} \frac{\delta Q_{\alpha,c}}{\delta C_\alpha} \right| = \left| \frac{C_\alpha}{Q_{\alpha,c}} \right| = \left| \frac{1}{n+1} \right| \end{aligned} \tag{7.19}$$

where we have set $q_{\alpha,c} = nC_\alpha$ for simplicity. The factor n is high because (C_α/ $q_{\alpha,c}$) is small (i.e. $n = 35.6$ for $\alpha = 0$) and the major contributor is $u(q_\alpha)$. The $u(q_\alpha)$ for the comparator is obtained from employing the sensitivity coefficients:

$$\begin{aligned} c_{q_{\alpha,c},q_{0,c}} &\equiv \left| \frac{q_{0,c}}{q_{\alpha,c}} \frac{\delta q_{\alpha,c}}{\delta q_{0,c}} \right| = 1 \\ c_{q_{\alpha,c},\bar{E}_{r,c}} &\equiv \left| \frac{\bar{E}_{r,c}}{q_{\alpha,c}} \frac{\delta q_{\alpha,c}}{\delta \bar{E}_{r,c}} \right| = |\alpha| \\ c_{q_{\alpha,c},\alpha} &= \left| \frac{\alpha}{q_{\alpha,c}} \frac{\delta q_{\alpha,c}}{\delta \alpha} \right| = \left| \alpha \ln\left(\bar{E}_{r,c} \right) \right| \end{aligned} \tag{7.20}$$

That is, the major contributor to the uncertainty in the calculated q_α is $u(q_0)$, while the contributions from $u(\bar{E}_r)$ and $u(\alpha)$ are greatly reduced. The

uncertainty in the q_0 factor for the comparator is obtained from the sensitivity coefficients:

$$c_{q_{0,c},Q_{0,c}} \equiv \left| \frac{Q_{0,c}}{q_{0,c}} \frac{\delta q_0}{\delta Q_{0,c}} \right| = \left| \frac{Q_{0,c}}{q_{0,c}} \right| = |n| \, c_{q_{0,c},C_0}$$
$$c_{q_{0,c},C_0} \equiv \left| \frac{C_0}{q_{0,c}} \frac{\delta q_{0,c}}{\delta C_0} \right| = \left| \frac{C_0}{q_{0,c}} \right| = \left| \frac{1}{n-1} \right| \qquad (7.21)$$

where we have set $Q_{0,c} = nC_0$ for simplicity. Since the ratio $(Q_{0,c}/C_0)$ is high (i.e. $n = 36.6$) the first sensitivity coefficient remains close to unity and while the second one close to 0. This demonstrates that (for the comparator) the major contributor to the uncertainty in Q_α is the uncertainty in its Q_0 factor (see Table 7.11).

Table 7.11: Combined standard uncertainty $u(Q_\alpha)$ for the ultimate comparator from the uncertainty contributions described in the section 7.7.3.

Contribution from:	*s (%)*	Distribution	*u (%)*	Type / Comment
C_0	0.20	triangular	**0.08**	B
α	20.0	normal	**20.0**	A; k=2.571; N=6; S84
	2.3	normal	**2.30**	A; k=2.306; N=9; Y4
	10.0	triangular	**4.08**	B; X26
C_α	0.20		**0.08**	B
Ultimate comparator				
$\bar{E}_r$	7.0	triangular	**2.86**	B; $\bar{E}_r$ = 5.7 eV
$\bar{E}_{r,\alpha}$	0.12		**0.12**	S84
	2.34		**0.32**	Y4
	3.87		**0.83**	X26
Q_0	2.00	triangular	**0.82**	B; Q_0 = 15.7
q_0	2.01		**0.84**	
q_α	2.02		**0.85**	S84
	3.09		**0.90**	Y4
	4.37		**1.19**	X26
Q_α	*2.1*		***0.9***	*S84*
	3.2		***0.9***	*Y4*
	4.5		***1.2***	*X26*

No correlation was considered between the variables.

For the analyte

Once the uncertainty in q_α is computed from the previous two sections, the $u(q_0)$ can be obtained from eq. (2.54). The sensitivity coefficients are:

$$\begin{aligned} c_{q_0,q_\alpha} &\equiv \left| \frac{q_\alpha}{q_0} \frac{\delta q_0}{\delta q_\alpha} \right| = 1 \\ c_{q_0,\bar{E}_r} &\equiv \left| \frac{\bar{E}_r}{q_0} \frac{\delta q_0}{\delta \bar{E}_r} \right| = |\alpha| \\ c_{q_0,\alpha} &= \left| \frac{\alpha}{q_0} \frac{\delta q_0}{\delta \alpha} \right| = \left| \alpha \ln\left(\bar{E}_r\right) \right| \end{aligned} \tag{7.22}$$

Finally, once the uncertainty in the q_0 factor is determined, the $u(Q_0)$ is found from the sensitivity coefficients:

$$\begin{aligned} c_{Q_0,q_0} &\equiv \left| \frac{q_0}{Q_0} \frac{\delta Q_0}{\delta q_0} \right| = \left| \frac{q_0}{Q_0} \right| = |n| c_{Q_0,C_0} \\ c_{Q_0,C_0} &\equiv \left| \frac{C_0}{Q_0} \frac{\delta Q_0}{\delta C_0} \right| = \left| \frac{C_0}{Q_0} \right| = \left| \frac{1}{n+1} \right| \end{aligned} \tag{7.23}$$

The factor n is usually high when the ratio (C_0/Q_0) is small. For low Q_0 isotopes with $Q_0 \approx C_0$ (i.e. ^{45}Sc) one has $n \approx 1$ and up to half of $u(C_0)$ is added. The major contributor to the uncertainty in a Q_0 determination is therefore $u(q_\alpha)$.

The Table 7.12 shows that in this work the precision for a Q_0 determination varies between 2.2 to 2.7% depending on the irradiation channel employed, with an average precision of $u(Q_0)$ = 2.4%. This budget is bound to the same considerations summarized previously for a single k_0 determination, but for a target isotope with a Q_0 and $\bar{E}_r$ factor like that of the ultimate comparator and $s(\bar{E}_r)$= 25% which corresponds to our worst estimate. For an isotope such as ^{114}Cd we should consider a $s(F_{Cd})$= 6% uncertainty in the observed F_{Cd} =

0.40, meaning a precision of $u(Q_0)$ = 4.4% for the determination of this isotope Q_0 factor.

Table 7.12: Relative *s* and *u* for the components leading to the $u(Q_0)$ in a Q_0 factor determined on 3 irradiation channels.

Contribution from:	*s (%)*	Distribution	*u (%)*	Type / Comment
Analyte				
q_α	2.89		**2.14**	S84
	3.80		**2.16**	Y4
	5.01		**2.31**	X26
$\bar{E}_r$	25.0	triangular	**10.21**	B; worst estimate
$\bar{E}_{r,\alpha}$	0.15		**0.12**	S84
	2.83		**0.72**	Y4
	4.67		**1.36**	X26
q_0	2.89		**2.14**	S84
	4.74		**2.28**	Y4
	6.85		**2.68**	X26
Q_0	*3.0*		***2.2***	*S84*
	4.9		***2.3***	*Y4*
	7.0		***2.8***	*X26*

The uncertainty budget was estimated for a target isotope with Q_0 and $\bar{E}_r$ factors like the ultimate comparator.

No correlation was considered between the variables.

7.8 In a k_0 determination with *f* and α

The *f* parameter can be estimated from the ultimate comparator Cd-ratios and Q_α factor according to eq. (2.56) or from other calibration monitors results in this work (see section 4.5). The $u(f)$ can be estimated from the previous sources as given in Table 7.13. The average $u(f)$ = 2.2% in Table 7.13 confirms the uncertainty obtained from the SD of the mean of the historic records in Table 6.4 for channels S84 and Y4. This estimate is also applicable to $u(\beta_\alpha)$ since this parameter is just proportional to *f* (see sections 2.11 and 6.5).

The sensitivity coefficients for the normalized reaction rate R in either convention can be written as:

$$\begin{aligned} c_{R,Q_\alpha} &= c_{R,f} = \left| \frac{G_e}{R_H} \frac{Q_\alpha}{f} \right| = \left| 1 - \frac{G_{th} g_T}{R_{H,W}} \right| \\ c_{R,s_\alpha} &= c_{R,\beta_\alpha} = \left| \frac{G_r}{R_W} \frac{s_\alpha}{\beta_\alpha} \right| = \left| 1 - \frac{G_{th} g_T}{R_W} \right| \\ c_{R,G_e} &= \left| 1 - \frac{G_{th} g_T}{R_{H,W}} \right| \\ c_{R,G_{th}} &= c_{R,g_T} = \left| \frac{G_{th} g_T}{R_{H,W}} \right| \end{aligned} \tag{7.24}$$

For a channel like S84 with $\alpha \approx 0$ and the ultimate comparator which has a mid-range Q_0 factor, one can roughly approximate $Q_\alpha \approx f$ if one disregards neutron self-shielding and non-1/v behaviour, meaning that the sensitivity coefficients are all $c \approx 0.5$. Therefore, half of each uncertainty component is added quadratically. The major contributors are $u(f)$ and $u(Q_\alpha)$ or $u(\beta_\alpha)$ and $u(s_\alpha)$. Then one is posed with 2 extreme cases for the analyte: low or high Q_0 factors.

If Q_α is approximately four times the magnitude of f (i.e. ^{98}Mo or ^{116}Sn) the sensitivity coefficients are $c \approx 4/5 = 0.8$ and $u(k_0) \approx 3.3\%$ for any material. On the other hand, if Q_α is 10% the magnitude of f factor the sensitivity coefficients are $c \approx 0.1/1.1 = 0.091$ and $u(k_0) \approx 2\%$. Finally, with a Q_α factor for the analyte similar in magnitude to that of the comparator (i.e. ^{124}Sn), the sensitivity coefficients are again $c \approx 0.5$ and a mid-range precision is estimated at $u(k_0) \approx 2.6\%$.

These estimates were calculated assuming a $s(g_T) = 0.5\%$ leading to $u(g_T) = 0.3\%$ per a triangular distribution. It was necessary to adopt the Q_0 (or s_0) and $\bar{E}_r$ factors for: ^{96}Zr, ^{116}Sn, ^{125}Sb (from ^{124}Sn(n,γ)^{125m}Sn) which are high-Q_0 factors and for ^{153}Eu, ^{168}Yb and ^{151}Eu which are mid-low to low values.

For the non-1/*v* nuclides ^{151}Eu and ^{168}Yb and although the g_T values taken from [2, 16, 48] have no associated uncertainty, one can adopt $s(g_T)$ = 2% leading to $u(g_T)$ = 1.15%. By noting that their epithermal-to-thermal contribution is expected to be small ($c < 0.25$) the precision for these isotopes would reach $u(k_0)$ = 2.2%. Adoption of β_α, s_α and α is therefore more suited for k_0 determination of non-1/v isotopes than the Cd-subtraction method.

Table 7.13: Combined standard uncertainty in the *f* or β_α parameter calculated from the ultimate comparator or another monitor nuclear data.

Contribution from:	*s (%)*	*u (%)*	Type / Comment
***f* or β_α**	4.0	**1.6**	from comparator Cd-ratios
	5.6	**2.8**	from other isotopes with $u(Q_0)$ = 2.5%
Mean	*4.8*	***2.2***	

See the uncertainty contributions reported in Table 7.1 to Table 7.12 for more information on components.

7.8.1 Estimate for a ^{238}U k_0 factor and ^{235}U k_0-fission factor

In this work we adopted the following values and half-width uncertainties from the recommended literature [3, 20, 54, 85]:

- for the ^{238}U(n,γ)^{239}U→^{239}Np reaction*:* $Q_0 = 103.4 \pm 1.3$ and $\bar{E}_r = 16.9 \pm 1.2$ eV and,

- for ^{235}U fission: $Q_0 = 0.47 \pm 0.05$ and $\bar{E}_r = 0.59 \pm 0.08$ eV.

From the previous discussion and sensitivity coefficients reported in this section:

- the precision for a single determination of a ^{238}U k_0 factor is $u(k_0)$ = 2.5% ($c \leq 3/4$) while,

- for a single determination of a ^{235}U k_0-fission factor it is $u(k_0) = 1.8\%$ due to its low Q_0 factor ($c \leq 0.014$).

The previous estimate is given for determinations in a channel Y4, as done in this work (see sections 6.7, 6.8.2 and 6.11).

Table 7.14: Relative *s* and *u* contributions from the different influence quantities involved in a single k_0 determination by means of *f* and *α*.

Contribution from:	*s (%)*	Distribution	*u (%)*	Type / Comment
Ultimate comparator				
G_e	0.30	triangular	**0.12**	B
Westcott g_T factor (non-1/v isotopes)	0.50	uniform	**0.29**	B
G_{th} *effective* = G_{th} * G_{mod}	0.54	triangular	**0.22**	B
f (or β_α)	4.82		**2.21**	see Table 7.13
Q_α *(or s_α)*	3.25		**1.01**	see Table 7.11
R	*2.94*		***1.23***	
Analyte				
G_e	0.30	triangular	**0.12**	B
Westcott g_T factor (non-1/v isotopes)	0.50	uniform	**0.29**	B
G_{th} *effective* = G_{th} * G_{mod}	0.54	triangular	**0.22**	B
f (or β_α)	4.82		**2.20**	see Table 7.13
Q_α *(or s_α)*	4.96		**2.43**	see Table 7.11
R	*1.74*		***0.83***	

Contribution from:	*s (%)*	Distribution	*u (%)*	Type / Comment
Fluence variability (spatial)	0.25		**0.25**	see Table 7.6
Ratio of reaction rates for standard and comparator	3.42		**1.50**	
Ratio of a=A/ŵ values for standard and comparator	2.58		**1.33**	PD
	2.25		**1.23**	FW
	2.27		**1.24**	C
Material			→	terms in Table 7.7
				Single determination
k_0 factor	*3.2*		***2.1***	*PD*
	3.0		***2.1***	*FW & C*
	3.1		***2.3***	*IRMM NOC & AA*

See the uncertainty contributions reported in Table 7.1 to Table 7.13 for more information on components, symbols and abbreviations.

No correlation was considered between the variables.

A single determination is for 1 channel exercise with 1 material studied on 1 detector.

All sensitivity values estimated for channel S84, with:

$c \approx 0.5$ for the comparator reaction rate ($f \approx Q_\alpha$; $R \approx 2$) and,

$c \approx 0.25$ for an analyte with a Q_0 factor such as ^{95}Zr, ^{153}Eu or ^{187}Re ($R \approx 1.3$; $Q_\alpha \approx 30\%$ of f).

7.9 In the k_0 determination with a highly-thermalized channel

The precision for a k_0 determination improves for higher (f/Q_α) ratio as shown by eq. (7.16) and the sensitivity coefficients for Δa in eq. (7.15). This is shown numerically and graphically in the Table 7.9.

For highly thermalized channels where the epithermal contribution is negligible (i.e. $f >> Q_\alpha$) the k_0 factor computation depends only on the factors listed in eq. (2.64) with G_{th} to be considered an "effective" correction factor due to thermal neutron self-shielding and moderation: $G_{th,\text{eff}} = G_{th}.G_{\text{mod}}$. The uncertainty of the contributing components is listed in Table 7.15, from which we obtained $u(k_0) = 1.8\%$ for a determination in our Cavity channel and for a compound or pure metal sample.

This precision estimate was found from:

- a 1% and 2% half-width uncertainty in the correction factor for the analyte ($G_{th,\text{eff}} = 0.9$) and the comparator ($G_{th,\text{eff}} = 0.8$) leading to $u(G_{th,\text{eff}}) \leq 0.82\%$ contribution per a triangular distribution.

- a $s(g_T) = 0.5\%$ uncertainty in the Westcott g_T factor for the analyte and the comparator leading to a $u(g_T) = 0.29\%$ contribution from this parameter (uniform distribution).

Table 7.15: Relative *s* and *u* leading to the $u(k_0)$ for a k_0 determination with a highly thermalized channel as e.g. the channel Cavity employed in this work.

Contribution from:	*s (%)*	Distribution	*u (%)*	Type / Comment
Analyte				
Westcott g_T factor (non-1/v isotopes)	0.50	uniform	0.29	B
*G_{th} effective = G_{th} * G_{mod}*	1.00	triangular	0.41	B
Ultimate comparator				
Westcott g_T factor (non-1/v isotopes)	0.50	uniform	0.29	B
*G_{th} effective = G_{th} * G_{mod}*	2.00	triangular	0.82	B
Sub-total	*2.35*		***1.00***	
Fluence variability (spatial)	0.25		0.25	see Table 7.6
Material	0.94		0.54	see Table 7.7 (FW, C)
Ratio of activity concentrations (A/ŵ)	2.27		1.24	see Table 7.4 (FW, C)
Sub-total	*2.64*		***1.48***	
k_0 factor	*3.5*		***1.8***	FW, C

C = Compound; FW = metal samples such as foils and wires (Pure / Alloy).

7.10 In a thermal neutron cross-section

From the definition of a k_0 factor given in eq. (2.38) the uncertainty in a σ_0 value derived from this formula contains the uncertainty contributions from the atomic weight $s(M)$, I_γ values $s(I_\gamma)$ and isotopic abundances $s(\theta)$ of the comparator and the analyte. The *s* and *u* of these parameters are given in Table 7.16. Assuming a $u(k_0)$ that varies between 1.8 and 4% and a moderate $s(I_\gamma) \leq 1\%$ for the analyte, the table reports that $u(\sigma_0) \approx u(k_0)$ for a single determination: 1 material irradiated in 1 channel and measured with 1

detector. This estimate includes a standard uncertainty of 0.33% due to isotopic variability in the $u(k_0)$ value (see Table 7.7). If we adopt the $s(I_\gamma)$ = 5% as in the case of a poor yield γ-ray, then the combined uncertainty increases to $u(\sigma_0)$ = 2.7 to 4.5%.

Table 7.16: Relative *s* and *u* for the terms contributing to the uncertainty in a single determination of a thermal neutron cross-section. Estimate $u(\sigma_0)$ based on k_0 factors with $u(k_0)$ = 1.8 to 4% and a moderate $s(I_\gamma)$ = 1% value.

Contribution from:	*s (%)*	Distribution	*u (%)*	Type / Comment
Comparator				
isotopic abundance	0.00	uniform	0.00	B
γ-ray abundance	0.10	triangular	0.04	B
atomic weight	0.00	triangular	0.00	B
thermal neutron cross-section	0.10	triangular	0.04	B
Sub-total	*0.14*		***0.06***	
Analyte				
isotopic abundance	0.50	uniform	0.29	B
γ-ray abundance	1.00	triangular	0.41	B
atomic weight	0.05	triangular	0.02	B
Sub-total	*1.12*		***0.50***	
k_0 factor		min	**1.8**	low Q_0; X26; Cavity
		max	**4.0**	Cd-114, high Q_0 on S84; strong $g_T \neq 1$
thermal neutron cross-section for the analyte		***min***	***1.9***	1 determination
		max	***4.0***	

The uncertainties in the nuclear data are taken from [6, 8, 10, 17].

7.11 Estimate from multiple exercises with different materials, detectors and channels

The uncertainty budgets for k_0 and Q_0 factors given in the previous sections were estimated for a single determination, that is, 1 material tested in 1 irradiation channel with 1 detector at mid-range sample-detector distance. However, in this work we are interested in a way to estimate the final uncertainty for these factors when averaging the results from exercises performed with replicates of different materials irradiated in different channels and measured at different positions on different detectors.

The uncertainty in a k_0 or Q_0 factor can be decomposed into 2 components. For estimating the combined standard uncertainty u_{multi} in a quantity F from these kind of experiments, we employed:

$$u_{multi}(F) = \sqrt{u_A(F)^2 + u_B(F)^2} \tag{7.25}$$

The standard uncertainty u_A is found from a type-A evaluation, that is:

$$u_A(F) = \frac{SD_F}{\sqrt{N_{Ch}N_m}} \tag{7.26}$$

This standard uncertainty $u_A(F)$ is estimated from the SD of the mean from these multiple channel, detector and material results with $(N_{Ch}N_m) - 1$ degrees of freedom. The sample size $N_{Ch}N_m$ is calculated from the number of channels (N_{Ch}) and the number of bare samples only (N_m; N_m = 4 to 6), i.e. half the total number of samples per channel ($N_s = 2N_m$) because the Cd-covered replicates are also necessary for calculating a Q_0 or a k_0 factor per the Cd-subtraction.

The other (standard uncertainty) component $u_B(F)$ must be found from a type-B evaluation as done in the previous sections. It is not possible to adopt $u_B(F)$ directly from these estimates for a single determination of a k_0 or Q_0

factor since one should not add the same uncertainty twice [109]. There are several uncertainties from the previous sections that can be evaluated by means of the SD of the mean of eq. (7.26). Therefore, the next step is to reduce our uncertainty budgets for a single determination by withdrawing the components that can be evaluated by $u_A(F)$ instead, leaving into u_B(F) only those uncertainty contributions that are (inherently) common to all channel experiments.

For instance, the uncertainty due to efficiency calibration, half-life, background subtraction, sample weighing and the certified elemental content is common to all detectors and samples results irrespectively of the channel employed. These components cannot be evaluated by means of $u_A(F)$, hence must be accounted into $u_B(F)$. See next.

7.11.1 Estimate of $u_A(F)$

For our purposes, we can fix N_m = 4 from 8 samples per channel (4 bare) prepared from different materials. Since we employed up to N_{Ch} = 4 irradiation channels, the number of degrees of freedom varies between 3 to 15. This gives a k = 3.182 to 2.131 (respectively) for a 95% confidence level. The typical observed SD in a k_0 or Q_0 factor was < 1%, although a conservative approach would be to adopt SD ≤ 2%. If it was determined in 1 irradiation channel (with different detectors and materials) then $u_A(F) \leq$ 1% (k =3.182; $N_{Ch}N_m$ =4).

For 2 channels (k = 2.365; $N_{Ch}N_m$ =8), 3 channels (k = 2.201; $N_{Ch}N_m$ =12) and 4 channels (k = 2.131; $N_{Ch}N_m$ =16) the reader can verify from eq. (7.26) that $u_A(F) \leq 0.71\%$, 0.58% and ≤ 0.5% respectively. Coverage factors given for a 95% confidence level.

7.11.2 Estimate of $u_B(F)$

The isotopic variability, all mass losses mechanisms, X-ray and γ-ray self-absorption and sample positioning are typical effects that vary per studied sample/material, therefore their uncertainty contributions can be evaluated instead by means of the SD in the results, i.e. by means of $u_A(F)$. Other uncertainties that can be evaluated this way are the contributions of $u(t_d)$ and $u(t_c)$ to $u(D)$, $u(C)$ and the uncertainty from counting statistics $u(N_p)$, because the replicates samples were measured at different decay and cooling times several times (4 to 6 times per position) at 2 to 3 different positions.

The thermal and epithermal neutron self-shielding, neutron scattering, neutron moderation and geometry differences between replicates are other examples of effects that vary between different sample sizes/matrices, therefore these components can be evaluated from the variance of repeated (and reproducible) experiments. Uncertainty components that vary per detector system such as detector fine-tuning or per sample-detector position such as the COI corrections, can be evaluated by means of the observed $u_A(F)$.

If one employs different irradiations channels with a big spread in neutron fluence characteristics, i.e. φ_{th}, φ_e, α and temperature, as well as different sample-loading mechanisms, then the uncertainty due to: neutron fluence variability, g_T factors, burn-up of target nuclide, irradiation timing, the ramping up/down of the fluence at the start/end of the irradiation as well as all sources of interferences (primary and/or secondary) can also be evaluated by means of the SD of these results. The impact of the different Cd-covers sizes (same thickness) employed per rabbit-sample configuration it is also assumed to vary between channels.

The impact of pulse pile-up and detector dead-time depends on the measured count-rate (i.e. sample-detector position) and the correction method applied (e.g. LFC or ZDT). Therefore, one must consider that the impact of these

count loss mechanisms will be different even in the case of replicate samples measured at the same detector and position if these where irradiated on different channels, i.e. at different neutron fluence rate magnitudes, because the induced activities will differ.

Therefore, the standard uncertainty component $u_B(F)$ can be calculated from the estimates in Table 7.1 to Table 7.16 after the previous listed contributions are subtracted. These (uncertainty) contributions will be obtained later from $u_A(F)$ to determine the $u_{\text{multi}}(F)$ (see the next section).

- For 1 irradiation channel with different detectors and materials:

The $u_B(k_0)$ = 1.7% per the Cd-subtraction technique but remains at $u_B(k_0)$ = 2.1% for determinations with f and α. The uncertainty from f and α remains fixed, while most components showing up on Cd-ratios are now unaccounted in the new type-B evaluation. The average between the 2 methods is $u_B(k_0)$ = 1.9%.

The $u_B(Q_0)$ is 2%, but one must note that both estimates are for an analyte with a Q_0 factor like that of the comparator, which covers almost all studied cases with a few exceptions. For a worst estimate, such as an isotope with a high Q_0 factor as Cd-114 and F_{Cd} = 0.40, one has $u_B(k_0) \approx u_B(Q_0)$ = 2.7%.

- For ≥ 2 irradiation channels (with different detectors and materials):

The $u_B(k_0)$ = 1.44% per the Cd-subtraction technique but remains at $u_B(k_0) \approx$ 1.74% for determinations with f and α. The average between the 2 methods is $u_B(k_0)$ = 1.6%.

The precision for a Q_0 does not improve much, it is estimated at $u_B(Q_0)$ = 1.85% for an analyte with a Q_0 factor like that of the comparator. For Cd-114, due to the high uncertainty in F_{Cd}, and one has $u_B(k_0) \approx u_B(Q_0)$ = 2.5% as an extreme example.

7.11.3 Estimate of $u_{multi}(F)$

From the previous estimates $u_A(F)$ in section 7.11.1 and for an analyte with a Q_0 factor like the comparator one has the following final combined standard uncertainty estimate for multiple samples/materials measured with different detectors (at different positions):

- For N_{Ch} = 1 channel → $u_{multi}(k_0) \leq 2\%$ and $u_{multi}(Q_0) \leq 2.2\%$. The coverage factor for a 95% confidence level is k = 3.182.

Clearly, the precision should be better than our previous estimate $u(k_0) \approx u(Q_0) \approx 2.4\%$ for a single determination on a channel like S84 with only 1 detector and 1 sample/material.

- For N_{Ch} = 2, N_{Ch} = 3 and N_{Ch} = 4 channels → $u_{multi}(k_0) \leq 1.6\%$ and $u_{multi}(Q_0) \leq 2\%$. The coverage factor for a 95% confidence level is k = 2.365, k = 2.201 and k = 2.131 respectively.

Once more, this budget is suited for all studied cases except for high Q_0 factors and a strong F_{Cd} deviation from unity like Cd-114.

7.12 Statistical significance test

When one wishes to compare mean values for statistical significance, the One-sample two-tailed Student t-test states that between a mean value X with variance s^2 (N-1 degrees of freedom) and a mean value μ with unknown variance, a t-value can be computed as:

$$t = \frac{X - \mu}{\frac{s_X}{\sqrt{N}}} \tag{7.27}$$

When multiplying the numerator (signal) and denominator (noise) by X, one obtains:

$$t = \frac{\left(1 - \frac{\mu}{X}\right)}{\left(\frac{s_{r,X}}{\sqrt{N}}\right)} = \frac{\Delta}{u_{multi}(F)} \tag{7.28}$$

with Δ the relative (percent) difference between X and μ and $u_{\text{multi}}^2(F)$ as the substitute for the variance (or noise) in the denominator. The degrees of freedom $N - 1$ in the eq. (7.27) are included in our estimate of $u_{\text{multi}}(F)$ as shown in the previous section (i.e. $N_{Ch}N_m - 1$).

The Table 7.17 shows the resulting t-values from applying eq. (7.28) with the estimate $u_{\text{multi}}(k_0)$ given in the section 7.11 for up to 4 channel determinations and 3 to 15 degrees of freedom ($N_{Ch}N_m - 1$). This is tabulated when assuming Δ = 3 to 6% values between our results and the recommended literature.

One can conclude from this table that when employing 1 irradiation channel only the results with ≥ 6% difference will be statistically significant at the 95% confidence level. On the other hand, the results with relative differences of ≥ 4% will be statistically significant when determined in 2 to 4 irradiations channels. Finally, it is clear that ≤ 3% differences are not statistically significant per our estimate uncertainty and degrees of freedom.

The Table 7.18 on the other hand shows that statistical significance in the relative differences between Q_0 results is possible when it is ≥ 7% and the determination was performed in 1 irradiation channel. For ≥ 2 channels, only ≥ 5% relative differences will be statistically significant (at 95% confidence level).

Table 7.17: The t-values for a two-tailed Student t-test for finding statistical significance in the experimental k_0 factor results, when comparing the relative difference between our mean values and the literature recommended ones.

				Δ= Relative difference			
Channels	**k for p = 0.05**			**3%**	**4%**	**5%**	**≥ 6%**
N_{Ch}	**(95% confidence)**	$N_{Ch}N_m$ **- 1**	u_{multi}	**t-value**			
1	3.182	3	2.0%	1.50	2.00	2.50	*3.60*
2	2.365	7	1.6%	1.88	*2.50*	*3.13*	*4.50*
3	2.201	11	1.5%	2.00	*2.67*	*3.33*	*4.80*
4	2.131	15	1.5%	2.00	*2.67*	*3.33*	*4.80*

Table 7.18: The t-values for a two-tailed Student t-test for finding statistical significance in the experimental Q_0 factor results, when comparing the relative difference between our mean values and the literature recommended ones.

				Δ= Relative difference			
Channels	**k for p = 0.05**			**3%**	**4%**	**5%**	**≥ 7%**
N_{Ch}	**(95% confidence)**	$N_{Ch}N_m$ **- 1**	u_{multi}	**t-value**			
1	3.182	3	2.2%	1.36	1.82	2.27	3.27
2	2.365	7	2.1%	1.46	1.95	*2.44*	*3.51*
3	2.201	11	2.0%	1.51	2.01	*2.51*	*3.61*
4	2.131	15	2.0%	1.53	2.04	*2.54*	*3.66*

A relative difference would be statistically significant at the given p = 0.05 or 95% confidence level when the calculated p value (derived from the calculated t-value) is equal or lower than our confidence level p value (i.e. $p \leq 0.05$). This occurs for the underlined t-values in the tables.

Estimates obtained asuming a SD ≤ 2%.

8. Discussion

This chapter aims at providing a discussion of the experimental k_0, Q_0 and $\bar{E}_r$ factors obtained in this work. The tables and figures are located and described in Chapter 10 and a summary of the following discussion is also given at the end of that chapter (section 10.8). Chapter 6 provides the information about the materials, models and methods employed for obtaining the results. For the calculation of uncertainties refer to the previous chapter.

8.1 The α-vector method for Q_0 and $\bar{E}_r$ determination

Figure 10.1 to Figure 10.11 show the resulting Y_α vs. α plots from the monitoring of 41 (n,γ) reactions. The dashed curves correspond to polynomial fits ($p_3 \neq 0$) to our experimental results, while the points represent the expected (or theoretical) lines based on the latest recommended values in [20, 23] (with $p_3 = 0$).

These Y_α vs. α plots show that the $\bar{E}_r$ concept, its assumed α-independence and the linearity of α are valid assumptions since most of the observed biases in intercept/slope between the theoretical and expected lines seem to be related only to differences in Q_0 and $\bar{E}_r$ absolute magnitudes and not to inconsistencies in the underlying assumed linearity. This is because when

$p_3 \neq 0$ is assumed, we observe that the p_3 value is constrained within >-9 and <4 for the majority of the depicted cases, meaning that for our rather extreme channel X26 (α = 0.110±0.05) the $\bar{E}_{r,p3,\alpha}$ value calculated according to eq. (6.8) and $p_3 = \pm 10$ would result in a final contribution to the Q_α factor (from the term $(\bar{E}_{r,p3,\alpha})^{-\alpha}$) that is ±12% different than it would be expected if $p_3 = 0$. The effect of p_3 is described in the following paragraphs.

Solving the α-vector problem with $p_3 \neq 0$ gives a different set of p_1 and p_2 values than solving it when forcing $p_3 = 0$. Still, the difference in p_1 values (or Q_0 factors) will be small, as the term is associated with the constant term of the polynomial, but the difference in p_2 values (or $\bar{E}_r$ factors) can be considerable.

Table 10.6 summarizes the P-vectors or (p_1,p_2,p_3)-tuples obtained for 36 target isotopes when assuming: A) a non-zero p_3 value as in eq. (6.14) with $N = 3$ and; B) when forcing the condition $p_3 = 0$ (no α-dependence) as in eq. (6.15).

As expected, the differences between Q_0 (or s_0) factors obtained by methods A or B are small (typically within 1%), except for the s_0 factors for the non-1/v cases ^{168}Yb and ^{151}Eu (3-6%), for which the application of the modified Westcott formalism was not truly meant, but as an approximation. The quoted $\bar{E}_r$ values in Table 10.6 are different in orders of magnitude in some cases between the methods A and B.

A functional relationship must be established between the different $\bar{E}_r$ values of Table 10.6, as the idea of reporting "one set of values for $p_3 = 0$ and one set for $p_3 \neq 0$" is against the concept of a standardization. We could take eq. (6.8) as the general shape of $\bar{E}_r$ as a function of α, apply the index p_3 for labelling a $\bar{E}_r$ factor determined with $p_3 \neq 0$, and rewrite the eq. as:

$$\bar{E}_{r,p_3,\alpha} = \left\{ \bar{E}_{r,p_3} \right\} e^{-\alpha p_3} \tag{8.1}$$

and express the $\bar{E}_{r,p3}$ value as a similar exponential function of the $\bar{E}_{r,0}$ value (found with $p_3 = 0$).

$$\bar{E}_{r,p_3} = \bar{E}_{r,0} e^{-\alpha_0 p_3} \tag{8.2}$$

The α_0 parameter is determined from a linear fit on a Z_{p3} vs. p_3 plot:

$$Z_{p_3} = \ln\left\{\frac{\bar{E}_{r,0}}{\bar{E}_{r,p_3}}\right\} = \alpha_0 p_3 \tag{8.3}$$

By means of eq. (8.3) we can obtain only one set of $\bar{E}_{r,0}$ values, that are consistent (in order of magnitude) to the recommended ones in references [20, 23]. The analyst would then have two ways to employ the $\bar{E}_{r,0}$ values in the calculation of the Q_α factor: 1) either by direct substitution in eq. (2.41) when assuming $p_3 = 0$ (no α-dependence) or; 2) through the following eq. that uses the p_3 and α_0 values:

$$\bar{E}_{r,p_3,\alpha} = \left\{\bar{E}_{r,0}\right\} e^{-p_3(\alpha+\alpha_0)} \tag{8.4}$$

followed by the substitution of this $\bar{E}_{r,p3,\alpha}$ in the eq. (2.41) for Q_α calculation, as usual.

The Figure 8.1 shows the Z_{p3} vs. p_3 plot obtained from the 2 sets of $\bar{E}_r$ values reported in Table 10.6. From a linear fit, eq. (8.3) gives $\alpha_0 = -0.1$, allowing us to drop one set of $\bar{E}_r$ values from Table 10.6, namely those tabulated with $p_3 \neq 0$ (method A) and to preserve only one set of $\bar{E}_{r,0}$ values, which are those tabulated under the method B.

It should be noted that although the $\bar{E}_r$ factor calculated with eq. (8.4) is different from a raw one (i.e. $\bar{E}_{r,0}$), what is actually employed in the computation of Q_α is the factor $(\bar{E}_r)^{-\alpha}$, as shown in eq. (2.41).

The Figure 8.2 shows the percent relative difference between a $(\bar{E}_r)^{-\alpha}$ factor obtained when inputting a $\bar{E}_{r,p,\alpha}$ value from eq. (8.4) with $\alpha_0 = -0.1$ ($p_3 \neq 0$) and, when inputting a raw $\bar{E}_{r,0}$ value ($p_3 = 0$) instead, for 36 target isotopes of interest studied on three irradiation channels (X26, Y4 and S84).

For the two extreme channels S84 (α = -0.003) and X26 (α = 0.11) the relative differences are within 1 and 2%, while it can be up to 5% for isotopes studied in the intermediate channel Y4 (α = 0.066).

Only ^{23}Na, ^{45}Sc and ^{151}Eu gave relative differences higher than 10%, since their data points were greatly scattered. In the case of ^{23}Na and ^{45}Sc their low Q_0 factors are close to C_0, which corresponds to a singularity in the eq. (6.10) . Both isotopes were investigated in 3 channels therefore the difference is statistically significant at the 95% confidence level assuming $u(Q_0)$ = 2% (t-value = 5; N_m =11); see sections 7.11 and 7.12. However, since their Q_0 (or s_0) factors are low, the $\bar{E}_{r,0}$ factor will have a small impact on Q_α. For ^{151}Eu, the recommended literature is adopted and bears a high uncertainty.

It seems then that the application of eq. (8.4) is not strictly necessary in virtue of the small impact on the Q_α factor and, considering that the Q_α contribution will be further reduced into the final analytical result (e.g. the elemental content or the k_0 factor). If $Q_0 > f$ and the relative difference in $(\bar{E}_r)^{-\alpha}$ factors is > 5%, the employment of p_3 values would be advisable.

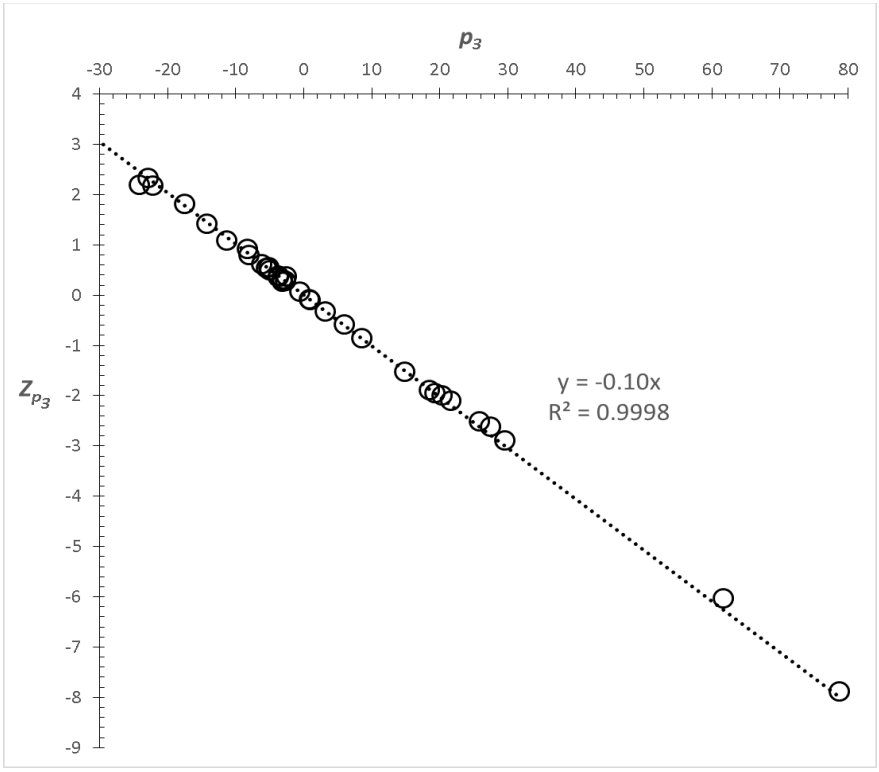

Figure 8.1: Graph of Z_{p3} values vs. p_3 for 36 (n,γ) target isotopes investigated on 3 irradiation channels. From a linear regression (*dashed line*) the optimal value α_0 = -0.1 was found from the slope, for which an experimental $\bar{E}_r$ value determined with $p_3 \neq 0$ can be transformed to an experimental $\bar{E}_r$ factor that is p_3 (or α) independent.

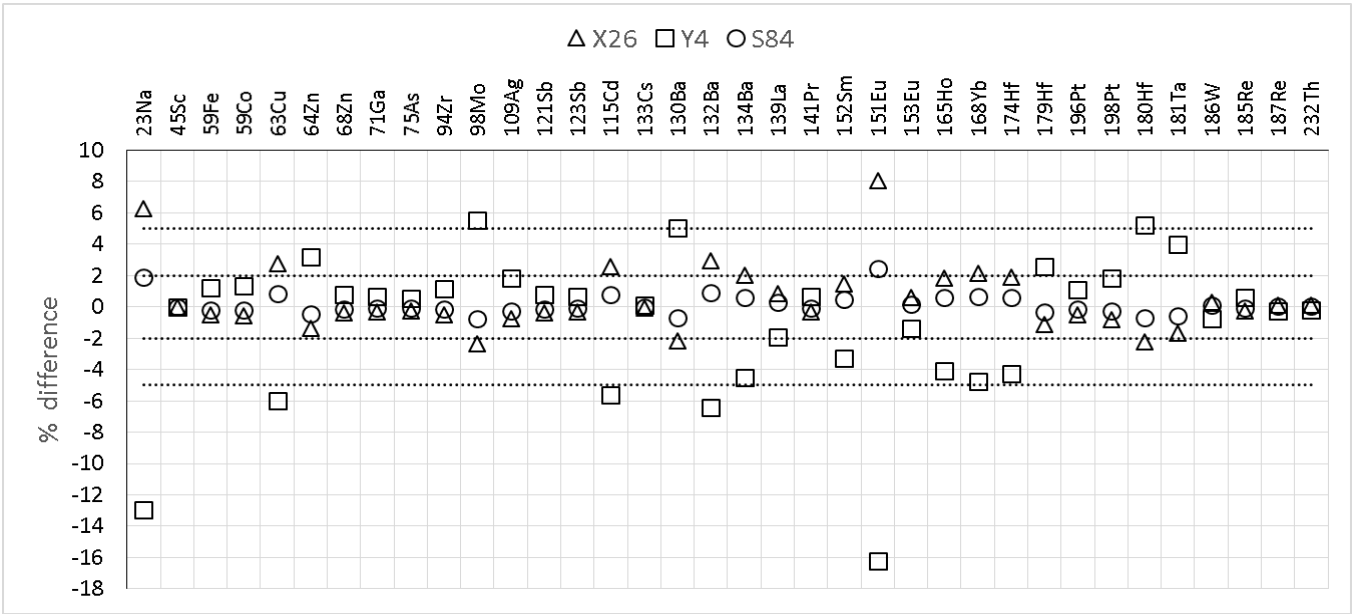

Figure 8.2: Percent relative difference in the calculated $(\bar{E}_r)^{-\alpha}$ factor obtained with $\bar{E}_{r,p,\alpha}$ from eq. (8.4) with α_0 = -0.1 ($p_3 \neq 0$) and a raw $\bar{E}_{r,0}$ value (p_3 = 0), for 36 target isotopes of interest studied on 3 irradiation channels of the BR1. The α values for channels X26, Y4 and S84 are reported in Table 6.6, while Table 10.6 contains the source $\bar{E}_r$ and p_3 values.

8.2 On Q_0 and $\bar{E}_r$ factors

The experimental Q_0 (or s_0) and $\bar{E}_r$ factors obtained in this work (TW) are summarized in Table 10.7 and Table 10.8. These values are reported for the respective activation-decay scheme (ADS) and are compared to values from the recommended compilations (Lit) in references [20–23]. The Q_0 (or s_0) values were found by means of:

A) the α-vector method applied to the 3 irradiation channels (S84, Y4, X26);

B) from the mean (AVG) of the results of all samples irradiated on each channel (Table 10.7) and from the mean of all channels employed (Table 10.8) when inputting the recommended $\bar{E}_r$ value in Lit [20, 23].

The uncertainty evaluation for a single Q_0 determination, i.e. a 1 channel exercise with 1 material measured in 1 detector, is given in section 7.7 while for a $\bar{E}_r$ value it is estimated from the standard error in the α-vector method (see section 6.3).

8.2.1 Differences in the $\bar{E}_r$ factors

From a total of 54 experimental $\bar{E}_r$ factors reported in this work, 32 values were consistent with the recommended literature within <25% relative difference. For 23 target isotopes, the relative difference was just 10-15%, meaning that in general, for half of the studied (n,γ) reactions the α-vector method gave us $\bar{E}_r$ factors in good agreement with the recommended literature at 95% confidence level, giving the quoted uncertainties (see Table 10.8; min 3%; max 33%; mean 13% at 1*s*).

Similarly, when comparing our $\bar{E}_r$ values to those reported for instance by A. Trkov in a personal communication to the International k_0 Scientific Committee members which were calculated with data from the ENDSF [4, 6] and JENDL [7] nuclear databases, we observed differences of <25% for

approximately half of the studied isotopes (25 isotopes) and of <10% for a third of the cases reported in Table 10.8. (19 isotopes).

The recommended $\bar{E}_r$ values in references [20, 23] and those calculated for instance by A. Trkov in his personal communication are semi-empirical ones, calculated from experimental resonance data available in the literature but according to two different approaches.

The recommended $\bar{E}_r$ values were first computed in [106, 107] assuming that a Breit-Wigner distribution accurately describes the resonance phenomena. These were calculated by making use of eq. (2.48) for computing $\bar{E}_r$ values from the weighted average of actual resonances known at that time.

A. Trkov opted for finding Q_α values numerically for several values of α, by employing the more accurate and recent Reich-Moore distribution [199], but assuming later the same $Q_\alpha \rightarrow \bar{E}_r$ conversion formula as proposed in eq. (2.41). This formula is reciprocally employed for $Q_\alpha \rightarrow Q_0$ conversion when inputting an $\bar{E}_r$ parameter, meaning that the recommended literature [20, 23] cannot be upgraded with the modern set of values from A. Trkov, for it would not reproduce the same Q_0 factor. In some cases, the difference between the recommended values in [20, 23] and the values from A. Trkov is significant but in any case the adoption of Q_0 and $\bar{E}_r$ values from the same source is strongly advised.

For cases such as: ^{23}Na, ^{45}Sc, ^{134}Ba (after correction for the (n, n') interference), ^{138}Ba and ^{174}Yb, our experimental $\bar{E}_r$ factors gave us Q_0 factors in better agreement between irradiation channels than when inputting the recommended literature $\bar{E}_r$ values (i.e. a lower observed SD).

Since the effective resonance energy is an idealized concept, the adoption of experimental $\bar{E}_r$ values seems justified, if these were determined over a large spread in α values and/or with at least $N \geq 3$ channels.

8.2.2 Differences in the Q_0 (or s_0) factors

The Figure 8.3 and Figure 8.4 show the ratios between our experimental Q_0 (or s_0) factors quoted in Table 10.8 under methods A (the α-vector) and B (the classical approach) against the recommended values from the literature [20, 23].

The observed relative differences between our Q_0 values and the reccommended literature can be separated into three groups (see Table 8.1).

The group of reactions or target isotopes showing relative differences of < 5% are not explicitely quoted in Table 8.1 because these are not statistically significant at the 95% confidence level from the point of view of a two-tailed Student t-test (see Table 7.18).

Table 8.1: Typical ranges of observed relative differences between the Q_0 factors in this work and the recommended values [23].

1)	< 5% difference	According to a two-tailed Student t-test there is no statistical significance at the 95% confidence level for < 7% difference in 1 channel, except for ≥ 5% difference for ≥ 2 channels results (see Table 7.18)
2)	5 - 11% difference	^{75}As, ^{87}Rb, ^{84}Sr, ^{102}Ru, ^{107}Ag and ^{181}Ta (6 targets)
3)	> 11% difference	low Q_0 factors: ^{26}Mg, ^{27}Al, ^{37}Cl, ^{41}K, ^{50}Ti, ^{50}Cr, ^{64}Ni, ^{152}Gd, ^{174}Yb (9 targets) medium to high Q_0 factors: ^{89}Y, ^{133}Cs (for ^{134}Cs production), all Ba isotopes and ^{196}Pt non-1/v isotopes: ^{151}Eu, ^{153}Eu, ^{164}Dy, ^{174}Hf and ^{168}Yb (5 targets)

1/v or moderate-1/v cases

For the second group in Table 8.1 (5-11% difference) it must be noted that except for ^{87}Rb, all other Q_0 factors in the latest k_0-libraries are "adopted", from literature available before 1980 [13, 20] and therefore bear a high uncertainty, i.e. $s(Q_0)$ = 10% according to these references. This leads to $u(Q_0)$ = 4.1% per a triangular distribution or to $u(Q_0)$ = 5.8% per a rectangular one. We opt for the conservative approach and will assume a $u(Q_0)$ = 5.8% for adopted values from the recommended literature, because these values were computed with I_0 and σ_0 values from different sources, as shown in [13].

The ^{107}Ag and ^{87}Rb were investigated in 1 channel (6% and 11% difference). Our result is not significant for ^{107}Ag but on the contrary, it is significant for ^{87}Rb (at the 95% confidence level; see Table 7.18). The ^{75}As and ^{181}Ta determination was performed in 3 channels and for ^{84}Sr and ^{102}Ru in 2 channels, therefore the observed relative differences ≤ 11% are statistically significant as well.

Our values for ^{75}As, ^{84}Sr, ^{102}Ru, ^{107}Ag and ^{181}Ta are recommendable by virtue of their experimental nature, lower uncertainty and because these are also agreement with the experimental values reported by Kennedy et al. [18, 19] (K1, K2 and K3), as shown in Table 8.2 and Figure 8.5. Our results for these cases are within 5% relative difference to at least one of the results reported by Kennedy et al. from the Cd-ratio and the two-channel methods applied in these references and for almost all quoted nuclides in Table 8.2, including ^{87}Rb. Therefore, our results for the mentioned cases are not significant when compared to Kennedy et al.

It is important to remark that for ^{84}Sr, our Q_0 factors leading to ^{85m}Sr and ^{85}Sr may suggest that an isotope "ID-swap" occurred between the results for the ground state and the isomer during the development of the first compilations, since our values are quite similar to the recommended ones for ^{85}Sr and ^{85m}Sr

instead [20, 23]. We obtained Q_0 = 13.0(4) for ^{85m}Sr and Q_0 = 14.5(3) for ^{85}Sr monitoring under the ADS IV/b (with $\bar{E}_r$ values from the recommended literature [20, 23]). The latter Q_0 value is in good agreement with the Cd-ratio results from Kennedy et al. of Table 8.2 (3% lower in there).

For production of ^{115}Cd, ^{134m}Cs and ^{170}Tm we obtained ≥ 10% difference to the Kennedy et al. results but this time for ^{134m}Cs and ^{170}Tm our results were not significant when compared to the recommended literature (< 4% relative difference). The result for ^{115}Cd production is discussed later.

For the third and last group of target isotopes with Q_0 values with >11% relative difference (see Table 8.1), once more almost all the recommended Q_0 factors are adopted (see Table 10.8 or references [20, 23]) and therefore bear a high uncertainty. The only exceptions are ^{41}K and ^{89}Y, for which the results would be statistically significant when compared to the recommended literature.

For the subset of ^{26}Mg, ^{27}Al, ^{37}Cl, ^{41}K, ^{50}Ti, ^{50}Cr, ^{64}Ni, ^{152}Gd, ^{164}Dy, ^{174}Yb and ^{174}Hf, all target isotopes with a (small) Q_0 < 0.9, the adoption of either our values or the recommended ones will not impact significantly the analytical result in high *f* channels. For bare irradiations and a channel such as Y4, one can estimate < 1.2% impact in the reaction rate and for channel X26 just < 0.5%. However, for an epithermal channel like S84 one has < 2.8% impact in the reaction rate. Clearly, when Cd-covered irradiations are performed (ENAA) the > 11% relative difference propagates fully to the analytical result.

Irradiations under Cd are useful for avoiding spectral interferences from activation of unwanted nuclides such as ^{27}Al, ^{51}V, ^{23}Na. This is sometimes necessary for instance when performing trace analysis on pure Al, Na, V and/or Ti matrices, etc. The motivation of employing a Cd-cover in routine analysis is to substantially reduce the activation of these unwanted nuclides, but one can be still interested in accurately quantifying these elements for

practical reasons, for which the accurate knowledge of the Q_0 factor would be fundamental. Thus, even if a Q_0 factor is rather small, for ENAA our Q_0 values nowadays provide lower uncertainties and better metrological traceability than those compiled 30 years ago from imprecise data.

For (n,γ) production of ^{197m}Pt and ^{197}Pt for instance, our experimental Q_0 factors from the α-vector method were compared to calculated values from nuclear data found in references [1, 2, 6], which are imprecise.

It must be remarked that in the case of ^{130}Ba, the reported Lit value in Table 10.8 is in principle incorrect, as warned by De Corte in 2010 [187], but unfortunately as of 2015 it is still quoted as such in all the recommended references since 1989 [20, 23, 38]. The correct recommended value of Q_0 = 21.3(9) at 68% confidence level was obtained by Smodis et al. in their first 1994 redetermination [49] noted by De Corte [187], and is quoted instead in Table 8.2. Our Q_0 factor is in agreement with the value reported by Smodis et al. [49] and Kennedy et al. [19] (2006).

Our Q_0 result for ^{94}Zr confirms the results obtained by the INW and DTU Risø during the development of the k_0-method [13] within < 1%. It also confirms within < 1% the results from Smodis et al. in reference [200]. Our result is however 5% lower than expected from the Q_0 factor reported in the latest recommended compilations [20, 23] and statistically significant at the 95% confidence level (studied in 3 channels). Our result was obtained by means of ^{95}Zr (index *p*) but also by analysis of its daughter ^{95}Nb (index *d*) after at least 67 days of decay (t_d), for which parent-daughter "transient equilibrium" (index *trans*) has been reached according to [34]:

$$t_{d,trans} = \left(\frac{1.44 T_{1/2,p} T_{1/2,d}}{T_{1/2,p} - T_{1/2,d}} \right) \ln \left(\frac{T_{1/2,p}}{T_{1/2,d}} \right) \qquad (8.5)$$

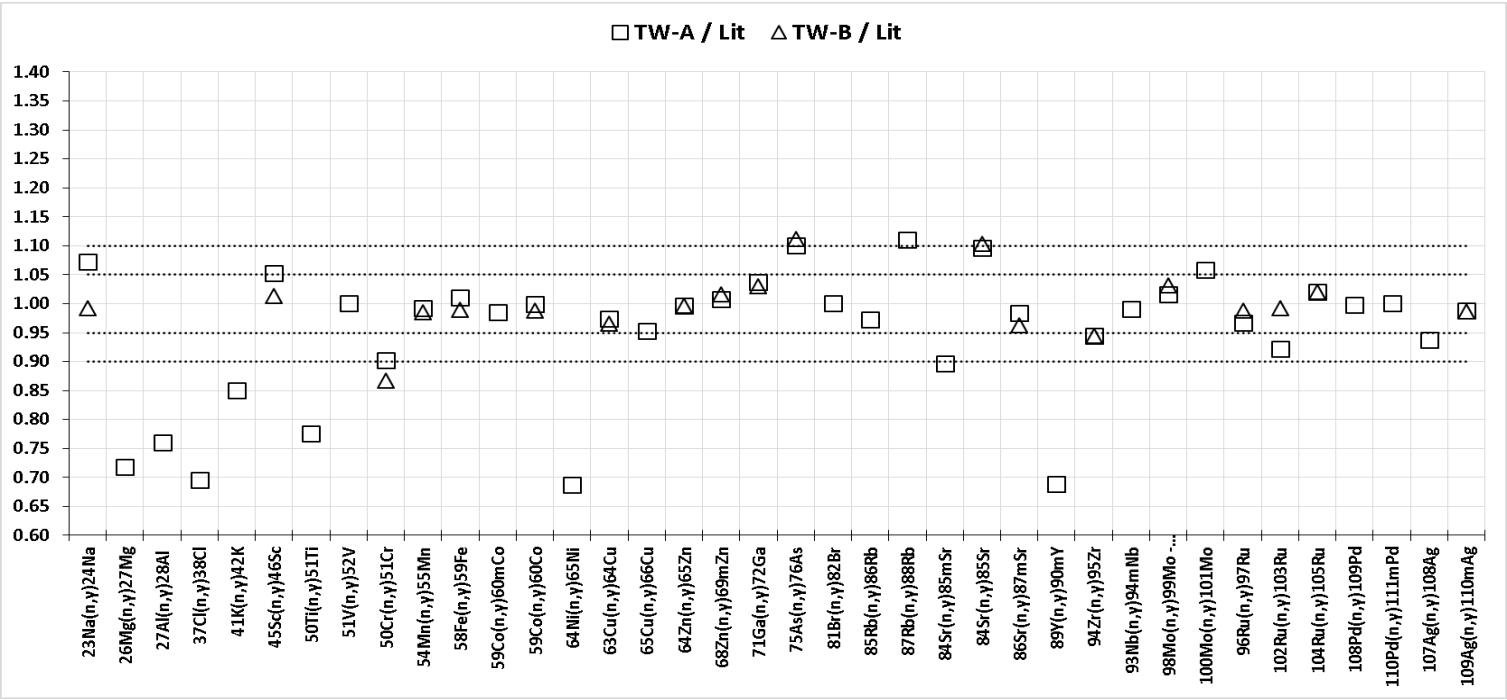

Figure 8.3: Ratios between the Q_0 (or s_0) factors found in TW (methods A and B) and the recommended Lit values. Ratios calculated from the values in Table 10.8 for the target isotopes ^{23}Na to ^{109}Ag.

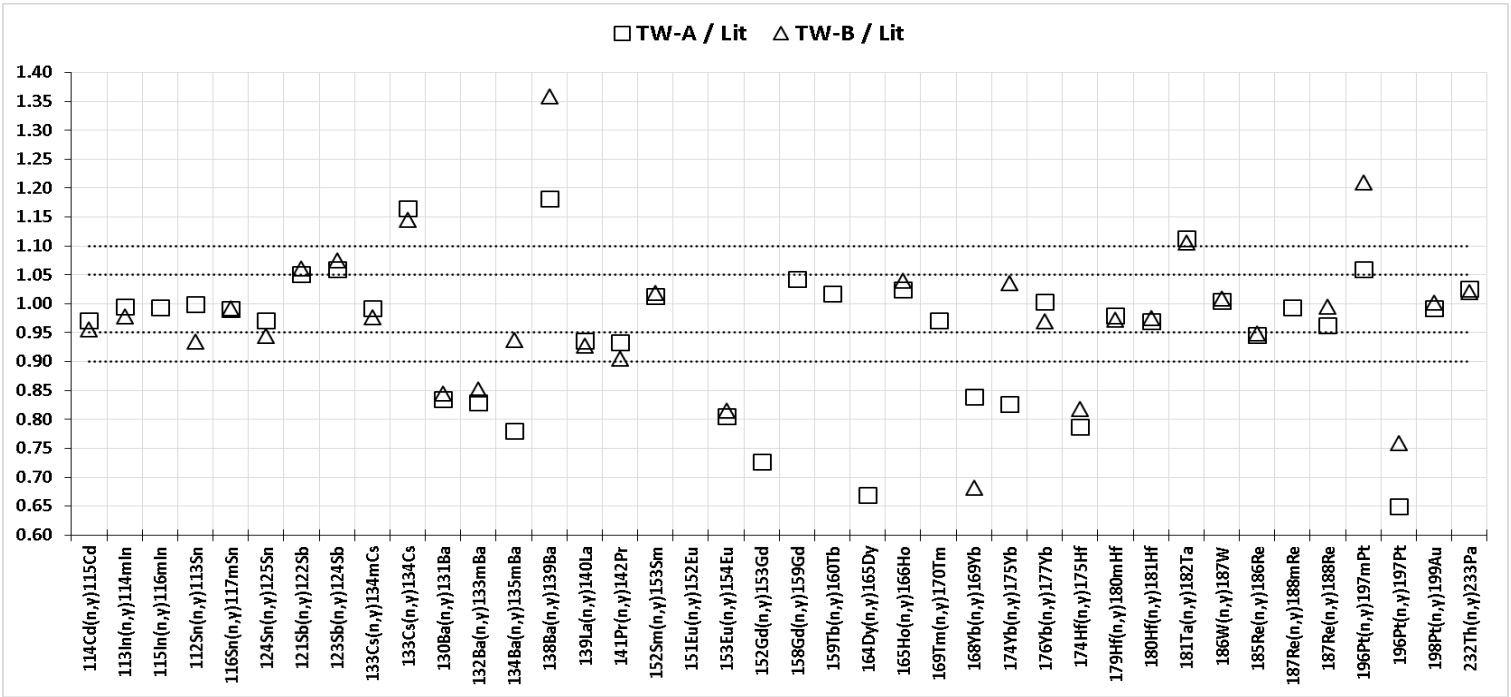

Figure 8.4: Ratios between the Q_0 (or s_0) factors found in TW (methods A and B) and the recommended Lit values. Ratios calculated from the values in Table 10.8 for the target isotopes ^{114}Cd to ^{232}Th.

Table 8.2: Comparison between the Q_0 factors in: TW, Lit and as reported by K1 (2003), K2 (Cd-ratio) and K3 (two-channel method; 2006) when adopting the same $\bar{E}_r$ values from Lit.

			Q_0 (%; 1s)					
TI	**FN**	**ADS**	**Lit**		**TW**		**K1, K2, K3**	
^{75}As	^{76}As	I	13.6	*	15.0	(2)	16.6	(8)
							14.7	(3)
							15.0	(7)
^{87}Rb	^{88}Rb	I	23.3	(3)	25.9	(2)	25.7	(8)
							24.8	(4)
							21.8	(7)
^{84}Sr	^{85}Sr	IV/b	13.2	*	14.5	(2)	12.2	(8)
							14.1	(4)
							10.8	(11)
^{108}Pd	^{109}Pd	IV/b	26.6	(2)	26.6	(4)	30.5	(8)
							25.0	(4)
							27.8	(6)
^{109}Ag	^{110m}Ag	I	16.7	(4)	16.5	(2)	14.9	(8)
							16.4	(3)
							14.9	(6)
^{114}Cd	^{115}Cd	I	32.4	*	31.4	(4)	46.2	(8)
							43.7	(4)
							38.0	(3)
^{115}In	^{116m}In	IV/b	16.8	(2)	16.7	(2)	16.3	(8)
							16.9	(1)
							17.1	(1)
^{133}Cs	^{134m}Cs	I	11.8	(3)	11.7	(2)	13.7	(8)
							12.6	(2)
							13.5	(6)

			Q_0 (%; 1*s*)					
TI	**FN**	**ADS**	**Lit**		**TW**		**K1, K2, K3**	
^{133}Cs	^{134}Cs	IV/b	12.7	*	14.8	(2)	15.6	(8)
							15.5	(3)
							15.3	(6)
^{130}Ba	^{131}Ba	IV/b	24.8	**	20.7	(3)	-	
			<u>21.3</u>	**(4)**			21.4	(3)
							22.5	(5)
^{169}Tm	^{170}Tm	I	13.7	(2)	13.3	(3)	15.4	(8)
							14.8	(2)
							15.5	(6)
^{181}Ta	^{182}Ta	IV/b	33.3	*	37.0	(4)	37.6	(8)
							37.2	(5)
							36.4	(6)
^{185}Re	^{186}Re	I	15.4	(3)	14.6	(2)	15.2	(8)
							15.4	(3)
							15.5	(6)

Uncertainties from Lit and K1, K2 and K3 as quoted in these references.

* Values adopted from imprecise literature available before 1980.

** See text for comments on this value, which is incorrect. The correct value Q_0 = 21.3(9) at the 68% confidence level is given underlined in the next row from reference [49].

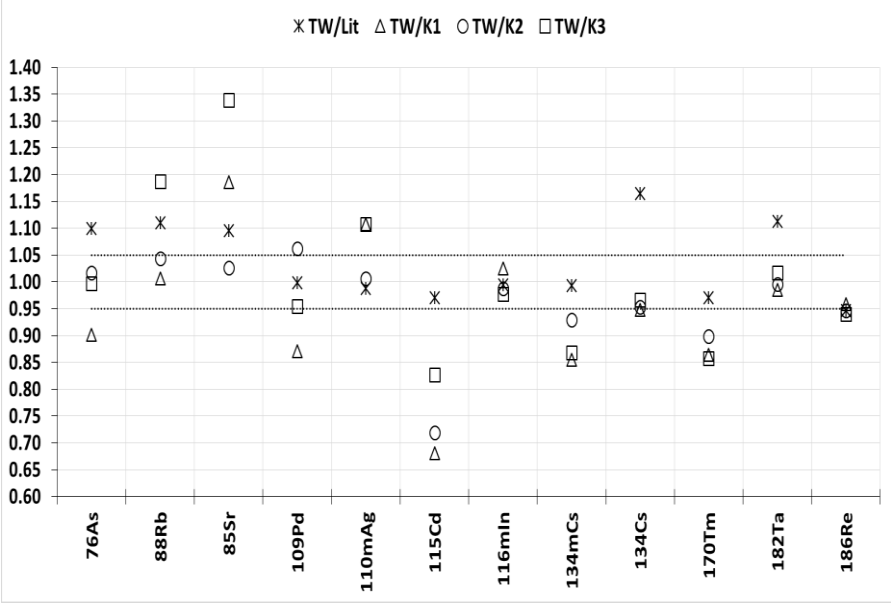

Figure 8.5: Q_0 factors ratios between the values found in TW against the recommended values from Lit and from K1, K2 and K3. For all these cases, the results in TW are < 5% different than at least 1 source (not significant at the 95% confidence level).

Non-1/v cases

For the non-1/v strong absorbers: ^{151}Eu, ^{153}Eu and ^{168}Yb from Table 2.1we adopted the Westcott formalism because of the considerable errors that would be expected from the application of the Høgdahl convention (see Table 2.2). However, the s_0 factor is not a true nuclear constant as its definition in eq. (2.71) shows that it is still a function of the channel temperature. Additionally, the accepted Cd cut-off energy E_{Cd} = 0.55 eV is bound to the condition that the neutron cross-section of the isotope must follow the 1/v-law up to ~1.5 eV [48], which is clearly not the case for these isotopes. Because of this reason we did not expect to obtain accurate s_0 factors from the Cd-ratio determinations.

For example, for ^{151}Eu we obtained "trivial solutions" to our α-vector system of equations, as s_0 = 0.05 ± 0.01 and $\bar{E}_r$ = 0.17 ± 0.03 eV are both values sufficiently close to zero. The same s_0 factor was obtained by adopting the recommended $\bar{E}_r$ = 0.45 eV value. For ^{153}Eu we obtained s_0 = 4.75±0.14 by inputting the recommended $\bar{E}_r$ = 5.8±0.2 eV value and a similar s_0 = 4.81±0.14 with $\bar{E}_r$ = 7.24±1.45 eV from the α-vector method. Although the recommended $\bar{E}_r$ value was confirmed by means of the α-vector method, our s_0 results were 19% lower than expected. For ^{168}Yb we obtained s_0 = 4.17±0.50 when inputting the recommended $\bar{E}_r$ = 0.61 eV value, and s_0 = 3.39±0.27 with $\bar{E}_r$ = 0.026±0.007 eV from the α-vector method, meaning that both experimental s_0 factors are lower than the recommended literature s_0 value by 17% and 32% (respectively). Clearly all these results are statistically significant at the 95% confidence level (see Table 7.18).

A contribution to these discrepancies could be due to the choice of W' = 0 in our computations. In order to match the s_0 factors from the recommended literature one would need to adopt W' = 1.16 for ^{151}Eu, W' = 0.9 for ^{153}Eu and W' = 0.65 for ^{168}Yb, but since it has been mentioned in reference [48] that the W' parameter is expected to be a small correction factor, we concluded that our choice of W' = 0 contributes poorly to these observed

differences. Therefore, for ^{151}Eu, ^{153}Eu and ^{168}Yb we recommend the adoption of the recommended literature s_0 and $\bar{E}_r$ factors, as done in this work for k_0 determination.

As mentioned in sections 2.11 and 6.5, when performing analytical determinations of non-1/v nuclides with 1-2% g_T variation over the typical 20–100 ºC temperature range of interest (see Table 2.3), the analyst should in principle adopt the (β_α,s_0) nomenclature given by the Westcott formalism (R_W). This is because the strict adoption of the Høgdahl convention (R_H) would yield analytical results that can be up to 2% biased (at 20 ºC) for some of these nuclides (see Table 2.4). Fortunately, the "hybrid" relation of eq. eq. (6.32) offers an accurate alternative for modelling the dimensionless reaction rate $R_{W\to H}$ while maintaining the (f_α,Q_0) nomenclature.

For ^{164}Dy and when adopting the modified Westcott formalism, we obtained a negative s_0 factor of s_0 = -0.33(7) with the $\bar{E}_r$ = 224(11) eV value from the recommended literature. This negative s_0 factor is maybe due to the adoption of W' = 0 in the calculation of eq. (2.73) of section 2.10, as there are no W' values currently tabulated in the literature, except for ^{197}Au [48]. To obtain a positive s_0 factor then one would need to adopt $W' \geq 0.28$ per our results.

The Q_0 = 0.13(3) factor is proposed for this isotope instead, obtained from applying the Cd-ratio with the g_T-dependent relation of eq. (6.32). Despite the high uncertainty of this result (21%; 1*s*), it is an experimental value of the same order of magnitude as the Q_0 = 0.19(2) factor proposed in the literature, which is adopted. On the contrary, from the α-vector method results we obtained Q_0 = 0.723) (or s_0 = 0.33 for W' = 0) and $\bar{E}_r$ = 28.9(72) eV, which are both considerably different to the recommended values by 380% and -775% (respectively). These high discrepancies are probably due to the fact that if $Q_0 \leq C_0$ is true for this isotope then the α-vector method is subject to the mathematical singularity in eq. (6.10): logarithm of ≤ 0. We do not recommend our α-vector method Q_0 result due to an observed overestimation of the reaction rate in channel S84. Instead, we recommend

the adoption of our "classic" Q_0 result or the recommended literature value, noting however that we observed a better agreement between channels by adopting $\bar{E}_r$ = 29(7) eV (from the α-vector method).

Based on the (f^*/f) results from van Sluijs et al. [74] and our results in Table 6.1 a mean can be calculated resulting in (f^*/f) = 1.025. For practical reasons, we believe the analyst can adopt this approximation if no β_α determination has been performed. The Table 8.3 shows the expected % differences (Δ) that would be obtained for k_0 (or analytical) determinations when applying the "hybrid" relation of eq. (6.32), that is, when employing $R_{W\to H}$ as compared to values obtained from employing R_W. The Table 8.3 indicates that the expected differences are lower than 0.6% for any of the irradiation channels employed (negligible). This demonstrates the improvement in the accuracy provided by the "hybrid" relation, as compared to the rigid Høgdahl convention (see Table 2.4). The Table 8.3 also offers the Q_0 and $\bar{E}_r$ values found in this work which we found to be in better agreement with the k_0 results from the Cd-subtraction technique.

Table 8.3: Expected % relative differences (Δ) in experimental k_0 factors for some investigated nuclides of Table 2.3 (having "flat g_T factors"; see section 2.11), when adopting the modified Westcott formalism (R_W) as compared to the "hybrid" relation ($R_{W\rightarrow H}$) given by eq. (6.32).

							S84			*Y4*			*X26*		
TI	**FN**	$\bar{E}_r$ **(eV)**		Q_0		g_{20}	$R_{W\rightarrow H}$	R_W	**Δ**	$R_{W\rightarrow H}$	R_W	**Δ**	$R_{W\rightarrow H}$	R_W	**Δ**
^{115}In	^{116m}In	1.56	(7)	16.7	(3)	1.021	1.99	1.99	0.4%	1.43	1.43	0.5%	1.18	1.18	0.6%
^{185}Re	^{186}Re	3.4	(4)	15.4*	(3)	1.007	1.90	1.90	0.4%	1.37	1.36	0.5%	1.14	1.14	0.6%
^{113}In	^{114m}In	6.41	(15)	24.1	(2)	1.006	2.42	2.42	0.4%	1.55	1.55	0.6%	1.20	1.20	0.6%
^{187}Re	^{188m}Re	41.1	(3.9)	4.56	(3)	0.996	1.24	1.24	0.3%	1.08	1.08	0.4%	1.02	1.02	0.6%
	^{188}Re	70.2	(3.0)	4.33	(10)		1.23	1.23	0.3%	1.07	1.07	0.3%	1.02	1.02	0.6%
^{164}Dy	^{165}Dy	29	(25)	0.13	(21)	0.988	0.97	0.97	0.3%	0.98	0.98	0.3%	0.99	0.99	0.6%
^{174}Hf	^{175}Hf	200	(22)	0.64	(2)	0.986	1.00	1.00	0.3%	0.99	0.99	0.3%	0.99	0.99	0.6%
^{197}Au	^{198}Au	5.65	(7)	15.7	(2)	1.007	1.91	1.92		1.36	1.36		1.13	1.13	

Values for irradiations on 3 channels with extreme f^*, β_α and α parameters but same average neutron temperature (of 20 ºC).

* Adopted from the 2012 recommended literature [23].

Δ calculated by eq. (2.83) with the use of $R_{W\rightarrow H}$ parameter instead of the R_H parameter from the modified Høgdahl convention.

The f^*/f values are given in Table 6.1. The f, β_α and α values are given in Table 6.6.

The Q_0 and $\bar{E}_r$ values quoted were determined in this work (see Table 10.15).

Not confirmed cases

Finally, from all observed relative differences and, excluding those nuclides:

- that have adopted Q_0 factors (high uncertainty) from the literature;

- with Q_0 factors so small that under bare irradiations their impact will be negligible (except in ENAA);

- for which the adoption of s_0 factors from the literature is advised instead (^{151}Eu and ^{168}Yb);

- with significant relative differences but confirmed by at least one independent source;

we can conclude that the only nuclides for which we obtained significant differences that could not be verified by another source are: ^{89}Y, ^{134}Ba and ^{114}Cd.

For ^{89}Y, we tested first the same compound (pure yttrium oxide) employed by DC. In virtue of the discrepancy, another matrix (pure yttrium foil) was tested, which confirmed our first results. The observed difference could not be explained in terms of self-shielding effects (negligible), decay scheme (*I*; the simplest) and half-life (not changed). Unfortunately, it was tested on the sole irradiation channel suited for short-lived nuclides for which the induced activity was high enough as to precisely determine it (S84). Therefore, the accuracy of the assumed F_{Cd} could not be validated.

In the case of ^{134}Ba, after correction for the (n,n') interference (see section 2.13.4) by means of eq. (2.118) and the *L* values obtained from the analysis of the (n, n') intereference on ^{117m}Sn, we obtained a Q_0 factor which is 23% lower than the one reported by DC. This nuclide was excluded from the Lit compilations in [20, 23] but no reason was given.

In the case of ^{114}Cd we obtained F_{Cd} = 0.400(24) by application of the α-vector method and, by letting this parameter vary until we observed a

matching $\bar{E}_r$ value to the one reported in the recommended literature. On the other hand, by application of the F_{Cd} = 0.45 reported by DC we obtained a 23% lower Q_0 value than the one in Table 10.8. It must be noted however that DC reported Q_0 = 39.6(5) in his Habilitation thesis [13] instead of the Q_0 = 32.4(32) final adopted value in the latest compilations.

Kennedy et al. proposed Q_0 = 39.6(5) for F_{Cd} = 0.45 based on their results in [19], confirming the previous value from DC. It follows that this Q_0 factor should be adopted in our k_0-computations for consistency with other authors. Strangely, we obtained a confirmation of our derived σ_0 with other independent nuclear databases (i.e. 1% difference; Table 10.21) when applying the (f, α) method with our Q_0 value in Table 10.8. It remains puzzling.

8.2.3 About the two sets of (Q_0, $\bar{E}_r$) values from this work

In this work 2 sets of experimental Q_0 (or s_0) factors are tabulated for 54 cases of analytical interest, which were determined by means of 2 different methods. These factors are correlated to $\bar{E}_r$ values that may differ significantly in magnitude (see Table 10.8 or Table 10.15). Two questions then follow:

- how different are these 2 sets of Q_0 factors, i.e. what is the impact of the chosen $\bar{E}_r$ value?

- what would be the impact of the chosen (Q_0, $\bar{E}_r$) values on the dimensionless (n,γ) reaction rate R_H or R_W? That is, one is interested in the impact on the analytical result (e.g. the elemental content or a k_0 factor).

Although for k_0 determination most of the reactions studied in this work were dealt with by means of the Cd-subtraction technique and therefore the adoption of Q_0 and $\bar{E}_r$ values was not required, a third question is inevitable:

- to which set of values the reported k_0 factors are more correlated, i.e. which set of Q_0 (or s_0) and $\bar{E}_r$ values better reproduces the k_0 factors from this work?

One must note that independently of the accuracy of either set, the Q_0 (or s_0) factors obtained by means of the α-vector method (TW-A; see Table 10.8) were up to ± 4% different than the corresponding values obtained with $\bar{E}_r$ values from the recommended literature (TW-B; same table) for 43 of these cases. The Figure 8.6 show these differences in terms of ratios between the sets of factors. For these cases the choice of our experimental $\bar{E}_r$ values instead of the recommended ones was not statistically significant for a Q_0 determination, since the uncertainty is at least 4% at 2*s*.

The Figure 8.8 show that for 29 reactions the difference on the R_H (or R_W) parameter computed with either set of (Q_0, $\bar{E}_r$) values, for irradiation channels covering the typical (f, α) values of interest, would be usually lower than 0.5% for a poorly thermalized channel such as S84 and lower than 0.3% for moderate and well-thermalized channels such as Y4 and X26 (respectively). This would correspond to a negligible impact on k_0 factors determined by the bare method, as given by eq. (2.37) with R_H or R_W. The Figure 8.9 and Figure 8.10 shows that for another 22 cases, the differences would be lower than 1.5% for a channel as S84 and negligible (lower than 0.6%) for channels such as Y4 and X26. These differences are well within the typical uncertainty in a k_0 factor at the 2*s* confidence level (~5%).

On the other hand, 11 studied cases showed significant relative differences between Q_0 factors of the order of 5-25%, as shown in Figure 8.7. For ^{165}Dy production the difference is approximately 550% and it is not shown in the figure due to its scale.

Nonetheless, it is important to realize as shown by Figure 8.11, that although differences in Q_0 (or s_0) factors of 5 to 25% are considered significant, from that set of 11 reactions we observed that:

- for production of ^{24}Na, ^{103}Ru, ^{139}Ba, ^{152}Eu and ^{175}Yb production, the relative differences in the R_H (or R_W) parameter were ≤1% on average for an epithermal channel (S84), and lower for the thermalized channels (under bare conditions);

- for production of ^{113m}Sn/^{113}In, ^{164}Dy, ^{169}Yb, ^{197}Pt/^{197m}Pt and ^{135m}Ba the relative differences were on average ≤5% for an epithermal channel and ≤2% for the thermalized channels (under bare conditions).

Since these differences are within our expected k_0 uncertainty for a single determination at 2*s* confidence level (≤ 5%) the adoption of either set of (Q_0, $\bar{E}_r$) values will not be statistically significant for a single k_0 determination. Yet, it seems logic to provide some recommendations on which set of Q_0 and $\bar{E}_r$ values should be adopted by the analyst.

For production of ^{113m}Sn/^{113}In we recommend the adoption of the values $\bar{E}_r$ = 107(3) eV and Q_0 = 48.4(5) from the recommended literature [23] (1*s*) since our experimental Q_0 factor confirmed this result (0.2% lower).

The Q_0 factors for ^{197m}Pt/^{197}Pt and ^{135m}Ba production were determined with $\bar{E}_r$ values from Jovanović et al. [107] since there is no recommended k_0 nuclear data tabulated for these reactions. The adopted $\bar{E}_r$ values of 291(44) eV for ^{196}Pt and 155(6) eV for ^{134}Ba are small in comparison to our experimental $\bar{E}_r$ values of 5319(277) eV and 5503(1100) eV (respectively; at 1*s*) and hence the reason for the 15-20% difference in the resulting Q_0 factors. For these cases, we strongly recommend the adoption of our experimental values from the α-vector method (see Table 10.8), as the k_0 factors computed through the bare method were later consistent with the k_0 factors found through the Cd-subtraction technique.

For the non-1/v nuclides studied in this work, the recommendations were given in the previous section.

.

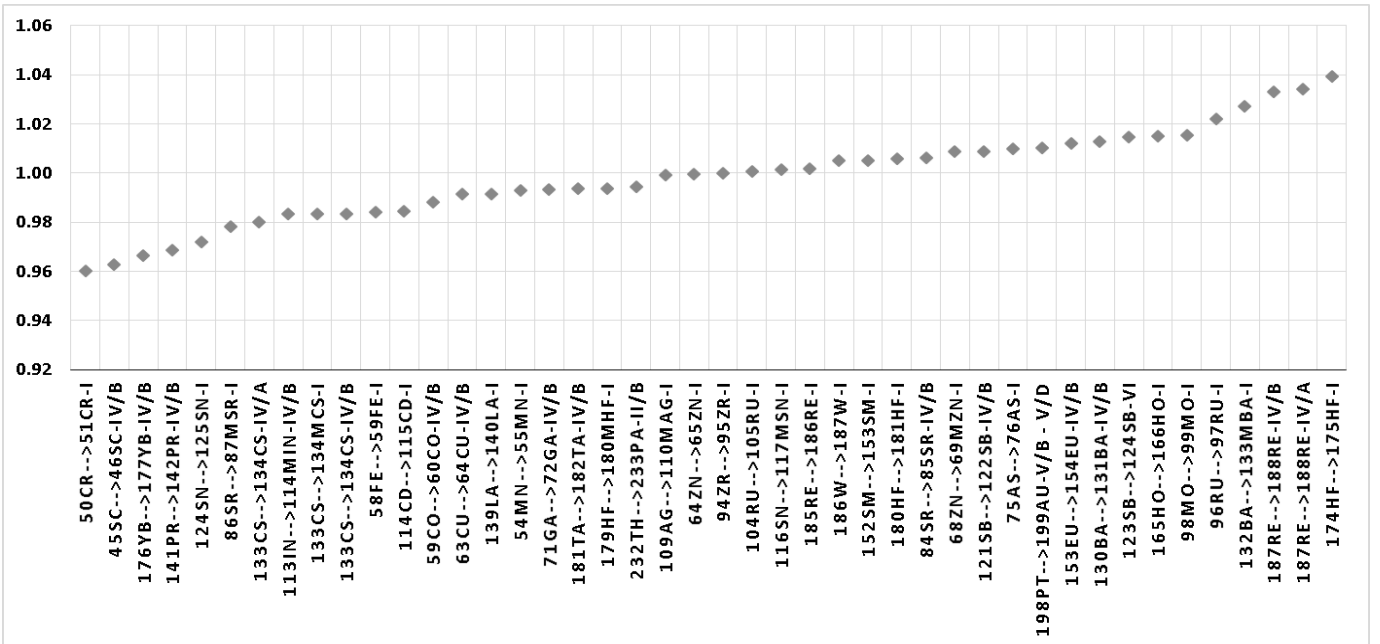

Figure 8.6: Ratios between the Q_0 or s_0 factors obtained in TW by means of the $\bar{E}_r$ values from the α-vector method (TW-A) and the values in TW with $\bar{E}_r$ values from Lit (TW-B; see Table 10.8). Up to ±4% relative difference is observed between the Q_0 or s_0 factors for 44 cases.

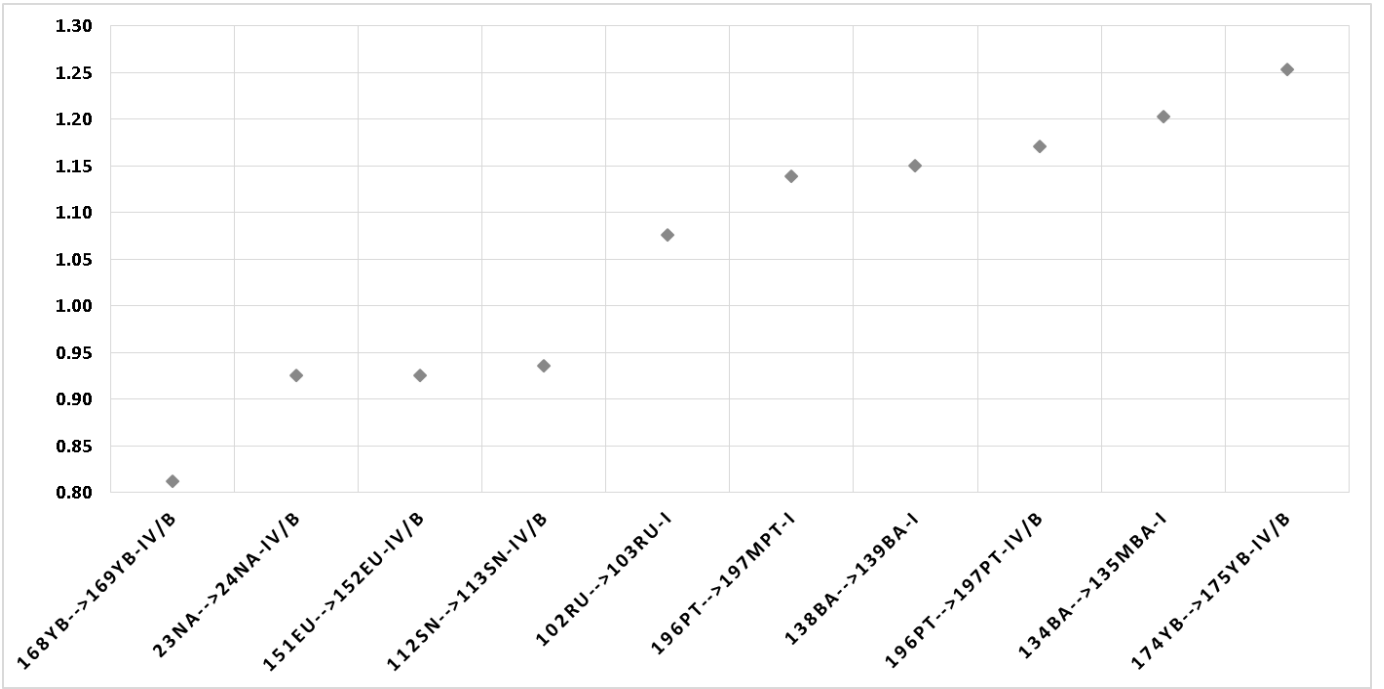

Figure 8.7: Extension of Figure 8.6 for the 10 isotopes (or reactions) that showed more than 5% and up to 25% relative difference between Q_0 (or s_0) factors.

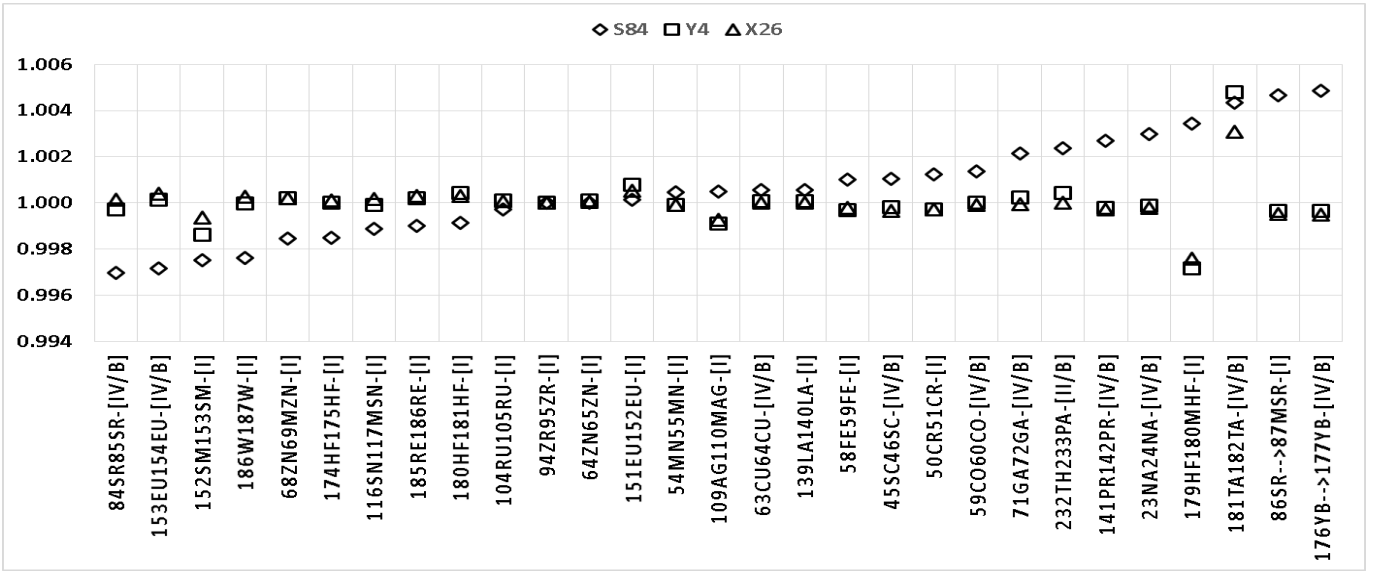

Figure 8.8: Ratios between the R_i parameters ($i = H$ or W) calculated with Q_0 (or s_0) and $\bar{E}_r$ values found in TW with the α-vector method (TW-A), against the R_i for Q_0 (or s_0) values in TW from adoption of the $\bar{E}_r$ values from Lit (TW-B; see Table 10.8).
Values calculated for 3 irradiations channels covering the typical f, β_α and α range of interest (see Table 6.6).
Up to ± 0.5% relative differences are observed for the 29 listed cases.

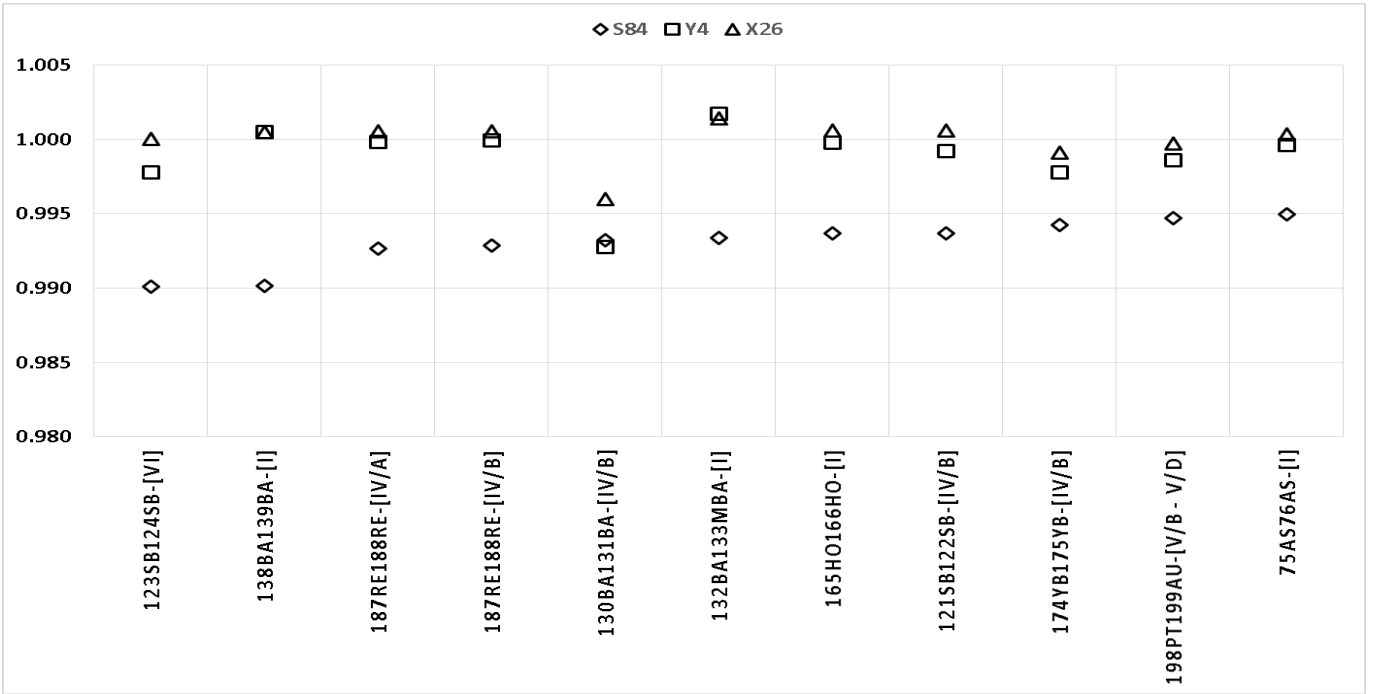

Figure 8.9: Extension of Figure 8.8. This graph shows relative differences of 0.5 to 1% for 11 isotopes in an epithermal channel (S84) and lower than 0.3% on average in thermalized channels (Y4 and X26).

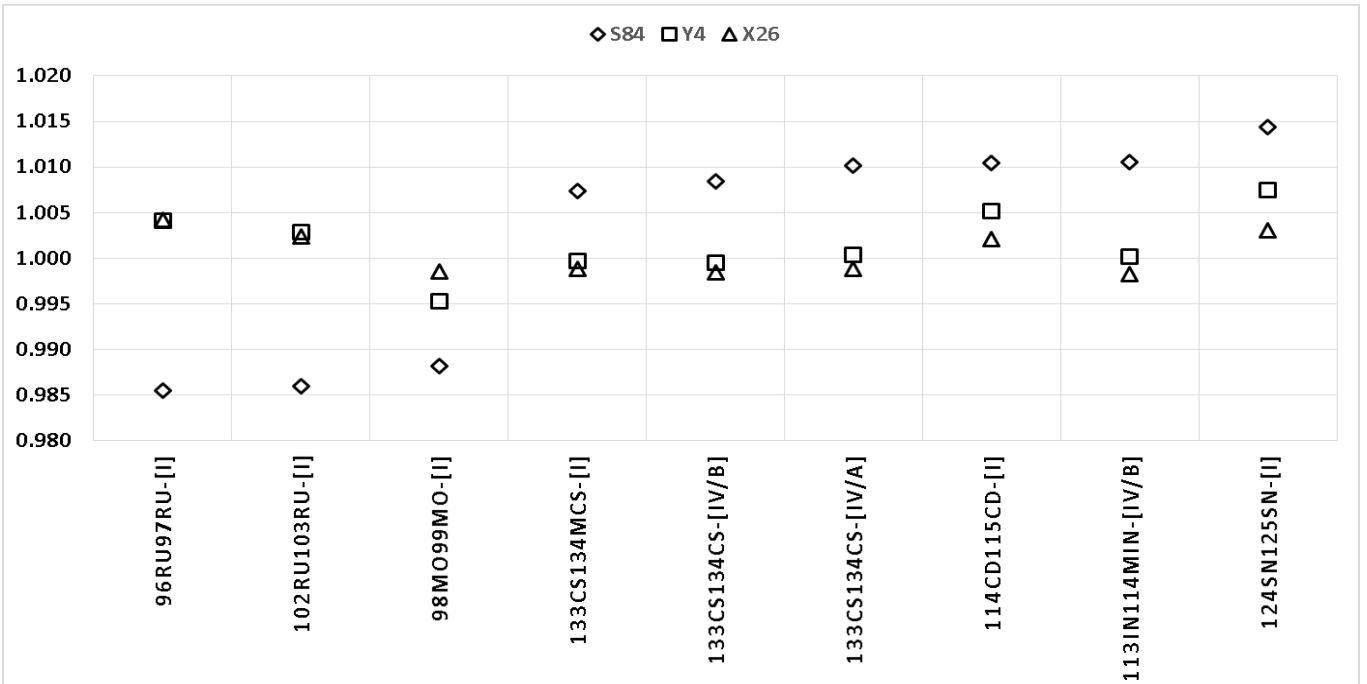

Figure 8.10: Extension of Figure 8.8. This graph shows relative differences in the 0.5-1.5% range for 9 isotopes in an epithermal channel (S84) and lower than 0.6% in thermalized channels (Y4 and X26).

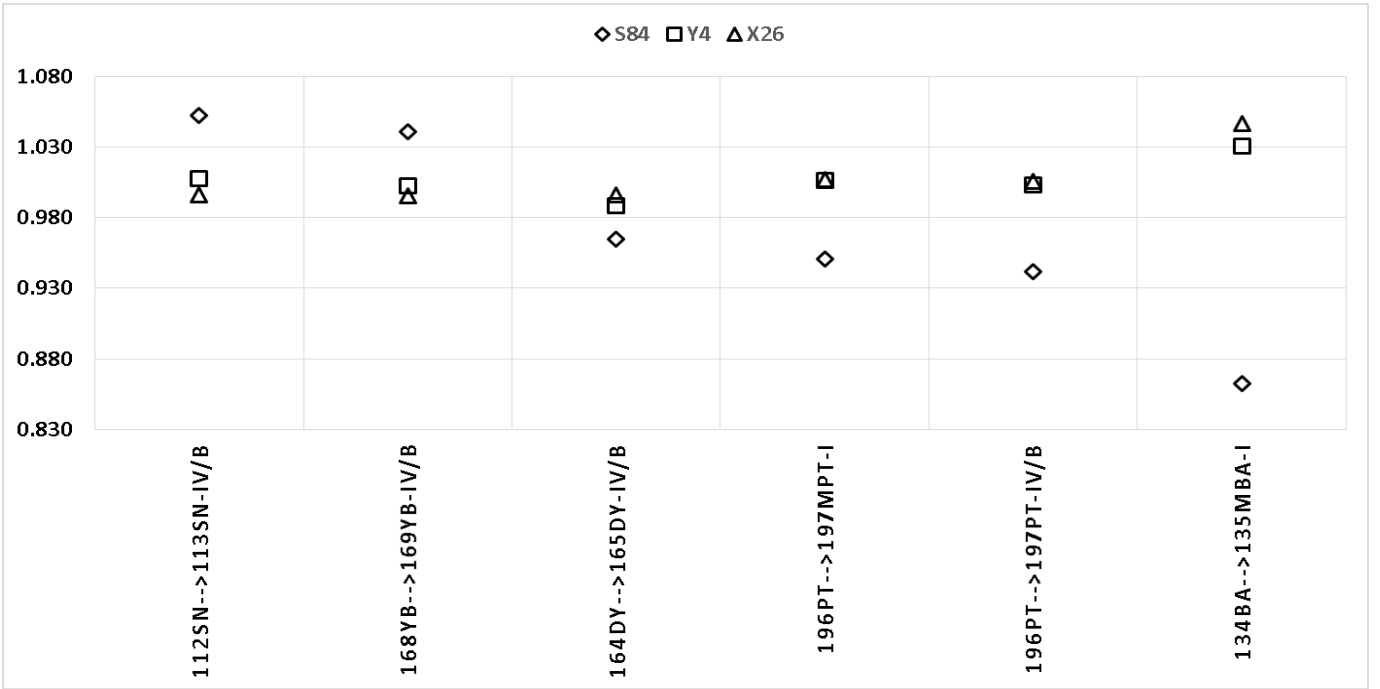

Figure 8.11: Extension of Figure 8.8. This graph shows relative differences of up to ± 5% for 5 reactions in an epithermal channel (S84) and up to ± 2% in thermalized channels (Y4 and X26). For ^{135m}Ba the differences are higher.

8.3 On the k_0 factors and thermal neutron cross-sections

The section 10.4.1 provides the k_0 nuclear data results obtained in TW per irradiation channel while the section 10.6.1 provides the final compendium for 76 (n,γ) target isotopes leading to 96 measured radionuclides states. The thermal neutron cross-sections are given in section 10.7. The results for ^{238}U and ^{235}U are given separately in section 10.6.2 and are discussed at the end of this chapter (section 8.5).

The different number of standards or materials employed and their typical self-shielding correction factors are listed in Table 6.3. These values were determined with the aid of up to 4 irradiation channels described in Figure 6.7 and with channel characteristics given in Table 6.4 and Table 6.6.

According to our k_0 results reported in Table 10.15, for at least 54 radionuclides the values for the main γ-rays were in agreement with the recommended literature in [20, 23] within 3%. This was normal to expect considering the uncertainty associated to these recommended lines (≤ 2%; 1*s*). When considering ≤ 5% difference between k_0 results then two thirds of the studied radionuclides are within this range (66).

In general, a third of our k_0 factors are only 1% different than those reported in the recommended k_0-literature, confirming thus the accuracy of our efficiency transfer computations (30 radionuclides). When considering secondary γ-lines, the differences between our values and the recommended ones were typically in the 3-4% range, sometimes higher for the lowest-yield lines.

As stated before in section 7.12, for k_0-results determined in at least 2 channels a two-tailed Student t-test will report statistical significance at the 95% confidence level only when ≥ 4% relative difference is observed

compared to other authors values. This is shown in Table 7.17. For determinations in 1 channel, the condition for statistical significance is observed at ≥ 6% relative difference.

Our k_0 factor for the ^{42}K 1524 keV line was just 1% different to the Lit value, but the result for the 312.7 keV line was 10% higher than expected [20, 23] (significant). Since our k_0-ratio and k_0 factors are consistent with values derived from [1, 2, 6], we would like to recommend our results.

For ^{51}Cr, its sole k_0 factor seems 5% lower. This was systematically observed for 2 different standards on 2 irradiation channels even after repetitions. The derived neutron cross-section value is 7% lower when compared to [1, 2]. Still, it must be remarked that even today some of the data in these compilations:

1) has not quoted uncertainty or proper identification (i.e. if the data corresponds to the isomer, ground or compound state);
2) is not traceable or is sometimes correlated to the first k_0 compilations and/or to deprecated/imprecise nuclear data;
3) was determined without considering neutron self-shielding effects or other sample-matrix undesirable effects;
4) is partially (or completely) unknown or, has been deduced from crude theoretical models.

The Figure 8.12 show the experimental and/or evaluated cross-sections for ^{50}Cr(n,γ)^{51}Cr compiled in the EXFOR database [121]. The nuclear data in for ^{51}Cr in the JEFF, CENDL and EAF [2] libraries is also imprecise, but so far the k_0-community has not reported major discrepancies in the analysis of chromium with the current radioisotope nuclear data. In reference [60] this radioisotope was employed as the comparator, obtaining k_0 factors for ^{110m}Ag that are only 1% different than our results. In summary, it was not possible to clarify the source of our systematic difference for ^{51}Cr. Yet, the more

recent result in 1997 from Venturini et al. [201] is in agreement with our result within 1.5%. Our result disagrees by up to 7% with results from other authors before 1980.

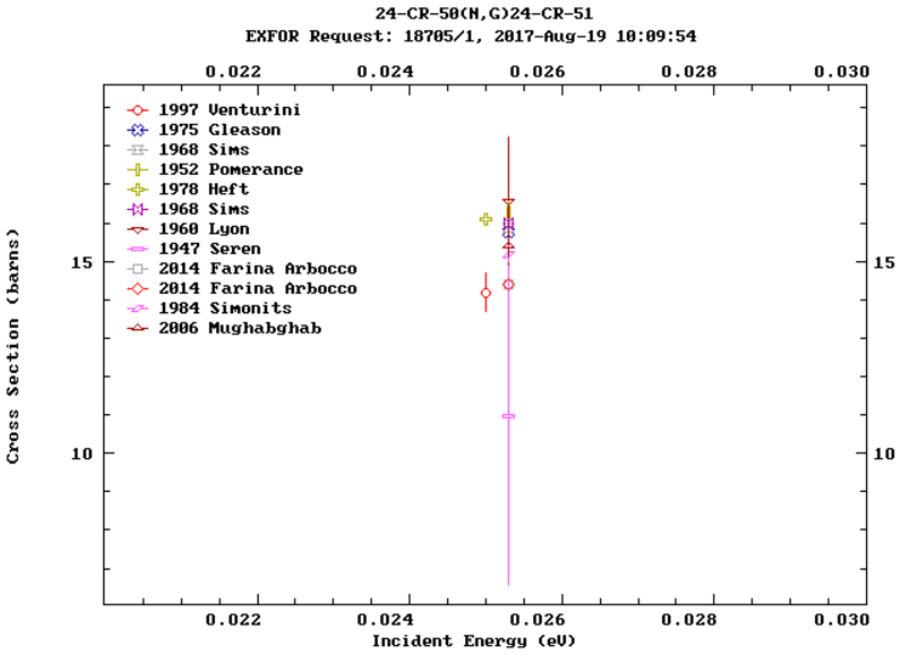

Figure 8.12: Experimental and/or evaluated thermal neutron cross-section for ^{50}Cr(n,γ)^{51}Cr from several authors as compiled in the EXFOR database [121]**. Our mean value is within 1.5% in agreement with the more recent result (1997) from Venturini et al.** [201] **and in disagreement up to 7% with the value from older results (<1980).**

The 511 keV k_0 factors for ^{64}Cu and ^{65}Zn are 10% different and have always represented a spectrometric challenge. We aimed at $u(N_p) \leq 0.7\%$ uncertainty since in practice the longer this emission is measured for better counting statistics the broader the resulting photo-peak becomes, for which the

FWHM detector calibration curve used by the typical γ-ray spectrometry software usually does not accurately work. We tripled the number of measurements to compensate for our higher photo-peak uncertainty.

Although our results are from one independent laboratory, we had a clear advantage on several technological improvements and knowledge of nuclear data over researchers from 30 years ago. For instance, a typical ^{75}As spectrum is almost entirely made up of duplets, a limiting factor depending on the resolution of the detectors employed. We recommend the use of the 657.1 keV line over the other lines.

For ^{85m}Sr, our k_0 factors for the 151.2 and 231.9 keV lines are 3 and 7% higher than the recommended literature [20, 23]. A 3% variation is justified because of our 11% lower Q_0 factor. On the other hand, our k_0 factor for the 514 keV of ^{85}Sr was coherent with Lit (within 1%) [20, 23] and it was just 1% lower than the one reported by Kennedy et al. [19]. This means that the assumed $F_{Cd} = 1$ cannot be the source of the discrepancy. If our accuracy for the ground state is to be trusted and we employ it as an internal comparator, we would obtain again the same results for its isomer (independently of the thermal self-shielding effects). Secondly, our resulting k_0-ratio for ^{85m}Sr is in good agreement with the expected $I_\gamma/I_{\gamma,ref}$ value, therefore the excess difference may be only attributable to efficiency calibration inaccuracies at this energy region, imprecisions in the resulting peak deconvolutions, gamma-ray coincidence effects, pulse losses or to simple systematic errors during the first determinations.

Our k_0-results for ^{88}Rb are > 5% different than expected and also in disagreement with the values reported by Kennedy et al. [19]. Unfortunately, we could only perform this kind of short-lived experiments on channel S84 and with 1 material, as our sensitivity would be null on channels X26 and the Cavity for this material, because of dilution and the low neutron cross-section for the target (^{87}Rb). More independent experiments are necessary for a clarification of these discrepancies.

For ^{95}Zr, the values are in agreement with Lit values within 2% and within 1 to 5% to the first determinations during 1976-89 reported in [13, 42, 194]. The 765.8 keV factor for ^{95}Nb is 1% different when adopting the Lit F_i values into the ADS. Nonetheless, it recalls our attention that coherence with its mother nuclide (^{95}Zr) is not observed in terms of derived cross-sections. Instead, when the more recent and accurate F_i values from reference [8] are employed (i.e. a F_{24}/F_2F_3 value 5% lower than Lit), the agreement is finally reached between mother and daughter σ_0 values, but the relative difference with the k_0 values from Lit is now 3%. We computed this k_0 factor for both cases (see Table 10.9) but we recommend the use of the updated F_i values and the corresponding k_0 result.

Our k_0 factors for ^{97m}Nb and ^{110m}Ag are only 1% different than those reported by Lin et al. [58, 60] (see Table 8.5).

Our results for ^{99}Mo are 3% different than expected except for the 181.0 keV line. These results are in contrast with the 140.5 keV sole line of the daughter ^{99m}Tc for which we observed <1% difference. Only the result for the 777 keV line is statistically significant (4%; 3 channels).

Our k_0 factor for the ^{101}Tc 184.1 keV line is 25% higher than the recommended value but consistent with the other γ-rays and, with the calculated k_0 value from nuclear data in [1, 2, 6]. The Lit value for this line has a $s(k_0)$ = 5% uncertainty, thus our result is more precise. Our k_0 factors for the main γ-lines of ^{101}Mo are 6-8% higher than Lit and statistically significant (1 channel), but the derived σ values are just 1% higher than expected from references [1, 2, 6] and in line with our ^{101}Tc results.

The k_0 factors for the ^{97}Ru 215.7 keV and ^{103}Ru 497.1 keV lines were 8% higher than expected. The derived σ values for ^{96}Ru and ^{102}Ru are in good agreement with the values reported in [1, 2, 6] (<1% difference) and the k_0-ratios are consistent as well.

For ^{104}Ru, our σ value was just 2% higher than in [1, 2, 6] while the differences with the Lit values ranged between 1-5% on average. The main discrepancy is a 12% difference in the 129.6 keV line of the daughter ^{105m}Rh. Comparison of this line result to the ones from ^{105}Ru or ^{105}Rh allowed us to estimate the ^{105}Ru decay branching factors F_2 = 0.264 and F_{24} = 0.736 (7% uncertainty), as compared to the F_2 = 0.25 and F_{24} = 0.76 adopted in [20–23].

For the 434 keV line of ^{108}Ag we obtained a 6% higher k_0 but the other lines agree with Lit within 1%. The corresponding k_0 ratio is 2% different than expected but in better agreement than the ratio between literature values (see Table 10.9).

For the Pd radioisotopes the differences were in the 1-5% range, except for the ^{109m}Ag line at 88 keV (10% lower). We employed a pure Pd wire and the attenuation of the 88 keV line was perhaps underestimated in our efficiency transfer model, as this line does not confirm the σ value derived from the mother nuclide ^{109}Pd lines. The ^{109}Pd lines are on the other hand in agreement with references [1, 2, 6]. Still, its imprecise nuclear data should not be used as reference.

The ^{109m}Ag result reported by Kennedy et al. [18] suggest a k_0 factor 15.7% lower than the Lit value as well. Our k_0 result, which corresponds to the ADS type V/c is instead closer to the recommended value for the ADS type V/a. Strangely, in the 2003 recommended data tables the 88 keV line is quoted first for the ADS type V/c and later for the type V/a [20], being the only one exceptional case observed among all nuclides in the provided sequential order. However, if an accidental swap of factors has indeed occurred, it would contradict the fact that a k_0 factor for the ADS V/c should be higher in magnitude than one for the ADS type V/a. It remains puzzling, since Blaauw et al. also found an inconsistency in the ratio between the k_0 factors for both ADS types scenarios ($k_{0,Vc}/k_{0,Va}$) when employing the Lit values [3].

We opted for adding more uncertainty due to γ attenuation effects to our result.

The k_0 factors for ^{111}Ag are introduced in this work, since these are not reported in the recommended literature [20, 23]. Production of ^{111}Ag follows the ADS type VII/c which cannot be found in [20–23], but has been described in the section 2.12. The resulting σ seems to be 27% higher than expected from data in [1, 2, 6], although it is not clear if the quoted values in these compilations correspond to the ground state or, to a combination of the metastable and ground states.

The k_0 factors for ^{115}Cd and its daughter ^{115m}In were 4% higher than expected [20], but are only 1% different than those found by Lin et al. [60] by means of a highly-thermalized channel. The difference with the recommended value [20, 23] is mostly due to our 12% lower F_{Cd} = 0.400(24) adoption and 3% lower Q_0 factor. The k_0 result for the 336 keV line of ^{115m}In reported by Kennedy et al. [18] is 22% lower than our result, mostly due to their adopted Q_0 factor, which is 48% higher than the one found in this work (see the previous section).

The data for ^{125}Sb (from activation of ^{124}Sn) is not available in the recommended literature [20, 23]. It is given in this work assuming an ADS of the VII/b kind. Our results for ^{125}Sb required the adoption of the Q_0 factor for ^{125m}Sn production from Lit because of the ADS calculations. The σ value for ^{124}Sn (derived from ^{125}Sb) was confirmed by the ^{125}Sn results as well, which are in good agreement with data from references [1, 2, 6, 20, 23].

Our k_0 results for ^{122}Sb and ^{124}Sb are 9 and 5% lower than the Lit values. These results were systematically observed over the 3 different channels. The σ values for ^{121}Sb and ^{123}Sb are consistent (≤1% difference) with references [1, 2, 6] but in discrepancy with the derivable σ values from Lit. Our k_0-ratios for both isotopes are consistent as well.

The sole k_0 factor at 127.5 keV for ^{134m}Cs was found to be 7% higher than expected. The difference could not be attributed to the Q_0 factor alone or other nuclear data inputted in the calculations. We believe it might be due to differences in the efficiency transfer and gamma attenuation corrections. At such gamma energy, the efficiency transfer is very sensitive to the linear attenuation coefficients employed. Also, the assumption that the photon crosses perpendicularly every absorber until it reaches the detector, does not necessarily hold for low gamma energies and close counting geometries [13]. Our k_0 factor is 2.3% higher than the one reported in by Kennedy et al. [19], but their employed Q_0 factor was ~5% higher than our observed value (or the Lit one). If their results are renormalized per the recommended Q_0 factor, this difference becomes negligible. On the other hand our result is just 2.7% higher than reported by Stopic et al. [66] (not significant), from irradiations under highly thermalized channels for which they obtained a better uncertainty of < 1%.

The k_0 factors for ^{134}Cs under the ADS type *IV/a* and *IV/b* were ~5% (significant) and ~3% (not significant) lower than the Lit ones, respectively. These differences can be attributed to the adopted (and lower) Q_0 factors employed at the time of their determination and, to a lesser extent, to the adopted η value for the *IV/a* case (see eq. (2.124)). By applying eq. (6.7) between k_0 factors under the ADS *IV/a* and *IV/b,* the extrapolated η values are summarized in Table 8.4 for the literature and our experimental data. Table 8.4 shows dispersion in the Lit results between gamma lines when combining the k_0 factors and to the computed average η value.

The mean η from our experimental data converged to the last η = 0.105 inputted in the iterative process, while the consistency is dully observed between pair of γ lines. We propose η = 0.105 for calculations related to the ADS type *IV/a,* since it is exactly the mean value resulting from the ratio between derived neutron cross-sections in Table 10.21.

The k_0 standardization of ^{131}Ba has been a historical problem, worsened because of accidental typos or inaccurate Q_0 adoptions, as has been explained by De Corte [187]. Our k_0 factors for this reaction are also in better agreement with Kennedy et al. [19] and Lin et al. [60] for all γ-rays except for the 123.8 keV line (5%). Our 123.8 keV line is instead in agreement with Smodis et al. [49] within 1% (see Table 8.6).

For ^{152}Sm, the 97.4 keV line is not reliable, as it is severely affected by the Compton from the more prominent 103.2 keV line, which in turn is more recommendable. Our result for the 103.2 keV is 2.6% lower than expected, which is not statistically significant, but is instead 6.6% higher than reported by Lin et al. [60].

As previously mentioned, the k_0 determination for ^{152}Eu required the adoption of s_0 = 1.25 and $\bar{E}_r$ = 0.448 eV for ^{151}Eu from Lit, as we doubted our (almost trivial) s_0 results. The resulting k_0 factors are in good agreement with the Lit values when employing the g_T factors from Holden [48] at the channel temperatures provided (except for the low energy gamma lines; see Table 6.5). This could be due to unaccounted or underestimated γ-interferences from ^{154}Eu. The derived σ is up to 12% different than in references [1, 2, 6] but one needs to take into account that the Atlas value has not been updated since 1984. On the other hand the recent (2014) results from [202] are encouraging, since their reported σ is 18% higher than in these references but just 6% higher than our result, hence we recommended the use of our k_0 values for channel temperature monitoring.

For ^{165}Dy, ^{180m}Hf and ^{181}Hf the k_0 discrepancies were on average 5% and cannot be attributed on Q_0 adoptions. The derived σ values are within the range found in [1, 2, 6], and our k_0-ratios are within 1% of the expected ones, hence we are encouraged by our results.

The k_0-data for ^{188}Re under the ADS type *IV/b* is proposed here for the first time. The η = 0.0283 value obtained from the ratios between the k_0 factors

for the ADS types *IV/a* and *IV/b* confirms the recommended value $\eta = 0.028$ within 1% [20]. However, the uncertainty in the η values is twice the $u(k_0)$ uncertainty (by definition).

The k_0 data for ^{197m}Pt and ^{197}Pt was introduced for the first time in this work. The σ is within the range reported in [1, 2, 6], but it is not clear if this data corresponds to the ground or to the metastable plus ground case. The k_0 factors for ^{199}Pt are also introduced in TW. Our σ leading to this radioisotope (and its daughter ^{199}Au) is 9% lower than expected [1, 2, 6] but the result is still in line considering the high uncertainty on the isotopic abundance of ^{198}Pt [9, 10]. Our results for the daughter (^{199}Au) are in agreement with the Lit values within 1% [20, 23].

Table 8.4: Observed η values for ^{134}Cs (see eq. (2.124)) derived from the ratios between k_0 factors for the ADS IV/a and IV/b obtained in this work (TW) [81] **or, as reported in the recommended literature (Lit) [20].**

Energy (keV)	TW	Lit
563.2	0.107	0.075
569.3	0.108	0.100
604.7	0.105	0.072
795.9	0.101	0.059
802	0.089	0.059
1365.2	0.101	-
Average	**0.102**	**0.073**

The uncertainty in η is twice the uncertainty in the k_0 factors ($u(\eta) = 2.3\%$).

Table 8.5: The k_0 factors for ^{110m}Ag as reported by several sources [19, 20, 23, 60] **and this work under identical Q_0 = 16.7 adoption. Recommended k_0 factors from the AVG and SD from all quoted sources (N = 4). All uncertainties given in %, at the 1*s* confidence level.**

Energy (keV)	k_0-library (2003/2012) [20, 23]		Kennedy et al. (2006) [19]		Lin et al. (2012) [60]		TW (2012) [62]		AVG	
446.8	1.36E-03	(1.7)					1.37E-03	(1.6)	**1.37E-03**	**(0.6)**
620.4	1.02E-03	(0.7)					1.01E-03	(1.6)	**1.02E-03**	**(0.4)**
657.8	3.50E-02	(0.7)	3.65E-02	(1.7)	3.56E-02	(1.9)	3.53E-02	(1.6)	**3.56E-02**	**(1.8)**
677.6	3.93E-03	(1.2)			4.00E-03	(1.9)	3.93E-03	(1.6)	**3.95E-03**	**(1.0)**
687.0	2.43E-03	(1.1)					2.43E-03	(1.6)	**2.43E-03**	**(0.0)**
706.7	6.03E-03	(0.8)					6.20E-03	(1.6)	**6.11E-03**	**(1.9)**
744.3	1.69E-03	(1.2)					1.77E-03	(1.6)	**1.73E-03**	**(3.3)**
763.9	8.27E-03	(0.7)	8.72E-03	(1.7)	8.40E-03	(1.9)	8.35E-03	(1.6)	**8.44E-03**	**(2.3)**
818.0	2.69E-03	(0.8)					2.73E-03	(1.6)	**2.71E-03**	**(0.9)**
884.7	2.69E-02	(0.8)	2.83E-02	(1.9)	2.74E-02	(1.9)	2.75E-02	(1.6)	**2.75E-02**	**(2.1)**
937.5	1.27E-02	(0.8)			1.29E-02	(1.9)	1.29E-02	(1.6)	**1.28E-02**	**(0.9)**
1384.3	9.12E-03	(0.8)	9.52E-03	(2.6)	9.21E-03	(1.9)	9.22E-03	(1.6)	**9.27E-03**	**(1.9)**
1475.8	1.50E-03	(0.7)					1.51E-03	(1.6)	**1.51E-03**	**(0.5)**
1505.0	4.84E-03	(0.8)			4.92E-03	(1.9)	4.93E-03	(1.6)	**4.90E-03**	**(1.0)**
1562.3	4.35E-04	(1.0)					4.54E-04	(1.6)	**4.44E-04**	**(3.0)**

For most AVG lines the SD of the mean is $\leq (2\%/\sqrt{4}) \rightarrow u(k_0) \leq 1\%$ and k = 3.182 for a 95% confidence level.

Table 8.6: The k_0 factors for ^{131}Ba as reported by several sources [19, 20, 23, 49, 60] **and this work under identical Q_0 = 21.3 adoption. Recommended k_0 factors from the AVG and SD from all quoted sources. All uncertainties given in %, at the 1*s* confidence level.**

Energy (keV)	k_0-library (2003/2012) [20, 23]		Smodis et al. (1994) [49]		Kennedy et al. (2006) [19]		Lin et al. (2012) [60]		TW (2012) [62]		AVG	
123.8	3.90E-05	(0.7)	3.90E-05	(0.7)	3.75E-05	(2.6)	3.66E-05	(2.3)	3.94E-05	(1.5)	**3.83E-05**	**(3.1)**
133.6	3.24E-06	(5.0)							2.97E-06	(1.5)	**3.10E-06**	**(6.2)**
216.1	2.75E-05	(1.4)	2.75E-05	(1.4)	2.59E-05	(1.9)	2.52E-05	(2.3)	2.59E-05	(1.5)	**2.64E-05**	**(3.9)**
239.6									3.23E-06	(1.5)	**3.23E-06**	**(1.9)**
249.4									3.69E-06	(1.5)	**3.69E-06**	**(2.3)**
373.2	1.92E-05	(0.4)	1.92E-05	(0.4)	1.81E-05	(1.8)	1.80E-05	(2.3)	1.82E-05	(1.5)	**1.85E-05**	**(3.3)**
404.0									1.73E-06	(1.5)	**1.73E-06**	**(2.1)**
486.5	3.44E-06	(5.0)							2.78E-06	(1.5)	**3.11E-06**	**(15)**
496.3	6.48E-05	(0.2)	6.48E-05	(0.2)	6.19E-05	(1.4)	6.07E-05	(2.3)	6.15E-05	(1.5)	**6.27E-05**	**(3.1)**
585.0									1.61E-06	(1.5)	**1.61E-06**	**(2.0)**
620.1	2.34E-06	(5.0)							1.88E-06	(1.5)	**2.11E-06**	**(15)**
1047.6									1.72E-06	(1.5)	**1.72E-06**	**(2.0)**

For most lines the SD of the mean is $\leq (3\%/\sqrt{5}) \rightarrow u(k_0) \leq 1.34\%$ and k = 2.776 for a 95% confidence level.

8.4 Differences due to the adopted F_{Cd} factor

During the Q_0, $\bar{E}_r$ and k_0 determination by means of the Cd-subtraction method on several irradiation channels, it was soon realized that although several nuclear constants employed in our calculations were easily available in the digital or written literature, such as half-lives, decay branching factors, gamma-ray intensities, etc. [1, 2, 5, 6, 8], other nuclear constants such as the Cadmium transmission factors (F_{Cd}) for typical Cd-covers of 1 mm thickness and 2:1 cylindrical geometrical ratio are apparently not readily compiled in any official form. Furthermore, what is currently available (as of 2014) in terms of reactions or independent sources is still rather scarce.

The choice of F_{Cd} factors in this work for all the related calculations was simple. The values from the latest recommended compilations were to be adopted for most of the reactions to maintain the traceability, unless there were enough reasons to doubt or suspect the accuracy of the value. However, both the 2003 and 2012 recommended libraries do not provide the F_{Cd} factors associated to their reported values. We therefore opted to adopt the values from the IUPAC electronic compilation [24] and to check their traceability to the first generations (or compilations) of experimental k_0 nuclear data [36, 38, 40, 44, 45]

Dedicated experiments involving irradiation of samples under Cd-covers of different thickness were outside our capabilities due to time and budget limitations. As shown by the IUPAC electronic database, most of the target nuclides involved in our study have F_{Cd} factors equal to unity, with just a few isotopes deviating from this norm. Thus, the costly and cumbersome experiments for F_{Cd} determination with the method of Cd-cover thickness variation seemed not relevant. Nonetheless, it was still possible to study the impact on our Q_0 and k_0 factors from the adoption of F_{Cd} factors from other sources.

The Table 10.12 shows the Q_0 and $\bar{E}_r$ factors found in this work by means of the α vector method [62, 80, 89] and the F_{Cd} factors from the recommended literature [24]. These values are also compared to the ones derived by Trkov et al (Tkv) with the aid of the Evaluated Nuclear Data File database ENDF/B-VII.1b4 and compiled in an report to the International Atomic Energy (IAEA; Austria)[25]. Most of the F_{Cd} values adopted in our calculations from Lit differ from the ones proposed by Tkv in typically 5%, because the values from Tkv are typically within a ± 5% deviation from unity.

The Table 10.12 contains 38 reactions from which up to 15 of our $\bar{E}_r$ values agree within a ± 10% relative difference (40% of the reactions). A total of 22 of our Q_0 factors or 58% of the reactions analysed are within a ±10% relative difference to the values reported by them, while 33 of our Q_0 factors (87% of the reactions) are within a 20%.

The Table 10.13 on the other hand contains the Q_0 factors found in this work by means of the F_{Cd} and $\bar{E}_r$ factors from Lit (classic approach) and are also compared to the values reported by Tkv. The Table 10.13 contains 62 reactions and it can be readily seen that up to 24 of the $\bar{E}_r$ values adopted from the 2012 recommended k_0 compilation agree within a ± 20% relative difference to the values from them (39% of the sample). A total of 42 Q_0 factors found in this work are within a 10% relative difference to the values reported by them (68% of the reactions). A total of 51 Q_0 factors reported in this work are within a ±20% relative difference (82% of the reactions).

The ^{114}Cd, ^{164}Dy and ^{176}Yb target nuclides are the extreme cases, with a 20%, 9% and 11% deviation from unity respectively.

The clear next step was to recalculate several of our experimental Q_0 (or s_0) and k_0 factors quoted in Table 10.15 by adopting the F_{Cd} factors from Tkv instead.

The Table 10.14 summarizes the ratios ΔQ_0 and Δk_0 between the original Q_0 and k_0 factors and the ones computed after the adoption of the F_{Cd} factors from Tkv. In contrast, the k_0 factors do not depend on the adopted Q_0 and $\bar{E}_r$ values but on the F_{Cd} factors when employing the Cd-subtraction method for their determination.

The Table 10.14 shows that after inputting the F_{Cd} factors from Tkv most of the new (or recalculated) Q_0 factors were within ± 6% relative difference to the previous values. From the 65 reactions reported in the table, we found that 16 of them resulted in Q_0 factors with relative differences higher than ± 6%. The more extreme cases were ^{87}Rb (+12%), ^{98}Mo (+15%), ^{104}Ru (+13%), ^{108}Pd (+14%), ^{114}Cd (-63%) and ^{164}Dy (-13%).

The relative differences on the Q_0 factors for the previous 6 target isotopes may seem significant, but for irradiation of samples inside a Cd-cover (ENAA), the full impact on the analytical result (the analyte content) can only be assessed when considering the relative differences in their correlated k_0 and F_{Cd} factors. Under ENAA, the overall impact on the analytical result when employing the F_{Cd} factors from Tkv is just ± 3% for ^{65}Cu, ^{87}Rb, ^{98}Mo and ^{108}Pd and it is usually lower for the rest of the quoted reactions. For the extreme cases ^{114}Cd, ^{115}In, ^{164}Dy, ^{176}Yb and ^{187}W, the overall impact on the analytical result would be -60%, -8%, -5%, -6% and -9% (respectively).

Under normal (bare) NAA irradiation conditions, the impact on the analytical result from the recalculated Q_0 factors will vary from channel to channel. For low f (or mildly thermalized channels), the impact of the new Q_0 factors will be the highest, while the impact of the k_0 factors will propagate directly to the analytical result irrespectively of the chosen irradiation channel.

The average (AVG) and SD of the Δk_0 factors for our 3 irradiation channels showed us that the newly determined k_0 factors with F_{Cd} values from Tkv are in general ± 3% different than the values from Table 10.15 for all the quoted

radioisotopes, except for 4 cases: ^{88}Rb, ^{99}Mo, ^{115}Cd /^{115}In and ^{109}Pd/^{109m}Ag. These 4 cases showed instead relative differences of -4%, -7%, +37% and -5% (respectively). These differences in k_0 factors would be propagated to the analytical result in full if $f >> Q_\alpha$ as in the case of highly thermalized or "pure thermal" irradiation channels (such as "the Cavity"). Only the ^{99}Mo and ^{115}Cd /^{115}In cases are statistically significant and require further attention, i.e. a F_{Cd} determination by irradiations with Cd-covers of different thicknesses should be appropriate.

8.5 On the nuclear data for k_0-UNAA

The k_0 and k_0-fission factors determined in this work are given per material in section 10.4.2, while the final recommended results from the average of up to 3 different authors and nuclear data for the application of k_0-UNAA are given in section 10.6.2.

Several fission products interfere mutually in the typical γ-ray spectrum. We aimed at determining the k_0-fission factors for ^{85m}Kr (4.48 h half-life) at 151.2 and 304.9 keV, but it was not possible to obtain reliable results since the first line is interfered by the emission of the 149.7 keV line by both ^{131}Te and its isomer, while the second line is interfered by emission of ^{140}Ba at 304.9 keV. Both interfering nuclides live longer, and although we subtracted the ^{140}Ba contribution by using our k_0-fission factors from the other lines of this nuclide, our results for ^{85m}Kr had a SD greater than 10%. We suspect that since it is in gas form at room conditions, the required efficiency transfer calculations are beyond our current computational capabilities because the gas probably abandoned the lying sample matrix to reach the top of the sample container.

For other medium to long-lived fission products of interest, such as ^{89}Sr, ^{91}Sr (or ^{91}Y), ^{129}Sb, ^{136}Cs, and ^{144}Ce, we could not determine their k_0 fission

factors because of: a) their spectrum was completely interfered during its lifespan or; b) our sensitivity was not high enough for a precise determination.

The nuclides for which we determined new (effective) k_0-fission factors, that is, those that are not reported in the current (2012) k_0-library [23], were: ^{97}Zr, ^{131m}Te, ^{132}Te, ^{133}I, ^{135}I, ^{137m}Ba (the 661.7 keV line is usually assigned to its mother ^{137}Cs), and ^{140}Ba. The remaining k_0-factors found in this work correspond to nuclides that have been already investigated in the k_0-literature.

For ^{95}Zr our k_0 factors were 2 and 1% higher than in the recommended k_0-literature [20, 23] and Blaauw et al. [3] (respectively), within the expected uncertainty. For its daughter ^{95}Nb, the difference with the recommended k_0-literature was 4%. This is probably due to our adoption of the more recent experimental decay branching factors F_i from reference [8] into the ADS scheme. Blaauw et al. did not report a result for this nuclide [3]. For ^{97}Nb and its isomer, our results were within 1% of the recommended k_0-literature and Blaauw et al. values. [3, 20, 23].

For ^{99}Mo our results for the main γ-lines were in agreement with the other sources and up to 3% different in the case of the secondary γ-lines [3, 20, 23]. Our k_0 ratios for this nuclide are more consistent with the expected ratio between I_γ values than the other sources. On the other hand, our result for the 140.5 keV line of ^{99m}Tc is in line with Blaauw et al. [3] but is 4% higher than in the recommended k_0-literature [20, 23]. The same can be observed from our results for both ^{103}Ru lines. Our k_0 factor for the main γ-line of ^{105}Rh is in agreement with both sources, while our value for the secondary 306.1 keV line seems to be lower than the recommended k_0-literature by 6% [20, 23].

For ^{131}I our results are consistent with both sources except for the 364.5 keV line which is 4% higher than in recommended k_0-literature. Our differences

for the ^{140}La lines varied between 1-3% as compared to both sources [3, 20, 23]. For the ^{141}Ce and ^{147}Nd main lines there were no statistical significant differences in the results. However, for ^{143}Ce we observed differences of up to 5% between our results and those from references [3, 20, 23], for most γ-lines.

In general, the new k_0-fission results for the nuclides that are not tabulated in the current recommended k_0-library [23] are consistent with the calculated values obtained from absolute nuclear data compilations (within a max. 3% relative difference), although these compilations [1, 2, 4–10] usually contain imprecise data and/or no uncertainty is given. Several k_0-factors are proposed for these fission products.

The neutron capture of ^{238}U was only studied in this work through ^{239}Np from the decay of the mother nuclide ^{239}U. All our observed k_0 factors for ^{239}Np were within 1% relative difference with the values reported in the recommended k_0-literature, except for a 5% difference observed for the 106.1 and 228.2 keV lines. The first line is usually difficult to resolve due to the overlapping of the 103.7 keV ^{239}Np line and the high Compton-background in this energy region. The second line was interfered by the ^{132}Te 228.2 keV line, but it was possible to work out a solution.

From the ^{235}U-depleted material we computed a tentative k_0 factor for the ^{239}Np 228.2 keV line. This k_0 factor would be only slightly interfered due to the low ^{235}U content. On the other hand, with this value it was possible to calculate the ^{239}Np contribution in the photo-peak of the ^{235}U-enriched material, and subtract it to obtain a k_0-fission factor for the ^{132}Te 228.2 keV line. Finally, with the ^{132}Te k_0-fission factor, we calculated its contribution in the photo-peak of the ^{235}U depleted material (neglected at the beginning), and after the due subtraction a new k_0 factor for the ^{239}Np 228.2 keV line was obtained. The iteration continued until the convergence was quickly observed.

If we take the average from all our relative differences to the Lit values, our characterization of ^{235}U would require ~2% higher k_0-factors. For ^{238}U characterization with the 277.6 keV ^{239}Np line, we would require a 1% lower k_0 factor. Hence, after a complete recalibration of all our laboratory parameters, the determination of the $n(^{235}U)/n(^{238}U)$ isotopic ratio by means of the highly-recommended 277.6 keV line shows 3% overestimation, similarly to what we found in our 2010 work for some prominent gamma lines [85]. As mentioned before, the results from Blaauw et al. [3] are consistent with this overall 2% observed discrepancy for several fission products, although they did not report k_0-measurements on ^{239}Np in their work.

At 3% difference, none of these results are statistically significant at 95% confidence level because we only employed one channel for these determinations. Therefore, we propose the mean and SD from the 3 authors of information as a new set of recommended k_0 factors for k_0-UNAA application (see Table 10.17 and Table 10.18).

8.5.1 About the effective k_0-fission factors

The first determinations of k_0 factors were performed under the Høgdahl convention [13].The Westcott g_T factors reported in [16] show that the ^{235}U deviation from the 1/v law differs from unity in the 0 to 100 °C range, with g_T = 0.9815 at our Y4 channel temperature of 27 ± 2°C (see Table 6.5). During the first k_0-fission factors determination in reference [54], the non-1/v variation of the ^{235}U cross section was considered to be only of a few percent (although no exact number was given) and the application of the Høgdahl convention seemed justified.

When comparing both conventions, in the case of sufficiently thermalized channels and low Q_α (or s_α) values, the Q_α/f fraction in the Høgdahl

convention can be as negligible as the s_α/β_α corresponding quantity that is employed in the Westcott formalism, meaning that a k_0 factor determined per a pure Høgdahl formula would be equivalent to g_T times the k_0 value found through the Westcott formula. Thus, one can only assume that the k_0-fission factors reported in [54] are actually $\sim g_T.k_0$ factors, because of their applied convention and because no g_T factor (or channel temperature) and g_T normalization process was mentioned in that work. On the other hand, the method applied by Blaauw et al. for k_0 determination is based on its holistic approach and differs considerably in the way the overall computations are made [3]. There was no mention of which formalism was employed in that work as well, nor a reference to g_T factors and/or channel temperatures, therefore we concluded that the k_0 factors reported in these references are "effective" ($g_T.k_0$) values as well, that we assume are tabulated at the room temperature range of 20-30 °C.

For consistency with other authors we reported effective k_0-fission factors ($g_T.k_0$) as well at our Y4 channel temperature of 27°C, which can be inputted directly in the commonly applied Høgdahl formalism for not too extreme irradiation channels. Between 20-100°C the g_T factor for ^{235}U varies by just 1.1%, thus the renormalization of the literature (or our) values would not be strictly necessary unless the use of the Westcott formalism is preferred. For ^{238}U on the other hand, the Westcott g_T factor is ≈1 between 20 to 100°C [16] and k_0 factors are thus provided.

9. Summary and conclusions

The success of the k_0-standardization of Neutron Activation Analysis relies in the continuous revision of its core values. Although the k_0 and Q_0 factors are defined as "nuclear constants", it is clear from their experimental nature and correlation to adopted nuclear data that these "constants" can change in time. It has been shown that part of the current recommended k_0-library has been determined experimentally only once, 30 years ago, and that it is correlated to nuclear data adopted from unconfirmed literature available before 1980. Several authors have identified systematic differences in their analysis of reference materials when employing certain sub-datasets in the current k_0-literature (2012) but the task of identifying the source of these inaccuracies can be difficult or even inconclusive, until more experimental data is made available to the k_0-community. A review of the traceability of the current k_0-library showed us: that the F_{Cd} factors are missing from the latest references or that a few of these F_{Cd} values (adopted) might be inaccurate and need validation for ENAA purposes; that some radionuclides are not reported anymore (^{135m}Ba; ^{125}Sb) or that new radionuclides could be added to the recommended library (e.g. ^{197}Pt, ^{111}Ag, ^{235}U fission products; additional γ-lines). Also, it has been shown that some sub-sets of data could be improved (^{134}Cs, ^{186}Re for both "a" and "b" ADS type IV scenarios).

The Universiteit Gent and the SCK•CEN Belgian Nuclear Research Centre (Belgium) considered that it was time to take advantage from the advances in technology and nuclear chemistry over the last 20 years (e.g. better radiation detectors, standard certificates) for launching a redetermination of

k_0 nuclear data for 76 (n,γ) target isotopes, leading to the formation of 96 radionuclides states (364 γ-rays of analytical interest). To improve the $n(^{235}U)/n(^{238}U)$ determination method at the SCK•CEN, it was felt necessary to redetermine and introduce new k_0 factors for both ^{238}U neutron capture and ^{235}U fission as well. The k_0 nuclear data for these 2 additional target isotopes leading to ^{239}Np and 20 fission products was explored to provide information about the uranium enrichment levels in multi-elemental samples, with useful application in neutron forensics for safeguards and/or in environmental monitoring.

The determination of k_0 nuclear data was a metrological work that required the accurate recalibration of all irradiation channels and detectors employed. For achieving this, sufficiently diluted, homogenous standards and certified radioactive sources of great quality and metrological traceability were acquired from e.g. IRMM, NIST, Goodfellow and AREVA, while an adaptation/modification of the SOLCOI code allowed us to perform an accurate efficiency transfer by means of the more recent and smooth X and γ-ray linear attenuation curves from the NIST XCOM online database. For instance, a 0.6% minimum relative difference was observed between our computed and experimental efficiency data-points for small cylindrical paper filters and for abundant γ-rays in the 300-1300 keV energy range, measured at 20-30 cm detector-sample separations which would later serve as k_0 determination positions.

We studied and validated recent experimental methods proposed in the literature for the calculation of neutron self-shielding correction factors (e.g. the Sigmoid, Chilian et al. and MATSSF methods), to account for undesired matrix self-absorption of thermal and resonance neutrons, which are the main source of biases in the estimated (n,γ) reaction rate.

From our self-shielding validation experiments for samples with high Na, Dy and H content, the Chilian et al. method for thermal neutron self-shielding correction was apparently more suited for our work due to its

accuracy and versatility (k_{th} adaptable parameter) than the MATSSF thermal calculation method, since the latter does not allow (yet) for a tuning of their proposed W parameter (or the Bell factor), which could in principle provide a way to improve its overall accuracy and versatility for these cases.

On the other hand, the MATSSF epithermal calculation method is more rigorous, versatile (allowing for three neutron-source/sample configurations) and is apparently more accurate than the Chilian et al. method for ^{96}Zr and ^{98}Mo resonance self-shielding corrections, mainly because of observed differences in the experimental effective resonance absorption cross-sections they proposed. It is clearly erroneous to conclude which method is more accurate than the other based on a few studied elements, but because of our validation results, time and budget limitations and, given that for the majority of the prepared samples the self-shielding corrections were negligible or at worst up to 5% for few cases, we opted for employing the Chilian et al. method for thermal self-shielding and the MATSSF method for epithermal self-shielding corrections in all our k_0 nuclear data determinations. From channel calibration experiments on small polyethylene vials (1 mm wall thickness) it was clear that all kind of polyethylene spacers had to be avoided in our k_0 and Q_0 determination experiments. This was especially true for samples inside Cd-covers since further thermalization of the neutron fluence rate by the polyethylene was feared and observed (e.g. significant changes in f, α).

All the experiments were performed at the BR1 reactor of the SCK•CEN, by employing up to four irradiation channels with a high spread in (f, α) values (i.e. neutron parameters) and up to six HPGe detectors with diverse absolute γ-detection efficiencies, to obtain as many independent results in terms of the neutronics and γ-spectrometry parameters as we could. In some cases, more than one certified material of a given element was employed. Specialized software for all our relevant computations was developed in C# 4.0 language before and during our experiments, exploiting state-of-the-art

algorithms and data-relations to link efficiently several k_0-NAA & laboratory SQL databases and to handle great amounts of data-points in a redundancy-free manner, aiming at minimizing the chances of systematic errors during data input. Evidently the analyst, the laboratory team and other variables of the overall determination setup (e.g. some hardware, weighting/drying room, the software and software developer) remained constant during these experiments. This means that even after all metrological aspects have been taken with great care, the need for a confirmation of our results by other parties remains, at least for these nuclides with significantly different results reported in this work.

A multi-channel method for Q_0 and $\bar{E}_r$ determination that was introduced by Simonits et al. in 1984, but that has not been exploited in the literature since then, was re-derived here for the general case of the $\bar{E}_r$ as a function of α and, an isotope-specific parameter p, which was proposed later by Jovanović et al. in 1987. The method was employed in this work for the determination of 54 $\bar{E}_r$ factors in up to three irradiation channels, obtaining 32 values within a 25% relative difference (within the uncertainty range) and 23 values within a 10-15% relative difference to the expected values. This means that the latter group of (radioisotopes) values are highly recommendable for α-calibration (accurate $\bar{E}_r$ values). Given that the majority of the literature $\bar{E}_r$ factors were calculated assuming a Breit-Wigner resonance distribution with nuclear data available at that time (1979-1989), this multi-channel approach not only provided a way for validating several of these values, but in overall it showed that the previously assumed α-independence of the $\bar{E}_r$ during the launch of the k_0-method was correct within their expected 20% $\bar{E}_r$ uncertainty range and that the impact (of this assumption) on the Q_α factor was in our case typically 1 - 2% for our extreme channels ($\alpha \approx 0$ or $\alpha \approx 0.1$) and up to 5% for a few isotopes at α = [0.06;0.07]. Thus, the impact in the analytical results would be negligible unless $Q_\alpha >> f$ or ENAA is performed.

The reported Q_0 results for 24 isotopes agreed with the recommended values within 4%, which is in line with our expected uncertainty at the 2*s* confidence level. Our Q_0 findings corroborate significant discrepancies found by Kennedy et al. during the last decade (e.g. Sr, As, Ru and Ta). From our results, we suggested that the latest recommended Q_0 factors for ^{85m}Sr and ^{85}Sr production should be swapped. Differences of 10-30% were observed for low-Q_0 values (e.g. ^{27}Al, ^{174}Hf, ^{164}Dy, etc.) which had adopted literature data. For these nuclides, the Q_0 factor will have a negligible impact on the analytical result. On the other hand, several of our Q_0 results had lower uncertainties than in the literature.

For 54 radioisotopes, our k_0 factors agree with the latest references within 2 - 4% (1% for most recommended lines). For the Cr, Rb, Pd, ^{114}In, Cs, Sb and Pt radionuclides the discrepancies with the main lines were >5% and require further attention. We introduced the k_0 factors for ^{197m}Pt, ^{197}Pt, ^{199}Pt and ^{125}Sb and for ^{134}Cs and ^{188}Re under the more natural ADS type IV/b. Several recommended new k_0-factors are proposed for multi-γ radioisotopes (e.g. ^{72}Ga, ^{140}La, ^{76}As, ^{181}Ta, etc.). It was shown that the derived thermal neutron cross-sections were usually in agreement with the literature while our k_0 factors were also in good proportion when compared to the ratio between the respective γ-ray abundances.

Our reported ^{235}U k_0-fission factors were on average 2% higher than the values in the current literature and in line with the recent results by Blaauw et al. (with a few exceptions). The 2% difference, combined with our 1% lower observed k_0 factor for the 277.6 keV line of ^{239}Np, accounted for a 3% overestimation of the $n(^{235}\text{U})/n(^{238}\text{U})$ isotopic ratio that we observed when employing the current recommended k_0-literature even after a complete recalibration of all employed instruments. However, this difference is not statistically significant.

From the experimental k_0 factors it was possible to extrapolate some fundamental nuclear constants. Therefore, the k_0 standardization plays an

important role in the traceability of the nuclear data libraries for related disciplines. Unfortunately, these fundamental constants would need to be recalculated any time that a strongly-correlated parameter is updated (e.g. γ-ray or isotopic abundances, decay branching factors). Methods such as the Cd-subtraction technique or the employment of highly thermalized channels were especially suited for this metrological work and are recommendable for future work, in virtue of the lower chances of introducing systematic errors by minimizing the adoption of calibrated/modelled parameters. In this work, only 6 cases: ^{96}Zr, ^{116}Sn, ^{125}Sb (from ^{124}Sn(n,γ)^{125m}Sn), ^{151}Eu, ^{153}Eu and ^{168}Yb required the adoption of strongly-correlated values such as the Q_0 or s_0 factors from the literature and of modelled parameters (i.e. f, α) for k_0 determination.

After more than 30 years of development and applications of this technique, several improvements in instrumentation, software, concepts, etc., we achieved at our institutes a precision of ~3% (at the 95% confidence level) for multiple k_0 determinations on up to 4 channels. We believe that more laboratories should embrace in a re-determination of the statistically significant factors found in this work (i.e. with relative differences of ≥ 5%) and of new ones when feasible, desirable and possible, to obtain accurate and robust k_0 factors from the average of several authors with expected uncertainties better than 4% at the 95% confidence level.

10. A compendium

This chapter contains a compendium of tables and figures with the main results of this work and/or nuclear data adopted in or derived from our calculations. Each section provides information about the content of these figures and tables.

The experimental k_0, Q_0 and $\bar{E}_r$ values of this work were determined at the BR1 reactor in the SCK•CEN by means of up to 4 irradiation channels (S84, Y4, X26 and the thermal Cavity). This work was performed in close collaboration with the Universiteit Gent (Belgium) and were reported in references [62, 80, 81].

The following results are reported for the respective activation-decay scheme relating the target isotope with the corresponding formed (and measured) nuclide and are typically compared to values from the recommended k_0 compilations in references [20–23] or to other sources of nuclear data [1, 2, 4–10].

The reader is advised to follow the list of abbreviations given at the beginning of this book for more information about the table symbols and sources of literature values employed.

A summary of our findings is given at the end of this chapter.

10.1 Half-lives

The Table 10.1 compiles the half-lives employed in this work for all determinations (underlined values). These values were quoted as compiled in the ND database, by DC and in Lit. Most of the k_0 factors in the recommended literature are correlated to the $T_{1/2}$ values from DC, although these are nowadays quoted as correlated to the $T_{1/2}$ values in the latest recommended literature.

After a careful examination of all sources, it was realized that these constants have not changed significantly since then and thus, one can safely adopt the latest values from the recommended k_0-literature, as done in this work. The only exceptions are listed in the same table, from which the values were rather adopted from recent data (> 2008) compiled by the DDEP and/or from the ND database when not listed in this source. The changes in $T_{1/2}$ values for these exceptional cases are not significant (e.g. ^{95}Zr) and are not considered to influence the results (< 0.2% variation).

Table 10.1: Half-lives ($T_{1/2}$) employed in this work (underlined values) for the formed nuclides as reported by several sources. Uncertainties in absolute value for the last significant digit as reported by these sources (e.g. a half-width uncertainty)

FN	ND		DC		Lit			FN	ND		DC		Lit		
^{24m}Na	20.2	(-)	20.18	(10)	20.2	(-)	ms	^{60m}Co	10.47	(1)	10.47	(1)	10.47	(-)	m
^{24}Na	14.959	(3)	14.997	(12)	14.96	(-)	h	^{60}Co	5.271	(8)	5.271	(8)	5.271	(8)	y
^{27}Mg	9.458	(9)	9.458	(12)	9.462	(-)	m	^{65}Ni	2.520	(2)	2.5175	(5)	2.517	(-)	h
^{28}Al	2.240	(1)	2.2414	(12)	2.2414	(-)	m	^{64}Cu	12.701	(3)	12.701	(2)	12.70	(-)	h
^{38m}Cl	700	(-)	715	(3)	715	(-)	ms	^{66}Cu	5.10	(2)	5.120	(14)	5.12	(-)	m
^{38}Cl	37.21	(3)	37.240	(5)	37.24	(-)	m	^{65}Zn	244.01	(1)	243.93 *	(9)	244.3	(-)	d
^{41}K	12.360	(12)	12.360	(12)	12.36	(-)	h	^{69m}Zn	13.76	(15)	13.76	(2)	13.76	(-)	h
^{46m}Sc	18.7	(-)	18.75	(4)	18.75	(-)	s	^{72m}Ga	39.7	(-)	39.7	(-)	39.7	(-)	ms
^{46}Sc	83.82	(2)	83.79	(4)	83.8	(-)	d	^{72}Ga	14.1 *	(2)	14.10	(2)	14.10	(-)	h
^{51}Ti	5.752	(7)	5.76	(1)	5.76	(-)	m	^{76}As	26.32	(3)	26.261	(17)	26.24	(-)	h
^{52}V	3.75	(1)	3.743	(1)	3.75	(-)	m								
^{51}Cr	27.69	(1)	27.701	(1)	27.70	(-)	d	^{82m}Br	6.10	(-)	6.130	(5)	6.13	(-)	m
^{56}Mn	2.5785	(5)	2.5789	(1)	2.579	(-)	h	^{82}Br	35.30	(3)	35.282	(7)	35.30	(-)	h
^{59}Fe	44.63	(9)	44.495	(9)	44.5	(-)	d	^{99}Mo	2.751	(2)	2.748	(1)	2.7475	(-)	(d)
^{86m}Rb	1.02	(-)	1.017	(3)	1.02	(-)	m	^{99m}Tc	6.02	(30)	6.007	(1)	6.01	(-)	(h)
^{86}Rb	18.66	(2)	18.642	(18)	18.63	(-)	d	^{101}Mo	14.60	(14)	14.61	(3)	14.61	(-)	(m)
^{88}Rb	17.8	(1)	17.773	(11)	17.78	(-)	m	^{101}Tc	14.20	(14)	14.02	(1)	14.20	(-)	(m)

FN	ND		DC		Lit			FN	ND		DC		Lit		
^{85m}Sr	67.66	(7)	67.63	(4)	67.63	(-)	m	^{97}Ru	2.9	(1)	2.83	(23)	2.90	(-)	(d)
^{85}Sr	64.84 *	(3)	64.850	(7)	64.84	(-)	d	^{103}Ru	39.26	(2)	39.247	(3)	39.35	(-)	(d)
^{87m}Sr	2.805	(2)	2.815	(12)	2.803	(-)	h	^{105}Ru	4.44	(2)	4.44	(2)	4.44	(-)	(h)
^{90m}Y	3.19	(1)	3.19	(6)	3.19	(-)	h	^{105m}Rh	45	(-)	42.9	(3)	42.3	(-)	(s)
^{95}Zr	64.02	(1)	64.032 *	(6)	64.02	(1)	d	^{105}Rh	35.36	(6)	35.36	(6)	35.36	(-)	(h)
^{95m}Nb	3.61	(4)	3.61 *	(3)	3.61	(4)	d	^{109m}Pd	4.69	(1)	4.696	(3)	4.69	(-)	(m)
^{95}Nb	34.97	(9)	34.991 *	(3)	34.97	(9)	d	^{109}Pd	13.7	(1)	13.701	(3)	13.46	(-)	(h)
^{96}Zr	16.74	(2)	16.749	(8)	16.74	(-)	h	^{109m}Ag	39.6	(2)	39.6	(2)	39.6	(-)	(s)
^{97m}Nb	60	(8)	58.7	(8)	52.7	(-)	s	^{111m}Pd	5.5	(1)	5.5	(1)	5.5	(-)	(h)
^{97}Nb	72.1	(7)	72.1	(7)	72.1	(-)	m	^{111}Pd	23.4	(2)	-		-		(m)
^{94m}Nb	6.26	(1)	6.263	(4)	6.26	(-)	m	^{111}Ag	7.5	(1)	-		-		(d)
^{108}Ag	2.37	(1)	2.382	(11)	2.37	(-)	m	^{125m}Sn	9.52	(5)	9.53	(1)	9.52	(-)	(m)
^{110m}Ag	249.76	(4)	249.76	(4)	249.8	(-)	d	^{125}Sn	9.64	(2)	9.64	(3)	9.64	(-)	(d)
^{115}Cd	53.47	(10)	53.46	(5)	53.5	(-)	h	^{125}Sb	2.7586	(1)	2.7617	(1)			(y)
^{115m}In	4.486	(1)	4.486	(1)	4.486	(-)	h	^{122m}Sb	4.2	(-)	4.191	(3)	4.191	(-)	(m)
^{114m2}In	43.1	(-)	43.1	(6)	43.1	(-)	ms	^{122}Sb	2.70	(2)	2.7238	(2)	2.724	(-)	(d)
^{114m}In	49.51	(1)	49.51	(1)	49.51	(-)	d	^{124m2}Sb	20.2	(2)	20.2	(2)	20.2	(-)	(m)
^{116m2}In	2.16	(-)	2.18	(4)	2.18	(-)	s	^{124m}Sb	93	(5)	93	(5)	93	(-)	(s)
^{116m}In	54.15	(5)	54.29	(17)	54.41	(-)	m	^{124}Sb	60.20	(3)	60.20	(3)	60.20	(-)	(d)

FN	ND		DC		Lit		
^{113m}Sn	21.4	(4)	21.4	(4)	21.4	(-)	m
^{113}Sn	115.09	(3)	115.09	(3)	115.1	(-)	d
^{113m}In	99.48	(6)	99.476	(23)	99.48	(-)	m
^{117m}Sn	13.61	(4)	13.76	(4)	13.6	(-)	d
^{140}La	1.67855 *	(1)	1.676	(1)	1.678	(-)	m
^{142m}Pr	14.6	(5)	14.6	(5)	14.6	(-)	m
^{142}Pr	19.12	(4)	19.12	(4)	19.12	(-)	h
^{152}Sm	1.9285 *	(1)	1.946	(8)	1.9375	(-)	h
^{152}Eu	13.5280	(14)			13.54	(-)	y
^{154m}Eu	46.0	(4)	46.0	(4)	46.0	(-)	m
^{154}Eu	8.561	(8)	8.601	(10)	8.593	(-)	y
^{153}Gd	240.4	(10)	240.4	(10)	240.4	(-)	d
^{159}Gd	18.56	(7)	18.479	(4)	18.56	(-)	h
^{160}Tb	72.1	(3)	72.3	(2)	72.3	(-)	d
^{165m}Dy	1.258	(6)	1.257	(6)	1.257	(-)	m
^{165}Dy	2.334	(1)	2.334	(1)	2.334	(-)	h
^{166}Ho	26.80	(2)	26.824	(12)	26.83	(-)	h
^{186}Re	3.777	(4)	3.72	(-)	3.718 *	(-)	d

FN	ND		DC		Lit		
^{134m}Cs	2.910	(8)	2.912	(2)	2.903 *	(-)	(h)
^{134}Cs	2.062	(4)	2.0652	(4)	2.065 *	(-)	(y)
^{131m}Ba	14.6	(2)	14.6	(2)	14.6	(-)	(m)
^{131}Ba	11.8	(2)	11.50	(6)	11.50	(-)	(d)
^{133m}Ba	38.9	(1)	38.93	(10)	38.9	(-)	(h)
^{135m}Ba	28.7	(2)	28.7	(2)			(h)
^{139}Ba	83.06	(25)	83.06	(21)	83.06	(-)	m
^{170}Tm	128.6	(3)	128.6	(3)	128.6	(-)	(d)
^{169m}Yb	46	(2)			46	(-)	(s)
^{169}Yb	32.018 *	(5)			32.03	(-)	(d)
^{175m}Yb	68.2	(-)	68.20	(3)	68.2	(-)	(ms)
^{175}Yb	4.19	(1)	4.185	(1)	4.185	(-)	(d)
^{177m}Yb	11.4	(-)	6.41	(2)	6.41	(-)	(s)
^{177}Yb	1.9	(9)	1.911	(3)	1.911	(-)	(h)
^{177}Lu	6.647	(4)			6.73	(-)	(d)
^{175}Hf	70	(2)	70	(2)	70	(-)	(d)
^{180m}Hf	5.519	(4)	5.47	(4)	5.5	(-)	(h)
^{181}Hf	42.39	(6)	42.39	(6)	42.39	(-)	(d)

FN	ND		DC		Lit			FN	ND		DC		Lit		
^{188m}Re	18.59	(4)	18.59	(-)	18.59	(-)	m	^{182m}Ta	15.8	(-)	15.84	(10)	15.8	(-)	(m)
^{188}Re	17.005	(4)	17.01	(-)	17.01	(-)	h	^{182}Ta	114.43	(3)	114.74	(12)	114.4	(-)	(d)
^{197m}Pt	95.41	(18)					m	^{187}W	23.9	(1)	24.00	(1)	23.72 *	(6)	(h)
^{197}Pt	19.892	(2)					h	^{233}Th	22.30	(9)	21.83	(4)	22.3	(-)	(m)
^{199m}Pt	14	(-)	13.6	(4)	13.6	(-)	s	^{233}Pa	27.00	(11)	26.975	(13)	26.97	(-)	(d)
^{199}Pt	30.8	(-)	30.8	(4)	30.8	(-)	m	^{239}U	23.500	(5)	23.45	(2)	23.450	(-)	(m)
^{199}Au	3.139	(7)	3.139	(7)	3.139	(-)	d	^{239}Np	2.355	(5)	2.356	(3)	2.357	(-)	(d)
^{198}Au	2.695	(3)	2.6948	(12)	2.695 *	(-)	d								

* Values reported by the DDEP.

10.2 Summary of ADS related formulae and definitions

The ADS equations from references [20, 21] were rewritten in terms of the Lamda and Temporal factors introduced in the section 2.12 of this work. These auxiliary parameters are compiled in Table 10.2, while the relationships between the Temporal factors T_i and the $f(S,D,C)_{yz}$ functions for each ADS type-*y* and *z*-scenario from eqs. (2.125) to (2.146) are summarized in Table 10.3.

Each ADS type and scenario requires an adjustment of the k_0 and a Q_α "standard definitions" [20, 21]:

$$k_{0,s,S,c} \equiv \frac{\left(I_{\gamma,S}\theta_s\sigma_{0,s,S}/M\right)}{\left(I_{\gamma,C}\theta_c\sigma_{0,c}/M\right)} \qquad (10.1)$$
$$Q_{\alpha,s} \equiv I_{\alpha,s}/\sigma_{0,s}$$

The index *s* is associated to target nuclides (*s* = 1 to 4) while the index *S* is associated to formed radionuclides (*S* = 2 to 4). The index *c* corresponds to the comparator. The Table 10.4 and Table 10.5 summarize the relationships between the k_0 and Q_α standard definitions (eq. (10.1)) and their definition given in [20, 21] for each ADS type and scenario.

Table 10.2: Compilation of practical auxiliary parameters in the calculation of the ADS of a given reaction.

Lamda factors	**Temporal factors**
$\lambda_i \equiv \ln(2)/T_{1/2,i}$ $\lambda_{ij} \equiv \lambda_i - \lambda_j \equiv -\lambda_{ji}$ $\lambda_{ijk} = \frac{\lambda_j \lambda_k}{\lambda_{ij} \lambda_{ik}} = \lambda_{ikj}$	$T_i \equiv S_i D_i C_i$ $T_{ij} \equiv \frac{\lambda_i T_j - \lambda_j T_i}{\lambda_{ij}} \equiv T_{ji}$ $T_{ijk} \equiv T_i \lambda_{ijk} = T_{ikj}$
Auxiliary ratios	$\iota_{ij} \equiv \frac{I_{\gamma,i}}{I_{\gamma,j}}; \quad \eta_{ij} \equiv \frac{\sigma_{0,i}}{\sigma_{0,j}}; \quad \mathrm{O}_{ij} \equiv \eta_{ij} \frac{R_{H,i}}{R_{H,j}}$

Table 10.3: Relationships between 7 Temporal factors T_i (i = 1, …, 7) defined in eq. (2.122) and the $f(S,D,C)_{yz} = T_{yz}$ function for each ADS type-y and scenario-z (y = I,II,…,VII and z = a, b, c, d) reported in the recommended literature [20, 21].

III	**II**	**I**
$T_{IIIa} = T_{IIIb} + F_{234}T_{24}$ $T_{IIIb} = T_{234} + T_{324} + T_{423}$ $T_{IIIc} = T_{24}$	$T_{IIa} = T_{23}$ $T_{IIb} = T_3$ $T_{IIc} = T_2\left(\lambda_3/\lambda_{32}\right)$ $T_{IId} = T_2\left(\iota_{23}/F_2\right) + T_{23}$	$T_I = T_2$
IV	**V**	
$T_{IVa} = T_3 + \mathrm{O}_{23}F_2T_{23}$ $T_{IVb} = T_3$ $T_{IVc} = T_2\left(\lambda_3/\lambda_{32}\right)$ $T_{IVd} = T_2\mathrm{O}_{23}\iota_{23} + \left(T_3 + \mathrm{O}_{23}F_2T_{23}\right)$	$T_{Va} = \left(\left\{T_{234} + T_{324} + T_{423}\right\}\mathrm{O}_{23}F_2\right) + T_{34}$ $T_{Vb} = T_4$ $T_{Vc} = T_3$ $T_{Vd} = T_{34}$	
VI		
$T_{VIa} = T_{34}\mathrm{O}_{34}F_3 + T_4 + \mathrm{O}_{24}\left\{F_{24}T_{24} + F_2F_3\left(T_{234} + T_{324} + T_{423}\right)\right\}$ $T_{VIb} = T_{VIc} = T_4$		
VII		
$T_{VIIa} = \left(\left\{T_{234} + T_{324} + T_{423}\right\}\mathrm{O}_{23}F_2 + T_{34}\right) + \left(T_{24}\mathrm{O}_{23}\left\{F_{24}/F_3\right\}\right)$ $T_{VIIb} = T_{24}\mathrm{O}_{23}\left\{F_{24}/F_3\right\} + T_{34}$ $T_{VIIc} = T_4$		

Table 10.4: Relationships between the k_0 standard definition in eq. (10.1) and the corresponding definition for each ADS type-*y* and scenario-*z* from references [20, 21] (*y = I, II, …, VII*; *z = a, b, c, d*).

<table>
<tr><th>I</th><th>II</th><th>III</th></tr>
<tr><td>$k_{0,I} \equiv k_{0,1,2,c}$</td><td>$k_{0,IIz} \equiv F_2 k_{0,1,3,c}$
with z = a, b, c, d</td><td>$k_{0,IIIa} = k_{0,IIIb} \equiv F_2 F_3 k_{0,1,4,c}$
$k_{0,IIIc} \equiv k_{0,1,4,c}$</td></tr>
<tr><th>IV</th><th colspan="2">V</th></tr>
<tr><td>$k_{0,IVa} = k_{0,IVd} \equiv k_{0,3,3,c}$
$k_{0,IVc} = F_2 \eta_{23} k_{0,3,3,c} \equiv F_2 k_{0,2,3,c}$
$k_{0,IVb} = \{F_2 \eta_{23} + 1\} k_{0,3,3,c}$</td><td colspan="2">$k_{0,Va} \equiv F_3 k_{0,3,4,c}$
$k_{0,Vz} = \{F_2 \eta_{23} + 1\} F_3 k_{0,3,4,c}$
with z = b, c, d</td></tr>
<tr><th colspan="3">VI</th></tr>
<tr><td colspan="3">$k_{0,VIa} \equiv k_{0,4,4,c}$
$k_{0,VIb} = \left(F_{24}\eta_{24} + F_3\{F_2\eta_{24} + \eta_{34}\} + 1\right) k_{0,4,4,c}$
$k_{0,VIc} = \left(F_3\{F_2\eta_{24} + \eta_{34}\} + 1\right) k_{0,4,4,c}$</td></tr>
<tr><th colspan="3">VII</th></tr>
<tr><td colspan="3">$k_{0,VIIa} \equiv k_{0,VIIb} = F_3 k_{0,3,4,c}$
$k_{0,VIIc} = \left(\eta_{23}\{(F_{24}/F_3) + F_2\} + 1\right) F_3 k_{0,3,4,c}$</td></tr>
</table>

Table 10.5: Relationships between the Q_0 standard definition in eq. (10.1) and the corresponding definition for each ADS type-*y* and scenario-*z* from references [20, 21] (*y = I, II, …, VII*; *z = a, b, c, d*).

<table>
<tr><td>I</td><td>II</td><td>III</td></tr>
<tr><td>$Q_{\alpha,I} \equiv Q_{\alpha,1}$</td><td>$Q_{\alpha,IIz} \equiv Q_{\alpha,1}$
with z = a, b, c, d</td><td>$Q_{\alpha,IIIz} \equiv Q_{\alpha,1}$
with z = a, b, c</td></tr>
<tr><td>IV</td><td colspan="2">V</td></tr>
<tr><td>$Q_{\alpha,IVa} = Q_{\alpha,IVd} \equiv Q_{\alpha,3}$
$Q_{\alpha,IVc} \equiv Q_{\alpha,2}$
$Q_{\alpha,IVb} = \dfrac{F_2\eta_{23}Q_{\alpha,2} + Q_{\alpha,3}}{F_2\eta_{23}+1}$</td><td colspan="2">$Q_{\alpha,Va} \equiv Q_{\alpha,3}$
$Q_{\alpha,Vz} \equiv \dfrac{F_2\eta_{23}Q_{\alpha,2} + Q_{\alpha,3}}{F_2\eta_{23}+1}$
with z = b, c, d</td></tr>
<tr><td colspan="3">VI</td></tr>
<tr><td colspan="3">$Q_{\alpha,VIa} \equiv Q_{\alpha,4}$
$Q_{\alpha,VIb} = \dfrac{\left[F_3\left\{F_2\eta_{24}Q_{\alpha,2} + \eta_{34}Q_{\alpha,3}\right\} + Q_{\alpha,4}\right] + F_{24}Q_{\alpha,2}}{\left(F_3F_2 + F_{24}\right)\eta_{24} + F_3\eta_{34} + 1}$
$Q_{\alpha,VIc} = Q_{\alpha,VIb}\Big\vert_{F_{24}=0}$</td></tr>
<tr><td colspan="3">VII</td></tr>
<tr><td colspan="3">$Q_{\alpha,VIIa} = Q_{\alpha,VIIb} \equiv Q_{\alpha,3}$
$Q_{\alpha,VIIc} = \dfrac{\eta_{23}\left\{\left(F_{24}/F_3\right) + F_2\right\}Q_{\alpha,2} + Q_{\alpha,3}}{\eta_{23}\left\{\left(F_{24}/F_3\right) + F_2\right\} + 1}$</td></tr>
</table>

10.3 The α-vector method results

The method is presented in section 6.3 and a discussion is given in section 8.1.

The Y_α vs. α plots

Figure 10.1 to Figure 10.11 show the resulting Y_α vs. α plots from the monitoring of 41 (n,γ) reactions. The dashed curves correspond to polynomial fits ($p_3 \neq 0$) to our experimental results, while the points represent the expected (or theoretical) lines based on the latest recommended values in [20, 23] (with $p_3 = 0$). From a given polynomial regression (dashed line) the $\bar{E}_r$ and Q_0 factors are obtained from the slope and the intercept, respectively. A dotted line corresponds to the regression one would expect from the Lit values.

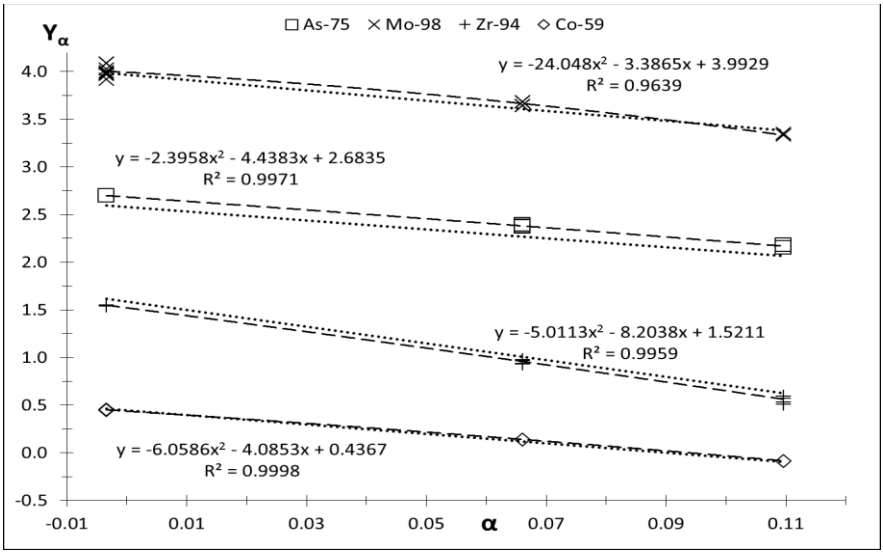

Figure 10.1: Graph of experimental Y_α values for ^{75}As(n,γ)^{76}As, ^{98}Mo(n,γ)^{99}Mo, ^{94}Zr(n,γ)^{95}Zr and ^{59}Co(n,γ)^{60}Co vs. α.

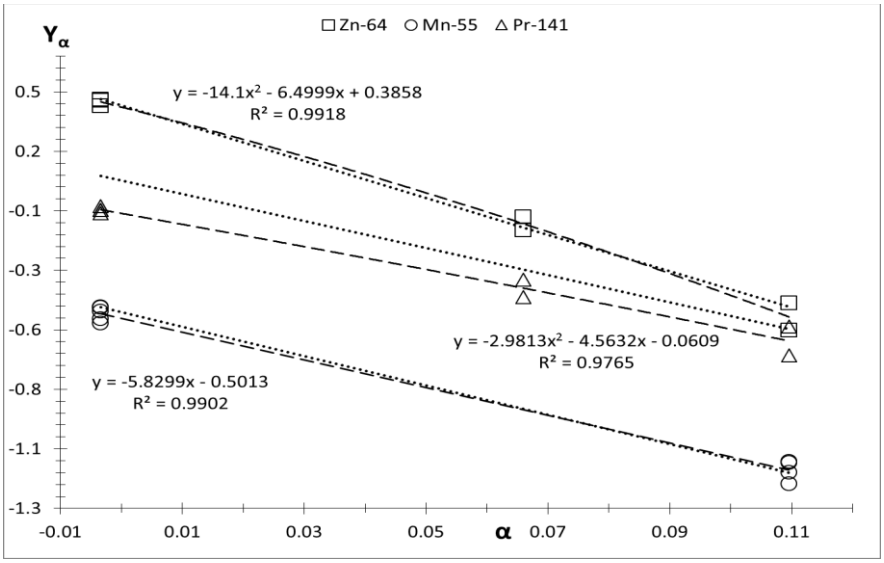

Figure 10.2: Graph of experimental Y_α values for ^{64}Zn(n,γ)^{65}Zn, ^{55}Mn(n,γ)^{56}Mn, ^{141}Pr(n,γ)^{142}Pr vs. α.

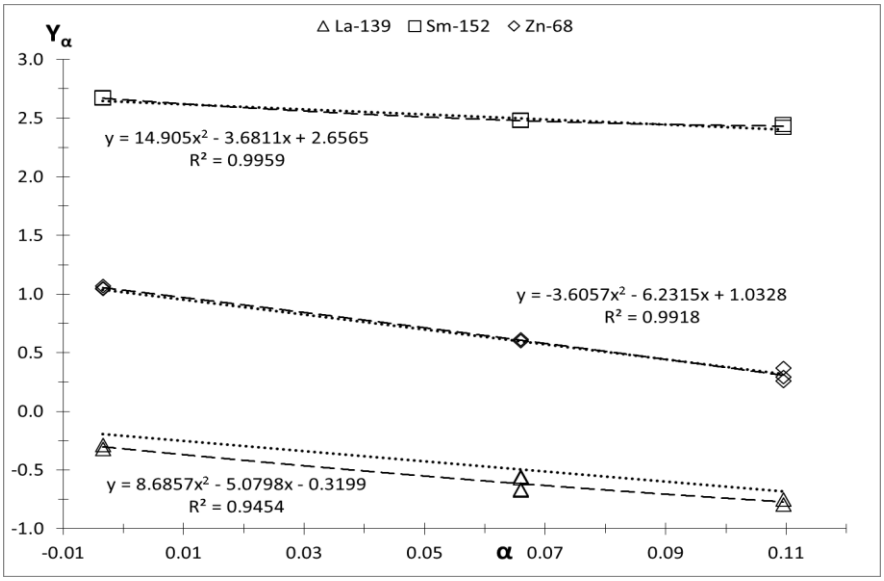

Figure 10.3: Graph of experimental Y_α values for ^{139}La(n,γ)^{140}La, ^{152}Sm(n,γ)^{153}Sm, ^{68}Zn(n,γ)^{69m}Zn vs. α.

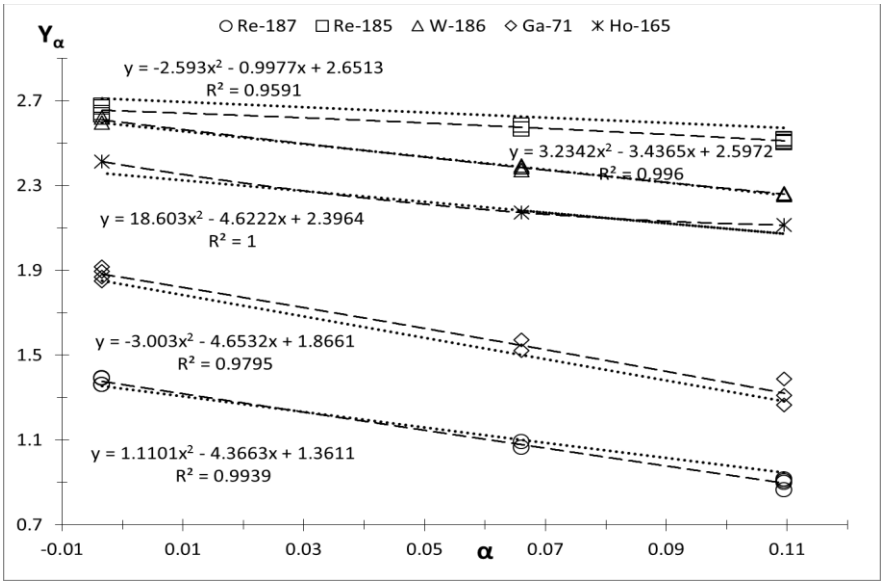

Figure 10.4: Graph of experimental Y_α values for $^{187}Re(n,\gamma)^{188}Re$, $^{185}Re(n,\gamma)^{186}Re$, $^{186}W(n,\gamma)^{187}W$ and $^{165}Ho(n,\gamma)^{166}Ho$ vs. α.

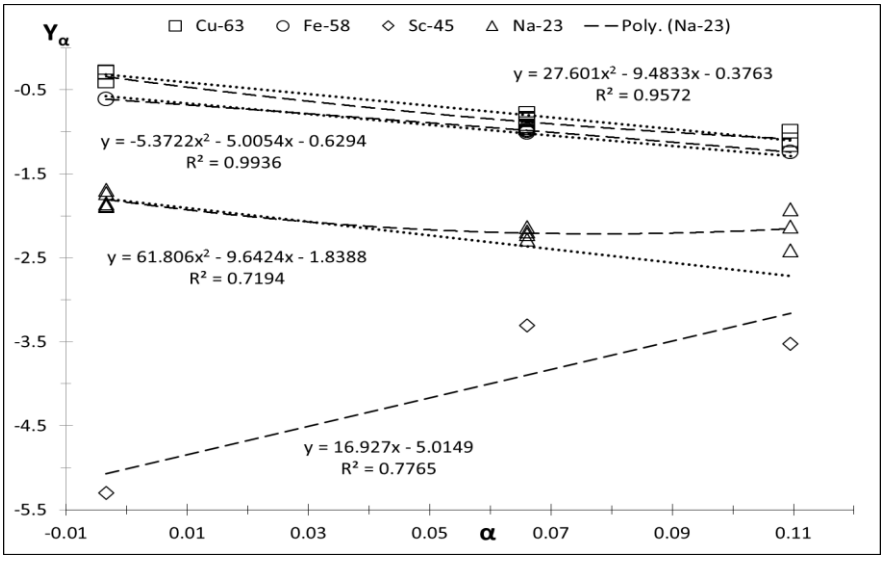

Figure 10.5: Graph of experimental Y_α values for $^{63}Cu(n,\gamma)^{64}Cu$, $^{58}Fe(n,\gamma)^{59}Fe$, $^{45}Sc(n,\gamma)^{46}Sc$ and $^{23}Na(n,\gamma)^{24}Na$ vs. α.

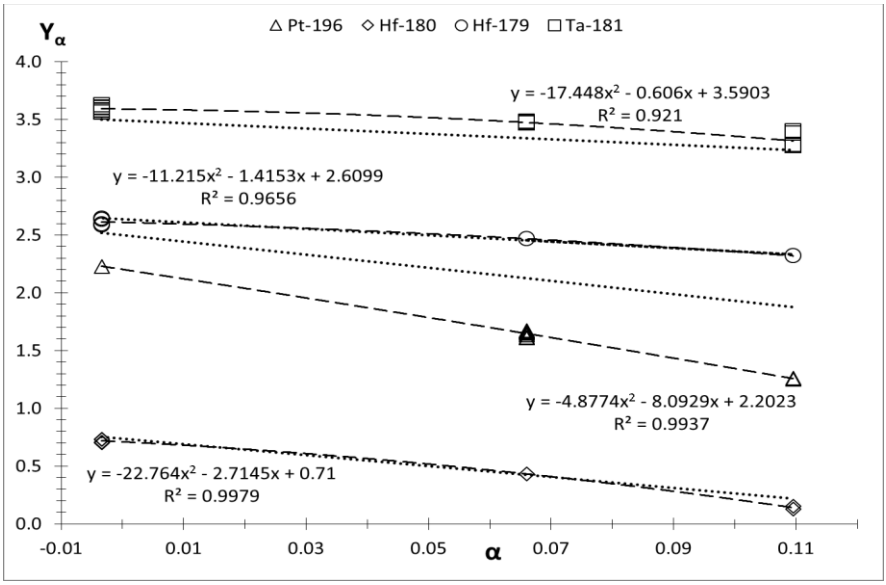

Figure 10.6: Graph of experimental Y_α values for ^{179}Hf(n,γ)^{180m}Hf, ^{180}Hf(n,γ)^{181}Hf, ^{181}Ta(n,γ)^{182}Ta and ^{196}Pt(n,γ)$^{197(m+g)}$Pt vs. *α*.

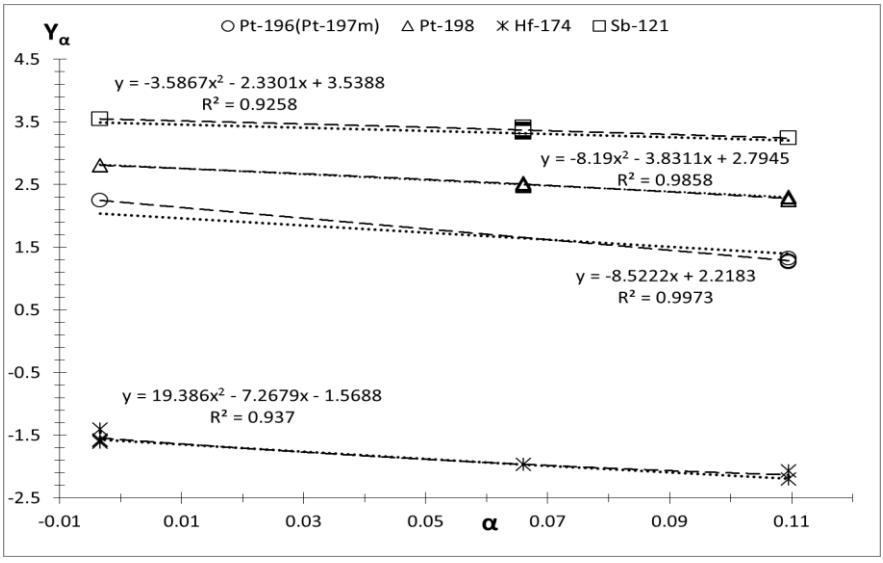

Figure 10.7: Graph of experimental Y_α values for ^{174}Hf(n,γ)^{175}Hf, ^{196}Pt(n,γ)^{197m}Pt, ^{198}Pt(n,γ)^{199}Pt →^{199}Au and ^{121}Sb(n,γ)^{122}Sb vs. *α*.

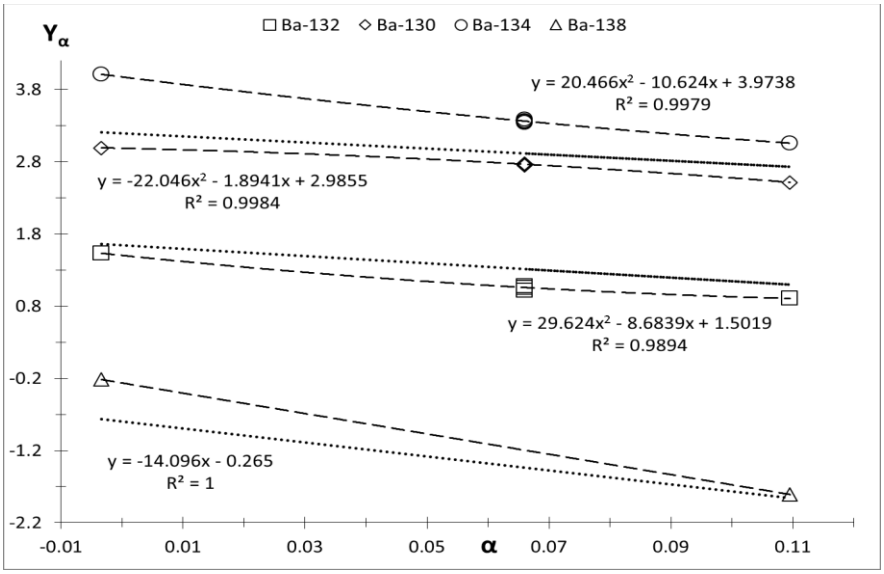

Figure 10.8: Graph of experimental Y_α values for $^{132}Ba(n,\gamma)^{133m}Ba$, $^{130}Ba(n,\gamma)^{131}Ba$, $^{134}Ba(n,\gamma)^{135m}Ba$ and $^{138}Ba(n,\gamma)^{139}Ba$ vs. α.

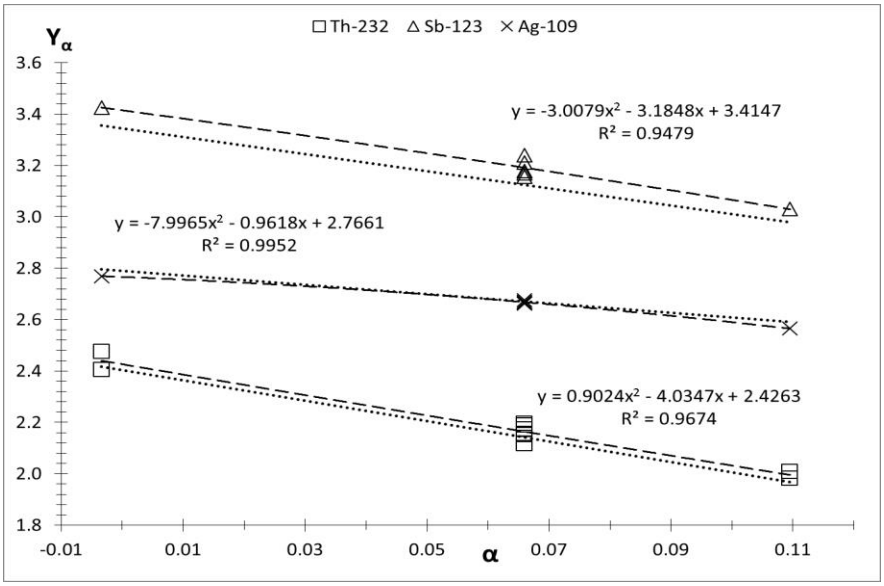

Figure 10.9: Graph of experimental Y_α values for $^{109}Ag(n,\gamma)^{110m}Ag$, $^{123}Sb(n,\gamma)^{124}Sb$ and $^{232}Th(n,\gamma)^{233}Th \rightarrow ^{233}Pa$ vs. α.

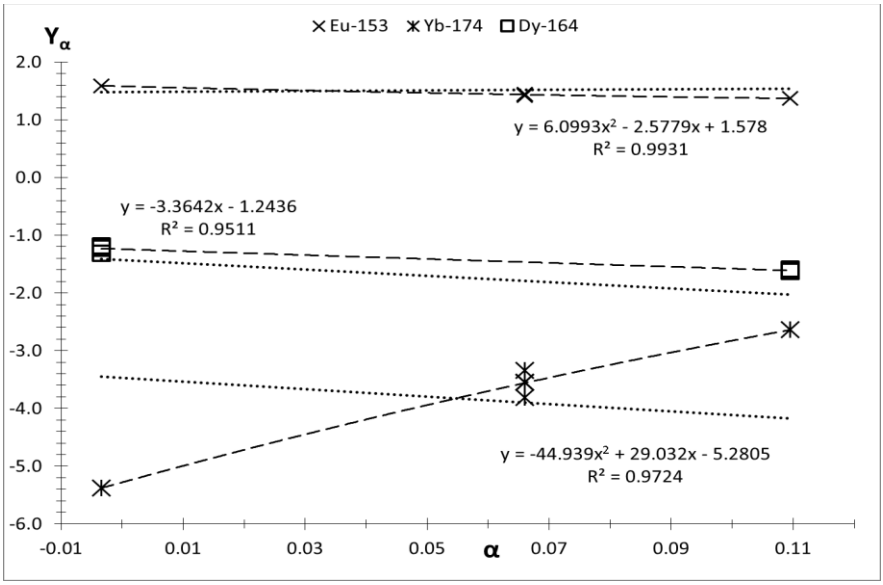

Figure 10.10: Graph of experimental Y_α values for ^{153}Eu(n,γ)^{154}Eu, ^{174}Yb(n,γ)^{175}Yb and ^{164}Dy(n,γ)^{165}Dy vs. α.

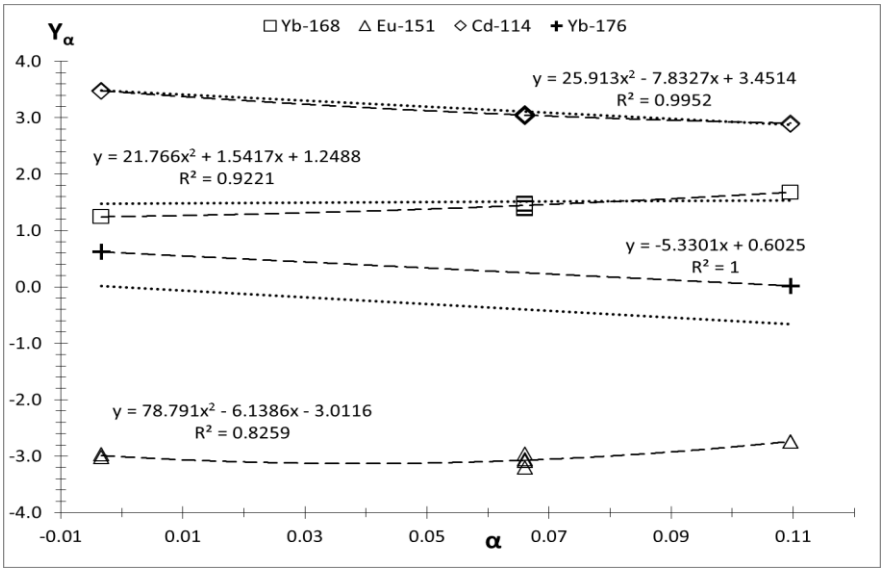

Figure 10.11: Graph of experimental Y_α values for ^{151}Eu(n,γ)^{152}Eu, ^{168}Yb(n,γ)^{169}Yb, ^{176}Yb(n,γ)^{177}Yb and ^{114}Cd(n,γ)^{115}Cd vs. α.

P-vectors or (p_1, $p2$, $p3$)-tuples

The Table 10.6 summarizes the P-vectors or (p_1,p_2,p_3)-tuples obtained for 36 target isotopes when assuming: A) a non-zero p_3 value as in eq. (6.14) with $N = 3$ and; B) when forcing the condition $p_3 = 0$ (no α-dependence) as in eq. (6.15).

Table 10.6: P-vectors or (p_1,p_2,p_3)-tuples obtained from the application of the α-vector method to 36 target isotopes and for the ADS in question, when: A) the p_3 is allowed to be non-zero (matrix form); B) the condition $p_3 = 0$ is enforced (least-squares linear method). From each P-vector a pair of Q_0, $\bar{E}_r$ and p values are obtained. A relationship between the 2 sets of $\bar{E}_r$ values is given in eq. (8.4).

	TI	^{23}Na	^{45}Sc	^{59}Fe	^{59}Co	^{63}Cu	^{64}Zn	^{68}Zn	^{71}Ga
	ADS	**IV/b**	**IV/b**	**I**	**IV/b**	**IV/b**	**I**	**I**	**IV/b**
A	p_1	-1.839	-5.136	-0.629	0.437	-0.376	0.386	1.033	1.866
	p_2	-9.642	47.478	-5.005	-4.085	-9.483	-6.500	-6.232	-4.653
	p_3	61.8	-299.2	-5.37	-6.1	27.6	-14.1	-3.6	-3.0
	$\bar{E}_r$ (in eV)	*15404*	*0.0*	*149*	*59.5*	*13138*	*665*	*509*	*105*
	Q_0 (or s_0)	*0.59*	*0.43*	*0.96*	*1.98*	*1.12*	*1.90*	*3.24*	*6.9*
B	p_1	-1.853	-5.015	-0.623	0.429	-0.398	0.388	1.034	1.866
	p_2	-3.604	16.927	-5.533	-4.688	-6.859	-7.905	-6.603	-4.959
	p_3	0	0	0	0	0	0	0	0
	$\bar{E}_r$ (in eV)	*36.7*	*0.0*	*253*	*109*	*952*	*2711*	*737*	*142*
	Q_0 (or s_0)	*0.59*	*0.44*	*0.97*	*1.96*	*1.10*	*1.90*	*3.24*	*6.9*
	$\bar{E}_{rA}/\bar{E}_{rB}$	419	0	0.59	0.55	13.8	0.25	0.69	0.74
	Q_{0A}/Q_{0B}	1.00	1.00	1.00	1.01	1.01	1.00	1.00	1.00
	Z_{p3}	-6.04	30.55	0.53	0.60	-2.62	1.41	0.37	0.31

	TI	^{75}As	^{94}Zr	^{98}Mo	^{109}Ag	^{121}Sb	^{123}Sb	^{115}Cd	^{133}Cs
	ADS	**I**	**I**	**I**	**I**	**IV/b**	**VI/c**	**I**	**I**
A	p_1	2.684	1.521	3.993	2.766	3.539	3.415	3.451	2.406
	p_2	-4.438	-8.204	-3.387	-0.962	-2.330	-3.185	-7.833	-1.883
	p_3	-2.4	-5.0	-24.1	-8.0	-3.6	-3.0	25.9	-0.5
	$\bar{E}_r$ *(in eV)*	*85*	*3655*	*30*	*2.62*	*10.3*	*24.2*	*2522*	*6.6*
	Q_0 *(or s_0)*	*15.1*	*5.01*	*54.6*	*16.3*	*34.9*	*30.8*	*32.0*	*11.5*
B	p_1	2.687	1.523	3.995	2.776	3.543	3.419	3.419	2.406
	p_2	-4.794	-8.742	-5.569	-1.743	-2.681	-3.479	-5.310	-1.937
	p_3	0	0	0	0	0	0	0	0
	$\bar{E}_r$ *(in eV)*	*121*	*6261*	*262*	*5.71*	*14.6*	*32.4*	*202*	*6.9*
	Q_0 *(or s_0)*	*15.1*	*5.02*	*54.8*	*16.5*	*35.0*	*31.0*	*31.0*	*11.5*
	$\bar{E}_{rA}/\bar{E}_{rB}$	0.70	0.58	0.11	0.46	0.70	0.75	12.46	0.95
	Q_{0A}/Q_{0B}	1.00	1.00	1.00	0.99	1.00	1.00	1.03	1.00
	Z_{p3}	0.36	0.54	2.18	0.78	0.35	0.29	-2.52	0.05

	TI	^{130}Ba	^{132}Ba	^{134}Ba	^{139}La	^{141}Pr	^{152}Sm	^{151}Eu *
	ADS	**IV/b**	**I**	**I**	**I**	**IV/b**	**I**	**IV/b**
A	p_1	2.986	1.502	3.974	-0.320	-0.061	2.657	-3.012
	p_2	-1.894	-8.684	-10.624	-5.080	-4.563	-3.681	-6.139
	p_3	-22.0	29.6	20.5	8.7	-3.0	14.9	78.8
	$\bar{E}_r$ *(in eV)*	*6.6*	*5907*	*41110*	*161*	*96*	*40*	*463*
	Q_0 *(or s_0)*	*20.2*	*4.92*	*53.6*	*1.16*	*1.37*	*14.7*	*0.05*
B	p_1	3.022	1.468	3.950	-0.327	-0.065	2.657	-3.073
	p_2	-4.060	-5.774	-8.613	-4.210	-4.810	-2.138	1.753
	p_3	0	0	0	0	0	0	0
	$\bar{E}_r$ *(in eV)*	*58.0*	*322*	*5503*	*67.3*	*122.7*	*8.5*	*0.17*
	Q_0 *(or s_0)*	*21.0*	*4.77*	*52.4*	*1.15*	*1.37*	*14.7*	*0.05*
	$\bar{E}_{rA}/\bar{E}_{rB}$	0.11	18.36	7.47	2.39	0.78	4.68	2675
	Q_{0A}/Q_{0B}	0.97	1.03	1.02	1.00	1.00	1.00	1.06
	Z_{p3}	2.17	-2.91	-2.01	-0.87	0.25	-1.54	-7.89

* s_0 factors ($W' = 0$ was assumed)

	TI	^{153}Eu *	^{165}Ho	^{168}Yb *	^{174}Hf	^{179}Hf	^{196}Pt	^{198}Pt
	ADS	**IV/b**	**I**	**IV/b**	**I**	**I**	**IV/b**	**V/b-d**
A	p_1	1.578	2.396	1.249	-1.569	2.610	2.205	2.795
	p_2	-2.578	-4.622	1.542	-7.268	-1.415	-8.093	-3.831
	p_3	6.1	18.6	21.8	19.4	-11.2	-4.9	-8.2
	$\bar{E}_r$ *(in eV)*	*13.2*	*102*	*0.21*	*1434*	*4.12*	*3271*	*46.1*
	Q_0 *(or* s_0*)*	*5.27*	*11.4*	*3.49*	*0.21*	*14.0*	*9.5*	*16.8*
B	p_1	1.570	2.389	1.220	-1.567	2.609	2.213	2.810
	p_2	-1.980	-2.723	3.660	-5.300	-2.496	-8.579	-4.734
	p_3	0	0	0	0	0	0	0
	$\bar{E}_r$ *(in eV)*	*7.24*	*15.2*	*0.03*	*200*	*12.1*	*5319*	*113.7*
	Q_0 *(or* s_0*)*	*5.24*	*11.3*	*3.39*	*0.21*	*14.0*	*9.6*	*17.0*
	$\bar{E}_{rA}/\bar{E}_{rB}$	1.82	6.68	8.32	7.16	0.34	0.62	0.41
	Q_{0A}/Q_{0B}	1.01	1.01	1.03	1.00	1.00	0.99	0.99
	Z_{p3}	-0.60	-1.90	-2.12	-1.97	1.08	0.49	0.90

* s_0 factors. We assumed $W' = 0$ for all these cases

	TI	**^{180}Hf**	**^{181}Ta**	**^{186}W**	**^{185}Re**	**^{187}Re**	**^{232}Th**
	ADS	**I**	**IV/b**	**I**	**I**	**IV/b**	**II/b**
A	p_1	0.710	3.590	2.597	2.651	1.361	2.426
	p_2	-2.715	-0.606	-3.437	-0.998	-4.366	-4.035
	p_3	-22.8	-17.4	3.2	-2.6	1.1	0.9
	$\bar{E}_r$ *(in eV)*	*15.1*	*1.83*	*31*	*2.7*	*79*	*56.5*
	Q_0 *(or* s_0*)*	*2.46*	*36.7*	*13.9*	*14.6*	*4.33*	*11.7*
B	p_1	0.707	3.594	2.595	2.651	1.361	2.425
	p_2	-5.026	-2.405	-3.095	-1.267	-4.251	-3.945
	p_3	0	0	0	0	0	0
	$\bar{E}_r$ *(in eV)*	*152*	*11.1*	*22.1*	*3.5*	*70.2*	*51.7*
	Q_0 *(or* s_0*)*	*2.46*	*36.8*	*13.8*	*14.6*	*4.33*	*11.7*
	$\bar{E}_{rA}/\bar{E}_{rB}$	0.10	0.17	1.41	0.76	1.12	1.09
	Q_{0A}/Q_{0B}	1.00	1.00	1.00	1.00	1.00	1.00
	Z_{p3}	2.31	1.80	-0.34	0.27	-0.12	-0.09

10.4 Results per irradiation channel

10.4.1 Results for (n,γ) reactions

The experimental Q_0 (or s_0) and $\bar{E}_r$ factors obtained in TW are summarized in Table 10.7 and Table 10.8 next to the Lit and Trkov values. The Q_0 (or s_0) values were found by means of:

A) the α-vector method applied to the 3 irradiation channels (S84, Y4, X26);

B) from the AVG of the results of all samples irradiated on each channel (Table 10.7) and from the mean of all channels employed (Table 10.8) when inputting the recommended $\bar{E}_r$ value in Lit [20, 23].

The uncertainty evaluation for a single Q_0 determination, i.e. a 1 channel exercise with 1 material measured in 1 detector, is given in section 7.7 while for a $\bar{E}_r$ value it is estimated from the standard error in the α-vector method (see section 6.3).

The Table 10.9 compiles the experimental k_0 values obtained in this work for the investigated formed nuclides from the mean and SD (in %) of all samples irradiated per irradiation channel but tabulated as ratios against the Lit or to the C value (theoretical). The AVG value in this case corresponds to the mean ratio from all channels employed. The uncertainty evaluation for a single k_0 determination is given in sections 7.6, 7.8 and 7.9.

Table 10.7: The Q_0 factors obtained in this work from eq. (2.59) applied in up to three different channels. Results from the AVG and SD (in %) of all materials employed when adopting the $\bar{E}_r$ factors from Lit.

TI	FN	ADS	Ch AVG		SD	TI	FN	ADS	Ch AVG		SD
^{23}Na	**^{24}Na**	**IV/b**	*S84*	*0.59*	*(2)*	**^{64}Ni**	**^{65}Ni**	**I**	*S84*	*0.46*	*(1)*
			Y4	*0.62*	*(2)*	**^{63}Cu**	**^{64}Cu**	**IV/b**	*S84*	*1.12*	*(4)*
			X26	*0.72*	*(10)*				*Y4*	*1.08*	*(3)*
^{26}Mg	**^{27}Mg**	**I**	*S84*	*0.46*	*(4)*				*X26*	*1.15*	*(5)*
^{27}Al	**^{28}Al**	**I**	*S84*	*0.54*	*(3)*	**^{65}Cu**	**^{66}Cu**	**I**	*S84*	*1.01*	*(1)*
^{37}Cl	**^{38}Cl**	**IV/b**	*S84*	*0.48*	*(6)*	**^{64}Zn**	**^{65}Zn**	**I**	*S84*	*1.89*	*(1)*
^{41}K	**^{42}K**	**I**	*Y4*	*0.74*	*(2)*				*Y4*	*1.93*	*(3)*
^{45}Sc	**^{46}Sc**	**IV/b**	*S84*	*0.42*	*(1)*				*X26*	*1.85*	*(6)*
			Y4	*0.49*	*(1)*	**^{68}Zn**	**^{69m}Zn**	**I**	*S84*	*3.24*	*(1)*
			X26	*0.50*	*(1)*				*Y4*	*3.22*	*(1)*
^{50}Ti	**^{51}Ti**	**I**	*S84*	*0.52*	*(2)*				*X26*	*3.17*	*(5)*
^{51}V	**^{52}V**	**I**	*S84*	*0.55*	*(4)*	**^{71}Ga**	**^{72}Ga**	**IV/b**	*S84*	*6.89*	*(3)*
^{50}Cr	**^{51}Cr**	**I**	*S84*	*0.46*	*(2)*				*Y4*	*6.97*	*(3)*
			Y4	*0.50*	*(2)*				*X26*	*6.94*	*(6)*

TI	FN	ADS	Ch AVG		SD	TI	FN	ADS	Ch AVG		SD
^{54}Mn	**^{55}Mn**	**I**	*S84*	*1.03*	*(3)*	**^{75}As**	**^{76}As**	**I**	*S84*	*15.0*	*(1)*
			X26	*1.06*	*(3)*				*Y4*	*15.1*	*(1)*
^{58}Fe	**^{59}Fe**	**I**	*S84*	*0.96*	*(1)*				*X26*	*14.8*	*(4)*
			Y4	*1.00*	*(1)*	**^{81}Br**	**^{82}Br**	**IV/b**	*Y4*	*19.3*	*(2)*
			X26	*1.01*	*(1)*	**^{85}Rb**	**^{86}Rb**	**IV/b**	*Y4*	*14.4*	*(2)*
^{59}Co	**^{60m}Co**	**I**	*S84*	*1.97*	*(3)*	**^{87}Rb**	**^{88}Rb**	**I**	*S84*	*25.9*	*(2)*
	^{60}Co	**IV/b**	*S84*	*1.96*	*(1)*						
			Y4	*2.01*	*(1)*						
			X26	*1.99*	*(1)*						

TI	FN	ADS	Ch AVG		SD	TI	FN	ADS	Ch AVG		SD
^{84}Sr	**^{85m}Sr**	**I**	*S84*	*13.0*	*(3)*	**^{108}Pd**	**^{109}Pd**	**IV/b**	*Y4*	*26.3*	*(4)*
	^{85}Sr	**IV/b**	*S84*	*14.6*	*(4)*		**^{109m}Ag**	**V/c**	*Y4*	*26.8*	*(4)*
			Y4	*14.5*	*(2)*	**^{110}Pd**	**^{111m}Pd**	**I**	*Y4*	*11.9*	*(3)*
^{86}Sr	**^{87m}Sr**	**I**	*S84*	*3.97*	*(2)*		**^{111}Ag**	**VII/c**	*Y4*	*9.9*	*(3)*
			Y4	*4.06*	*(1)*	**^{107}Ag**	**^{108}Ag**	**I**	*S84*	*2.72*	*(2)*
^{89}Y	**^{90m}Y**	**I**	*S84*	*4.08*	*(3)*	**^{109}Ag**	**^{110m}Ag**	**I**	*S84*	*16.3*	*(2)*
^{94}Zr	**^{95}Zr**	**I**	*S84*	*4.98*	*(2)*				*Y4*	*16.7*	*(1)*
			Y4	*5.06*	*(2)*				*X26*	*16.3*	*(1)*
			X26	*4.99*	*(3)*	**^{114}Cd**	**^{115}Cd**	**I**	*S84*	*31.8*	*(7)*
^{93}Nb	**^{94m}Nb**	**I**	*S84*	*7.28*	*(4)*				*Y4*	*30.3*	*(5)*
^{98}Mo	**^{99}Mo**	**I**	*S84*	*54.5*	*(6)*				*X26*	*32.5*	*(4)*
	^{99m}Tc	**II/d**	*Y4*	*56.0*	*(2)*		**^{115m}In**	**II/a**	*S84*	*32.3*	*(7)*
			X26	*50.9*	*(1)*				*Y4*	*30.4*	*(5)*
^{100}Mo	**^{101}Mo**	**I**	*S84*	*19.9*	*(1)*				*X26*	*33.1*	*(4)*
	^{101}Tc	**II/a**	*S84*	*19.9*	*(1)*						

TI	FN	ADS	Ch AVG		SD	TI	FN	ADS	Ch AVG		SD
^{96}**Ru**	^{97}**Ru**	**I**	*S84*	*26.3*	*(2)*	^{113}**In**	^{114m}**In**	**IV/b**	*Y4*	*24.0*	*(3)*
			Y4	*25.3*	*(2)*				*X26*	*24.2*	*(2)*
^{102}**Ru**	^{103}**Ru**	**I**	*S84*	*3.62*	*(2)*	^{115}**In**	^{116m}**In**	**IV/b**	*S84*	*16.7*	*(1)*
			Y4	*3.20*	*(3)*						
^{104}**Ru**	^{105}**Ru**	**I**	*S84*	*13.2*	*(1)*	^{112}**Sn**	^{113}**Sn**	**IV/b**	*Y4*	*47.6*	*(3)*
			Y4	*13.2*	*(2)*				*X26*	*49.1*	*(1)*
	^{105m}**Rh**	**II/a**	*S84*	*12.9*	*(1)*		^{113m}**In**	**V/c**	*Y4*	*47.5*	*(3)*
			Y4	*12.9*	*(1)*				*X26*	*49.1*	*(2)*
	^{105}**Rh**	**III/c**	*S84*	*13.2*	*(1)*	^{116}**Sn**	^{117m}**Sn**	**I**	*Y4*	*55.8*	*(3)*
			Y4	*13.1*	*(1)*				*X26*	*55.7*	*(3)*

TI	FN	ADS	Ch AVG		SD	TI	FN	ADS	Ch AVG		SD
^{124}Sn	^{125m}Sn	I				^{134}Ba	^{135m}Ba	I	*S84*	*54.7*	*(2)*
	^{125}Sn	I	*Y4*	*16.7*	*(4)*				*Y4*	*39.9*	*(1)*
			X26	*16.3*	*(3)*				*X26*	*36.0*	*(1)*
	^{125}Sb	VII/b	*Y4*	*16.3*	*(2)*	^{138}Ba	^{139}Ba	I	*S84*	*1.20*	*(1)*
			X26	*17.1*	*(1)*				*X26*	*0.90*	*(1)*
^{121}Sb	^{122}Sb	IV/b	*S84*	*34.8*	*(2)*	^{139}La	^{140}La	I	*S84*	*1.16*	*(2)*
			Y4	*34.9*	*(1)*				*Y4*	*1.15*	*(4)*
			X26	*34.3*	*(1)*				*X26*	*1.17*	*(2)*
^{123}Sb	^{124}Sb	VI/c	*S84*	*30.8*	*(2)*	^{141}Pr	^{142}Pr	IV/b	*S84*	*1.36*	*(1)*
			Y4	*30.8*	*(1)*				*Y4*	*1.43*	*(4)*
			X26	*30.2*	*(1)*				*X26*	*1.46*	*(6)*
^{133}Cs	^{134m}Cs	I	*S84*	*11.5*	*(1)*	^{152}Sm	^{153}Sm	I	*S84*	*14.8*	*(1)*
			Y4	*11.7*	*(2)*				*Y4*	*14.3*	*(1)*
			X26	*11.9*	*(2)*				*X26*	*14.8*	*(2)*

TI	FN	ADS	Ch AVG		SD	TI	FN	ADS	Ch AVG		SD
^{133}Cs	**^{134}Cs**	**IV/b**	*S84*	*14.5*	*(1)*	**^{151}Eu** *	**^{152}Eu**	**IV/b**	*S84*	*0.05*	*(5)*
			Y4	*14.8*	*(3)*				*Y4*	*0.04*	*(3)*
			X26	*15.0*	*(2)*				*X26*	*0.06*	*(4)*
		IV/a	*from I and IV/b*			**^{153}Eu** *	**^{154}Eu**	**IV/b**	*S84*	*4.86*	*(5)*
^{130}Ba	**^{131}Ba**	**IV/b**	*S84*	*20.1*	*(1)*				*Y4*	*4.71*	*(3)*
			Y4	*21.4*	*(1)*				*X26*	*4.77*	*(4)*
			X26	*20.1*	*(1)*	**^{152}Gd**	**^{153}Gd**	**I**	*Y4*	*0.56*	*(3)*
^{132}Ba	**^{133m}Ba**	**I**	*S84*	*5.0*	*(1)*	**^{158}Gd**	**^{159}Gd**	**I**	*Y4*	*31.2*	*(2)*
			Y4	*4.4*	*(1)*	**^{159}Tb**	**^{160}Tb**	**I**	*Y4*	*18.2*	*(4)*
			X26	*4.7*	*(1)*						

* s_0 factors instead of Q_0 factors, calculated by means of eq. (2.69) with $W' = 0$.

TI	FN	ADS	Ch AVG		SD	TI	FN	ADS	Ch AVG		SD
^{164}Dy	^{165}Dy	IV/b	*S84*	*0.14*	*(8)*	^{181}Ta	^{182}Ta	IV/b	*S84*	*36.5*	*(4)*
			X26	*0.07*	*(7)*				*Y4*	*38.1*	*(2)*
^{165}Ho	^{166}Ho	I	*S84*	*11.5*	*(2)*				*X26*	*36.0*	*(5)*
			Y4	*10.8*	*(1)*	^{186}W	^{187}W	I	*S84*	*13.9*	*(2)*
			X26	*11.3*	*(2)*				*Y4*	*13.7*	*(1)*
^{169}Tm	^{170}Tm	I	*Y4*	*13.3*	*(3)*				*X26*	*13.8*	*(1)*
^{168}Yb *	^{169}Yb	IV/b	*S84*	*3.47*	*(3)*	^{185}Re	^{186}Re	I	*S84*	*14.6*	*(2)*
			Y4	*4.11*	*(2)*				*Y4*	*14.6*	*(1)*
			X26	*5.08*	*(5)*				*X26*	*14.5*	*(1)*
^{174}Yb	^{175}Yb	IV/b	*S84*	*0.39*	*(5)*		^{188m}Re	I	*S84*	*4.54*	*(6)*
			Y4	*0.34*	*(3)*	^{187}Re	^{188}Re	IV/b	*S84*	*4.34*	*(2)*
			X26	*0.53*	*(5)*				*Y4*	*4.17*	*(2)*
^{176}Yb	^{177}Yb	IV/b	*S84*	*2.42*	*(3)*				*X26*	*4.07*	*(2)*
			X26	*2.60*	*(3)*			IV/a	*from I and IV/b*		

TI	FN	ADS	Ch AVG		SD	TI	FN	ADS	Ch AVG		SD
^{174}**Hf**	^{175}**Hf**	**I**	*S84*	*0.64*	*(2)*	^{196}**Pt**	^{197m}**Pt**	**I**	*S84*	*9.71*	*(3)*
			Y4	*0.60*	*(2)*				*X26*	*7.16*	*(2)*
			X26	*0.60*	*(4)*		^{197}**Pt**	**IV/b**	*S84*	*9.55*	*(3)*
^{179}**Hf**	^{180m}**Hf**	**I**	*S84*	*14.0*	*(1)*				*Y4*	*7.98*	*(2)*
			Y4	*14.6*	*(3)*				*X26*	*6.97*	*(2)*
			X26	*14.2*	*(2)*	^{198}**Pt**	^{199}**Au**	**V/b**	*S84*	*16.7*	*(2)*
^{180}**Hf**	^{181}**Hf**	**I**	*S84*	*2.45*	*(2)*			**V/d**	*Y4*	*17.1*	*(2)*
			Y4	*2.54*	*(3)*				*X26*	*16.7*	*(3)*
			X26	*2.36*	*(3)*	^{232}**Th**	^{233}**Pa**	**II/b**	*S84*	*11.8*	*(4)*
									Y4	*11.8*	*(3)*
									X26	*11.8*	*(2)*

* s_0 factors instead of Q_0 factors, calculated by means of eq. (2.69) with $W' = 0$.

The Table 10.8 provides a summary of these results and other adopted correlated values.

Table 10.8: Experimental Q_0 (or s_0) values obtained in TW by two approaches: A) the α-vector method: applied on three irradiation channels (S84, Y4 and X26) for simultaneous $\bar{E}_r$ and p_3 determination (see section 6.3 and Table 10.6); B) the classical method: through the AVG from the results of all channels after adopting the $\bar{E}_r$ factor from Lit (see eqs. (2.59), (2.73) and Table 10.7).

				$\bar{E}_r$ (%; 1s)						Q_0 (%; 1s)*					
				Lit B)		TW A)		Trkov	Others	Lit		TW			
												A)		B)	
Target	**FN**	**ADS**	p_3 **												
^{23}Na	**^{24}Na**	**IV/b**	**61.8**	3380	(11)	**36.7**	**(4)**	2178	2246	0.59	(10)	**0.59**	**(2)**	**0.63**	**(8)**
^{26}Mg	**^{27}Mg**	**I**		257000	(13)			376395	471341	0.64	(10)			**0.46**	**(2)**
^{27}Al	**^{28}Al**	**I**		11800	(6)			11628	12067	0.71	(10)			**0.54**	**(2)**
^{37}Cl	**^{38}Cl**	**IV/b**		13700	(14)			18267	35200	0.69	(10)			**0.48**	**(2)**
^{41}K	**^{42}K**	**I**		2960	(7)			3278	3303	0.87	(3)			**0.74**	**(2)**
^{45}Sc	**^{46}Sc**	**IV/b**	**(-)**	5130	(17)	**0.00**	**(25)**	1.15	0.79	0.43	(10)	**0.44**	**(2)**	**0.45**	**(8)**
^{50}Ti	**^{51}Ti**	**I**		63200	(13)			75074	81694	0.67	(10)			**0.52**	**(2)**
^{51}V	**^{52}V**	**I**		7230	(4)			2463	5359	0.55	(10)			**0.55**	**(2)**
^{50}Cr	**^{51}Cr**	**I**		7530	(16)	**0.027**	**(25)**	21295	155930	0.53	(10)	**0.46**	**(3)**	**0.48**	**(2)**

				$\bar{E}_r$ (%; 1s)						Q_0 (%; 1s)*					
				Lit B)		TW A)		Trkov	Others	Lit		TW			
												A)		B)	
Target	**FN**	**ADS**	p_3 **												
^{54}Mn	**^{55}Mn**	**I**	**0**	468	(11)	**341**	**(4)**	380	381	1.05	(6)	**1.03**	**(2)**	**1.04**	**(2)**
^{58}Fe	**^{59}Fe**	**I**	**-5.4**	637	(24)	**253**	**(9)**	489	518	0.975	(2)	**0.97**	**(2)**	**0.99**	**(2)**
^{59}Co	**^{60m}Co**	**I**	**6.06**	136	(5.1)	**109**	**(4)**	122	122	2.0	(10)			**1.97**	**(2)**
	^{60}Co	**IV/b**								1.99	(6)	**1.96**	**(2)**	**1.99**	**(2)**
^{64}Ni	**^{65}Ni**	**I**		14200	(12)			29471	13741	0.67	(10)			**0.46**	**(2)**
^{63}Cu	**^{64}Cu**	**IV/b**	**27.6**	1040	(5)	**952**	**(6)**	1274	1281	1.14	(10)	**1.10**	**(2)**	**1.11**	**(3)**
^{65}Cu	**^{66}Cu**	**I**		766	(17)			765	771	1.06	(10)			**1.01**	**(2)**
F_{Cd} = 1.03															
^{64}Zn	**^{65}Zn**	**I**	**-14.1**	2560	(10)	**2711**	**(7)**	3009	2798	1.91	(5)	**1.90**	**(2)**	**1.90**	**(2)**
^{68}Zn	**^{69m}Zn**	**I**	**-3.6**	590	(10)	**737**	**(4)**	597	605	3.19	(1.4)	**3.24**	**(2)**	**3.21**	**(2)**
^{71}Ga	**^{72}Ga**	**IV/b**	**-3.0**	154	(12)	**142**	**(3)**	166	166	6.69	(1.2)	**6.89**	**(2)**	**6.94**	**(2)**
^{75}As	**^{76}As**	**I**	**-2.4**	106	(34)	**121**	**(3)**	127	127	13.6	(10)	**15.1**	**(2)**	**15.0**	**(2)**
^{81}Br	**^{82}Br**	**IV/b**		152	(9)			168	168	19.3	(3)			**19.3**	**(2)**
^{85}Rb	**^{86}Rb**	**IV/b**		839	(9)			1413	1416	14.8	(3)			**14.4**	**(2)**

				$\bar{E}_r$ (%; 1s)						Q_0 (%; 1s)*					
				Lit B)		TW A)		Trkov	Others	Lit		TW			
												A)		B)	
Target	**FN**	**ADS**	p_3 **												
^{87}Rb	**^{88}Rb**	**I**		364	(3)			413	413	23.3	(3)			**25.9**	**(2)**
^{84}Sr	**^{85m}Sr**	**I**		469	(7)	**506**	**(25)**	930		14.5	(2)			**13.0**	**(3)**
	^{85}Sr	**IV/b**								13.2	(10)	**14.6**	**(2)**	**14.5**	**(2)**
^{86}Sr	**^{87m}Sr**	**I**		795	(2)	**502**	**(25)**	932		4.11	(2)	**3.95**	**(2)**	**4.04**	**(2)**
^{89}Y	**^{90m}Y**	**I**		4300	(8)			9694	11059	5.93	(2)			**4.08**	**(2)**
^{94}Zr	**^{95}Zr**	**I**	**-5.0**	6260	(5)	**6261**	**(5)**	12927		5.31	(3)	**5.02**	**(3)**	**5.02**	**(2)**
^{96}Zr	**^{97}Zr**	**I**		338	(2)			343		251.6	(1)			recommended; adopted because Q_0>>f for any channel in TW	
	^{97m}Nb	**II/a**													
	^{97}Nb	**III/a**													
^{93}Nb	**^{94m}Nb**	**I**		574	(8)			826	938	7.35	(3)			**7.28**	**(2)**
^{98}Mo	**^{99}Mo - ^{99m}Tc**	**I - II/d**	**-24.1**	241	(10)	**262**	**(5)**	319.5	266.1	53.1	(6)	**54.8**	**(3)**	**54.0**	**(4)**
^{100}Mo	**^{101}Mo**	**I**		672	(14)			878.9		18.8	(4)			**19.9**	**(2)**
	^{101}Tc	**II/a**													

				$\bar{E}_r$ (%; 1s)						Q_0 (%; 1s)*					
				Lit B)		TW A)		Trkov	Others	Lit		TW			
												A)		B)	
Target	**FN**	**ADS**	p_3 **												
^{96}Ru	**^{97}Ru**	**I**		776	(16)	**1343**	**(25)**	1452		26.5	(4)	**26.2**	**(2)**	**25.6**	**(2)**
^{102}Ru	**^{103}Ru**	**I**		181	(4)	**1556**	**(25)**	526		3.63	(10)	**3.60**	**(2)**	**3.35**	**(3)**
^{104}Ru	**^{105}Ru**	**I**		495	(10)	**504**	**(25)**	737.5		12.8	(3)	**13.1**	**(2)**	**13.1**	**(2)**
	^{105m}Rh	**II/a**													
	^{105}Rh	**III/c**													
^{108}Pd	**^{109}Pd**	**IV/b**		39.7	(5)			40.2		26.6	(2)			**26.6**	**(4)**
	^{109m}Ag	**V/c**													
^{110}Pd	**^{111m}Pd**	**I**		950	(9)			1635		11.9	(15)			**11.9**	**(3)**
	^{111}Ag	**VII/c**								10-14 [e]	(15)			**9.9**	**(3)**
^{107}Ag	**^{108}Ag**	**I**		39	(5)					2.90	(10)			**2.72**	**(2)**
^{109}Ag	**^{110m}Ag**	**I**	**-8**	6.08	(1)	**5.7**	**(7)**	6.03		16.7	(4)	**16.5**	**(2)**	**16.5**	**(2)**
^{114}Cd	**^{115}Cd**	**I**	**25.9**	207	(19)	**202**	**(33)**	288		32.4	(10)	**31.0**	**(4)**	**31.4**	**(4)**
F_{Cd} = 0.40 [a]	**^{115m}In**	**II/a**													
^{113}In	**^{114m}In**	**IV/b**		6.41	(15)	**5.0**	**(25)**	8.55		24.2	(2)	**23.7**	**(2)**	**24.1**	**(2)**

				$\bar{E}_r$ (%; 1s)						Q_0 (%; 1s)*					
				Lit B)		TW A)		Trkov	Others	Lit		TW A)		TW B)	
Target	**FN**	**ADS**	p_3 **												
^{115}In	**^{116m}In**	**IV/b**		1.56	(7)			1.52		16.8	(2)			**16.7**	**(2)**
F_{Cd} = **0.927**															
^{112}Sn	**^{113}Sn**	**IV/b**		107	(3)	**49.9**	**(25)**	148.5		48.4	(1)	**45.2**	**(3)**	**48.3**	**(3)**
	^{113m}In	**V/c**													
^{116}Sn	**^{117m}Sn**	**I**		128	(3)	**130**	**(25)**	183		56.3	(2)	**55.9**	**(3)**	**55.8**	**(3)**
^{124}Sn	**^{125m}Sn**	**I**		74	(7)	**76.6**	**(25)**	69.2		60.1 **	(3)				
	^{125}Sn	**I**								17.2	(11)	**16.2**	**(2)**	**16.7**	**(2)**
	^{125}Sb	**VII/b**													
^{121}Sb	**^{122}Sb**	**IV/b**	**-3.6**	13.1	(4)	**14.6**	**(4)**	14.45		33.0	(4)	**35.0**	**(3)**	**34.7**	**(2)**
F_{Cd} = **0.99**															
^{123}Sb	**^{124}Sb**	**VI/c**	**-3.0**	28.2	(6)	**32.4**	**(5)**	31.93		28.8	(4)	**31.0**	**(3)**	**30.5**	**(2)**
^{133}Cs	**^{134m}Cs**	**I**	**-0.42**	9.27	(11)	**6.93**	**(4)**	9.92		11.8	(3)	**11.5**	**(2)**	**11.7**	**(2)**
	^{134}Cs	**IV/b**								12.7	(10)	**14.5**	**(2)**	**14.8**	**(2)**
		IV/a								13.2	(10)	**14.8**	**(3)**	**15.1**	**(2)**

				$\bar{E}_r$ (%; 1s)						Q_0 (%; 1s)*					
				Lit B)		TW A)		Trkov	Others	Lit		TW			
												A)		B)	
Target	**FN**	**ADS**	p_3 **												
^{130}Ba	**^{131}Ba**	**IV/b**	**-22**	69.9	(5)	**58.0**	**(3)**	87.8	88.3	24.8 ***	(10)	**21.0**	**(2)**	**20.7**	**(3)**
^{132}Ba	**^{133m}Ba**	**I**	**29.6**	143	(10)	**322**	**(3)**	219.7	219.7	5.6	(10)	**4.8**	**(2)**	**4.6**	**(5)**
^{134}Ba	**^{135m}Ba**	**I**	**20.5**	115	(-)	**5503**	**(20)**	177	115	55.8	(-)	**52.4**	**(3)**	**43.5**	**(12)**
^{138}Ba	**^{139}Ba**	**I**		15700	(3.2)	**1323778**	**(25)**	5238	5342	0.88	(10)	**1.20**	**(3)**	**1.04**	**(15)**
^{139}La	**^{140}La**	**I**	**8.7**	76.0	(3.9)	**67.3**	**(3)**	92.6	92.1	1.24	(10)	**1.15**	**(2)**	**1.16**	**(2)**
^{141}Pr	**^{142}Pr**	**IV/b**	**-3.0**	296	(4.1)	**123**	**(5)**	442		1.51	(10)	**1.37**	**(2)**	**1.41**	**(3)**
^{152}Sm	**^{153}Sm**	**I**	**14.9**	8.53	(1.1)	**8.48**	**(5)**	8.26		14.4	(2)	**14.7**	**(2)**	**14.6**	**(2)**
^{151}Eu	**^{152}Eu**	**IV/b**	**78.8**	0.448	(-)	**0.17**	**(20)**	4.93		1.25	(-)	**0.05**	**(5)**	**0.05**	**(18)**
^{153}Eu	**^{154}Eu**	**IV/b**	**6.1**	5.8	(4)	**7.24**	**(20)**	9.54		5.90	(10)	**4.81**	**(3)**	**4.75**	**(3)**
^{152}Gd	**^{153}Gd**	**I**		16.7	(9)			119.6		0.77	(15)			**0.56**	**(3)**
^{158}Gd	**^{159}Gd**	**I**		48	(8)			48.0		29.9	(3)			**31.2**	**(2)**
^{159}Tb	**^{160}Tb**	**I**		18.1	(15)			25	25	17.9	(4)			**18.2**	**(2)**
^{164}Dy	**^{165}Dy**	**IV/b**		224	(5)	**28.9**	**(25)**	6.27		0.19	(10)	**0.72**	**(4)**	**0.13**	**(22)**

				$\bar{E}_r$ (%; 1s)						Q_0 (%; 1s)*					
				Lit B)		TW A)		Trkov	Others	Lit		TW			
												A)		B)	
Target	**FN**	**ADS**	p_3 **												
^{165}Ho	**^{166}Ho**	**I**	**18.6**	12.3	(3.3)	**15.23**	**(6)**	14.64	14.63	10.9	(3)	**11.3**	**(2)**	**11.2**	**(3)**
F_{Cd} = 0.99															
^{169}Tm	**^{170}Tm**	**I**		4.8	(2)			5.2		13.7	(2)			**13.3**	**(3)**
^{168}Yb	**^{169}Yb**	**IV/b**	**21.8**	0.61	(-)	**0.026**	**(25)**	0.58	0.61	4.97	(-)	**3.39**	**(4)**	**4.17**	**(12)**
^{174}Yb	**^{175}Yb**	**IV/b**		602	(8)	**0.115**	**(30)**	0.114	602.5	0.46	(10)	**0.48**	**(4)**	**0.38**	**(19)**
^{176}Yb	**^{177}Yb**	**IV/b**		412	(5)	**190**	**(25)**	593	421	2.50	(2)	**2.43**	**(3)**	**2.51**	**(3)**
^{176}Lu	**^{177}Lu**	**I**		0.158	(-)			999999		1.67	(10)	*Temperature monitor*			
^{174}Hf	**^{175}Hf**	**I**	**19.4**	29.6	(7)	**200**	**(22)**	212		0.78	(10)	**0.64**	**(3)**	**0.61**	**(3)**
^{179}Hf	**^{180m}Hf**	**I**	**-11.2**	16	(12)	**12.1**	**(15)**	21.7		14.4	(3)	**14.0**	**(2)**	**14.1**	**(2)**
^{180}Hf	**^{181}Hf**	**I**	**-22.8**	115	(6)	**152**	**(8)**	158.4		2.52	(4)	**2.46**	**(2)**	**2.44**	**(3)**
^{181}Ta	**^{182}Ta**	**IV/b**	**-17.4**	10.4	(6)	**11.1**	**(15)**	11.55		33.3	(10)	**36.8**	**(3)**	**37.0**	**(4)**
F_{Cd} = 0.972															
^{186}W	**^{187}W**	**I**	**3.2**	20.5	(1)	**22.1**	**(3)**	20.2	20.2	13.7	(2)	**13.8**	**(2)**	**13.8**	**(2)**
F_{Cd} = 0.91															

				$\bar{E}_r$ (%; 1s)						Q_0 (%; 1s)*					
				Lit B)		TW A)		Trkov	Others	Lit		TW			
												A)		B)	
Target	FN	ADS	p_3 **												
^{185}Re	^{186}Re	I	**-2.6**	3.40	(4.1)	**3.55**	**(4)**	3.64		15.4	(3)	**14.6**	**(3)**	**14.6**	**(2)**
F_{Cd} = 0.98															
	^{188m}Re	I	**1.1**							4.57	(3)			**4.54**	**(3)**
^{187}Re	^{188}Re	IV/b		41.1	(3.9)	**70.2**	**(3)**	58.9		4.35	(10)	**4.33**	**(2)**	**4.19**	**(3)**
		IV/a								4.34	(3)	**4.32**	**(3)**	**4.18**	**(4)**
^{196}Pt	^{197m}Pt	I	**-4.9**	*from Others*		**5319**	**(5)**		291	7.95 [b]		**9.62**	**(4)**	**8.44** [c]	**(15)**
	^{197}Pt	IV/b								12.6 [b]		**9.57**	**(4)**	**8.17** [c]	**(12)**
^{198}Pt	^{199}Au	V/b - V/d	**-8.2**	106	(3)	**114**	**(8)**	523	106	17.0	(2)	**17.0**	**(2)**	**16.9**	**(2)**
^{232}Th	^{233}Pa	II/b	**0.9**	54.4	(1)	**51.7**	**(3)**	72.6		11.5	(4)	**11.7**	**(2)**	**11.8**	**(2)**

				$\bar{E}_r$ (%; 1s)				Q_0 (%; 1s)*		
				Lit B)	TW A)	Trkov	Others	Lit	TW	
Target	**FN**	**ADS**	p_3 **						**A)**	**B)**
^{197}Au [d] **F_{Cd} = 0.991**	**^{198}Au**	**I**		5.65 (7)		5.631	5.86	15.7 (2)	*The comparator*	

The typical uncertainty on our experimental $\bar{E}_r$ values is ~25% when not mentioned (determined with 2 channels). All uncertainties in % at the 1*s* confidence level.

* s_0 factors are reported for ^{151}Eu, ^{153}Eu, ^{168}Yb and ^{176}Lu instead of Q_0 factors. We assumed $W' = 0$ for all these cases.

** The use of p_3 values is not compulsory. These could be employed along the $\bar{E}_r$ factors and the eq. (8.4) with α_0 = -0.1 as obtained in this work (see Figure 8.1).

*** Erroneous value identified and redetermined (Q_0 = 21.3 ± 0.9) by Smodis et al. in reference [49] (1994). It was not updated into the 2003 k_0-library [20] or 2012 k_0-library [23].

[a] The F_{Cd} =0.400(24) value for ^{114}Cd was found in this work. All other F_{Cd} values were adopted from reference [13] since these factors are not compiled anymore in the latest recommended compilations [20, 23].

[b] Q_0 factors calculated according to the Q_0 definition (for the given ADS) with nuclear data from [1].

[c] Q_0 factors calculated with $\bar{E}_r$ = 291 ± 44 eV from reference [107].

[d] For the comparator s_0 = 17.2 and W' = 0.055 [20, 23, 48]. The s_0 factor has a 10% half-width uncertainty per these references.

Table 10.9: Ratios of experimental k_0 factors found in TW from the mean and SD of all samples studied on channels Y4, S84, X26 and the thermal Cavity (double underlined) against the Lit or C values. The AVG values are the mean ratios from all channels.

	γ	k_0 (%; 1s)			TW / [Lit or C] (% SD)						I_γ / $I_{\gamma,ref}$		σ (b)
FN	**(keV)**	**C**	**Lit**		**AVG**	**Y4 /Cavity**		**S84**		**X26**	I_γ	**TW / C**	**Lit / C**	**TW**
^{24}Na [IV/b] <- F_2 - ^{24m}Na [I]	**1368.6**	4.70E-02	4.68E-02	(1.0)	***1.01***	1.02	(1.5)	1.02	(1.5)		*99.994*	reference		**0.518**
						0.99	(1.4)	0.99	(1.4)					
	2754.0	4.69E-02	4.62E-02	(0.5)	***1.02***	1.04	(1.8)	1.04	(1.8)		*99.855*	1.00	1.01	**0.520**
						1.01	(1.7)	1.01	(1.7)					
^{27}Mg [I]	**170.7**	3.12E-06	3.02E-06	(1.0)	***1.00***			1.00	(1.2)		*0.86*	1.01	1.00	**0.0371**
	843.8	2.60E-04	2.53E-04	(0.5)	***1.00***			1.00	(0.8)		*71.8*	reference		**0.0374**
	1014.4	1.02E-04	9.80E-05	(0.2)	***1.01***			1.01	(0.7)		*28.2*	1.01	1.01	**0.0371**

FN	γ (keV)	k_0 (%; 1s) C	k_0 (%; 1s) Lit		TW / [Lit or C] (% SD) AVG	Y4 /Cavity		S84		X26	I_γ	I_γ / $I_{\gamma,ref}$ TW / C	I_γ / $I_{\gamma,ref}$ Lit / C	σ (b) TW
^{28}Al [I]	**1778.9**	1.79E-02	1.75E-02	(0.8)	***1.01***			1.03	(0.5)		*100*	reference		**0.2298**
								1.00	(0.5)					
^{38}Cl [IV/b] <-F_2 = 1- ^{38m}Cl [I]	**1642.7**	2.06E-03	1.97E-03	(1.4)	***0.99***			0.99	(1.5)		*33.3*	1.01	1.01	**0.410**
	2167.4	2.75E-03	2.66E-03	(1.3)	***0.99***			0.99	(1.5)		*44.4*	reference		**0.415**
^{42}K [I]	**312.7**	1.76E-05	1.59E-05	(1.1)	***1.10***	1.10	(1.0)	1.10	(1.1)		*0.336*	1.00	1.11	**1.449**
	1524.7	9.49E-04	9.46E-04	(0.6)	***1.00***	1.00	(0.4)	1.00	(0.9)		*18.08*	reference		**1.453**

FN	γ (keV)	k_0 (%; 1s) C	k_0 (%; 1s) Lit		TW / [Lit or C] (% SD) AVG	Y4 /Cavity		S84		X26		I_γ	I_γ / $I_{\gamma,ref}$ TW / C	I_γ / $I_{\gamma,ref}$ Lit / C	σ (b) TW
^{46}Sc [IV/b] <- F_2 = 1 - ^{46m}Sc															
^{46}Sc	**889.3**	1.26E+00	1.22E+00	(0.4)	***1.03***	1.02	(0.5)	1.02	(0.7)	1.03	(1.0)	*99.984*	1.00	1.00	**27.0**
	1120.5	1.26E+00	1.22E+00	(1.1)	***1.02***	1.02	(0.4)	1.02	(0.7)	1.02	(1.0)	*99.987*	reference		**26.8**
^{51}Ti [I]	**320.1**	3.77E-04	3.74E-04	(1.0)	***0.99***			0.99	(1.0)			*93.1*	reference		**0.1757**
	928.0	2.79E-05	2.65E-05	(1.3)	***1.00***			1.00	(1.5)			*6.9*	1.04	1.05	**0.1692**
^{52}V [I]	**1434.0**	2.00E-01	1.96E-01	(1.2)	***1.00***			1.00	(1.1)			*100*	reference		**4.77**

FN	γ (keV)	k_0 (%; 1s) C	k_0 (%; 1s) Lit		TW / [Lit or C] (% SD) AVG	Y4 /Cavity		S84		X26		I_γ	I_γ / $I_{\gamma,ref}$ TW / C	I_γ / $I_{\gamma,ref}$ Lit / C	σ (b) TW
^{51}Cr [I]	**320.1**	2.66E-03	2.62E-03	(0.4)	***0.95***	0.95	(0.8)	0.96	(0.8)		**IRMM**	*9.91*	reference		**14.41**
		Average between the IRMM (up) and the Goodfellow (down) material				0.95	(0.7)	0.94	(0.9)						
						0.96	(1.9)	0.96	(1.8)						
						0.95	(1.6)	0.94	(1.7)		**GF**				
						0.96	(1.9)	0.96	(1.9)						
^{56}Mn [I]	**846.8**	5.02E-01	4.96E-01	(0.6)	***1.00***	0.99	(0.5)	0.99	(0.6)	1.00	(0.7)	*98.85*	reference		**13.14**
	1810.7	1.37E-01	1.35E-01	(0.4)	***0.98***	0.98	(0.7)	0.99	(0.7)	0.98	(0.8)	*26.9*	1.02	1.00	**12.93**
	2113.1	7.22E-02	7.17E-02	(0.2)	***0.98***	0.98	(0.2)	0.98	(0.7)	0.98	(0.8)	*14.2*	1.01	0.99	**13.04**
^{59}Fe [I]	**142.7**	1.42E-06	1.33E-06	(1.6)	***1.00***	1.00	(1.2)	0.98	(2.0)	1.02	(1.8)	*1.02*	1.05	1.05	**1.24**
	192.3	4.29E-06	3.78E-06		***1.02***	1.02	(0.7)	1.03	(1.0)	1.01	(0.8)	*3.08*	1.10	1.12	**1.19**
	1099.3	7.87E-05	7.77E-05	(0.5)	***1.00***	1.00	(0.5)	1.00	(1.1)	1.00	(0.7)	*56.50*	reference		**1.30**
	1291.6	6.02E-05	5.93E-05	(0.4)	***0.99***	1.00	(0.7)	0.99	(1.2)	0.99	(0.8)	*43.20*	1.01	1.00	**1.29**

FN	γ (keV)	k_0 (%; 1s) C	k_0 (%; 1s) Lit		TW / [Lit or C] (% SD) AVG	Y4 /Cavity		S84		X26		I_γ	I_γ / $I_{\gamma,ref}$ TW / C	I_γ / $I_{\gamma,ref}$ Lit / C	σ (b) TW
^{60}Co [IV/d]-[IV/b] <- F_2=1- ^{60m}Co [I]	**58.6**	1.47E-02	1.51E-02	(0.8)	***0.97***			0.97	(1.2)			*2.036*	reference		**20.4**
	1332.5	1.74E-03	1.75E-03	(1.4)	***1.02***			1.02	(1.4)			*0.240*	0.97	1.02	**21.0**
	1173.2	1.32E+00	1.32E+00	(0.4)	***1.00***	1.00	(0.3)	1.00	(0.6)	0.99	(1.0)	*99.850*	1.00	1.00	**37.17**
	1332.5	1.32E+00	1.32E+00	(0.5)	***1.00***	0.99	(0.4)	1.00	(0.7)	1.00	(1.0)	*99.983*	reference		**37.14**
	1332.5		5.93E-01		***1.00***			1.00	(1.0)			γ_2 / γ_3	**0.0E+00**		**16.7**
													2.4E-03		
^{65}Ni [I]	**366.3**	2.60E-05	2.51E-05	(1.0)	***1.01***			1.01	(1.1)			*4.81*	1.01	1.03	**1.61**
	1115.5	8.34E-05	8.14E-05	(0.5)	***1.00***			1.00	(1.0)			*15.43*	1.01	1.02	**1.60**
	1481.8	1.27E-04	1.27E-04	(0.6)	***0.99***			0.99	(1.3)			*23.59*	reference		**1.62**

	γ	k_0 (%; 1s)			TW / [Lit or C] (% SD)							I_γ / $I_{\gamma,ref}$			σ (b)
FN	**(keV)**	**C**	**Lit**		**AVG**	**Y4 /Cavity**		**S84**		**X26**		I_γ	**TW / C**	**Lit / C**	**TW**
^{64}Cu [I]	**511.0**	3.58E-02	3.70E-02		***0.90***	0.90	(0.7)	0.90	(1.1)	0.90	(1.0)	*35.00*	reference		**4.17**
	1345.8	4.86E-04	4.98E-04	(0.9)	***0.98***	0.98	(0.7)	0.98	(0.8)	0.98	(2.0)	*0.475*	0.92	1.01	**4.52**
^{66}Cu [I]	**1039.2**	2.03E-03	1.86E-03	(0.5)	***1.04***			1.04	(1.0)			*9.23*	reference		**2.06**
^{65}Zn [I]	**511.0**	3.53E-04			***0.91***	0.91	(2.0)					*2.842*	1.00		**0.718**
	1115.5	6.23E-03	5.72E-03	(0.4)	***0.99***	1.00	(0.5)	0.98	(2.0)	0.99	(1.3)	*50.22*	reference		**0.718**
^{69m}Zn [I]	**438.6**	4.02E-04	3.98E-04	(0.6)	***1.00***	1.00	(1.0)	1.01	(0.4)	0.99	(0.6)	*94.77*	reference		**0.071**

	γ	k_0 (%; 1s)			TW / [Lit or C] (% SD)								I_γ / $I_{\gamma,ref}$		σ (b)
FN	**(keV)**	**C**	**Lit**		**AVG**	**Y4 /Cavity**		**S84**		**X26**		I_γ	**TW / C**	**Lit / C**	**TW**
^{72}Ga [IV/b] <-------- F_2=1 --- ^{72m}Ga [I]	**289.5**	1.10E-04			***0.99***	1.02	(1.2)	0.98	(2.0)	0.98	(0.3)	*0.199*	1.01		**4.58**
	381.7	1.68E-04			***0.99***	0.99	(0.6)	1.00	(5.7)	0.99	(1.0)	*0.304*	1.01		**4.55**
	428.6	1.19E-04			***0.99***	0.99	(0.7)	0.99	(1.0)	1.00	(1.3)	*0.216*	1.01		**4.55**
	600.9	3.21E-03			***0.99***	0.99	(0.3)	0.98	(1.9)	1.01	(0.5)	*5.822*	1.01		**4.57**
	630.0	1.44E-02	1.49E-02		***0.97***	0.97	(0.4)	0.97	(0.6)	0.98	(0.6)	*26.13*	0.99	0.96	**4.64**
	786.5	1.84E-03			***1.00***	0.99	(0.6)	0.99	(2.3)	1.01	(0.7)	*3.34*	1.00		**4.60**
	810.3	1.15E-03			***1.00***	0.99	(0.4)	0.99	(1.9)	1.01	(1.1)	*2.087*	1.00		**4.60**
	834.1	5.26E-02	5.23E-02	(0.6)	***1.01***	1.01	(0.3)	1.00	(0.5)	1.01	(0.6)	*95.45*	reference		**4.61**
	894.3	5.59E-03	5.46E-03	(0.9)	***1.02***	1.03	(0.6)	1.01	(1.2)	1.03	(1.1)	*10.14*	1.00	1.02	**4.60**
	970.8	6.08E-04			***1.00***	1.00	(0.3)	1.00	(0.5)	0.99	(0.4)	*1.103*	1.00		**4.63**
	1050.8	3.85E-03	3.83E-03	(0.8)	***1.01***	1.01	(0.4)	1.00	(0.4)	1.01	(0.3)	*6.991*	1.00	1.00	**4.61**
	1215.1	4.47E-04			***0.99***	0.99	(0.4)	0.97	(0.9)	1.01	(1.4)	*0.811*	1.01		**4.58**
	1230.9	7.85E-04			***1.01***	1.03	(0.3)	1.02	(1.8)	0.98	(0.8)	*1.425*	0.99		**4.67**
	1260.1	6.44E-04			***0.99***	0.99	(0.8)	0.98	(2.3)	1.01	(0.4)	*1.169*	1.01		**4.56**
	1276.8	8.75E-04			***1.01***	1.01	(0.9)	1.02	(0.8)	1.00	(0.8)	*1.587*	0.99		**4.66**
	1464.1	1.99E-03			***1.01***	1.01	(0.5)	1.01	(1.2)	1.00	(1.3)	*3.609*	0.99		**4.66**
	1596.7	2.42E-03			***1.00***	1.00	(0.4)	1.00	(1.2)	1.00	(1.1)	*4.39*	1.00		**4.62**
	1862.0	2.98E-03			***1.01***	1.01	(0.3)	1.02	(1.5)	1.01	(0.8)	*5.41*	0.99		**4.65**
	2201.6	1.48E-02	1.48E-02	(1.0)	***1.02***	1.02	(0.5)	1.01	(1.3)	1.02	(0.8)	*26.87*	0.98	0.99	**4.68**
	2491.0	4.26E-03	4.19E-03	(1.7)	***1.02***	1.02	(0.4)	1.02	(1.0)	1.03	(0.7)	*7.73*	1.00	1.01	**4.63**
	2507.7	7.35E-03	7.29E-03	(1.3)	***1.02***	1.02	(0.4)	1.01	(1.0)	1.02	(0.9)	*13.33*	0.99	1.00	**4.66**

FN	γ (keV)	k_0 (%; 1s) C	k_0 (%; 1s) Lit		TW / [Lit or C] (% SD) AVG	Y4 /Cavity		S84		X26		I_γ	I_γ / $I_{\gamma,ref}$ TW / C	I_γ / $I_{\gamma,ref}$ Lit / C	σ (b) TW
^{76}As [I]	**559.1**	5.13E-02	4.83E-02	(1.6)	***1.01***	1.00	(0.1)	1.01	(0.1)	1.01	(0.6)	*45*	reference		**3.88**
	563.2	1.37E-03	1.40E-03		***0.95***	0.94	(0.3)	0.96	(0.1)	0.96	(1.0)	*1.2*	0.97	0.92	**3.99**
	571.5	1.60E-04			***0.95***	0.93	(1.1)	0.95	(0.2)	0.96	(3.0)	*0.14*	1.00		**3.87**
	657.1	7.07E-03	6.61E-03	(1.3)	***1.02***	1.02	(0.2)	1.02	(0.1)	1.02	(0.3)	*6.2*	0.99	1.01	**3.90**
	665.3	4.56E-04			***1.01***	1.01	(0.3)	1.02	(0.1)	1.01	(0.3)	*0.4*	0.94		**4.14**
	740.1	1.33E-04			***0.96***	0.96	(1.1)	0.95	(0.4)	0.96	(3.9)	*0.117*	0.99		**3.91**
	771.7	1.39E-04			***0.89***	0.89	(1.0)	0.89	(0.2)	0.91	(3.7)	*0.122*	1.06		**3.66**
	867.6	1.49E-04			***0.94***	0.92	(0.6)	0.94	(0.3)	0.95	(3.1)	*0.131*	1.01		**3.83**
	1212.9	1.64E-03	1.52E-03	(1.3)	***1.02***	1.01	(0.2)	1.02	(0.1)	1.02	(2.3)	*1.44*	1.01	1.02	**3.85**
	1228.5	1.39E-03			***0.92***	0.91	(0.6)	0.92	(0.1)	0.93	(2.2)	*1.22*	1.03		**3.76**
	1439.1	3.18E-04			***0.93***	0.92	(0.6)	0.94	(0.3)	0.93	(1.2)	*0.279*	1.02		**3.80**
	1216.1	3.90E-03	3.73E-03	(0.9)	***0.98***	0.97	(0.2)	0.99	(0.1)	0.98	(0.8)	*3.42*	1.01	0.98	**3.84**
	2096.3	6.27E-04			***0.96***	0.98	(0.9)	0.96	(0.2)	0.96	(1.5)	*0.55*	0.98		**3.94**
	1453.6	1.23E-04			***0.93***	0.93	(0.5)	0.94	(0.3)	0.92	(1.1)	*0.108*	1.02		**3.81**
	1787.7	3.34E-04			***0.93***	0.94	(0.6)	0.95	(0.2)	0.92	(2.0)	*0.293*	1.01		**3.82**

	γ	k_0 (%; 1*s*)			TW / [Lit or C] (% SD)							I_γ / $I_{\gamma,\mathrm{ref}}$		σ (b)
FN	**(keV)**	**C**	**Lit**		**AVG**	**Y4 /Cavity**		**S84**		**X26**	I_γ	**TW / C**	**Lit / C**	**TW**
^{82}Br [IV/b] <- F_2=1 - ^{82m}Br [I]	**554.3**	2.16E-02	2.38E-02	(1.1)	***1.00***	1.00	(1.0)	0.99	(1.3)		*71.10*	1.00	0.99	**2.60**
	619.1	1.32E-02	1.45E-02	(0.8)	***1.00***	1.01	(0.9)	0.99	(1.5)		*43.50*	1.00	0.99	**2.60**
	698.4	8.61E-03	9.38E-03	(0.9)	***1.00***	1.01	(1.0)	0.99	(1.5)		*28.30*	1.01	1.00	**2.59**
	776.5	2.54E-02	2.76E-02	(0.8)	***1.00***	1.01	(0.9)	0.99	(1.3)		*83.40*	reference		**2.60**
	827.8	7.30E-03	7.99E-03	(0.9)	***0.99***	1.01	(1.0)	0.98	(1.3)		*24.00*	1.00	0.99	**2.60**
	1044.0	8.61E-03	9.14E-03	(0.7)	***1.00***	1.01	(1.2)	0.99	(1.4)		*28.30*	1.03	1.02	**2.52**
	1317.5	8.16E-03	8.91E-03	(0.4)	***1.01***	1.01	(1.1)	1.00	(1.2)		*26.80*	1.00	1.00	**2.61**
	1474.9	5.05E-03	5.42E-03	(0.5)	***1.00***	1.02	(1.2)	0.99	(1.4)		*16.60*	1.01	1.01	**2.58**

	γ	k_0 (%; 1s)			TW / [Lit or C] (% SD)					I_γ / $I_{\gamma,ref}$		σ (b)
FN	**(keV)**	**C**	**Lit**		**AVG**	**Y4 /Cavity**		**S84**	**X26**	I_γ	**TW / C**	**Lit / C**	**TW**
^{86}Rb [IV/b] <- F_2=1 ^{86m}Rb [I]													
^{86}Rb	**1077.0**	7.53E-04	7.65E-04	(1.0)	***1.04***	1.04	(0.7)			*8.64*	reference		**0.521**
^{88}Rb [I]	**898.0**	1.02E-04	1.01E-04	(1.5)	***0.93***			0.93	(0.5)	*14.68*	1.01	1.00	**0.0943**
	1382.5	5.42E-06			***0.89***			0.89	(1.5)	*0.781*	1.06	1.05	**0.0907**
	1836.0	1.58E-04	1.57E-04	(1.1)	***0.94***			0.94	(0.6)	*22.73*	reference		**0.0957**
	2677.9	1.47E-05	1.47E-05		***0.95***			0.95	(0.8)	*2.123*	0.99	1.00	**0.0969**

FN	γ (keV)	k_0 (%; 1s) C	k_0 (%; 1s) Lit		TW / [Lit or C] (% SD) AVG	Y4 /Cavity		S84		X26		I_γ	I_γ / $I_{\gamma,ref}$ TW / C	I_γ / $I_{\gamma,ref}$ Lit / C	σ (b) TW
^{85}Sr [IV/b] <- F_2 - ^{85m}Sr [I]	**151.2**	1.02E-05	1.05E-05		***1.03***	1.03	(2.0)	1.03	(2.0)			*12.3*	1.01	0.96	**0.657**
	231.9	7.00E-05	6.92E-05		***1.07***	1.08	(0.9)	1.07	(0.8)			*84.1*	reference		**0.661**
	514.0	9.08E-05	9.15E-05	(0.9)	***1.01***	1.01	(0.8)	1.00	(0.9)			*98.5*	reference		**0.700**
^{87m}Sr [I]	**388.5**	1.49E-03	1.49E-03	(0.5)	***1.03***	1.03	(1.1)	1.03	(1.2)	1.03	(1.5)	*82.4*	reference		**0.791**
		Negligible (n,n') interference				1.03	(1.5)	1.02	(1.2)	1.03	(1.0)				
^{90m}Y [I]	**202.5**	2.29E-05	2.36E-05	(2.0)	***1.04***			1.04	(0.5)			*97.30*	reference		**0.0011**
	479.5	2.13E-05	2.23E-05	(0.9)	***1.01***			1.01	(0.5)			*90.74*	1.01	0.99	**0.0011**

FN	γ (keV)	k_0 (%; 1s) C	k_0 (%; 1s) Lit		TW / [Lit or C] (% SD) AVG	Y4 /Cavity		S84		X26		I_γ	I_γ / $I_{\gamma,ref}$ TW / C	I_γ / $I_{\gamma,ref}$ Lit / C	σ (b) TW
^{95}Zr [I]	**724.2**	8.71E-05	8.90E-05	(1.3)	***1.02***	1.02	(0.5)	1.02	(1.6)	1.02	(0.7)	*44.270*	1.01	1.01	**0.0515**
	756.7	1.07E-04	1.10E-04	(1.3)	***1.02***	1.03	(0.3)	1.03	(1.5)	1.02	(1.1)	*54.380*	reference		**0.0520**
<-------- F24 -------- <- F3 - ^{95m}Nb <- F2 -			*F2*	0.0111	[13]	0.0112	(1)	[8]							
			F3	0.9444	***old***	0.9775	(1)	***new***							
			F24	0.9889	***data***	0.9889	(1)	***data***							
			F24 / F2F3	94.38		90.55	(-)								
^{95}Nb [III/a]	**765.8**	2.18E-06	2.17E-06	(1.5)	***0.99***	0.99	(1.2)	1.00	(1.0)	0.98	(1.2)	*99.808*	*old data*		**0.0495**
		2.20E-06			***1.03***	1.03	(0.4)	1.03	(1.0)	1.03	(0.8)		***new data***		**0.0515**

FN	γ (keV)	k_0 (%; 1s) C	k_0 (%; 1s) Lit		TW / [Lit or C] (% SD) AVG	Y4 /Cavity		S84		X26		I_γ	I_γ / $I_{\gamma,ref}$ TW / C	I_γ / $I_{\gamma,ref}$ Lit / C	σ (b) TW
^{97}Zr [I] <---------- F_{24} ---------- <- F_3 - ^{97m}Nb [II/a] <- F_2 -	**743.4**	1.39E-05	1.24E-05	(0.3)	***1.03***	1.03	(0.5)			1.03	(1.8)	*97.9*	reference		**0.0211**
						1.03	(0.7)			1.04	(2.0)				
^{97}Nb [III/a]	**657.9**	1.40E-05	1.24E-05	(0.9)	***1.05***	1.05	(1.2)			1.05	(1.8)	*98.2*	0.99	1.00	**0.0213**
						1.05	(0.7)			1.04	(2.0)				
^{94m}Nb [I]	**871.0**		9.70E-05	(1.6)	***0.99***			0.99	(0.9)			*0.50*	reference		**0.853**

	γ	k_0 (%; 1s)			TW / [Lit or C] (% SD)							I_γ / $I_{\gamma,ref}$		σ (b)
FN	**(keV)**	**C**	**Lit**		**AVG**	**Y4 /Cavity**		**S84**		**X26**		I_γ	**TW / C**	**Lit / C**	**TW**
^{99m}Tc [II/d] <-- F_2=0.88 -- ^{99}Mo [I]	**181.0**	4.15E-05	4.15E-05	(0.6)	***1.00***	1.01	(0.2)	1.01	(0.8)	0.99	(0.3)	*6.01*	0.98	1.01	**0.130**
	366.4	8.24E-06	8.36E-06	(1.3)	***0.97***	0.96	(0.2)	0.96	(1.0)	0.97	(0.3)	*1.19*	1.00	1.00	**0.127**
	739.0	8.37E-05	8.46E-05	(0.7)	***0.97***	0.97	(0.3)	0.98	(1.2)	0.96	(0.5)	*12.12*	reference		**0.127**
	777.0	2.96E-05	2.97E-05	(1.1)	***0.96***	0.96	(0.3)	0.96	(1.4)	0.96	(0.4)	*4.28*	1.01	1.01	**0.126**
	140.5	5.38E-04	5.27E-04	(0.5)	***1.00***	1.00	(0.5)	1.00	(1.0)	1.01	(0.8)	*88.5*			**0.128**

FN	γ (keV)	k_0 (%; 1s) C	k_0 (%; 1s) Lit		TW / [Lit or C] (% SD) AVG	Y4 /Cavity	S84	X26	I_γ	I_γ / $I_{\gamma,ref}$ TW / C	I_γ / $I_{\gamma,ref}$ Lit / C	σ (b) TW
^{101}Tc [II/a] <--- F_2=1 --- ^{101}Mo [I]	**191.9**	7.75E-05	7.25E-05	(1.6)	***1.08***		1.08	(0.9)	*18.21*	1.00	1.02	**0.201**
	505.1	4.94E-05	4.71E-05	(1.9)	***1.06***		1.06	(0.9)	*11.62*	1.00	1.00	**0.200**
	590.1	8.72E-05	8.30E-05	(1.8)	***1.06***		1.06	(0.9)	*20.5*	reference		**0.200**
	695.6	2.83E-05	2.79E-05	(1.6)	***1.02***		1.02	(0.9)	*6.65*	1.00	0.97	**0.200**
	1011.1	6.21E-05	6.18E-05	(2.2)	***1.02***		1.02	(2.2)	*14.6*	0.99	0.96	**0.201**
	127.2	1.12E-05	1.20E-05		***1.03***		1.03	(0.9)	*2.63*	0.92	0.92	**0.219**
	184.1	6.81E-06	5.50E-06		***1.25***		1.25	(0.9)	*1.60*	1.00	1.22	**0.201**
	306.8	3.79E-04	3.73E-04	(1.3)	***1.03***		1.03	(0.9)	*89.0*	reference		**0.201**
	545.1	2.54E-05	2.49E-05	(1.0)	***1.03***		1.03	(0.9)	*5.96*	1.00	1.00	**0.201**

FN	γ (keV)	k_0 (%; 1s) C	k_0 (%; 1s) Lit		TW / [Lit or C] (% SD) AVG	Y4 /Cavity		S84		X26	I_γ	I_γ / $I_{\gamma,ref}$ TW / C	I_γ / $I_{\gamma,ref}$ Lit / C	σ (b) TW
^{97}Ru [I]	**215.7**	2.84E-04	2.25E-04	(0.5)	***1.08***	1.07	(0.6)	1.09	(0.7)		*85.6*	reference		**0.2478**
						1.08	(1.2)	1.08	(1.5)					
	324.5	3.58E-05			***0.85***	0.85	(0.5)	0.85	(0.8)		*10.79*	1.00		**0.2478**
						0.86	(1.6)	0.86	(0.8)					
^{103}Ru [I]	**497.1**	7.54E-03	6.89E-03	(0.4)	***1.07***	1.07	(1.1)	1.07	(1.1)		*91.0*	reference		**1.241**
						1.07	(0.6)							
	610.3	4.77E-04	4.30E-04	(0.5)	***1.08***	1.09	(0.8)	1.09	(1.1)		*5.76*	1.00	1.01	**1.242**
						1.07	(0.6)							

FN	γ (keV)	k_0 (%; 1s) C	k_0 (%; 1s) Lit		TW / [Lit or C] (% SD) AVG	Y4 /Cavity		S84		X26	I_γ	I_γ / $I_{\gamma,ref}$ TW / C	I_γ / $I_{\gamma,ref}$ Lit / C	σ (b) TW
^{105}Rh [III/c] <-- F_3 --- ^{105m}Rh [II/a] <---- F_2 ---- ^{105}Ru [I]	**262.8**	1.24E-04	1.31E-04	(1.8)	***0.98***	0.98	(0.9)	0.98	(2.0)		*6.57*	1.00	0.94	**0.507**
	316.4	2.10E-04			***1.04***	1.04	(1.3)	1.03	(1.7)		*11.1*	1.00		**0.508**
	469.4	3.31E-04	3.26E-04	(1.4)	***1.05***	1.05	(1.3)	1.04	(1.9)		*17.5*	1.01	1.01	**0.506**
	676.4	2.97E-04	2.95E-04		***1.03***	1.03	(1.2)	1.04	(1.7)		*15.7*	1.01	1.00	**0.505**
	724.3	8.94E-04	8.87E-04	(1.7)	***1.04***	1.04	(0.7)	1.05	(1.7)		*47.3*	reference		**0.508**
<---------- F_{24} ----------	**129.6**	9.99E-05	9.20E-05	(1.3)	***1.12***	1.13	(1.3)	1.12	(1.0)		*20.0*	reference		**0.134**
	306.1	9.64E-05	1.01E-04	(1.5)	***0.99***	1.00	(1.1)	0.99	(1.0)		*5.1*	0.98	0.94	**0.508**
						0.98	(1.2)	0.98	(1.2)					
	318.9	3.61E-04	3.57E-04	(2.1)	***1.03***	1.03	(1.2)	1.04	(1.7)		*19.1*	reference		**0.499**
						1.02	(0.9)	1.02	(0.9)					

	γ	k_0 (%; 1s)			TW / [Lit or C] (% SD)							I_γ / $I_{\gamma,ref}$			σ (b)
FN	**(keV)**	**C**	**Lit**		**AVG**	**Y4 /Cavity**		**S84**		**X26**		I_γ	**TW / C**	**Lit / C**	**TW**
^{109m}Ag [V/c] <- F$_3$=1 - ^{109}Pd [IV/b] <- F$_2$=1 - ^{109m}Pd [I]															**Lit**
	188.9	5.38E-04	4.94E-04	(0.3)								*56*			**0.170**
	311.4	1.44E-05	1.48E-05	(1.4)	***0.95***	0.95	(0.3)	0.95	(0.5)	0.96	(1.2)	*0.032*	1.00	1.00	**8.49**
	602.5	3.60E-06			***1.00***	1.00	(1.3)	0.99	(1.2)			*0.008*	0.99		**8.62**
	636.3	4.50E-06			***1.00***	1.01	(1.0)	1.00	(1.0)			*0.010*	0.98		**8.70**
	647.3	1.10E-05	1.13E-05	(0.5)	***0.95***	0.95	(0.4)	0.95	(0.3)	0.96	(1.4)	*0.0244*	reference		**8.51**
	781.4	5.04E-06			***0.98***	0.98	(0.6)	0.99	(0.8)			*0.0112*	1.00		**8.53**
	88.0	1.67E-03	1.71E-03		***0.89***	0.90	(0.6)			0.89	(0.5)	*3.7*	reference		**7.96**
						0.90	(0.6)			0.89	(0.5)				

	γ	k_0 (%; 1s)			TW / [Lit or C] (% SD)						I_γ / $I_{\gamma,ref}$		σ (b)
FN	**(keV)**	**C**	**Lit**		**AVG**	**Y4 /Cavity**		**S84**		**X26**	I_γ	**TW / C**	**Lit / C**	**TW**
^{111}Ag [VII/c] <-- F_3 -- ^{111}Pd <-- F_2 -- ^{111m}Pd [I] <-------- F_{24} ----------	**172.2**	2.58E-05	1.07E-05	(1.4)	***0.95***	0.96	(1.0)	0.94	(3.0)		*34.0*	reference		**0.0130**
						0.96	(1.0)	0.94	(3.1)					
								-						
								-						
						-								
	245.4	6.53E-06			***1.20***	1.19	(2.0)	1.21	(2.0)		*1.24*	1.12		**0.2753**
	342.0	3.53E-05			***1.34***	1.33	(1.0)	1.35	(1.0)		*6.70*	reference		**0.3075**

	γ	k_0 (%; 1s)			TW / [Lit or C] (% SD)							I_γ / $I_{\gamma,ref}$		σ (b)
FN	**(keV)**	**C**	**Lit**		**AVG**	**Y4 /Cavity**		**S84**		**X26**		I_γ	**TW / C**	**Lit / C**	**TW**
^{108}Ag [I]	**434.0**	1.89E-03	1.59E-03	(1.8)	***1.06***			1.06	(1.0)			*0.50*	1.02	1.07	**33.5**
	618.9	9.86E-04	9.33E-04		***0.99***			0.99	(1.0)			*0.26*	0.97	0.96	**35.2**
	633.0	6.65E-03	6.01E-03	(1.9)	***1.01***			1.01	(0.9)			*1.76*	reference		**34.2**
^{110m}Ag [I]	**446.8**	1.36E-03	1.36E-03	(1.7)	***1.01***	1.02	(1.2)			1.00	(1.5)	*3.7*	1.00	1.00	**3.98**
	620.4	1.01E-03	1.02E-03	(0.7)	***0.99***	1.01	(1.3)			0.98	(1.6)	*2.73*	0.99	0.98	**3.98**
	657.8	3.52E-02	3.50E-02	(0.7)	***1.01***	1.01	(0.3)			1.01	(0.5)	*95.61*	reference		**3.96**
	677.6	3.94E-03	3.93E-03	(1.2)	***1.00***	0.99	(0.8)			1.01	(0.8)	*10.7*	1.01	1.00	**3.93**
	687.0	2.41E-03	2.43E-03	(1.1)	***1.00***	1.00	(0.9)			1.00	(1.6)	*6.53*	0.99	0.98	**3.99**
	706.7	6.15E-03	6.03E-03	(0.8)	***1.03***	1.03	(0.7)			1.03	(1.1)	*16.69*	0.99	1.01	**3.98**
	744.3	1.76E-03	1.69E-03	(1.2)	***1.05***	1.04	(1.0)			1.06	(1.3)	*4.77*	0.99	1.03	**3.98**
	763.9	8.33E-03	8.27E-03	(0.7)	***1.01***	1.01	(0.7)			1.02	(1.0)	*22.6*	1.00	1.00	**3.96**
	818.0	2.74E-03	2.69E-03	(0.8)	***1.01***	1.02	(1.0)			1.01	(1.6)	*7.43*	1.01	1.01	**3.93**
	884.7	2.76E-02	2.69E-02	(0.8)	***1.02***	1.01	(0.5)			1.03	(1.0)	*75.0*	1.01	1.02	**3.93**
	937.5	1.29E-02	1.27E-02	(0.8)	***1.02***	1.02	(0.7)			1.02	(0.9)	*35.0*	1.00	1.01	**3.95**
	1384.3	9.25E-03	9.12E-03	(0.8)	***1.01***	1.00	(1.0)			1.03	(1.5)	*25.1*	1.01	1.01	**3.94**
	1475.8	1.50E-03	1.50E-03	(0.7)	***1.01***	1.02	(1.3)			1.00	(2.0)	*4.08*	1.00	1.00	**3.97**
	1505.0	4.91E-03	4.84E-03	(0.8)	***1.02***	1.01	(1.5)			1.03	(2.0)	*13.33*	1.00	1.01	**3.97**
	1562.3	4.50E-04	4.35E-04	(1.0)	***1.04***	1.05	(2.2)			1.04	(2.4)	*1.22*	0.99	1.03	**3.99**

FN	γ (keV)	k_0 (%; 1s) C	k_0 (%; 1s) Lit		TW / [Lit or C] (% SD) AVG	Y4 /Cavity		S84		X26		I_γ	I_γ / $I_{\gamma,ref}$ TW / C	I_γ / $I_{\gamma,ref}$ Lit / C	σ (b) TW
^{115m}In [II/a] <-F_2=1- ^{115}Cd [I]	**527.9**	4.85E-04	4.77E-04	(1.3)	***1.04***	1.04	(1.2)	1.05	(1.3)	1.05	(1.8)	*27.5*	reference		**0.339**
	336.2	8.07E-04	7.73E-04	(1.7)	***1.04***	1.05	(1.2)	1.04	(1.2)	1.05	(1.8)	*45.8*	reference		**0.330**

	γ	k_0 (%; 1s)			TW / [Lit or C] (% SD)						I_γ / $I_{\gamma,ref}$			σ (b)
FN	**(keV)**	**C**	**Lit**		**AVG**	**Y4 /Cavity**		**S84**	**X26**		I_γ	**TW / C**	**Lit / C**	**TW**
^{114m}In [IV/b] <-F_2=1- ^{114m2}In [I]														
	190.3	9.84E-04	1.06E-03	(0.8)	***0.97***	0.96	(1.1)		0.97	(1.3)	*15.56*	reference		**8.4**
	558.4	2.78E-04	2.86E-04	(0.7)	***0.94***	0.94	(1.1)		0.94	(1.2)	*4.39*	1.00	1.01	**7.9**
	725.2	2.78E-04	2.90E-04	(0.6)	***0.93***	0.93	(1.4)		0.93	(1.4)	*4.39*	reference		**7.9**

	γ	k_0 (%; 1s)			TW / [Lit or C] (% SD)						I_γ / $I_{\gamma,ref}$		σ (b)
FN	**(keV)**	**C**	**Lit**		**AVG**	**Y4 /Cavity**		**S84**		**X26**	I_γ	**TW / C**	**Lit / C**	**TW**
^{116m}In [IV/b] <-F_2=1- ^{116m2}In [I]	**138.3**	1.05E-01	1.01E-01	(1.4)	***1.01***	1.02	(0.9)	1.01	(0.3)		*3.7*	0.99	0.99	**159**
	416.9	7.69E-01	7.54E-01	(1.1)	***1.01***	1.01	(0.3)	1.00	(0.4)		*27.2*	0.98	0.97	**160**
	818.7	3.43E-01	3.36E-01	(1.2)	***1.01***	1.02	(0.3)	1.00	(0.3)		*12.13*	0.98	0.97	**160**
	1097.3	1.65E+00	1.60E+00	(1.3)	***1.00***	1.01	(0.2)	1.00	(0.4)		*58.5*	1.00	0.99	**157**
	1293.5	2.40E+00	2.29E+00	(0.8)	***1.01***	1.02	(0.2)	1.01	(0.4)		*84.8*	reference		**157**
	1507.4	2.80E-01	2.69E-01	(1.4)	***1.01***	1.00	(0.2)	1.01	(0.5)		*9.92*	1.01	1.00	**156**
	2112.1	4.27E-01	4.18E-01	(1.2)	***0.99***	1.00	(0.5)	0.99	(0.4)		*15.09*	0.99	0.97	**158**

FN	γ (keV)	k_0 (%; 1s) C	k_0 (%; 1s) Lit		TW / [Lit or C] (% SD) AVG	Y4 /Cavity		S84	X26		I_γ	I_γ / $I_{\gamma,ref}$ TW / C	I_γ / $I_{\gamma,ref}$ Lit / C	σ (b) TW
^{113m}In [V/c] <-F$_3$- ^{113}Sn [IV/b] <-F$_2$- ^{113m}Sn	**255.1**	1.95E-06	1.95E-06	(1.2)	***1.00***	1.00	(1.0)		1.00	(1.5)	*2.11*	1.00	1.00	**0.541**
						1.00	(1.2)		1.00	(1.2)				
	391.7	6.00E-05	5.99E-05	(0.8)	***1.00***	1.00	(1.0)		1.00	(1.5)	*64.97*	reference		**0.540**
						1.00	(1.2)		1.00	(1.2)				
^{117m}Sn [I]	**156.0**	3.24E-07	3.23E-07	(1.5)	***1.03***	1.03	(1.0)		1.04	(1.2)	*2.113*	1.00	1.03	**0.0062**
	158.4	1.33E-05	1.36E-05	(1.0)	***1.00***	1.00	(0.5)		1.00	(0.6)	*86.4*	reference		**0.0062**
	Strong (n,n') primary interference													

FN	γ (keV)	k_0 (%; 1s) C	k_0 (%; 1s) Lit	TW / [Lit or C] (% SD) AVG	Y4 /Cavity	S84	X26	I_γ	I_γ / $I_{\gamma,ref}$ TW / C	I_γ / $I_{\gamma,ref}$ Lit / C	σ (b) TW
^{125m}Sn [I] (F_2=0)	**331.9**		1.18E-04 (2.0)					*97.3*	reference		**0.1190**
<---------- F_{24} =1 ----------	**822.5**	1.97E-07	2.10E-07	***0.99***	0.99 (0.8)		1.00 (2.0)	*4.3*	0.96	0.95	**0.0048**
^{125}Sn [I]	**915.6**	1.88E-07	1.97E-07	***0.96***	0.95 (2.8)		0.96 (2.0)	*4.1*	1.01	0.97	**0.0045**
<--- F_3=1 ----	**1067.1**	4.59E-07	4.64E-07	***1.00***	1.00 (3.7)		1.00 (1.5)	*10.0*	1.00	1.00	**0.0045**
^{125}Sb [VII/b]	**1089.2**	2.11E-07	2.63E-07	***0.95***	0.96 (1.2)		0.95 (2.0)	*4.6*	0.85	0.81	**0.0053**
	176.3	3.14E-07		***1.02***	1.02 (5.5)		1.02 (5.0)	*6.84*	1.00		**0.0046**
	427.9	1.36E-06		***1.03***	1.02 (0.9)		1.05 (1.6)	*29.60*	0.99		**0.0046**
	463.4	4.81E-07		***1.03***	1.02 (3.0)		1.04 (2.3)	*10.49*	0.99		**0.0046**
	600.5	8.10E-07		***1.02***	1.02 (1.1)		1.03 (1.8)	*17.65*	reference		**0.0046**
	606.6	2.28E-07		***1.02***	1.02 (3.3)		1.02 (2.0)	*4.98*	1.01		**0.0046**
	635.9	5.15E-07		***1.03***	1.04 (1.6)		1.02 (2.2)	*11.22*	0.99		**0.0046**

	γ	k_0 (%; 1s)			TW / [Lit or C] (% SD)							I_γ / $I_{\gamma,ref}$		σ (b)
FN	**(keV)**	**C**	**Lit**		**AVG**	**Y4 /Cavity**		**S84**		**X26**		I_γ	**TW / C**	**Lit / C**	**TW**
^{122}Sb [IV/b] <- F_2=1- ^{122m}Sb [I]															
	564.2	4.00E-02	4.38E-02	(1.5)	***0.91***	0.91	(0.8)	0.91	(0.4)	0.92	(1.2)	*70.67*	reference		**5.772**
	692.7	2.18E-03	2.38E-03	(2.0)	***0.92***	0.92	(1.2)	0.91	(0.2)	0.92	(1.8)	*3.85*	1.00	1.00	**5.761**

	γ	k_0 (%; 1s)			TW / [Lit or C] (% SD)							I_γ / $I_{\gamma,ref}$		σ (b)
FN	**(keV)**	**C**	**Lit**		**AVG**	**Y4 /Cavity**		**S84**		**X26**		I_γ	**TW / C**	**Lit / C**	**TW**
^{124}Sb [VI/c] <- F_3 - ^{124m}Sb <-F_2 - ^{124m2}Sb	**602.7**	2.82E-02	2.96E-02	(0.6)	***0.95***	0.95	(0.9)	0.94	(0.9)	0.95	(1.5)	*97.8*	reference		**3.90**
	645.9	2.14E-03	2.21E-03	(0.7)	***0.96***	0.96	(1.3)	0.95	(1.1)	0.96	(1.8)	*7.42*	1.01	1.02	**3.88**
	709.3	3.90E-04			***0.99***	0.99	(1.4)	0.99	(0.5)			*1.353*	1.00		**3.90**
	713.8	6.56E-04			***0.99***	0.99	(1.2)	0.98	(0.5)			*2.276*	1.01		**3.87**
	722.8	3.10E-03	3.19E-03	(0.8)	***0.96***	0.96	(1.6)	0.97	(0.8)	0.97	(1.7)	*10.76*	1.00	1.02	**3.89**
	968.2	5.42E-04			***1.00***	1.00	(2.2)	1.00	(0.5)			*1.882*	0.99		**3.93**
	1045.1	5.28E-04			***0.99***	1.00	(2.1)	0.98	(0.5)			*1.833*	1.01		**3.88**
	1325.5	4.55E-04			***0.98***	0.98	(1.2)	0.98	(0.5)			*1.58*	1.02		**3.84**
	1368.2	7.56E-04			***0.99***	0.99	(1.7)	0.99	(0.5)			*2.624*	1.00		**3.89**
	1436.6	3.51E-04			***0.99***	1.01	(0.7)	0.97	(0.5)			*1.217*	1.00		**3.90**
	1691.0	1.37E-02	1.41E-02	(1.1)	***0.98***	0.97	(0.9)	0.98	(1.4)	0.97	(1.6)	*47.57*	0.99	1.02	**3.94**
	2090.9	1.58E-03	1.58E-03	(2.0)	***1.00***	1.00	(1.2)	1.00	(4.9)			*5.49*	1.00	1.05	**3.91**

	γ	k_0 (%; 1s)			TW / [Lit or C] (% SD)								I_γ / $I_{\gamma,ref}$		σ (b)
FN	**(keV)**	**C**	**Lit**		**AVG**	**Y4 /Cavity**		**S84**		**X26**		I_γ	**TW / C**	**Lit / C**	**TW**
^{134}Cs [IV/b] ---------- ^{134}Cs [IV/a] < -- F_2=1 -- ^{134m}Cs [I]	**127.5**	5.15E-03	5.48E-03	(1.7)	***1.07***	1.07	(0.8)	1.08	(0.6)	1.07	(1.0)	*12.60*	reference		**2.97**
	563.2	3.63E-02	3.85E-02		***0.93***	0.92	(1.2)	0.93	(1.6)			*8.34*	1.00	0.99	**27.2**
	569.3	6.70E-02	6.67E-02		***0.99***	0.99	(1.2)	0.98	(1.5)			*15.37*	1.00	1.05	**27.2**
	604.7	4.25E-01	4.44E-01	(0.3)	***0.94***	0.95	(1.0)	0.94	(1.2)	0.94	(1.5)	*97.62*	reference		**27.3**
	795.9	3.72E-01	3.92E-01	(1.2)	***0.95***	0.94	(1.1)	0.94	(1.2)	0.95	(1.6)	*85.46*	0.99	0.99	**27.6**
	802.0	3.78E-02	3.88E-02		***0.97***	0.97	(1.3)	0.97	(1.7)			*8.69*	0.99	1.02	**27.6**
	1365.2	1.31E-02			***1.00***	1.00	(1.3)	1.00	(1.5)			*3.02*	0.98		**27.7**
	475.4	7.04E-03			***1.00***	0.99	(0.9)	1.01	(0.8)	1.00	(1.2)	*1.48*	0.99		**30.4**
	563.2	3.97E-02	4.14E-02	(1.7)	***0.95***	0.95	(0.8)	0.96	(0.8)	0.95	(1.2)	*8.34*	1.00	0.98	**30.1**
	569.3	7.32E-02	7.34E-02	(1.5)	***0.99***	0.99	(0.7)	0.99	(0.8)	1.00	(1.0)	*15.37*	1.00	1.02	**30.1**
	604.7	4.65E-01	4.76E-01	(2.0)	***0.97***	0.97	(0.5)	0.98	(0.6)	0.97	(1.0)	*97.62*	reference		**30.1**
	795.9	4.07E-01	4.15E-01	(2.0)	***0.98***	0.98	(0.6)	0.99	(0.6)	0.99	(1.0)	*85.46*	0.99	1.00	**30.4**
	802.0	4.14E-02	4.11E-02	(2.0)	***1.00***	1.00	(0.9)	0.99	(0.7)	1.00	(1.2)	*8.69*	1.00	1.03	**30.0**
	1038.6	4.72E-03			***1.00***	1.00	(1.0)	1.00	(1.2)	1.00	(1.3)	*0.99*	0.99		**30.4**
	1168.0	8.53E-03			***0.99***	0.99	(1.1)	0.98	(1.2)	0.99	(1.2)	*1.79*	1.00		**30.0**
	1365.2	1.44E-02			***1.01***	1.01	(1.3)	1.01	(1.0)	1.00	(2.6)	*3.02*	0.99		**30.5**

FN	γ (keV)	k_0 (%; 1s) C	k_0 (%; 1s) Lit		TW / [Lit or C] (% SD) AVG	Y4 /Cavity		S84		X26		I_γ	I_γ / $I_{\gamma,ref}$ TW / C	Lit / C	σ (b) TW
^{131}Ba [IV/b] <---- F_2=1 ----- ^{131m}Ba [I]	**123.8**	4.18E-05	3.90E-05	(0.7)	***1.01***	1.01	(0.6)	1.01	(0.3)	1.01	(1.5)	*29.80*	0.97	1.03	**8.19**
	133.6	3.06E-06	3.24E-06		***0.92***	0.92	(0.8)	0.91	(0.4)	0.91	(1.5)	*2.18*	0.94	0.91	**8.44**
	216.1	2.86E-05	2.75E-05	(1.4)	***0.94***	0.96	(0.5)	0.94	(0.5)	0.93	(1.7)	*20.40*	1.01	1.00	**7.89**
	239.6	3.51E-06			***0.92***	0.92	(0.6)	0.93	(1.3)	0.91	(1.8)	*2.50*	0.99		**8.00**
	249.4	4.15E-06			***0.89***	0.91	(0.4)	0.88	(0.9)	0.88	(1.9)	*2.96*	1.03		**7.72**
	373.2	2.02E-05	1.92E-05	(0.4)	***0.95***	0.96	(0.7)	0.95	(0.4)	0.93	(1.7)	*14.40*	1.02	1.01	**7.82**
	404.0	1.89E-06			***0.92***	0.92	(0.4)	0.92	(0.5)	0.90	(1.8)	*1.34*	1.00		**7.97**
	486.5	3.01E-06	3.44E-06		***0.81***	0.82	(0.2)	0.81	(0.3)	0.80	(1.5)	*2.15*	0.99	0.84	**8.04**
	496.3	6.74E-05	6.48E-05	(0.2)	***0.95***	0.96	(0.8)	0.94	(0.2)	0.94	(1.8)	*48.00*	reference		**7.94**
	585.0	1.72E-06			***0.93***	0.95	(0.7)	0.93	(0.4)	0.93	(1.5)	*1.22*	0.98		**8.13**
	620.1	2.07E-06	2.34E-06		***0.81***	0.81	(1.2)	0.80	(1.0)	0.81	(2.0)	*1.47*	1.00	0.85	**7.92**
	1047.6	1.88E-06			***0.92***	0.92	(1.2)	0.92	(0.3)	0.90	(2.0)	*1.34*	1.00		**7.97**

	γ	k_0 (%; 1s)		TW / [Lit or C] (% SD)							I_γ / $I_{\gamma,ref}$		σ (b)
FN	**(keV)**	**C**	**Lit**	**AVG**	**Y4 /Cavity**		**S84**		**X26**		I_γ	**TW / C**	**Lit / C**	**TW**
^{133m}Ba [I]														
	275.9	1.36E-06	2.27E-06	***0.90***	0.91	(0.7)	0.89	(1.0)	0.90	(1.5)	*17.69*	reference		**0.752**
^{135m}Ba [I]														
	268.3	7.89E-06	3.12E-06	***1.03***	1.04	(2.0)	1.01	(2.3)	1.04	(2.0)	*16.0*	reference		**0.054**
	Strong (n,n') primary interference													
^{139}Ba [I]														
	165.9	1.05E-03	1.05E-03 (0.7)	***1.00***	1.00	(1.5)	1.01	(0.9)	0.99	(1.6)	*23.76*	reference		**0.404**
	1420.5	1.15E-05		***1.00***			0.99	(2.0)	1.00	(2.0)	*0.261*	1.00	1.00	**0.402**

	γ	k_0 (%; 1s)			TW / [Lit or C] (% SD)							I_γ / $I_{\gamma,ref}$		σ (b)
FN	**(keV)**	**C**	**Lit**		**AVG**	**Y4 /Cavity**		**S84**		**X26**		I_γ	**TW / C**	**Lit / C**	**TW**
^{140}La [I]	**328.8**	2.83E-02	2.87E-02	(1.0)	***1.00***	1.00	(0.2)	1.00	(1.7)	1.02	(0.6)	*20.8*	0.99	1.00	**9.22**
	432.5	4.07E-03			***1.02***	1.01	(0.2)	1.02	(0.7)	1.04	(1.2)	*2.995*	0.99		**9.23**
	487.0	6.26E-02	6.37E-02	(0.9)	***1.00***	1.00	(0.3)	1.00	(0.8)	1.00	(1.2)	*46.1*	reference		**9.16**
	751.6	5.97E-03			***1.03***	1.01	(0.2)	1.02	(1.4)	1.04	(0.6)	*4.392*	0.99		**9.27**
	815.8	3.22E-02	3.32E-02	(0.6)	***0.99***	0.98	(0.2)	0.99	(1.1)	1.00	(0.3)	*23.72*	0.99	0.99	**9.24**
	867.8	7.58E-03			***1.03***	1.02	(0.2)	1.02	(0.3)	1.03	(0.2)	*5.58*	0.99		**9.27**
	919.6	3.71E-03			***1.02***	1.02	(0.3)	1.01	(1.5)	1.03	(1.2)	*2.73*	0.99		**9.22**
	925.2	9.57E-03			***1.03***	1.02	(0.1)	1.02	(1.2)	1.04	(1.1)	*7.04*	0.99		**9.29**
	1596.2	1.30E-01	1.34E-01	(1.1)	***0.99***	0.99	(0.2)	0.99	(2.1)	1.00	(0.2)	*95.4*	0.99	0.98	**9.30**

FN	γ (keV)	k_0 (%; 1s) C	k_0 (%; 1s) Lit		TW / [Lit or C] (% SD) AVG	Y4 /Cavity		S84		X26		I_γ	I_γ / $I_{\gamma,ref}$ TW / C	I_γ / $I_{\gamma,ref}$ Lit / C	σ (b) TW
^{142}Pr [IV/b] <- F_2=1 - ^{142m}Pr [I]			-												
	1575.6	6.31E-03	6.12E-03	(0.6)	***1.01***	1.02	(0.2)	1.01	(0.3)	1.01	(1.1)	*3.7*	1.00	1.00	**11.3**
^{153}Sm [I]	**69.7**	3.59E-02	3.52E-02	(1.0)	***1.02***	1.02	(1.5)	1.01	(0.4)	1.03	(2.0)	*4.691*	1.01	1.05	**206**
	97.4	5.97E-03			***1.14***	1.16	(1.0)	1.14	(1.2)	1.12	(2.5)	*0.779*	0.88		**235**
	103.2	2.24E-01	2.31E-01	(0.4)	***0.97***	0.98	(0.5)	0.97	(0.7)	0.97	(1.2)	*29.19*	reference		**207**

	γ	k_0 (%; 1*s*)		TW / [Lit or C] (% SD)							I_γ / $I_{\gamma,\mathrm{ref}}$		σ (b)
FN	**(keV)**	**C**	**Lit**	**AVG**	**Y4 /Cavity**		**S84**		**X26**		I_γ	**TW / C**	**Lit / C**	**TW**
^{152}Eu [IV/b] <-- F_2=1 -- ^{152m2}Eu [I]	**121.8**		1.28E+01 (0.8)	***0.97***	0.97	(2.0)	0.99	(3.0)	0.95	(2.0)	*28.7*	1.00	1.00	**6589**
	244.7		3.44E+00 (0.3)	***0.96***	0.96	(1.0)	0.95	(1.3)	0.96	(1.7)	*7.61*	1.00	0.98	**6574**
	344.3		1.19E+01 (0.9)	***0.97***	0.98	(0.9)	0.96	(1.0)	0.97	(1.5)	*26.6*	1.00	0.99	**6604**
	444.0		1.39E+00 (1.2)	***1.00***	1.00	(1.0)	0.99	(1.5)	1.00	(1.7)	*3.158*	0.99	1.01	**6671**
	778.9		5.70E+00 (0.8)	***1.00***	1.00	(0.9)	0.98	(1.1)	1.01	(2.0)	*12.96*	0.99	1.01	**6669**
	867.4		1.88E+00 (0.9)	***0.99***	0.99	(1.0)	0.98	(1.5)	0.99	(2.0)	*4.26*	0.99	1.01	**6637**
	963.4		6.46E+00 (0.4)	***0.99***	1.00	(0.9)	0.98	(1.1)	1.00	(1.5)	*14.79*	1.00	1.02	**6598**
	1084.0		4.57E+00 (0.4)	***0.98***	0.97	(1.0)	0.97	(1.1)	0.99	(1.0)	*10.24*	0.99	1.00	**6631**
	1112.1		6.07E+00 (0.8)	***0.98***	0.98	(0.9)	0.97	(1.0)	0.98	(2.0)	*13.69*	1.00	1.00	**6583**
	1408.0		9.36E+00 (0.6)	***0.98***	0.98	(1.3)	0.97	(1.0)	0.98	(1.0)	*21.07*	reference		**6591**

Negligible contribution from ^{152m}Eu --> ^{152}Eu; Strong non-1/v absorber
Temperature monitor; modified Westcott formalism; Lit values are theoretical

	γ	k_0 (%; 1s)			TW / [Lit or C] (% SD)							I_γ / $I_{\gamma,ref}$		σ (b)
FN	**(keV)**	**C**	**Lit**		**AVG**	**Y4 /Cavity**		**S84**		**X26**		I_γ	**TW / C**	**Lit / C**	**TW**
^{154}Eu [IV/b] <-- F_2=1 -- ^{154m}Eu [I]	**123.1**	9.05E-01			***1.00***	1.00	(0.6)	0.99	(1.2)	1.01	(1.1)	*40.4*	1.00		**312**
	248.0	1.54E-01	1.55E-01		***0.99***	1.00	(0.6)	0.99	(1.6)	0.99	(1.5)	*6.89*	1.00	0.99	**311**
	591.8	1.11E-01	1.08E-01	(1.5)	***1.01***	1.01	(0.9)	0.99	(1.7)	1.02	(1.6)	*4.95*	1.02	1.02	**306**
	692.4	3.98E-02			***1.01***	1.01	(1.1)					*1.777*	0.99		**315**
	723.3	4.49E-01	4.46E-01	(1.5)	***1.01***	1.02	(0.7)	1.00	(1.4)	1.01	(1.3)	*20.06*	reference		**313**
	756.9	1.01E-01	1.08E-01		***0.98***	0.99	(0.8)	0.98	(1.8)			*4.52*	0.95	0.93	**327**
	873.2	2.70E-01	2.72E-01	(1.4)	***1.00***	1.01	(0.7)	0.99	(1.5)	0.99	(1.8)	*12.08*	1.00	0.99	**312**
	996.4	2.35E-01	2.30E-01		***1.02***	1.03	(0.6)	1.01	(0.6)	1.03	(2.0)	*10.48*	1.00	1.01	**313**
	1274.4	7.79E-01	7.77E-01	(1.1)	***1.00***	1.01	(0.7)	0.99	(1.6)	1.00	(1.5)	*34.80*	1.01	1.00	**311**
	1596.5	4.02E-02			***1.01***	1.01	(1.4)					*1.797*	0.99		**315**

	γ	k_0 (%; 1s)			TW / [Lit or C] (% SD)							I_γ / $I_{\gamma,ref}$		σ (b)
FN	**(keV)**	**C**	**Lit**		**AVG**	**Y4 /Cavity**		**S84**		**X26**	I_γ	**TW / C**	**Lit / C**	**TW**
^{153}Gd [I]	**97.4**	5.66E-03	5.86E-03	(1.4)	***1.01***	1.01	(0.6)	1.01	(0.9)		*29.0*	reference		**771**
	103.2	4.12E-03	4.21E-03	(1.4)	***1.03***	1.04	(0.6)	1.03	(0.9)		*21.1*	1.00	1.01	**773**
^{159}Gd [I]	**363.5**	8.55E-04	8.49E-04	(1.6)	***1.02***	1.02	(0.6)	1.02	(0.9)		*11.78*	reference		**2.22**
^{160}Tb [I]	**86.8**	4.06E-02	4.20E-02	(1.1)	***1.00***	1.00	(0.6)				*13.2*	0.99	0.98	**24.1**
	197.0	1.59E-02	1.62E-02	(0.5)	***1.00***	1.00	(1.0)				*5.18*	1.00	1.00	**23.8**
	215.6	1.24E-02	1.27E-02	(0.4)	***1.01***	1.01	(0.7)				*4.02*	0.99	0.99	**24.2**
	298.6	8.03E-02	8.25E-02	(1.2)	***1.00***	1.00	(0.8)				*26.10*	0.99	0.99	**24.1**
	879.4	9.26E-02	9.42E-02	(0.9)	***1.00***	1.00	(0.7)				*30.10*	reference		**23.9**
	962.3	3.02E-02	3.05E-02		***1.00***	1.00	(0.7)				*9.81*	1.01	1.01	**23.6**
	1178.0	4.58E-02	4.71E-02	(1.1)	***1.00***	1.00	(0.6)				*14.90*	0.99	0.99	**24.0**
	1199.9	7.32E-03	7.53E-03	(1.3)	***0.99***	0.99	(0.8)				*2.38*	1.01	0.99	**23.7**
	1271.9	2.29E-02	2.35E-02	(0.8)	***1.00***	1.00	(0.7)				*7.44*	0.99	0.99	**24.1**
	1312.1	8.80E-03	8.98E-03	(0.9)	***1.00***	1.00	(0.7)				*2.86*	1.00	1.00	**23.9**

FN	γ (keV)	k_0 (%; 1s) C	k_0 (%; 1s) Lit		TW / [Lit or C] (% SD) AVG	Y4 /Cavity		S84		X26		I_γ	I_γ / $I_{\gamma,ref}$ TW / C	I_γ / $I_{\gamma,ref}$ Lit / C	σ (b) TW
^{165}Dy [IV/b] <-F$_2$-^{165m}Dy [I]	**94.7**	3.66E-01	3.57E-01	(1.4)	***1.01***	1.01	(0.4)	1.01	(0.8)	1.02	(1.1)	*3.80*	reference		**2621**
	279.8	5.14E-02	4.88E-02	(0.8)	***1.05***	1.04	(0.6)	1.05	(0.9)	1.07	(1.8)	*0.53*	0.99	1.03	**2645**
	361.7	8.71E-02	8.36E-02	(0.7)	***1.04***	1.03	(0.5)	1.03	(0.9)	1.04	(1.2)	*0.90*	0.99	1.02	**2635**
	633.4	5.90E-02	5.62E-02	(1.5)	***1.03***	1.03	(0.6)	1.03	(1.5)	1.04	(2.0)	*0.61*	1.01	1.02	**2600**
	715.3	5.57E-02	5.23E-02	(1.2)	***1.04***	1.03	(0.9)	1.03	(1.6)	1.06	(2.0)	*0.58*	1.01	1.04	**2584**
^{166}Ho [I]	**80.6**	5.09E-02	4.94E-02	(1.0)	***1.04***	1.04	(1.0)	1.03	(0.9)	1.05	(0.6)	*6.56*	reference		**61.7**
						1.03	(0.4)								
	1379.4	7.15E-03	6.95E-03	(1.6)	***1.02***	1.01	(0.6)	1.01	(0.6)	1.02	(1.2)	*0.92*	1.02	1.00	**60.4**
						1.01	(2.0)								
	1581.9	1.41E-03	1.40E-03	(2.1)	***1.01***	1.01	(0.6)	1.00	(0.5)	1.01	(1.2)	*0.18*	1.01	0.98	**61.3**
	1662.5	9.23E-04	8.75E-04	(0.7)	***1.04***	1.04	(0.9)	1.02	(1.5)	1.04	(1.3)	*0.12*	1.03	1.03	**60.0**

FN	γ (keV)	k_0 (%; 1s) C	k_0 (%; 1s) Lit		TW / [Lit or C] (% SD) AVG	Y4 /Cavity		S84		X26		I_γ	I_γ / $I_{\gamma,ref}$ TW / C	I_γ / $I_{\gamma,ref}$ Lit / C	σ (b) TW
^{170}Tm [I]	**84.3**	3.22E-02	3.26E-02	(1.7)	***1.01***	1.01	(3.0)	1.01	(5.0)			*2.48*	reference		**107**
^{169}Yb [IV/b] <- F_2=1 - ^{169m}Yb [I]	**93.6**	8.78E-04	1.18E-03		***1.02***	1.01	(3.1)	1.03	(1.1)	1.01	(3.0)	*2.57*	1.00	0.99	**3151**
	109.8	5.93E-03	7.79E-03		***1.06***	1.06	(2.2)	1.05	(1.2)	1.07	(1.5)	*17.36*	0.98	1.02	**3203**
	130.5	3.89E-03	5.17E-03		***1.02***	1.02	(1.3)	1.02	(1.4)	1.02	(2.0)	*11.38*	1.01	1.00	**3121**
	177.2	7.62E-03	1.04E-02		***1.00***	1.02	(0.8)	0.98	(1.4)	1.01	(1.7)	*22.32*	1.00	0.98	**3141**
	198.0	1.23E-02	1.64E-02		***1.02***	1.04	(0.6)	1.00	(1.6)	1.03	(1.5)	*35.93*	reference		**3148**
	307.7	3.43E-03	4.34E-03		***1.07***	1.07	(0.1)	1.04	(1.5)	1.08	(1.9)	*10.046*	1.01	1.06	**3101**

Strong non-1/v absorber
Temperature monitor; modified Westcott formalism; Lit values are theoretical

	γ	k_0 (%; 1s)			TW / [Lit or C] (% SD)							I_γ / $I_{\gamma,ref}$		σ (b)
FN	**(keV)**	**C**	**Lit**		**AVG**	**Y4 /Cavity**		**S84**		**X26**		I_γ	**TW / C**	**Lit / C**	**TW**
^{175}Yb [IV/b]<- F_2=1-^{175m}Yb [I]															
	113.8	9.46E-03	9.42E-03	(1.3)	***1.01***	1.01	(0.4)	1.00	(1.0)			*3.87*	0.98	0.97	**63.3**
	137.7	5.74E-04	5.69E-04	(0.6)	***1.01***	1.00	(0.9)	1.02	(0.4)			*0.235*	0.98	0.98	**63.2**
	144.9	1.64E-03	1.59E-03	(1.5)	***1.03***	1.03	(0.5)	1.02	(1.0)			*0.672*	0.99	1.00	**62.9**
	282.5	1.50E-02	1.46E-02	(0.3)	***1.03***	1.03	(0.6)	1.02	(0.4)	1.04	(1.2)	*6.13*	0.98	0.99	**63.4**
	396.3	3.23E-02	3.12E-02	(0.6)	***1.02***	1.03	(0.1)	1.01	(0.4)	1.01	(0.7)	*13.2*	reference		**62.2**

FN	γ (keV)	k_0 (%; 1s) C	k_0 (%; 1s) Lit	TW / [Lit or C] (% SD) AVG	Y4 /Cavity		S84		X26	I_γ	I_γ / $I_{\gamma,ref}$ TW / C	I_γ / $I_{\gamma,ref}$ Lit / C	σ (b) TW
^{177}Yb [IV/b] <- F_2=1- ^{177m}Yb [I]													
	150.3	9.17E-04	8.94E-04	***1.01***	1.01	(1.2)	1.01	(1.2)		*20.5*	reference		**2.80**
	941.8	4.83E-05	4.87E-05	***1.01***	1.01	(1.2)	1.00	(1.2)		*1.08*	0.97	0.97	**2.89**
	1080.2	2.64E-04	2.68E-04	***0.99***	0.98	(1.2)	0.99	(1.2)		*5.9*	0.98	0.96	**2.85**
	1241.2	1.57E-04	1.62E-04	***0.98***	0.98	(1.2)	0.99	(1.2)		*3.50*	0.96	0.94	**2.90**
^{177}Lu [I]	**112.9**	4.00E-02	4.15E-02							*6.17*		1.02	**2167**
	208.4	6.72E-02	7.14E-02							*10.36*	reference		**2220**
													Lit

Negligible contribution from ^{177m}Lu --> ^{177}Lu; Strong non-1/v absorber
Temperature monitor; modified Westcott formalism; Lit values are theoretical

	γ	k_0 (%; 1s)			TW / [Lit or C] (% SD)								I_γ / $I_{\gamma,ref}$		σ (b)
FN	**(keV)**	**C**	**Lit**		**AVG**	**Y4 /Cavity**		**S84**		**X26**		I_γ	**TW / C**	**Lit / C**	**TW**
^{175}Hf [I]															
	343.4	8.95E-03	9.06E-03	(1.0)	***0.99***	0.98	(0.2)	1.00	(0.6)	0.98	(0.7)	*87.0*	reference		**549**
						5% wire		0.1% wire							
^{180m}Hf [I]	**93.3**	1.21E-04	1.24E-04	(0.5)	***0.96***	0.97	(1.2)	0.95	(1.1)			*17.1*	0.98	0.99	**0.437**
	215.4	5.77E-04	5.91E-04	(1.5)	***0.95***	0.95	(0.9)	0.95	(1.0)			*81.3*	0.99	0.99	**0.433**
	332.3	6.68E-04	6.74E-04	(2.0)	***0.95***	0.96	(0.8)	0.95	(0.8)			*94.1*	reference		**0.428**
	443.2	5.81E-04	5.88E-04	(1.9)	***0.96***	0.96	(1.0)	0.95	(1.0)			*81.9*	0.99	1.00	**0.430**
	500.7	1.01E-04	1.02E-04	(0.9)	***0.95***	0.95	(1.1)	0.94	(1.5)			*14.3*	1.01	1.00	**0.424**
^{181}Hf [I]	**133.0**	2.32E-02	2.37E-02	(0.6)	***0.98***	0.96	(2.0)	0.99	(0.5)	1.00	(1.3)	*43.3*	1.00	1.03	**13.08**
	345.9	8.10E-03	7.93E-03		***1.01***	1.01	(1.1)	1.01	(0.5)	1.02	(1.2)	*15.12*	1.01	1.08	**12.93**
	482.2	4.31E-02	4.56E-02	(0.9)	***0.94***	0.94	(0.8)	0.95	(0.3)	0.95	(1.2)	*80.5*	reference		**13.03**

	γ	k_0 (%; 1s)			TW / [Lit or C] (% SD)							I_γ / $I_{\gamma,\mathrm{ref}}$		σ (b)
FN	**(keV)**	**C**	**Lit**		**AVG**	**Y4 /Cavity**		**S84**		**X26**		I_γ	**TW / C**	**Lit / C**	**TW**
^{182}Ta [IV/b] <-F$_2$=1- ^{182m}Ta [I]	**84.7**	6.28E-03			***0.99***	1.00	(1.5)	0.99	(1.6)	0.98	(1.5)	*2.65*	1.00		**20.3**
	100.1	3.36E-02	3.18E-02		***1.03***	1.03	(1.0)	1.03	(1.0)	1.02	(0.9)	*14.2*	1.02	1.05	**19.9**
						1.02	(1.5)								
	113.7	4.43E-03			***0.99***	0.99	(0.9)	1.00	(1.5)	0.98	(1.6)	*1.87*	1.00		**20.3**
						0.99	(1.5)								
	152.4	1.66E-02	1.62E-02	(0.7)	***1.01***	1.01	(1.0)	1.01	(0.9)	1.00	(1.0)	*7.02*	1.01	1.02	**20.2**
						1.01	(1.5)								
	156.4	6.32E-03			***0.99***	0.99	(1.0)	1.00	(0.4)	0.98	(0.5)	*2.67*	1.00		**20.3**
						0.99	(1.5)								
	179.4	7.38E-03			***0.99***	0.99	(0.9)	0.99	(1.2)	0.98	(1.3)	*3.12*	1.00		**20.2**
						0.98	(1.5)								
	198.4	3.47E-03			***0.98***	0.98	(1.2)	0.98	(1.2)	0.98	(1.3)	*1.47*	1.01		**20.1**
						0.99	(1.5)								
	222.1	1.79E-02	1.78E-02	(0.9)	***1.00***	1.01	(0.8)	1.01	(1.3)	0.99	(1.6)	*7.57*	1.00	1.00	**20.3**
						0.99	(1.5)								
	229.3	8.63E-03			***0.99***	0.99	(0.8)	1.00	(0.8)	0.99	(1.2)	*3.64*	1.00		**20.4**
						0.99	(1.5)								
	264.1	8.55E-03			***0.98***	0.99	(0.7)	0.98	(0.9)	0.99	(1.1)	*3.61*	1.01		**20.2**
						0.97	(1.5)								
	1001.7	4.94E-03			***0.98***	0.97	(1.5)	0.98	(1.5)	0.97	(1.0)	*2.09*	1.01		**20.0**

	γ	k_0 (%; 1s)			TW / [Lit or C] (% SD)							I_γ / $I_{\gamma,ref}$		σ (b)
FN	**(keV)**	**C**	**Lit**		**AVG**	**Y4 /Cavity**		**S84**		**X26**		I_γ	**TW / C**	**Lit / C**	**TW**
						0.99	(1.5)								
	1121.3	8.34E-02	8.27E-02	(0.8)	***1.00***	1.01	(1.0)	1.01	(0.9)	0.99	(1.1)	*35.24*	reference		**20.3**
						1.00	(1.5)								
	1157.5		2.33E-03		***1.01***	1.00	(1.4)	1.01	(1.0)	1.01	(1.0)	*(S)*			
	1189.1	3.90E-02	3.88E-02	(0.7)	***0.99***	0.99	(0.8)	0.99	(0.5)	0.98	(1.2)	*16.49*	1.01	1.00	**20.1**
						0.99	(1.5)								
	1221.4	6.45E-02	6.45E-02	(0.8)	***0.99***	1.00	(1.0)	1.00	(0.4)	0.98	(1.1)	*27.23*	1.00	0.99	**20.3**
						0.99	(1.5)								
	1231.0	2.75E-02	2.72E-02	(0.7)	***1.00***	1.00	(1.0)	1.01	(0.2)	0.98	(1.2)	*11.62*	1.01	1.00	**20.2**
						1.00	(1.5)								
	1257.4	3.57E-03			***0.99***	0.99	(1.2)	0.98	(0.8)	0.98	(1.0)	*1.51*	1.00		**20.2**
						0.99	(1.5)								
	1289.2	3.25E-03			***0.99***	1.00	(1.0)	0.98	(0.5)	0.98	(1.0)	*1.37*	1.00		**20.2**
						0.99	(1.5)								

FN	γ (keV)	k_0 (%; 1s) C	k_0 (%; 1s) Lit		TW / [Lit or C] (% SD) AVG	Y4 /Cavity		S84		X26		I_γ	I_γ / $I_{\gamma,ref}$ TW / C	Lit / C	σ (b) TW
^{187}W [I]	**134.2**	1.28E-02	1.13E-02	(0.7)	***1.03***	1.03	(0.2)	1.03	(0.3)	1.03	(1.0)	*10.36*	0.99	1.02	**34.8**
	479.6	3.28E-02	2.97E-02	(1.0)	***1.02***	1.02	(1.2)	1.01	(0.5)	1.02	(0.8)	*26.60*	0.99	1.00	**35.1**
	551.5	7.56E-03	6.91E-03	(0.5)	***1.00***	1.01	(0.4)	0.99	(0.7)	1.01	(1.6)	*6.14*	0.99	0.99	**34.9**
	618.3	9.32E-03	8.65E-03	(0.5)	***0.99***	1.00	(1.4)	0.98	(0.1)	1.00	(1.4)	*7.57*	0.99	0.98	**35.1**
	625.5	1.62E-03			***0.91***	0.92	(0.3)	0.91	(0.3)			*1.31*	0.99		**34.8**
	685.7	4.09E-02	3.71E-02	(0.5)	***1.00***	1.01	(1.2)	0.99	(0.3)	1.00	(0.8)	*33.20*	reference		**34.6**
	772.9	6.18E-03	5.61E-03	(0.7)	***1.01***	1.01	(1.2)	0.99	(0.1)	1.02	(1.9)	*5.02*	0.99	1.00	**34.8**
^{186}Re [I]	**122.6**	2.84E-03	2.79E-03	(1.1)	***1.01***	1.02	(0.9)	1.01	(0.5)	1.02	(0.5)	*0.603*	1.01	0.99	**110.9**
	137.2	4.43E-02	4.33E-02	(0.7)	***1.04***	1.04	(0.2)	1.03	(0.5)	1.04	(0.9)	*9.420*	reference		**112.4**

	γ	k_0 (%; 1s)			TW / [Lit or C] (% SD)							I_γ / $I_{\gamma,ref}$		σ (b)
FN	**(keV)**	**C**	**Lit**		**AVG**	**Y4 /Cavity**		**S84**		**X26**		I_γ	**TW / C**	**Lit / C**	**TW**
^{188}Re [IV/b] ---------- ^{188}Re [IV/a] <---- F_2 = 1 ---- ^{188m}Re [I]	**92.4**	7.34E-04	7.77E-04	(1.5)	***0.96***			0.96	(1.2)			*5.1*	0.98	0.91	**2.09**
	106.0	1.56E-03	1.50E-03	(1.6)	***1.03***			1.03	(1.5)			*10.8*	reference		**2.04**
	155.0	8.16E-02	7.77E-02	(0.6)	***1.00***			1.00	(0.8)			*15.20*	reference		**73.4**
	478.0	5.47E-03	5.29E-03	(0.8)	***1.00***			1.00	(1.3)			*1.02*	0.99	0.99	**74.2**
	633.0	6.87E-03	6.83E-03	(1.3)	***1.00***			1.00	(1.6)			*1.28*	0.96	0.96	**76.2**
	829.5	2.20E-03	2.17E-03		***1.02***			1.02	(5.0)			*0.41*	0.95	0.97	**77.6**
	931.3	2.95E-03	2.85E-03		***1.02***			1.02	(5.0)			*0.55*	0.97	0.99	**75.9**
	155.0	8.39E-02	7.99E-02		***1.00***	1.01	(0.3)	0.99	(0.2)	1.01	(0.5)		reference		**73.4**
	478.0	5.63E-03	5.44E-03		***1.00***	1.01	(0.7)	0.99	(1.1)	1.00	(2.0)		0.99	0.99	**74.2**
	633.0	7.06E-03	7.02E-03		***1.00***	0.99	(1.8)	0.98	(1.8)	1.01	(1.1)		0.96	0.96	**76.1**
	829.5	2.26E-03	2.23E-03		***1.02***	1.03	(3.0)	1.01	(2.0)	1.03	(1.5)		0.95	0.97	**77.6**
	931.3	3.03E-03	2.93E-03		***1.02***	1.03	(0.9)	1.01	(3.0)	1.03	(1.2)		0.97	0.99	**75.9**

	γ	k_0 (%; 1*s*)		TW / [Lit or C] (% SD)							I_γ / $I_{\gamma,ref}$		σ (b)
FN	**(keV)**	**C**	**Lit**	**AVG**	**Y4 /Cavity**		**S84**		**X26**		I_γ	**TW / C**	**Lit / C**	**TW**
^{197}Pt [IV/b] < - F_2 - ^{197m}Pt [I]	**346.5**	1.32E-05		***0.80***			0.80	(1.0)	0.80	(1.3)	*11.10*	reference		**0.035**
	191.4	5.79E-05		***1.30***	1.30	(1.3)	1.27	(1.5)	1.32	(1.3)	*3.70*	reference		**0.752**
	268.8	3.60E-06		***1.30***	1.28	(1.6)	1.31	(1.7)			*0.23*	1.00		**0.751**

	γ	k_0 (%; 1s)			TW / [Lit or C] (% SD)								I_γ / $I_{\gamma,ref}$		σ (b)
FN	**(keV)**	**C**	**Lit**		**AVG**	**Y4 /Cavity**		**S84**		**X26**		I_γ	**TW / C**	**Lit / C**	**TW**
^{199}Au [V/b,V/d] <- F_3=1 - ^{199}Pt [IV/b] <- F_2=1 - ^{199m}Pt [I]	**391.9**	2.34E-04						<-	**calculated only**			*84.94*	reference		**0.35**
	493.8	1.27E-04			***0.90***			0.90	(0.5)			*4.47*	1.00		**3.25**
	543.0	3.34E-04			***0.90***			0.90	(0.5)			*11.74*	reference		**3.25**
	714.6	4.12E-05			***0.90***			0.90	(0.5)			*1.45*	1.00		**3.26**
	158.4	1.14E-03	1.03E-03	(1.4)	***1.01***	1.01	(0.9)	1.00	(1.0)	1.01	(1.2)	*40.0*	reference		**3.30**
	208.2	2.48E-04	2.26E-04	(1.0)	***1.00***	1.00	(1.1)	1.00	(1.1)	1.00	(0.9)	*8.72*	1.00	0.99	**3.29**

FN	γ (keV)	k_0 (%; 1s) C	k_0 (%; 1s) Lit		TW / [Lit or C] (% SD) AVG	Y4 /Cavity		S84		X26	I_γ	I_γ / $I_{\gamma,ref}$ TW / C	I_γ / $I_{\gamma,ref}$ Lit / C	σ (b) TW
^{233}Pa [II/b] <- F_2=1 - ^{233}Th [I]	**300.1**	4.39E-03	4.37E-03	(0.3)	***1.01***	1.01	(1.0)	1.01	(1.3)		*6.63*	1.00	0.99	**7.409**
	311.9	2.55E-02	2.52E-02	(0.5)	***1.02***	1.02	(0.9)	1.02	(1.4)		*38.5*	reference		**7.400**
	340.5	2.95E-03	2.95E-03	(0.7)	***1.01***	1.01	(1.1)	1.01	(1.4)		*4.45*	1.00	0.99	**7.435**
	375.4	4.49E-04	4.49E-04	(0.6)	***1.00***	1.00	(1.9)	1.01	(2.0)		*0.679*	1.00	0.99	**7.371**
	398.5	9.21E-04	9.26E-04	(0.5)	***1.00***	1.00	(1.0)	1.01	(1.3)		*1.391*	1.00	0.98	**7.420**
	415.8	1.15E-03	1.16E-03	(1.0)	***1.00***	0.99	(1.5)	1.00	(1.4)		*1.73*	1.00	0.98	**7.411**
^{198}Au [I]	**411.8**		1.00	(-)	**($\sigma_0 \theta I_\gamma$) / AW**	**0.4786**					*95.54*	the comparator		**98.66**

The last 4 columns contain the reported I_γ values from references [6, 8] and their ratios against the most prominent line (reference) of the same radioisotope ($I_\gamma / I_{\gamma,\mathrm{ref}}$). The ($I_\gamma / I_{\gamma,\mathrm{ref}}$) ratios were found from the ratios between k_0 factors in TW and Lit (respectively) and were tabulated against the calculated ratios from the γ-ray intensities (TW/C and Lit/C).

The σ values are effective thermal neutron cross-sections (i.e. metastable, ground or combined; see ADS) computed with the aid of nuclear data from several sources [1, 2, 4–10]. See Table 10.21 for the mean values.

All the F_{Cd}, F_i factors and typical Westcott g_T factors are provided in the final compendium of Table 10.15.

10.4.2 Results for ^{235}U and ^{238}U

The experimental "effective" k_0-fission factors (see section 6.7) obtained in this work from the natural-U (NIST SRM 3164) and the ^{235}U-enriched (IRMM SP 89010) materials compiled in Table 10.10. The k_0 factors for ^{239}Np obtained from the NIST and the ^{235}U-depleted (IRMM NS 20017) materials are compiled in Table 10.11. The uncertainties in both tables correspond to the SD from the results of all irradiated samples of a given material. Final values are given in section 10.6.

Table 10.10: The k_0-fission factors found in this work from the natural-U (NIST SRM 3164) and ^{235}U-enriched (IRMM SP 89010) materials. The results were obtained from the mean and SD of all (replicate). The results from the NIST samples are separated per irradiation (irr) for comparison. The final values are reported in Table 10.17.

FN ADS	Energy (keV)	TW (% SD)					
		NIST 1st irr		IRMM enriched		NIST 2nd irr	
Zr-95	724.2	1.04E-03	(2.5)	1.05E-03	(2.3)	1.04E-03	(2.4)
I	756.7	1.28E-03	(0.6)	1.27E-03	(1.7)	1.31E-03	(1.0)
Nb-95 III/a	765.8	2.56E-05	(4.6)	2.56E-05	(0.5)	2.51E-05	(1.9)
Zr-97	507.6			1.12E-04	(5.3)	1.13E-04	(5.0)
I	703.8	2.39E-05	(5.1)	2.20E-05	(2.0)	2.36E-05	(4.0)
	1021.3	2.33E-05	(5.2)	2.28E-05	(2.0)	2.27E-05	(3.0)
	1276.1	2.06E-05	(5.0)	1.99E-05	(1.0)	2.00E-05	(2.6)
Nb-97m II/a	743.4	2.01E-03	(0.8)	2.02E-03	(1.3)	2.01E-03	(0.8)
Nb-97 III/a	657.9	2.03E-03	(0.6)	2.03E-03	(0.9)	2.04E-03	(0.7)

FN ADS	Energy (keV)	TW (% SD)					
		NIST 1st irr		IRMM enriched		NIST 2nd irr	
Mo-99	181.1			1.35E-04	(2.0)		
I	366.4	2.72E-05	(4.0)	2.60E-05	(3.0)	2.70E-05	(5.1)
	739.5	2.71E-04	(0.8)	2.70E-04	(1.4)	2.79E-04	(1.0)
	777.9	9.60E-05	(4.0)	9.50E-05	(2.0)	9.40E-05	(4.0)
Tc-99m II/d	140.5	1.74E-03	(1.6)	1.74E-03	(1.0)	1.75E-03	(1.5)
Ru-103	497.1	9.99E-04	(2.8)	9.79E-04	(1.5)	1.03E-03	(1.9)
I	610.3	6.39E-05	(5.0)	6.29E-05	(3.0)	6.48E-05	(7.0)
Rh-105	306.1	1.83E-05	(2.3)	1.80E-05	(3.0)	1.76E-05	(9.4)
III/c	318.9	6.62E-05	(2.6)	6.65E-05	(1.8)	6.64E-05	(1.5)
Te-131m	793.8			2.05E-05	(4.6)		
I	852.0			3.03E-05	(5.0)		
	1125.5			1.71E-05	(4.2)		
I-131	284.3			6.30E-05	(1.9)		
VI/b	364.5			8.40E-04	(1.0)		
	636.9			7.37E-05	(5.0)		
Te-132 I	228.2			1.38E-03	(0.8)		
I-133 VI/b	529.9	2.11E-03	(4.4)	2.14E-03	(1.3)	2.16E-03	(1.7)
I-135	288.5			7.00E-05	(5.0)	7.12E-05	(6.6)
I	836.8			1.56E-04	(2.5)	1.49E-04	(1.8)
	1038.8			1.80E-04	(1.0)	1.83E-04	(1.7)
	1131.5			5.16E-04	(4.5)	5.38E-04	(1.9)
	1260.4			6.44E-04	(1.8)	6.49E-04	(3.0)
	1457.6			2.02E-04	(4.6)	2.00E-04	(2.8)
	1502.8			2.50E-05	(1.5)	2.44E-05	(1.3)
	1678.0			2.16E-04	(1.3)	2.19E-04	(1.5)
	1706.5			9.14E-05	(2.7)	9.52E-05	(1.7)
	1791.2			1.78E-04	(2.0)	1.80E-04	(3.6)
Cs-137 (Ba-137m) II/c	661.7	1.91E-03	(4.0)	1.95E-03	(3.0)	1.93E-03	(3.0)

FN ADS	Energy (keV)	TW (% SD)					
		NIST 1st irr		IRMM enriched		NIST 2nd irr	
Ba-140	162.7	1.46E-04	(2.8)	1.45E-04	(6.5)	1.44E-04	(2.0)
I	304.9	9.47E-05	(2.5)	9.67E-05	(4.6)	9.76E-05	(1.8)
	423.7	7.43E-05	(8.0)	7.33E-05	(8.0)	7.20E-05	(3.2)
	437.6	4.54E-05	(1.1)	4.53E-05	(8.1)	4.45E-05	(5.6)
	537.3	5.57E-04	(0.8)	5.61E-04	(2.0)	5.56E-04	(2.9)
La-140	328.8	4.68E-04	(2.9)	4.60E-04	(2.1)	4.67E-04	(2.2)
II/a	432.5	6.59E-05	(2.2)	6.78E-05	(2.0)	6.95E-05	(2.0)
	487.0	1.06E-03	(2.4)	1.04E-03	(2.2)	1.07E-03	(1.7)
	751.6	1.01E-04	(2.3)	9.87E-05	(2.0)	1.02E-04	(2.3)
	815.8	5.40E-04	(2.4)	5.37E-04	(2.2)	5.51E-04	(0.8)
	867.8	1.27E-04	(2.0)	1.25E-04	(2.2)	1.30E-04	(2.5)
	919.6	6.01E-05	(2.5)	6.13E-05	(1.9)	6.34E-05	(2.0)
	925.2	1.55E-04	(2.0)	1.59E-04	(2.0)	1.63E-04	(2.3)
	1596.2	2.15E-03	(1.3)	2.15E-03	(1.0)	2.22E-03	(0.5)
Ce-141 I	145.4	1.03E-03	(0.7)	1.02E-03	(1.0)	1.06E-03	(2.0)
Ce-143	231.6	4.52E-05	(3.7)	4.55E-05	(1.8)	4.44E-05	(3.7)
I	293.3	9.30E-04	(0.6)	9.32E-04	(1.0)	9.43E-04	(0.9)
	350.6	7.12E-05	(1.9)	7.12E-05	(2.7)	7.09E-05	(2.0)
	664.6	1.26E-04	(1.7)	1.27E-04	(1.3)	1.23E-04	(0.7)
	721.9	1.21E-04	(1.7)	1.17E-04	(2.1)	1.19E-04	(0.7)
Nd-147	91.1	2.29E-04	(5.0)	2.20E-04	(3.8)	2.33E-04	(1.5)
I	319.4			1.74E-05	(6.0)	1.68E-05	(5.0)
	439.9			9.86E-06	(3.9)	1.11E-05	(6.1)
	531.0	1.08E-04	(5.0)	1.08E-04	(4.1)	1.10E-04	(3.8)

For ^{235}U fission: Q_0 = 0.47(5) and $\bar{E}_r$ = 0.59(8) eV from Lit.

Table 10.11: The k_0 factors for ^{239}Np found in this work from the natural-U (NIST SRM 3164) and ^{235}U-depleted (IRMM NS 20017) materials in Table 6.3. The results from the NIST samples are separated per irradiation (irr) for comparison. The mean results are given in Table 10.18.

FN ADS	Energy (keV)	TW (% SD)					
		NIST 1st irr		IRMM depleted		NIST 2nd irr	
Np-239	106.1	6.20E-03	(1.9)	6.12E-03	(0.9)	6.24E-03	(2.0)
II/b	209.8	7.81E-04	(0.9)	7.93E-04	(1.6)	7.90E-04	(0.9)
	228.2	2.60E-3	(2.5)	2.59E-03	(2.0)	2.62E-3	(2.5)
	277.6	3.37E-03	(0.8)	3.32E-03	(0.6)	3.40E-03	(1.9)
	285.8	1.85E-04	(1.0)	1.82E-04	(0.6)	1.85E-04	(2.0)
	315.9	3.70E-04	(0.8)	3.63E-04	(0.6)	3.75E-04	(0.9)
	334.2	4.75E-04	(1.2)	4.79E-04	(0.7)	4.83E-04	(1.6)

For ^{238}U(n,γ)^{239}U→^{239}Np*:* Q_0 = 103.4(13) and $\bar{E}_r$ = 16.9(12) eV from Lit.

10.5 Differences due to the choice of F_{Cd} factors

The Table 10.12 shows the Q_0 and $\bar{E}_r$ factors found in this work by means of the α vector method [62, 80, 89] with the adoption of the F_{Cd} factors from the recommended literature [24]. These values are also compared to the ones derived by Tkv. The comparison is made by means of the ratio Δ = TW/Tkv between the quantities (i.e. ΔQ_0 or $\Delta \bar{E}_r$). In the Table 10.13 on the other hand the comparison was done between the Q_0 factors found in this work by means of the $\bar{E}_r$ factors from the recommended literature [24] and the Tkv values.

The Table 10.14 summarizes the ratios ΔQ_0 and Δk_0 between the original Q_0 and k_0 factors and the ones computed after the adoption of the F_{Cd} factors from Tkv. The ΔQ_0 and Δk_0 values were defined as:

$$\begin{aligned} \Delta Q_0 &= \frac{Q_0^*}{Q_0}; \\ \Delta k_0 &= \frac{k_0^*}{k_0}; \end{aligned} \tag{10.2}$$

with the asterisk * denoting the values obtained by adopting the F_{Cd} factors from Tkv. The Q_0^* factor was computed by inputting:

- A) the $\bar{E}_r$ value adopted from the recommended literature [23, 203] or,

- B) with the $\bar{E}_r$ factor reported by Trkov et al. (see Table 10.13).

The Δk_0 values are given for each irradiation channel employed (S84, Y4 and X26) per the Cd-subtraction technique of eq. (2.62).

For ^{114}Cd the reported F_{Cd} factor was determined experimentally in this work by varying $\bar{E}_r$ until the SD between Q_0 results from the different channels is minimized (multi-channel approach).

Table 10.12: The Q_0 and $\bar{E}_r$ factors found in this work by means of the α vector method in [62, 80, 89] **with F_{Cd} factors adopted from Lit as compared to the values derived by Tkv.**

			TW				Tkv			Δ = Tkv/TW	
TI	**FN**	**ADS**	F_{Cd}	$\bar{E}_r$ (1s; %)		Q_0 (1s; %)	F_{Cd}	$\bar{E}_r$	Q_0	ΔQ_0	$\Delta \bar{E}_r$
^{89}Y	^{90m}Y	I	1.000	4300	(8)	4.08 (2)	0.977	11059	0.656	0.16	2.57
^{138}Ba	^{139}Ba	I	1.000	15700	(3.2)	1.04 (15)	0.992	5600	0.66	0.63	0.36
^{112}Sn	^{113}Sn - ^{113m}In	IV/b - V/c	1.000	107	(3)	48.3 (3)	0.958	148.8	35.16	0.73	1.39
^{68}Zn	^{69m}Zn	I	1.000	590	(10)	3.21 (1)	0.972	605.4	2.521	0.78	1.03
^{198}Pt	^{199}Au	V/b - V/d	1.000	106	(3)	16.9 (2)	0.943	523.8	13.74	0.81	4.94
^{153}Eu	^{154}Eu	IV/b	1.000	5.8	(4)	4.75 (3)	0.970	9.54	3.954	0.83	1.64
^{181}Ta	^{182}Ta	IV/b	0.972	10.4	(6)	37.0 (4)	0.970	11.55	31.9	0.86	1.11
^{179}Hf	^{180m}Hf	I	1.000	16	(12)	14.1 (2)	0.965	21.7	12.33	0.87	1.34

			TW				Tkv			Δ = Tkv/TW	
TI	**FN**	**ADS**	F_{Cd}	$\bar{E}_r$ (1s; %)	Q_0 (1s; %)		F_{Cd}	$\bar{E}_r$	Q_0	ΔQ_0	$\Delta \bar{E}_r$
^{180}Hf	^{181}Hf	I	1.000	115	(6)	2.44 (3)	0.982	160.5	2.218	0.91	1.40
^{50}Ti	^{51}Ti	I	1.000	63200	(13)	0.52 (2)	0.999	81694	0.473	0.91	1.29
^{51}V	^{52}V	I	1.000	7230	(4)	0.55 (2)	0.998	5359	0.501	0.91	0.74
^{23}Na	^{24}Na	IV/b	1.000	3380	(11)	0.63 (8)	0.990	2246	0.58	0.92	0.66
^{164}Dy	^{165}Dy	IV/b	1.000	224	(5)	0.13 (22)	1.092	6.268	0.1171	0.92	0.03
^{186}W	^{187}W	I	0.910	20.5	(1)	13.8 (1)	0.968	20.26	12.69	0.92	0.99
^{45}Sc	^{46}Sc	IV/b	1.000	5130	(17)	0.45 (8)	1.000	0.786	0.42	0.93	0.00
^{64}Zn	^{65}Zn	I	1.000	2560	(10)	1.90 (2)	0.970	2798	1.784	0.94	1.09
^{165}Ho	^{166}Ho	I	0.990	12.3	(3.3)	11.2 (3)	0.967	14.69	10.51	0.94	1.19
^{50}Cr	^{51}Cr	I	1.000	7530	(16)	0.48 (2)	1.002	21295	0.451	0.94	2.83

			TW				Tkv			Δ = Tkv/TW	
TI	**FN**	**ADS**	F_{Cd}	$\bar{E}_r$ (1s; %)		Q_0 (1s; %)	F_{Cd}	$\bar{E}_r$	Q_0	ΔQ_0	$\Delta \bar{E}_r$
^{37}Cl	^{38}Cl	IV/b	1.000	13700	(14)	0.48 (2)	1.000	35203	0.453	0.94	2.57
^{115}In	^{116m}In	IV/b	0.927	1.56	(7)	16.7 (2)	0.949	1.524	15.89	0.95	0.98
^{123}Sb	^{124}Sb	VI/c	1.000	28.2	(6)	30.5 (2)	0.967	31.93	29.2	0.96	1.13
^{109}Ag	^{110m}Ag	I	1.000	6.08	(1)	16.5 (2)	0.975	6.03	15.81	0.96	0.99
^{54}Mn	^{55}Mn	I	1.000	468	(11)	1.04 (2)	0.976	381.1	0.999	0.96	0.81
^{58}Fe	^{59}Fe	I	1.000	637	(24)	0.99 (2)	0.977	518.3	0.946	0.96	0.81
^{98}Mo	^{99}Mo - ^{99m}Tc	I - II/d	1.000	241	(10)	54.0 (4)	0.964	266.1	52.25	0.97	1.10
^{96}Ru	^{97}Ru	I	1.000	776	(16)	25.6 (2)	0.952	1452	24.94	0.97	1.87
^{130}Ba	^{131}Ba	IV/b	1.000	69.9	(5)	20.7 (3)	0.975	88.35	20.14	0.97	1.26
^{176}Yb	^{177}Yb	IV/b	1.000	412	(5)	2.51 (3)	0.887	593	2.446	0.97	1.44

			TW				Tkv			Δ = Tkv/TW	
TI	**FN**	**ADS**	F_{Cd}	$\bar{E}_r$ (1s; %)		Q_0 (1s; %)	F_{Cd}	$\bar{E}_r$	Q_0	ΔQ_0	$\Delta \bar{E}_r$
^{159}Tb	^{160}Tb	I	1.000	18.1	(15)	18.2 (2)	0.966	25.02	17.74	0.97	1.38
^{100}Mo	^{101}Mo - ^{101}Tc	I - II/a	1.000	672	(14)	19.9 (2)	0.967	878.9	19.41	0.98	1.31
^{63}Cu	^{64}Cu	IV/b	1.000	1040	(5)	1.11 (3)	0.980	1281	1.091	0.98	1.23
^{71}Ga	^{72}Ga	IV/b	1.000	154	(12)	6.94 (1)	0.955	166	6.898	0.99	1.08
^{27}Al	^{28}Al	I	1.000	11800	(6)	0.54 (2)	0.996	12067	0.537	0.99	1.02
^{158}Gd	^{159}Gd	I	1.000	48	(8)	31.2 (2)	0.975	48.16	31.03	1.00	1.00
^{65}Cu	^{66}Cu	I	1.030	766	(17)	1.01 (2)	0.961	770.5	1.01	1.00	1.01
^{174}Yb	^{175}Yb	IV/b	1.000	602	(8)	0.38 (19)	1.010	0.114	0.3845	1.01	0.00
^{81}Br	^{82}Br	IV/b	1.000	152	(9)	19.3 (2)	0.961	168.2	19.58	1.01	1.11
^{26}Mg	^{27}Mg	I	1.000	257000	(13)	0.46 (2)	0.999	471341	0.47	1.02	1.83

			TW				Tkv			Δ = Tkv/TW	
TI	**FN**	**ADS**	F_{Cd}	$\bar{E}_r$ (1s; %)		Q_0 (1s; %)	F_{Cd}	$\bar{E}_r$	Q_0	ΔQ_0	$\Delta \bar{E}_r$
^{59}Co	^{60m}Co	I	1.000	136	(5.1)	1.97 (2)	1.000	121.9	2.018	1.02	0.90
^{75}As	^{76}As	I	1.000	106	(34)	15.0 (1)	0.965	127.2	15.33	1.02	1.20
^{121}Sb	^{122}Sb	IV/b	0.990	13.1	(4)	34.7 (2)	0.961	14.45	35.69	1.03	1.10
^{85}Rb	^{86}Rb	IV/b	1.000	839	(9)	14.4 (2)	0.962	1416	15.39	1.07	1.69
^{104}Ru	^{105}Ru - ^{105m}Rh - ^{105}Rh	I - II/a - III/c	1.000	495	(10)	13.1 (2)	0.921	737.5	13.99	1.07	1.49
^{139}La	^{140}La	I	1.000	76.0	(3.9)	1.16 (1)	0.985	94.73	1.247	1.08	1.25
^{84}Sr	^{85m}Sr	I	1.000	469	(7)	13.0 (3)	0.972	929.6	14	1.08	1.98
^{107}Ag	^{108}Ag	I	1.000	39	(5)	2.72 (2)	0.980	62.8	2.927	1.08	1.63
^{93}Nb	^{94m}Nb	I	1.000	574	(8)	7.28 (2)	0.945	937.9	7.844	1.08	1.63
^{108}Pd	^{109}Pd - ^{109m}Ag	IV/b - V/c	1.000	39.7	(5)	26.6 (4)	0.896	40.2	28.70	1.08	1.01

			TW				Tkv			Δ = Tkv/TW	
TI	**FN**	**ADS**	F_{Cd}	$\bar{E}_r$ (1s; %)		Q_0 (1s; %)	F_{Cd}	$\bar{E}_r$	Q_0	ΔQ_0	$\Delta \bar{E}_r$
^{64}Ni	^{65}Ni	I	1.000	14200	(12)	0.46 (2)	0.975	2786	0.502	1.09	0.20
^{132}Ba	^{133m}Ba	I	1.000	143	(10)	4.6 (5)	0.953	220.5	5.173	1.11	1.54
^{86}Sr	^{87m}Sr	I	1.000	795	(2)	4.04 (2)	0.972	931.8	4.593	1.14	1.17
^{113}In	^{114m}In	IV/b	1.000	6.41	(15)	24.1 (2)	0.957	6.556	27.87	1.16	1.02
^{169}Tm	^{170}Tm	I	1.000	4.8	(2)	13.3 (3)	0.974	5.19	15.42	1.16	1.08
^{124}Sn	^{125}Sn - ^{125}Sb	I - VII/b	1.000	74	(7)	16.7 (2)	0.977	69.34	19.76	1.18	0.93
^{114}Cd	^{115}Cd - ^{115m}In	I - II/a	0.400	207	(19)	31.4 (4)	0.791	287.9	39.1	1.24	1.39
^{102}Ru	^{103}Ru	I	1.000	181	(4)	3.35 (3)	0.969	525.8	4.272	1.28	2.90
^{174}Hf	^{175}Hf	I	1.000	29.6	(7)	0.61 (3)	0.980	212	0.7988	1.30	7.15
^{152}Gd	^{153}Gd	I	1.000	16.7	(9)	0.56 (3)	0.990	119.6	0.7459	1.33	7.16

			TW				**Tkv**			**Δ = Tkv/TW**	
TI	**FN**	**ADS**	F_{Cd}	$\bar{E}_r$ **(1s; %)**	Q_0 **(1s; %)**		F_{Cd}	$\bar{E}_r$	Q_0	ΔQ_0	$\Delta \bar{E}_r$
^{41}K	^{42}K	I	1.000	2960 (7)	0.74 (2)		0.962	3278	1.063	1.44	1.11
^{116}Sn	^{117m}Sn	I	1.000	128 (3)	55.8 (3)		0.974	183	86	1.54	1.43
^{110}Pd	^{111m}Pd	I	1.000	950 (9)	11.9 (3)		0.947	1636	149.5	12.56	1.72

The Δ = Tkv/TW values are the ratios between the results reported by both authors.

Table 10.13: The Q_0 factors found in this work [62, 80, 89] **by means of the $\bar{E}_r$ and F_{Cd} factors adopted from Lit as compared to the values derived by Tkv.**

			TW				Tkv			Δ = Tkv/TW	
TI	**FN**	**ADS**	F_{Cd}	$\bar{E}_r$ (1s; %)		Q_0 (1s; %)		F_{Cd}	$\bar{E}_r$	Q_0	ΔQ_0	$\Delta \bar{E}_r$
^{89}Y	^{90m}Y	I	1.000	4300	(8)	4.08	(2)	0.977	11059	0.656	0.16	0.11
^{138}Ba	^{139}Ba	I	1.000	15700	(3.2)	1.04	(15)	0.992	5600	0.66	0.63	0.04
^{112}Sn	^{113}Sn - ^{113m}In	IV/b - V/c	1.000	107	(3)	48.3	(3)	0.958	148.8	35.16	0.73	0.24
^{68}Zn	^{69m}Zn	I	1.000	590	(10)	3.21	(1)	0.972	605.4	2.521	0.78	0.71
^{198}Pt	^{199}Au	V/b - V/d	1.000	106	(3)	16.9	(2)	0.943	523.8	13.74	0.81	0.41
^{153}Eu	^{154}Eu	IV/b	1.000	5.8	(4)	4.75	(3)	0.970	9.54	3.954	0.83	0.28
^{181}Ta	^{182}Ta	IV/b	0.972	10.4	(6)	37.0	(4)	0.970	11.55	31.9	0.86	0.22
^{179}Hf	^{180m}Hf	I	1.000	16	(12)	14.1	(2)	0.965	21.7	12.33	0.87	0.58

			TW				Tkv			Δ = Tkv/TW	
TI	**FN**	**ADS**	F_{Cd}	$\bar{E}_r$ (1s; %)		Q_0 (1s; %)	F_{Cd}	$\bar{E}_r$	Q_0	ΔQ_0	$\Delta \bar{E}_r$
^{180}Hf	^{181}Hf	I	1.000	115	(6)	2.44 (3)	0.982	160.5	2.218	0.91	0.36
^{50}Ti	^{51}Ti	I	1.000	63200	(13)	0.52 (2)	0.999	81694	0.473	0.91	0.57
^{51}V	^{52}V	I	1.000	7230	(4)	0.55 (2)	0.998	5359	0.501	0.91	0.57
^{23}Na	^{24}Na	IV/b	1.000	3380	(11)	0.63 (8)	0.990	2246	0.58	0.92	0.12
^{164}Dy	^{165}Dy	IV/b	1.000	224	(5)	0.13 (22)	1.092	6.268	0.1171	0.92	0.04
^{186}W	^{187}W	I	0.910	20.5	(1)	13.8 (1)	0.968	20.26	12.69	0.92	0.92
^{45}Sc	^{46}Sc	IV/b	1.000	5130	(17)	0.45 (8)	1.000	0.786	0.42	0.93	0.12
^{64}Zn	^{65}Zn	I	1.000	2560	(10)	1.90 (2)	0.970	2798	1.784	0.94	0.47
^{165}Ho	^{166}Ho	I	0.990	12.3	(3.3)	11.2 (3)	0.967	14.69	10.51	0.94	0.38
^{50}Cr	^{51}Cr	I	1.000	7530	(16)	0.48 (2)	1.002	21295	0.451	0.94	0.47

			TW				Tkv			Δ = Tkv/TW	
TI	**FN**	**ADS**	F_{Cd}	$\bar{E}_r$ (1s; %)		Q_0 (1s; %)	F_{Cd}	$\bar{E}_r$	Q_0	ΔQ_0	$\Delta \bar{E}_r$
^{37}Cl	^{38}Cl	IV/b	1.000	13700	(14)	0.48 (2)	1.000	35203	0.453	0.94	0.59
^{115}In	^{116m}In	IV/b	0.927	1.56	(7)	16.7 (2)	0.949	1.524	15.89	0.95	0.48
^{123}Sb	^{124}Sb	VI/c	1.000	28.2	(6)	30.5 (2)	0.967	31.93	29.2	0.96	0.48
^{109}Ag	^{110m}Ag	I	1.000	6.08	(1)	16.5 (2)	0.975	6.03	15.81	0.96	0.64
^{54}Mn	^{55}Mn	I	1.000	468	(11)	1.04 (2)	0.976	381.1	0.999	0.96	0.48
^{58}Fe	^{59}Fe	I	1.000	637	(24)	0.99 (2)	0.977	518.3	0.946	0.96	0.48
^{98}Mo	^{99}Mo - ^{99m}Tc	I - II/d	1.000	241	(10)	54.0 (4)	0.964	266.1	52.25	0.97	0.24
^{96}Ru	^{97}Ru	I	1.000	776	(16)	25.6 (2)	0.952	1452	24.94	0.97	0.49
^{130}Ba	^{131}Ba	IV/b	1.000	69.9	(5)	20.7 (3)	0.975	88.35	20.14	0.97	0.32
^{176}Yb	^{177}Yb	IV/b	1.000	412	(5)	2.51 (3)	0.887	593	2.446	0.97	0.32

			TW				Tkv			Δ = Tkv/TW	
TI	**FN**	**ADS**	F_{Cd}	$\bar{E}_r$ (1s; %)		Q_0 (1s; %)	F_{Cd}	$\bar{E}_r$	Q_0	ΔQ_0	$\Delta \bar{E}_r$
^{159}Tb	^{160}Tb	I	1.000	18.1	(15)	18.2 (2)	0.966	25.02	17.74	0.97	0.65
^{100}Mo	^{101}Mo - ^{101}Tc	I - II/a	1.000	672	(14)	19.9 (2)	0.967	878.9	19.41	0.98	0.49
^{63}Cu	^{64}Cu	IV/b	1.000	1040	(5)	1.11 (3)	0.980	1281	1.091	0.98	0.39
^{71}Ga	^{72}Ga	IV/b	1.000	154	(12)	6.94 (1)	0.955	166	6.898	0.99	0.97
^{27}Al	^{28}Al	I	1.000	11800	(6)	0.54 (2)	0.996	12067	0.537	0.99	0.62
^{158}Gd	^{159}Gd	I	1.000	48	(8)	31.2 (2)	0.975	48.16	31.03	1.00	0.50
^{65}Cu	^{66}Cu	I	1.030	766	(17)	1.01 (2)	0.961	770.5	1.01	1.00	0.50
^{174}Yb	^{175}Yb	IV/b	1.000	602	(8)	0.38 (19)	1.010	0.114	0.3845	1.01	0.05
^{81}Br	^{82}Br	IV/b	1.000	152	(9)	19.3 (2)	0.961	168.2	19.58	1.01	0.68
^{26}Mg	^{27}Mg	I	1.000	257000	(13)	0.46 (2)	0.999	471341	0.47	1.02	0.64

			TW				Tkv			Δ = Tkv/TW	
TI	**FN**	**ADS**	F_{Cd}	$\bar{E}_r$ (1s; %)		Q_0 (1s; %)	F_{Cd}	$\bar{E}_r$	Q_0	ΔQ_0	$\Delta \bar{E}_r$
^{59}Co	^{60m}Co	I	1.000	136	(5.1)	1.97 (2)	1.000	121.9	2.018	1.02	0.51
^{75}As	^{76}As	I	1.000	106	(34)	15.0 (1)	0.965	127.2	15.33	1.02	1.02
^{121}Sb	^{122}Sb	IV/b	0.990	13.1	(4)	34.7 (2)	0.961	14.45	35.69	1.03	0.51
^{85}Rb	^{86}Rb	IV/b	1.000	839	(9)	14.4 (2)	0.962	1416	15.39	1.07	0.71
^{104}Ru	^{105}Ru - ^{105m}Rh - ^{105}Rh	I - II/a - III/c	1.000	495	(10)	13.1 (2)	0.921	737.5	13.99	1.07	0.71
^{139}La	^{140}La	I	1.000	76.0	(3.9)	1.16 (1)	0.985	94.73	1.247	1.08	1.08
^{84}Sr	^{85m}Sr	I	1.000	469	(7)	13.0 (3)	0.972	929.6	14	1.08	0.43
^{107}Ag	^{108}Ag	I	1.000	39	(5)	2.72 (2)	0.980	62.8	2.927	1.08	0.54
^{93}Nb	^{94m}Nb	I	1.000	574	(8)	7.28 (2)	0.945	937.9	7.844	1.08	0.72
^{108}Pd	^{109}Pd - ^{109m}Ag	IV/b - V/c	1.000	39.7	(5)	26.6 (4)	0.896	40.2	28.70	1.08	0.31

			TW				Tkv			Δ = Tkv/TW	
TI	**FN**	**ADS**	F_{Cd}	$\bar{E}_r$ (1s; %)		Q_0 (1s; %)	F_{Cd}	$\bar{E}_r$	Q_0	ΔQ_0	$\Delta \bar{E}_r$
^{64}Ni	^{65}Ni	I	1.000	14200	(12)	0.46 (2)	0.975	2786	0.502	1.09	0.68
^{132}Ba	^{133m}Ba	I	1.000	143	(10)	4.6 (5)	0.953	220.5	5.173	1.11	0.25
^{86}Sr	^{87m}Sr	I	1.000	795	(2)	4.04 (2)	0.972	931.8	4.593	1.14	0.57
^{113}In	^{114m}In	IV/b	1.000	6.41	(15)	24.1 (2)	0.957	6.556	27.87	1.16	0.77
^{169}Tm	^{170}Tm	I	1.000	4.8	(2)	13.3 (3)	0.974	5.19	15.42	1.16	0.46
^{124}Sn	^{125}Sn - ^{125}Sb	I - VII/b	1.000	74	(7)	16.7 (2)	0.977	69.34	19.76	1.18	0.59
^{114}Cd	^{115}Cd - ^{115m}In	I - II/a	0.400	207	(19)	31.4 (4)	0.791	287.9	39.1	1.24	0.31
^{102}Ru	^{103}Ru	I	1.000	181	(4)	3.35 (3)	0.969	525.8	4.272	1.28	0.43
^{174}Hf	^{175}Hf	I	1.000	29.6	(7)	0.61 (3)	0.980	212	0.7988	1.30	0.43
^{152}Gd	^{153}Gd	I	1.000	16.7	(9)	0.56 (3)	0.990	119.6	0.7459	1.33	0.44

			TW			Tkv			Δ = Tkv/TW	
TI	**FN**	**ADS**	F_{Cd}	$\bar{E}_r$ (1s; %)	Q_0 (1s; %)	F_{Cd}	$\bar{E}_r$	Q_0	ΔQ_0	$\Delta \bar{E}_r$
^{41}K	^{42}K	I	1.000	2960 (7)	0.74 (2)	0.962	3278	1.063	1.44	0.72
^{116}Sn	^{117m}Sn	I	1.000	128 (3)	55.8 (3)	0.974	183	86	1.54	0.62
^{110}Pd	^{111m}Pd	I	1.000	950 (9)	11.9 (3)	0.947	1636	149.5	12.56	5.03

The Δ = Tkv/TW values are the ratios between the results reported by both authors.

Table 10.14: The ratios between the Q_0 and k_0 factors found in this work [62, 80, 89] **with F_{Cd} factors adopted from Lit against the resulting values with F_{Cd} factors adopted from Tkv. The ΔQ_0 ratios were calculated twice: by inputting the $\bar{E}_r$ values from Lit (A) or, by inputting the $\bar{E}_r$ values proposed by Trv (B).**

				ΔQ_0		Δk_0				
TI	**FN**	**ADS**	F_{Cd}	**A**	**B**	**Y4**	**X26**	**S84**	**AVG**	**SD (%)**
^{23}Na	^{24}Na	IV/b	0.990	1.00	1.00	1.00	1.00	1.00	1.00	0.0
^{26}Mg	^{27}Mg	I	0.999	1.00	1.00	1.00	1.00	1.00	1.00	0.0
^{27}Al	^{28}Al	I	0.996	1.00	1.00	1.00	1.00	1.00	1.00	0.0
^{37}Cl	^{38}Cl	IV/b	1.000	1.00	1.00	1.00	1.00	1.00	1.00	0.0
^{41}K	^{42}K	I	0.962	1.05	1.05	1.00	1.00	1.00	1.00	0.1
^{45}Sc	^{46}Sc	IV/b	1.000	1.00	1.00	1.00	1.00	1.00	1.00	0.0
^{50}Ti	^{51}Ti	I	0.999	1.00	1.00	1.00	1.00	1.00	1.00	0.0
^{51}V	^{52}V	I	0.998	1.00	1.00	1.00	1.00	1.00	1.00	0.0
^{50}Cr	^{51}Cr	I	1.002	1.00	1.00	1.00	1.00	1.00	1.00	0.0
^{54}Mn	^{55}Mn	I	0.976	1.03	1.03	1.00	1.00	1.00	1.00	0.1
^{58}Fe	^{59}Fe	I	0.977	1.03	1.03	1.00	1.00	1.00	1.00	0.1

				ΔQ_0		Δk_0				
TI	**FN**	**ADS**	F_{Cd}	**A**	**B**	**Y4**	**X26**	**S84**	**AVG**	**SD (%)**
^{59}Co	^{60m}Co	I	1.000	1.00	1.00	1.00	1.00	1.00	1.00	0.0
	^{60}Co	IV/b		1.00	1.00	1.00	1.00	1.00	1.00	0.0
^{64}Ni	^{65}Ni	I	0.975	1.02	1.02	1.00	1.00	1.00	1.00	0.0
^{63}Cu	^{64}Cu	IV/b	0.980	1.02	1.03	1.00	1.00	1.00	1.00	0.1
^{65}Cu	^{66}Cu	I	0.961	1.08	1.08	1.00	1.00	1.00	1.00	0.2
^{64}Zn	^{65}Zn	I	0.970	1.03	1.04	1.00	1.00	1.00	1.00	0.2
^{68}Zn	^{69m}Zn	I	0.972	1.03	1.03	1.00	1.00	0.99	1.00	0.2
^{71}Ga	^{72}Ga	IV/b	0.955	1.06	1.05	0.99	1.00	0.98	0.99	0.7
^{75}As	^{76}As	I	0.965	1.06	1.07	0.99	0.99	0.97	0.98	1.2
^{81}Br	^{82}Br	IV/b	0.961	1.06	1.06	0.99	0.99	0.97	0.98	1.2
^{85}Rb	^{86}Rb	IV/b	0.962	1.05	1.09	0.99	1.00	0.98	0.99	1.0
^{87}Rb	^{88}Rb	I	0.958	1.12	1.12	0.96	0.98	0.93	0.96	2.9
^{84}Sr	^{85m}Sr	I	0.972	1.05	1.05	0.99	1.00	0.98	0.99	1.0
	^{85}Sr	IV/b		1.05	1.08	0.99	1.00	0.98	0.99	0.9

				ΔQ_0		Δk_0				
TI	**FN**	**ADS**	F_{Cd}	**A**	**B**	**Y4**	**X26**	**S84**	**AVG**	**SD (%)**
^{86}Sr	^{87m}Sr	I	0.972	1.02	1.03	1.00	1.00	1.00	1.00	0.2
^{89}Y	^{90m}Y	I	0.977	1.03	1.03	1.00	1.00	0.99	1.00	0.3
^{93}Nb	^{94m}Nb	I	0.945	1.09	1.08	0.99	1.00	0.97	0.99	1.2
^{98}Mo	^{99}Mo - ^{99m}Tc	I - II/d	0.964	1.15	1.15	0.93	0.97	0.90	0.93	3.7
^{100}Mo	^{101}Mo - ^{101}Tc	I - II/a	0.967	1.08	1.08	0.98	0.99	0.96	0.98	1.8
^{96}Ru	^{97}Ru	I	0.952	1.09	1.12	0.97	0.99	0.95	0.97	2.1
^{102}Ru	^{103}Ru	I	0.969	1.02	1.07	1.00	1.00	1.00	1.00	0.2
^{104}Ru	^{105}Ru - ^{105m}Rh - ^{105}Rh	I - II/a - III/c	0.921	1.13	1.14	0.98	0.99	0.95	0.97	2.4
^{108}Pd	^{109}Pd - ^{109m}Ag	IV/b - V/c	0.896	1.14	1.14	0.95	0.98	0.92	0.95	3.1
^{110}Pd	^{111m}Pd	I	0.947	1.07	1.11	0.99	1.00	0.97	0.99	1.3
	^{111}Ag	VII/c		1.07	1.11	0.99	1.00	0.97	0.99	1.2
^{107}Ag	^{108}Ag	I	0.980	1.03	1.02	1.00	1.00	1.00	1.00	0.2
^{109}Ag	^{110m}Ag	I	0.975	1.04	1.04	0.99	1.00	0.98	0.99	0.7

				ΔQ_0		Δk_0				
TI	**FN**	**ADS**	F_{Cd}	**A**	**B**	**Y4**	**X26**	**S84**	**AVG**	**SD (%)**
^{114}Cd	^{115}Cd - ^{115m}In	I - II/a	0.791	0.37	0.38	1.30	1.11	1.71	1.37	22.4
^{113}In	^{114m}In	IV/b	0.957	1.06	1.09	0.98	0.99	0.96	0.98	1.3
^{115}In	^{116m}In	IV/b	0.949	0.95	0.95	1.01	1.01	1.02	1.02	0.9
^{112}Sn	^{113}Sn - ^{113m}In	IV/b - V/c	0.958	1.07	1.10	0.97	0.98	0.95	0.97	1.8
^{116}Sn	^{117m}Sn	I	0.974	1.05	1.08	0.98	0.99	0.96	0.98	1.2
^{124}Sn	^{125}Sn - ^{125}Sb	I - VII/b	0.977	1.03	1.02	0.99	1.00	0.99	0.99	0.6
^{121}Sb	^{122}Sb	IV/b	0.961	1.06	1.07	0.97	0.99	0.96	0.97	1.4
^{123}Sb	^{124}Sb	VI/c	0.967	1.07	1.08	0.97	0.99	0.96	0.97	1.6
^{130}Ba	^{131}Ba	IV/b	0.975	1.05	1.07	0.98	0.99	0.97	0.98	1.2
^{132}Ba	^{133m}Ba	I	0.953	1.04	1.06	1.00	1.00	0.99	1.00	0.4
^{138}Ba	^{139}Ba	I	0.992	1.02	1.00	1.00	1.00	1.00	1.00	0.1
^{139}La	^{140}La	I	0.985	1.02	1.03	1.00	1.00	1.00	1.00	0.1
^{153}Eu	^{154}Eu	IV/b	0.970	1.04	1.07	1.00	1.00	0.99	1.00	0.3
^{152}Gd	^{153}Gd	I	0.990	1.02	1.05	1.00	1.00	1.00	1.00	0.0
^{158}Gd	^{159}Gd	I	0.975	1.04	1.04	0.98	0.99	0.97	0.98	1.0

				ΔQ_0		Δk_0				
TI	**FN**	**ADS**	F_{Cd}	**A**	**B**	**Y4**	**X26**	**S84**	**AVG**	**SD (%)**
^{159}Tb	^{160}Tb	I	0.966	1.04	1.07	0.99	0.99	0.98	0.99	0.9
^{164}Dy	^{165}Dy	IV/b	1.092	0.87	1.10	1.00	1.00	1.00	1.00	0.1
^{165}Ho	^{166}Ho	I	0.967	1.04	1.05	0.99	1.00	0.99	0.99	0.6
^{169}Tm	^{170}Tm	I	0.974	1.02	1.03	0.99	1.00	0.99	0.99	0.4
^{174}Yb	^{175}Yb	IV/b	1.010	0.97	1.03	1.00	1.00	1.00	1.00	0.0
^{176}Yb	^{177}Yb	IV/b	0.887	1.06	1.08	1.00	1.00	0.99	1.00	0.4
^{174}Hf	^{175}Hf	I	0.980	1.04	1.06	1.00	1.00	1.00	1.00	0.1
^{179}Hf	^{180m}Hf	I	0.965	1.06	1.07	0.99	0.99	0.97	0.98	1.1
^{180}Hf	^{181}Hf	I	0.982	1.02	1.03	1.00	1.00	1.00	1.00	0.1
^{181}Ta	^{182}Ta	IV/b	0.970	1.00	1.00	1.00	1.00	1.00	1.00	0.1
^{186}W	^{187}W	I	0.968	0.92	0.92	1.02	1.01	1.04	1.02	1.6
^{198}Pt	^{199}Au	V/b - V/d	0.943	1.09	1.21	0.98	0.99	0.96	0.98	1.8

AVG = mean of the reported Δk_0 ratios, which are given per irradiation channel following the Cd-subtraction method.

10.6 An experimental k_0-library

10.6.1 For (n,γ) reactions

A compendium of k_0 nuclear data for 76 (n,γ) target isotopes and the monitoring of 96 formed radionuclides states is given in Table 10.15. These values were determined with $N_{Ch} \leq 4$ irradiation channels with characteristics given in Table 6.6. and Figure 6.7. The different number of standards (m; materials) employed and their typical self-shielding correction factors are listed in Table 6.3.

The Q_0 factors were found by inputting the $\bar{E}_r$ from Lit (first line), or by means of the α-vector method ($\bar{E}_r$ determination; underlined values; second line) [89]. The relative difference with the Lit or C value is tabulated by means of:

$$\Delta = \left[\left(\frac{k_{0,TW}}{k_{0,literature}} \right) - 1 \right] \tag{10.3}$$

with Δ expressed in percentage.

The provided uncertainties for the k_0 and Q_0 factors in TW are combined standard uncertainties. The uncertainties from the Lit values are quoted as given in these references (i.e. these are not standard uncertainties). A discussion of the uncertainty evaluation and estimates for a single determination and (later) for multiple determinations, i.e. different materials, channels and detectors is given in Chapter 7. In the last part of that chapter, coverage k factors for a 95% confidence level are given depending on the number of channels employed for the determination. The uncertainty in the $\bar{E}_r$ was obtained from eq. (6.17), i.e. the standard error from the polynomial regressions in the graphs reported in section 10.3.

The next section deals with the recommended k_0 and k_0-fission factors for ^{235}U (20 fission products) and ^{238}U (^{239}Np) determination. These values are not reported in Table 10.15.

Table 10.15: Compendium of k_0 nuclear data for 76 nuclides investigated at the SCK•CEN & Universiteit Gent in references [62, 80, 81] **as compared to those reported in Lit. The Q_0 factors were found by inputting the $\bar{E}_r$ from Lit (first line), or by means of the α-vector method ($\bar{E}_r$ determination; underlined values; second line)** [89]**. See bottom caption for more information.**

Target	$\bar{E}_r$ in eV (%; 1*s*)		Q_0 (%; 1*s*)* TW		Q_0 (%; 1*s*)* Lit		FI F_i; effective state (bold)	ADS $T_{1/2}$	γ (keV)	k_0 (%; 1*s*)		m	N_{Ch}	Δ%
^{23}Na	3380	(11)					^{24m}Na	I						
	<u>36.7</u>	(4)					F_2=0.995; **m**	20.2 ms						
			0.63	(8)	0.59	(10)	^{24}Na	IV/b	1368.6	4.71E-02	(1.5)	3	3	1
			<u>0.59</u>	(2)			**F_2m+g**	14.96 h	2754.0	4.72E-02	(1.5)			2
^{26}Mg	257000	(13)	0.46	(2)	0.64	(10)	^{27}Mg	I	170.7	3.02E-06	(1.7)	1	1	0
							g	9.462 m	843.8	2.54E-04	(1.7)			0
									1014.4	9.90E-05	(1.7)			1
^{27}Al	11800	(6)	0.54	(2)	0.71	(10)	^{28}Al	I	1778.9	1.77E-02	(1.5)	10	1	1
							g	2.241 m						
^{37}Cl	13700	(14)					^{38m}Cl	I						
							F_2=1; **m**	715 ms						
			0.48	(2)	0.69	(10)	^{38}Cl	IV/b	1642.7	1.95E-03	(1.8)	1	1	-1
							F_2m+g	37.24 m	2167.4	2.63E-03	(1.8)			-1

Target	$\bar{E}_r$ in eV (%; 1*s*)		Q_0 (%; 1*s*)* TW		Q_0 (%; 1*s*)* Lit		FI F_i; effective state (bold)	ADS $T_{1/2}$	γ (keV)	k_0 (%; 1*s*)		m	N_{Ch}	Δ%
^{41}K	2960	(7)	0.74	(4)	0.87	(3)	^{42}K	I	312.7	1.75E-05	(1.6)	1	1	10
							g	12.36 h	1524.7	9.45E-04	(1.6)			0
^{45}Sc	5130	(17)					^{46m}Sc	I						
	0.00						F_2=1; **m**	18.75 s						
			0.45	(8)	0.43	(10)	^{46}Sc	IV/b	889.3	1.25E+00	(1.4)	1	3	3
			0.44	(2)			**F_2m+g**	83.8 d	1120.5	1.25E+00	(1.4)			2
^{50}Cr	7530	(16)	0.48	(2)	0.53	(10)	^{51}Cr	I	320.1	2.49E-03	(1.6)	2	2	-5
	0.027	(25)	0.46	(3)			**g**	27.7 d						
^{50}Ti	63200	(13)	0.52	(2)	0.67	(10)	^{51}Ti	I	320.1	3.70E-04	(1.7)	1	1	-1
							g	5.76 m	928.0	2.64E-05	(1.7)			1
^{51}V	7230	(4)	0.55	(2)	0.55	(10)	^{52}V	I	1434.0	1.96E-01	(1.6)	1	1	0
							g	3.75 m						
^{55}Mn	468	(11)	1.04	(2)	1.05	(3)	^{56}Mn	I	846.8	4.94E-01	(1.5)	1	3	0
	341	(4)	1.03	(2)			**g**	2.579 h	1810.7	1.32E-01	(1.5)			-2
									2113.1	7.04E-02	(1.5)			-2

Target	$\bar{E}_r$ in eV (%; 1*s*)		Q_0 (%; 1*s*)* TW		Q_0 (%; 1*s*)* Lit		FI F_i; effective state (bold)	ADS $T_{1/2}$	γ (keV)	k_0 (%; 1*s*)		m	N_{Ch}	Δ%
	637	(24)	0.99	(2)	0.98	(1)	^{59}Fe	I	142.7	1.33E-06	(1.5)	3	3	0
^{58}Fe	253	(9)	0.97	(2)			**g**	44.5 d	192.3	3.86E-06	(1.5)			2
									1099.3	7.76E-05	(1.5)			0
									1291.6	5.89E-05	(1.5)			-1
	136	(5)	1.97	(2)	2.00	(10)	^{60m}Co	I	58.6	1.47E-02	(1.7)	1	1	-3
	109	(4)					F_2=0.998; **m**	10.47 m	1332.5	1.79E-03	(1.7)			2
			1.99	(2)	1.99	(3)	^{60}Co	IV/b	1173.2	1.32E+00	(1.5)		3	0
^{59}Co			1.96	(2)			**F_2m+g**	5.271 y	1332.5	1.32E+00	(1.5)			0
					2.00	(10)	^{60}Co	IV/d	1332.5	5.92E-01	(1.8)		1	0
							g		1173.2	**$I_{\gamma,m}/(F_2 I_{\gamma,g})$=0.0**				
							$\sigma_{0,m}/\sigma_{0,g}$=1.23		1332.5	**$I_{\gamma,m}/(F_2 I_{\gamma,g})$=0.0024**				
	14200	(12)	0.46	(2)	0.67	(10)	^{65}Ni	I	366.3	2.55E-05	(1.6)	1	1	1
^{64}Ni							**g**	2.517 h	1115.5	8.14E-05	(1.6)			0
									1481.8	1.26E-04	(1.6)			-1
^{63}Cu	1040	(5)	1.11	(2)	1.14	(10)	^{64}Cu	I	511.0	3.32E-02	(1.7)	3	3	-10
	952	(6)	1.10	(2)			**g**	12.7 h	1345.8	4.88E-04	(1.5)			-2

Target	$\bar{E}_r$ in eV (%; 1*s*)	Q_0 (%; 1*s*)* TW	Q_0 (%; 1*s*)* Lit	FI F_i; effective state (bold)	ADS $T_{1/2}$	γ (keV)	k_0 (%; 1*s*)	m	N_{Ch}	Δ%
^{65}Cu	766 (17)	1.01 (2)	1.06 (10)	^{66}Cu	I	1039.2	1.93E-03 (1.6)	3	1	4
	F_{Cd} =1.034			**g**	5.12 m					
^{64}Zn	2560 (10)	1.90 (2)	1.91 (5)	^{65}Zn	I	511.0	3.20E-04 (1.8)	1	1	-9
	2711 (7)	1.90 (2)		**g**	244.3 d	1115.5	5.66E-03 (1.5)		3	-1
^{68}Zn	590 (10)	3.21 (2)	3.19 (1)	^{69m}Zn	I	438.6	3.98E-04 (1.5)	1	3	0
	737 (4)	3.24 (2)		**m**	13.76 h					

Target	$\bar{E}_r$ in eV (%; 1*s*)		Q_0 (%; 1*s*)* TW		Q_0 (%; 1*s*)* Lit		FI F_i; effective state (bold)	ADS $T_{1/2}$	γ (keV)	k_0 (%; 1*s*)		m	N_{Ch}	Δ%
	154	(12)					^{72m}Ga	I						
	142	(2)					F_2=1; **m**	39.7 ms						
			6.94	(2)	6.69	(1)	^{72}Ga	IV/b	289.5	1.09E-04	(1.5)	1	3	-1
			6.89	(2)			**F_2m+g**	14.1 h	381.7	1.65E-04	(1.5)			-1
									428.6	1.17E-04	(1.5)			-1
									600.9	3.18E-03	(1.5)			-1
									630.0	1.45E-02	(1.5)			-3
									786.5	1.84E-03	(1.5)			0
									810.3	1.15E-03	(1.5)			0
									834.1	5.26E-02	(1.5)			1
									894.3	5.57E-03	(1.5)			2
^{71}Ga									970.8	6.10E-04	(1.5)			0
									1050.8	3.85E-03	(1.5)			1
									1215.1	4.44E-04	(1.5)			-1
									1230.9	7.95E-04	(1.5)			1
									1260.1	6.37E-04	(1.5)			-1
									1276.8	8.84E-04	(1.5)			1
									1464.1	2.01E-03	(1.5)			1
									1596.7	2.42E-03	(1.5)			0
									1862.0	3.01E-03	(1.5)			1
									2201.6	1.50E-02	(1.5)			2
									2491.0	4.28E-03	(1.5)			2
									2507.7	7.43E-03	(1.5)			2

Target	$\bar{E}_r$ in eV (%; 1*s*)		Q_0 (%; 1*s*)* TW		Q_0 (%; 1*s*)* Lit		FI F_i; effective state (bold)	ADS $T_{1/2}$	γ (keV)	k_0 (%; 1*s*)		m	N_{Ch}	Δ%
	106	(34)	15.0	(2)	13.6	(10)	^{76}As	I	559.1	4.86E-02	(1.5)	1	3	1
	121	(3)	15.1	(2)			**g**	26.24 h	563.2	1.33E-03	(1.5)			-5
									571.5	1.51E-04	(1.5)			-5
									657.1	6.75E-03	(1.5)			2
									665.3	4.62E-04	(1.5)			1
									740.1	1.28E-04	(1.5)			-4
									771.7	1.24E-04	(1.5)			-11
									867.6	1.40E-04	(1.5)			-6
^{75}As									1212.9	1.54E-03	(1.5)			2
									1228.5	1.28E-03	(1.5)			-8
									1439.1	2.96E-04	(1.5)			-7
									1216.1	3.66E-03	(1.5)			-2
									2096.3	6.05E-04	(1.5)			-4
									1129.9	1.39E-04	(1.5)			-3
									1453.6	1.15E-04	(1.5)			-7
									1787.7	3.12E-04	(1.5)			-7

Target	$\bar{E}_r$ in eV (%; 1*s*)		Q_0 (%; 1*s*)* TW		Q_0 (%; 1*s*)* Lit		FI F_i; effective state (bold)	ADS $T_{1/2}$	γ (keV)	k_0 (%; 1*s*)		m	N_{Ch}	Δ%
	152	(9)					^{82m}Br	I						
							F_2=0.976; **m**	6.13 m						
			19.3	(2)	19.3	(3)	^{82}Br	IV/b	554.3	2.39E-02	(1.6)	2	2	0
							F_2m+g	35.3 h	619.1	1.46E-02	(1.6)			0
^{81}Br									698.4	9.44E-03	(1.6)			0
									776.5	2.80E-02	(1.6)			0
									827.8	8.03E-03	(1.6)			-1
									1044.0	9.19E-03	(1.6)			0
									1317.5	9.04E-03	(1.6)			1
									1474.9	5.52E-03	(1.6)			0
	839	(9)					^{86m}Rb	I						
							F_2=1; **m**	1.02 m						
^{85}Rb			14.4	(2)	14.8	(3)	^{86}Rb	IV/b	1077.0	7.94E-04	(1.6)	1	1	4
							F_2m+g	18.63 d						

Target	$\bar{E}_r$ in eV (%; 1*s*)		Q_0 (%; 1*s*)* TW		Q_0 (%; 1*s*)* Lit		FI F_i; effective state (bold)	ADS $T_{1/2}$	γ (keV)	k_0 (%; 1*s*)		m	N_{Ch}	Δ%
^{87}Rb	364	(3)	25.9	(2)	23.3	(3)	^{88}Rb	I	898.0	9.42E-05	(1.6)	1	1	-7
							g	17.78 m	1382.5	4.82E-06	(1.7)			-11
									1836.0	1.48E-04	(1.6)			-6
									2677.9	1.40E-05	(1.6)			-5
^{84}Sr	469	(7)	13.0	(5)	14.5	(3)	^{85m}Sr	I	151.2	1.08E-05	(1.6)	1	2	3
	<u>506</u>	(25)					F_2=0.866; **m**	67.63 m	231.9	7.43E-05	(1.6)			7
			14.5	(2)	13.2	(10)	^{85}Sr	IV/b	514.0	9.21E-05	(1.6)	1	2	1
			<u>14.6</u>	(2)			**F_2m+g**	64.84 d						
^{86}Sr	795	(2)	4.04	(2)	4.11	(2)	^{87m}Sr	I	388.5	1.54E-03	(1.5)	1	3	4
	<u>502</u>	(25)	<u>3.95</u>	(2)			**m**	2.803 h						
^{89}Y	4300	(8)	4.08	(3)	5.93	(2)	^{90m}Y	I	202.5	2.45E-05	(1.7)	2	1	4
							m	3.19 h	479.5	2.26E-05	(1.7)			1

Target	$\bar{E}_r$ in eV (%; 1*s*)		Q_0 (%; 1*s*)* TW		Q_0 (%; 1*s*)* Lit		FI F_i; effective state (bold)	ADS $T_{1/2}$	γ (keV)	k_0 (%; 1*s*)		m	N_{Ch}	Δ%
	6260	(5)	5.02	(2)	5.31	(3)	^{95}Zr	I	724.2	9.08E-05	(1.5)	1	3	2
	6261	(5)	5.02	(3)			F_2=0.0112; **g**	64.032 d	756.7	1.13E-04	(1.5)			2
							F_{24}=0.989							
^{94}Zr							^{95m}Nb	II/a						
							F_3=0.975; **F_2g**	3.61 d						
							^{95}Nb	III/a	765.8	2.15E-06 **	(1.6)	1	3	-1
							F_2F_3g	34.991 d		2.24E-06	(1.6)		3	3
	338	(2)			251.6	(1)	^{97}Zr	I						
							F_2=0.968; **g**	16.74 d						
							F_{24}=0.032							
^{96}Zr							^{97m}Nb	II/a	743.4	1.28E-05	(1.7)	1	2	3
							F_3=1; **F_2g**	52.7 s						
							^{97}Nb	III/a	657.9	1.30E-05	(1.7)	1	2	5
							F_2F_3g	72.1 m						
^{93}Nb	574	(8)	7.28	(2)	7.35	(3)	^{94m}Nb	I	871.0	9.59E-05	(1.6)	3	1	-1
							m	6.26 m						

Target	$\bar{E}_r$ in eV (%; 1*s*)		Q_0 (%; 1*s*)* TW		Q_0 (%; 1*s*)* Lit		FI F_i; effective state (bold)	ADS $T_{1/2}$	γ (keV)	k_0 (%; 1*s*)		m	N_{Ch}	Δ%
	241	(10)	54.0	(4)	53.1	(6)	^{99}Mo	I	181.0	4.16E-05	(1.6)	1	3	0
	262	(5)	54.8	(3)			F_2=0.88; **g**	2.7475 d	366.4	8.07E-06	(1.6)			-3
									739.0	8.20E-05	(1.6)			-3
^{98}Mo									777.0	2.86E-05	(1.6)			-4
							^{99m}Tc	II/d	140.5	5.29E-04	(1.6)	1	3	0
							F_2g	6.01 h	140.5	**$I_{\gamma,Mo}/(F_2 I_{\gamma,Tc})$=0.0675**				
	672	(14)	19.9	(2)	18.8	(4)	^{101}Mo	I	191.9	7.82E-05	(1.9)	1	1	8
							F_2=1; **g**	14.61 m	505.1	4.98E-05	(1.9)			6
									590.1	8.76E-05	(1.9)			6
									695.6	2.85E-05	(1.9)			2
^{100}Mo									1011.1	6.29E-05	(1.9)			2
							^{101}Tc	II/a	127.2	1.23E-05	(1.9)	1	1	3
							F_2g	14.2 m	184.1	6.88E-06	(1.9)			25
									306.8	3.83E-04	(1.9)			3
									545.1	2.56E-05	(1.9)			3

Target	$\bar{E}_r$ in eV (%; 1*s*)		Q_0 (%; 1*s*)* TW		Q_0 (%; 1*s*)* Lit		FI F_i; effective state (bold)	ADS $T_{1/2}$	γ (keV)	k_0 (%; 1*s*)		m	N_{Ch}	Δ%
^{96}Ru	776	(16)	25.6	(2)	26.5	(4)	^{97}Ru	I	215.7	2.43E-04	(1.6)	2	2	8
	1343	(25)	26.2	(2)			**g**	2.9 d	324.5	3.06E-05	(1.6)			-15
^{102}Ru	181	(4)	3.35	(6)	3.63	(10)	^{103}Ru	I	497.1	7.36E-03	(1.6)	2	2	7
	1556	(25)	3.60	(2)			**g**	39.35 d	610.3	4.67E-04	(1.6)			8
^{104}Ru	495	(10)	13.1	(2)	12.8	(3)	^{105}Ru	I	262.8	1.28E-04	(1.6)	2	2	-2
	504	(25)	13.1	(2)			F_2=0.264; **g**	4.44 h	316.4	2.17E-04	(1.6)			4
							F_{24}=0.736		469.4	3.41E-04	(1.6)			4
									676.4	3.05E-04	(1.6)			3
									724.3	9.26E-04	(1.6)			4
							^{105m}Rh	II/a	129.6	1.03E-04	(1.6)	2	2	12
							F_3=1; **F_2g**	42.3 s						
							^{105}Rh	III/c	306.1	9.98E-05	(1.6)	2	2	-1
							(F_2F_3+F_{24})g	35.36 h	318.9	3.67E-04	(1.6)			3

Target	$\bar{E}_r$ in eV (%; 1*s*)	Q_0 (%; 1*s*)* TW	Q_0 (%; 1*s*)* Lit	FI F_i; effective state (bold)	ADS $T_{1/2}$	γ (keV)	k_0 (%; 1*s*)	m	N_{Ch}	Δ%
	39.7 (5)	-		^{109m}Pd	I					
				F_2=1; **m**	4.69 m					
		26.6 (7)	26.6 (2)	^{109}Pd	IV/b	311.4	1.41E-05 (1.6)	1	3	-5
				F_3=1; **F_2m+g**	13.46 h	602.5	3.58E-06 (1.6)			-1
^{108}Pd						636.3	4.52E-06 (1.6)			0
						647.3	1.08E-05 (1.6)			-5
						781.4	4.96E-06 (1.6)			-2
				^{109m}Ag	V/c	88.0	1.53E-03 (2.5)	1		-11
				(F_2m+g)F_3	39.6 s					
	950 (9)	11.9 (5)	11.9 (7)	^{111m}Pd	I	172.2	1.02E-05 (1.8)	1	1	-5
				F_2=0.73; **m**	5.5 h					
				F_{24}=0.27						
^{110}Pd				^{111}Pd	IV/a					
				F_3=1; **g**	23.4m					
				^{111}Ag	VII/c	245.4	7.86E-06 (1.8)	1	1	
				({(F_{24})+F_2F_3}m)+(F_3g)	7.45d	342.0	4.74E-05 (1.8)			

Target	$\bar{E}_r$ in eV (%; 1*s*)		Q_0 (%; 1*s*)* TW		Q_0 (%; 1*s*)* Lit		FI F_i; effective state (bold)	ADS $T_{1/2}$	γ (keV)	k_0 (%; 1*s*)		m	N_{Ch}	Δ%
	39	(5)	2.72	(2)	2.9	(10)	^{108}Ag	I	434.0	1.68E-03	(1.7)	2	1	6
^{107}Ag							**g**	2.37 m	618.9	9.22E-04	(1.7)			-1
									633.0	6.05E-03	(1.7)			1
	6.08	(1)	16.5	(2)	16.7	(4)	^{110m}Ag	I	446.8	1.37E-03	(1.6)	4	2	1
	5.7	(7)	16.5	(2)			**m**	249.8 d	620.4	1.01E-03	(1.6)			-1
									657.8	3.53E-02	(1.6)			1
									677.6	3.93E-03	(1.6)			0
									687.0	2.43E-03	(1.6)			0
									706.7	6.20E-03	(1.6)			3
									744.3	1.77E-03	(1.6)			5
^{109}Ag									763.9	8.35E-03	(1.6)			1
									818.0	2.73E-03	(1.6)			1
									884.7	2.75E-02	(1.6)			2
									937.5	1.29E-02	(1.6)			2
									1384.3	9.22E-03	(1.6)			1
									1475.8	1.51E-03	(1.6)			1
									1505.0	4.93E-03	(1.6)			2
									1562.3	4.54E-04	(1.6)			4

Target	$\bar{E}_r$ in eV (%; 1*s*)		Q_0 (%; 1*s*)* TW		Q_0 (%; 1*s*)* Lit		FI F_i; effective state (bold)	ADS $T_{1/2}$	γ (keV)	k_0 (%; 1*s*)		m	N_{Ch}	Δ%
^{114}Cd	207	(19)	31.4	(4)	32.4	(10)	^{115}Cd	I	527.9	4.97E-04	(2.0)	1	2-3	4
	202	(33)	31.0	(4)			F_2=1; **g**	53.5 h						
	F_{Cd} =0.40						^{115m}In	II/a	336.2	8.07E-04	(2.0)	1	2-3	4
							F_2g	4.486 h						
^{113}In	6.41	(15)					^{114m2}In	I						
	5.0	(25)					F_2=1; **m_2**	43.1 ms						
			24.1	(2)	24.2	(2)	^{114m1}In	IV/b	190.3	1.02E-03	(1.6)	2	2	-3
			23.7	(2)			**F_2m_2+m_1**	49.51 d	558.4	2.70E-04	(1.6)			-6
									725.2	2.70E-04	(1.6)			-7

Target	$\bar{E}_r$ in eV (%; 1*s*)	Q_0 (%; 1*s*)* TW	Q_0 (%; 1*s*)* Lit	FI F_i; effective state (bold)	ADS $T_{1/2}$	γ (keV)	k_0 (%; 1*s*)		m	N_{Ch}	Δ%
	1.56 (7)			^{116m2}In	I						
	F_{Cd} =0.927			F_2=1; **m_2**	2.18 s						
		16.7 (3)	16.8 (2)	^{116m1}In	IV/b	138.3	1.02E-01	(1.6)	2	2	1
		s_0= 18.0		**F_2m_2+m_1**	54.41 m	416.9	7.59E-01	(1.6)			1
^{115}In			Non-1/v absorber			818.7	3.39E-01	(1.6)			1
			1.5% var. between 20-100 ºC			1097.3	1.60E+00	(1.6)			0
			g_{20}=1.021; g_{60}=1.028; g_{100}=1.036			1293.5	2.32E+00	(1.6)			1
						1507.4	2.70E-01	(1.6)			1
						2112.1	4.15E-01	(1.6)			-1
	107 (3)			^{113m}Sn	I						
	49.9 (25)			F_2=0.911; **m**	21.4 m						
		48.3 (4)	48.4 (1)	^{113}Sn	IV/b	255.1	1.95E-06	(1.6)	2	2	0
^{112}Sn		45.2 (4)		F_3=1; **F_2m+g**	115.1 d						
				^{113m}In	V/c	391.7	5.99E-05	(1.6)	2	2	0
				$(F_2m+g)F_3$	99.48 m						

Target	$\bar{E}_r$ in eV (%; 1*s*)		Q_0 (%; 1*s*)* TW		Q_0 (%; 1*s*)* Lit		FI F_i; effective state (bold)	ADS $T_{1/2}$	γ (keV)	k_0 (%; 1*s*)		m	N_{Ch}	Δ%
^{116}Sn	128	(3)	55.8	(3)	56.3	(2)	^{117m}Sn	I	156.0	3.33E-07	(1.6)	2	2	3
	130	(25)	55.9	(3)			n,n' interf.; **m**	13.6 d	158.4	1.36E-05	(1.6)			0
	74.2	(7)			60.1	(3)	^{125m}Sn	I						
	76.6	(25)					F_2=0.0; **m**	9.52 m						
							F_{24}=1							
			16.7	(2)	17.2	(12)	^{125}Sn	I	822.5	2.08E-07	(1.6)	2	2	-1
			16.2	(4)			F_3=1; **g**	9.64 d	915.6	1.88E-07	(1.6)			-4
									1067.1	4.64E-07	(1.6)			0
^{124}Sn									1089.2	2.50E-07	(1.6)			-5
							^{125}Sb	VII/b	176.3	3.19E-07	(1.6)	2	2	2
							F_3g	2.7586 y	427.9	1.40E-06	(1.6)			3
									463.4	4.95E-07	(1.6)			3
									600.5	8.28E-07	(1.6)			2
									606.6	2.32E-07	(1.6)			2
									635.9	5.31E-07	(1.6)			3

Target	$\bar{E}_r$ in eV (%; 1*s*)	Q_0 (%; 1*s*)* TW	Q_0 (%; 1*s*)* Lit	FI F_i; effective state (bold)	ADS $T_{1/2}$	γ (keV)	k_0 (%; 1*s*)	m	N_{Ch}	Δ%
	13.1 (4)			^{122m}Sb	I					
	14.6 (4)			F_2=1; **m**	4.191 m					
^{121}Sb	F_{Cd} =0.99	34.7 (2)	33.0 (4)	^{122}Sb	IV/b	564.2	4.00E-02 (1.5)	1	3	-9
		35.0 (3)		**F_2m+g**	2.724 d	692.7	2.18E-03 (1.5)			-9

Target	$\bar{E}_r$ in eV (%; 1*s*)		Q_0 (%; 1*s*)* TW		Q_0 (%; 1*s*)* Lit		FI F_i; effective state (bold)	ADS $T_{1/2}$	γ (keV)	k_0 (%; 1*s*)		m	N_{Ch}	Δ%
	28.2	(7)					^{124m2}Sb	I						
	32.4	(5)					F_2=1; F_{24}=0; **m_2**	20.2 m						
							^{124m1}Sb	IV/a						
							F_3=0.75; **m_1**	93 s						
			30.5	(2)	28.8	(4)	^{124}Sb	VI/c ***	602.7	2.80E-02	(1.5)	1	3	-5
			31.0	(3)			**$F_3(F_2m_2+m_1)+g$**	60.2 d	645.9	2.11E-03	(1.5)			-4
									709.3	3.87E-04	(1.5)			-1
^{123}Sb									713.8	6.47E-04	(1.5)			-1
									722.8	3.08E-03	(1.5)			-4
									968.2	5.43E-04	(1.5)			0
									1045.1	5.22E-04	(1.5)			-1
									1325.5	4.46E-04	(1.5)			-2
									1368.2	7.50E-04	(1.5)			-1
									1436.6	3.48E-04	(1.6)			-1
									1691.0	1.38E-02	(1.5)			-2
									2090.9	1.58E-03	(1.5)			0

Target	$\bar{E}_r$ in eV (%; 1*s*)		Q_0 (%; 1*s*)* TW		Q_0 (%; 1*s*)* Lit		FI F_i; effective state (bold)	ADS $T_{1/2}$	γ (keV)	k_0 (%; 1*s*)		m	N_{Ch}	Δ%
	9.27	(5)	11.7	(2)	11.8	(3)	^{134m}Cs	I	127.5	5.88E-03	(1.6)	1	3	7
	6.93	(4)	11.5	(2)			F_2=1; **m**	2.903 h						
			15.1	(2)	13.2	(10)	^{134}Cs	IV/a	563.2	3.57E-02	(1.6)	1	3	-7
			14.8	(3)			**g**	2.065 y	569.3	6.57E-02	(1.6)			-1
							$\sigma_{0,m}/\sigma_{0,g}$=0.105		604.7	4.19E-01	(1.6)			-6
									795.9	3.71E-01	(1.6)			-5
									802.0	3.76E-02	(1.6)			-3
									1365.2	1.31E-02	(1.6)			0
^{133}Cs			14.8	(2)	12.7	(10)	^{134}Cs	IV/b	475.4	7.06E-03	(1.5)	1	3	0
			14.5	(4)			**F_2m+g**		563.2	3.95E-02	(1.5)			-5
									569.3	7.28E-02	(1.5)			-1
									604.7	4.63E-01	(1.5)			-3
									795.9	4.08E-01	(1.5)			-2
									802.0	4.10E-02	(1.5)			0
									1038.6	4.73E-03	(1.5)			0
									1168.0	8.45E-03	(1.5)			-1
									1365.2	1.45E-02	(1.5)			1

Target	$\bar{E}_r$ in eV (%; 1*s*)		Q_0 (%; 1*s*)* TW		Q_0 (%; 1*s*)* Lit		FI F_i; effective state (bold)	ADS $T_{1/2}$	γ (keV)	k_0 (%; 1*s*)		m	N_{Ch}	Δ%
	69.9	(5)					^{131m}Ba	I						
	58.0	(5)					F_2=1; **m**	14.6 m						
			20.7	(3)	24.8	(10)	^{131}Ba	IV/b	123.8	3.94E-05	(1.5)	1	3	1
			21.0	(4)			**F_2m+g**	11.5 d	133.6	2.97E-06	(1.5)			-8
									216.1	2.59E-05	(1.5)			-6
									239.6	3.23E-06	(1.5)			-8
^{130}Ba									249.4	3.69E-06	(1.5)			-11
									373.2	1.82E-05	(1.5)			-5
									404.0	1.73E-06	(1.5)			-8
									486.5	2.78E-06	(1.5)			-19
									496.3	6.15E-05	(1.5)			-5
									585.0	1.61E-06	(1.5)			-7
									620.1	1.88E-06	(1.5)			-19
									1047.6	1.72E-06	(1.5)			-8
^{132}Ba	143	(10)	4.64	(5)	5.60	(10)	^{133m}Ba	I	275.9	2.04E-06	(1.5)	1	3	-10
	322	(2)	4.77	(2)			**m**	38.9 h						

Target	$\bar{E}_r$ in eV (%; 1*s*)		Q_0 (%; 1*s*)* TW		Q_0 (%; 1*s*)* Lit		FI F_i; effective state (bold)	ADS $T_{1/2}$	γ (keV)	k_0 (%; 1*s*)		m	N_{Ch}	Δ%
^{134}Ba	115	(-)	43.5	(23)	55.8	(-)	^{135m}Ba	I	268.3	3.21E-06	(1.6)	1	3	3
	5503	(20)	52.4	(3)			**m**	28.7 h						
^{138}Ba	15700	(3)	1.04	(14)	0.88	(10)	^{139}Ba	I	165.9	1.05E-03	(1.5)	1	3	0
	1324000	(25)	1.20	(3)			**g**	83.06 m	1420.5	1.15E-05	(1.5)			0
^{139}La	76	(4)	1.16	(2)	1.24	(10)	^{140}La	I	328.8	2.88E-02	(1.5)	1	3	0
	67.3	(3)	1.15	(2)			**g**	1.6786 d	432.5	4.16E-03	(1.5)			2
									487.0	6.35E-02	(1.5)			0
									751.6	6.12E-03	(1.5)			3
									815.8	3.29E-02	(1.5)			-1
									867.8	7.78E-03	(1.5)			3
									919.6	3.78E-03	(1.5)			2
									925.2	9.83E-03	(1.5)			3
									1596.2	1.33E-01	(1.5)			-1
^{141}Pr	296	(4)					^{142m}Pr	I						
	123	(5)					F_2=1; **m**	14.6 m						
			1.41	(2)	1.51	(10)	^{142}Pr	IV/b	1575.6	6.19E-03	(1.5)	1	3	1
			1.37	(2)			**F_2m+g**	19.12 h						

Target	$\bar{E}_r$ in eV (%; 1*s*)		Q_0 (%; 1*s*)* TW		Q_0 (%; 1*s*)* Lit		FI F_i; effective state (bold)	ADS $T_{1/2}$	γ (keV)	k_0 (%; 1*s*)		m	N_{Ch}	Δ%
	8.53	(1)	14.6	(2)	14.4	(2)	^{153}Sm	I	69.7	3.59E-02	(1.6)	1	3	2
^{152}Sm	8.48	(4)	14.7	(2)			**g**	1.9375 d	97.4	6.80E-03	(1.6)			14
									103.2	2.25E-01	(1.6)			-3
	0.45	(-)					^{152m2}Eu	I						
	0.17	(20)					F_2=1; $\mathbf{m_2}$	96 m						
							^{152m1}Eu	I						
			s_0 given; adoption from Lit is recommended				F_3=0; $\mathbf{m_1}$	9.312 h						
			0.05	(18)	***1.25***	***(-)***	^{152}Eu	IV/b	121.8	1.23E+01	(1.7)	1	3	-4
			0.05	(5)			$\mathbf{F_2 m_2 + g}$	13.54 y	244.7	3.29E+00	(1.7)			-4
^{151}Eu									344.3	1.15E+01	(1.7)			-3
			^{152m1}Eu γ-ray interfered, requires cooling (^{152m1}Eu decay)						444.0	1.39E+00	(1.7)			0
			Strong non-1/v absorber; Temp. monitor						778.9	5.68E+00	(1.7)			0
			Westcott convention is required						867.4	1.86E+00	(1.7)			-1
			7.8 % var. between 20-100 °C						963.4	6.42E+00	(1.7)			-1
			g_{20}=0.901; g_{60}=0.863; g_{100}=0.831						1084.0	4.46E+00	(1.7)			-2
									1112.1	5.92E+00	(1.7)			-2
									1408.0	9.13E+00	(1.7)			-2

Target	$\bar{E}_r$ in eV (%; 1*s*)		Q_0 (%; 1*s*)* TW		Q_0 (%; 1*s*)* Lit		FI F_i; effective state (bold)	ADS $T_{1/2}$	γ (keV)	k_0 (%; 1*s*)		m	N_{Ch}	Δ%
	5.80	(4)					^{154m}Eu	I						
	7.24	(20)	s_0 given in TW; Q_0 in Lit				F_2=1; **m**	46 m						
			4.75	(3)	5.90	(10)	^{154}Eu	IV/b	123.1	9.04E-01	(1.6)	1	3	0
			4.81	(3)			**F_2m+g**	8.593 y	248.0	1.54E-01	(1.5)			-1
									591.8	1.09E-01	(1.5)			1
^{153}Eu			Non-1/v absorber; 2.3 % var. between 20-100 °C						692.4	4.02E-02	(1.6)			1
			g_{20}=0.974; g_{60}=0.963; g_{100}=0.952						723.3	4.50E-01	(1.6)			1
									756.9	1.06E-01	(1.5)			-2
									873.2	2.71E-01	(1.5)			0
									996.4	2.35E-01	(1.5)			2
									1274.4	7.77E-01	(1.5)			0
									1596.5	4.07E-02	(1.5)			1
^{152}Gd	16.7	(9)	0.56	(5)	0.77	(15)	^{153}Gd	I	97.4	5.94E-03	(1.7)	1	1	1
							g	240.4 d	103.2	4.34E-03	(1.7)			3
^{158}Gd	48.2	(8)	31.2	(5)	29.9	(3)	^{159}Gd	I	363.5	8.63E-04	(1.7)	1	1	2
							g	18.56 h						

Target	$\bar{E}_r$ in eV (%; 1*s*)		Q_0 (%; 1*s*)* TW		Q_0 (%; 1*s*)* Lit		FI F_i; effective state (bold)	ADS $T_{1/2}$	γ (keV)	k_0 (%; 1*s*)		m	N_{Ch}	Δ%
	18.1	(15)	18.2	(2)	17.9	(4)	^{160}Tb	I	86.8	4.18E-02	(1.7)	1	1	0
							g	72.3 d	197.0	1.62E-02	(1.7)			0
									215.6	1.28E-02	(1.7)			1
									298.6	8.26E-02	(1.7)			0
^{159}Tb									879.4	9.45E-02	(1.7)			0
									962.3	3.05E-02	(1.7)			0
									1178.0	4.71E-02	(1.7)			0
									1199.9	7.43E-03	(1.7)			-1
									1271.9	2.36E-02	(1.7)			0
									1312.1	8.97E-03	(1.7)			0
	224	(5)					^{165m}Dy	I						
	28.9	(25)					F_2=0.9776; **m**	1.257 m						
			0.13	(21)	0.19	(10)	^{165}Dy	IV/b	94.7	3.62E-01	(1.5)	3	3	1
			0.72	(3)			**F_2m+g**	2.334 h	279.8	5.13E-02	(1.5)			5
^{164}Dy									361.7	8.66E-02	(1.5)			4
							Non-1/v absorber		633.4	5.79E-02	(1.5)			3
							1 % var. between 20-100 °C		715.3	5.43E-02	(1.6)			4
							g_{20}=0.988; g_{60}=0.983; g_{100}=0.978							

Target	$\bar{E}_r$ in eV (%; 1*s*)		Q_0 (%; 1*s*)* TW		Q_0 (%; 1*s*)* Lit		FI F_i; effective state (bold)	ADS $T_{1/2}$	γ (keV)	k_0 (%; 1*s*)		m	N_{Ch}	Δ%
^{165}Ho	12.3	(3)	11.2	(3)	10.9	(2)	^{166}Ho	I	80.6	5.13E-02	(1.4)	1	4	4
	<u>15.23</u>	(6)	<u>11.3</u>	(2)			**g**	26.83 h	1379.4	7.06E-03	(1.4)			2
	F_{Cd} =0.99								1581.9	1.41E-03	(1.4)			1
									1662.5	9.06E-04	(1.4)			4
^{169}Tm	4.8	(2)	13.3	(3)	13.7	(2)	^{170}Tm	I	84.3	3.29E-02	(3.0)	1	1	1
							g	128.6 d						
^{168}Yb	0.61	(-)					^{169m}Yb	I						
	<u>0.026</u>	(25)					F_2=1; **m**	46 s						
			4.17	(12)	4.97	(-)	^{169}Yb	IV/b	93.6	1.20E-03	(1.6)	1	3	2
			<u>3.39</u>	(8)			**F_2m+g**	32.03 d	109.8	8.26E-03	(1.6)			6
									130.5	5.28E-03	(1.6)			2
			Strong non-1/v absorber; Temp. monitor						177.2	1.04E-02	(1.6)			0
			3.3 % var. between 20-100 °C						198.0	1.68E-02	(1.6)			2
			g_{20}=1.057; g_{60}=1.075; g_{100}=1.092						307.7	4.63E-03	(1.6)			7

Target	$\bar{E}_r$ in eV (%; 1*s*)		Q_0 (%; 1*s*)* TW		Q_0 (%; 1*s*)* Lit		FI F_i; effective state (bold)	ADS $T_{1/2}$	γ (keV)	k_0 (%; 1*s*)		m	N_{Ch}	Δ%
	602	(8)					^{175m}Yb	I						
	0.115	(30)					F_2=1; **m**	68.2 ms						
			0.38	(18)	0.46	(10)	^{175}Yb	IV/b	113.8	9.47E-03	(1.5)	1	3	0
^{174}Yb			0.48	(3)			**F_2m+g**	4.185 d	137.7	5.74E-04	(1.5)			1
									144.9	1.63E-03	(1.5)			3
									282.5	1.50E-02	(1.5)			3
									396.3	3.18E-02	(1.5)			2
	412	(5)					^{177m}Yb	I						
	190	(25)					F_2=1; **m**	6.41 s						
			2.51	(4)	2.50	(2)	^{177}Yb	IV/b	150.3	9.01E-04	(1.6)	1	2	1
^{176}Yb			2.43	(4)			**F_2m+g**	1.911 h	941.8	4.89E-05	(1.6)			0
									1080.2	2.64E-04	(1.6)			-1
									1241.2	1.59E-04	(1.6)			-2
	0.16	(-)			1.67	(10)	^{177}Lu	I	112.9	4.15E-02		1	4	
							g	6.73 d	208.4	7.14E-02				
^{176}Lu	Strong non-1/v absorber; Temp. monitor; adopted values 34.2 % var. between 20-100 °C g_{20}=1.746; g_{60}=2.099; g_{100}=2.344													

Target	$\bar{E}_r$ in eV (%; 1*s*)		Q_0 (%; 1*s*)* TW		Q_0 (%; 1*s*)* Lit		FI F_i; effective state (bold)	ADS $T_{1/2}$	γ (keV)	k_0 (%; 1*s*)		m	N_{Ch}	Δ%
	29.6	(7)	0.61	(3)	0.78	(10)	^{175}Hf	I	343.4	8.95E-03	(1.5)	2	3	-1
			s_0=0.22				**g**	70 d						
^{174}Hf	200	(22)	0.64	(2)	Non-1/v absorber									
			s_0=0.25		1.1% var. between 20-100 °C									
					g_{20}=0.986; g_{60}=0.981; g_{100}=0.975									
	16.2	(12)	14.1	(2)	14.4	(2)	^{180m}Hf	I	93.3	1.19E-04	(1.7)	2	1	-4
	12.1	(15)	14.0	(2)			**m**	5.5 h	215.4	5.61E-04	(1.6)			-5
^{179}Hf									332.3	6.42E-04	(1.6)			-5
									443.2	5.62E-04	(1.6)			-4
									500.7	9.67E-05	(1.6)			-5
	115	(6)	2.44	(3)	2.52	(4)	^{181}Hf	I	133.0	2.33E-02	(1.5)	2	3	-2
^{180}Hf	152	(8)	2.46	(2)			**g**	42.39 d	345.9	8.03E-03	(1.5)			1
									482.2	4.31E-02	(1.5)			-6

Target	$\bar{E}_r$ in eV (%; 1*s*)	Q_0 (%; 1*s*)* TW	Q_0 (%; 1*s*)* Lit	FI F_i; effective state (bold)	ADS $T_{1/2}$	γ (keV)	k_0 (%; 1*s*)		m	N_{Ch}	Δ%
	10.4 (6)			^{182m}Ta	I						
	11.1 (15)			F_2=1; **m**	15.8 m						
	F_{Cd} =0.972	37.0 (3)	33.3 (10)	^{182}Ta	IV/b	84.7	6.23E-03	(1.3)	3	4	-1
		36.8 (2)		**F_2m+g**	114.4 d	100.1	3.26E-02	(1.3)			2
						113.7	4.38E-03	(1.3)			-1
						152.4	1.63E-02	(1.3)			1
						156.4	6.26E-03	(1.3)			-1
						179.4	7.27E-03	(1.3)			-1
						198.4	3.40E-03	(1.3)			-2
^{181}Ta						222.1	1.78E-02	(1.3)			0
						229.3	8.56E-03	(1.3)			-1
						264.1	8.41E-03	(1.3)			-2
						1001.7	4.82E-03	(1.3)			-2
						1121.3	8.26E-02	(1.3)			0
						1157.5	2.35E-03	(1.3)			1
						1189.1	3.83E-02	(1.3)			-1
						1221.4	6.39E-02	(1.3)			-1
						1231.0	2.71E-02	(1.3)			0
						1257.4	3.52E-03	(1.3)			-1
						1289.2	3.20E-03	(1.3)			-1

Target	$\bar{E}_r$ in eV (%; 1*s*)	Q_0 (%; 1*s*)* TW	Q_0 (%; 1*s*)* Lit	FI F_i; effective state (bold)	ADS $T_{1/2}$	γ (keV)	k_0 (%; 1*s*)		m	N_{Ch}	Δ%
	20.5 (1)	13.8 (2)	13.7 (2)	^{187}W	I	134.2	1.17E-02	(1.5)	4	3	3
	22.1 (3)	13.8 (2)		**g**	23.72 h	479.6	3.02E-02	(1.5)			2
	F_{Cd} =0.908					551.5	6.92E-03	(1.5)			0
^{186}W						618.3	8.58E-03	(1.5)			-1
						625.5	1.48E-03	(1.5)			-9
						685.7	3.71E-02	(1.5)			0
						772.9	5.65E-03	(1.5)			1
	3.40 (4)	14.6 (2)	15.4 (3)	^{186}Re	I	122.6	2.83E-03	(1.5)	1	3	1
	3.55 (4)	*s*$_0$= *16.9*		**g**	3.718 d	137.2	4.48E-02	(1.5)			4
^{185}Re		14.6 (2)	Non-1/v absorber								
		s$_0$= 16.9	0.4% var. between 20-100 ºC								
	F_{Cd} =0.98		g_{20}=1.007; g_{60}=1.009; g_{100}=1.011								

Target	$\bar{E}_r$ in eV (%; 1*s*)	Q_0 (%; 1*s*)* TW	Q_0 (%; 1*s*)* Lit	FI F_i; effective state (bold)	ADS $T_{1/2}$	γ (keV)	k_0 (%; 1*s*)	m	N_{Ch}	Δ%
	41.1 (4)	4.54 (3)	4.57 (3)	^{188m}Re	I	92.4	7.43E-04 (1.6)	1	1	-4
		s_0=4.64		F_2=1; **m**	18.59 m	106.0	1.54E-03 (1.6)			3
		4.18 (4)	4.34 (3)	^{188}Re	IV/a	155.0	7.79E-02 (1.6)	1	3	0
		s_0=4.23		**g**	17.01 h	478.0	5.29E-03 (1.6)			0
	70.2 (3)	4.32 (4)		**$\sigma_{0,m}/\sigma_{0,g}$=0.028**		633.0	6.81E-03 (1.6)			0
		s_0=4.39				829.5	2.22E-03 (1.7)			2
^{187}Re						931.3	2.91E-03 (1.7)			2
		4.19 (3)	4.35 (10)	^{188}Re	IV/b	155.0	8.01E-02 (1.5)	1	3	0
		s_0=4.24		**F_2m+g**		478.0	5.43E-03 (1.5)			0
		4.33 (2)				633.0	6.99E-03 (1.5)			0
		s_0=4.40	Non-1/v absorber			635.0	8.32E-04 (1.5)			0
			0.4% var. between 20-100 ºC			829.5	2.28E-03 (1.5)			2
			g_{20}=0.996; g_{60}=0.994; g_{100}=0.992			931.3	2.99E-03 (1.5)			2
	291 (-)	8.44 [a] (15)	7.95 [b]	^{197m}Pt	I	346.5	1.06E-05 (1.5)	3	2	-20
	5319 (5)	9.62 (4)		F_2=0.967; **m**	95.41 m					
^{196}Pt		8.17 [a] (12)	12.6 [b]	^{197}Pt	IV/b	191.4	7.51E-05 (1.5)	3	3	30
		9.57 (4)		**F_2m+g**	19.892 h	268.8	4.67E-06 (1.5)			30

Target	$\bar{E}_r$ in eV (%; 1*s*)		Q_0 (%; 1*s*)* TW		Q_0 (%; 1*s*)* Lit		FI F_i; effective state (bold)	ADS $T_{1/2}$	γ (keV)	k_0 (%; 1*s*)		m	N_{Ch}	Δ%
	106	(3)					^{199m}Pt	I						
	114	(8)					F_2=1; **m**	13.6 s						
			16.9	(2)	17.0	(2)	^{199}Pt	IV/b	493.8	1.15E-04	(1.6)	3	1	-10
^{198}Pt			17.0	(2)			F_3=1; **F_2m+g**	30.8 m	543.0	3.00E-04	(1.6)			-10
									714.6	3.72E-05	(1.6)			-10
							^{199}Au	V/b - V/d	158.4	1.04E-03	(1.5)	3	3	1
							F_3(F_2m+g)	3.139 d	208.2	2.26E-04	(1.5)			0
	54.4	(3)					^{233}Th	I						
	51.7	(3)					F_2=1; **g**	22.3 m						
			11.8	(2)	11.5	(4)	^{233}Pa	II/b	300.1	4.42E-03	(1.5)	1	2	1
^{232}Th			11.7	(2)			**F_2g**	26.97 d	311.9	2.57E-02	(1.5)			2
									340.5	2.98E-03	(1.5)			1
									375.4	4.51E-04	(1.5)			0
									398.5	9.29E-04	(1.5)			0
									415.8	1.15E-03	(1.5)			0

Target	$\bar{E}_r$ in eV (%; 1*s*)	Q_0 (%; 1*s*)* TW	Q_0 (%; 1*s*)* Lit	FI F_i; effective state (bold)	ADS $T_{1/2}$	γ (keV)	k_0 (%; 1*s*)	m	N_{Ch}	Δ%
^{197}Au [c]	5.7 (7)		15.7 (2)	^{198}Au	I	411.8	1.00E+00	5	4	
	F_{Cd} =0.991		s_0=17.2	**g**	2.695 d					
			Non-1/v absorber;							
			0.4% var. between 20-100 ºC							
			g_{20}=1.007; g_{60}=1.009; g_{100}=1.011							

[*] For ^{151}Eu, ^{153}Eu, ^{168}Yb and ^{176}Lu s_0 factors are reported instead of Q_0 factors. W'=0 was assumed for all these cases.

Westcott g_T factors available in references [2, 16, 48].

[**] Value obtained when employing the F_i factors reported by DC. The second value is obtained with the more recent F_i factors reported in [8] (see Table 10.9).

[***] According to the recommended literature the k_0 factors for ^{124}Sb are quoted under the ADS type VI (no scenario) [20]. Our three proposed scenarios (a, b and c) for the ADS type VI are described in section 2.12.

[a] Q_0 factors calculated with the $\bar{E}_r$ value adopted from Trkov.

[b] Q_0 factors calculated according to their definition for the given ADS, with nuclear data from [1, 2].

[c] For the comparator s_0=17.2 [20] and W'=0.055 [48] and 10% relative half-width uncertainty.

F_{Cd} factors adopted from [13], half-lives adopted from Table 10.1 and/or from references [6, 8].

m = Number of materials (standards) tested; Ch = Number of (irradiation) channels employed.

The uncertainties from Lit values are given as quoted in these references (at 1*s*). These are not standard uncertainties.

The uncertainties in the values from TW are combined standard uncertainties. See section 7.11 for the coverage factors to employ per the number of channels employed for a 95% confidence level.

10.6.2 Recommended data for k_0-UNAA

The Table 10.16 contains the half-life $T_{1/2}$ and decay branching factor F_i (i = 2, 3, 24) adopted for each investigated formed nuclide in the fission of ^{235}U (20 radioisotopes) and the radiative neutron capture of ^{238}U (^{239}Np production) along the source for this data.

For ^{95}Zr and its daughters ^{95m}Nb and ^{95}Nb we adopted different F_i values than in the recommended k_0-literature [20, 23], from more recent and precise determinations reported in [8]. These F_i values were also employed for the determination of the k_0 factors for (n,γ) production of the same nuclides in this work [62].

The following values and half-width uncertainties from Lit were adopted for the calculations:

- for the ^{238}U(n,γ)^{239}U→^{239}Np reaction: Q_0 = 103.4(13) and $\bar{E}_r$ = 16.9(12) eV and,

- for ^{235}U fission: Q_0 = 0.47(5) and $\bar{E}_r$ = 0.59(8) eV.

An average and final set of results is compiled in Table 10.17 for ^{235}U k_0-fission factors and in Table 10.18 for ^{239}Np k_0 factors. The results shown in TW were obtained from the mean and the SD of the mean for N = 2 different standards tested in channel Y4 (8 samples; 4 samples per material) but an uncertainty budget for a single determination is given in section 7.8.1. The values from Lit correspond to the average and SD of one material irradiated in up to 4 channels, with the sample number not mentioned; presumably one per channel [54]. The uncertainty treatment on the B results is not mentioned. Their results correspond to one material (5 samples) irradiated in one channel [3].

We propose a new set of k_0 and k_0-fission factors from the mean and SD of the results from 3 different authors: TW, Lit and B. Considering that the results between TW, Lit and B were obtained from the analysis of N = 17 samples (8 + 4 + 5), one can estimate the precision of the AVG factors from the SD of the mean, i.e. $u(k_0) = SD/\sqrt{17}$ and a coverage factor k = 2.12 for a 95% confidence level. That is, assuming a SD ≤ 3% as most values in the table, then the expanded standard uncertainty would be $U(k_0) \leq 1.54\%$.

As mentioned in the section 8.5.1, the listed effective k_0-fission factors ($g_T.k_0$) of Table 10.17 are tabulated at the channel temperature range of 20-30 °C.

Our results in Table 10.17 and Table 10.18 are also expressed in terms of the Lit and B values or in terms of the C ones (Δ = TW/Lit; TW/B or TW/C). The calculated k_0 factors were determined with the definitions in eq. (5.4).

After computing k_0-ratios for each radioisotope against a reference line ($z = k_0/k_{0,ref}$) these were compared to the ratios between the I_γ values ($x = I_\gamma/I_{\gamma,ref}$) adopted from references [6, 8]. This was performed for the results in this work in Table 10.17 and Table 10.18, the Lit and B values. These results are summarized in Table 10.19. Unless inaccurate I_γ or k_0 factors are employed, both ratios should be equal ($z = x$; by definition), therefore observed systematic differences are probably due to imperfections in detector efficiency modelling and/or to unresolved γ-ray interferences. However, the I_γ values reported in the literature bear a high uncertainty for most the secondary γ-rays investigated, therefore this comparison might not be always a reliable indicator of the accuracy of the results.

By means of the CFY factors and nuclear data from the different sources [1, 2, 4–10] the σ_0 values for the $^{235}U(n,f)$ and $^{238}U(n,\gamma)$ reactions were obtained from the result of each γ-line. The Table 10.20 summarizes the absolute nuclear data employed in this work and the average σ_0 result obtained from all involved γ-lines.

Table 10.16: Adopted half-lives ($T_{1/2}$) and decay branching factors (F_i) for each formed nuclide. Uncertainties are expressed in absolute value for the last significant digit and correspond to half-widths.

FN	$T_{1/2}$				Decay branching factors			
Zr-95	64.032	(6)	d	RV	F_2	0.0112	(1)	RV
Nb-95m	3.61	(3)	d		F_3	0.975	(1)	
Nb-95	34.991	(6)	d		F_{24}	0.989	(1)	
Zr-97	16.74	(-)	h	Lit	F_2	0.968	(-)	Lit
Nb-97m	52.7	(-)	s		F_3	1.000	(-)	
Nb-97	72.1	(-)	m		F_{24}	0.032	(-)	
Mo-99	65.94	(-)	h	Lit	F_2	0.876	(19)	RV
Tc-99m	6.01	(-)	h	Lit				
Ru-103	39.35	(-)	d	Lit				
Ru-105	4.44	(-)	h	Lit	F_2	0.25	(5)	DC
Rh-105m	45	(-)	s		F_3	1.00	(-)	
Rh-105	35.36	(-)	h		F_{24}	0.76	(1)	
Te-131m	33	(-)	h	Lit	F_2	0.259	(-)	Lit
Te-131	25	(-)	m		F_3	1.000	(-)	
I-131	8.021	(-)	d		F_{24}	0.741	(-)	
Te-132	3.204	(13)	d	ND				
Te-133m	55.4	(4)	m	ND	F_2	0.165	(-)	ND
Te-133	12.5	(3)	m		F_3	1.000	(-)	
I-133	20.83	(8)	h		F_{24}	0.835	(-)	
I-135	6.58	(3)	h	ND				

FN	$T_{1/2}$			Decay branching factors				
Cs-137	30.08	(9)	y	ND	F_2	1.000	(-)	ND
Ba-137m	2.552	(1)	m					
Ba-140	12.75	(-)	d	Lit	F_2	1.000	(-)	ND
La-140	1.678	(-)	d					
Ce-141	32.51	(-)	d	Lit				
Ce-143	33.10	(-)	h	Lit				
Nd-147	10.98	(-)	d	Lit				
U-239	23.45	(-)	m	Lit	F_2	1.000	(-)	ND
Np-239	2.357	(-)	d					
Au-198	2.695	(-)	d	Lit				

Table 10.17: Effective k_0-fission factors (g_T x k_0) found in this as compared to the values in Lit, B or C. AVG and SD (in %) from all quoted authors results, next to the ratios between values obtained in TW against the other sources (Δ = TW / others). See this section text for more information.

	Energy	g_T x k_0 (%; 1s)					Δ = TW /	
FN	(keV)	C	Lit	TW	B	AVG	Lit or C	B
Zr-95	724.2	1.04E-03	1.02E-03 (2.1)	**1.05E-03 (1.5)**	1.03E-03 (3.0)	1.03E-03 (1.2)	1.02	1.01
	756.7	1.28E-03	1.26E-03 (2.4)	**1.28E-03 (1.7)**	1.27E-03 (2.0)	1.27E-03 (0.9)	1.02	1.01
Nb-95	765.8	2.57E-05	2.44E-05 (0.4)	**2.55E-05 (1.5)**		2.49E-05 (3.0)	1.04	
Zr-97	507.6	1.09E-04		**1.12E-04 (1.5)**			1.03	
	703.8	2.19E-05		**2.29E-05 (4.1)**			1.05	
	1021.3	2.19E-05		**2.29E-05 (1.5)**			1.05	
	1276.1	2.04E-05		**2.01E-05 (1.7)**			0.99	
Nb-97m	743.4	1.93E-03	2.01E-03 (1.2)	**2.01E-03 (1.4)**	2.00E-03 (0.4)	2.01E-03 (0.3)	1.00	1.01
Nb-97	657.9	2.07E-03	2.02E-03 (0.7)	**2.03E-03 (1.4)**	2.01E-03 (0.2)	2.02E-03 (0.6)	1.01	1.01

FN	Energy (keV)	g_T x k_0 (%; 1s) C	Lit	TW	B	AVG	Δ = TW / Lit or C	Δ = TW / B
Mo-99	181.1	1.33E-04	1.34E-04 (2.2)	**1.35E-04 (2.0)**	1.38E-04 (3.0)	1.36E-04 (1.6)	1.00	0.97
	366.4	2.64E-05	2.75E-05 (4.2)	**2.66E-05 (2.5)**	2.64E-05 (0.9)	2.68E-05 (2.2)	0.97	1.01
	739.5	2.68E-04	2.72E-04 (2.2)	**2.73E-04 (1.7)**	2.76E-04 (0.9)	2.74E-04 (0.8)	1.00	0.99
	777.9	9.48E-05	9.19E-05 (1.8)	**9.50E-05 (1.4)**	9.91E-05 (4.0)	9.53E-05 (3.8)	1.03	0.96
Tc-99m	140.5	1.72E-03	1.68E-03 (2.4)	**1.74E-03 (1.4)**	1.75E-03 (0.2)	1.72E-03 (2.2)	1.04	1.00
Ru-103	497.1	1.00E-03	9.68E-04 (5.0)	**9.98E-04 (2.4)**	1.00E-03 (1.3)	9.89E-04 (1.8)	1.03	1.00
	610.3	6.33E-05	6.05E-05 (5.0)	**6.36E-05 (1.8)**	6.39E-05 (2.0)	6.27E-05 (3.0)	1.05	1.00
Rh-105	306.1	1.75E-05	1.91E-05 (5.0)	**1.80E-05 (1.4)**	1.77E-05 (11.0)	1.83E-05 (4.1)	0.94	1.02
	318.9	6.55E-05	6.57E-05 (5.0)	**6.64E-05 (1.4)**	6.57E-05 (1.3)	6.59E-05 (0.6)	1.01	1.01
Te-131m	793.8	2.00E-05		**2.05E-05 (3.5)**			1.02	
	852.0	2.97E-05		**3.03E-05 (3.8)**			1.02	
	1125.5	1.64E-05		**1.71E-05 (3.3)**			1.04	
I-131	284.3	6.41E-05	6.38E-05 (5.0)	**6.30E-05 (2.0)**	6.20E-05 (0.9)	6.29E-05 (1.4)	0.99	1.02
	364.5	8.54E-04	8.05E-04 (5.0)	**8.40E-04 (1.6)**	8.31E-04 (1.0)	8.25E-04 (2.2)	1.04	1.01
	636.9	7.50E-05		**7.37E-05 (3.8)**			0.98	

FN	Energy (keV)	g_T x k_0 (%; 1s) C	Lit	TW	B	AVG	Δ = TW / Lit or C	B
Te-132	228.2	1.37E-03		**1.38E-03 (1.5)**			1.01	
I-133	529.9	2.11E-03		**2.14E-03 (1.4)**			1.01	
I-135	288.5	7.06E-05		**7.06E-05 (1.7)**			1.00	
	836.8	1.52E-04		**1.52E-04 (2.8)**			1.00	
	1038.8	1.80E-04		**1.81E-04 (1.6)**			1.01	
	1131.5	5.15E-04		**5.27E-04 (2.5)**			1.02	
	1260.4	6.53E-04		**6.47E-04 (1.5)**			0.99	
	1457.6	1.98E-04		**2.01E-04 (1.5)**			1.02	
	1502.8	2.46E-05		**2.47E-05 (1.8)**			1.00	
	1678.0	2.19E-04		**2.17E-04 (1.6)**			0.99	
	1706.5	9.33E-05		**9.33E-05 (2.5)**			1.00	
	1791.2	1.76E-04		**1.79E-04 (1.5)**			1.02	
Cs-137	661.7	1.91E-03		**1.94E-03 (1.6)**			1.01	

FN	Energy (keV)	g_T x k_0 (%; 1s) C	Lit	TW	B	AVG	Δ = TW / Lit or C	Δ = TW / B
Ba-140	162.7	1.40E-04		**1.45E-04 (1.4)**			1.04	
	304.9	9.66E-05		**9.64E-05 (1.4)**			1.00	
	423.7	7.09E-05		**7.32E-05 (1.4)**			1.03	
	437.6	4.34E-05		**4.51E-05 (1.5)**			1.04	
	537.3	5.49E-04		**5.59E-04 (1.5)**			1.02	
La-140	328.8	4.69E-04	4.57E-04 (1.3)	**4.64E-04 (1.6)**	4.60E-04 (1.0)	4.60E-04 (0.7)	1.01	1.01
	432.5	6.75E-05		**6.78E-05 (1.4)**			1.00	
	487.0	1.04E-03	1.01E-03 (1.0)	**1.05E-03 (2.1)**	1.02E-03 (0.9)	1.03E-03 (2.1)	1.04	1.03
	751.6	9.90E-05		**1.00E-04 (2.1)**			1.01	
	815.8	5.35E-04	5.17E-04 (0.8)	**5.41E-04 (1.6)**	5.24E-04 (1.8)	5.27E-04 (2.4)	1.05	1.03
	867.8	1.26E-04		**1.27E-04 (1.8)**			1.01	
	919.6	6.16E-05		**6.15E-05 (1.5)**			1.00	
	925.2	1.59E-04		**1.59E-04 (1.4)**			1.00	
	1596.2	2.15E-03	2.10E-03 (0.5)	**2.17E-03 (1.6)**	2.12E-03 (0.8)	2.13E-03 (1.7)	1.03	1.02
Ce-141	145.4	1.02E-03	1.03E-03 (0.5)	**1.03E-03 (1.9)**	1.01E-03 (1.1)	1.02E-03 (1.2)	1.00	1.02

FN	Energy (keV)	g_T x k_0 (%; 1s) C	Lit	TW	B	AVG	Δ = TW / Lit or C	Δ = TW / B
Ce-143	231.6	4.43E-05	4.51E-05 (2.9)	**4.52E-05 (1.6)**	4.38E-05 (11.0)	4.47E-05 (1.7)	1.00	1.03
	293.3	9.24E-04	9.05E-04 (1.0)	**9.34E-04 (1.4)**	9.11E-04 (0.2)	9.17E-04 (1.7)	1.03	1.03
	350.6	6.97E-05	6.77E-05 (5.0)	**7.11E-05 (1.4)**	7.29E-05 (1.5)	7.06E-05 (3.7)	1.05	0.98
	664.6	1.23E-04	1.20E-04 (0.8)	**1.26E-04 (1.7)**	1.14E-04 (1.8)	1.20E-04 (4.9)	1.05	1.10
	721.9	1.16E-04	1.15E-04 (0.9)	**1.19E-04 (1.9)**	1.11E-04 (1.8)	1.15E-04 (3.3)	1.03	1.07
Nd-147	91.1	2.27E-04	2.31E-04 (5.0)	**2.26E-04 (2.8)**	2.30E-04 (8.0)	2.29E-04 (1.3)	0.98	0.98
	319.4	1.72E-05	1.61E-05 (5.0)	**1.71E-05 (2.2)**	1.61E-05 (1.3)	1.64E-05 (3.5)	1.06	1.06
	439.9	1.04E-05	1.00E-05 (5.0)	**1.05E-05 (6.1)**	9.88E-06 (15.0)	1.01E-05 (3.1)	1.05	1.06
	531.0	1.08E-04	1.08E-04 (5.0)	**1.08E-04 (1.5)**	1.08E-04 (0.5)	1.08E-04 (0.2)	1.00	1.00

For TW results g_T = 0.9815 should we employed for the renormalization to k_0 factors (if needed).

The ADS for the monitoring of each fission product is given in Table 10.10.

Underlined values under the column AVG are recommended (≤ 2% uncertainty).

Table 10.18: The k_0 factors found in this work for ^{239}Np as compared to the values in Lit or C. See this section text for more information.

FN ADS	Energy (keV)	k_0 (%; 1*s*) C	Lit	TW	AVG	Δ = TW / Lit	Δ = TW / C
Np-239	106.1	6.20E-03	6.52E-03 (0.6)	**6.19E-03 (1.8)**	6.35E-03 (3.7)	0.95	1.00
II/b	209.8	8.19E-04	7.80E-04 (0.5)	**7.88E-04 (1.7)**	7.84E-04 (0.7)	1.01	0.96
	228.2	2.67E-03	2.71E-03 (0.7)	**2.60E-03 (1.7)**	2.66E-03 (2.9)	0.95	0.98
	277.6	3.45E-03	3.40E-03 (0.8)	**3.37E-03 (1.9)**	3.38E-03 (0.7)	0.99	0.98
	285.8	1.87E-04	1.83E-04 (5.0)	**1.84E-04 (1.8)**	1.84E-04 (0.4)	1.00	0.99
	315.9	3.81E-04	3.68E-04 (1.5)	**3.69E-04 (2.1)**	3.69E-04 (0.2)	1.00	0.97
	334.2	4.88E-04	4.81E-04 (1.0)	**4.79E-04 (1.6)**	4.80E-04 (0.3)	1.00	0.98

Underlined values under the column AVG are recommended (≤ 2% uncertainty).

Table 10.19: The k_0-fission factors ratios against a reference γ-line ($k_0/k_{0,ref}$). Values computed for the TW (Table 10.17 and Table 10.18), Lit and B values. These ratios should be equal to the respective I_γ ratios ($x = I_\gamma/I_{\gamma,ref}$; same reference).

		Energy			$(k_0/k_{0,ref})$ / x			σ_0 (b)
FN	**CFY %**	**(keV)**	I_γ	$x = (I_\gamma/I_{\gamma,ref})$	**Lit/*x***	**B/*x***	**TW/*x***	**TW**
Zr-95	6.500	724.2	44.27	1.2	1.01	1.00	1.00	585
		756.7	54.38		ref			585
Nb-95	6.500	765.8	99.81		ref			580
Zr-97	5.98	507.6	5.03		ref			603
		703.8	1.01	5.0			0.99	611
		1021.3	1.01	5.0			0.99	611
		1276.1	0.94	5.4			1.05	576
Nb-97m	5.63	743.4	97.9		ref			608
Nb-97	6.00	657.9	98.23		ref			575
Mo-99	6.11	181.1	6.01	2.0	1.01	0.99	1.00	590
		366.4	1.19	10.2	0.97	1.03	1.01	587
		739.5	12.12		ref			593
		777.9	4.28	2.8	1.05	0.98	1.01	586
Tc-99m	6.11	140.5	88.5		ref			593

FN	CFY %	Energy (keV)	I_γ	$x = (I_\gamma/I_{\gamma,ref})$	$(k_0/k_{0,ref})$ / x Lit/x	B/x	TW/x	σ_0 (b) TW
Ru-103	3.03	497.1	91.0		ref			583
		610.3	5.76	15.8	1.01	0.99	0.99	588
Rh-105	0.946	306.1	5.1	3.7	0.92	0.99	0.99	601
		318.9	19.1		ref			593
Te-131m	0.412	793.8	13.4	1.5			1.00	598
		852.0	19.9		ref			596
		1125.5	11.0	1.8			0.98	608
I-131	2.89	284.3	6.12	13.3	0.95	1.01	1.00	574
		364.5	81.5		ref			575
		636.9	7.16	11.4			1.00	574
Te-132	4.28	228.2	88.0		ref			591
I-133	6.70	529.9	87.0		ref			591

		Energy			$(k_0/k_{0,ref})$ / x			σ_0 (b)
FN	**CFY %**	**(keV)**	I_γ	$x = (I_\gamma/I_{\gamma,ref})$	**Lit/*x***	**B/*x***	**TW/*x***	**TW**
I-135	6.28	288.5	3.1	7.3			1.02	585
		836.8	6.69	3.4			1.02	585
		1038.8	7.9	2.9			1.02	589
		1131.5	22.6		ref			599
		1260.4	28.7	0.8			1.04	578
		1457.6	8.7	2.6			1.01	593
		1502.8	1.08	20.9			1.02	587
		1678.0	9.6	2.4			1.03	580
		1706.5	4.1	5.5			1.03	584
		1791.2	7.72	2.9			1.01	594
Cs-137	6.19	661.7	85.1		ref			592
Ba-140	6.21	162.7	6.22	3.9			0.98	605
		304.9	4.29	5.7			1.02	583
		423.7	3.15	7.7			0.99	603
		437.6	1.93	12.6			0.98	607
		537.3	24.39		ref			595

		Energy			$(k_0/k_{0,ref})$ / x			σ_0 (b)
FN	**CFY %**	**(keV)**	I_γ	$x = (I_\gamma/I_{\gamma,ref})$	**Lit/*x***	**B/*x***	**TW/*x***	**TW**
La-140	6.22	328.8	20.8	4.6	1.00	1.00	1.02	578
		432.5	3.0	31.9			1.01	586
		487.0	46.1	2.1	1.00	1.00	1.00	591
		751.6	4.39	21.7			1.00	591
		815.8	23.72	4.0	1.01	1.01	1.00	591
		867.8	5.58	17.1			1.00	589
		919.6	2.73	34.9			1.01	584
		925.2	7.04	13.6			1.01	586
		1596.2	95.4		ref			589
Ce-141	5.85	145.4	48.29		ref			589
Ce-143	5.954	231.6	2.05	20.9	0.96	1.00	0.99	596
		293.3	42.8		ref			591
		350.6	3.23	13.3	1.01	0.94	0.99	596
		664.6	5.69	7.5	1.00	1.06	0.99	599
		721.9	5.39	7.9	0.99	1.03	0.99	595

		Energy			$(k_0/k_{0,ref})$ / x			σ_0 (b)
FN	**CFY %**	**(keV)**	I_γ	$x = (I_\gamma/I_{\gamma,ref})$	**Lit/*x***	**B/*x***	**TW/*x***	**TW**
Nd-147	2.232	91.1	28.1	0.5	0.98	0.98	1.01	579
		319.4	2.13	6.3	1.07	1.07	1.01	580
		439.9	1.28	10.5	1.03	1.04	0.99	591
		531.0	13.4		ref			584
Np-239		106.1	25.9	0.6	0.94		0.98	2.67
ADS = II/b		209.8	3.4	4.2	1.04		1.01	2.58
		228.2	11.1	1.3	0.97		1.00	2.61
		277.6	14.4		ref			2.61
		285.8	0.8	18.5	1.01		0.99	2.64
		315.9	1.6	9.1	1.02		1.01	2.60
		334.2	2.0	7.1	1.00		1.00	2.63

The ADS for the monitoring of each fission product is given in Table 10.10.

Table 10.20: Absolute nuclear data adopted for the determination of the σ_0 for the ^{238}U(n,γ) and ^{235}U(n,f) reactions studied in this work.

	U-238		U-235		Au-197		Ref.
AW	**238.02891**	**(3)**	**238.02891**	**(3)**	**196.96659**	**(1)**	**IUPAC1**
***θ* (%)**	**99.2745**	**(10)**	**0.72**	**(1)**	**100.0**	**(-)**	**IUPAC2**
σ_0 (b)	2.75	(6)			98.65	(9)	DC
	2.677	(13)	584.33	(99)	**98.66**	**(9)**	**A**
	2.683	(-)	585.0	(-)	98.7	(-)	ENDF
	2.684	(-)	585.0	(-)	98.74	(-)	JEFF
	2.683	(-)	585.1	(-)	98.7	(-)	ROSF
	2.718	(-)	585.0	(-)	98.74	(-)	CENDL
	2.72	(-)	583.2	(-)	98.71	(-)	EAF
	2.683	(-)	585.1	(-)	98.65	(-)	JENDL
	2.62	**(6)**	**589**	**(9)**	**adopted from A**		**TW**
g_{27}	**1.004**	**(-)**	**0.9815**	**(-)**	**1.007**	**(-)**	**H**
g_{40}	1.004	(-)	0.9792	(-)	1.008	(-)	
g_{60}	1.005	(-)	0.9755	(-)	1.009	(-)	
g_{100}	1.006	(-)	0.9692	(-)	1.011	(-)	

The σ_0 values in TW were found from the average of all the values per γ-line listed in Table 10.19 and their uncertainties from the discussion in section 7.8.1. All uncertainties are expressed in absolute value, for the last significant digit at 1*s* confidence level.

For our σ_0 results we recommend k=2.365 (N = 8 samples) for a 95% confidence level.

The I_γ = 95.54 value adopted in this work for the 411.8 keV line of ^{198}Au was taken from reference [8].

The Westcott g_T factor indexes are expressed in °C.

10.7 Thermal neutron cross-sections

The derived thermal neutron cross-sections at 2200 m/s neutron velocity for production of metastable, ground and/or "effective" (or compound) states from this work are summarized in Table 10.21 along the adopted absolute nuclear data for their calculation. The neutron cross-sections are compared to values from: DC, A and the EENL databases [1, 2, 4, 6–8, 13, 15].

All uncertainties in Table 10.21 are reported in absolute value for the last significant digit. In the case of the DC and A databases, these uncertainties are half-widths or approximate SDs. The reported values in TW are the AVG and SD of all the results per γ-ray listed in the last column of Table 10.15.

In section 7.10 it was calculated that the standard uncertainty in a single determination of σ_0 value is typically like that of a k_0 factor, i.e. $u(\sigma_0) \approx u(k_0)$ since the uncertainty in the atomic weights and isotopic abundances are usually negligible for most cases and that the major contributor to the combined uncertainty is usually $u(I_\gamma)$. The estimate $u(k_0)$ already includes some uncertainty contribution from isotopic variability from the standards employed (0.33%). In this work, the SD from the results of all available γ-lines is reported instead. The reader can combine the reported SD in TW from Table 10.21 with the $u(k_0)$ reported in Table 10.15 to obtain an estimate of the combined standard uncertainty $u(\sigma_0)$.

In section 7.11 an estimate for $u(k_0)$ ($\approx u(\sigma_0)$) from multiple determinations is given. The reader can apply the proposed coverage factors for a 95% confidence level depending on the number of irradiation channels and samples employed for a given target isotope (see Table 10.15). From the employment of up to 4 channels one can estimate a precision of ~3.5% in the reported σ_0 values (at the 95% confidence level).

Table 10.21: Absolute nuclear data and thermal neutron cross-sections for neutron capture and production of metastable, ground or compound states found in this work as compared to values by DC, A and the EENL databases.

						σ_0 (b; 1*s*)								
TI	**AW**		**θ (%)**		**State**	**DC**		**A**		**TW**		**ENDF**	**JEND**	**JEFF**	**EAF**
^{23}Na	22.990		100	-	**F_2m+g**	0.513	4	0.40	3	0.519	1	0.5281	0.5314	0.5314	0.4237
^{26}Mg	24.305	6	11.01	3	**g**	0.0372	3	0.0384	6	0.0372	2	0.0383	0.0383	0.0383	0.0384
^{27}Al	26.982		100	-	**g**	0.226	2	0.231	3	0.230	2	0.2335	0.2304	0.2335	0.2335
^{37}Cl	35.452	6	24.2	1	**m**			0.047	10						
					m+g	0.423	6	0.433	6	0.412	3	0.4332	0.4329	0.4331	0.4333
^{41}K	39.098	1	6.730	4	**g**	1.45	3	1.46	3	1.451	3	1.461	1.459	1.459	1.461
^{45}Sc	44.956		100	-	**m**			9.8	11						
					g			17.4	11						
					m+g	26.3	2	27.2	2	26.9	1	27.16	27.15	27.15	27.16
^{50}Ti	47.867	1	5.18	2	**g**	0.171	4	0.179	3	0.173	5	0.1795		0.1795	0.1784
^{51}V	50.942	1	99.75	4	**g**	4.79	8	4.88	6	4.77	5	4.919	4.919		4.91

						σ_0 (b; 1*s*)								
TI	**AW**		**θ (%)**		**State**	**DC**		**A**		**TW**		**ENDF**	**JEND**	**JEFF**	**EAF**
^{50}Cr	51.996	1	4.35	1	**g**	15.2	2	15.4	2	14.4	1	15.40	15.38	15.93	15.97
^{55}Mn	54.938		100	-	**g**	13.20	13	13.36	5	13.0	1	13.28	13.28	13.42	13.41
^{58}Fe	55.845	2	0.282	4	**g**	1.31	5	1.32	3	1.30	1	1.149	1.300	1.315	1.150
^{59}Co	58.933		100	-	**m**			20.4	8	20.7	5				
					g					16.7	2				
					F_2m+g	37.13	7	37.18	6	37.15	2	37.18	37.21	37.18	37.23
^{64}Ni	58.693	1	0.926	2	**g**	1.69	6	1.64	4	1.62	1	1.48	1.48	1.518	1.481
^{63}Cu	63.546	3	69.2	2	**g**	4.28	18	4.50	2	4.52	2	4.47	4.507	4.47	4.473
^{65}Cu			30.9	2	**g**	2.48	60	2.17	3	2.06	1	2.149	2.169	2.149	2.151
^{64}Zn	65.38	2	49.2	8	**g**	0.726	17	0.79	2	0.718	7	0.7875	0.7875		0.7642
^{68}Zn			18.5	6	**m**	0.070	2	0.072	4	0.071	1				
^{71}Ga	69.723	1	39.89	1	**m**			0.15	5						
					m+g	4.61	5	4.61	15	4.61	4	4.731	3.71		4.712

						σ_0 (b; 1*s*)								
TI	**AW**		**θ (%)**		**State**	**DC**		**A**		**TW**		**ENDF**	**JEND**	**JEFF**	**EAF**
^{75}As	74.922		100	-	**g**	3.86	17	4.09	8	3.8	1	4.502	4.153	4.302	4.504
^{81}Br	79.904	1	49.31	7	**m**			2.12	5						
					g			0.235	8						
					F_2m+g	2.58	3	2.36	5	2.59	3	2.365	2.356	2.776	2.778
^{85}Rb	85.468		72.2	1	**m**			0.056	3						
					g			0.438	8						
					m+g	0.494	7	0.494	7	0.521	5	0.4936	0.4802	0.4765	0.4769
^{87}Rb			27.83	2	**g**	0.10	3	0.102	4	0.094	3	0.120	0.120	0.120	0.120
^{84}Sr	87.62	1	0.56	1	**m**	0.61	-	0.623	60	0.659	3				
					g			0.2	1	0.130	9				
					m+g			0.8	1	0.79	6	0.822	0.828	0.8127	0.813
					F_2m+g	0.69	2	0.740		0.700	7				
^{86}Sr			9.86	1	**m**	0.770	7	0.77	6	0.791	9				

						σ_0 **(b; 1*s*)**								
TI	**AW**		**θ (%)**		**State**	**DC**		**A**		**TW**		**ENDF**	**JEND**	**JEFF**	**EAF**
^{89}Y	88.906		100		**m**	0.0010	1	0.0010	2	0.0012	1				
^{94}Zr	91.224	2	17.4	3	**g**	0.053	1	0.050	2	0.052	3	0.0499	0.0507	0.0498	0.0499
^{96}Zr			2.80	9	**g**	0.0213	1	0.0229	1	0.0211	2	0.0229	0.0203	0.0229	0.0230
^{93}Nb	92.906		100	-	**m**	0.86	10			0.853	8				
					m+g			1.15	5			1.156	1.142	1.156	1.156
^{98}Mo	95.96	2	24.4	4	**g**	0.131	1	0.130	6	0.128	2	0.130	1.321	0.130	0.1291
^{100}Mo			9.8	3	**g**	0.200	22	0.199	3	0.201	1	0.1991	0.1938	0.1991	0.1987
^{96}Ru	101.07	7	5.5	1	**g**	0.229	3	0.29	2	0.248	2	0.2901	0.2711	0.2487	0.2489
^{102}Ru			31.6	1	**g**	1.16	3	1.27	4	1.241	1	1.27	1.475	1.27	1.27
^{104}Ru			18.6	3	**g**	0.491	10	0.491	10	0.505	5	0.472	0.469	0.472	0.472
^{108}Pd	106.42	1	26.5	1	**m**			0.185	10						
					g			8.48	50			8.481	8.481	8.46	7.362
					m+g	8.77	-	8.665	-	8.57	9				

						σ_0 **(b; 1*s*)**									
TI	**AW**		**θ (%)**		**State**	**DC**		**A**		**TW**		**ENDF**	**JEND**	**JEFF**	**EAF**
^{110}Pd			11.7	1	**m**	0.0120	-	0.033	3	0.0130	2				
					m+g			0.73	17	0.291	4	0.229	0.225	0.227	0.273
^{107}Ag	107.868		51.84	1	**g**	33.1	17	37.6	12	34.3	9	37.61	37.65	37.62	37.64
^{109}Ag			48.16	1	**m**	3.90	3	3.95	5	3.96	2				
^{114}Cd	112.411	8	28.7	4	**g**	0.23	-	0.330	18	0.334	6	0.336	0.3405	0.336	0.3364
^{113}In	114.818	3	4.29	5	**m_2**			3.1	8						
					m_1			8.1	7						
					g			3.9	4						
					m_2+m_1	8.2	-	8.1	8	8.1	3				
					m_2+m_1+g	8.2	-	12.0	17			12.13	12.09	12.07	12.04

TI	AW	θ (%)	State	σ_0 (b; 1*s*) DC		A		TW		ENDF	JEND	JEFF	EAF
^{115}In		95.71 5	**m_2**			81	8						
			m_1			81	8						
			g			40	2						
			m_2+m_1	157	5	162.3	7	158	2				
			m_2+m_1+g							202.3	201.2	201.2	205
^{112}Sn	118.710 7	0.97 1	**m**			0.29	3						
			F_2m+g	0.541	10			0.541	1				
			m+g			0.85	4			0.8503	0.8607	1.009	0.7316
^{116}Sn		14.5 1	**m**	0.0060	1	0.0060	2	0.0061	2				
^{117}Sn		7.68 7	**n,n'**	0.095	-								
^{124}Sn		5.79 5	**m**	0.116	3								
			g	0.0042	-	0.0045	-	0.0046	1				
			m+g	0.120	3	0.134	6			0.1337	0.1357	0.1355	0.135

						σ_0 (b; 1*s*)								
TI	**AW**		**θ (%)**		**State**	**DC**		**A**		**TW**		**ENDF**	**JEND**	**JEFF**	**EAF**
^{121}Sb	121.760	1	57.21	5	**m+g**	6.33	15	5.77	11	5.766	8	5.773	5.994	5.994	5.920
^{123}Sb			42.79	5	**m_2**			0.019	10						
					m_1			0.037	10						
					g			3.880	12						
					$F_3(m_2+m_1)+g$	4.08	9	3.94	12	3.89	3	3.875	4.188	4.188	4.06
^{133}Cs	132.905		100	-	**m**	2.74	8	2.6	1	2.97	2				
					g			27.7	14	27.4	2				
					m+g	30.7	2	30.3	11	30.2	2	29.06	28.90	29.01	29.00
^{130}Ba	137.327	7	0.106	1	**m**			0.98	5						
					g			7.7	9						
					m+g	9.04	27	8.7	9	8.00	2	8.680	8.701		
^{132}Ba			0.101	1	**m**	0.82	-	0.5	-	0.75	1				
^{134}Ba			2.42	2	**m**	0.053	-	0.134	24	0.054	1				

						σ_0 (b; 1*s*)									
TI	**AW**		**θ (%)**		**State**	**DC**		**A**		**TW**		**ENDF**	**JEND**	**JEFF**	**EAF**
^{135}Ba			6.59	1	**n,n'**	0.30	-								
^{138}Ba			71.70	4	**g**	0.405	5	0.404	40	0.404	1	0.4035	0.4044	0.3592	0.3591
^{139}La	138.905		99.91		**g**	9.34	9	9.04	4	9.25	4	9.042	8.94	9.042	8.94
^{141}Pr	140.908		100	-	**m**			3.9	3						
					m+g	11.2	16	11.5	3	11.3	1	11.51	11.48	11.51	11.49
^{152}Sm	150.36	2	26.75	16	**g**	220	5	206	6	206	1	206	205.9	206	206.2
^{151}Eu	151.964	1	47.81	6	**m_2+g**					6612	36				
					m_2+m_1+g			9200	-			9184	9169	9167	9168
^{153}Eu			52.19	6	**m+g**	307	12	312	7	312	3	312.5	312.7	312.7	312.5
^{152}Gd	157.25	3	0.20	1	**g**			735	20	772	2	735	735	735	1057
^{158}Gd			24.8	1	**g**	2.40	-	2.20	2	2.22	2	2.20	2.20	2.501	2.50
^{159}Tb	158.925		100	-	**g**	23.8	2	23.4	4	23.9	2	23.36	23.13	23.36	23.23
^{164}Dy	162.500	1	28.26	5	**F_2m+g**	2725	354	2650	70	265	2	2653	2654	2651	2651

						σ_0 (b; 1*s*)									
TI	**AW**		**θ (%)**		**State**	**DC**		**A**		**TW**		**ENDF**	**JEND**	**JEFF**	**EAF**
^{165}Ho	164.930		100	-	**g**	58.1	23	61.2	11	60.9	8	64.70		63.46	61.1
^{169}Tm	168.934		100	-	**g**	107	-	105	2	107	8	105	105	105	104.9
^{168}Yb	173.054	5	0.123	3	**g**			2300	170			2300	2308	2308	2305
					m+g					3144	34				
^{174}Yb			32.0	1	**m+g**	128	9	63.2	15	63.0	5	63.2	63.2	63.21	69.2
^{176}Yb			13.0	1	**m+g**	3.11	-	2.85	5	2.85	7	2.85	2.82	2.823	2.86
^{176}Lu	174.967	1	2.60	1	**g**	2194	-	2090	70			2097	2097	2097	2097
^{174}Hf	178.49	2	0.16	1	**g**	549	10	549	7	549	6	561.7	562.3	651.5	403.8
^{179}Hf			13.62	2	**m**	0.450	12	0.445	3	0.430	5	0.428			
^{180}Hf			35.1	2	**g**	13.50	18	13.04	7	13.01	7	13.01	13.06	13.06	13.08
^{181}Ta	180.948		99.99	3	**m+g**	20.4	2	20.5	5	20.2	1	21.13	20.68	20.68	21.14
^{186}W	183.84	1	28.43	19	**g**	38.7	2	38.1	5	34.9	2	38.1	38.1	39.46	37.49
^{185}Re	186.207	1	37.4	2	**g**	106	17	112.1	2	112	1	112.2		112.2	112.3

						σ_0 (b; 1*s*)									
TI	**AW**		**θ (%)**		**State**	**DC**		**A**		**TW**		**ENDF**	**JEND**	**JEFF**	**EAF**
^{187}Re			62.6	2	**m**	2.05	9	2.05	9	2.06	3				
					m+g	73.2	3	76.4	10	74.6	14	76.71		76.71	74.86
^{196}Pt	195.084	9	25.2	3	**m**			0.044	4	0.0352	4				
					g					0.718	3				
					F_2m+g			0.58	3	0.753	15				0.737
^{198}Pt			7.36	13	**m**			0.35	4						
					m+g	3.58	14	3.61	11	3.30	1				3.44
^{197}Au	196.967		100	-	**g**	98.66	9	98.66	9	from A		98.7	0.9865	0.9874	0.9871
^{232}Th	232.038		100	-	**g**	7.26	8	7.35	3	7.41	2	7.337	7.338	7.405	7.401

For uranium, refer to Table 10.20.

The uncertainties are given in absolute value for the last significant digit, as quoted in these references.

The uncertainties reported in TW correspond to the SD from all available γ-lines. See text for more information about the estimated precision.

10.8 Summary of findings

About the nuclear data for (n,γ) reactions

In this chapter, we provided the k_0 nuclear data for 76 (n,γ) target isotopes, leading to the formation of 96 radionuclides (excluding uranium, comented further in this text).

The effective resonance energies for 54 (n,γ) reactions were found experimentally through the α-vector method, which allows to assume a given α-dependence of the $\bar{E}_r$ parameter on a constant p_3 empirical value or not (p_3=0). Our results for both cases allowed us to confirm that the α-independence of the $\bar{E}_r$ parameter assumed by Jovanovic and later by De Corte et al. in his Habitation thesis (during the first k_0 determinations) holds for half the investigated isotopes on average, since 32 values (60% of total) agreed with the literature within <25% relative difference, while for 23 values (43% of total) the difference was less than 10-15%. On the other hand, the maximum difference expected when neglecting the p_3 value was <5% for channel Y4 and, within 1-2% for our extreme channels S84 and X26. When the accuracy of the recommended values is suspected, our sets of $\bar{E}_r$ and Q_0 values might offer an alternative to this problem but further (independent) validations of this experimental data and the α-vector method generalization to N channels by other independent laboratories are required, as expected.

Apart from the half-lives and decay branching fractions, the $\bar{E}_r$ values are the only ones left that are still borrowed directly from the literature, thus the accuracy of a theoretical $\bar{E}_r$ value can be tested through the α-vector method. It can be reverse-engineered for α-calibration by inputting Q_0 and $\bar{E}_r$ values from the literature, obtaining a system of transcendental equations that is solved through an iterative process. The α-vector method allows for the Y_α values from several laboratories to be combined and from this multi-channel

graph, better estimates of the Q_0 and $\bar{E}_r$ values can be obtained each time a set of independent experimental results is made available to the k_0-community. Thus, it provides a practical approach for combining Q_0 and $\bar{E}_r$ results from different authors, while allowing for a smooth modelling of the Q_α factor with as many p_i-values as different channels are combined.

The reported Q_0 results for 24 isotopes agreed with the 2012 recommended values within 4%, which are only statistically significant when determined in at least 2 irradiation channels. Our Q_0 findings corroborate significant discrepancies found by Kennedy et al. during the last decade (e.g. Sr, As, Ru and Ta). From our results, we suggested that the 2012 recommended Q_0 factors for ^{85m}Sr and ^{85}Sr production could be swapped (since the pioneering determinations). The new result for ^{196}Pt was compared to calculated values from the literature as there is no recommended Q_0 factor associated with this isotope.

For the remaining elements, it was not possible to compare all our significant findings with more recent experimental data or, in the case of non-1/v absorbers, the modified Westcott formalism is not suited for s_0 determination. Differences of 10-30% were observed for low-Q_0 values (e.g. ^{27}Al, ^{174}Hf, ^{164}Dy, etc.) which have imprecise (adopted; <1980) values. For these nuclides with low-Q_0 factors, the observed impact on the k_0 determinations was negligible and the same effect is expected in the analytical result (i.e. the elemental content) under normal NAA, but the adoption of our Q_0 values will have a significant impact in routine analysis under Cd-covered irradiations (ENAA) as compared to the results that are obtained today with the latest recommended database. Several of our Q_0 results have lower uncertainties than in the literature and are recommendable.

The 364 k_0 factors reported were found experimentally by means of the Cd-subtraction technique and (for just a few cases) through the usual modified Høgdahl and/or Westcott conventions that required the adoption of Q_0 or s_0

factors from the recommended literature. Our k_0 factors are the average of the values found with all irradiation channels and materials employed in this work. The observed SD for these values was typically lower than our expected $u_{multi}(k_0)$ = 1.6% for multiple channels, detectors and materials (for a single k_0 determination $u(k_0)$ = 2.4% in i.e. channel S84). It was higher when in presence of F_{Cd}, g_T, G_t factors ≠1 and γ attenuation uncertainty contributions.

For 54 radioisotopes, our k_0 factors agree with the 2012 compilation within 2-4% (1% for most recommended lines). For the Cr, Rb, Pd, ^{114}In, Cs, Sb and Pt radionuclides the k_0 factors for the main lines were > 5% different (statistically significant) and require confirmation from independent laboratories. We reported k_0 factors that are not in the current library for ^{197m}Pt, ^{197}Pt, ^{199}Pt and ^{125}Sb. Due to the high uncertainty in the ^{198}Pt isotopic abundance, the data for ^{199}Pt requires further validations. The k_0 factors for ^{134}Cs and ^{188}Re under the more natural decay scheme IV/b were proposed for the first time as well. Additionally, several recommended new k_0-factors are proposed for multi-γ radioisotopes (e.g. ^{72}Ga, ^{140}La, ^{76}As, ^{181}Ta, etc.). The derived thermal neutron cross-sections agreed with the literature while our k_0 factors were also in good proportion when compared to the ratio between the respective γ abundances.

When considering how our factors would influence a previous analytical result (elemental concentration), differences in k_0 values will propagate entirely to it. The differences in Q_0 factors will propagate fully if α = 0 and Cd-covered irradiations are performed (f = 0; ENAA). The discrepancies on the Q_0 factors would become negligible if f is sufficiently high ($f >> Q_\alpha$).

About k_0-UNAA and the k_0-fission factors

The current k_0-fission literature was intended for corrections in the calculated content of e.g. rare earth elements from interferences arising from natural ^{235}U fission. In this work, we validated its applicability under the opposite perspective, i.e. the determination of the ^{235}U content in multi-elemental samples containing U. These results combined with the calculated ^{238}U content provided a means for determining the ^{235}U enrichment levels in samples.

The problem of (n,γ) interfering reactions was dealt in Chapter 5 by means of a filtering algorithm, described and tested in this work with the aid of several standards having low to high nominal $n(^{235}U)/n(^{238}U)$ values (0.5 to 10% ^{235}U enrichment). The radioisotopes ^{131}I and ^{140}La (after sufficient cooling times) were identified as unbiased (non-interfered) initial estimators for the filtering algorithm. However, a 2-3% overestimation of the $n(^{235}U)/n(^{238}U)$ value was observed with the current k_0-literature, which motivated the experimental redetermination of current and new k_0-fission factors, to improve the reliability of the overall method.

The k_0-fisison factors for 20 fission products were reported in this work, from which 7 nuclides are produced only by fission of ^{235}U (not interfered).

The derived thermal neutron cross-sections of 589(9) b for ^{235}U and 2.62(6) b for ^{238}U at the 1*s* confidence level agreed with the literature values within 1 and 2% (respectively). Our ratios of k_0 factors were also in agreement when compared to the ratio between the respective γ-ray abundances. For our σ_0 results we recommend k=2.365 (N = 8 samples) for a 95% confidence level.

Our reported k_0 fission factors were on average 2% higher than the values in the current k_0-literature and in line with the recent results by Blaauw et al. with a few exceptions. This 2% difference, combined with our 1% lower observed k_0 factor for the 277.6 keV line of ^{239}Np, accounts for a 3% overestimation of the $n(^{235}U)/n(^{238}U)$ isotopic ratio, which is consistent to

what we observed when employing the current recommended k_0-literature before the recalibration of all our detectors and irradiation channels. A new set of recommended k_0 and k_0-fission factors for k_0-UNAA is provided from the mean of the results of 3 authors.

11. Samenvatting en conclusie

Het succes van de k_0-standaardisatie in neutronenactiveringsanalyse wordt bepaald door de continue revisie van de fundamentele gegevens. Hoewel de k_0 en Q_0 factoren gedefinieerd zijn als "nucleaire constanten", is het duidelijk dat deze "constanten" in de tijd kunnen aangepast worden wegens hun experimentele natuur en correlatie van de aangenomen nucleaire gegevens. Een deel van de huidige aanbevolen k_0-bibliotheek werd slechts één maal experimenteel bepaald, 30 jaar geleden, en deze was gecorreleerd met nucleaire gegevens, die bekomen waren van niet-bevestigde literatuur, beschikbaar voor 1980. Verschillende auteurs hebben systematische verschillen vastgesteld bij de analyse van referentiematerialen bij het gebruik van sub-datasets van de huidige k_0-litteratuur (2012). Maar het is moeilijk of zelfs onmogelijk om de oorzaak van deze inaccuratesse te vinden, tenzij er meer experimentele gegevens beschikbaar zijn voor de k_0-gemeenschap. Een kritische revisie van de traceerbaarheid van de huidige k_0-bibliotheek toonde aan: dat de F_{Cd} factoren ontbreken in de laatste literatuurreferenties of dat sommige (aangenomen) F_{Cd} factoren zouden kunnen inaccuraat zijn en validatie vereisen voor ENAA toepassing; dat sommige radionucliden niet meer gerapporteerd worden (^{135m}Ba; ^{125}Sb) of dat nieuwe radionucliden zouden kunnen toegevoegd worden aan de aanbevolen bibliotheek (bv. ^{197}Pt, ^{111}Ag, ^{235}U fissie producten; bijkomende γ-lijnen). Bovendien werd aangetoond dat sommige subsets van gegevens zouden kunnen verbeterd worden (^{134}Cs, ^{186}Re voor zowel "a" als "b" ADS type IV scenario's).

Voor de Universiteit Gent (UGent) en het Studiecentrum voor Kernenergie (SCK•CEN) (België) was het tijd om gebruik te maken van de vorderingen in de technologie en de nucleaire chemie van de laatste 20 jaar (o.m. betere detectoren voor straling, gecertificeerde standaarden) om een project op te starten om k_0 nucleaire gegevens opnieuw te bepalen voor 76 (n,γ) doelwit isotopen, die 96 radionucliden vormen (364 γ-stralen met analytisch nut). Om de $n(^{235}U)/n(^{238}U)$ bepaling aan het SCK•CEN te verbeteren, was het noodzakelijk om ook de k_0 factoren voor zowel ^{238}U neutron vangst als voor ^{235}U fissie opnieuw te bepalen en in te voeren. De k_0 nucleaire gegevens voor deze 2 bijkomende doelwit isotopen die ^{239}Np en 20 fissie producten vormen, werd onderzocht om informatie te bekomen over de uranium aanrijkingsniveaus in multi-element monsters, met nuttige toepassingen in de neutron forensisch onderzoek en/of milieucontroles.

De bepaling van k_0 nucleaire gegevens was een metrologisch werk waarvoor alle bestralingskanalen en detectoren opnieuw accuraat dienden te worden gekalibreerd. Om dat te verwezenlijken werden voldoende verdunde, homogene standaarden en gecertificeerde radioactieve bronnen van goede kwaliteit en traceerbaarheid bekomen van o.m. IRMM, NIST, Goodfellow en AREVA. Bovendien liet een aangepaste/gemodificeerde SOLCOI code ons toe om accurate efficiëntie transfer uit te voeren d.m.v. meer recente en vloeiende X en γ-straal lineaire attenuatie curves van de NIST XCOM onlinedatabase. Minstens 0,6% relatief verschil werd bijvoorbeeld vastgesteld tussen onze berekende en experimentele gegevens-punten voor kleine cilindervormige papierfilters en voor abundante γ-stralen in het 300-1300 keV energiegebied, gemeten op 20-30 cm afstand tussen detector en monster, die later zullen gebruikt worden voorde k_0 bepalingen.

De in de literatuur recent voorgestelde experimentele methoden voor de berekening van de correctie factoren voor neutronen self-shielding (bv. de Sigmoid, Chilian et al. en MATSSF methoden) hebben we bestudeerd en gevalideerd, om de ongewenste matrix zelfabsorptie van thermische en

resonantie neutronen in rekening te brengen, die de belangrijkste bron zijn van afwijkingen in de geschatte (n,γ) reactiesnelheid.

Uit onze self-shielding experimenten en validering van monsters met hoge Na, Dy en H concentratie bleek de Chilian et al. methode voor thermische neutronen self-shielding correctie beter geschikt voor ons werk, wegens zijn accuratesse en ruime toepasbaarheid (k_{th} aanpasbare parameter) dan de MATSSF thermische berekeningsmethode, omdat deze laatste (nog) niet toeliet om de voorgesteld *W* parameter (of de Bell factor) aan te passen, wat in principe een mogelijkheid zou zijn om de accuratesse en ruime toepasbaarheid voor deze gevallen te verbeteren.

Anderzijds is de MATSSF epithermische berekeningsmethode nauwgezetter, ruimer toepasbaar (laat 3 neutronenbron/monster configuraties toe) en is duidelijk accurater dan de Chilian et al. methode voor ^{96}Zr en ^{98}Mo resonantie self-shielding correcties, vooral wegens de geobserveerde verschillen in de experimentele effectieve resonantie absorptie werkzame doorsnede die ze voorstelden. Het is duidelijk onjuist om te besluiten welke methode accurater is dan een andere, op basis van slechts enkele bestudeerde elementen. Op basis van onze validatie resultaten, tijd en budget beperkingen, en, gegeven dat voor de meeste voorbereide monsters de self-shielding correcties verwaarloosbaar waren of in het slechtste gevel tot 5% voor enkele gevallen, hebben we er voor gekozen om de Chilian et al. methode te gebruiken voor thermische self-shielding en de MATSSF methode voor epithermische self-shielding correcties voor al onze k_0 bepalingen van nucleaire gegevens. Uit de kanaal kalibratie experimenten met kleine polyetheen potjes (1 mm wanddikte) was het duidelijk dat alle soorten polyetheen tussenstukjes moeten vermeden worden in onze experimenten voor de bepaling van k_0 en Q_0. Dat was zeker het geval voor monsters in de Cd-doosjes, omdat meer thermalisering van de neutronen fluentietempo te verwachten en waargenomen werd (bv. significante veranderingen in *f*, *a*).

Alle experimenten werden uitgevoerd aan de BR1 reactor van het SCK•CEN, gebruik makend van tot vier bestralingskanalen met een grote spreiding in (f, α) waarden (d.i. neutron parameters) en gebruik makend van tot zes HPGe detectoren met verschillende absolute γ-detectie-efficiëntie, om zo veel mogelijk onafhankelijke resultaten te bekomen in termen van neutronen- en γ-spectrometrie-parameters als mogelijk. In sommige gevallen werd meer dan één gecertificeerd materiaal van een gegeven element gebruikt. Gespecialiseerde software voor alle relevante berekeningen werd ontwikkeld in de programmeertaal C# 4.0 voor en gedurende de experimenten. Om de kans op systematische fouten bij het invoeren van gegevens te minimaliseren, werd gebruik gemaakt van state-of-the-art algoritmes en gegevens-relaties om efficiënt verschillende k_0-NAA & labo SQL databases te koppelen en om een groot aantal gegevenspunten op een redundantie-vrije wijze te verwerken. Vanzelfsprekend bleven de analist, het labo team en andere variabelen van de gehele bepalingsstructuur en organisatie (bv. sommige apparatuur, weeg- en droogkamer, de software en de programmeur) constant gedurende deze experimenten. Bijgevolg, hoewel alle metrologische aspecten met grote zorg behandeld werden, blijft de noodzaak om onze resultaten te bevestigen door derden, ten minste voor de nucliden waarvoor significant verschillende resultaten bekomen werden.

De multikanaalsmethode voor de Q_0 en $\bar{E}_r$ bepaling die geïntroduceerd werd door Simonits et al. in 1984, maar sindsdien niet verder ontwikkeld werd in de literatuur, werd in dit werk opnieuw afgeleid voor het algemeen geval van $\bar{E}_r$ in functie van α en een isotoop specifieke parameter p, die later voorgesteld werd door Jovanovic et al. in 1987. De methode werd in dit werk gebruikt voor de bepaling van 54 $\bar{E}_r$ factoren in tot 3 bestralingskanalen, waarbij 32 waarden bekomen werden binnen 25% relatief verschil (binnen het onzekerheidsinterval) en 23 waarden binnen 10-15% relatief verschil met de verwachte waarden. Bijgevolg is de laatste groep van (radio-isotoop)

waarden ten zeerste aanbevolen is voor α-kalibratie (accurate $\bar{E}_r$ waarden). Gegeven dat de meeste $\bar{E}_r$ factoren in de literatuur berekend werden in de veronderstelling van een Breit-Wigner resonantie distributie met de nucleaire gegevens die beschikbaar waren in die tijd (1979-1989), maakte deze multikanaalsmethode het niet alleen mogelijk om verschillende van deze gegevens te valideren, maar bovendien toomde deze methode aan dat de eerder, ten tijde van het lanceren van de k_0 methode, veronderstelde α-onafhankelijkheid van $\bar{E}_r$ was correct binnen hun verwachtte 20% $\bar{E}_r$ onzekerheidsinterval en dat de impact (of de veronderstelling) op Q_0 was in ons geval typisch 1 - 2% voor onze extreme kanalen ($\alpha \approx 0$ of $\alpha \approx 0.1$) en tot 5% voor enkele isotopen voor a = [0,06:0,07]. Bijgevolg zou de impact op de analytische resultaten verwaarloosbaar zijn, tenzij $Q_0 >> f$ of ENAA toegepast wordt.

De gerapporteerde Q_0 resultaten voor 24 isotopen waren in overeenstemming met de aanbevolen waarden binnen 4%, hetgeen overeenkomt met onze verwachte onzekerheid op het 2s betrouwbaarheidsniveau. Onze Q_0 resultaten bevestigen significante verschillen aan met Kennedy et al. in de laatste decade (bv. Sr, AS, Ru en Ta). Met onze resultaten suggereren wij om de laatste aanbevolen Q_0 factoren voor de ^{85m}Sr en ^{85}Sr productie te vervangen. Verschillen van 10-30% werden vastgesteld voor lage- Q_0 waarden (bv. ^{27}Al, ^{174}Hf, ^{164}Dy, enz.) die aangenomen literatuurwaarden gebruikten.

De Q_0 factor heeft, voor deze nucliden, een verwaarloosbare invloed op het analyseresultaat. Anderzijds hebben onze Q_0 resultaten een lagere onzekerheid dan in de literatuur.

Voor 54 radio-isotopen komen onze k_0 factoren binnen 2-4% (1% voor de meeste aanbevolen lijnen) met de laatste referenties. Voor de radionucliden Cr, Rb, Pd, 114In, Cs, Sb en Pt zijn de afwijkingen > 5% en vereisen verdere studie. Wij hebben k_0 factoren voorgesteld voor ^{197m}Pt, ^{197}Pt, ^{199}Pt en ^{125}Sb en voor ^{134}Cs en ^{188}Re voor het meer natuurlijke ADS type IV/b.

Verschillende aanbevolen nieuwe k_0 factoren werden voorgesteld voor multi-γ radio-isotopen (bv. ^{72}Ga, ^{140}La, ^{76}As, ^{181}Ta, enz.). Er werd aangetoond dat de afgeleide thermische neutronen werkzame doorsnede meestal in overeenkomst waren met de literatuur, terwijl onze k_0 factoren ook in goede verhouding waren, vergeleken met de verhouding tussen de respectievelijke γ-straal abundanties.

Onze gerapporteerde ^{235}U k_0-fissie factoren waren gemiddeld 2% hoger dan de waarden van de huidige literatuur en in overeenstemming met de recente resultaten van Blaauw et al. (op enkele uitzonderingen na). Het 2% verschil, in combinatie met onze 1% lagere k_0 factor voor de 277,6 keV lijn van ^{239}Np, gaven aanleiding tot een 3% overschatting van de $n(^{235}U)/n(^{238}U)$ isotopische verhouding die we bekomen hebben, gebruik makend van de huidige aanbevolen k_0-literatuur, zelfs na een volledige herkalibratie van alle gebruikte instrumenten. Het verschil is echter niet statisch significant.

Het was mogelijk om, uit de experimenteel bepaalde k_0 factoren, sommige fundamentele nucleaire constanten te extrapoleren. Daarom speelt de k_0 standaardisatie een belangrijke rol in de traceerbaarheid van nucleaire gegevens voor aanverwante disciplines. Helaas zouden deze nucleaire constanten opnieuw moeten berekend worden, telkens een strek gecorreleerde parameter (bv. γ-straal of isotopische abundantie, verval probabiliteit) bijgewerkt wordt. Methoden zoals de Cd-aftrek techniek of het gebruik van zeer gethermaliseerde kanalen waren bijzonder geschikt voor dit metrologisch werk en zijn aanbevolen voor toekomstig werk, omwille van de lagere kans om systematische fouten in te voeren, wegens minder aanvaarde of gekalibeerde/gemodelleerde parameters. In dit werk was het voor slechts 6 gevallen (^{96}Zr, ^{116}Sn, ^{125}Sb (via ^{124}Sn(n,γ)^{125m}Sn), ^{151}Eu, ^{153}Eu en ^{169}Yb) nodig om sterk gecorreleerde waarden, zoals Q_0 of s_0 factoren uit de literatuur en gemodelleerde parameters (d.i. f, α) voor de k_0 bepaling, aan te nemen.

Na meer dan 30 jaar van ontwikkeling en toepassing van deze techniek, verschillende verbeteringen in instrumentatie, software, concepten, enz., hebben we in onze instituten een precisie van circa 3% bereikt voor multipele k_0 bepalingen in tot 4 kanalen (voor het 95% betrouwbaarheidsniveau). Wij menen dat meer laboratoria zich zouden moeten engageren in het opnieuw bepalen van de statisch significante verschillende factoren (d.i. met een relatief verschil van $\geq 5\%$) die in dit werk gevonden zijn en in het bepalen van nieuwe, indien haalbaar, wenselijk en mogelijk, om accurate en robuuste k_0 factoren te bekomen uit het gemiddelde van verschillende auteurs met een verwachte onzekerheid die beter is dan 4% voor het 95% betrouwbaarheidsniveau.

.

12. Bibliography

1. Mughabghab SF (2006) Atlas of Neutron Resonances, 5th ed. Elsevier, Amsterdam, The Netherlands

2. Pritychenko B, Mughabghab SF (2012) Neutron Thermal Cross Sections, Westcott Factors, Resonance Integrals, Maxwellian Averaged Cross Sections and Astrophysical Reaction Rates Calculated from the ENDF/B-VII.1, JEFF-3.1.2, JENDL-4.0, ROSFOND-2010, CENDL-3.1 and EAF-2010 Evaluated Data Librari. Nucl Data Sheets 113:3120–3144.

3. Blaauw M, De Corte F (2010) Consistency of nuclear data in the fundamental databases for use in the k0 method. Nucl Instruments Methods Phys Res A 622:377–380.

4. Chadwick MB, Herman M, Obložinský P, Dunn ME, Danon Y, Kahler AC, Smith DL, Pritychenko B, Arbanas G, Arcilla R, Brewer R, Brown DA, Capote R, Carlson AD, Cho YS, Derrien H, Guber K, Hale GM, Hoblit S et al. (2011) ENDF/B-VII.1 Nuclear Data for Science and Technology: Cross Sections, Covariances, Fission Product Yields and Decay Data. Nucl Data Sheets 112:2887–2996.

5. BNL-National Nuclear Data Center (2012) Nuclear Structure Data File Retrieval, USA. http://www.nndc.bnl.gov/ensdf/. Accessed 1 Feb 2014

6. BNL-National Nuclear Data Center (2013) NuDat 2.6: Nuclear Structure and Decay Data. USA. http://www.nndc.bnl.gov/nudat2/. Accessed 1 Dec 2013

7. JAEA - Nuclear Data Center (2014) Japanese Evaluated Nuclear Data Library. Japan. http://wwwndc.jaea.go.jp/jendl/jendl.html.

8. CEA -Laboratoire National Henri Becquerel (2012) Recommended Data. France. http://www.nucleide.org/DDEP_WG/DDEPdata.htm.

Accessed 1 Jun 2013

9. Wieser ME, Coplen TB (2010) Atomic weights of the elements 2009 (IUPAC Technical Report). Pure Appl Chem 83:359–396.

10. Berglund M, Wieser ME (2011) Isotopic compositions of the elements 2009 (IUPAC Technical Report). Pure Appl Chem 83:397–410.

11. Firestone RB (2005) Fission. In: Lawrence Berkeley Natl. Lab. http://ie.lbl.gov/fission.html. Accessed 1 Jan 2013

12. Nichols AL, Aldama DL, Verpelli M (2008) Handbook of Nuclear Data for Safeguards: Database Extensions. International Atomic Energy Agency, Vienna, Austria

13. De Corte F (1987) The k0-standardization method: a move to the optimization of neutron activation analysis. Habilitation (geaggregeerde voor het hoger onderwijs). Thesis. Rijksuniversiteit Gent, Belgium

14. Forrest RA, Kopecky J, Sublet J (2007) The European Activation File : EAF-2007 neutron-induced cross section library.

15. BNL-National Nuclear Data Center (2010) Evaluated Nuclear Data File (ENDF) Retrieval & Plotting. http://www.nndc.bnl.gov/sigma/index.jsp. Accessed 1 Jan 2011

16. Holden NE (1999) Temperature Dependence of the Westcott g-factor for Neutron Reactions in Activation Analysis. Pure Appl Chem 71:2309–2315.

17. Wieser ME, Holden N, Coplen TB, Böhlke JK, Berglund M, Brand WA, De Bièvre P, Gröning M, Loss RD, Meija J, Hirata T, Prohaska T, Schoenberg R, O'Connor G, Walczyk T, Yoneda S, Zhu X-K (2013) Atomic weights of the elements 2011 (IUPAC Technical Report). Pure Appl Chem 85:1047–1078.

18. Kennedy G, St-Pierre J (2003) Is the k0 method accurate for elements with high Q0 values? J Radioanal Nucl Chem 257:475–480.

19. St-Pierre J, Kennedy G (2006) Re-measurement of Q0 and k0 values for 14 nuclides. Nucl Instruments Methods Phys Res A 564:669–674.

20. De Corte F, Simonits A (2003) Recommended nuclear data for use in the k0 standardization of neutron activation analysis. At Data Nucl Data Tables 85:47–67.

21. Kolotov VP, De Corte F (2003) An electronic database with a compilation of k0 and related data for NAA. J Radioanal Nucl Chem 257:501–508.

22. k0-International Scientific Committee (2012) Classic k0 Database. International. http://www.kayzero.com/k0naa/k0naa/News/Artikelen/2012/3/25_The_IUPAC_databasa.html. Accessed 1 May 2012

23. Jaćimović R, De Corte F, Kennedy G, Vermaercke P, Revay Z (2014) The 2012 recommended k0 database. J Radioanal Nucl Chem 300:589–592.

24. Kolotov VP, De Corte F (2004) Compilation of k0 and related data for NAA in the form of electronic database (IUPAC Technical Report). Pure Appl Chem 76:1921–1925.

25. Trkov A, Kaiba T, Žerovnik G, Revay Z, Firestone R, Jacímović R, Radulovič V (2015) Supplementary Data for Neutron Activation Analysis (IAEA - NDS Technical Report). Vienna, Austria

26. de Rupescissa J The book of Quintessence or the Fifth Being: That is to Say Mortal Heaven. The British Library MS 73

27. Heindel M (1919) Freemasonry and Catholicism. L. N. Fowler & CO., London, UK

28. Paneth FA (1936) Role of Chemistry in the Study of Atomic Transmutation. Nature 137:560–562.

29. Chadwick J (1932) Possible Existence of a Neutron. Nature 129:312–312.

30. Fermi E (1934) Radioattività prodotta da bombardamento di neutroni. Nuovo Cimentio 11:429–441.

31. Amaldi E, Fermi E, Rasetti F, Segrè E (1934) Nuovi Radioelementi Prodotti Con Bombardamento di Neutroni. Nuovo Cim 11:442–451.

32. Levi H (1976) George Hevesy and his concept of radioactive indicators?In retrospect. Eur J Nucl Med 1:3–10.

33. Hein RE (1957) Description and Application of Activation Analysis. Trans Kansas Acad Sci 60:320.

34. Rakovic M (1970) Activation Analysis, 1st ed. ACADEMIA, Prague, Czech Republic

35. Institute of Isotopes - Hungarian Academy of Sciences (2012) Neutrons for elemental analysis. http://www.iki.kfki.hu/nuclear/research/index_en.shtml. Accessed 14 Nov 2017

36. Simonits A, Moens L, De Corte F, Wispelaere A, Elek A, Hoste J (1980) k0-Measurements and related nuclear data compilation for (n,γ) reactor neutron activation analysis. J Radioanal Nucl Chem 60:461–516.

37. De Corte F, Speecke A, Hoste J (1969) Reactor neutron activation analysis by a triple comparator method. J Radioanal Chem 3:205–215.

38. De Corte F, Simonits A, Wispelaere A, Elek A (1989) k0-Measurements and related nuclear data compilation for (n,γ) reactor neutron activation analysis. J Radioanal Nucl Chem 133:3–41.

39. Simonits A, De Corte F, Hoste J (1975) Single-comparator methods in reactor neutron activation analysis. J Radioanal Nucl Chem 24:31–46.

40. Moens L, De Corte F, Wispelaere A, Hoste J, Simonits A, Elek A, Szabo E (1984) k0-Measurements and related nuclear data compilation for (n,γ) reactor neutron activation analysis. J Radioanal Nucl Chem 82:385–452.

41. Francesco G, Giampaolo G, Jules P (1965) Reactor Neutron Activation Analysis by the Single Comparator Method. Anal Chem 37:1085–1092.

42. De Corte F, Simonits A, Wispelaere A, Hoste J (1987) Accuracy and applicability of the k0-standardization method. J Radioanal Nucl Chem 113:145–161.

43. Simonits A, De Corte F, Moens L, Hoste J (1982) Status and recent developments in the k0-standardization method. J Radioanal Chem 72:209–230.

44. De Corte F, Simonits A (1989) k0-Measurements and related nuclear data compilation for (n,γ) reactor neutron activation analysis. J Radioanal Nucl Chem 133:43–130.

45. De Corte F, Simonits A, Bellemans F, Freitas MC, Jovanović S, Smodiš B, Erdtmann G, Petri H, Wispelaere A (1993) Recent advances in the k0-standardization of neutron activation analysis: Extensions, applications, prospects. J Radioanal Nucl Chem 169:125–158.

46. De Corte F (1998) A survey of recentk 0-NAA developments and

applications in Europe. J Radioanal Nucl Chem 234:9–16.

47. Roth S, Grass F, De Corte F, Moens L, Buchtela K (1993) Determination of k0 and Q0 factors of short-lived nuclides. J Radioanal Nucl Chem 169:159–175.

48. De Corte F, Bellemans F, Neve P, Simonits A (1994) The use of a modified Westcott-formalism in the k0-standardization of NAA: The state of affairs. J Radioanal Nucl Chem 179:93–103.

49. Smodiš B, De Corte F, Wispelaere A (1994) Nuclear data and measurements for the130Ba(n,γ)131Ba reaction. J Radioanal Nucl Chem Lett 186:183–188.

50. Simonits A, De Corte F, De Wispelaere A (1996) The 174Yb(n,γ)175Yb reaction: a convincing new argument for k0-standardization in absolute neutron activation analysis. Appl Radiat Isot 47:389–394.

51. De Corte F, Van Lierde S, Simonits A, Bossus D, van Sluijs R, Pommé S (1999) A re-evaluation of k0 and related nuclear data for the 555.8 keV gamma-line emitted by the 104mRh-104Rh mother–daughter pair for use in NAA. Appl Radiat Isot 51:701–706.

52. Van Lierde S, De Corte F, Bossus D, Van Sluijs R, Pommé S (1999) Determination of k0 and related nuclear data for short-lived radionuclides to be used in KAYZERO-NAA at DSM research. Nucl Instruments Methods Phys Res Sect A Accel Spectrometers, Detect Assoc Equip 422:874–879.

53. Van Lierde S, De Corte F, Van Sluijs R, Bossus D (2000) New Experimental k0 and Related Data for Generalized Activation/Decay Cases Implemented in the “Kayzero” Software Package. J Radioanal Nucl Chem 245:179–184.

54. De Corte F, Van Lierde S (2001) Determination and evaluation of fission k0-factors for correctionof the 235U(n,f) interference in k0-NAA. J Radioanal Nucl Chem 248:97–101.

55. De Corte F, Van Lierde S (2001) Evaluation of (n,γ) cross sections from k0-factors for radionuclides with short half-life and/or a complex activation-decay scheme. J Radioanal Nucl Chem 248:103–107.

56. De Wispelaere A, De Corte F (2003) Some irregularities observed in the analysis results of k0-NAA. J Radioanal Nucl Chem 257:471–473.

57. De Corte F (2003) The updated NAA nuclear data library derived from

the Y2K k0-database. J Radioanal Nucl Chem 257:493–499.

58. Lin X, Gerstenberg H, Lierse von Gostomski C, Henkelmann R, Türler A, Rossbach M (2009) Determination of k0-values for the reactions 94Zr (n, gamma) 95Zr and 96Zr (n, gamma) 97Zr-97mNb by irradiation in highly thermalized neutron flux. Appl Radiat Isot 67:2092–6.

59. Jaćimović R, Stibilj V (2010) Determination of Q0 and k0 factors for 75Se and their validation using a known mass of Se on cellulose. Nucl Instruments Methods Phys Res A 622:415–418.

60. Lin X, Lierse von Gostomski C (2012) Determination of the k0-values for 75Se, 110mAg, 115Cd–115mIn, 131Ba, and 153Sm by irradiation in highly thermalized neutron flux. J Radioanal Nucl Chem 295:1921–1925.

61. Radulović V, Trkov A, Jaćimović R, Jeraj R (2013) Measurement of the neutron activation constants Q0 and k0 for the 27Al(n, γ)28Al reaction at the JSI TRIGA Mark II reactor. J Radioanal Nucl Chem 298:1791–1800.

62. Farina Arboccò F, Vermaercke P, Smits K, Sneyers L, Strijckmans K (2012) Experimental determination of k0, Q0, Er factors and neutron cross-sections for 41 isotopes of interest in Neutron Activation Analysis. J Radioanal Nucl Chem 296:931–938.

63. Acharya R, Holzbecher J, Chatt A (2012) Determination of k0-factors of short-lived nuclides and application of k0-NAA to selected trace elements. Nucl Instruments Methods Phys Res Sect A Accel Spectrometers, Detect Assoc Equip 680:1–5.

64. Lin X, Henkelmann R, Alber D (2007) Is there something wrong in the barium determination by k0-INAA? J Radioanal Nucl Chem 271:71–76.

65. Vermaercke P, Hult M, Verheyen L, Farina Arboccò F (2010) Measurement of the isotopic composition of germanium by k0-INAA and INAA. Nucl Instruments Methods Phys Res A 622:433–437.

66. Stopic A, Bennett JW (2014) Measurement of k0 values for caesium and iridium. J Radioanal Nucl Chem 300:593–597.

67. Canberra (2001) Model 556A Acquisition Interface Module User Guide. http://depni.sinp.msu.ru/~hatta/canberra/556A Acquisition Interface

Module User%27s Manual.pdf. Accessed 11 Dec 2015

68. Canberra (2012) Basic Counting Systems. http://users.df.uba.ar/sgil/labo5_uba/recursos/counting_Detection_syst_Canberra.htm. Accessed 1 Oct 2012

69. Canberra (2016) Lynx Digital Signal Analyzer. http://www.canberra.com/products/radiochemistry_lab/pdf/Lynx-SS-C38658.pdf. Accessed 11 Dec 2015

70. De Corte F, Wispelaere A, Sluijs R, Bossus D, Simonits A, Kučera J, Frána J, Smodis B, Jaćimović R (1997) The installation of KAYZERO-assisted NAA for use in industry and environmental sanitation in three Central European countries: Plans and achievements of a COPERNICUS project. J Radioanal Nucl Chem 215:31–37.

71. van Sluijs R (2011) Kayzero for Windows. k0-ware. The Netherlands. http://www.kayzero.com/. Accessed 1 Jun 2011

72. van Sluijs R, Bossus D, Blaauw M, Kennedy G, De Wispelaere A, Van Lierde S, De Corte F (2000) Evaluation of Three Software Programs for Calculating True-Coincidence Summing Correction Factors. J Radioanal Nucl Chem 244:675–680.

73. Verheijke ML (1994) Relation between the høgdahl convention and the modified Westcott formalism for (n, γ) reactions with a pure 1/v n cross-section behavior. J Radioanal Nucl Chem 183:293–299.

74. van Sluijs R, Jacimovic R, Kennedy G (2014) A simplified method to replace the Westcott formalism in k0-NAA using non-1/v nuclides. J Radioanal Nucl Chem 300:539–545.

75. Gonçalves IF, Martinho E, Salgado J (2001) Monte Carlo calculation of resonance self-shielding factors for epithermal neutron spectra. Radiat Phys Chem 61:461–462.

76. Salgado J, Martinho E (2004) Development of a Unique Curve for Thermal Neutron Self-Shielding Factors in Spherical Scattering Materials. Nucl Sci Eng 148:426–428.

77. Chilian C, Chambon R, Kennedy G (2010) Neutron self-shielding with k0-NAA irradiations. Nucl Instruments Methods Phys Res A 622:429–432.

78. Chilian C, St-Pierre J, Kennedy G (2008) Complete thermal and epithermal neutron self-shielding corrections for NAA using a

spreadsheet. J Radioanal Nucl Chem 278:745–749.

79. IAEA (2009) MATSSF Program. Austria.

80. Farina Arboccò F, Vermaercke P, Smits K, Sneyers L, Strijckmans K (2014) Experimental determination of k0, Q0 factors, effective resonance energies and neutron cross-sections for 37 isotopes of interest in NAA. J Radioanal Nucl Chem 302:655–672.

81. Farina Arboccò F, Vermaercke P, Smits K, Sneyers L, Strijckmans K (2012) Experimental determination of k0 nuclear data for the cesium radionuclides. J Radioanal Nucl Chem 295:2063–2069.

82. Farina Arboccò F, Strijckmans K, Vermaercke P, Verheyen L, Sneyers L (2010) The impact of polyethylene vials on reactor channel characterization in k0-NAA. J Radioanal Nucl Chem 286:569–575.

83. Farina Arboccò F, Vermaercke P, Sneyers L, Strijckmans K (2011) Experimental validation of some thermal neutron self-shielding calculation methods for cylindrical samples in INAA. J Radioanal Nucl Chem 291:529–534.

84. Farina Arboccò F, Vermaercke P, Verheyen L, Strijckmans K (2012) Experimental evaluation of epithermal neutron self-shielding for 96Zr and 98Mo. J Radioanal Nucl Chem 297:371–375.

85. Farina Arboccò F, Vermaercke P, Sneyers L, Soares Leal A, Gonçalves Bouças J (2010) The use of k0-NAA for the determination of the n(235U)/n(238U) isotopic ratio in samples containing uranium. Nucl Instruments Methods Phys Res A 622:443–448.

86. Vermaercke P, Farina Arboccò F, Sneyers L, Leal A, Bruggeman M (2009) Environmental monitoring for safeguards using k0-standardised Neutron Activation Analysis. 2009 1st Int. Conf. Adv. Nucl. Instrumentation, Meas. Methods their Appl. IEEE, pp 1–5

87. Vermaercke P, Sneyers L, Farina Arboccò F, Aleksiayenak Y (2011) Using k0-UNAA for the determination of depleted uranium in the moss biomonitoring technique. Int J Environ Heal 5:72–83.

88. Simonits A, Jovanović S, De Corte F, Moens L, Hoste J (1984) A method for experimental determination of effective resonance energies related to (n, γ) reactions. J Radioanal Nucl Chem 82:169–179.

89. Farina Arboccò F, Vermaercke P, Smits K, Sneyers L, Strijckmans K (2014) Experimental determination of Q0 factors and effective

resonance energies with a multi-channel approach: the α-vector method. J Radioanal Nucl Chem 302:631–646.

90. Microsoft (2010) C# Language specification 4.0. USA. http://www.microsoft.com/en-us/download/details.aspx?id=7029. Accessed 1 Jun 2011

91. Farina Arboccò F, Vermaercke P, Smits K, Sneyers L, Strijckmans K (2014) Experimental k 0 and k 0-fission factors for the determination of the n(235U)/n(238U) enrichment levels and correction for 235U fission interferences in samples containing uranium. J Radioanal Nucl Chem 302:721–735.

92. Morandi PJ (1998) Population Growth and Exponential Decay. http://www.math.nmsu.edu/~pmorandi/math210gs99/GrowthAndDecay.html. Accessed 1 Oct 2012

93. Tsishchanka K (2010) Exponential Growth and Decay. https://cims.nyu.edu/~kiryl/Calculus/Section_3.4--Exponential_Growth_and_Decay/Exponential_Growth_and_Decay.pdf. Accessed 1 Oct 2012

94. Watt B (1952) Energy Spectrum of Neutrons from Thermal Fission of U235. Phys Rev 87:1037–1041.

95. Trkov A, Radulović V (2015) Nuclear reactions and physical models for neutron activation analysis. J Radioanal Nucl Chem 304:763–778.

96. Høgdahl OT (1964) Proceed Symp Radiochemical Methods of Analysis, Salzburg, October 19-23. IAEA, Vienna. p 23

97. Nisle RG, Harker YD (1960) Self-shielding in stacked foils. Nucleonics 14:86.

98. Fleming RF (1982) Neutron self-shielding factors for simple geometrics. Int J Appl Radiat Isot 33:1263–1268.

99. Baumann NP (1963) Resonance Integrals and self-shielding factors for detectors and foils. Report DP-817. Aiken, SC, USA

100. Kennedy G, Chilian C, Jaćimović R, Žerovnik G, Snoj L, Trkov A (2011) Neutron self-shielding in irradiation channels of small reactors is isotropic. J Radioanal Nucl Chem 291:555–559.

101. Trkov A, Žerovnik G, Snoj L, Ravnik M (2009) On the self-shielding factors in neutron activation analysis. Nucl Instruments Methods Phys

Res A 610:553–565.

102. Rinard P (1991) Neutron interactions with matter: Passive Nondestructive Assay of Nuclear Materials. Report NUREG/CR-5550.

103. Beyster JR, Young JA (1967) Thermalization of Neutrons in Condensed Matter. Annu Rev Nucl Sci 17:97–128.

104. Chilian C, St-Pierre J, Kennedy G (2006) Dependence of thermal and epithermal neutron self-shielding on sample size and irradiation site. Nucl Instruments Methods Phys Res A 564:629–635.

105. Ryves TB (1969) A New Thermal Neutron Flux Convention. Metrologia 5:119–124.

106. Moens L, Simonits A, De Corte F, Hoste J (1979) Comparative study of measured and critically evaluated resonance integral to thermal cross-section ratios. Part I. J Radioanal Nucl Chem 54:377–390.

107. Jovanović S, De Corte F, Simonits A, Moens L, Vukotić P, Hoste J (1987) The effective resonance energy as a parameter in (n, γ) activation analysis with reactor neutrons. J Radioanal Nucl Chem 113:177–185.

108. De Corte F, Moens L, Simonits A, Wispelaere A, Hoste J (1979) Instantaneous α-determination without Cd-cover in the 1/E1+α epithermal neutron spectrum. J Radioanal Chem 52:295–304.

109. BIPM (2008) Evaluation of measurement data - Guide to the expression of uncertainty in measurement JCGM 100:2008. http://www.bipm.org/utils/common/documents/jcgm/JCGM_100_2008_E.pdf. Accessed 1 Oct 2013

110. Westcott CH (1970) Effective cross section values for well-moderated thermal neutron reactor spectra, AECL--1101-REV. Chalk River, Ontario, Canada

111. IAEA (2007) Database of Prompt Gamma Rays from Slow Neutron Capture for Elemental Analysis, STI/PUB/1263. International Atomic Energy Agency, Vienna, Austria

112. Holden N (1991) Temperature dependence of the Westcott g-factor for the actinide nuclides in ENDF/B-VI. Report BNL 45256. New York, USA

113. van Sluijs R, Stopic A, Jacimovic R (2015) Evaluation of Westcott g(T

n)-factors used in k 0-NAA for “non-1/v” (n,γ) reactions. J Radioanal Nucl Chem 306:579–587.

114. Simonits A, De Corte F, Nimr T El, Moens L, Hoste J (1984) Comparative study of measured and critically evaluated resonance integral to thermal cross-section ratios. Part II. J Radioanal Nucl Chem Artic 81:397–415.

115. Lin X, De Corte F, Moens L, Simonits A, Hoste J (1984) Computer-assisted reactor NAA of geological and other reference materials, using the k0-standardization method: Evaluation of the accuracy. J Radioanal Nucl Chem Artic 81:333–343.

116. Beets C, Deckers H (1962) The fission neutron spectrum of U235. Nucl Phys 30:232–238.

117. U.S. Department of Energy (1993) DOE Fundamentals Handbook DOE-HDBK-1019/1-93: Nuclear Physics and Reactor Theory. Washington. USA

118. Lin X, Renterghem D, De Corte F, Cornelis R (1989) Correction for neutron induced reaction interferences in the NAA k0-standardization method. J Radioanal Nucl Chem 133:153–165.

119. De Corte F, Moens L, Simonits A, Wispelaere A, Hoste J (1983) The reaction117Sn (n, n′)117mSn as a primary interference in (n, γ) neutron activation analysis. J Radioanal Chem 79:255–263.

120. Shibata K, Iwamoto O, Tsuneo N, Iwamoto N, Ichihara A, Kunieda S, Chiba S, Furutaka K, Otuka N, Ohasawa T, Murata T, Matsunobu H, Zukeran A, Kamada S, Katakura J (2011) JENDL-4.0: A New Library for Nuclear Science and Engineering. J Nucl Sci Technol 48:1–30.

121. IAEA-National Nuclear Data Center (2014) Experimental Nuclear Reaction Data. https://www-nds.iaea.org/exfor/exfor.htm.

122. Pommé SG, Hardeman FEMC, Robouch PB, Etxebarria N, De Corte FA, De Wispelaere AHMJ, van Sluijs R, Simonits AP (1996) General Activation and Decay Formulas and Their Application in Neutron Activation Analysis with k0 Standardization. Anal Chem 68:4326–4334.

123. De Corte F, Hammami KS-E, Moens L, Simonits A, Wispelaere A, Hoste J (1981) The accuracy and precision of the experimental α-determination in the 1/E1+α epithermal reactor-neutron spectrum. J

Radioanal Nucl Chem 62:209–255.

124. Nimr T, De Corte F, Moens L, Simonits A, Hoste J (1981) Epicadmium neutron activation analysis (ENAA) based on the k0-comparator method. J Radioanal Chem 67:421–435.

125. Planck M (1901) Ueber das Gesetz der Energieverteilung im Normalspectrum. Ann Phys 309:553–563.

126. Einstein A (2003) Physics & reality. Daedalus 132:22–25.

127. Einstein A (1905) Über einen die Erzeugung und Verwandlung des Lichtes betreffenden heuristischen Gesichtspunkt. Ann Phys 322:132–148.

128. KDictionaries (2010) Random House Kernerman Webster's College Dictionary, 1st ed. Random House, New York. USA

129. Faulkner K (2012) Physics for diagnostic radiology. 3rd edition. Br J Radiol 85:290–290.

130. Compton A (1923) A Quantum Theory of the Scattering of X-rays by Light Elements. Phys Rev 21:483–502.

131. Christillin P (1986) Nuclear Compton scattering. J Phys G Nucl Phys 12:837–851.

132. Hubbell JH (2006) Electron–positron pair production by photons: A historical overview. Radiat Phys Chem 75:614–623.

133. Nave CR (2012) Photoelectric effect. In: Hyperphysics. http://hyperphysics.phy-astr.gsu.edu/hbase/mod1.html#c2. Accessed 1 Oct 2012

134. Nave CR (2012) Compton scattering. In: Hyperphysics. http://hyperphysics.phy-astr.gsu.edu/hbase/quantum/comptint.html. Accessed 1 Oct 2012

135. Pease CS, Goode AR, McGraw JK, Baker D, Jackson J, Gay SB (2012) Basic Radiobiology. http://www.med-ed.virginia.edu/courses/rad/radbiol/images/basic-rad-bio-scan-pair-production.gif. Accessed 1 Oct 2012

136. Guthrie F (1873) On a new relation between heat and electricity. Proc R Soc London 21:168–169.

137. Cyprus University (2013) Nuclear and Heavy-Ion Physics Website.

http://www-np.ucy.ac.cy/radio_isotopes/wwwen/gamma/Eu152.png. Accessed 1 Oct 2012

138. HyperLabs Software (2009) HyperLab 2009 product information. http://hlabsoft.com/web/hl2005/productinfo.php. Accessed 1 Jan 2011

139. HyperLabs Software (2011) HyperLab Reference Guide. http://www.hlabsoft.com/web/hl2009/docs/HyperLab2009.1Manuals.pdf. Accessed 12 Nov 2015

140. STC Radek (2012) Photomanager module. http://www.radek.ru/upload/modules_photomanager_module211/13601832638.jpg. Accessed 1 Oct 2012

141. Moens L, Hoste J (1983) Calculation of the peak efficiency of high-purity germanium detectors. Int J Appl Radiat Isot 34:1085–1095.

142. Moens L, De Donder J, Lin X, De Corte F, De Wispelaere A, Simonits A, Hoste J (1981) Calculation of the absolute peak efficiency of gamma-ray detectors for different counting geometries. Nucl Instruments Methods Phys Res 187:451–472.

143. NIST (2011) XCOM: Photon cross sections database. http://www.nist.gov/pml/data/xcom/index.cfm. Accessed 1 Dec 2011

144. k0-ware. The Netherlands (2005) Kayzero for Windows: for reactor neutron activation analysis (NAA) using the k0 standardization method. Version 2.

145. Vasil'ev SI, Gromov KY, Klimenko AA, Samatov ZK, Smol'nikov AA, Fominykh VI, Chumin VG (2006) Coincidence summing in γ-ray spectra and determination of the intensity of weak crossover γ transitions. Instruments Exp Tech 49:34–40.

146. Moens L, De Corte F, Simonits A, Lin X, Wispelaere A, Donder J, Hoste J (1982) Calculation of the absolute peak efficiency of Ge and Ge(Li) detectors for different counting geometries. J Radioanal Chem 70:539–550.

147. Leo WR (1994) Techniques for Nuclear and Particle Physics Experiments. Springer

148. Pommé S (2006) Dead Time, Pile-Up, and Counting Statistics. pp 218–233

149. Knoll G Radiation Detection and Measurement.

150. Pommé S, Fitzgerald R, Keightley J (2015) Uncertainty of nuclear counting. Metrologia 52:S3–S17.

151. Pommé S, Alzetta J-P, Uyttenhove J, Denecke B, Arana G, Robouch P (1999) Accuracy and precision of loss-free counting in γ-ray spectrometry. Nucl Instruments Methods Phys Res Sect A Accel Spectrometers, Detect Assoc Equip 422:388–394.

152. Westphal GP, Lemmel H, Grass F, Gwozdz R, Jöstl K, Schröder P, Hausch E (2001) A gamma-spectrometry system for activation analysis. J Radioanal Nucl Chem 248:53–60.

153. van Sluijs R, Bossus DAW, Konings J, De Corte F, De Wispelaere A, Simonits A (1997) Loss-free counting in NAA using KAYZERO evaluation software. J Radioanal Nucl Chem 215:283–285.

154. Case KM, de Hoffmann F, Placzek G (1953) Introduction to the Theory of Neutron Diffussion. U.S. Govt. Printing Office, Washington. USA

155. Dwork J, Hofmann PL, Hurwitz H, Clancy EF (1955) Self-Shielding factors for infinitely long, hollow cylinders. Report KAPL-1262. New York. USA

156. Stewart JC, Zweifel PF (1958) Self-shielding and Doppler effects in the absorption of neutrons. New York. USA

157. Zweifel PF (1978) Twenty years of transport theory. Transp Theory Stat Phys 7:173–190.

158. Wachspress EL (1958) Thin regions in Diffussion Theory calculations. Nucl Sci Eng 3:186.

159. Gilat J, Gurfinkel Y (1963) Self-shielding in Activation Analysis. Nucleonics 21:143–144.

160. Gilat J, Gurfinkel Y (1962) Self-shielding Effects in Activation Analysis. Israel Atomic Energy Commission

161. Wolfram - MathWorld (2010) Modified Bessel function of the First Kind. In: Wolfram Res. Inc. http://mathworld.wolfram.com/ModifiedBesselFunctionoftheFirstKind.html. Accessed 1 Jan 2010

162. Wolfram - MathWorld (2010) Modified Bessel function of the Second Kind. In: Wolfram Res. Inc. http://mathworld.wolfram.com/ModifiedBesselFunctionoftheSecond

Kind.html. Accessed 1 Jan 2010

163. Wolfram - MathWorld (2010) En function. In: Wolfram Res. Inc. http://mathworld.wolfram.com/En-Function.html. Accessed 1 Jan 2010

164. Blaauw M (1996) The Derivation and Proper Use of Stewart's Formula for Thermal Neutron Self-Shielding in Scattering Media. Nucl Sci Eng 124:431–435.

165. Blaauw M (1995) The confusing issue of the neutron capture cross-section to use in thermal neutron self-shielding computations. Nucl Instruments Methods Phys Res A 356:403–407.

166. Martinho E, Salgado J, Gonçalves IF (2004) Universal curve of the thermal neutron self-shielding factor in foils, wires, spheres and cylinders. J Radioanal Nucl Chem 261:637–643.

167. Chilian C, Kassakov M, St-Pierre J, Kennedy G (2006) Extending NAA to materials with high concentrations of neutron absorbing elements. J Radioanal Nucl Chem 270:417–423.

168. Gonçalves IF, Martinho E, Salgado J (2004) Extension to cylindrical samples of the universal curve of resonance neutron self-shielding factors. Nucl Instruments Methods Phys Res B 213:186–188.

169. Salgado J, Martinho E, Gonçalves IF (2004) The calculation of neutron self-shielding factors of a group of isolated resonances. J Radioanal Nucl Chem 260:317–320.

170. Salgado J, Gonçalves IF, Martinho E (2004) Epithermal neutron self-shielding factors in foils for collimated beams. Appl Radiat Isot 60:677–81.

171. Gonçalves IF, Martinho E, Salgado J (2002) Monte Carlo calculation of epithermal neutron resonance self-shielding factors in foils of different materials. Appl Radiat Isot 56:945–951.

172. Pommé S, Simonits A, Lindstrom R, De Corte F, Robouch P (2000) Determination of Burnup Effects in $^{197}Au(n,\gamma)^{198}Au$ Prior to Reactor Neutron Field Characterisation. J Radioanal Nucl Chem 245:223–227.

173. Vermaercke P, Sneyers L, Bruggeman M, Wispelaere A, De Corte F (2008) Neutron spectrum calibration using the Cd-ratio for multi-monitor method with a synthetic multi-element standard. J Radioanal Nucl Chem 278:631–636.

174. Vermaercke P, Robouch P, Sneyers L, De Corte F (2007) Using synthetic multi-element standards (SMELS) for calibration and quality control of the irradiation facilities in the BR1 reactor. J Radioanal Nucl Chem 276:235–241.

175. Dung HM, Sasajima F (2003) Determination of α and f for k0-NAA in irradiation sites with high thermalized neutrons. J Radioanal Nucl Chem 257:509–512.

176. Op de Beeck J (1985) Energy dependence of the epithermal neutron spectrum shape parameter α with respect to application of comparator-type NAA. J Radioanal Nucl Chem 90:167–187.

177. Greenberg RR, Bode P, De Nadai Fernandes EA (2011) Neutron activation analysis: A primary method of measurement. Spectrochim Acta Part B At Spectrosc 66:193–241.

178. Sears VF (1992) Neutron scattering lengths and cross sections. Neutron News 3:26–37.

179. Gebauhr W (1962) Störungen bei Aktivierungsanalysen durch Neutronenbeschuss. Fresenius' Zeitschrift für Anal Chemie 185:339–356.

180. Landsberger S (1986) Spectral interferences from uranium fission in neutron activation analysis. Chem Geol 57:415–421.

181. Landsberger S (1989) Update of uranium fission interferences in neutron activation analysis. Chem Geol 77:65–70.

182. Orlov V V., Sharapov VN, Vaimugin AA, Galanin AN, Kisil' IM (1974) Resonant neutron absorption in tubular fuel elements. Sov At Energy 36:623–628.

183. Emsley J (2003) Nature's building blocks: an A-Z guide to the elements. "Tellurium." Oxford University Press

184. US Geological Survey (2009) Minerals Information: "Rare Earths." http://minerals.usgs.gov/minerals/pubs/commodity/rare_earths. Accessed 3 Mar 2009

185. HyperLabs Software (2005) HyperLab 2005 product information. http://hlabsoft.com/web/hl2005/productinfo.php. Accessed 3 Mar 2009

186. Vermaercke P, Farina F, Sneyers L, Bruggeman M, Bouças JG (2009)

Validation of the determination of tin by k0-instrumental neutron activation analysis in foodstuff. J Radioanal Nucl Chem 281:35–39.

187. De Corte F (2010) Towards an international authoritative system for coordination and management of a unique recommended k0-NAA database. Nucl Instruments Methods Phys Res A 622:373–376.

188. Wolfram - MathWorld (2012) Least Squares Fitting. http://mathworld.wolfram.com/LeastSquaresFitting.html. Accessed 1 Jun 2011

189. International Standardisation Organization (2015) ISO 30:2015 Reference materials - Selected terms and definitions. https://www.iso.org/obp/ui/#iso:std:iso:guide:30:ed-3:v1:en. Accessed 20 Jun 2016

190. Lamberty A, Emons H (2011) Reference materials: from CBNM to IRMM. Accredit Qual Assur 16:393–398.

191. Mettler Toledo (2014) XP Micro and Ultra-microbalances. https://www.mt.com/int/en/home/products/Laboratory_Weighing_Solutions/Micro_Ultra_Balances/XP_Micro_Ultramicro.tabs.documents.html. Accessed 1 Dec 2015

192. Sartorius (2014) Infrared Moisture Analyser. https://www.sartorius.com/sartorius/en/EUR/Applications/Quality-Control/Moisture-Analyzers/Infrared-Moisture-Analyser/p/MA100H-000115V1. Accessed 1 Dec 2015

193. LAF Technologies (2014) Aura Mini Vertical Laminar Flow Cabinets. http://laftech.com.au/product/aura-mini/. Accessed 13 Dec 2012

194. Simonits A, De Corte F, Van Lierde S, Pommé S, Robouch P, Eguskiza M (2000) The k0 and Q0 values for the Zr-isotopes: A re-investigation. J Radioanal Nucl Chem 245:199–203.

195. De Wispelaere A, De Corte F, Bossus DAW, Swagten JJMG, Vermaercke P (2006) Re-determination and re-evaluation of the f and α parameters in channels Y4 and S84 of the BR1 reactor, for use in k0-NAA at DSM Research. Nucl Instruments Methods Phys Res A 564:636–640.

196. ISO (2011) ISO/IEC 9075-1:2011, Information technology - Database languages - SQL - Part 1: Framework. Switzerland. http://www.iso.org/iso/home/store/catalogue_ics/catalogue_detail_ics

.htm?csnumber=53681. Accessed 1 Jun 2012

197. Microsoft (2010) Lamda Expressions (C# Programming Guide). USA. http://msdn.microsoft.com/en-us/library/bb397687(v=vs.100).aspx. Accessed 1 Jun 2010

198. Van Audenhove J, Joyeux J, Audenhove J Van, Van Audenhove J, Joyeux J (1966) The preparation by levitation melting in argon of homogeneous aluminium alloys for neutron measurements. J Nucl Mater 19:97–102.

199. Los Alamos National Laboratory (1998) Reich-Moore Resonance Format. In: Introd. to ENDF Formats. http://t2.lanl.gov/nis/endf/rm.html. Accessed 26 Jul 2011

200. Smodiš B, Trkov A, Jaćimović R (2003) Effects of the neutron spectrum on the neutron activation analysis constants for 94Zr and 96Zr. J Radioanal Nucl Chem 257:481–487.

201. Venturini L, Pecequilo BRS (1997) Thermal neutron capture cross-section of 48Ti, 51V, 50,52,53Cr and 58,60,62,64Ni. Appl Radiat Isot 48:493–496.

202. Basunia MS, Firestone RB, Révay Z, Choi HD, Belgya T, Escher JE, Hurst AM, Krtička M, Szentmiklósi L, Sleaford B, Summers NC (2014) Determination of the 151Eu(n,γ)152mEu and 153Eu(n,γ)154Eu Reaction Cross Sections at Thermal Neutron Energy. Nucl Data Sheets 119:88–90.

203. De Corte F (2007) Exit reactor Thetis/Ghent (1967–2003): A recollection of its significant contribution to NAA and its leading role in the development of the k0-standardization. J Radioanal Nucl Chem 271:37–41.

13. Appendix

13.1 List of A1 publications

1. Farina Arboccò F, Vermaercke P, Smits K, Sneyers L, Strijckmans K (2014) Experimental k0 and k0-fission factors for the determination of the n(235U)/n(238U) enrichment levels and correction for 235U fission interferences in samples containing uranium. J. Radioanal. Nucl. Chem. 302:721-735.
2. Farina Arboccò F, Vermaercke P, Smits K, Sneyers L, Strijckmans K (2014) Experimental determination of k0, Q0 factors, effective resonance energies and neutron cross-sections for 37 isotopes of interest in NAA. J. Radioanal. Nucl. Chem. 302:655-672.
3. Farina Arboccò F, Vermaercke P, Smits K, Sneyers L, Strijckmans K (2014) Experimental determination of Q0 factors and effective resonance energies with a multi-channel approach: the α-vector method. J. Radioanal. Nucl. Chem. 302:631-646.
4. Farina Arboccò F, Vermaercke P, Smits K, Sneyers L, Strijckmans K (2013) Experimental determination of k0 nuclear data for the cesium radionuclides. J. Radioanal. Nucl. Chem. 295:2063–2069.
5. Farina Arboccò F, Vermaercke P, Smits K, Sneyers L, Strijckmans K (2013) Experimental determination of k0, Q0, Er factors and neutron cross-sections for 41 isotopes of interest in Neutron Activation Analysis. J. Radioanal. Nucl. Chem. 296:931–938.

6. Farina Arboccò F, Vermaercke P, Verheyen L, Strijckmans K (2013) Experimental evaluation of epithermal neutron self-shielding for 96Zr and 98Mo. J. Radioanal. Nucl. Chem. 297:371–375.
7. Farina Arboccò F, Vermaercke P, Sneyers L, Strijckmans K (2012) Experimental validation of some thermal neutron self-shielding calculation methods for cylindrical samples in INAA. J. Radioanal. Nucl. Chem. 291:529–534.
8. Farina Arboccò F, Strijckmans K, Vermaercke P, Verheyen L, Sneyers L (2010) The impact of polyethylene vials on reactor channel characterization in k0-NAA. J. Radioanal. Nucl. Chem. 286:569–575.
9. Farina Arboccò F, Vermaercke P, Sneyers L, Soares Leal A, Gonçalves Bouças J (2010) The use of k0-NAA for the determination of the n(235U)/n(238U) isotopic ratio in samples containing uranium. Nucl. Instruments Methods Phys. Res. A 622:443–448.
10. Vermaercke P, Hult M, Verheyen L, Farina Arboccò F (2010) Measurement of the isotopic composition of germanium by k0-INAA and INAA. Nucl. Instruments Methods Phys. Res A 622:433–437.

13.2 List of A2 publications

1. Vermaercke P, Sneyers L, Farina Arboccò F, Aleksiayenak Y (2011) Using k0-UNAA for the determination of depleted uranium in the moss biomonitoring technique. Int. J. Environ. Heal. 5:72. doi: 10.1504/IJENVH.2011.039857.
2. Vermaercke P, Arbocco FF, Sneyers L, Leal A, Bruggeman M (2009) Environmental monitoring for safeguards using k0-standardised Neutron Activation Analysis. 2009 1st Int. Conf. Adv. Nucl. Instrumentation, Meas. Methods their Appl. IEEE, pp 1–5.

13.3 List of international conferences

1. Farina Arboccò F, Vermaercke P, Verheyen L, Strijckmans K. Experimental evaluation of epithermal neutron self-shielding for Zr and Mo foils. Nuclear Analytical Methods in the Life Sciences 10, Bangkok, Thailand, 2012 (poster presentation).
2. Farina Arboccò F, Vermaercke P, Smits K, Sneyers L, Strijckmans K. Re-determination of k0 and Q0 factors for 10 isotopes of analytical interest. Methods & Application of Radioanalytical Chemistry IX, Kona, HI, USA, 2012 (oral presentation).
3. Farina Arboccò F, Vermaercke P, Sneyers L, Strijckmans K. Experimental validation of some thermal neutron self-shielding calculation methods for cylindrical samples in INAA. The 13th Conference in Modern Trends in Activation Analysis, College Station, TX, USA, 2011 (oral presentation).
4. Farina Arboccò F, Strijckmans K, Vermaercke P, Verheyen L, Sneyers L. The impact of polyethylene vials on reactor channel characterization in k0-NAA. The 16th Radiochemical Conference, Mariánské Lázně, Czech Republic, 2010 (oral presentation).
5. Farina Arboccò F, Vermaercke P, Sneyers L, Soares Leal A, Gonçalves Bouças J. The use of k0-NAA for the determination of the n(235U)/n(238U) isotopic ratio in samples containing uranium. The 5th International k0-workshop, Bello Horizonte, Brazil, 2009 (oral presentation).